UNIVERSITY OF OKLAHOMA

GRADUATE COLLEGE

PLANETARY REMNANTS AROUND WHITE DWARF STARS

A DISSERTATION

SUBMITTED TO THE GRADUATE FACULTY

in partial fulfillment of the requirements for the

Degree of

DOCTOR OF PHILOSOPHY

By

SARA DIANN BARBER
Norman, Oklahoma
2015

PLANETARY REMNANTS AROUND WHITE DWARF STARS

A DISSERTATION APPROVED FOR THE
HOMER L. DODGE DEPARTMENT OF PHYSICS AND ASTRONOMY

BY

Dr. Mukremin Kilic, Chair

Dr. Katherine Pandora

Dr. Eddie Baron

Dr. Phillip Gutierrez

Dr. Richard Henry

© Copyright by SARA DIANN BARBER 2015
All Rights Reserved.

For Ginger.

Acknowledgements

This dissertation marks a huge milestone in my life. I have relied heavily on the support of many special people who have challenged, encouraged, and stuck with me along the way.

I would like to express deepest gratitude to my advisor, Dr. Mukremin Kilic, for his full support, expert guidance, and understanding throughout my study and research. Without his incredible responsiveness, patience, and well timed counsel, my thesis work would have been a frustrating and overwhelming pursuit.

I would also like to thank Dr. John Debes, Dr. John Cowan, and Dr. Gregory Parker for seeing me through the job search process. Their vested interest in my success bolstered my confidence and spurred me on through the seemingly endless cycle of deadlines, and I will be forever in their debt.

Thanks also go to my fellow graduate students in the Homer L. Dodge Department of Physics & Astronomy. Scientific research can be a lonely enterprise at times and the wonderful sense of camaraderie I shared with them was invaluably restorative.

Finally, I would like to thank my husband, parents, and sisters for their unconditional love and support during the years. I would not have been able to complete this dissertation without their unflagging willingness to cheer me on.

Contents

Acknowledgements **iv**

Abstract **xv**

1 Introduction **1**
1.1 Exoplanets . . . 1
1.2 Searching in Post-Main Sequence . . . 4
1.3 Dusty White Dwarfs . . . 7
1.4 My Dissertation . . . 11

2 Dusty WDs in the Palomar-Green Catalog **14**
2.1 The Palomar-Green Catalog . . . 14
2.2 Selecting WDs Hospitable to Dust . . . 15
2.3 Observations . . . 17
2.3.1 Near-infrared Photometry . . . 17
2.3.2 Near-infrared Spectroscopy . . . 26
2.3.3 *Spitzer* Photometry . . . 27
2.4 Results . . . 29
2.5 Discussion . . . 35
2.5.1 The Frequency of Debris Disks Around WDs . . . 35
2.5.2 Planets Around Intermediate-Mass Stars . . . 37
2.5.3 Disk Lifetimes . . . 38
2.6 Conclusions . . . 39
2.7 Acknowledgements . . . 40

3 Dusty WDs in the *WISE* All Sky Survey ∩ SDSS **42**
3.1 The Wide-Field Infrared Survey Explorer . . . 42
3.2 Observations and Data Analysis . . . 45
3.2.1 Near-infrared Photometry . . . 45
3.2.2 Disk Modeling . . . 46
3.3 Results . . . 51
3.3.1 Blended Targets . . . 51
3.3.2 New Dusty WDs . . . 54
3.4 The Frequency of Disks in the *WISE* All Sky Survey . . . 58
3.5 Conclusions . . . 60
3.6 Acknowledgements . . . 61

4 A *Spitzer* Search for Massive Dusty WDs **62**
4.1 Introduction . . . 62
4.2 Observations and Data Analysis . . . 67
4.2.1 *Spitzer*+IRAC . . . 67
4.2.2 MMT+SWIRC . . . 68
4.2.3 Gemini+NIRI . . . 68
4.3 Results . . . 69
4.3.1 Galaxy Contamination . . . 76
4.3.2 Debris Disks . . . 77
4.4 Notes on Individual Objects . . . 82
4.5 Merger Remnants . . . 87
4.6 Conclusions . . . 89
4.7 Acknowledgements . . . 90

5 Dusty WDs in the McCook & Sion Catalog **92**
5.1 The McCook & Sion White Dwarf Catalog . . . 92
5.2 Cross-Correlation . . . 93
5.3 IRAC Photometry . . . 94
5.4 Disk Fitting . . . 95
5.5 Results . . . 98
5.5.1 Known Disks . . . 98
5.5.2 New Disks . . . 98
5.5.3 Centroid Positions . . . 103
5.5.4 Frequency Dependence on WD Mass . . . 106
5.6 Conclusions . . . 107
5.7 Acknowledgements . . . 109

6 Conclusions **112**

Bibliography **122**

APPENDICES **126**

A Massive WD SEDs **127**

B McCook & Sion IRAC Photometry **137**

C McCook & Sion IRAC SEDs **151**

D McCook & Sion non-IRAC SEDs **152**

List of Tables

2.1 Sample Properties 20
2.1 Sample Properties 22
2.1 Sample Properties 23
2.1 Sample Properties 24
2.1 Sample Properties 25
2.2 *Spitzer* IRAC Photometry 29

3.1 SWIRC Photometry 53
3.2 Best Fit Disk Parameters 55

4.1 IRAC Ch 1 and Ch 2 Photometry 70
4.1 IRAC Ch 1 and Ch 2 Photometry 71
4.1 IRAC Ch 1 and Ch 2 Photometry 72
4.1 IRAC Ch 1 and Ch 2 Photometry 73
4.2 Ground-based JHK Photometry 74
4.3 Best Fit Disk Parameters 82

5.1 Cross-Correlation Results 94
5.2 IRAC Detections 95
5.3 Input Disk Parameter Grid 97
5.4 Best Fit Disk Parameters 105
5.5 Frequency-Mass Variation 107

6.1 White Dwarfs with Debris Disks 119
6.1 White Dwarfs with Debris Disks 120
6.1 White Dwarfs with Debris Disks 121

B.1 IRAC Ch1 and Ch2 Photometry 138
B.1 IRAC Ch1 and Ch2 Photometry 139
B.1 IRAC Ch1 and Ch2 Photometry 140
B.1 IRAC Ch1 and Ch2 Photometry 141
B.1 IRAC Ch1 and Ch2 Photometry 142
B.1 IRAC Ch1 and Ch2 Photometry 143
B.1 IRAC Ch1 and Ch2 Photometry 144
B.1 IRAC Ch1 and Ch2 Photometry 145
B.1 IRAC Ch1 and Ch2 Photometry 146
B.1 IRAC Ch1 and Ch2 Photometry 147
B.1 IRAC Ch1 and Ch2 Photometry 148
B.1 IRAC Ch1 and Ch2 Photometry 149

B.1 IRAC Ch1 and Ch2 Photometry 150

List of Figures

1.1 Histogram of (a) semi-major axis and (b) publication year for all known planets including unconfirmed Kepler Objects of Interest (KOI). Note that the maximum orbital separation is 5 AU. The 2011 and 2014 peaks are Kepler discoveries. All data downloaded from `exoplanets.org`. 2

1.2 Histogram of all confirmed planets discovered via transits and radial velocity variations (`exoplanets.org`). Note the strong cutoff in detections above 3 $M_{\odot}$. Sun-like stars have been the focus of main-sequence exoplanet searches, thus the massive stellar regime remains largely unexplored. 5

1.3 The canonical spectral energy distribution (SED) for a WD+disk system. The excess of a warm disk starts in the NIR and persists for all mid-IR photometric bands. Cooler disks may show no excess until the mid-IR and are therefore easy to miss. 6

1.4 All polluted WDs with O, Mg, Si, and Fe measurements resemble composition of bulk Earth (Xu et al. 2014). 8

2.1 The PAIRITEL vs. 2MASS photometry for our sample. The PAIRITEL data agrees fairly well with the 2MASS photometry. 18

2.2 $J-H$ and $J-K$ colors vs. temperature for our sample of DA WDs from the PG catalog. Red squares and blue triangles show the confirmed dusty WDs and objects with follow-up IRTF spectroscopy, respectively. Solid lines show the predicted sequences for DA WDs (Bergeron et al., 2011). 21

2.3 SED of the known dusty WD GALEX J1931+0117. Green points represent 2MASS photometry, while blue points represent the photometry from Melis et al. 2011. The IRTF spectrum is shown in black and the red line represents the predicted contribution from a blackbody stellar photosphere. The noise near 1.9 and 2.5 μm falls in regions of poor telluric correction. The 1.28 μm feature is Paβ absorption. The detection of slight K-band excess around this target demonstrates that our near-infrared observations and reductions are reliable. 28

2.4 Spectral energy distributions of 41 WDs observed at the IRTF. The PAIRITEL and 2MASS photometry are shown as blue and green points, respectively. The black lines show the observed spectra and the red solid lines show the predicted photospheric emission for each star assuming blackbody emission. The IRTF spectra display telluric correction problems around 1.4 and 1.9 μm. 31
2.5 SEDs of the 11 WDs with new *Spitzer* photometry (shown in purple). The symbols are the same as in Figure 2.3. The IRTF spectra display telluric correction problems around 1.4 and 1.9 μm. Our *Spitzer* observations confirm the results of the IRTF observations; only PG1541+651 shows a significant infrared excess. 32
2.6 SEDs of the five dusty WDs in our sample. The symbols are the same as in Figure 2.5. The IRTF spectra display telluric correction problems around 1.4 and 1.9 μm. 33
2.7 Color-color diagrams using PAIRITEL/2MASS and WISE photometry for our WD sample. Red triangles mark the dusty WDs. Four of the five dusty WDs in our sample clearly show infrared excesses in the WISE bands. The fifth dusty WD, PG 1457−086, is also detected in the WISE observations, but with large photometric errors. 34
2.8 Probability function for WDs with debris disks. Probability, $P_n(N, p)$, of finding $n = 5$ debris disks as a function of assumed true debris disk frequencies, p, where $N = 117$. Dashed lines delineate the region containing 68% probability, equivalent to 1σ Gaussian limits. The solid line indicates the peak of the distribution. The derived frequency is $4.3^{+2.7}_{-1.2}$%. 36

3.1 The spectral energy distribution of WDs with nearby point sources. Pure hydrogen atmosphere models (Tremblay & Bergeron 2009; Tremblay et al. 2010; Gianninas et al. 2011), shown in blue, are normalized to the SDSS *griz*-bands. SDSS, SWIRC, and *WISE* photometry are shown as magenta circles, orange squares (empty squares for nearest blending point source), and green diamonds, respectively. ALLWISE data are plotted where available. The SDSS i-band and SWIRC J- and H-band science images of the corresponding WD field are shown to the right. The yellow circle indicates the $6''$ *WISE* beam. The small magenta circle is centered on the WD's SDSS J2000 coordinates with a radius equal to the proper motion since the SDSS DR7 data were taken and is used to identify the WD. Extraneous objects within the yellow circle are likely the source of the excesses detected in the *WISE* data. 47

3.2 The $J-H$ and $H-W2$ colors of the contaminating sources near to the WDs in our sample are shown by red circles. The L/T dwarf and M dwarf colors are derived from the NIR and *WISE* photometry published in Table 1 of Kirkpatrick et al. 2011 and are represented by green squares/blue triangles and orange diamonds, respectively. The colors of the contaminating sources in our SWIRC images are generally redder than the known brown dwarf and M dwarf populations and are more likely background galaxies. 49
3.3 The SED of the four isolated WDs in our sample. The SED components are the same as those described in Figure 3.1 except for the disk model, which is shown in red and the WD+disk combination which is shown in black here. The science images of these WDs show no obvious sign of contamination that could explain the excesses found in the *WISE* data. These excesses are well reproduced by geometrically flat, optically thick disk models (Jura 2003). . . . 56
3.4 The $J-H$ and $H-W2$ colors of the naked WDs in the WIRED sample are shown as empty green circles, while the colors of known dusty WDs and our four new dusty WDs are shown as small blue and large red circles, respectively. The NIR and MIR photometry for the published WD+disk systems are taken from the 2MASS and *WISE* online databases. The colors of the four new dusty WDs are comparable to the colors of the dusty WD population from the literature and are therefore likely to have the same mechanism generating their infrared excesses. 57

4.1 Histogram of stellar host mass of all confirmed exoplanets (`exoplanets.org`; Han et al. 2014) detected via transits and radial velocity variations as well as WD progenitor masses from this sample. This work probes a region in parameter space currently devoid of planetary systems. . 63
4.2 (a) Histogram of SDSS g-band magnitude for our sample (cyan) compared with published dusty WDs (red). We are probing a relatively faint population of WDs compared to the known dusty WD population. (b) Histogram of effective temperatures for all published dusty WDs and WDs from this sample. We are selecting WDs most hospitable to solid dust by using a 9500-22,500 K temperature cut. 66
4.3 Histogram of photometry excesses in the NIRI K-band as well as both IRAC channels. 75

4.4 Probability of detecting a 3σ excess at WDs in our sample due to chance alignment with a background galaxy (Fazio et al., 2004a). At this flux level, we expect 8 WDs, at most, to exhibit spurious significant excesses out of our 100 WD sample. 78
4.5 Original (left) and PSF-subtracted (right) IRAC Ch 2 images show the clean subtraction of sources close the the WD. The black arrow indicates the position of the WD. 80
4.6 Three WDs exhibiting excess emission consistent with a dusty debris disk. The insets to the right are the SDSS *i*-, SWIRC/UKIDSS *J*-, NIRI *K*-, and IRAC 2-band images. All frames have a 2.4″ circle indicating the IRAC photometry aperture size. The small circles on the IRAC 2 inset indicate the SDSS *g*-band (cyan) and IRAC Ch 2 (magenta) centroid positions corrected for proper motion. All centroids are consistent and thus galaxy contamination is unlikely. . 83
4.7 Histogram of progenitor mass for WDs in our sample (cyan), known dusty WDs (red), and new dusty WDs identified in this work (blue). The 1.04 $M_\odot$ (5.4 $M_\odot$ progenitor mass) WD known to have a disk is the helium-atmosphere WD J1234 Barber et al. 2014, identified from the *WIRED* Survey. The 0.84 $M_\odot$ (4.1 $M_\odot$ progenitor mass) known dusty WD was discovered by Dufour et al. 2010. This work increases the number of massive (>0.8 $M_\odot$) dusty WDs to five with the discovery of the first three hydrogen-atmosphere massive WDs with circumstellar dust. 84
4.8 (a) All polluted WDs with O, Mg, Si, and Fe measurements resemble composition of bulk Earth (Xu et al. 2014). (b) Predicted chemical composition of the disk formed following a WD+WD merger (Lorén-Aguilar et al. 2009). 89

5.1 Histogram of IRAC 2 excess significance, *V* magnitude, effective temperature, mass, surface gravity, and distance for all 1265 WDs. The dark histogram indicates the parameter space occupied by the dusty WDs. 96
5.2 (a) Comparison between published IRAC photometry vs. photometry we measure for the ten known dusty WDs in our sample with publicly available IRAC images in the *Spitzer* Heritage Archive. Our IRAC photometry agrees with published values. (b) Comparison of published disk parameters and our best-fit disk parameters. Error bars show 200 K errors for disk temperatures and 25° errors for inclination. Grey lines indicate a one-to-one relation. 99

5.3 Infrared colors of our sample (black dots) compared with known dusty WDs (open red circles). WDs without IRAC data are shown as empty circles. 100
5.4 SEDs and our model WD+flat disks for the 12 previously known dusty WDs. All available photometry, including GALEX (right triangle), Johnson-Cousins (star), SDSS (circle), 2MASS (square), UKIDSS (up triangle), *WISE* (left triangle), and *Spitzer* (down triangle), is shown. 101
5.5 Original IRAC Ch 1 image (left) and PSF-subtracted image (right) for 0420+520. The blending source is successfully removed and the resultant photometry is virtually unchanged. 103
5.6 SED for three new dusty WDs. The blending source in the J0420 IRAC 1 image is removed before PSF photometry is performed. . . 104
5.7 2MASS vs IRAC centroid separations for each dusty WD corrected for proper motion. Centroids closer than $0.5''$, the pointing accuracy of IRAC, are considered consistent. 105
5.8 (a) Frequency of disks as a function of mass. The shaded region indicates the 1σ binomial confidence interval. (b) Probability of giant planet formation vs stellar mass (Kennedy & Kenyon, 2008). . 108

6.1 We've expanded the temperature and mass regime occupied by dusty debris disks. 115
6.2 All 42 debris disks with published disk parameters. Debris disks are pictured to scale relative to the sun. The colors of the disks indicate the WD mass. Blue WD names indicate disks presented by this work. For WDs without published masses, we assume 0.6 $M_{\odot}$. . 117
6.3 All 42 debris disks with published disk parameters. Debris disks pictured to scale relative to the sun. The colors of the disks indicate the WD effective temperature. Blue WD names indicate disks presented by this work. 118

Abstract

In this dissertation we present the results of four separate searches for infrared excess emission at white dwarf stars. Using spectra from the IRTF and photometry from PAIRITEL, MMT+SWIRC, Gemini+NIRI, and *Spitzer*+IRAC we discover 11 new dusty WD systems. These new systems increase the population of such systems by 33%, bringing the total to 45. These discoveries also significantly expand the mass-temperature parameter space available to circumstellar dust at WDs with the discovery of the hottest, coolest, and most massive WD with dust. Future searches for WD debris disks can exploit these results to streamline their target selection. Our three massive dusty WDs also illustrate that massive main-sequence stars do host planets, despite the dearth of detections in this regime using conventional planet detection methods. We find the frequency of disks at WDs to be 4.3% around a sample of typical WDs and that the frequency varies with mass. The frequency amongst our sample of massive WDs is 3%. The frequency of disks at WDs is also used to derive that WDs can accrete objects as large as the dwarf planet Ceres.

Chapter 1

Introduction

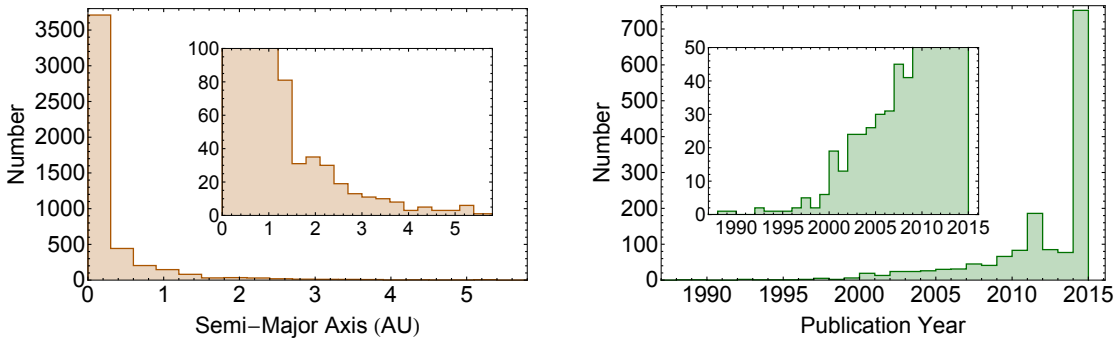
"And the earth withers, the moon crumbles, one by one stars flutter into dust."

– E. E. Cummings, *As Is The Sea Marvelous*

1.1 Exoplanets

Planets are signposts for life, thus the quest to answer one of the most profound questions facing humanity takes form as a hunt for planets. Over the last two decades, hundreds of planets have been discovered using a variety of techniques, each with its own set of advantages and shortcomings. The most intuitive method for detecting planets, of course, is to directly image them. Unfortunately, this method has also proven to be the most difficult. The small angular size of the orbit, in conjunction with the large contrast in brightness between the star and planet place most systems beyond the resolution and photometric accuracy limit of current observational facilities. From a distance of 5 parsecs, for instance, the greatest angular separation between Jupiter and the Sun would be just 1 arcsecond and the Sun's visible light would outshine Jupiter's by a factor of one billion (Mason, 2008). Indeed, very few planets have been discovered this way.

Instead, the vast majority of known exoplanets have been discovered indirectly − by measuring a planet's influence on the apparent brightness or motion of its host star. This is a very exciting time in the history of exoplanetary study. Searches for transits and radial velocity shifts have been extremely successful at finding planets interior to 5 AU to date. These two methods alone account for nearly 5000 planet discoveries (Figure 1.1), most of which have occurred in just the last five years. Despite the recent surge of exoplanet detections from the Kepler mission, there are several challenges facing main sequence exoplanetary searches.



(a) (b)

Figure 1.1: Histogram of (a) semi-major axis and (b) publication year for all known planets including unconfirmed Kepler Objects of Interest (KOI). Note that the maximum orbital separation is 5 AU. The 2011 and 2014 peaks are Kepler discoveries. All data downloaded from `exoplanets.org`.

Planetary transits, for instance, can be detected via the apparent decrease in stellar brightness as a planet passes between its star and the observer. Transit observations provide the planet's orbital period and is the only method for measuring its radius. The radius is required for calculating the mean density which

can give an estimate of the planet's bulk composition. Unfortunately, observing a planetary transit hinges on the slim chance of an alignment between the orbital plane and the observer's line of sight. For example, the probability of a Sun-like star being transited by a planet orbiting at 1 AU (Earth's orbital distance) is only 0.5%. More distant planets, like Jupiter, are even less likely to transit. Also, a small ratio of stellar to planetary cross-sectional area is required to produce a transit signal deep enough to detect. Even the transit of Jupiter, the largest planet in our Solar System, would decrease the sun's apparent brightness by just 1%. This places small planets and planets orbiting massive stars beyond our reach.

Radial velocity measurements, on the other hand, track the variations in stellar motion along the observer's line of sight due to the gravitational pull of a planet. This method can be used to obtain the planet's mass as well as its orbital semi-major axis. Similar to transits, radial velocity measurements require that the orbital plane be highly inclined. Furthermore, systems with low mass planets and/or high mass stars produce small velocity variation amplitudes, making them difficult to detect. Earth's gravitational pull, for example, produces a velocity shift in the sun of less than 0.1 m/s which is one fifth of the most precise radial velocity measurement ever recorded (Dumusque et al., 2012). Finally, for some systems, Doppler shifts due to variations in stellar activity can closely resemble the radial velocity signal of a planet. Many of the hurdles facing main sequence

planet detections are compounded with increasing stellar mass. In fact, virtually no planets have been detected at stars more massive than 3 $M_\odot$ (Figure 1.2).

Despite this bias in exoplanet detections, the frequency of Jovian planets increases from 3% for M dwarfs to 14% for 2 $M_\odot$ stars (Johnson et al. 2010; Bowler et al. 2010). Could it be that planets do not form around massive (>3 $M_\odot$) stars, or is this a selection effect? The planet formation models of Kennedy & Kenyon 2008 and Alibert et al. 2011 suggest the latter. They predict that the fraction of stars with giant planets shows a steady increase with mass up to 3 $M_\odot$. In addition, the mass of the planets and the width of the regions where they form are predicted to increase with stellar mass.

1.2 Searching in Post-Main Sequence

Since conventional planet detection techniques lose sensitivity in the massive (>3 $M_\odot$) regime, one can more easily search for planets by looking at these systems in post-main sequence. If planets survive post-MS evolution, they should be detectable around white dwarfs (WDs) (Burleigh et al., 2002; Gould & Kilic, 2008). Unfortunately, there are still no confirmed planets around single WDs (Burleigh et al., 2003; Friedrich et al., 2007). The candidate planet around the pulsating WD GD 66 (Mullally et al., 2007) is currently disputed (Hermes, 2013). Perhaps an easier way to detect remnant planetary systems around WDs is to look for the tidally

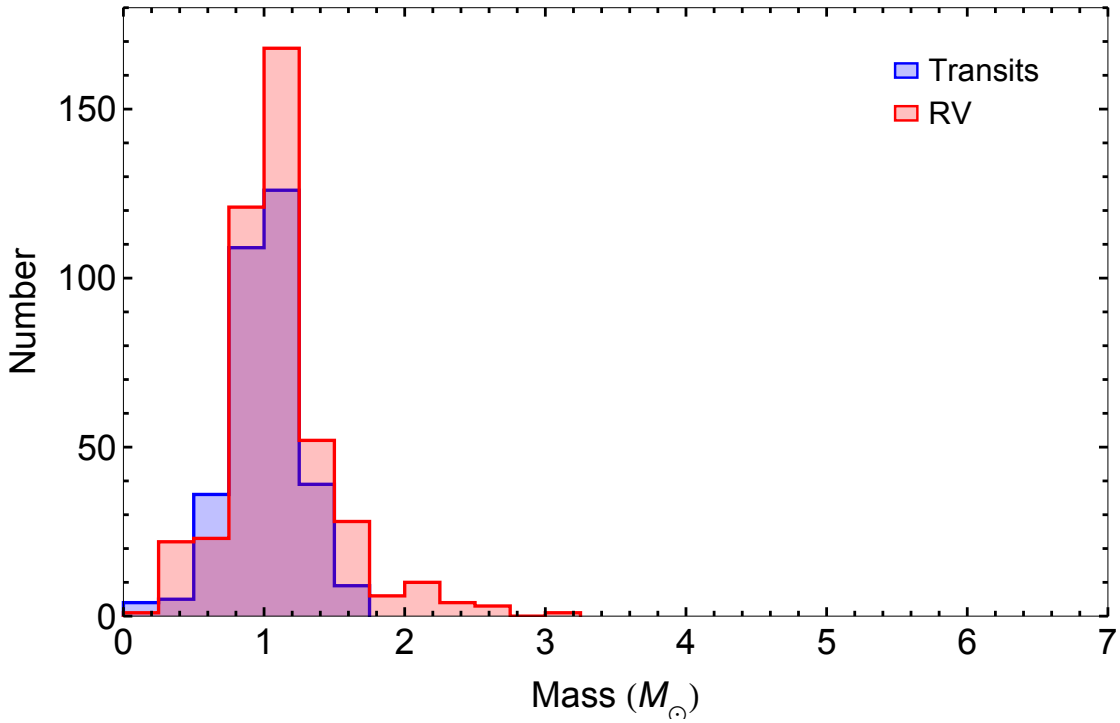


Figure 1.2: Histogram of all confirmed planets discovered via transits and radial velocity variations (`exoplanets.org`). Note the strong cutoff in detections above 3 $M_\odot$. Sun-like stars have been the focus of main-sequence exoplanet searches, thus the massive stellar regime remains largely unexplored.

disrupted remains of exoplanets, moons, and asteroids in the form of circumstellar debris disks (Debes & Sigurdsson, 2002; Jura, 2003; Kilic et al., 2006; Veras et al., 2013, 2014b,a). Take a planetary system consisting of a WD, an asteroid-belt analog and a Jupiter analog. In this scenario, minor bodies are sent into chaotic orbits through repeated mean-motion resonance interactions with the Jupiter-like giant planet (Debes & Sigurdsson, 2002; Jura, 2003). In the event where the planetesimal crosses the tidal radius of its host WD, it is ripped apart. Subsequent passes further degrade the debris and it eventually embodies a disk geometry. The

signature of a disk orbiting a white dwarf is excess emission in the infrared due to the reprocessed light from this dust (Figure 1.3). This emission is spread out over a much larger area than the cross-sectional area of any planet, making it much brighter and easier to detect.

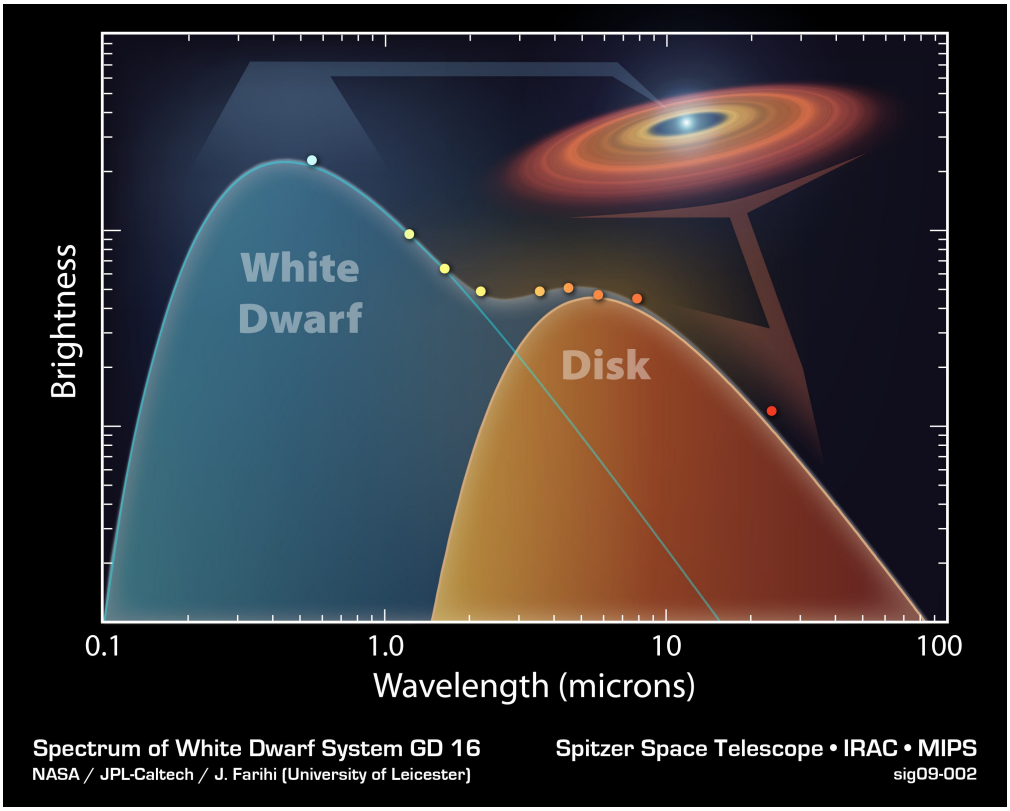


Figure 1.3: The canonical spectral energy distribution (SED) for a WD+disk system. The excess of a warm disk starts in the NIR and persists for all mid-IR photometric bands. Cooler disks may show no excess until the mid-IR and are therefore easy to miss.

Interestingly, this method of detecting planet hosting systems probes a parameter space complementary to that available to ordinary planet searches. For instance, the signal strength of a circumstellar disk orbiting a WD does not decrease

with increasing stellar mass. Also, contrary to transit and Doppler shift signals, the emission from a disk of tidally disrupted planetesimals is strongest when the orbital plane is face-on. Finally, planets that survive the red giant branch and asymptotic giant branch phases of stellar evolution likely lie several AU from the star (Burleigh et al., 2002). Thus, WD debris disks offer access to the otherwise elusive regime of planetary systems with massive host stars, face-on orbital planes, and large orbital separations.

1.3 Dusty White Dwarfs

Dust persists around a WD inside the tidal radius (radius where the gravitational force and tidal force are equal) of the WD and outside the radius at which the equilibrium temperature is such that the dust will sublimate (2100 K for pure carbon dust; Debes et al. 2011b). Some disks have been found to extend interior to this radius. Rafikov & Garmilla 2012 find that the dust sublimation temperature may be increased due to the vapor pressure of sublimated dust at the disk's inner rim. Poynting-Robertson drag carries dust from the tidal radius inward toward the WD where viscous torques cause the sublimated dust to accrete onto the WD's surface (Rafikov 2011a,b; Metzger et al. 2012; Veras et al. 2013). This accretion results in a spectroscopically detectable pollution of the otherwise pristine WD atmosphere. Photospheric abundance analyses of polluted WDs show that the accreted met-

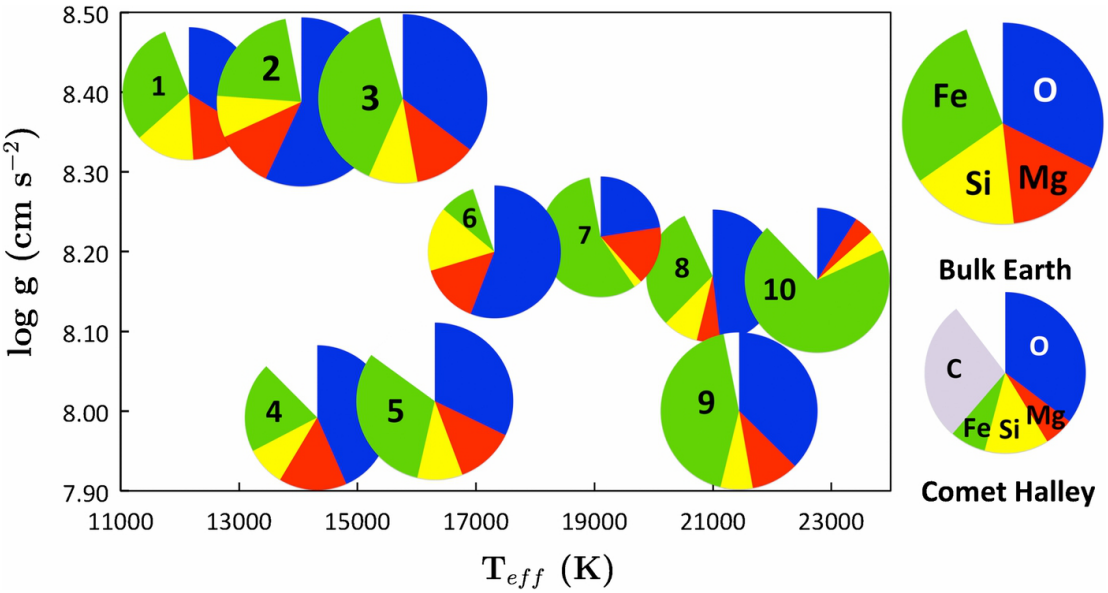


Figure 1.4: All polluted WDs with O, Mg, Si, and Fe measurements resemble composition of bulk Earth (Xu et al. 2014).

als originate from tidally disrupted minor bodies similar in composition to that of bulk Earth (Zuckerman et al. 2007; Dufour et al. 2010; Xu et al. 2014; Figure 1.4). Depleted levels of hydrogen and carbon rule out accretion of the interstellar medium (ISM) as a source of photospheric pollution (Jura 2006).

All known WDs with disks show metal absorption lines in their optical and ultraviolet spectra; DAZ and DBZ spectral types. The Poynting-Robertson drag timescale is significantly shorter than the evolutionary timescales for WDs (von Hippel et al., 2007; Rafikov, 2011b), hence we expect every WD with dust/gas disks to accrete metals from these disks and appear metal-rich. Zuckerman et al. (2003, 2010) find that about 30% of hydrogen (DA) and helium (DB) atmosphere WDs

show trace amounts of metals in their photospheres. However, only $\sim 20-30\%$ of DAZs, the ones with the highest accretion rates, host dust (Kilic et al., 2008; Farihi et al., 2009). The source of metals for the other DAZs remains unknown but it is likely that the majority of DAZs accrete many small asteroids that do not form a large, infrared-bright debris disk (Jura, 2008).

Dusty disks surrounding WDs are generally assumed to be geometrically flat and optically thick (Jura 2003; Rafikov 2011a,b) with properties similar to the rings of Saturn. Based on flat disk models, they vary in width from a narrow ring, extending only a few tenths of a solar radius, to a disk filling the entire region interior to the tidal disruption radius of the star and exterior to the radius of dust sublimation ($\sim R_{\odot}$). The WDs known to host debris disks typically range in temperature from 9500-22,500 K, in age from 0.05 - 1 Gyr, and in mass from 0.5-0.7 $M_{\odot}$.

The search for debris disks around WDs begins as a search for excess emission in the infrared. Over the last two decades, several hundreds of WDs have been surveyed for infrared excess due to substellar companions or circumstellar disks. The first dusty WD, G29-38, was identified by Zuckerman & Becklin (1987), see also Graham et al. (1990). Zuckerman & Becklin (1992) examined 200 WDs for excesses in the K-band, while Farihi et al. (2005) surveyed 371 WDs of all spectral types and constrained the frequency of companions to less than 0.5%. The dis-

covery of the second dusty WD, GD 362, (Kilic et al., 2005; Becklin et al., 2005) lead to the realization that dusty WDs may be found more readily by focusing the search on metal-rich WDs.

Mullally et al. (2007) survey 124 WDs with T_{eff}=5000-170,000 K using mid-infrared *Spitzer* photometry. Their search for infrared excess finds 2 dusty WDs for a disk frequency of 1.6%. However, this survey extends beyond the temperature range within which solid dust orbiting interior to the tidal radius can persist. Based on *Spitzer* observations of mostly metal-rich WDs, Farihi et al. (2009) estimate a debris disk frequency of 1% to 3% for WDs younger than 500 Myr. Debes et al. (2011b) recently searched for infrared excesses amongst an unbiased (in terms of metallicity) WD sample using the Wide-field Infrared Survey Explorer (WISE, Wright et al., 2010) data. They found about 1-5% of these WDs to be dusty. However, the large beam size of WISE allows for many false positives due to background contamination, and many of these dusty WD candidates need follow-up higher spatial resolution infrared imaging data to confirm the observed infrared excess. Just such a follow-up is presented in Chapter 3. In 2012, we conducted a NIR search for excesses around 117 DA WDs from the Palomar-Green survey and found 4.3% to have debris disks (Chapter 2). Most recently, Rocchetto et al. 2014 found five dusty WDs in their sample of 134 young DA WDs for a occurrence rate of 3.7%.

Prior to the publication of this dissertation, 39 WDs were known to host dust disks (Barber et al., 2014; Bergfors et al., 2014; Rocchetto et al., 2014). With this work, we explore the frequency of disks orbiting the greater DA WD population. We also probe, for the first time, a large number of massive WDs for disks. We significantly increase the dusty WD population with the discovery of 11 disks. We also expand the parameter space occupied by WD+disk systems with the discovery of the hottest, coolest, and most massive dusty WDs. While previous surveys have searched sample sizes in the tens to hundreds of WDs, this work presents a search for disks among thousands of WDs.

1.4 My Dissertation

As an undergraduate student I had the privilege of working on my senior project with Dr. William Romanishin. Over the summer of 2008 I used the University of Oklahoma campus observatory to study the opposition effect of solar system asteroids − a sharp peak in brightness caused by the sudden illumination of surface craters when an asteroid moves into opposition. This experience left me with a strong passion for observing and a keen interest in planetary systems. At the start of my third year of graduate school, Dr. Mukremin Kilic joined the Homer L. Dodge Department of Physics & Astronomy faculty. His work on tidally disrupted asteroids orbiting WDs was a perfect fit for me and, happily, he agreed to

take me on. What follows is the culmination of our nearly four year collaboration.

My dissertation project has focused on increasing the population of and expanding the parameter space occupied by WD+disk systems in order to better understand the formation, evolution, and pervasiveness of planetary systems in the galaxy. Much of this work has been previously published as first author papers in the Astrophysical Journal with the help of several collaborators, thus I have adopted "we" as the first person pronoun throughout. This dissertation is arranged as follows:

Chapter 2 presents near- and mid-infrared photometry and spectroscopy from PAIRITEL, IRTF, and *Spitzer* of a metallicity-unbiased sample of 117 cool, hydrogen atmosphere WDs from the Palomar-Green survey. We present a 4.3% disk occurrence rate in this sample and use this to calculate the average total mass accreted by planet-hosting WDs.

Chapter 3 describes the follow-up to a cross-correlation between the Sloan Digital Sky Survey (SDSS) Data Release 7 White Dwarf Catalog with the *Wide-Field Infrared Survey Explorer* (*WISE*) all-sky photometry which resulted in the identification of 52 WD+debris disk candidates. We present MMT+SAO Wide-Field InfraRed Camera J- and H-band imaging observations of 16 candidates and confirm four as bonafide disks.

Chapter 4 is a *Spitzer* search for circumstellar dust around 100 massive ($>0.8\,M_{\odot}$)

white dwarfs from the SDSS DR7 White Dwarf Catalog. We present three new debris disks in this sample, more than doubling the number of massive dusty WDs known in the literature.

Chapter 5 lays out the results from cross-correlation of archival GALEX, SDSS, UKIDSS, 2MASS, WISE, and *Spitzer* data for 1265 WDs from the Gianninas et al. 2011 spectroscopic survey of bright, hydrogen-rich WDs. We find 15 dusty WDs in the subset of this sample with *Spitzer* data (30%) which includes the discovery of three new disks.

Chapter 6 brings together a summary of the aforementioned results.

Chapter 2

Dusty WDs in the Palomar-Green Catalog

"Write your injuries in dust, your benefits in marble."

– Benjamin Franklin, *Poor Richard's Almanack*

2.1 The Palomar-Green Catalog

We start our search for dust with a selection of white dwarfs (WDs) from the Palomar-Green (PG) catalog. The PG catalog selects 1874 UV-bright objects down to B magnitudes of 16.1 (Green et al., 1986). The catalog is 84% complete and covers an area of 10,714 square degrees from 266 fields taken using the Palomar 18-inch Schmidt telescope in San Diego County, California. The catalog is dominated by hot subdwarf stars, however 21% of the sample is made up of hydrogen-atmosphere (DA) WDs. These bright WDs are great targets for disks because, if found to be dusty, they can easily be followed-up spectroscopically to determine their atmospheric abundances.

We present near- and mid-infrared photometry and spectroscopy from PAIRITEL, IRTF, and *Spitzer* of a metallicity-unbiased sample of 117 cool, DA WDs from the PG catalog and find five with excess radiation in the infrared, translating to a $4.3^{+2.7}_{-1.2}$% frequency of debris disks. This is slightly higher than, but

consistent with the results of previous surveys. Using an initial-final mass relation, we apply this result to the progenitor stars of our sample and conclude that 1-7 $M_{\odot}$ stars have at least a 4.3% chance of hosting planets; an indirect probe of the intermediate-mass regime eluding conventional exoplanetary detection methods. Alternatively, we interpret this result as a limit on accretion timescales as a fraction of WD cooling ages; WDs accrete debris from several generations of disks for $\sim$10 Myr. The average total mass accreted by these stars ranges from that of 200 km asteroids to Ceres-sized objects, indicating that WDs accrete moons and dwarf planets as well as Solar System asteroid analogues.

2.2 Selecting WDs Hospitable to Dust

Almost all known dusty WDs are relatively young, with cooling ages of $\lesssim 1$ Gyr and temperatures in the range 9500-22,500 K (with the exception of G166-58, Farihi et al. 2008). This is probably because a second heavy bombardment phase occurs around intermediate-mass stars in their post-main sequence (MS) evolution due to planetary migration around the mass-losing star (Debes et al., 2012; Bonsor & Wyatt, 2012). We would expect to see a peak in the frequency of collisions, tidal disruptions, and disks around the younger WD remnants of such stars (Debes & Sigurdsson, 2002).

Consider the disk around G29-38 ($T_{\rm eff}$=11,600 K) as a typical system. Jura

(2003) models the disk emission and obtains a ring of dust extending from R_{in}=0.1 $R_{\odot}$ to R_{out}=0.4-0.9 $R_{\odot}$ and T=300-600 K. Such a disk around a star twice or three times as hot as G29-38 would be sublimated and invisible in the IR. That's why a target selection using effective temperature gives a better measurement of the real frequency of disks.

To this end, we select 117 apparently single DA WDs from the PG catalog with T_{eff}=9500-22,500 K, where we are most efficient in finding disks using near- and mid-infrared data. Liebert et al. (2005) performed a detailed model atmosphere analysis of all DA WDs in the PG catalog and provided temperature, surface gravity, mass, and age estimates. Their spectroscopy did not have enough resolution to detect the metal-rich DAZs among these targets. Our survey does not have a metallicity bias, and hence it has the potential to reveal the true frequency of dusty disks without knowing the fraction of metal-rich WDs among the nearby WD population.

Section 2.3 describes our near- and mid-infrared photometry and spectroscopy data, while Section 2.4 presents the spectral energy distributions (SEDs) and the dusty WDs in the PG catalog. Section 2.6 presents a discussion of the frequency of disks and planets around WDs and their progenitor MS stars.

2.3 Observations

2.3.1 Near-infrared Photometry

We obtained simultaneous JHK_s imaging of 78 WDs using the Peters Automated Imaging Telescope (PAIRITEL, Bloom et al., 2006) between February 2009 and April 2010. PAIRITEL is the old Two Micron All Sky Survey (2MASS, Cutri et al., 2003) telescope and it uses the same camera and filter set. The total exposure time for our targets ranged from 70-1500 s depending on the expected brightness of each target. We use the PAIRITEL pipeline version 3.3 processed images and standard `IRAF DAOPHOT` routines to perform aperture photometry on every 2MASS source detected in the images. We use 2MASS stars to calibrate the photometry for each object.

Table 2.1 presents the PAIRITEL photometry (and the 2MASS photometry of a few relatively bright targets) for our sample along with the physical parameters obtained from the model atmosphere analysis of Liebert et al. (2005). We compare our PAIRITEL photometry to that of 2MASS in Figure 2.1. Only about half of our targets are detected by 2MASS in the K-band, and usually with large photometric errors. Our survey goes significantly deeper than 2MASS and provides improved photometry with smaller errors, which is essential for identifying objects with slight K-band excesses. This figure demonstrates that the PAIRITEL photometry

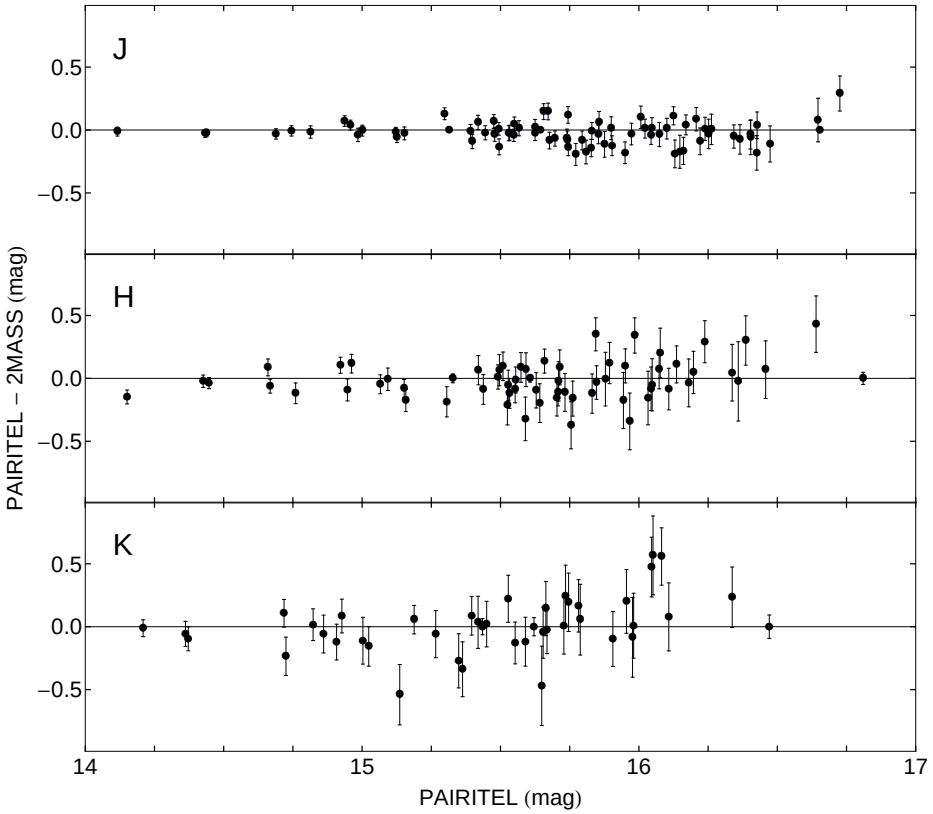


Figure 2.1: The PAIRITEL vs. 2MASS photometry for our sample. The PAIRITEL data agrees fairly well with the 2MASS photometry.

agrees fairly well with the 2MASS photometry and that it can be used reliably to constrain the near-infrared SEDs of our targets.

Figure 2.2 shows $J - H$ and $J - K$ colors of our sample of stars as a function of their effective temperatures. The colors for the majority of our targets follow the model predictions of $J - H = J - K \approx 0$ mag, though with some scatter. There are four WDs with $J - H$ excesses, though with relatively noisy 2MASS photometry. However, from the available mid-infrared photometry from *Spitzer*

and/or *WISE*, we conclude that there is no evidence of excess in these objects. The $J-H$ photometry for the rest of the targets are consistent with the emission from single WDs. Several of these apparently single WDs have positive $J-K$ colors, suggesting extra emission from a cool companion or a circumstellar debris disk. We chose to further examine those objects with positive $J-K$ colors by obtaining near-infrared spectra and mid-infrared photometry. Objects with apparently red colors were targeted however, depending on the timing of the observing runs and conditions, some of the objects with blue colors were also followed up as a sanity check.

Table 2.1. Sample Properties

PG	T_{eff} (K)	log g	WD Mass ($M_\odot$)	MS Mass ($M_\odot$)	τ (Myr)	J (mag)	H (mag)	K (mag)	Ref.	Data
0000+172	20210	7.99	0.62	2.1	85	16.262±0.016	16.299±0.035	16.237±0.154	1	I,P
0033+016	10980	8.83	1.12	6.7	2089	15.625±0.014	15.659±0.030	15.649±0.086	1	I,P
0048+202	20160	7.99	0.62	2.1	85	15.795±0.020	15.831±0.041	15.637±0.092	1	I,P
0059+258	21370	8.04	0.65	2.3	78	16.252±0.018	16.266±0.033	16.325±0.135	1	I,P
0107+268	13880	7.87	0.54	1.3	245	15.392±0.015	15.420±0.030	15.528±0.111	1	I,P
0132+254	19960	7.45	0.41	0.1	63	16.446±0.128	···	···	1,9	
0816+297	16660	7.84	0.53	1.2	129	16.141±0.105	15.921±0.184	···	1,10	
0819+364	18740	8.03	0.64	2.3	123	16.026±0.088	···	15.781±0.228	1,10	
0821+633	16770	7.82	0.52	1.2	123	16.221±0.009	16.238±0.018	16.342±0.045	1	P
0826+455	10370	7.86	0.52	1.2	513	15.001±0.006	14.947±0.009	14.927±0.018	1	I,S,P
0852+659	19070	8.13	0.70	2.8	141	15.876±0.079	15.826±0.184	···	1,8	
0854+405	22250	7.91	0.58	1.7	46	15.419±0.009	15.496±0.014	15.553±0.029	1	I,P
0908+171	17340	7.92	0.57	1.6	129	16.403±0.013	16.458±0.024	16.573±0.064	1	P
0915+526	15560	7.96	0.60	1.9	200	15.809±0.009	15.894±0.018	15.977±0.039	1	P
0933+729	17380	8.00	0.62	2.1	148	16.074±0.009	16.067±0.018	16.108±0.045	1	P
0938+286	14490	7.82	0.52	1.2	200	15.742±0.016	15.750±0.027	15.924±0.060	1	P
0938+550	18530	8.10	0.68	2.6	148	15.153±0.025	15.306±0.033	15.396±0.053	1	I,P
0943+441	12820	7.55	0.41	0.1	339	13.643±0.028	13.707±0.041	13.722±0.046	1,9	
0947+326	22060	8.31	0.82	3.9	117	16.022±0.015	16.044±0.023	15.841±0.069	1	I,P
0950+078	14770	7.95	0.59	1.8	229	16.148±0.011	16.280±0.021	16.280±0.049	1	P
0954+697	21420	7.91	0.58	1.7	54	16.427±0.016	16.612±0.042	16.548±0.078	1	P
0956+021	15670	7.80	0.51	1.1	151	16.007±0.012	16.073±0.022	16.130±0.049	1	S,P
1000−002	19470	7.99	0.62	2.1	98	16.474±0.019	16.558±0.054	16.614±0.094	1	P
1003−023	20340	7.95	0.60	1.9	76	15.677±0.014	15.733±0.030	15.845±0.057	1	P
1005+642	19660	7.93	0.58	1.7	81	14.232±0.029	14.330±0.050	14.356±0.052	1	
1015+161	19540	8.04	0.65	2.3	110	15.950±0.010	15.944±0.018	15.906±0.036	1,4	P
1017+125	21670	7.94	0.60	1.9	56	16.236±0.096	15.856±0.177	15.875±0.253	1,10	

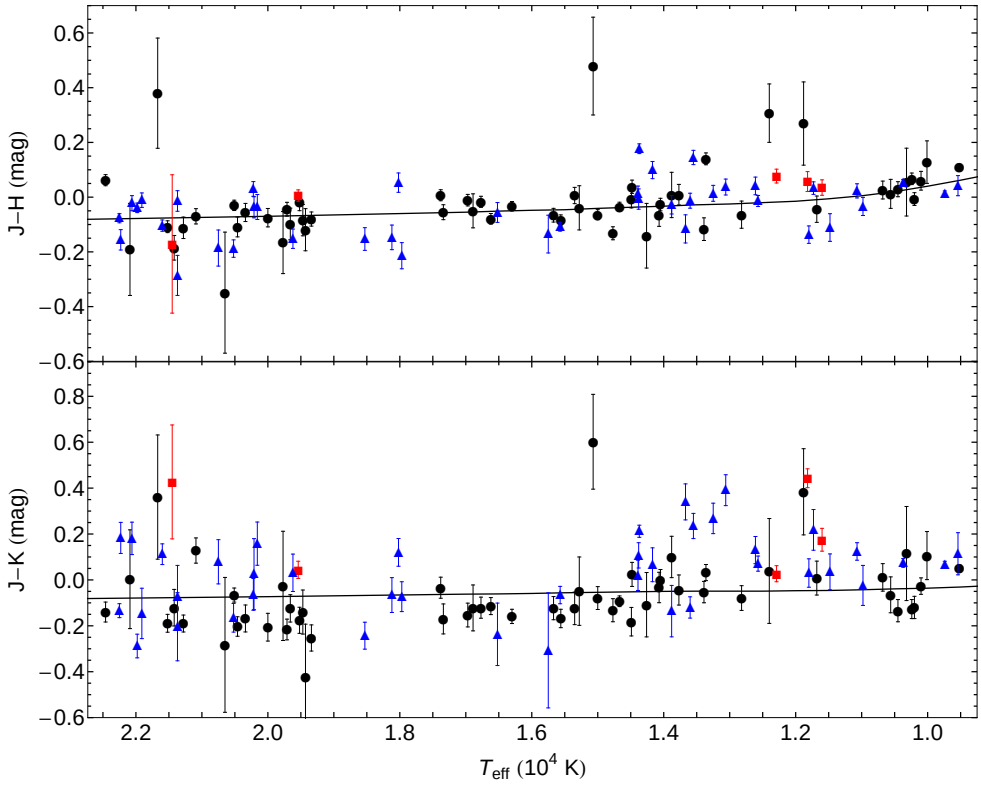


Figure 2.2: $J-H$ and $J-K$ colors vs. temperature for our sample of DA WDs from the PG catalog. Red squares and blue triangles show the confirmed dusty WDs and objects with follow-up IRTF spectroscopy, respectively. Solid lines show the predicted sequences for DA WDs (Bergeron et al., 2011).

Table 2.1 (cont'd)

PG	T_{eff} (K)	log g	WD Mass ($M_\odot$)	MS Mass ($M_\odot$)	τ (Myr)	J (mag)	H (mag)	K (mag)	Ref.	Data
1019+129	18020	8.00	0.62	2.1	132	16.101±0.017	16.048±0.031	15.981±0.058	1	I,P
1022+050	11680	7.64	0.44	0.4	490	14.193±0.035	14.237±0.033	14.185±0.065	1	
1026+024	12570	7.98	0.60	1.9	363	14.433±0.011	14.447±0.017	14.362±0.031	1	I,P
1031+063	20750	7.87	0.56	1.5	58	16.726±0.025	16.912±0.061	16.647±0.093	1	I,P
1031+234	15000	8.50	0.93	4.9	550	16.044±0.009	16.108±0.016	16.123±0.049	1	P
1034+492	20650	8.17	0.73	3.1	11	15.778±0.063	16.127±0.212	16.061±0.287	1,8	
1036+086	22230	7.49	0.42	0.2	46	16.654±0.015	16.810±0.034	16.471±0.066	1	I,S,P
1046+282	12610	7.97	0.59	1.8	363	15.479±0.016	15.438±0.028	15.349±0.057	1	I,P
1102+749	19710	8.36	0.85	4.2	182	15.530±0.010	15.574±0.023	15.746±0.044	1	P
1108+476	12400	8.31	0.80	3.7	603	15.657±0.054	15.350±0.092	15.618±0.222	1,8	
1115+166	22090	8.12	0.70	2.8	81	15.466±0.055	15.657±0.159	15.463±0.208	1	
1116+026	12290	8.05	0.63	2.2	427	14.745±0.014	14.668±0.021	14.718±0.032	1,4	P
1122+546	14380	7.83	0.52	1.2	209	15.697±0.015	15.704±0.034	15.590±0.053	1	I,S,P
1129+072	13360	7.91	0.56	1.5	288	15.298±0.012	15.158±0.018	15.266±0.033	1	P
1129+156	16890	8.19	0.73	3.1	224	14.443±0.034	14.493±0.052	14.565±0.094	1,8	
1134+301	21280	8.55	0.96	5.2	200	12.993±0.024	13.105±0.031	13.183±0.028	3	
1147+256	10200	8.14	0.69	2.7	794	15.548±0.012	15.555±0.020	15.668±0.047	1	P
1149+058	11070	8.15	0.69	2.7	646	14.985±0.015	14.962±0.021	14.861±0.035	1	I,S,P
1149+411	14070	7.84	0.53	1.2	224	16.365±0.017	16.431±0.037	16.398±0.064	1	P
1158+433	14050	7.85	0.53	1.2	224	16.170±0.011	16.197±0.020	16.169±0.043	1	P
1159−098	9540	8.81	1.10	6.5	2692	15.533±0.018	15.491±0.032	15.419±0.090	1	I,P
1201−001	19770	8.26	0.78	3.5	155	15.680±0.057	15.846±0.098	15.706±0.231	1,8	
1216+036	13800	7.85	0.53	1.2	245	16.284±0.101	16.198±0.187	···	1,10	
1229−013	19430	7.47	0.41	0.1	71	14.925±0.032	15.044±0.070	15.349±0.229	1,9	
1230+418	19520	7.98	0.61	2.0	95	16.161±0.014	16.180±0.027	16.337±0.055	1	P
1232+479	14370	7.82	0.52	1.2	204	14.937±0.011	14.760±0.014	14.725±0.024	1	I,P
1237−029	10240	8.58	0.98	5.4	1660	15.828±0.011	15.761±0.018	15.955±0.040	1	P

Table 2.1 (cont'd)

PG	T_{eff} (K)	log g	WD Mass ($M_\odot$)	MS Mass ($M_\odot$)	τ (Myr)	J (mag)	H (mag)	K (mag)	Ref.	Data
1244+149	10680	8.06	0.64	2.3	631	15.740±0.015	15.714±0.029	15.729±0.058	1	P
1257+032	17290	7.79	0.51	1.1	105	16.090±0.092	15.956±0.159	···	1,10	
1258+593	14480	7.87	0.54	1.3	214	15.645±0.012	15.607±0.021	15.621±0.051	1	P
1307+354	11180	8.15	0.70	2.8	631	15.344±0.051	15.398±0.096	···	1,8	
1310+583	10560	8.32	0.80	3.7	912	14.016±0.028	14.004±0.045	14.081±0.073	1,8	
1319+466	13880	8.19	0.73	3.1	398	14.867±0.035	14.859±0.075	14.767±0.083	1,8	
1325+168	17970	8.18	0.73	3.1	186	16.426±0.016	16.640±0.045	16.499±0.063	1	I,S,P
1328+344	16300	7.90	0.56	1.5	155	15.495±0.008	15.528±0.015	15.654±0.030	1	P
1330+473	22460	7.95	0.60	1.9	48	15.772±0.011	15.710±0.017	15.912±0.042	1	P
1335+369	20510	7.78	0.51	1.1	51	15.122±0.010	15.152±0.016	15.188±0.029	1	P
1337+705	20460	7.90	0.57	1.6	66	13.248±0.024	13.357±0.027	13.451±0.035	1,3,	
1344+573	13390	7.94	0.58	1.7	295	13.704±0.022	13.821±0.035	13.757±0.041	1	
1349+144	16620	7.68	0.46	0.6	145	15.550±0.009	15.629±0.017	15.664±0.036	1	P
1349+552	11800	7.87	0.54	1.3	380	15.830±0.015	15.967±0.028	15.800±0.060	1	I,P
1350+657	11880	7.91	0.55	1.4	389	15.688±0.068	15.419±0.136	15.304±0.175	1	
1350−090	9520	8.36	0.83	4.0	1318	14.191±0.007	14.082±0.009	14.140±0.013	1	P
1407+425	10010	8.21	0.73	3.1	912	14.998±0.044	14.870±0.064	14.892±0.095	1,5	
1408+324	18150	7.95	0.59	1.8	117	14.396±0.031	14.484±0.054	14.431±0.073	3	
1410+425	15350	7.87	0.54	1.3	178	16.343±0.016	16.337±0.025	16.467±0.069	1	P
1431+154	13550	7.95	0.58	1.7	302	16.130±0.014	15.985±0.022	15.895±0.053	1	I,P
1448+078	14170	7.75	0.48	0.8	195	15.854±0.016	15.755±0.027	15.788±0.072	1	I,P
1449+168	21600	7.88	0.56	1.5	49	15.973±0.010	16.077±0.018	15.861±0.044	1	I,P
1457−086	21450	7.97	0.62	2.1	63	16.041±0.098	16.212±0.233	15.614±0.228	1,7	
1501+032	13770	7.88	0.54	1.3	257	15.856±0.018	15.847±0.033	15.900±0.063	1	P
1502+351	18120	8.13	0.70	2.8	166	16.239±0.024	16.386±0.038	16.305±0.072	1	I,P
1507+021	19580	7.87	0.56	1.5	76	16.601±0.115	16.451±0.209	···	1,10	
1507+220	19340	7.91	0.57	1.6	85	15.445±0.015	15.525±0.021	15.698±0.055	1	P

Table 2.1 (cont'd)

PG	T_{eff} (K)	log g	WD Mass ($M_\odot$)	MS Mass ($M_\odot$)	τ (Myr)	J (mag)	H (mag)	K (mag)	Ref.	Data
1508+549	16970	7.86	0.54	1.3	126	16.125±0.009	16.136±0.019	16.278±0.051	1	P
1508+637	10450	8.12	0.68	2.6	724	14.689±0.015	14.660±0.023	14.823±0.046	1	P
1509+323	13970	7.98	0.60	1.9	282	14.436±0.030	14.574±0.055	14.572±0.089	3	
1515+669	10320	8.40	0.86	4.3	1122	15.295±0.053	15.240±0.112	15.180±0.198	1,8	
1519+384	19620	7.98	0.61	2.0	93	16.207±0.015	16.359±0.032	16.176±0.080	1	I,P
1527+091	21520	8.02	0.64	2.3	71	14.814±0.012	14.922±0.018	15.003±0.037	1	P
1531−023	18620	8.41	0.88	4.5	234	14.395±0.040	14.484±0.053	14.618±0.101	3	
1533−057	20000	8.50	0.94	5.0	245	15.876±0.013	15.951±0.031	16.082±0.059	1	P
1537+652	9740	8.15	0.69	2.7	912	14.438±0.006	14.426±0.009	14.372±0.014	1	IP
1541+651	11600	8.10	0.67	2.5	537	15.625±0.013	15.590±0.025	15.450±0.048	1	I,S,P
1548+149	20520	7.89	0.57	1.6	65	15.656±0.013	15.844±0.029	15.821±0.061	1	IP
1550+183	14260	8.25	0.77	3.4	389	15.170±0.050	15.311±0.107	15.278±0.131	1,8	
1601+581	14670	7.84	0.53	1.2	200	14.116±0.010	14.151±0.013	14.209±0.021	1	P
1605+684	21090	7.97	0.61	2.0	68	16.404±0.010	16.474±0.026	16.276±0.054	1	S,P
1610+167	14390	7.84	0.52	1.2	209	16.047±0.011	16.033±0.024	16.027±0.065	1	I,P
1614+137	22430	7.33	0.40	0.1	30	15.704±0.059	15.896±0.141	···	1	
1620+513	20890	7.92	0.58	1.7	63	16.251±0.093	16.181±0.213	···	1,10	
1626+409	21370	8.02	0.64	2.3	72	16.647±0.027	16.933±0.068	16.851±0.146	1	I,P
1632+177	10100	7.96	0.58	1.7	617	13.049±0.021	12.989±0.027	13.076±0.029	1,5	
1637+335	10150	8.17	0.71	2.9	832	14.551±0.031	14.467±0.045	14.424±0.081	3	
1641+388	15570	7.95	0.59	1.8	195	14.958±0.008	15.066±0.014	15.024±0.037	1	I,P
1647+376	21980	7.89	0.57	1.6	46	15.494±0.007	15.533±0.016	15.782±0.051	1	I,P
1654+637	15070	7.63	0.44	0.4	204	16.167±0.103	15.688±0.146	15.565±0.179	1,9	
1659+303	13600	7.95	0.58	1.7	295	15.315±0.011	15.328±0.025	15.435±0.045	1	IP
1720+361	13670	7.83	0.52	1.2	245	15.476±0.023	15.592±0.046	15.136±0.075	1	I,S,P
2226+061	15280	7.62	0.44	0.4	191	15.178±0.045	15.217±0.067	15.227±0.142	1,9	
2246+223	10650	8.80	1.10	6.5	2188	14.341±0.029	14.317±0.047	14.360±0.090	3	

Table 2.1 (cont'd)

PG	T_{eff} (K)	log g	WD Mass ($M_\odot$)	MS Mass ($M_\odot$)	τ (Myr)	J (mag)	H (mag)	K (mag)	Ref.	Data
2303+243	11480	8.09	0.66	2.4	550	15.398±0.028	15.509±0.042	15.363±0.073	1	S,P
2306+125	20220	8.05	0.66	2.4	98	15.672±0.012	15.642±0.024	15.735±0.068	1	I,P
2306+131	13250	7.92	0.56	1.5	295	15.567±0.013	15.553±0.026	15.299±0.065	1	I,S,P
2322+207	13060	7.84	0.52	1.2	282	15.745±0.013	15.708±0.026	15.354±0.066	1	I,P
2324+060	15750	7.90	0.56	1.5	174	15.744±0.028	15.879±0.063	16.051±0.249	1	I,P
2326+049	11820	8.15	0.70	2.8	550	13.132±0.029	13.075±0.022	12.689±0.029	1,2,3,5,6	
2328+108	21910	7.84	0.55	1.4	42	15.900±0.013	15.911±0.023	16.046±0.109	1	I,P
2329+267	11730	8.98	1.18	7.2	2042	15.126±0.011	15.093±0.020	14.908±0.088	1	I,P
2336+063	16520	8.03	0.63	2.2	186	15.903±0.017	15.959±0.032	16.140±0.135	1	I,P

Note. — Data sources: (I) IRTF; (S) *Spitzer*; (P) PAIRITEL

References. — (1) This work; (2) Reach et al. 2005a; (3) Mullally et al. 2007; (4) Jura et al. 2007a; (5) Farihi et al. 2008; (6) Reach et al. 2009; (7) Farihi et al. 2009; (8) Kilic et al. 2009a; (9) Kilic et al. 2010; (10) Xu & Jura 2012

2.3.2 Near-infrared Spectroscopy

We obtained low-resolution near-infrared spectra of 41 WDs over several nights in 2011 April, August, and September using the 3-m NASA InfraRed Telescope Facility (IRTF) equipped with the 0.8-5.4 Micron Medium-Resolution Spectrograph and Imager (SpeX; Rayner et al. 2003). We use a 0.5″ slit to obtain a resolving power of 90-210 over the 0.7-2.5 μm range. The observations are taken in two different positions on the slit separated by 10″. We use internal calibration lamps (a 0.1 W incandescent lamp and an Argon lamp) for flat-fielding and wavelength calibration, respectively. To correct for telluric features and flux calibrate the spectra, we use the observations of nearby A0V stars at a similar airmass to the target observations. We use the `IDL`-based package `SPEXTOOL` version 3.4 (Cushing et al. 2004) to reduce the data.

To demonstrate that our near-infrared observations and reductions are reliable, we also obtained a near-infrared spectrum of the previously known dusty WD GALEX J193156.8+011745 (hereafter J1931+0117; Vennes et al., 2010; Debes et al., 2011b; Melis et al., 2011). Figure 2.3 shows the near-infrared photometry and our IRTF spectrum of this object. There are two nearby red sources within 2″ of the WD (Melis et al., 2011). Our IRTF observations were obtained under average seeing conditions of 0.8″ and our 0.5″ slit minimizes the contamination from the nearby sources. A slight excess is clearly detected redward of 2.1 μm, typical

of dusty WDs (Kilic et al., 2006). Melis et al. (2011) also obtained a near-infrared spectrum of J1931+0117 on the Magellan 6.5 m Baade telescope, which shows a significantly larger excess redward of 1.6 μm. Those authors discuss the potential problems with the flux calibration of their spectra. They model the excess around J1931+0117 with a flat disk model with inner and outer temperatures of 1400 and 1200 K, respectively, essentially a narrow ring of dust. Our IRTF spectrum demonstrates that the excess around J1931+0117 mostly shows up redward of 2.1 μm and it is similar to the other dusty WDs with extended (up to 1 $R_{\odot}$) disks. Of course, the outer edge of the disk around J1931+0117 is currently unconstrained due to the lack of uncontaminated mid-infrared photometry. Regardless of these issues, this figure demonstrates that we are able to identify dusty WDs even with slight K-band excesses.

2.3.3 *Spitzer* Photometry

We used the warm *Spitzer* (Werner et al., 2004) equipped with the InfraRed Array Camera (IRAC; Fazio et al. 2004b) to obtain infrared photometry of 11 WDs between September 2010 and February 2011 for program number 70023. Based on our preliminary analysis of the PAIRITEL data, these 11 sources appeared to have slight K-band excesses indicative of debris disks. We obtained 3.6 and 4.5 μm images with integration times of 30 s or 100 s for nine dither positions. We

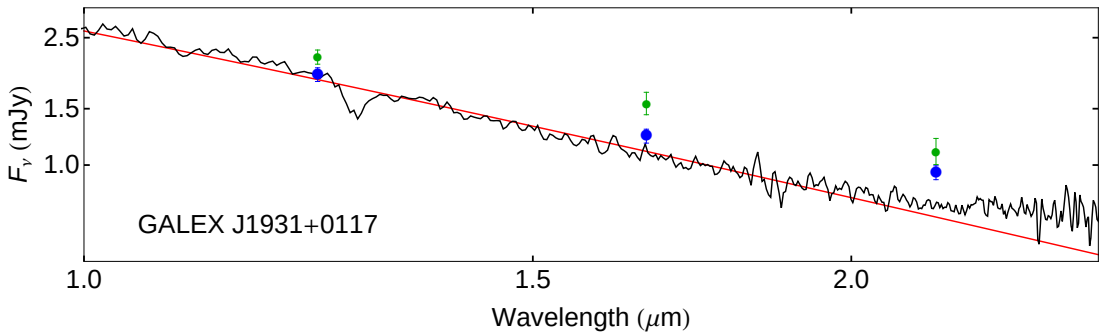


Figure 2.3: SED of the known dusty WD GALEX J1931+0117. Green points represent 2MASS photometry, while blue points represent the photometry from Melis et al. 2011. The IRTF spectrum is shown in black and the red line represents the predicted contribution from a blackbody stellar photosphere. The noise near 1.9 and 2.5 μm falls in regions of poor telluric correction. The 1.28 μm feature is Paβ absorption. The detection of slight K-band excess around this target demonstrates that our near-infrared observations and reductions are reliable.

use the `IDL ASTROLIB` packages to perform aperture photometry on the individual corrected basic calibrated data frames from the `S18.18.0` pipeline reduction.

Following the IRAC calibration procedures, we correct for the location of the source in the array before averaging the fluxes of each of the dithered frames at each wavelength. We also correct the Channel 1 (3.6 μm) photometry for the pixel phase dependence. We estimate the photometry error bars from the observed scatter in the nine images corresponding to the dither positions. We add the 3% absolute calibration error in quadrature (Reach et al., 2005b). Finally, we divide the estimated fluxes by the color corrections for a Rayleigh-Jeans spectrum, except for the dusty WDs in our sample. Table 2.2 presents our *Spitzer* IRAC photometry for 11 PG WDs.

Table 2.2. *Spitzer* IRAC Photometry

PG	3.6 μm (μJy)	4.5 μm (μJy)
0826+455	268.6±8.7	172.0±5.9
0956+021	88.6±3.5	53.7±2.8
1036+086	42.5±1.5	26.6±1.3
1122+546	118.2±4.3	77.6±3.1
1149+058	248.0±8.1	163.4±5.7
1325+168	64.7±2.2	42.3±1.7
1541+651	435.4±13.5	483.9±15
1605+684	60.9±2.7	41.2±2.2
1720+361	155.9±5.4	97.6±3.7
2303+243	170.8±5.9	110.1±4
2306+131	146.2±5.2	92.0±3.5

Note. — *Spitzer* Cycle 7 photometry fluxes in IRAC Channels 1 (3.6 μm) and 2 (4.5 μm).

2.4 Results

Our near-infrared photometric observations revealed several sources with potential K-band excesses. We followed up 11 of the most interesting targets with *Spitzer* IRAC and 41 stars in total at the IRTF. Figure 2.4 shows the SEDs of the 41 stars observed at the IRTF. Here, and in the rest of the figures, the PAIRITEL and 2MASS photometry are shown as blue and green points, respectively. The black lines show the observed spectra and the red solid lines show the predicted pho-

tospheric emission for each star assuming blackbody emission. The IRTF spectra display telluric correction problems around 1.4 and 1.9 μm, but otherwise they closely follow the predicted blackbody distributions for the majority of the targets in our sample. PG 0048+202 and PG 1720+361 are two of the stars for which our PAIRITEL photometry indicated K-band excesses, but our IRTF spectra show that there are no significant excesses in the K-band for these two stars. There is only one WD in our IRTF sample where a significant K-band excess is detected, PG 1541+651. The observed flux stays essentially constant between 2.0 and 2.5 μm, which is typical of dusty WDs.

Figure 2.5 shows the near- and mid-infrared data on 11 WDs that we targeted with *Spitzer*, including PG 1541+651. Eight of these stars also have IRTF spectroscopy available. Our *Spitzer* observations confirm the results from the IRTF observations; only PG 1541+651 shows a significant infrared excess that is compatible with a debris disk (see Kilic et al., 2012). The SEDs for the other ten objects in this figure are consistent with photospheric emission from each star.

There are four other previously known dusty WDs in our sample; PG 1015+161, PG 1116+026, PG 1457−086, and PG 2326+049. Figure 2.6 displays the SEDs for these four WDs plus PG 1541+651. PG 2326+049 has the most prominent excess, while the excess at PG 1457−086 is the most subtle. The difference in the strength of these excesses is likely due to a variation in the disk geometry from

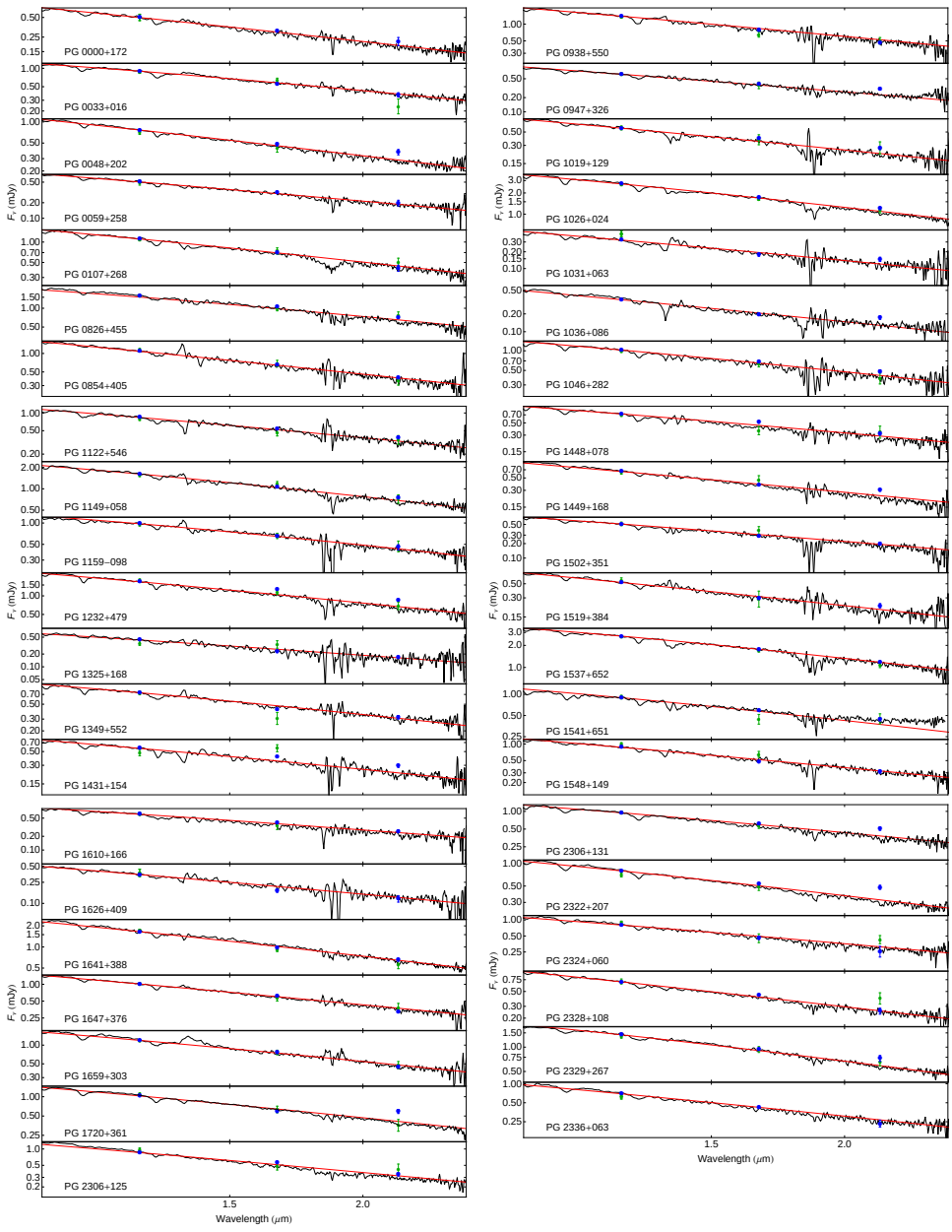


Figure 2.4: Spectral energy distributions of 41 WDs observed at the IRTF. The PAIRITEL and 2MASS photometry are shown as blue and green points, respectively. The black lines show the observed spectra and the red solid lines show the predicted photospheric emission for each star assuming blackbody emission. The IRTF spectra display telluric correction problems around 1.4 and 1.9 μm.

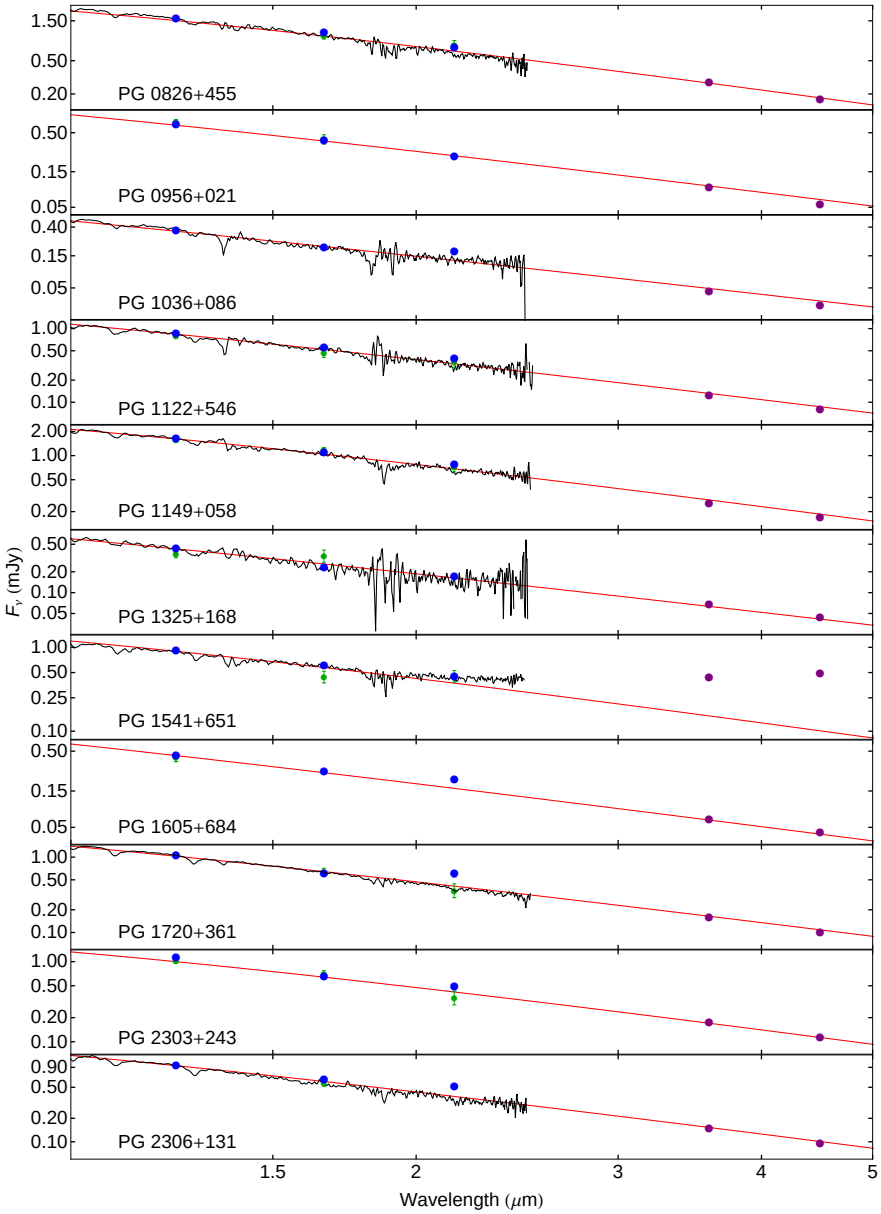


Figure 2.5: SEDs of the 11 WDs with new *Spitzer* photometry (shown in purple). The symbols are the same as in Figure 2.3. The IRTF spectra display telluric correction problems around 1.4 and 1.9 μm. Our *Spitzer* observations confirm the results of the IRTF observations; only PG1541+651 shows a significant infrared excess.

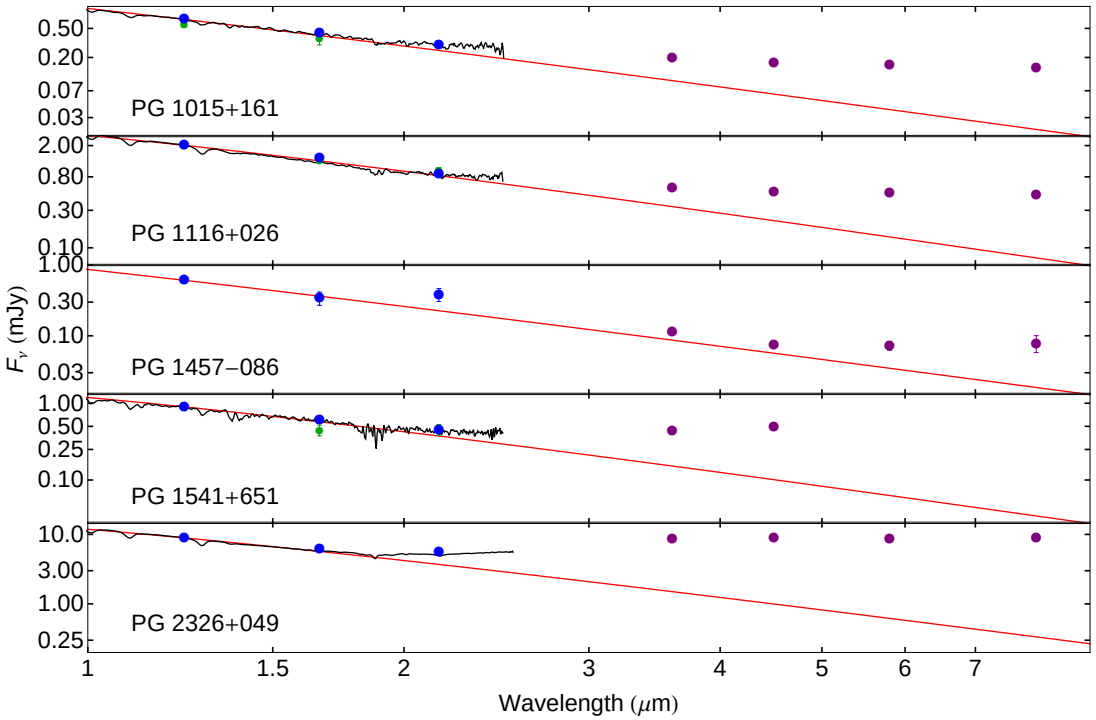


Figure 2.6: SEDs of the five dusty WDs in our sample. The symbols are the same as in Figure 2.5. The IRTF spectra display telluric correction problems around 1.4 and 1.9 μm.

object to object. There is another known dusty WD in the Liebert et al. (2005) DA WD sample, PG 1456+298 (G166-58, Farihi et al., 2008) that is cooler than the lower temperature limit of our sample and hence it is not included in Figure 2.6.

Out of the 117 DA WDs in our sample, the majority have SEDs that closely follow a single blackbody curve, while five WDs show a significant deviation from their blackbody model in the near- to mid-infrared (see Figure 2.6). In light of the recent WISE All-Sky Data Release, we examine our sample for infrared excesses

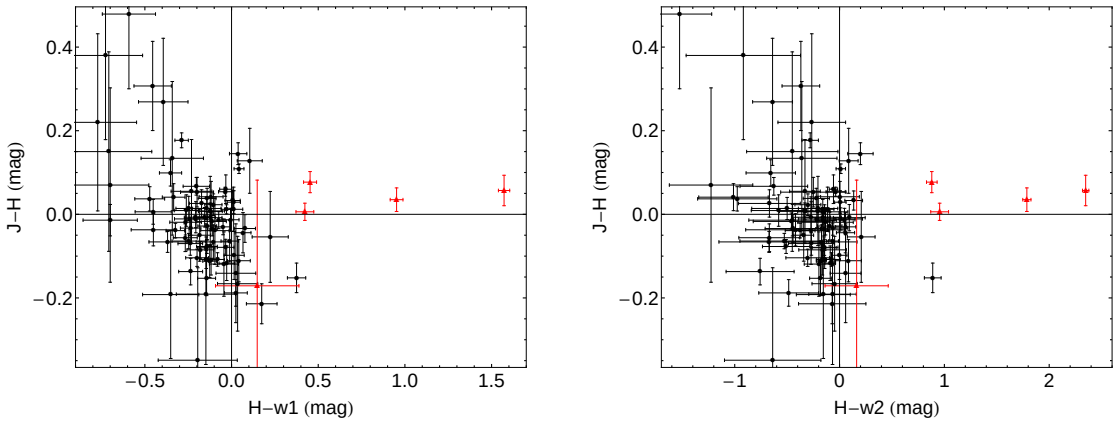


Figure 2.7: Color-color diagrams using PAIRITEL/2MASS and WISE photometry for our WD sample. Red triangles mark the dusty WDs. Four of the five dusty WDs in our sample clearly show infrared excesses in the WISE bands. The fifth dusty WD, PG 1457−086, is also detected in the WISE observations, but with large photometric errors.

in the WISE data and plot these results in Figure 2.7. Four of the five dusty WDs in our sample clearly show infrared excesses in the WISE bands. The fifth dusty WD, PG 1457−086, is also detected in the WISE observations, but with large photometric errors. There is another target, PG 1519+384, with positive $H-W1$ and $H-W2$ colors. However, there are two nearby sources within several arcseconds of this target in the Sloan Digital Sky Survey images. The WISE photometry for PG 1519+384 is likely contaminated by these background sources. Hence, the WISE data do not reveal any new dusty WDs in our sample other than the five systems known.

Farihi et al. (2005) finds a frequency of less than 0.5% for brown dwarf companions of WDs. Given our sample size of 117 we would expect to find less than one

brown dwarf companion in our sample. It is not surprising, then, that we do not find any substellar companions. Through the initial selection process, we excluded objects with potential M-dwarf companions.

2.5 Discussion

2.5.1 The Frequency of Debris Disks Around WDs

Out of the 348 DA WDs analyzed by Liebert et al. (2005), 308 are apparently single. Six of these PG WDs are known to host dust disks, corresponding to a debris disk frequency of 1.9%. This is similar to the frequency of disks, 1.6%, around the nearby bright WD sample of Mullally et al. (2007). Of course, these estimates ignore the fact that most disks occur around young WDs (see Kilic et al., 2009b). The process that creates the debris disks around WDs seem to be more efficient at younger ages.

We use the binomial probability distribution to compute the upper and lower limits on the frequency (p) of disks. The binomial distribution function gives the discrete probability distribution of obtaining exactly n successes out of N trials (where the result of each trial is true with probability p and false with probability $1 - p$). The probability, $P_n(N, p)$, that a survey of N WDs will detect n debris disks, when the true frequency of disks is p is given by (Burgasser et al., 2003, Appendix)

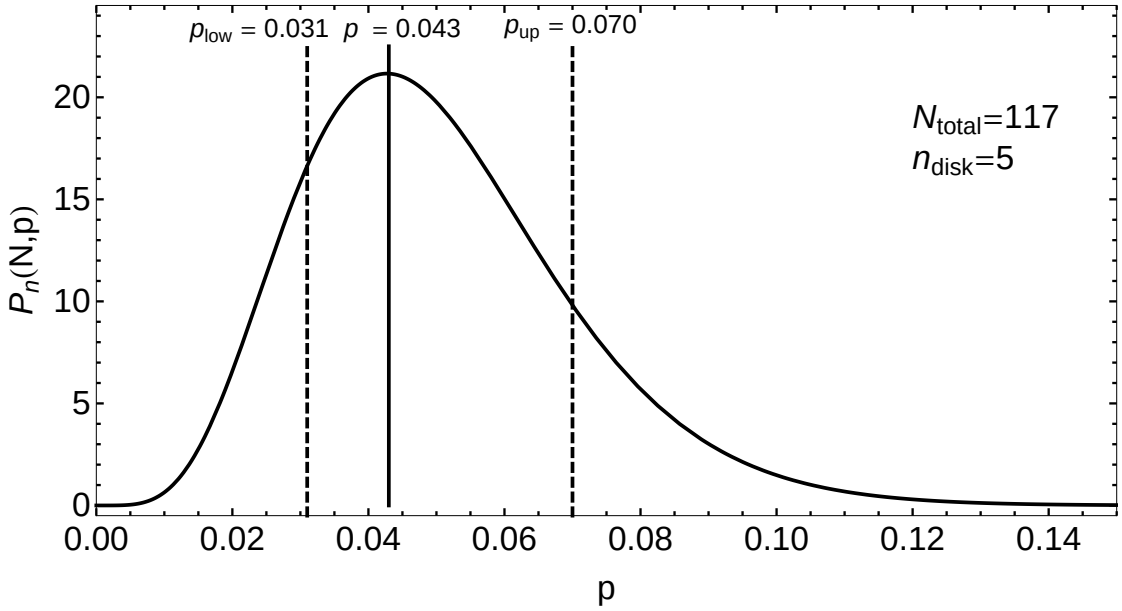


Figure 2.8: Probability function for WDs with debris disks. Probability, $P_n(N, p)$, of finding $n = 5$ debris disks as a function of assumed true debris disk frequencies, p, where $N = 117$. Dashed lines delineate the region containing 68% probability, equivalent to 1σ Gaussian limits. The solid line indicates the peak of the distribution. The derived frequency is $4.3^{+2.7}_{-1.2}$%.

$$P_n(N,p) = \left(\begin{array}{c} N \\ \\ n \end{array} \right) p^n (1-p)^{N-n} = \frac{N!}{n!(N-n)!} p^n (1-p)^{N-n}. \qquad (2.1)$$

Since this probability function is not symmetric about its maximum value, we report the range in p that delimits 68% of the integrated probability function, equivalent to 1σ Gaussian limits. For $N = 117$ and $n = 5$, there is a 68% chance of p being between 3.1% and 7% (see Figure 2.8). Thus, $p = 4.3^{+2.7}_{-1.2}$%. This frequency estimate is slightly higher than, but consistent with, the 3% disk frequency derived by Farihi et al. (2009) and the 3.7% frequency given by Rocchetto et al. 2014.

2.5.2 Planets Around Intermediate-Mass Stars

The 117 WDs in our sample have an average mass of 0.6 $M_{\odot}$ and mass range of 0.4-1.2 $M_{\odot}$. We estimate the progenitor MS masses using the initial-final mass relation derived by Kalirai et al. (2008) and Williams et al. (2009). We obtain an average progenitor mass of 2.4 $M_{\odot}$ and mass range of 1.1-7.2 $M_{\odot}$ (see Table 2.1) where we neglect WDs below 0.5 $M_{\odot}$. Based on the observed frequency of disks around our WD targets, we find that the probability of finding planetary systems around their progenitor 1-7 $M_{\odot}$ MS stars is at least $4.3^{+2.7}_{-1.2}$%. This result serves as an indirect probe of the intermediate-mass stellar systems which have thus far challenged conventional planetary detection techniques (Gould & Kilic, 2008).

The dusty WDs in our sample, PG 1015+161, 1116+026, 1457−086, 1541+651, and 2326+049 are the descendants of 2.1-2.8 $M_{\odot}$ MS stars. At first glance, this suggests that planet formation may be most efficient around 2-3 $M_{\odot}$ stars. However, given the age and star formation history of the Galactic disk, our sample is dominated by the $\sim$0.6 $M_{\odot}$ WD remnants of 2-3 $M_{\odot}$ MS stars. In fact, 80% of our sample consists of WD descendants of 1-3 $M_{\odot}$ MS stars. Hence, the lack of discoveries of dusty disks, and therefore remnant planetary systems, around the massive WD remnants of M>3 $M_{\odot}$ stars may be due to small number statistics. There are 22 systems in our sample with M>3 $M_{\odot}$ progenitors, we would expect to find 1 dusty WD in a sample of 22 stars. The probability of finding zero dusty WDs in a

sample of 22, when the expected number is one, is 30% (see Equation 1). Hence, larger surveys of massive WDs (see Chapter 4) are required to detect disks around them and to constrain the frequency of planets around their intermediate-mass progenitor MS stars.

2.5.3 Disk Lifetimes

An alternative interpretation of the 4.3% disk frequency around WDs is that perhaps 100% of WDs have remnant planetary systems that can create debris disks, but the disks only persist for 4.3% of the cooling age of the WD. For the average cooling age of our sample of WDs, 300 Myr, this implies that disks survive around typical WDs for $\sim$10 Myr. We note that this is the total time a WD accretes from circumstellar debris disks, even though individual disks may last for a significantly shorter amount of time. Kilic et al. (2008) and Farihi et al. (2009) estimate typical disk lifetimes of $\sim 10^5$ yr. Hence, up to 100 tidal disruption events that create circumstellar debris disks may occur for any given WD.

von Hippel et al. (2007) use a geometrically thin, optically thick disk model to determine typical accretion rates of WDs. Their result ($\sim 10^9$ g s^{-1}) means a WD with the disk lifetime typical of our sample will accrete a total mass equivalent to a 400 km Solar System asteroid (assuming an asteroid density of 3 g cm^{-3}). Rafikov (2011a) demonstrate that the Poynting-Robertson drag can explain accretion rates

of around 10^8 g s^{-1} from circumstellar debris disks onto the WDs. Taken at face value, this implies a total accreted mass of 10^{22} g, a 200 km asteroid, over the disk-hosting lifetime of a WD. However, dusty WDs show accretion rates of up to 10^{11} g s^{-1} (Dufour et al., 2012). To explain the observed high accretion rates, Rafikov (2011b) and Metzger et al. (2012) propose a runaway accretion scenario where rapid transport of metals from the disk results from interaction between spatially coexisting solid and gaseous disks. In this scenario, a WD accretes 10^{22} g of metals in 10^5 years. Hence, typical WDs may accrete up to 10^{24} g of metal over 10 Myr, the total time they host circumstellar disks. This is comparable to the mass of the dwarf planet Ceres and Pluto's moon Charon. Of course, if the tidally disrupted object is icy, the total accreted mass may be significantly higher (although see Jura & Xu, 2012). Therefore, the debris surrounding WDs is likely supplied through disruption of Solar System asteroid analogues, moons, and dwarf planets.

2.6 Conclusions

We present near- and mid-infrared observations and a comprehensive study of the SEDs of a metallicity-unbiased sample of 117 DA WDs from the PG catalog. Five of our targets show excess radiation from debris disks, indicating a debris disk frequency of $4.3^{+2.7}_{-1.2}$% which fits in well with previous surveys of this kind. We

interpret this frequency as a lower limit to the frequency of planets around the 1-7 $M_{\odot}$ progenitor MS stars; an indirect result for the intermediate-mass regime in which conventional exoplanetary detection methods are insensitive. Alternatively, we interpret the observed frequency of disks as the fraction of time a WD accretes from its debris disks over the entire cooling age of the star. We estimate that typical WDs may accrete metals from several generations of disks for $\sim$10 Myr, corresponding to accretion of metals up to 10^{24} g. This means WDs are capable of accreting bodies as large as dwarf planets as well as Solar System asteroid analogues.

2.7 Acknowledgements

This work is based, in part, on observations made with the *Spitzer Space Telescope*, which is operated by the Jet Propulsion Laboratory, California Institute of Technology under a contract with NASA. Support for this work was provided by NASA.

The PAIRITEL is operated by the Smithsonian Astrophysical Observatory (SAO) and was made possible by a grant from the Harvard University Milton Fund, the camera loan from the University of Virginia, and the continued support of the SAO and UC Berkeley. The PAIRITEL project and JSB are further supported by NASA/Swift Guest Investigator Grant no. NNG06GH50G. We thank

M. Skrutskie for his continued support of the PAIRITEL project.

The IRTF is operated by the University of Hawaii under Cooperative Agreement no. NNX-08AE38A with the National Aeronautics and Space Administration, Science Mission Directorate, Planetary Astronomy Program. We thank A. Giannas for his helpful comments, J. Farihi for useful discussions, and C. Blake, M. Skrutskie, and E. Falco for helping with the PAIRITEL observations. We also thank the referee, Marc Kuchner, for insightful suggestions.

We make use of the Bergeron WD cooling model grids (Holberg & Bergeron, 2006; Kowalski & Saumon, 2006; Tremblay et al., 2011) to calculate our debris disk models.

This chapter is reproduced by permission of the American Astronomical Society from Barber et al. 2012.

Chapter 3

Dusty WDs in the *WISE* All Sky Survey ∩ SDSS

"Beauty never slumbers, all is in her name. But the rose remembers the dust from which it came."

– Edna St. Vincent Millay, *Autumn Chant*

3.1 The Wide-Field Infrared Survey Explorer

In the previous chapter, we constrained the frequency of dusty WDs using the PG catalog which was submitted for publication in June of 1985, four months before my birth. Let's jump ahead and take advantage of the state-of-the-art space-based all-sky survey with coverage in the mid-infrared. The recently completed Wide-Field Infrared Survey Explorer (*WISE*) mission opens up new opportunities for detecting excess infrared light at WDs caused by orbiting planetary debris. *WISE* provides four bands of mid-infrared photometry from 3.4 to 22 μm. The *WISE* InfraRed Excesses around Degenerates (WIRED; Debes et al. 2011b) Survey reveals a large number of candidate WD+dust disk systems through a cross-correlation of ∼18,000 WDs from the Sloan Digital Sky Survey (SDSS) Data Release 7 WD catalog (Kleinman et al. 2013), the 2MASS All Sky Data Release Point Source Catalog (Skrutskie et al. 2006), and the UKIRT Infrared Deep Sky Survey (UKIDSS) Data

Release 5 Point Source Catalogs from the Large Area Survey and Galaxy Cluster Surveys (Lawrence et al. 2007). However, due to the large size of the *WISE* beam, some of these detections are likely the result of nearby contaminating sources.

We use the SDSS and UKIDSS observations to pare down the sample of 52 disk candidates identified by the WIRED survey to a target sample of 24 WDs. We removed a total of 28 of the 52 candidate dusty WDs from our target list for various reasons;

(1) We found 10 to have a blending source in their SDSS images.

085742.05+363526.6, 095337.97+493439.7, 100145.03+364257.3, 124455.15+040220.6, 131641.73+122543.8, 134800.05+282355.1, 141351.95+353429.6, 151747.51+342209.7, 155359.87+082131.3, 165012.47+112457.1

(2) Another seven have a blending source in their UKIDSS images.

024602.66+002539.2, 082624.40+062827.6, 084303.98+275149.6, 092528.22+044952.4, 133212.85+100435.2, 153149.04+025705.0, 224626.38−005909.2

(3) Six more are known in the literature to host circumstellar dust.

030253.09−010833.7, 084539.17+225728.0, 104341.53+085558.2, 122859.93+104032.9, 145806.53+293727.0, 161717.04+162022.3

(4) Two quasars were misidentified as WDs.

031343.07−001623.3, 103757.04+035023.6

(5) One final target is known to have a brown dwarf companion (Steele et al. 2009).

222030.69−004107.3

(6) Although 011055.06+143922.2 and 090522.93+071519.1 do not have obvious blends in their SDSS and UKIDSS images, we did not target them because NIR SWIRC observations in addition to UKIDSS data would not offer new information about the SEDs of those WDs. These two WDs will reenter our discussion when we consider the frequency of disks in the WISE sample.

These cuts reduce the number of true candidate disk systems in *WISE* from 52 to 24 WDs without an obvious nearby blending source, not already known to host disks or brown dwarf companions, without NIR data, and correctly identified as WDs. Hereafter, the WDs in the WIRED sample will be referred to with the letter "J" followed by the first four numbers of their WIRED name.

We present follow up near-infrared (NIR) J- and H-band photometry using the 6.5 m MMT with SWIRC of 16 WDs exhibiting a mid-infrared excess indicative of a debris disk detected by *WISE* (Debes et al. 2011b). We use the higher spatial resolution of SWIRC to confirm the presence of a debris disk or to identify a photometric contamination in the six arcsecond *WISE* beam. We start in Section 3.2 with a description of the observations and data reduction as well as the debris disk modeling of the detected excesses. We present our results in Section 3.3,

discuss the frequency of disks in Section 3.4, and summarize our conclusions in Section 3.5.

3.2 Observations and Data Analysis

3.2.1 Near-infrared Photometry

During two nights in May 2012, we imaged 16 of our 24 targets in the NIR J- and H-band using the SAO Wide-Field InfraRed Camera (SWIRC; Brown et al. 2008) with the MMT located on Mount Hopkins near Tucson, Arizona. SWIRC has a 2048×2048 pixel HAWAII-2 detector with a 0.15 arcsec/pixel plate scale and 5.12×5.12 arcmin field of view. Exposure times were adjusted to approach a signal-to-noise of 10. Each target was observed for two sets of a 3×5 dither pattern with offsets of 10 arcseconds to sample the sky background. We took dark frames for each exposure time and sky flats each evening. The weather conditions were good with an average seeing of 0.9 arcseconds.

We used the SWIRC data reduction pipeline to dark-subtract and flat-field the images. The images were then shifted to a common position and mean combined into one final image for each target. We calculated a zeropoint offset for each combined image by taking a weighted mean of the offsets for the 2MASS stars in the field. We used the `IRAF` aperture photometry package `apphot` to measure the flux of each isolated WD and comparison 2MASS stars. In many cases, the

presence of an additional point source very near to the target WD interfered with our aperture photometry measurements. We measured these blended targets using the `IRAF daophot` package, where we fit the point-spread-functions of the WD and nearest blending neighbor simultaneously.

3.2.2 Disk Modeling

We combine SDSS DR7 *ugriz* (Kleinman et al. 2013) and *WISE* 3.4 & 4.6 μm photometry with our SWIRC J- & H-band data to construct the SED of each WD. We model the flux of the WD in the NIR and MIR bands using pure hydrogen atmosphere models (Tremblay & Bergeron 2009; Tremblay et al. 2010; Gianninas et al. 2011) which we normalize to the SDSS *griz*-band data. In most cases, a secondary point source appears within six arcseconds of the WD of interest. The SEDs of these WDs are shown in Figure 3.1 where the SDSS, SWIRC, and *WISE* data appear as magenta circles, orange squares, and green diamonds, respectively. The SWIRC photometry of the blending point source (when present) is shown by empty orange squares. Two of the objects in this figure (J0914 and J1503) do not have obvious *WISE* contaminants but their SEDs are not consistent with a disk and they likely have unresolved background contaminants.

The colors of the blending sources do not resemble those of M dwarf stars or L/T brown dwarfs (see Figure 3.2). The average $J - H$, and $H - W2$ colors of

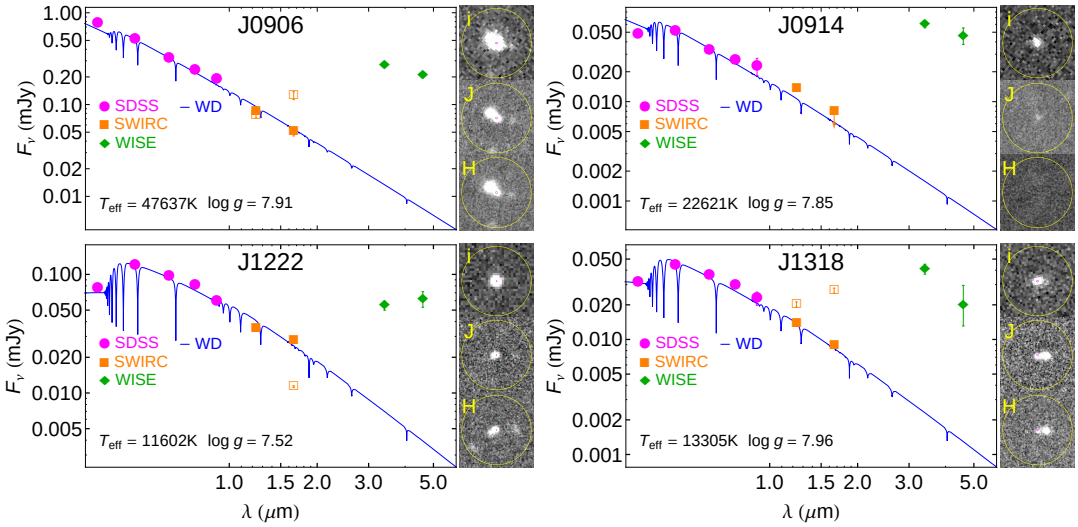
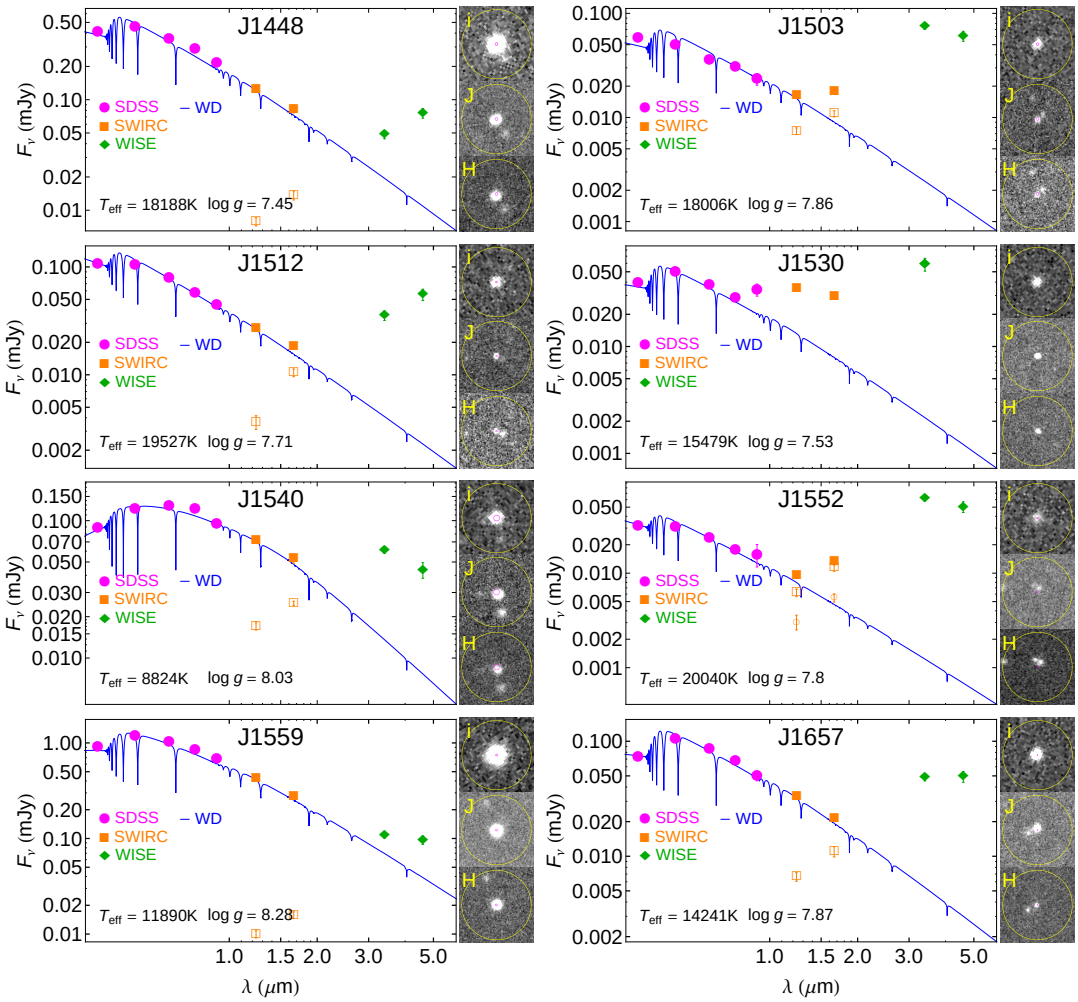


Figure 3.1: The spectral energy distribution of WDs with nearby point sources. Pure hydrogen atmosphere models (Tremblay & Bergeron 2009; Tremblay et al. 2010; Gianninas et al. 2011), shown in blue, are normalized to the SDSS *griz*-bands. SDSS, SWIRC, and *WISE* photometry are shown as magenta circles, orange squares (empty squares for nearest blending point source), and green diamonds, respectively. ALLWISE data are plotted where available. The SDSS *i*-band and SWIRC *J*- and *H*-band science images of the corresponding WD field are shown to the right. The yellow circle indicates the 6″ *WISE* beam. The small magenta circle is centered on the WD's SDSS J2000 coordinates with a radius equal to the proper motion since the SDSS DR7 data were taken and is used to identify the WD. Extraneous objects within the yellow circle are likely the source of the excesses detected in the *WISE* data.


J1448
SDSS
SWIRC
WISE
WD
$T_{\rm eff}$ = 18188K log g = 7.45
J1503
$T_{\rm eff}$ = 18006K log g = 7.86
J1512
$T_{\rm eff}$ = 19527K log g = 7.71
J1530
$T_{\rm eff}$ = 15479K log g = 7.53
J1540
$T_{\rm eff}$ = 8824K log g = 8.03
J1552
$T_{\rm eff}$ = 20040K log g = 7.8
J1559
$T_{\rm eff}$ = 11890K log g = 8.28
J1657
$T_{\rm eff}$ = 14241K log g = 7.87
F_ν (mJy)
λ (μm)

Continued.

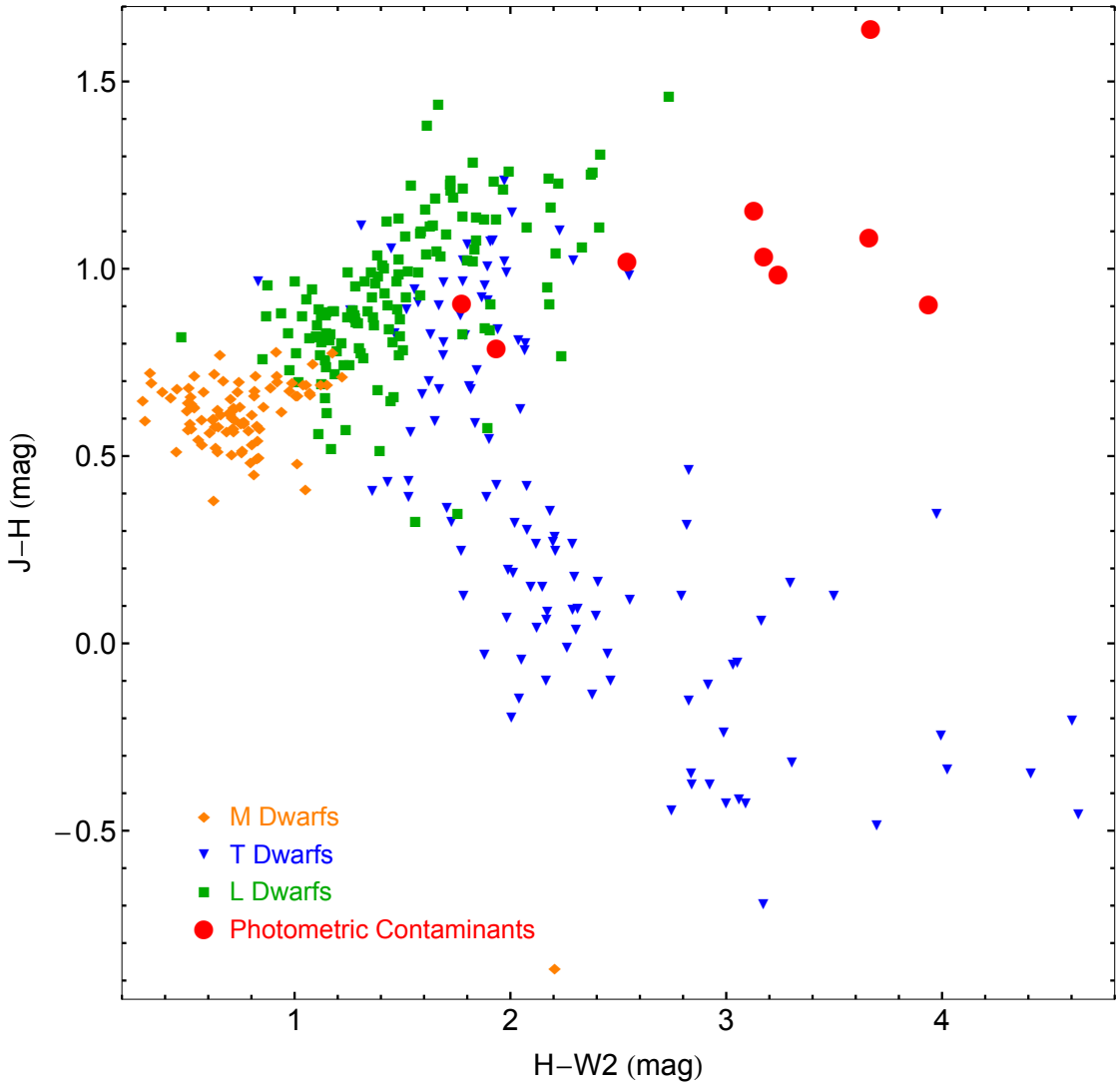


Figure 3.2: The $J - H$ and $H - W2$ colors of the contaminating sources near to the WDs in our sample are shown by red circles. The L/T dwarf and M dwarf colors are derived from the NIR and *WISE* photometry published in Table 1 of Kirkpatrick et al. 2011 and are represented by green squares/blue triangles and orange diamonds, respectively. The colors of the contaminating sources in our SWIRC images are generally redder than the known brown dwarf and M dwarf populations and are more likely background galaxies.

the blends in our images are 1.05 and 3.04 mag, respectively, while the $J-H$ and $H-W2$ colors for typical T dwarfs are 0.36 and 2.25 mag, for L dwarfs $J-H=0.92$ mag and $H-W2=1.49$ mag on average, and for typical M dwarfs $J-H=0.59$ mag and $H-W2=0.75$ mag (West et al. 2011; Lépine & Gaidos 2011; Kirkpatrick et al. 2011; Frith et al. 2013; Newton et al. 2014). Therefore, the blends in our sample are too red to be L/T brown dwarfs or M dwarf companions and are likely background galaxies.

In the cases where no obvious source of *WISE* contamination is present (J1147, J1234, J1507, J1537), we rule out the possibility of not detecting the presence of a dim resolved contaminant. If the excesses at these four WDs were due to an resolved contaminant with the same $J-H$ and $H-W2$ colors as the blending sources described above, we should have detected them. The limiting magnitudes of our J- and H-band images are fainter than the expected brightness of the typical blending sources for the other WD targets.

For these four WDs, we fit a geometrically flat, optically thick disk model (Jura 2003) to the SWIRC+*WISE* excesses using a χ^2 minimization method. Here χ^2 is defined as the square of the difference between the measured excess and the disk model flux over the square of the photometric error for the SWIRC J- & H- and the *WISE* 3.4 & 4.6 μm bands. We fit disk models with inner temperature of 800-2100 K and outer temperature 100-1200 K in steps of 10 K and inclination 0-90°

in steps of 10°. The SEDs are shown in Figure 3.3 where the best fit disk model appears in red and the WD+disk model combination appears in black. Debris disk models accurately reproduce the excesses found at the four isolated WDs in the sample. We compare the colors of these new dusty WDs to the previously known dusty WDs from the literature in Figure 3.4. The colors of the four new dusty WDs are comparable to the colors of the dusty WD population from the literature and are therefore likely to have the same mechanism generating their infrared excesses.

3.3 Results

3.3.1 Blended Targets

The SWIRC photometry of our sample along with physical characteristics of the WDs are tabulated in Table 3.1. The majority of our disk-candidate targets reveal extraneous sources of contamination when observed with high spatial resolution imaging in the NIR. We measured the photometry of the WD and primary blending source (closest to WD) simultaneously and plot them with filled and empty orange squares, respectively, in Figure 3.1. When considering the photometry of the blending source along with the *WISE* photometry, the resultant SEDs do not resemble that of an M dwarf or L/T brown dwarf, and are likely due to a background galaxy. The SWIRC data of the WD line up with the prediction for a hydrogen-dominated atmosphere for all but two of the blended targets, namely

J1503 and J1552. These targets likely have an additional blending target not resolved in the SWIRC data that contributes to this deviation from the WD model.

Table 3.1. SWIRC Photometry

WIRED	J (mag)	H (mag)	$J_{\rm blend}$ (mag)	$H_{\rm blend}$ (mag)	Dist. (pc)	$T_{\rm eff}$ (K)	log g	Mass ($M_\odot$)
090611.00+414114.3	18.20±0.07	18.27±0.11	18.30±0.07	17.29±0.11	469	47637	7.91	0.65
091411.11+434332.9	20.19±0.06	20.28±0.15	···	···	820	22621	7.85	0.56
114758.61+283156.2	17.52±0.07	17.55±0.07	···	···	134	12290	8.14	0.70
122220.88+395553.9	19.15±0.02	18.93±0.02	···	19.90±0.02	350	11602	7.52	0.37
123432.63+560643.0	18.30±0.04	18.13±0.05	···	···	133	13567	8.74	1.04
131849.24+501320.6	20.16±0.07	20.17±0.08	19.75±0.06	18.97±0.06	481	13305	7.96	0.59
144823.67+444344.3	17.78±0.07	17.74±0.09	20.77±0.09	19.70±0.1	267	18188	7.45	0.37
150347.29+615847.4	19.97±0.05	19.41±0.05	20.84±0.08	19.94±0.07	693	18006	7.86	0.53
150701.98+324545.1	18.15±0.06	18.02±0.08	···	···	114	7177	8.06	0.63
151200.04+494009.7	19.44±0.07	19.37±0.07	21.62±0.16	19.98±0.09	532	19527	7.71	0.49
153017.00+470852.4	19.15±0.05	18.87±0.05	···	···	703	15479	7.53	0.39
153725.71+515126.9	17.75±0.05	17.54±0.07	···	···	199	24926	8.20	0.73
154038.67+450710.0	18.36±0.06	18.23±0.08	19.93±0.07	19.03±0.04	154	8824	8.03	0.62
155206.11+391817.2	20.56±0.09	19.72±0.10	21.03±0.10	19.88±0.1	945	20040	7.80	0.53
155955.27+263519.2	16.44±0.05	16.42±0.06	20.52±0.09	19.54±0.09	67	11890	8.28	0.78
165747.02+624417.4	19.21±0.07	19.22±0.10	20.96±0.09	19.93±0.11	351	14241	7.87	0.55

Two targets (J0914 and J1530) have SEDs inconsistent with that of a debris disk and no neighboring point sources. While J0914 resembles a disk-hosting WD in that it has no NIR excess in conjunction with a MIR excess, the excess detected by *WISE* is too strong to be reproduced by any of the geometrically thin, optically thick debris disk models that we fit it with. The *WISE* excess is likely caused by a background red galaxy. The excess found at J1530, on the other hand, starts in the SDSS z-band which is uncharacteristic of a debris disk excess and enough to refute the presence of a disk.

3.3.2 New Dusty WDs

A quarter of the WDs in our sample show an excess consistent with that of a debris disk and have no obvious source of contamination within the *WISE* beam radius. The best fit disk parameters are listed in Table 3.3.2. To evaluate the uncertainties in the disk temperatures and inclinations we perform a Monte Carlo analysis where we replace the observed photometric fluxes f with $f + g\delta f$, where δf is the error in flux and g is a Gaussian deviate with zero mean and unit variance. For each of 7,000 sets of modified photometry, we repeat the analysis to derive best-fit parameters for the disk. We adopt the interquartile range of these parameters as the uncertainty. We find that the disk temperatures are uncertain by 200 K and the inclination by 20-25°. The lack of data beyond 5 μm contributes to the

Table 3.2. Best Fit Disk Parameters

WIRED	T_{in} (K)	T_{out} (K)	Incl. (°)	R_{in} ($R_\odot$)	R_{out} ($R_\odot$)
114758.61+283156.2	1400	600	60	0.126	0.389
123432.63+560643.0	1900	500	70	0.062	0.367
150701.98+324545.1	800	300	0	0.134	0.494
153725.71+515126.9	1200	800	30	0.414	0.711

Note. — Typical uncertainties for disk inner and outer temperatures are 200 K and 20-25° for inclination.

uncertainty in the outer temperature of the disks.

The inner and outer radii are obtained from the inner and outer temperatures of the disk using Equation 1 of Jura (2003). The four disks all have similar widths ($\sim$0.3 $R_\odot$), however the radius of the inner edge of the disk orbiting J1537 is three times that of the others. The most massive (J1234) and the coolest (J1507) dusty WDs have the hottest and the coolest disk inner edges; 1900 K and 800 K, respectively. The temperature of the inner edge of the disk surrounding J1234 is hotter than the sublimation temperature of dust ($\sim$ 1500 K; Rafikov & Garmilla 2012) and the flat disk model may need to be replaced with a warped disk in order to explain the SED (Jura et al. 2009).

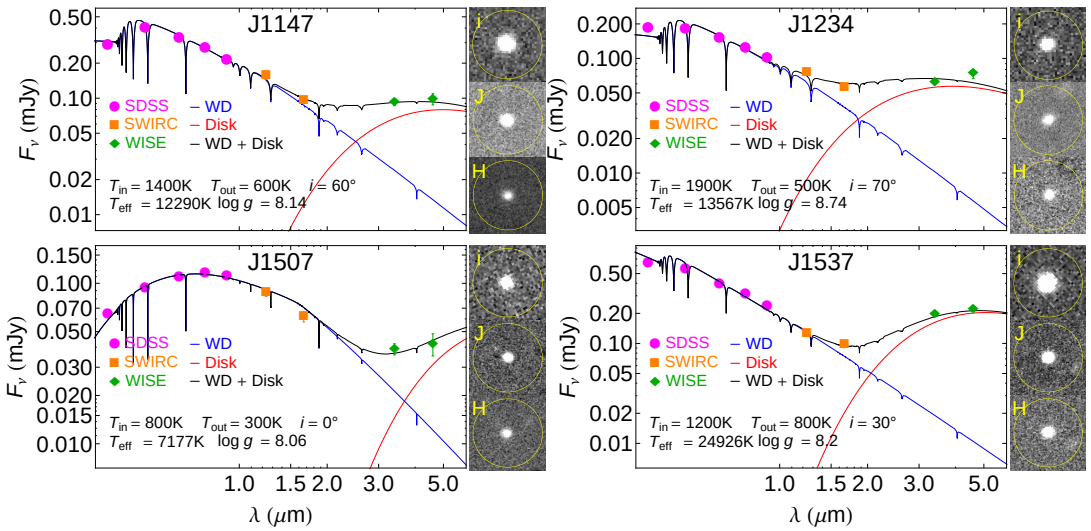


Figure 3.3: The SED of the four isolated WDs in our sample. The SED components are the same as those described in Figure 3.1 except for the disk model, which is shown in red and the WD+disk combination which is shown in black here. The science images of these WDs show no obvious sign of contamination that could explain the excesses found in the *WISE* data. These excesses are well reproduced by geometrically flat, optically thick disk models (Jura 2003).

J1507 is among the coolest dusty WDs known; WD 2115−560 (von Hippel et al. 2007; Farihi et al. 2009; Jura et al. 2009) and G166-58 (Farihi et al. 2008) are the only previously known WD+disk systems with host WDs cooler than 10,000 K. It is also worth noting that J1234 is a 1.04 $M_\odot$ dusty WD with an estimated progenitor main-sequence mass of 5.4 $M_\odot$ (Kalirai et al. 2008; Williams et al. 2009). J1234 is the most massive dusty WD currently known, and the discovery of its disk indicates that intermediate mass ∼5 $M_\odot$ main-sequence stars also host planets.

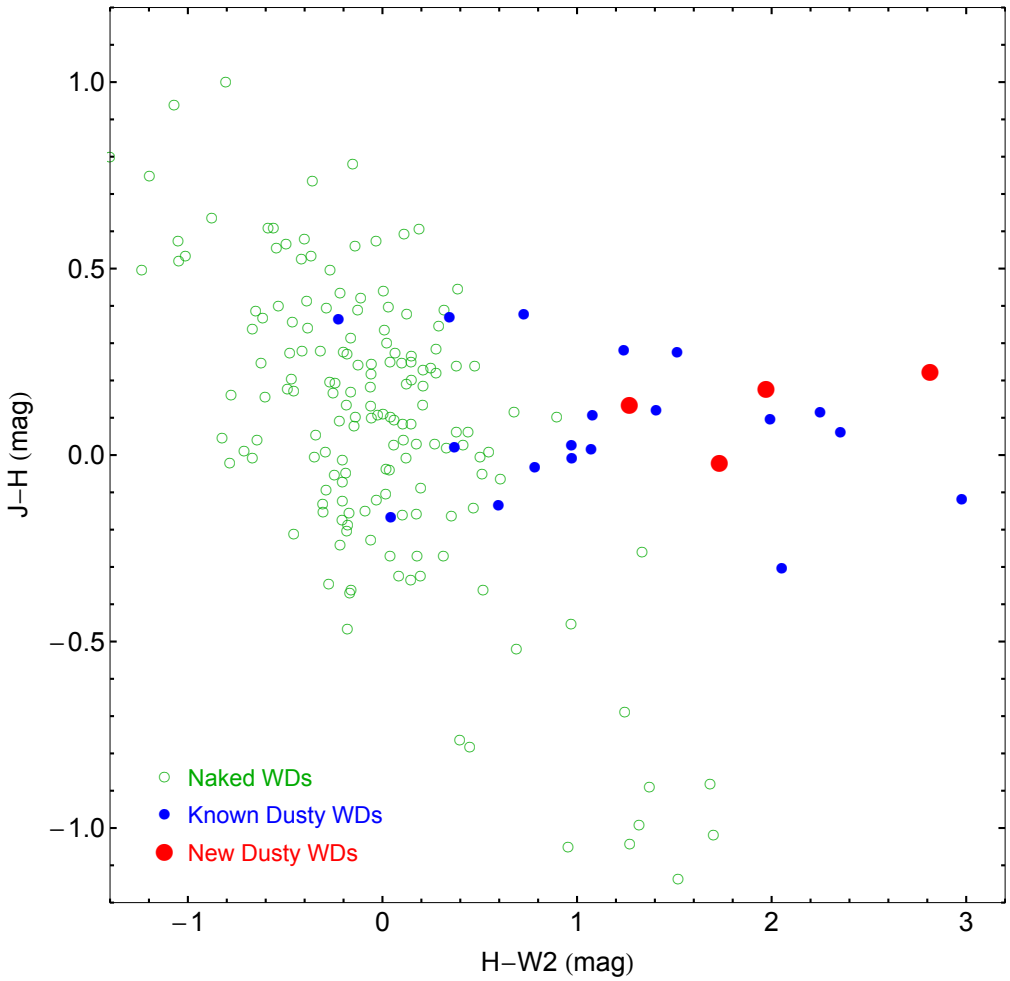


Figure 3.4: The $J-H$ and $H-W2$ colors of the naked WDs in the WIRED sample are shown as empty green circles, while the colors of known dusty WDs and our four new dusty WDs are shown as small blue and large red circles, respectively. The NIR and MIR photometry for the published WD+disk systems are taken from the 2MASS and *WISE* online databases. The colors of the four new dusty WDs are comparable to the colors of the dusty WD population from the literature and are therefore likely to have the same mechanism generating their infrared excesses.

3.4 The Frequency of Disks in the *WISE* All Sky Survey

Two WD+disk candidates identified by Debes et al. (2011b), J0110 and J0905, appear to be bonafide debris disks, due to the lack of an obvious contaminating source in the high resolution UKIDSS images, and must be included in the discussion of the frequency of disks in the WISE sample as a whole. Of the 12 WIRED disk candidates with UKIDSS data, only these two have no apparent contaminating source within a 6″ radius. With the inclusion of J0110 and J0905 there are now 12 confirmed debris disks in the *WISE* sample. These include six previously known dusty WDs, four new dusty WDs presented by this work, and two dusty WDs with UKIDSS data. Out of 1527 WDs in the *WISE* sample, 1020 are WD+M dwarf candidates and 42 are WD+brown dwarf candidates which leaves 465 single WDs observed by *WISE*. Thus, the frequency of disks around single WDs in the *WISE* sample is at least 2.6% which is consistent with the 1-3% disk frequency derived by Farihi et al. (2009). One of the eight WD+disk candidates in our target list that remain unobserved (J0813) was recently revealed by Wang et al. (2014) to have a nearby blending source. The remaining seven disk candidates without NIR data could bring the WISE disk frequency as high as 4.1%, consistent with the 4.3% frequency found by Barber et al. (2012).

If we restrict the frequency calculations to WDs with estimated W1 (3.4 μm)

fluxes above the 74% completeness limit of 50 μJy, we could not include any of the four new disks in the calculation. The seven WIRED disk candidates included in the flux limited sample can, however, be pared down to four candidates because J1037 was misidentified as a WD, J2220 is a known WD+BD system, and J1559 has contaminated *WISE* photometry. Therefore, the frequency of WD+disk systems in the flux limited WIRED sample is at most four out of 395 or 1%.

None of the four new dusty WDs is identified by Kleinman et al. (2013) as having an atmosphere polluted with metals, but this is most likely due to the low resolution and low S/N of the SDSS spectroscopy data. A metal-free atmosphere does not preclude the existence of a debris disk (Hoard et al. 2013), however follow-up high-resolution spectroscopy observations would be useful to confirm the state of pollution of these WD atmospheres. Hoard et al. (2013) report 7 WD+disk candidates, but 3 of them do not display pollution in their atmospheres. The warm inner disk temperatures in Table 3.3.2 imply that accretion is ongoing (Rafikov 2011a) and we expect that high quality, high resolution spectra will reveal the presence of metals. Also, the four new dusty WDs in our sample should show K-band excess from the disks (see Figure 3.3). K-band spectra would be useful to further characterize the source of the excess emission in these systems and to constrain the inner radii of the disks more precisely.

3.5 Conclusions

A recent cross-correlation between the SDSS DR7 White Dwarf Catalog with the Wide-Field Infrared Survey Explorer (*WISE*) all-sky photometry at 3.4, 4.6, 12, and 22 microns performed by Debes et al. (2011b) resulted in the discovery of 52 candidate dusty white dwarfs (WDs). The 6″ *WISE* beam allows for the possibility that many of the excesses exhibited by these WDs may be due to contamination from a nearby source, however. We present MMT+SWIRC J- and H-band imaging observations (0.5-1.5″ PSF) of 16 of these candidate dusty WDs and confirm that four have spectral energy distributions (SEDs) consistent with a dusty disk and are not accompanied by a nearby source contaminant. The remaining 12 WDs have contaminated *WISE* photometry and SEDs inconsistent with a dusty disk when the contaminating sources are not included in the photometry measurements. We find the frequency of disks around single WDs in the *WISE* ∩ SDSS sample to be 2.6-4.1%. One of the four new dusty WDs has a mass of 1.04 $M_{\odot}$ (progenitor mass 5.4 $M_{\odot}$) and its discovery offers the first confirmation that massive WDs (and their massive progenitor stars) host planetary systems.

We have confirmed the presence of dust surrounding four WDs with excess flux detected by *WISE*. These four new dusty WDs, including the two bonafide UKIDSS+WISE disks, increases the total number of confirmed WD+disk systems

from 29 to 35 (Farihi et al. 2009; Xu & Jura 2012; Hoard et al. 2013). The discovery of these four new debris disks enriches the current dusty WD population with one of the coolest (J1507), hottest (J1537), and the most massive (J1234) WDs known to host circumstellar dust. Expanding the parameter space known to be hospitable to circumstellar dust at WD stars will not only guide future infrared excess searches, but also enhance our understanding of the formation and evolution of these remnant planetary systems.

3.6 Acknowledgements

This chapter makes use of data products from the Wide-field Infrared Survey Explorer, which is a joint project of the University of California, Los Angeles, and the Jet Propulsion Laboratory/California Institute of Technology, funded by the National Aeronautics and Space Administration.

Observations reported here were obtained at the MMT Observatory, a joint facility of the Smithsonian Institution and the University of Arizona.

We make use of the Bergeron WD cooling model grids (Holberg & Bergeron, 2006; Kowalski & Saumon, 2006; Tremblay et al., 2011) to calculate our debris disk models.

This chapter is reproduced by permission of the American Astronomical Society from Barber et al. 2014.

Chapter 4

A *Spitzer* Search for Massive Dusty WDs

"You may trod me in the very dirt but still, like dust, I'll rise."

– Maya Angelou, *Still I Rise*

4.1 Introduction

We just presented the discovery of the most massive dusty white dwarf (WD) (J1234; M=1.04 $M_{\odot}$) to date in the last chapter. This discovery resulted from a broad survey of WDs selected by *WISE*. With this exciting system in mind, let's hone in on the massive WD population using *Spitzer* and see what more we can find. *Spitzer* (Werner et al., 2004), equipped with the InfraRed Array Camera (IRAC; Fazio et al. 2004b), has an advantage for finding disks over *WISE*. IRAC has a diffraction-limited beam size of 1.7″, about one quarter the size of the *WISE* beam. Thus, IRAC is much less likely to be contaminated by background sources.

To constrain the frequency of disks at massive WDs, and the frequency of planets at their massive progenitors for the first time, we assemble a sample of the 100 brightest hydrogen-atmosphere (DA) WDs from the Sloan Digital Sky Survey (SDSS) DR7 White Dwarf Catalog (Kleinman et al., 2013) with masses greater than 0.8 $M_{\odot}$ and temperatures between 9500 and 22,500 K (Figure 4.2b). This

sample hails from main sequence stars greater than 3.5 times the mass of the sun (Figure 4.1). They are cool enough that their dust sublimation radius is interior to their tidal disruption radius and, thus, they are hospitable to solid circumstellar dust. They are also young enough that their reservoir of planetesimals has not yet been exhausted. Assuming a similar disk frequency for normal and massive WDs (4.3%), we expect with 99.5% confidence that in our sample of 100 massive white dwarfs, at least one will be dusty.

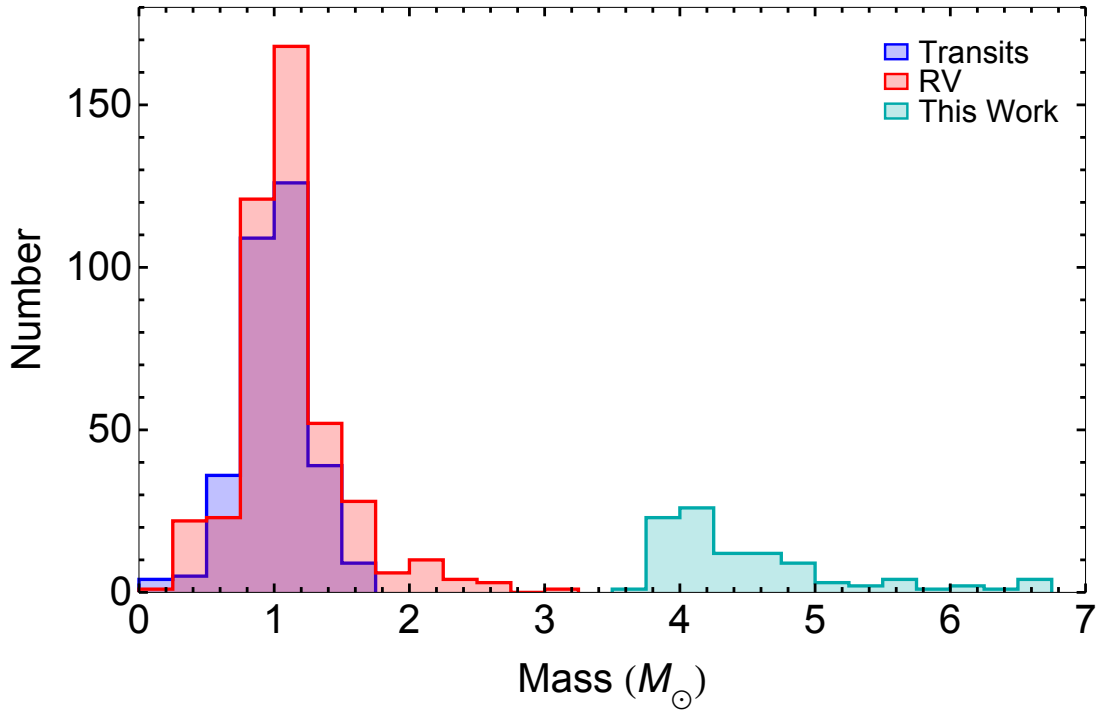


Figure 4.1: Histogram of stellar host mass of all confirmed exoplanets (`exoplanets.org`; Han et al. 2014) detected via transits and radial velocity variations as well as WD progenitor masses from this sample. This work probes a region in parameter space currently devoid of planetary systems.

Previous searches for infrared excesses at massive WDs have returned mostly null results. Hansen et al. (2006) examined 12 hot ($T_{\rm eff}$ >30,000 K), massive (M>1 $M_\odot$) WDs with *Spitzer* IRAC and found no instance of excess infrared emission. The authors were looking for planets, however, and we do not expect to find debris disks around stars this hot.

Mullally et al. (2007) survey 124 WDs with $T_{\rm eff} = 5000 - 170,000K$ using mid-infrared *Spitzer* photometry. Their search for infrared excess finds 2 dusty WDs for a disk frequency of 1.6%. However, this survey extends beyond the temperature range within which solid dust orbiting interior to the tidal radius can persist. While this sample was selected based on brightness, there are 6 white dwarfs with $T_{\rm eff}$=9500-22,500 K and M>0.8 $M_\odot$ (Gianninas et al., 2011). None of these six white dwarfs were found to have an infrared excess.

Farihi et al. (2008) conducted a *Spitzer* IRAC survey that focused on descendants of intermediate-mass stars with M>3 $M_\odot$ and $T_{\rm eff}$ >30,000 K. They found none of their 22 young, high-mass, field white dwarfs to be dusty. This sample is also too hot, however, for solid dust particles to persist within the stellar tidal radius.

Dufour et al. 2010 found the 0.84 $M_\odot$ helium-atmosphere (DB) WD J0738+1835 to be extremely polluted during a search for metal-rich WDs in the SDSS. With follow-up *Spitzer* and Gemini+NIRI photometry Dufour et al. 2012 confirmed the

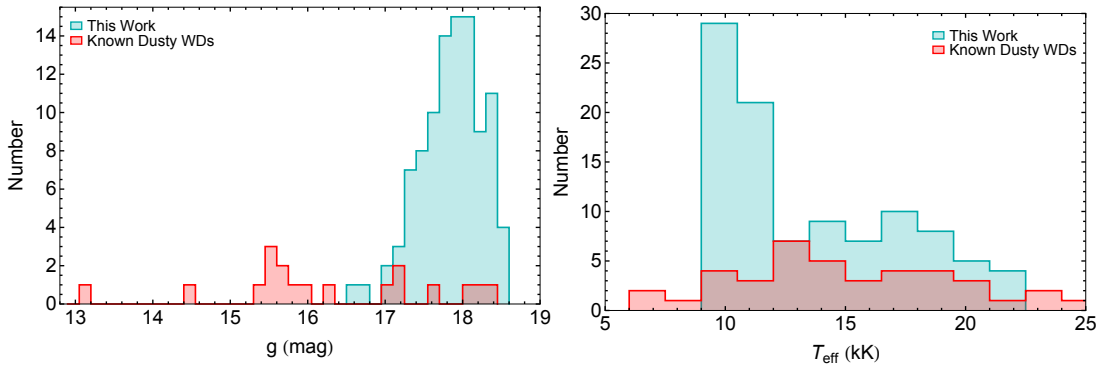
presence of dust. This is the only WD greater than 0.8 $M_{\odot}$ found to host dust prior to this work.

Debes et al. (2011b) recently searched for infrared excesses amongst an unbiased (in terms of metallicity) WD sample using the Wide-field Infrared Survey Explorer (WISE) (Wright et al., 2010) data. They found about 1-5% of these WDs to be dusty. However, 75% of these dusty WD candidates were found to be false positives due to chance alignment with background sources (Barber et al., 2014).

There are no known massive (M>0.8 $M_{\odot}$) dusty DA white dwarfs with $T_{\rm eff}$=9500-22,500 K in the WISE survey (Debes et al., 2011b). We cross-correlated the SDSS DR7 WD catalog (Kleinman et al., 2013), with WISE and found 322 massive SDSS DR7 white dwarfs detected in WISE. However, almost all are blends or objects with M dwarf companions. While WISE could potentially detect dusty WDs in this mass and temperature regime, what it has detected so far is objects with contaminated photometry. Our NIR follow-up of the WIRED survey using SWIRC (Barber et al. 2014; see also Chapter 3) turned up the most massive dusty WD to date, J1234+560 with M=1.04 $M_{\odot}$.

Koester et al. 2014 examine the abundances of a sample of 85 young (20-200 Myr), DA WD and find 56% to be polluted. Out of the 14 massive (>0.8 $M_{\odot}$) WDs in their sample, just one shows traces of heavy elements. This deficit in the WD pollution rate at massive WDs warrants further study.

The number of observations of massive DA white dwarfs hospitable to solid dust within the tidal radius of the WD (M>0.8 $M_{\odot}$ and T_{eff} = 9500-22,500 K) remains very small. There is no survey that has targeted these systems before. Our study will improve upon previous massive WD infrared searches because we will focus on objects that lie within the temperature range where dust orbiting within the stellar tidal radius can remain solid. Our sample also is unbiased towards metallicity, and will therefore identify the true frequency of disks at massive WDs. Figure 4.1 shows the mass distribution of our sample. This region in parameter space has been very under sampled thus far. We have a unique opportunity to constrain the frequency of disks at massive WDs, and thus the frequency of planets at their massive progenitor stars.



(a) (b)

Figure 4.2: (a) Histogram of SDSS *g*-band magnitude for our sample (cyan) compared with published dusty WDs (red). We are probing a relatively faint population of WDs compared to the known dusty WD population. (b) Histogram of effective temperatures for all published dusty WDs and WDs from this sample. We are selecting WDs most hospitable to solid dust by using a 9500-22,500 K temperature cut.

4.2 Observations and Data Analysis

4.2.1 *Spitzer*+IRAC

In Cycle 9 of the *Spitzer Space Telescope* (Werner et al., 2004) mission, we were awarded 15 hours (program 90212) to collect 4.5 μm observations of our entire sample using the InfraRed Array Camera (IRAC; Fazio et al. 2004b). 4.5 μm (IRAC Ch 2) data is sufficient to detect an excess. We were then awarded 3.5 hours (program 10062) to follow up the 23 most promising targets in the 3.6 μm (IRAC Ch 1) band during Cycle 10 to further characterize the excess. For both cycles each frame was exposed for 30s and dithered using a small scale (16 pixel maximum offset) 9-point random pattern for a total integration time of 270 seconds.

We measure the aperture photometry of most saturation corrected basic calibrated data (CBCD) long exposure mosaic frames in the same manner as Section 2.3.3. Unfortunately, some WDs are accompanied by point sources within 5-8$''$ that threaten to contaminate our measurements. We perform PSF-fitting photometry using the `IRAF daophot` package where we simultaneously fit the PSF of the WD and the neighboring point source with a PSF model created using several reference stars in the image.

4.2.2 MMT+SWIRC

Following two observing runs that were completely shut out due to weather, we conducted a successful two-night run in mid-May 2014 using the SAO Wide-Field InfraRed Camera (SWIRC; Brown et al. 2008) on the MMT. We imaged 12 WDs in the NIR J- and H-band where each target was observed for three sets of 3×5 dithers with offsets of 10 arcsec and exposure times of 25 s in both bands. We took dark frames and sky flats each evening. The sky was photometric with average seeing of 0.9 arcsec.

We used the SWIRC data reduction pipeline to dark and flat correct the images. We then shifted the images to a common reference position and mean combined them to create a final image in each band for each target. The zero-point offset for each final image was calculated using a weighted mean of the measured zero-point offsets of the 2MASS stars in the field. All photometry was performed using the `IRAF daophot` package where we fit the point spread function of the WD using several reference field stars.

4.2.3 Gemini+NIRI

We were awarded 2.3 hours (program GN-2014B-Q-6) to observe six of the WDs with the most compelling excesses using the 8 m Gemini telescope on Mauna Kea. We obtained K-band (2.2 μm) photometry using Gemini's Near InfraRed Imager

and Spectrometer (NIRI; Hodapp et al. 2003) between August and December of 2014. K-band data is critical for parameterizing the excess and constraining the inner radius of the debris disk. We used NIRI in f/6 imaging mode which has a 0.12 arcsec/pixel plate scale and a 120×120 arcsec field of view. We varied exposure times in order to achieve a S/N of 30. We used the Gemini/NIRI suite of `IRAF` packages to reduce the science and standard star images. We performed aperture photometry using the `IRAF apphot` package. The first image in each science, standard, dark, flat sequence was discarded due to an expected elevation in the dark level after sitting idle. We flux calibrated the WDs using the standard star K-band magnitudes published by Leggett et al. 2003 to calculate the zeropoint offset.

4.3 Results

In Tables 4.1 and 4.2 we present our mid- and near-infrared photometry, respectively, where the stellar parameters in Table 4.1 were obtained from Kleinman et al. 2013. Since a search for circumstellar dust around WDs is essentially a search for infrared excesses, we also present a histogram of the measured excesses in the NIRI/UKIDSS K-band and both IRAC channels in Figure 4.3.

Table 4.1. IRAC Ch 1 and Ch 2 Photometry

SDSSJ	T_{eff} (K)	log g	Mass ($M_\odot$)	$F_{3.6\ \mu m}$ (μJy)	$F_{4.5\ \mu m}$ (μJy)
000357.62−004939.0	9651	8.75	1.04	···	8±2
002516.45−095238.6	10995	8.41	0.85	···	12±2
003719.12+003139.3	10957	8.52	0.92	···	21±2
004610.37+133910.3	11012	8.34	0.81	···	9±4
005156.86+010052.2	10078	8.38	0.83	···	10±2
025200.98+004544.2	9992	8.41	0.85	···	12±2
025746.41+010106.0	17610	8.37	0.83	15±2	12±2
030243.80+062637.2	11447	8.54	0.93	···	12±2
032133.84+410134.6	13472	8.46	0.88	···	10±2
032727.52+001252.7	16755	8.61	0.98	···	10±2
034939.35+103649.9	11715	8.40	0.84	···	29±2
042017.89+052735.8	21132	8.33	0.81	9±2	7±2
055609.86+835754.5	15570	8.37	0.83	···	8±2
064754.29+363350.3	18116	8.39	0.85	6±3	10±3
072438.30+310729.0	10332	8.38	0.83	···	18±2
072723.02+413736.6	13629	8.37	0.83	···	14±2
073129.34+371444.9	12811	8.39	0.84	···	12±2
073612.36+222937.2	13858	8.49	0.90	25±2	24±2
074155.51+315347.5	18045	8.41	0.86	5±4	9±2
074712.63+452714.0	13692	8.88	1.11	···	14±2
080254.13+440945.3	15849	8.43	0.87	···	4±3
080456.47+194242.3	10058	8.39	0.84	···	23±2
080616.91+202602.4	16530	8.37	0.83	···	7±2
082608.99+542648.2	22183	8.45	0.89	···	9±3
082926.86−042021.9	16981	8.42	0.86	···	4±3
083602.91+303149.7	19193	8.84	1.09	···	7±2
084031.46+214042.7	17549	8.41	0.86	25±2	29±2
084321.98+204330.2	14758	8.42	0.86	10±2	10±2
085033.55+382717.2	17898	8.38	0.84	···	10±2
085828.81+441553.9	9724	8.38	0.83	···	13±2
085947.33+422113.1	14845	8.53	0.93	···	9±2

Table 4.1 (cont'd)

SDSSJ	$T_{\rm eff}$ (K)	log g	Mass ($M_\odot$)	$F_{3.6\ \mu m}$ (μJy)	$F_{4.5\ \mu m}$ (μJy)
090258.23+230640.2	13358	8.57	0.95	···	13±2
090621.64+380956.4	20192	8.90	1.12	···	8±2
091521.66+194939.7	19535	8.46	0.89	10±3	9±2
092329.81+012020.0	11280	8.6	0.97	···	7±2
092451.92+463341.5	18334	8.48	0.90	9±2	22±3
094000.27+005207.1	10692	8.42	0.86	20±2	14±2
094255.02+180328.6	11544	8.66	1.00	···	9±2
094324.04+300352.0	15580	8.52	0.92	19±2	15±2
094332.88+312454.9	10491	8.88	1.11	···	8±3
094804.30−000738.2	10034	8.42	0.86	···	11±2
100704.45+322947.0	9640	8.45	0.87	···	16±2
101218.09+610818.9	11778	8.37	0.83	···	12±2
102033.69+274137.4	11915	8.39	0.84	···	7±2
102128.30+393728.6	9629	8.42	0.85	···	14±2
102626.22+252342.1	10487	8.35	0.81	15±2	12±2
103044.56+191357.9	16227	8.45	0.88	···	3±3
103642.26+211527.9	11380	8.5	0.91	···	18±2
103744.65+523042.1	14302	8.47	0.89	···	7±2
104038.50+380822.9	19858	8.53	0.93	···	6±2
104243.00+651842.4	18261	8.35	0.82	···	7±2
105849.14+095750.0	9582	8.34	0.80	···	13±3
110314.74+070450.8	21668	8.5	0.92	18±2	15±2
110750.76+261351.8	11400	8.36	0.82	···	7±2
111743.92+182132.8	9978	8.69	1.01	···	11±2
113845.29+191952.5	17955	8.35	0.82	···	15±2
114348.09+483636.8	17690	8.89	1.12	13±2	8±2
114824.51+551934.6	9615	8.37	0.82	···	11±2
115315.77+635035.9	13362	8.44	0.87	···	9±2
120504.20+160746.9	9853	8.41	0.85	···	31±2
121205.11+140801.8	21212	8.37	0.84	···	17±2
121509.68+094847.2	9578	8.55	0.94	···	12±2

Table 4.1 (cont'd)

SDSSJ	$T_{\rm eff}$ (K)	log g	Mass ($M_\odot$)	$F_{3.6\ \mu m}$ (μJy)	$F_{4.5\ \mu m}$ (μJy)
122337.56+333806.5	10261	8.42	0.86	···	13±2
124836.84+433943.9	16557	8.42	0.86	···	6±2
130023.14+143635.2	9717	8.48	0.89	···	6±2
130407.75+004331.9	9925	8.65	1.00	···	13±2
130907.15+000626.4	10744	8.37	0.82	···	12±2
131446.20+383725.6	17433	8.39	0.84	16±2	12±2
132044.68+001854.9	19913	8.41	0.86	···	24±2
132118.11+551644.0	20008	8.34	0.82	···	10±2
133336.04+091704.9	13508	8.36	0.82	30±2	21±2
135922.66+490249.3	9910	8.39	0.84	···	20±2
140533.11+165049.2	13919	8.33	0.80	11±2	11±2
141356.52−002643.2	9553	8.40	0.84	···	23±2
141402.17+323208.6	10056	8.41	0.85	···	13±2
142152.21+093005.4	9576	8.35	0.81	74±3	49±3
143336.12+375140.1	10493	8.58	0.96	···	20±2
143349.02+640647.8	12197	8.33	0.80	···	10±2
145644.46+064352.0	9994	8.36	0.82	···	14±2
145901.10+412309.7	11118	8.36	0.82	···	8±1
150854.31+011613.6	16020	8.45	0.88	···	9±2
152912.18+533531.8	13383	8.51	0.92	···	8±2
154710.83+442848.2	9882	8.47	0.89	···	12±2
154832.76−001717.9	9817	8.49	0.90	27±2	19±2
155031.68+353824.5	10698	8.34	0.81	···	16±2
155438.35+241032.6	11632	8.58	0.96	···	15±2
161021.27+414346.5	10755	8.40	0.84	···	7±2
161218.08+083028.2	12026	8.46	0.88	19±2	15±2
161834.21+521810.8	14575	8.46	0.89	···	13±2
162752.26+332153.6	15036	8.49	0.90	···	6±2
162858.18+141508.6	10402	8.40	0.84	···	26±2
162918.99+004551.6	9773	8.53	0.92	···	17±2
163010.19+231735.0	11089	8.36	0.82	22±2	23±2

Table 4.1 (cont'd)

SDSSJ	T_{eff} (K)	log g	Mass ($M_\odot$)	$F_{3.6\ \mu m}$ (μJy)	$F_{4.5\ \mu m}$ (μJy)
164248.61+382411.2	19171	8.42	0.87	12±2	10±2
165020.53+301021.3	11021	8.65	1.00	···	6±2
180957.46+242535.9	16279	8.35	0.82	···	15±2
212930.65+114231.2	18855	8.40	0.85	···	4±2
214652.19+111237.7	18557	8.78	1.06	13±2	11±2
220830.02+065448.7	11104	8.49	0.90	···	10±2
220831.42+205909.7	11488	8.77	1.05	···	18±2

Note. — Stellar parameters (T_{eff}, log g, and mass) obtained from Kleinman et al. 2013.

Table 4.2. Ground-based JHK Photometry

SDSS	J (mag)	H (mag)	K (mag)
025746.41+010106.0	···	···	18.34 ± 0.01
042017.89+052735.8	···	···	18.79 ± 0.02
073612.36+222937.2	18.02 ± 0.04	18.37 ± 0.09	18.09 ± 0.02
084031.46+214042.7	18.31 ± 0.05	18.49 ± 0.07	18.25 ± 0.02
092451.92+463341.5	18.72 ± 0.03	18.74 ± 0.04	···
110314.74+070450.8	17.79 ± 0.02	17.65 ± 0.05	18.02 ± 0.02
131446.20+383725.6	18.07 ± 0.02	18.09 ± 0.03	18.29 ± 0.02
133336.04+091704.9	18.29 ± 0.04	18.05 ± 0.04	···
140533.11+165049.2	18.70 ± 0.02	18.63 ± 0.04	···
142152.21+093005.4	17.01 ± 0.05	16.84 ± 0.05	···
154832.76−001717.9	18.02 ± 0.03	17.87 ± 0.04	···
161218.08+083028.2	17.84 ± 0.05	17.71 ± 0.07	···
163010.19+231735.0	17.65 ± 0.03	17.46 ± 0.04	···
164248.61+382411.2	18.65 ± 0.04	18.46 ± 0.05	···

Note. — J- and H-band data were taken using MMT+SWIRC while K-band data were taking with Gemini+NIRI.

To determine if an excess originates from circumstellar dust, we examine the shape of the SED. Half of the known dusty WDs have an excess that starts in the K-band. A dust disk typically creates no excess blue-ward of the K-band. The SED redward of the K-band is fairly level initially, and then falls off slowly.

We compare the near- and mid-infrared data to the emission expected from a naked WD using the model DA atmospheres of (Tremblay & Bergeron, 2009; Tremblay et al., 2010; Gianninas et al., 2011) for the appropriate effective tem-

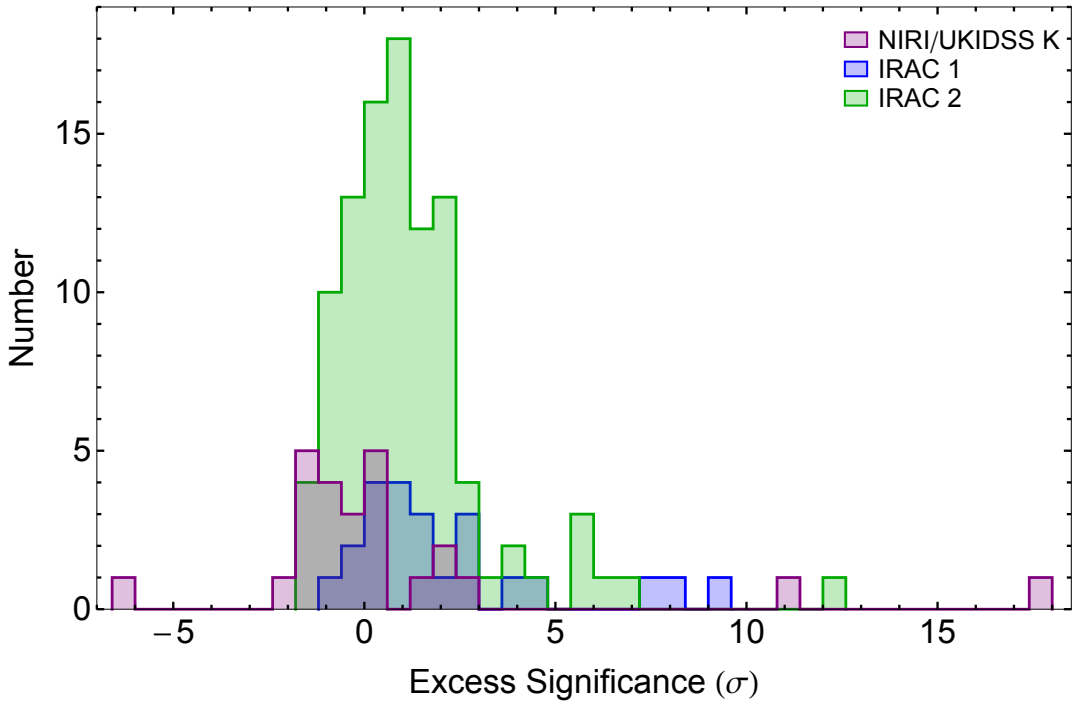


Figure 4.3: Histogram of photometry excesses in the NIRI K-band as well as both IRAC channels.

perature and surface gravity. The model is scaled to the SDSS *griz* photometry and the excess infrared emission is then fit with a flat, opaque disk model (Jura, 2003) using a chi-squared minimization between synthetic photometry of the disk models and the excesses observed in the SWIRC/UKIDSS J- and H-bands, the NIRI/UKIDSS K-band, and both IRAC Channels. In the case where PSF-fitting was required, we use the photometry of the WD from the PSF-subtracted image for the disk fit, although we ultimately plot both sets of photometry (Figure 4.6). The input parameters for the dusty disk models (WD distance and radius) are interpolated from the Bergeron cooling model grid (Holberg & Bergeron, 2006; Kowalski & Saumon, 2006; Tremblay et al., 2011).

4.3.1 Galaxy Contamination

Before we explore the results of disk model fitting to our measured excesses we need to examine the potential for extraneous sources of excess emission. Fazio et al. 2004a determine the galaxy count rate as a function of flux. We convert the count rate to a cumulative count rate to determine the probability of catching a galaxy in our photometry aperture and mistaking a galaxy for a debris disk. The chance of alignment with a background galaxy depends on the flux level we are probing (galaxies are more numerous at lower flux levels) and the size of our photometry aperture. Figure 4.2a shows that we probe a relatively faint population

of WDs and thus we run a real risk of interference from a background galaxy. We calculate the chance of alignment with a galaxy bright enough to create a three sigma excess at each of our WDs and find that we can expect to detect a spurious excess 3.9% of the time in IRAC Ch 1 and 7.5% of the time in Ch 2 (Figure 4.4). This means, statistically speaking, we should expect to detect 4-8 significant excesses due to background galaxies in our sample of 100 WDs. Thus, the 17-18 g-band magnitude regime is nearing the flux level where galaxies become quite numerous and dusty disks orbiting WDs are likely to be confused with emission from background galaxies.

After PSF-subtraction, we find five and ten WDs with significant ($>3\sigma$) excesses in IRAC Channels 1 and 2, respectively. These numbers are slightly higher than the 4-8 predicted spurious excesses based on the galaxy counts of Fazio et al. 2004a. Perhaps the additional 1-2 excesses are due to dust.

4.3.2 Debris Disks

We find three WDs with significant ($>3\sigma$) excesses consistent with circumstellar dust. Figure 4.6 shows the spectral energy distributions (SEDs) for these three WDs. For the remainder of this chapter I will refer to each WD with the first four numbers of its SDSS DR7 White Dwarf Catalog name preceded by the letter "J".

The excess emission found at J0736 is best fit by a fairly average sized disk,

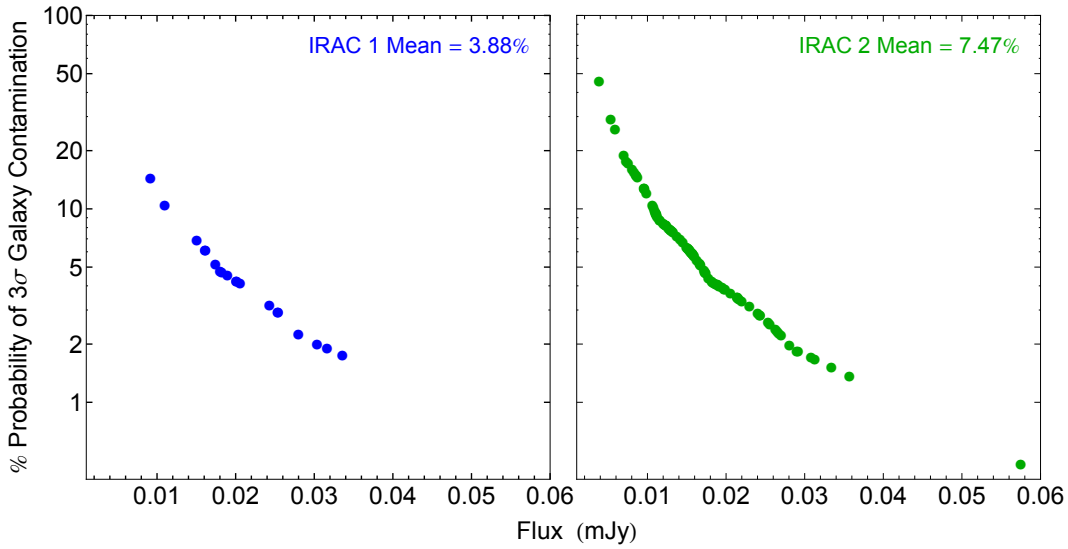


Figure 4.4: Probability of detecting a 3σ excess at WDs in our sample due to chance alignment with a background galaxy (Fazio et al., 2004a). At this flux level, we expect 8 WDs, at most, to exhibit spurious significant excesses out of our 100 WD sample.

extending from 800-300 K and inclined 70°. All images (SDSS, SWIRC, NIRI, IRAC) reveal a close (within 4″) neighboring source that threatens photometric contamination. This point source is successfully removed from both IRAC images and a significant excess (4σ in IRAC Ch 1, 7.2σ in IRAC Ch 2) persists. The result of PSF-subtraction on the IRAC Ch 2 image can be seen in Figure 4.5, where the original image is on the left and the subtracted image is on the right. The nearby source is satisfactorily removed. The photometry from the PSF-subtracted image (empty magenta boxes in Figure 4.6), is then used to find the best-fit disk. At 0.9 $M_{\odot}$, J0736 is the most massive WD in our sample with circumstellar dust, and the second most massive dusty WD to date behind the 1.04 $M_{\odot}$ J1234 (Barber et al., 2014).

Using the measured excess flux at J0736 and the galaxy counts of Fazio et al. 2004a, we calculate the chance of alignment within the 2.4″ aperture for each IRAC band. J0736 has an 11% chance of aligning with a galaxy bright enough to produce its measured excess. We can also check for the presence of a background galaxy by examining how the the centroid position of the WD varies (or doesn't vary) as a function of wavelength. Unlike a WD, which peaks in brightness in the optical, a background galaxy peaks in brightness in the mid-infrared. Thus, in all cases except for an exact alignment between the galaxy and the WD, a background galaxy will shift the centroid of the WD in the infrared with respect to the optical.

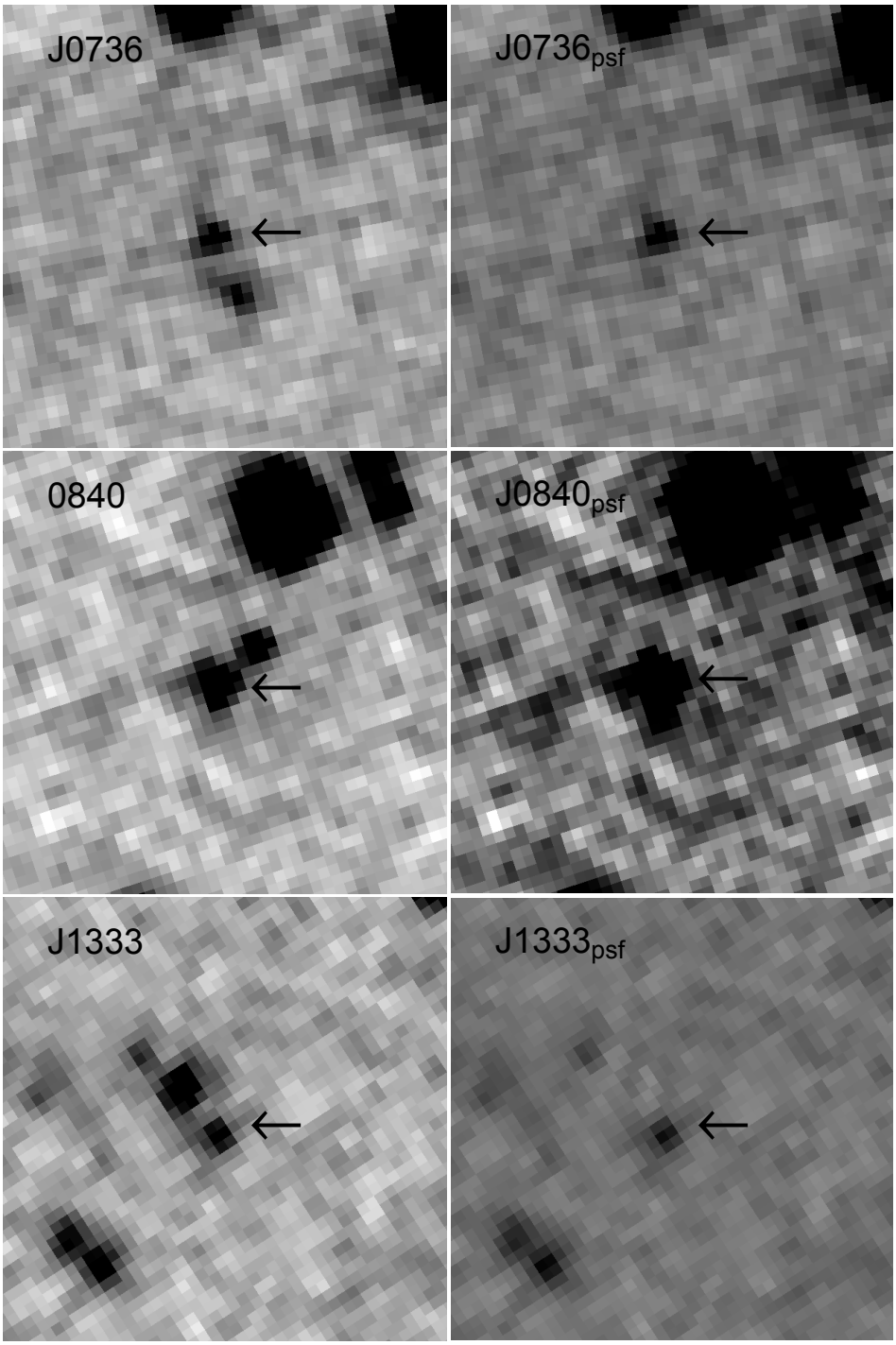


Figure 4.5: Original (left) and PSF-subtracted (right) IRAC Ch 2 images show the clean subtraction of sources close the the WD. The black arrow indicates the position of the WD.

To determine if there is a centroid shift between the optical and infrared images due to the presence of a background galaxy, we measure the centroid of the J0736 in the SDSS i- and IRAC Ch 2-band images using the `IRAF` PSF-fitting package `daophot`. We will consider two centroids to be consistent if they are closer than the $0.5''$ pointing accuracy of IRAC. Since there is no proper motion data available for J0736, we do not correct the SDSS i-band centroid position for proper motion. Nonetheless, we find that the two centroids are separated by only $0.32''$. We've plotted the location of both centroids (SDSS i-band in cyan and IRAC Ch 2 in magenta) on the IRAC Ch 2 inset in Figure 4.6. The radii of both circles is $0.25''$, half of the IRAC pointing accuracy. Thus, if the two circles meet, the centroids are consistent and it is unlikely that a background galaxy is present.

The SED of J0840 is successfully reproduced with the inclusion of an extended disk, ranging from 1200-300 K, and inclined 30°. This is one of the larger disks in the literature and the largest disk in this sample, extending more than a solar radius from the interior disk cavity to its outer edge. A nearby point source appears in both IRAC images but is not visible in the SDSS, SWIRC, or NIRI images. This neighboring point source is successfully subtracted out using standard `IRAF` PSF-fitting techniques (Figure 4.5) and the photometry is unchanged (empty magenta squares in Figure 4.6). We calculate that the excess found at J0840 has a 5% chance of originating from a background galaxy. Additionally, the SDSS i-band and non-

Table 4.3. Best Fit Disk Parameters

SDSS J2000	T_{in} (K)	T_{out} (K)	Incl. (°)	R_{in} ($R_\odot$)	R_{out} ($R_\odot$)
073612.36+222937.2	800	300	70	0.25	0.92
084031.46+214042.7	1200	300	30	0.21	1.35
133336.04+091704.9	1600	1200	0	0.13	0.49

Note. — Typical uncertainties for disk inner and outer temperatures are 200 K and 20-25° for inclination.

PSF subtracted IRAC 2-band centroids, corrected for proper motion, are separated by 0.53″ (Figure 4.6), only slightly higher than the IRAC pointing accuracy.

The large excess seen at J1333 agrees with the presence of a face-on narrow ring of dust. A nearby point source seen in all images is successfully removed via PSF-fitting with no significant reduction in the excess (see Figure 4.6). We calculate that this excess has an 11% chance of originating from a galaxy alignment. Furthermore, the proper motion corrected SDSS and IRAC centroids differ by just 0.47″ (Figure 4.6).

4.4 Notes on Individual Objects

The SEDs for all non-dusty WDs in this sample can be found in Appendix A.

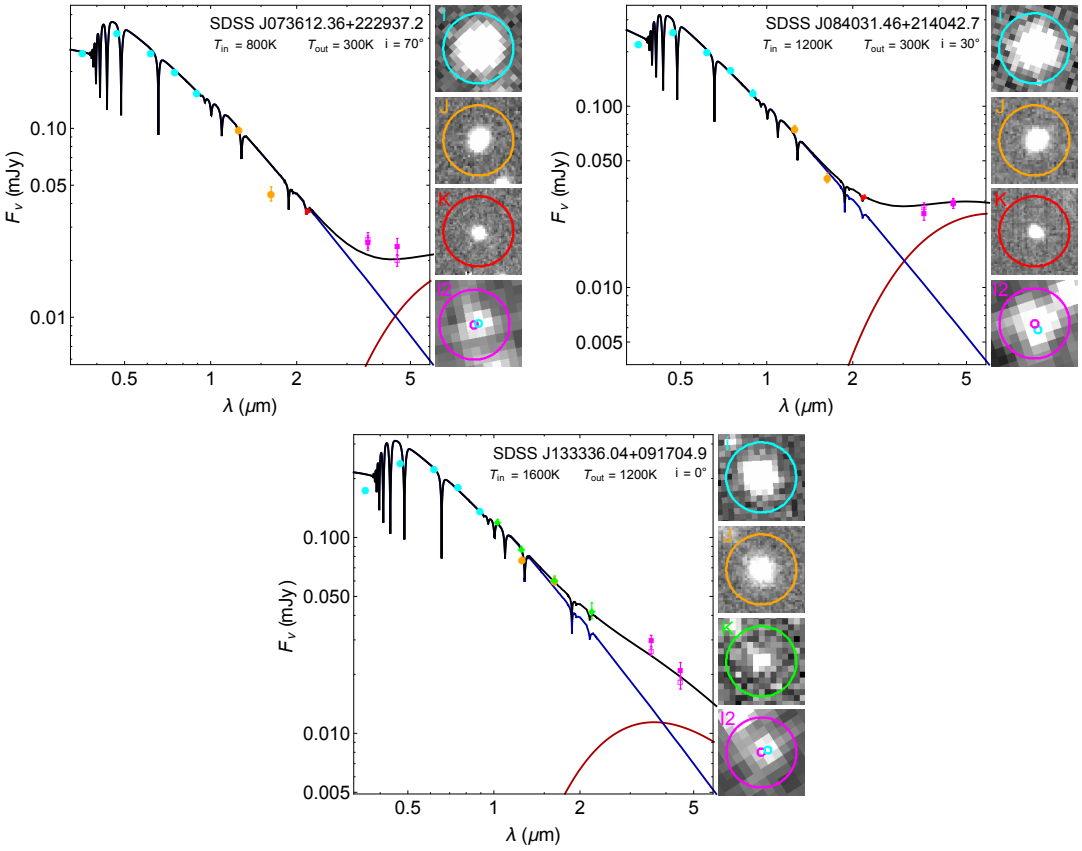


Figure 4.6: Three WDs exhibiting excess emission consistent with a dusty debris disk. The insets to the right are the SDSS i-, SWIRC/UKIDSS J-, NIRI K-, and IRAC 2-band images. All frames have a 2.4″ circle indicating the IRAC photometry aperture size. The small circles on the IRAC 2 inset indicate the SDSS g-band (cyan) and IRAC Ch 2 (magenta) centroid positions corrected for proper motion. All centroids are consistent and thus galaxy contamination is unlikely.

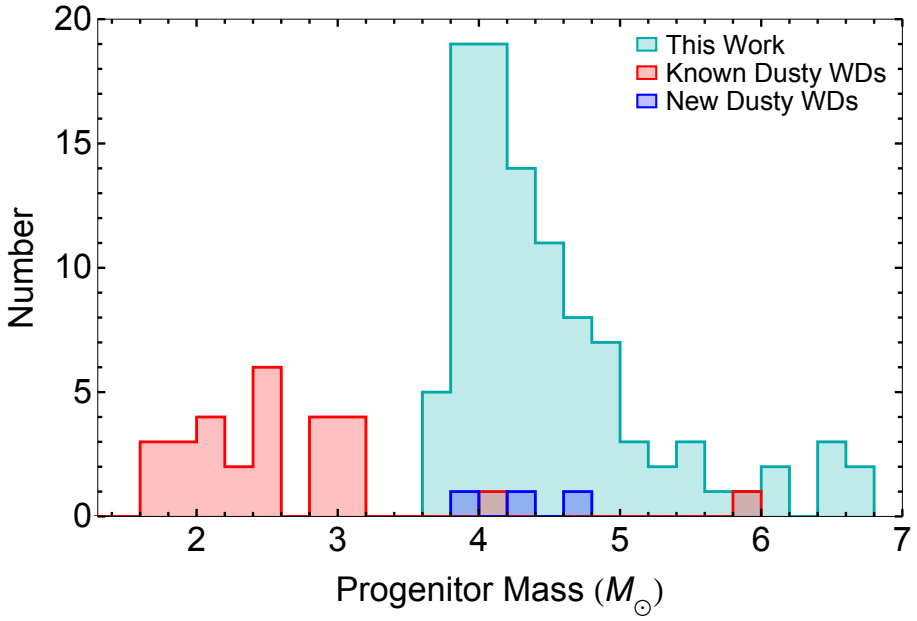


Figure 4.7: Histogram of progenitor mass for WDs in our sample (cyan), known dusty WDs (red), and new dusty WDs identified in this work (blue). The 1.04 $M_\odot$ (5.4 $M_\odot$ progenitor mass) WD known to have a disk is the helium-atmosphere WD J1234 Barber et al. 2014, identified from the *WIRED* Survey. The 0.84 $M_\odot$ (4.1 $M_\odot$ progenitor mass) known dusty WD was discovered by Dufour et al. 2010. This work increases the number of massive (>0.8 $M_\odot$) dusty WDs to five with the discovery of the first three hydrogen-atmosphere massive WDs with circumstellar dust.

025746.41+010106.0: J0257 has a subtle (1.7σ) excess in IRAC Ch 2 which is not reproduced with a debris disk.

085828.81+441553.9: While J0858 exhibits excess (2.1σ) emission in the IRAC 2 band, this photometry is likely contaminated as a nearby extended source can be seen in the image. Since this excess is already quite subtle, the removal of any contamination from this neighbor would render the excess thoroughly insignificant.

091521.66+194939.7: J0915 exhibits 1.7σ excess in the IRAC 2 band, but is consistent with the WD emission in the IRAC 1 band. This could be a cool, faint disk, but we chose not to follow it up in the NIR due to the subtlety of the excess.

094000.27+005207.1: J0940 has subtle excess (2.7σ in Ch1 and 2.9σ in Ch2) emission in both IRAC bands, however the best-fit optically thick, geometrically thin dust disk (Jura, 2003) does not successfully reproduce the observed SED.

102626.22+252342.1: The subtle excess (2.4σ in IRAC Ch 1 and 2.7σ in IRAC Ch 2) found at J1026 is likely contaminated by the adjoining object clearly visible in the IRAC Ch 2 image. Since this excess is already subtle, any contribution from the contaminating source would render the IRAC photometry essentially consistent with the expected WD emission. However, it's possible that this WD hosts a highly inclined extended disk or a narrow ring that would not produce emission significantly in excess of the WD.

110314.74+070450.8: The 2σ excess found at J1103 could not be reproduced by the inclusion of a dusty debris disk.

114348.09+483636.8: J1143, slightly elongated in the SDSS images, is clearly accompanied by nearby point sources in both IRAC images and thus the already subtle excess (2.6σ) is likely not associated with the WD.

131446.20+383725.6: The subtle (1.9σ) excess found at J1314 is not reproduced with the best-fit debris disk model.

132044.68+001854.9: We refer to Farihi et al. 2012 who cite enlarged FWHM and modest elongation as indication of likely contamination due to chance alignment with a background galaxy.

140533.11+165049.2: The 2.8σ excess exhibited by J1405 is not consistent with the emission from a dusty disk.

142152.21+093005.4: The 9.2σ excess found at J1412 is undoubtedly entirely due to the contamination from a nearby bright star.

154832.76-001717.9: J1548, while exhibiting a 4.7σ excess, has a blending source visible in both IRAC bands. PSF-subtraction of this blend leaves a 4σ excess in IRAC Ch 1 and a 2.1σ excess in Ch 2. The IRAC Ch 2 centroid is shifted by $1''$ to the west compared to the SDSS i-band centroid so perhaps an unresolved background source is responsible for the measured excess. Nonetheless, we fit the PSF-subtracted SED with a debris disk extending from 1800-1200 K and inclined

to 80°, however this would fall under the new class of faint debris disks put forth by Bergfors et al. 2014.

155031.68+353824.5: J1550 exhibits IRAC Ch 2 emission 2.2σ in excess of what is expected for a naked WD and was not followed-up in the NIR for this work. The SDSS and IRAC Ch 2 images show no obvious blends, so this is an interesting target for NIR follow-up that could reveal a faint disk.

161218.08+083028.2: This object has a subtle excess in both the IRAC 1 (1.2σ) and IRAC 2 (2.4σ), however, both IRAC images are severely blended by multiple objects so we attribute this excess emission to inextricably polluted photometry.

164248.61+382411.2: This WD has a subtle excess in both the IRAC 1 (1.6σ) and IRAC 2 (2.3σ). The images are unblended and the excess can be reproduced with the inclusion of the emission from an inclined, thin ring of dust (T_{in}=1300 K, T_{out}=1200 K, Incl.=80°). Perhaps this is a faint disk detection along with J1548, but the subtlety of the excess prevents us from claiming it as a bonafide dusty WD.

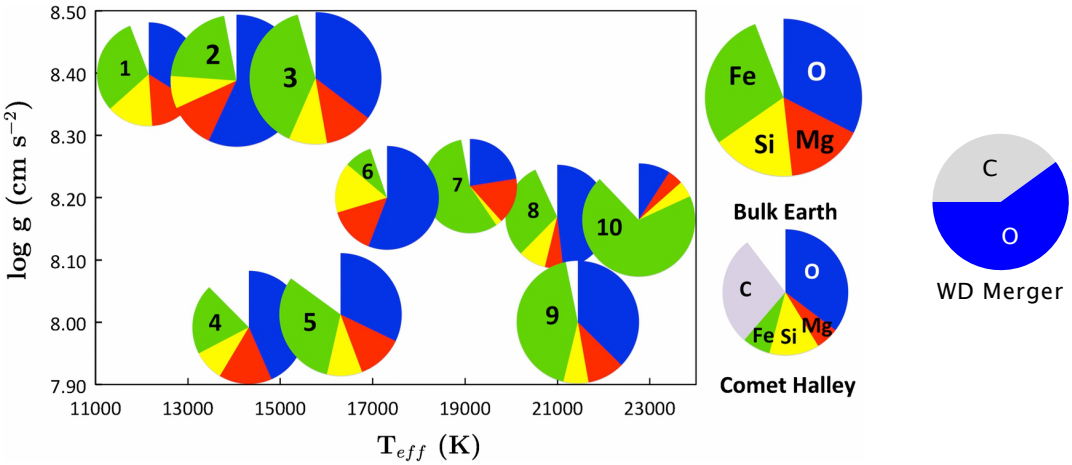
4.5 Merger Remnants

To explore planet formation around massive stars we need to go a step further than assembling a collection of massive WDs exhibiting excess IR emission consistent

with a dust disk. We need to verify that the composition of such a disk resembles bulk Earth. In the case of massive WDs, a second origin for circumstellar dust exists and must be eliminated from consideration. The merger of two WDs can result in the formation of a disk via conservation of angular momentum. Further, this disk can produce planets in an environment vastly different from that of a first generation proto-planetary disk (Livio et al. 2005). These planets form a reservoir of raw material for a second generation dusty debris disk around a massive WD merger remnant.

The compositions of these two flavors of massive WD dust disks should differ and high-resolution spectroscopy in the ultraviolet and optical can discern between them. Normal dusty WDs exhibit abundances dominated by refractory elements and depleted in carbon relative to solar levels (Zuckerman et al. 2007; Klein et al. 2010; Dufour et al. 2010; Xu et al. 2014; Jura & Young 2014). Conversely, the high-resolution smoothed particle hydrodynamics simulations of WD+WD mergers (Lorén-Aguilar et al. 2009) predict that the disk resulting from the merger will be depleted of refractory elements and dominated by carbon and oxygen (Figure 4.8). Additionally, the radial extent of these WD+WD merger disks resemble that of normal WD dust disks, eliminating the spectral energy distribution as a possible method of identifying the disk origin. Thus, abundance measurements of massive dusty WDs are critical for assigning broader implications for the frequency of disks,

and ultimately planets, in this mass regime. To date, no WD+WD merger disks have been observed, so if this is shown to be the origin of the disks put forth in this Chapter, these discoveries would be breaking new ground.



(a) (b)

Figure 4.8: (a) All polluted WDs with O, Mg, Si, and Fe measurements resemble composition of bulk Earth (Xu et al. 2014). (b) Predicted chemical composition of the disk formed following a WD+WD merger (Lorén-Aguilar et al. 2009).

4.6 Conclusions

We examine 100 massive (>0.8 $M_{\odot}$) WDs with 9500 <T_{eff} <22,500 K for dust and find three disks. We expect 8 spurious signifiant excesses due to chance alignment with background galaxies, and find ten WDs with significant infrared excesses. We rule out contamination due to chance alignment with a background galaxy for the three new dusty WDs by comparing the optical and infrared centroids of these WDs. The proper motion corrected centroid shifts we measure at these three WDs

is smaller than or consistent with the IRAC pointing accuracy. All three new disks have nearby point sources in their IRAC images, but these are successfully removed and a significant excess persists. These three new disks are the first known massive DA WDs with circumstellar dust. They increase the population of massive dusty WDs from two to five and constrain the occurrence rate of planet formation at 3.7-6.7 $M_{\odot}$ stars to be at least 3%.

4.7 Acknowledgements

This research has made use of the Exoplanet Orbit Database and the Exoplanet Data Explorer at `exoplanets.org`.

Observations reported here were obtained at the MMT Observatory, a joint facility of the Smithsonian Institution and the University of Arizona.

Based on program GN-2014B-Q-57 observations obtained at the Gemini Observatory, which is operated by the Association of Universities for Research in Astronomy, Inc., under a cooperative agreement with the NSF on behalf of the Gemini partnership: the National Science Foundation (United States), the National Research Council (Canada), CONICYT (Chile), the Australian Research Council (Australia), Ministério da Ciência, Tecnologia e Inovação (Brazil) and Ministerio de Ciencia, Tecnología e Innovación Productiva (Argentina).

This work is based, in part, on observations made with the *Spitzer Space Tele-*

scope, which is operated by the Jet Propulsion Laboratory, California Institute of Technology under a contract with NASA.

We make use of the Bergeron WD cooling model grids (Holberg & Bergeron, 2006; Kowalski & Saumon, 2006; Tremblay et al., 2011) to calculate our debris disk models.

Chapter 5

Dusty WDs in the McCook & Sion Catalog

"The seeker after truth should be humbler than the dust."

– Mahatma Gandhi, *The Story of My Experiments With Truth*

5.1 The McCook & Sion White Dwarf Catalog

We've discovered that when searching for debris disks around WDs in the 17-18 magnitude regime, we assume a significant risk of confusion with background galaxies. With this lesson in mind, let's look at a sample of bright (15-17 magnitude) WDs, where the risk of galaxy contamination is negligible. Gianninas et al. 2011 conducted a spectroscopic survey of ≈1300 bright, hydrogen-atmosphere WDs from the 1999 incarnation of the McCook & Sion WD Catalog (McCook & Sion, 1999). The digital McCook & Sion WD Catalog is the seminal catalog of spectroscopically confirmed WDs available to researchers today. At the time of this writing, accurate coordinates, spectral classes, photometry, proper motions, and finding charts for nearly 14,300 WDs are compiled here.

5.2 Cross-Correlation

We complement the broad-band UBV and Strömgren *uby* photometry presented in the McCook & Sion Catalog with a cross-correlation between several sources of archival data:

(1) Far- and near-UV photometry from the NASA Galaxy Evolution Explorer (GALEX) General Release 7

(2) *ugriz* photometry from the Sloan Digital Sky Survey (SDSS; Ahn et al. 2014) Data Release 10

(3) JHK photometry from the Two Micron All Sky Survey (2MASS; Skrutskie et al. 2006)

(4) $YJHK$ photometry from the UKIRT Infrared Deep Sky Survey (UKIDSS; Warren et al. 2007) Data Release 8

(5) 3.4 and 4.6 μm photometry from the Wide-field Infrared Survey Explorer (WISE; Wright et al. 2010) All-Sky Release

The results of our cross-correlation can be found in Table 5.1.

Table 5.1. Cross-Correlation Results

Survey	Detections
GALEX	1055
SDSS	708
2MASS	970
UKIDSS	166
WISE	1019

5.3 IRAC Photometry

Mid-infrared photometry, like the 3.4 and 4.6 μm photometry available from *WISE*, is necessary to detect emission from a debris disk orbiting a WD. *WISE*, however, has poor spatial resolution (6″ beam size) and is known to have a 75% false positive rate for detecting dusty disks around WDs (Barber et al., 2014). To mitigate this high rate of spurious detections, we compile higher spatial resolution archival data from the InfraRed Array Camera (IRAC; Fazio et al. 2004b) on the *Spitzer Space Telescope*. We query the *Spitzer* Heritage Archive for any observations within 10″ of the 1265 WDs from Gianninas et al. 2011 and find 907 Astronomical Observing Requests (AORs) for 381 WDs. Table 5.2 shows the number of detections we found in each IRAC band.

We use the `IRAF phot` and `IDL astrolib` packages to perform aperture photometry on the saturation corrected basic calibrated data (CBCD) frames. We

Table 5.2. IRAC Detections

Channel	Detections
1	304
2	377
3	156
4	228

use a 2 pixel aperture and all Ch 1 photometry is corrected for the pixel-phase-dependence. The IRAC photometry for all 381 WDs can be found in Appendix B.

A thorough analysis of all 1265 SEDs is beyond the scope of this work. Here, we focus only on those 381 WDs with *Spitzer* IRAC imaging as this data set is best suited for our goal, finding dusty debris disks. For those interested, spectral energy distributions (SEDs) using all available photometry of all 1265 WDs can be found in Appendix D. The parameter space spanned by our sample is presented in the histograms in Figure 5.1, where the dark histogram represents the WDs we find to host dust.

5.4 Disk Fitting

We start by computing a synthetic spectrum for each WD (Gianninas, priv. comm.) and scale it to the SDSS *griz* photometry. If no SDSS data is available, we use the

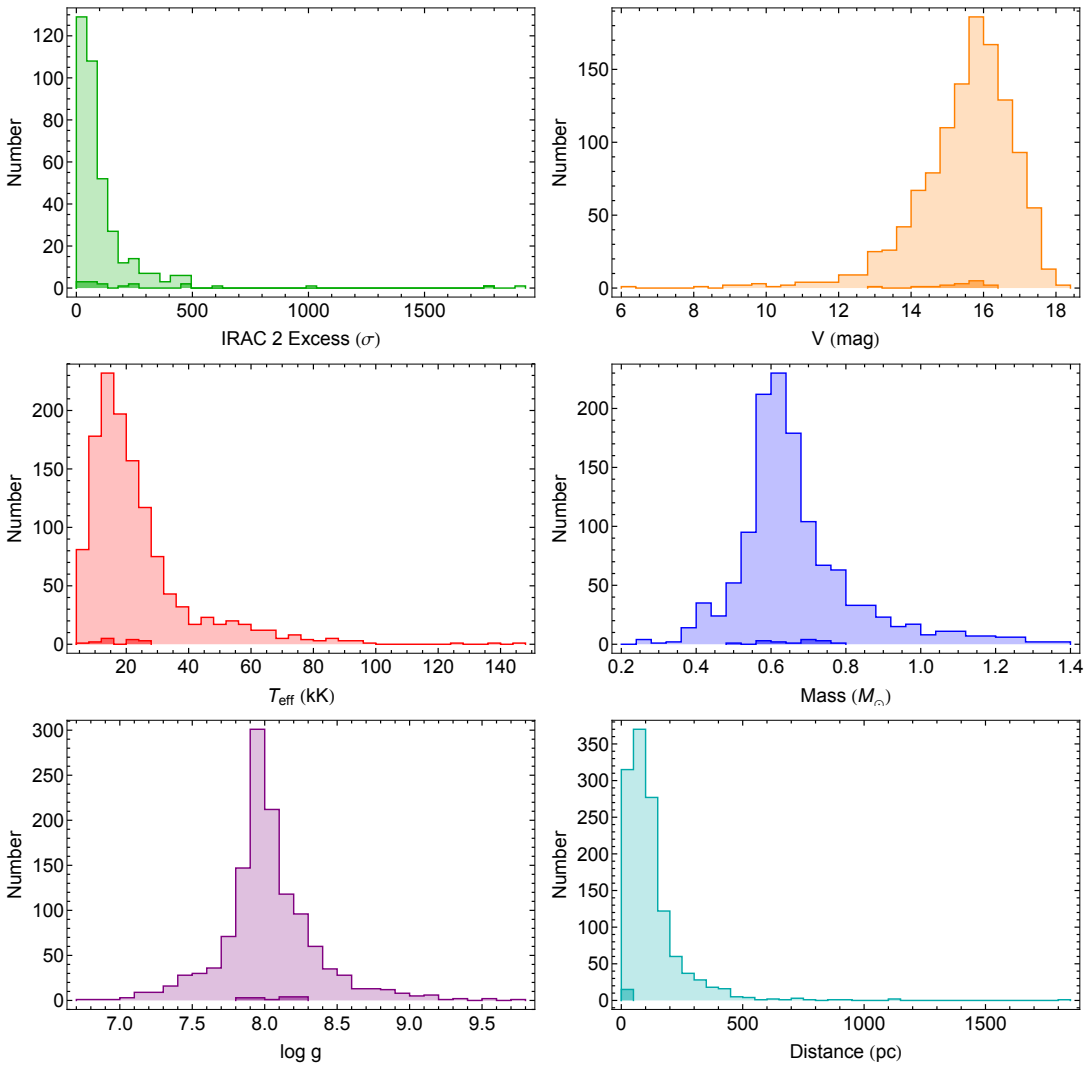


Figure 5.1: Histogram of IRAC 2 excess significance, V magnitude, effective temperature, mass, surface gravity, and distance for all 1265 WDs. The dark histogram indicates the parameter space occupied by the dusty WDs.

Table 5.3. Input Disk Parameter Grid

Disk Parameter		Value
Inner Temp.	Min.	800 K
	Max.	2100 K
	Step Size	100 K
Outer Temp.	Min.	100 K
	Max.	1200 K
	Step Size	100 K
Inclination	Min.	0°
	Max.	90°
	Step Size	10°

Strömgren y-band or broad-band V-band magnitude, where Strömgren photometry is prioritized over broad-band photometry. In the case where more than one epoch of data is available, we plot all epochs rather than a weighted mean. Once the spectrum is scaled to the optical photometry, we measure any excess emission in the 2MASS, UKIDSS, WISE, and IRAC data. We then use a chi-squared minimization between the measured excess and a selection of dusty disk models with the parameter set displayed in Table 5.3.

We use 2MASS JHK and/or UKIDSS JHK photometry to constrain the inner radius of the disk. In all cases, the measured IRAC photometry is used. If PSF-fitting is required to remove a blend from the IRAC data, the photometry from the PSF-subtracted image is used. Any available *WISE* data is not used in the fit

but is still plotted.

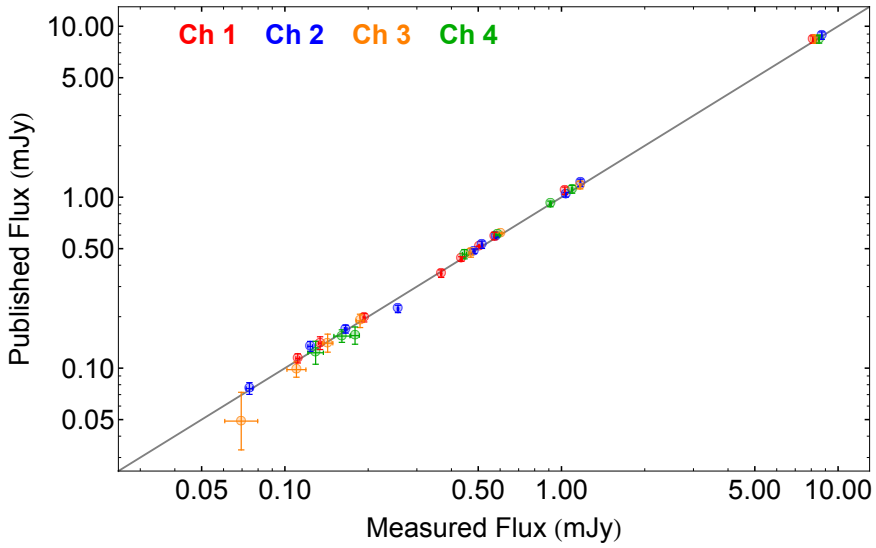
5.5 Results

5.5.1 Known Disks

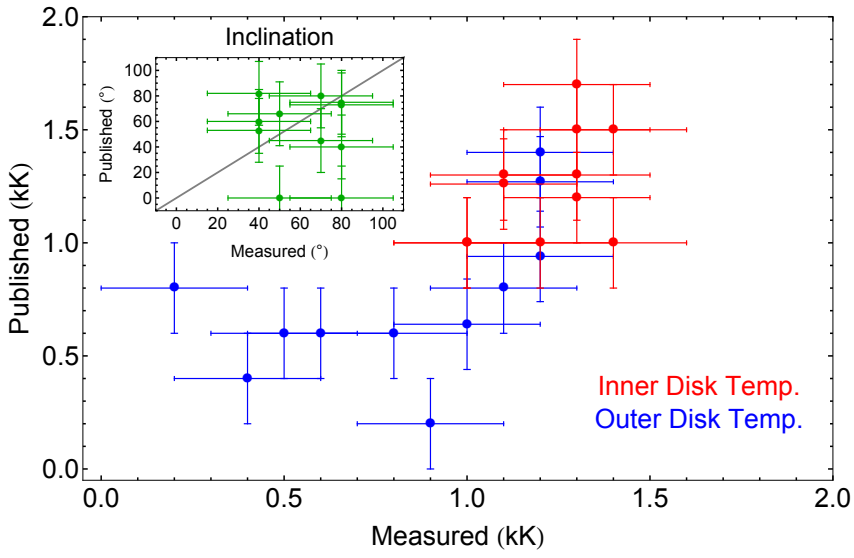
We find 15 WDs with circumstellar dust, 12 of which have been previously published. The color-color diagram in Figure 5.3 shows that the dusty WDs in our sample have a relatively flat J−H color and positive H−W2 color. To display the robustness of our IRAC photometry and disk models, we check our IRAC photometry against the published photometry for the 12 previously known dusty WDs in Figure 5.2a. Our measurements agree with published values in all cases. We also compare our best-fit disk parameters with published values in Figure 5.2b and find general agreement. The previously known dusty WD SEDs are shown in Figure 5.4.

5.5.2 New Disks

Our search also returns three new dusty WDs, all with thin rings of circumstellar dust. The SED at WD 0010+280 matches that of a highly inclined disk, extending only 0.13 $R_{\odot}$ from the inner to outer radii. There are no nearby sources threatening to contaminate the photometry. Furthermore, the *Spitzer* and *WISE* photometry are consistent. We measure the centroid position of the WD in the 2MASS *J*-



(a)



(b)

Figure 5.2: (a) Comparison between published IRAC photometry vs. photometry we measure for the ten known dusty WDs in our sample with publicly available IRAC images in the *Spitzer* Heritage Archive. Our IRAC photometry agrees with published values. (b) Comparison of published disk parameters and our best-fit disk parameters. Error bars show 200 K errors for disk temperatures and 25° errors for inclination. Grey lines indicate a one-to-one relation.

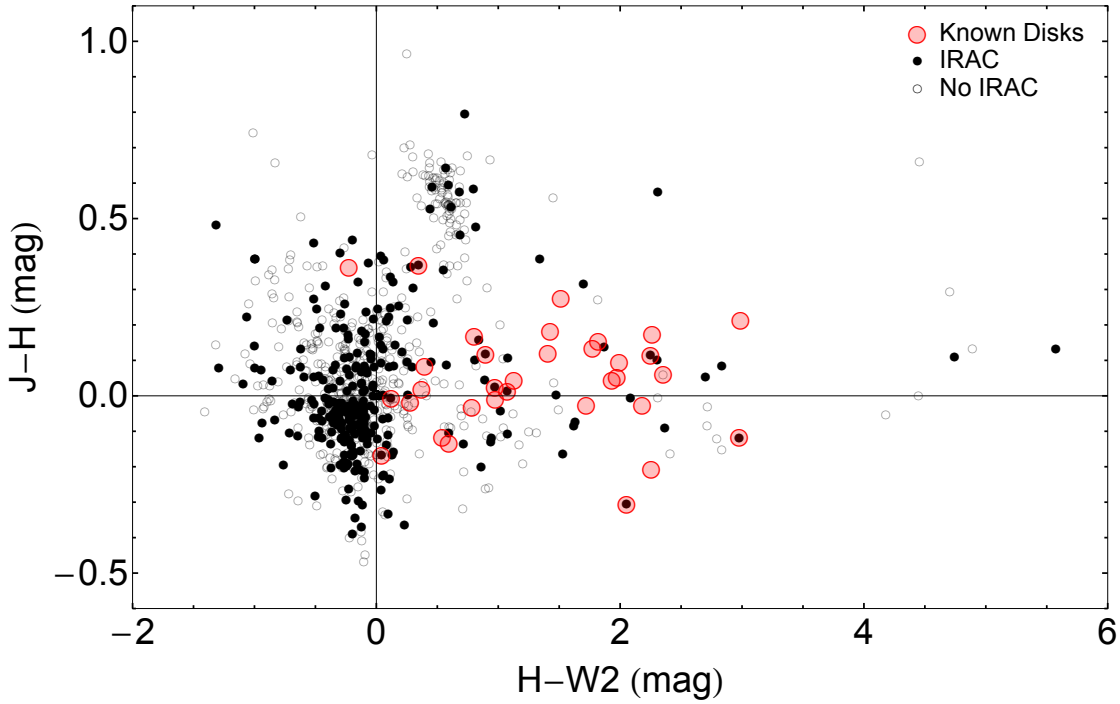


Figure 5.3: Infrared colors of our sample (black dots) compared with known dusty WDs (open red circles). WDs without IRAC data are shown as empty circles.

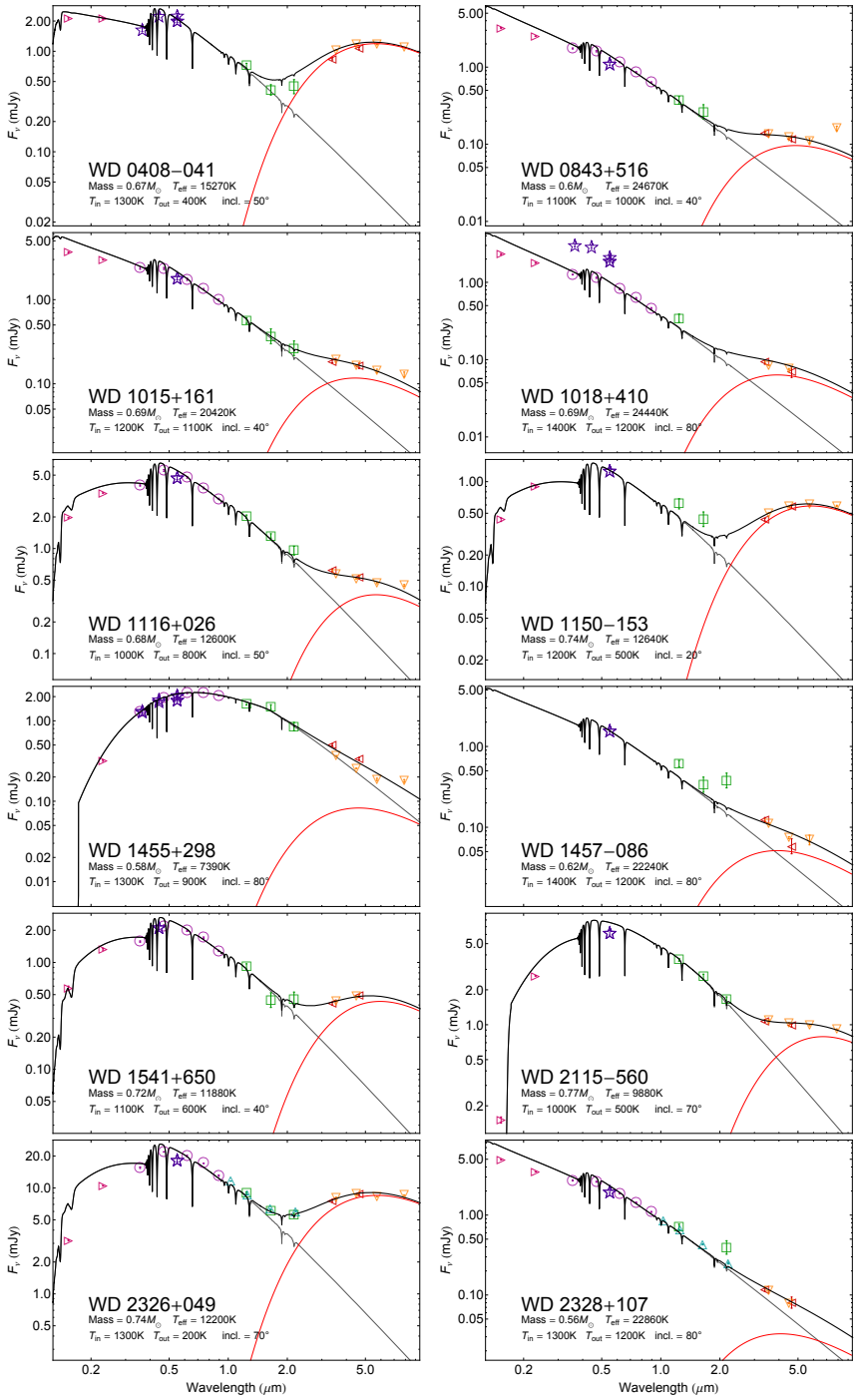


Figure 5.4: SEDs and our model WD+flat disks for the 12 previously known dusty WDs. All available photometry, including GALEX (right triangle), Johnson-Cousins (star), SDSS (circle), 2MASS (square), UKIDSS (up triangle), *WISE* (left triangle), and *Spitzer* (down triangle), is shown.

band image and compare it with the position of the WD in the IRAC Ch 2 image and find that they are separated by 0.2″. Furthermore, according to the galaxy counts from Fazio et al. 2004a, there is a 1.3% chance of an alignment within our 2.4 μm aperture with a background galaxy bright enough to create the measured excess. Thus, we eliminate background galaxy contamination from consideration. WD 0010+280 is by far the hottest dusty WD found to date, a full 200 Kelvin hotter than the 25,000 K WD 1537+515 (Barber et al., 2014). Therefore, with this discovery we greatly expand the parameter space occupied by dusty WDs.

We find that WD 0420+520 is surrounded by a thin, 0.05 $R_\odot$ wide, dusty disk. This object was first identified as a candidate WD+disk system using *WISE* by Hoard et al. 2013 and was recently found to have Ca absorption lines in its Keck+HIRES spectrum (Debes, priv. comm.). There is a blended source in the IRAC Ch 1 photometry, but is cleanly subtracted (Figure 5.5). We plot the photometry from the PSF-subtracted image in Figure 5.6 and use it to fit the debris disk. The excess observed at WD 0420+520 has a 0.4% chance of originating from a background galaxy. Further, we deem the 2MASS and IRAC centroids, separated by 0.47″, to be consistent.

The disk orbiting WD 0950-572 is the most narrow disk of the three, extending only 0.04 $R_\odot$. We examine the dependence of the WD centroid position on wavelength to see if a background galaxy might be the cause of the observed excess.

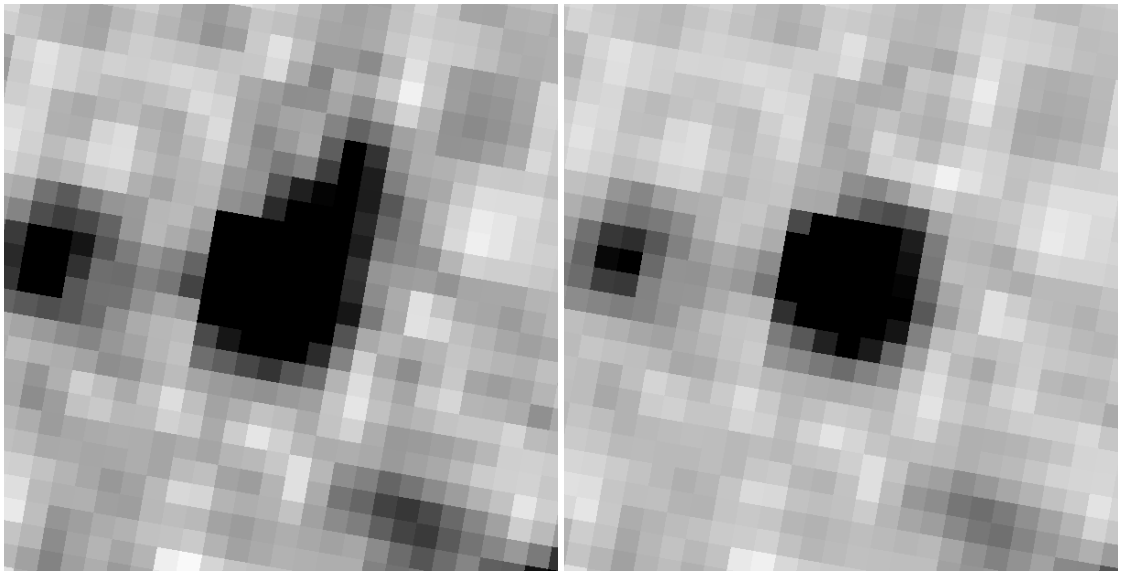


Figure 5.5: Original IRAC Ch 1 image (left) and PSF-subtracted image (right) for 0420+520. The blending source is successfully removed and the resultant photometry is virtually unchanged.

After correcting the 2MASS J-band centroid for proper motion, we find that it differs from the IRAC Ch 2 centroid position by $0.44''$. We also calculate that there is a 1.7% chance of an alignment with a galaxy of the brightness needed to create the excess. Thus, we conclude that WD 0950-572 is a bonafide dusty WD. All of the new best-fit disk parameters are listed in Table 5.5.2.

5.5.3 Centroid Positions

We plot the 2MASS-IRAC centroid separations for all 15 dusty WDs in our sample in Figure 5.7. The known dusty WDs appear as blue circles and the three new disks are red stars. We show the IRAC pointing accuracy as a green line and the mean separation for the known dusty WDs as a blue line, with a 1σ shaded area

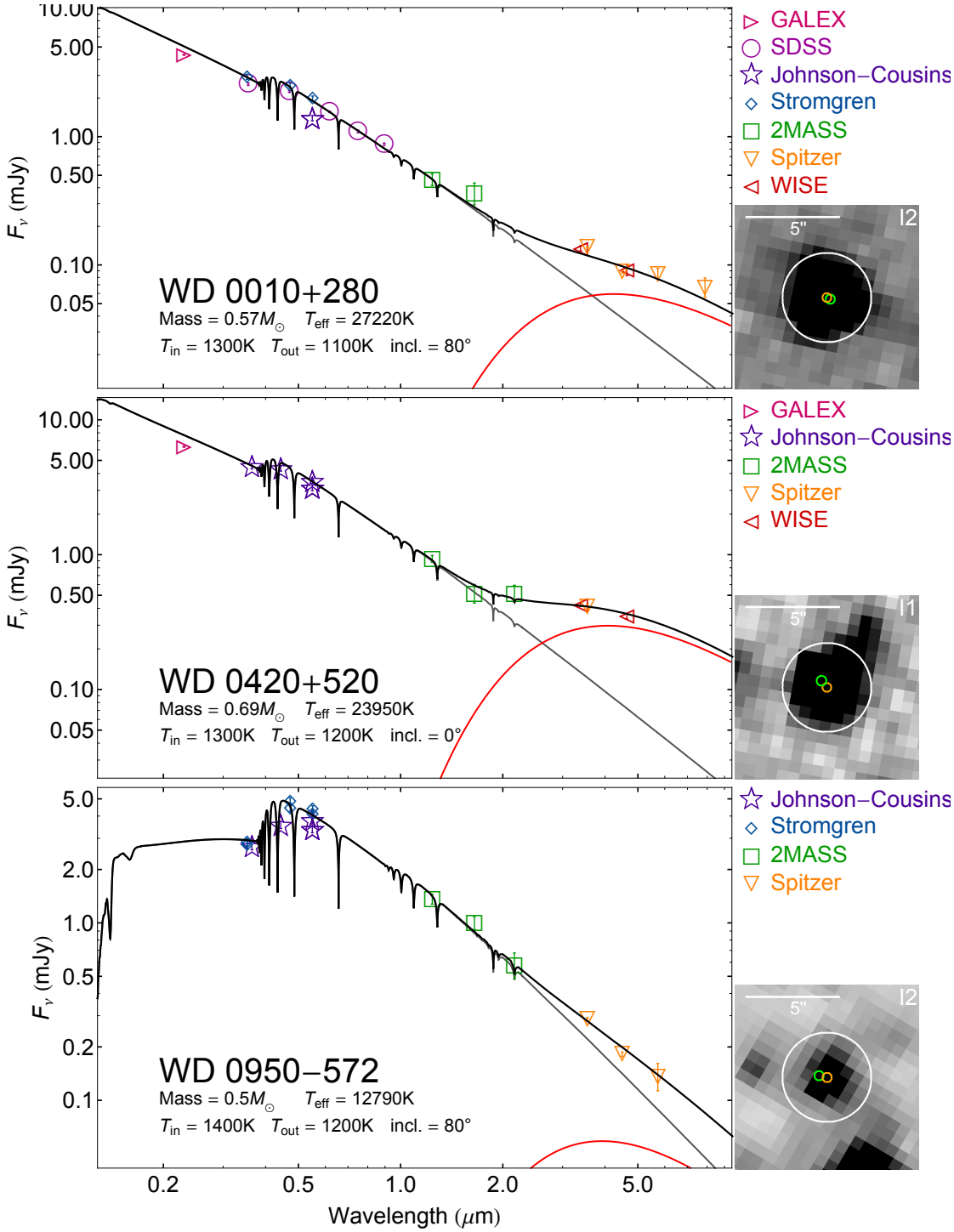


Figure 5.6: SED for three new dusty WDs. The blending source in the J0420 IRAC 1 image is removed before PSF photometry is performed.

Table 5.4. Best Fit Disk Parameters

WD	T_{in} (K)	T_{out} (K)	Incl. (°)	R_{in} ($R_\odot$)	R_{out} ($R_\odot$)
0010+280	1300	1100	80	0.52	0.65
0420+520	1300	1200	0	0.35	0.39
0950−572	1400	1200	80	0.17	0.21

Note. — Typical uncertainties for disk inner and outer temperatures are 200 K and 20-25° for inclination.

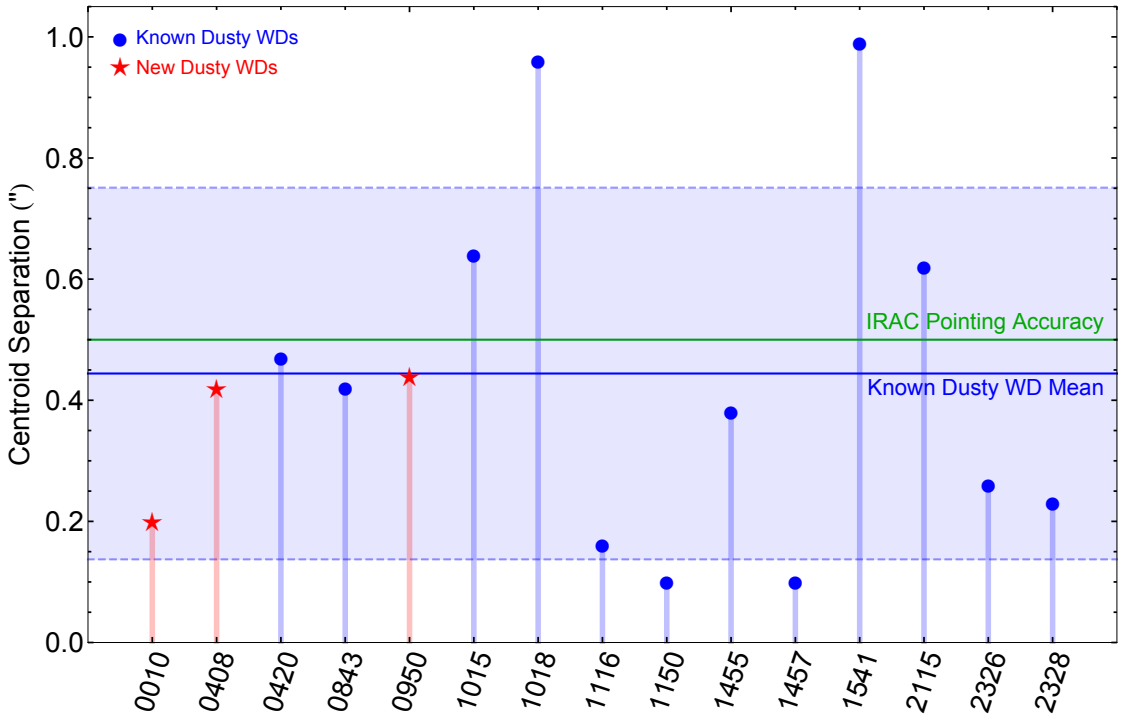


Figure 5.7: 2MASS vs IRAC centroid separations for each dusty WD corrected for proper motion. Centroids closer than 0.5″, the pointing accuracy of IRAC, are considered consistent.

on either side. It is clear that the 2MASS-IRAC separations found for the three new disk hosting WDs are consistent. The risk of contamination due to the chance alignment with a background galaxy is of little concern with a sample of bright WDs.

5.5.4 Frequency Dependence on WD Mass

We report an overall disk frequency of 3.9%, consistent with the 1-5% disk frequency of previous surveys. Out of 381 WDs with IRAC data, 69 are massive (>0.8 $M_{\odot}$). We find a signature for dust around none of these massive WDs. If we separate our IRAC sample into bins of 0.05 solar masses, the frequency of disks peaks at 12% for the 0.70-0.75 $M_{\odot}$ bin and drops off on either side (Figure 5.8a). To first order, this frequency-mass dependence of the disks occurrence rate resembles the dependence of giant planet formation on stellar mass put forth by Kennedy & Kenyon 2008 (Figure 5.8b), however larger sample sizes are required to reduce uncertainties. The number of WDs and disk detections in each bin and corresponding frequency with 1σ binomial confidence intervals can be found in Table 5.5. We find a 3.5% frequency of disks in the most massive bin (0.75-0.8 $M_{\odot}$) which is consistent with the 3% disk rate in our sample of massive WDs (0.8-1.12 $M_{\odot}$) observed with *Spitzer* (Chapter 4).

This large data set reveals three new debris disk, including the hottest WD

Table 5.5. Frequency-Mass Variation

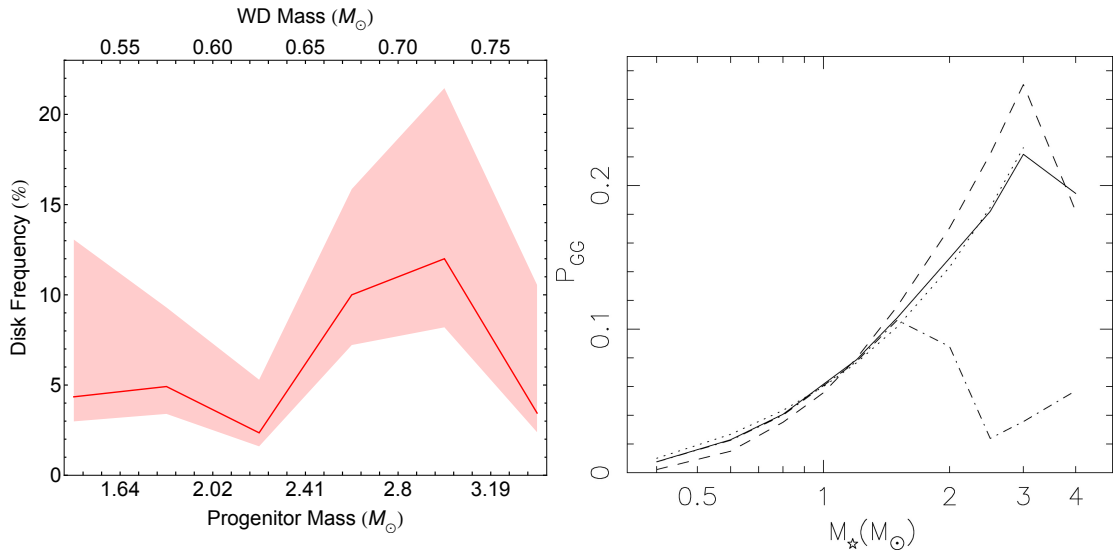
Mass Bin ($M_\odot$)	WDs	Disks	Frequency (%)	Lower Limit (%)	Upper Limit (%)
$0.50 \leq M < 0.55$	23	1	4.35	2.99	13.96
$0.55 \leq M < 0.60$	61	3	4.92	3.40	9.30
$0.60 \leq M < 0.65$	85	2	2.35	1.60	5.30
$0.65 \leq M < 0.70$	50	5	10.00	7.22	15.86
$0.70 \leq M < 0.75$	25	3	12.00	8.20	21.46
$0.75 \leq M < 0.80$	29	1	3.45	2.39	10.55

Note. — Frequency-mass bins with a 68% (1σ) binomial confidence interval.

known to host dust. We find that the frequency of debris disks at WDs varies with mass. It peaks at 12% for 0.7 $M_\odot$ WDs and falls off quickly for WDs more massive than this, which mirrors the planet formation models of Kennedy & Kenyon 2008 and the rate of disks for massive WDs presented in Chapter 4.

5.6 Conclusions

We present SEDs of 15 dusty WDs, 12 previously known and three new. Our measured IRAC photometry of the 12 previously known dusty WDs as well as our best-fit disk parameters agree with published values. All three new disks are narrow rings. We rule out contamination from chance alignment with background



(a) (b)

Figure 5.8: (a) Frequency of disks as a function of mass. The shaded region indicates the 1σ binomial confidence interval. (b) Probability of giant planet formation vs stellar mass (Kennedy & Kenyon, 2008).

galaxies by comparing the centroid position of each WD in their 2MASS J and IRAC Ch 2 images. The presence of a galaxy, in all cases save an exact alignment with the WD, will shift the IRAC Ch 2 centroid (where an excess is measured) relative to the 2MASS J band centroid (where there is no excess). Centroids for all three new WDs are separated by less than $0.5''$, the pointing accuracy of IRAC, and are thus considered consistent. We compare centroid separations for the new disks with the 12 previously known disks and find that the mean separation of these centroids is also less than the IRAC pointing accuracy.

We find a disk frequency of 3.9% for the subsample with *Spitzer* IRAC imaging, which is consistent with the 1-5% frequency found in previous surveys (Mullally

et al., 2007; Farihi et al., 2009; Debes et al., 2011b; Barber et al., 2012; Rocchetto et al., 2014). We also find that the frequency varies with WD mass. The frequency climbs slowly, peaks at 12% in the 0.70-0.75 $M_{\odot}$ mass bin and falls off steeply for WDs more massive. This dependence closely mirrors the predicted frequency of giant planet formation as a function of main-sequence mass put forth by Kennedy & Kenyon 2008. We find no dust around the massive WDs in our sample, however the disk frequency in our most massive bin (0.75-0.80 $M_{\odot}$) is 3.5%, consistent with the 3% disk frequency found in the massive WD sample from Chapter 4.

5.7 Acknowledgements

This research has made use of the NASA/IPAC Infrared Science Archive, which is operated by the Jet Propulsion Laboratory, California Institute of Technology, under contract with the National Aeronautics and Space Administration.

This publication makes use of data products from the Two Micron All Sky Survey, which is a joint project of the University of Massachusetts and the Infrared Processing and Analysis Center/California Institute of Technology, funded by the National Aeronautics and Space Administration and the National Science Foundation.

Based on observations made with the NASA Galaxy Evolution Explorer. GALEX is operated for NASA by the California Institute of Technology under NASA con-

tract NAS5-98034.

This project uses UKIDSS data. The UKIDSS project is defined in Lawrence et al. 2007. UKIDSS uses the UKIRT Wide Field Camera (WFCAM; Casali et al. 2007). The photometric system is described in Hewett et al. 2006, and the calibration is described in Hodgkin et al. 2009. The pipeline processing and science archive are described in Irwin et al (2009, in prep) and Hambly et al. 2008.

Funding for SDSS-III has been provided by the Alfred P. Sloan Foundation, the Participating Institutions, the National Science Foundation, and the U.S. Department of Energy Office of Science. The SDSS-III web site is http://www.sdss3.org/. SDSS-III is managed by the Astrophysical Research Consortium for the Participating Institutions of the SDSS-III Collaboration including the University of Arizona, the Brazilian Participation Group, Brookhaven National Laboratory, Carnegie Mellon University, University of Florida, the French Participation Group, the German Participation Group, Harvard University, the Instituto de Astrofisica de Canarias, the Michigan State/Notre Dame/JINA Participation Group, Johns Hopkins University, Lawrence Berkeley National Laboratory, Max Planck Institute for Astrophysics, Max Planck Institute for Extraterrestrial Physics, New Mexico State University, New York University, Ohio State University, Pennsylvania State University, University of Portsmouth, Princeton University, the Spanish Participation Group, University of Tokyo, University of Utah, Vanderbilt University, University

of Virginia, University of Washington, and Yale University.

This publication makes use of data products from the Wide-field Infrared Survey Explorer, which is a joint project of the University of California, Los Angeles, and the Jet Propulsion Laboratory/California Institute of Technology, and NEOWISE, which is a project of the Jet Propulsion Laboratory/California Institute of Technology. WISE and NEOWISE are funded by the National Aeronautics and Space Administration.

We make use of the Bergeron WD cooling model grids (Holberg & Bergeron, 2006; Kowalski & Saumon, 2006; Tremblay et al., 2011) to calculate our debris disk models.

Chapter 6

Conclusions

"Dust in the air suspended marks the place where a story ended."

– T. S. Eliot, *Little Gidding*

In this thesis we present four photometric/spectroscopic surveys in search of infrared excess emission at WDs. These surveys have allowed us to:

(1) Enrich the population of dusty WDs

(2) Explore the frequency of debris disks and how this frequency varies with WD mass

(3) Constrain the total mass accreted from these disks

(4) Expand the parameter space hospitable to dust around WDs

(5) Systematically probe the massive (>3.7 $M_{\odot}$) stellar regime for planets for the first time

We start with a study of the SEDs of a metallicity-unbiased sample of 117 DA WDs from the PG catalog. Five of our targets show excess radiation from debris disks, indicating a debris disk frequency of $4.3^{+2.7}_{-1.2}\%$. We interpret this frequency as a lower limit to the frequency of planets around the 1-7 $M_{\odot}$ progenitor MS

stars; an indirect result for the intermediate-mass regime in which conventional exoplanetary detection methods are insensitive. Alternatively, we interpret the observed frequency of disks as the fraction of time a WD accretes from its debris disks over the entire cooling age of the star. We estimate that typical WDs may accrete metals from several generations of disks for ∼10 Myr, corresponding to accretion of metals up to 10^{24} g. This means WDs are capable of accreting bodies as large as dwarf planets as well as Solar System asteroid analogues.

Next, we follow-up a cross-correlation between the SDSS DR7 White Dwarf Catalog with (*WISE*) performed by Debes et al. (2011b), which resulted in the discovery of 52 candidate dusty white dwarfs (WDs). We find that the 6″ *WISE* beam results in a 75% false-positive rate for debris disks at WDs. We present MMT+SWIRC *J*- and *H*-band imaging observations of 16 of these candidate dusty WDs and confirm that four have SEDs consistent with a dusty disk. We find the frequency of disks around single WDs in the *WISE* ∩ SDSS sample to be 2.6-4.1%. One of the four new dusty WDs is the most massive WD known to host dust, with a mass of 1.04 $M_{\odot}$ (progenitor mass 5.4 $M_{\odot}$). Its discovery offers the first confirmation that massive WDs (and their massive progenitor stars) host planetary systems.

The discovery of these four new debris disks further enriches the current dusty WD population with one of the coolest (J1507) and hottest (J1537) WDs known

to host circumstellar dust (Figure 6.1). Expanding the parameter space known to be hospitable to circumstellar dust at WD stars will not only guide future infrared excess searches, but also enhance our understanding of the formation and evolution of these remnant planetary systems.

To constrain the frequency of disks at massive WDs in particular, and the frequency of planets at their massive progenitors for the first time, we assemble a sample of the 100 brightest hydrogen-atmosphere (DA) WDs from the SDSS DR7 White Dwarf Catalog (Kleinman et al., 2013) with masses greater than 0.8 $M_{\odot}$ and temperatures between 9500 and 22,500 K. We find a 3% occurrence rate for disks among this sample, consistent with the frequency of disks orbiting normal WDs. We also discuss WD/WD mergers an alternative origin for dust at massive WDs.

Finally, we cross-correlate several sources of archival photometry with 1265 WDs from the McCook & Sion WD Catalog. While this work only focuses on 381 WDs with *Spitzer* data, the SEDs for all 1265 WDs are presented for use by the WD community. This large data set reveals three new debris disks, including the hottest WD known to host dust (WD0010+280). We find that the frequency of debris disks at WDs varies as a function of mass. It peaks at 12% for 0.7-0.75 $M_{\odot}$ WDs and falls off quickly for WDs more massive than this, which mirrors the planet formation models of Kennedy & Kenyon 2008 and the rate of disks for

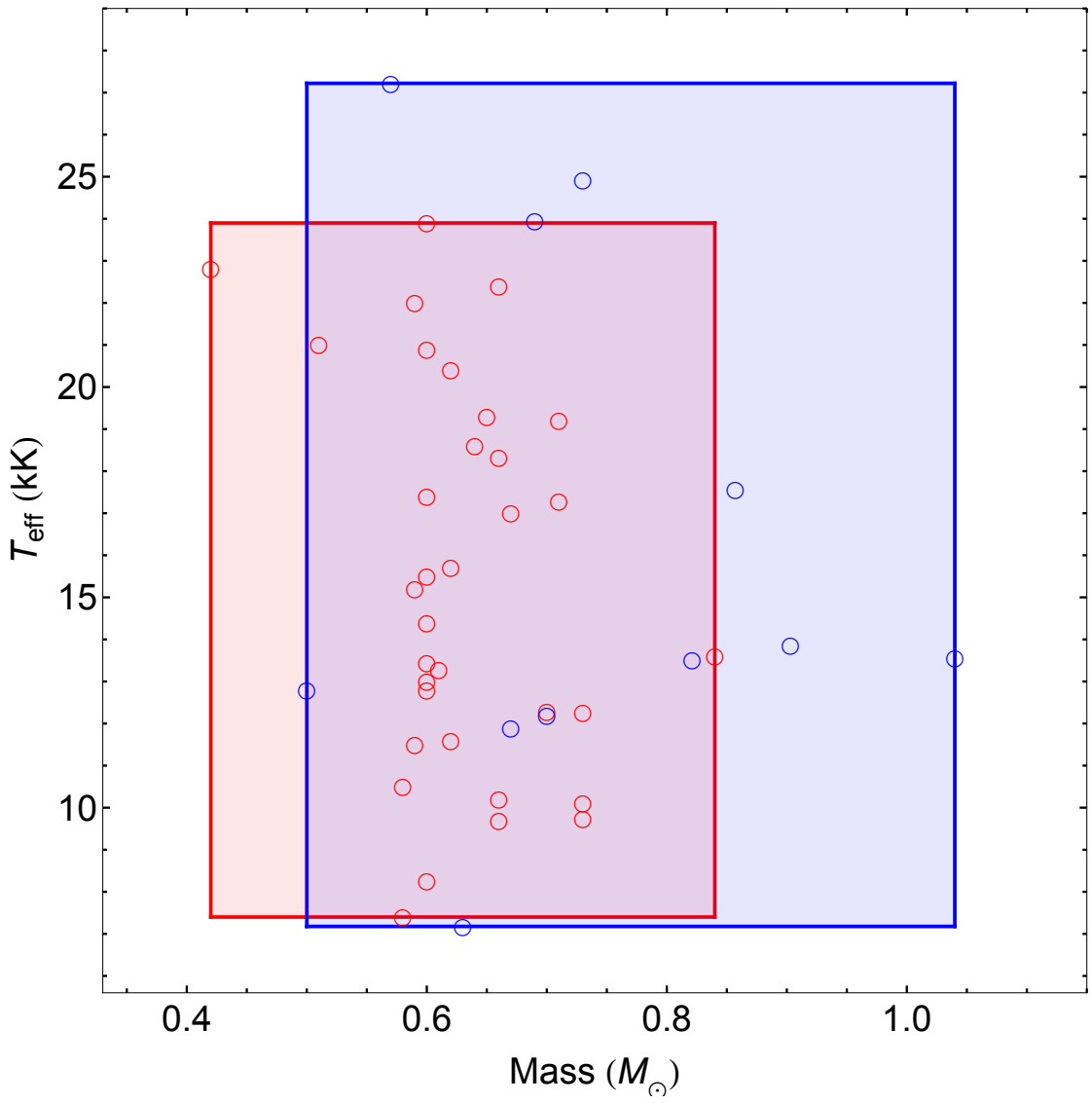


Figure 6.1: We've expanded the temperature and mass regime occupied by dusty debris disks.

massive WDs presented in Chapter 4.

We present illustrations of all known dusty WDs based on published disk parameters in Figure 6.2. The 11 disks with names in blue indicate the debris disks which were discovered as a part of this thesis. This work expands the parameter space available to dust orbiting WDs with the discovery of four new massive dusty WDs (J0736, J0840, J1234, J1333), including the first three massive DA WDs found to host dust. We also expand the temperature regime hospitable for circumstellar dust at WDs with three hot WDs (WD0010+280, WD0420+520, WD1537+515) and one cool WD (WD1507+324). The disk parameters used to construct this figure come from the literature and are listed in Table 6.1.

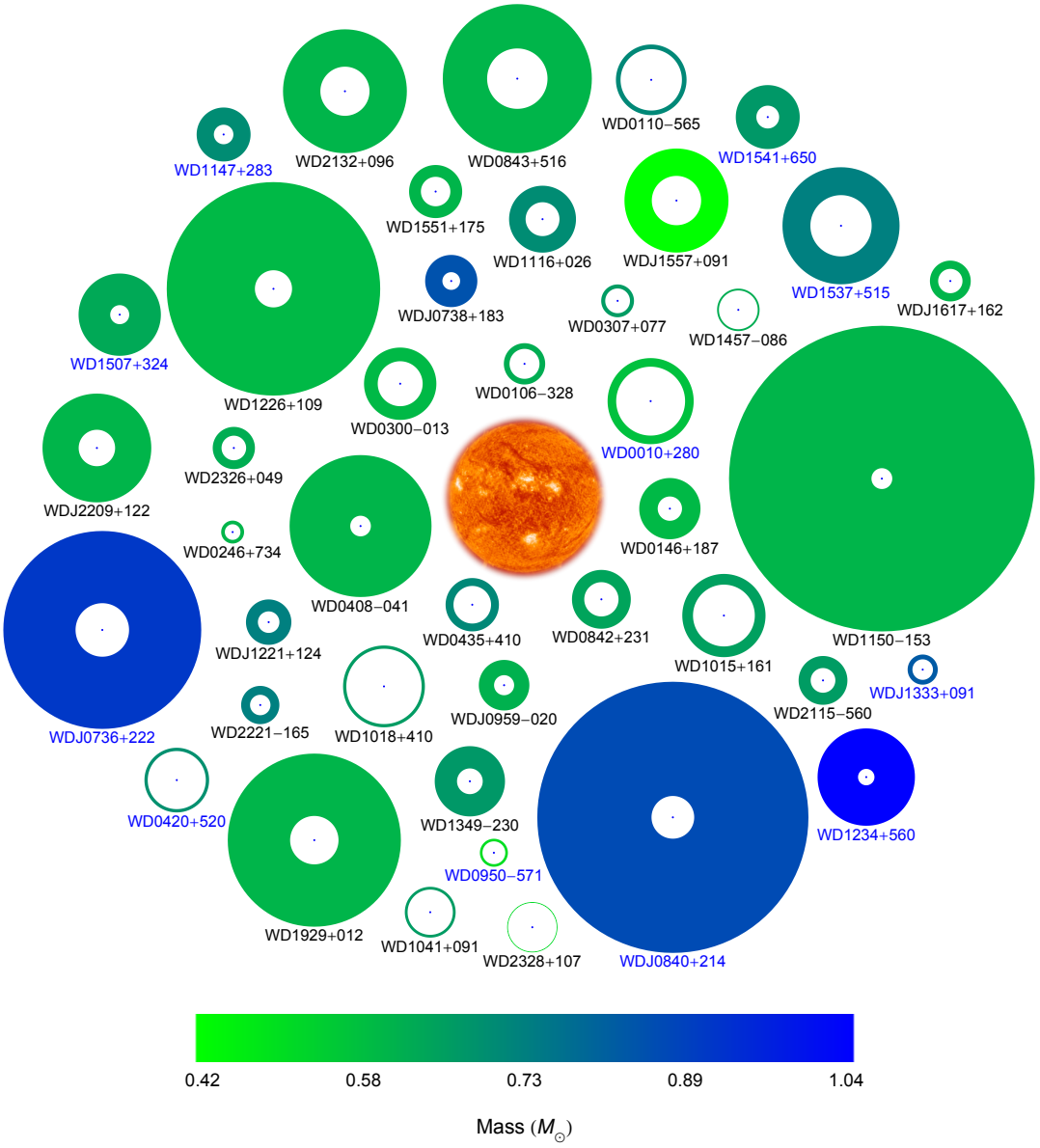


Figure 6.2: All 42 debris disks with published disk parameters. Debris disks are pictured to scale relative to the sun. The colors of the disks indicate the WD mass. Blue WD names indicate disks presented by this work. For WDs without published masses, we assume 0.6 $M_\odot$.

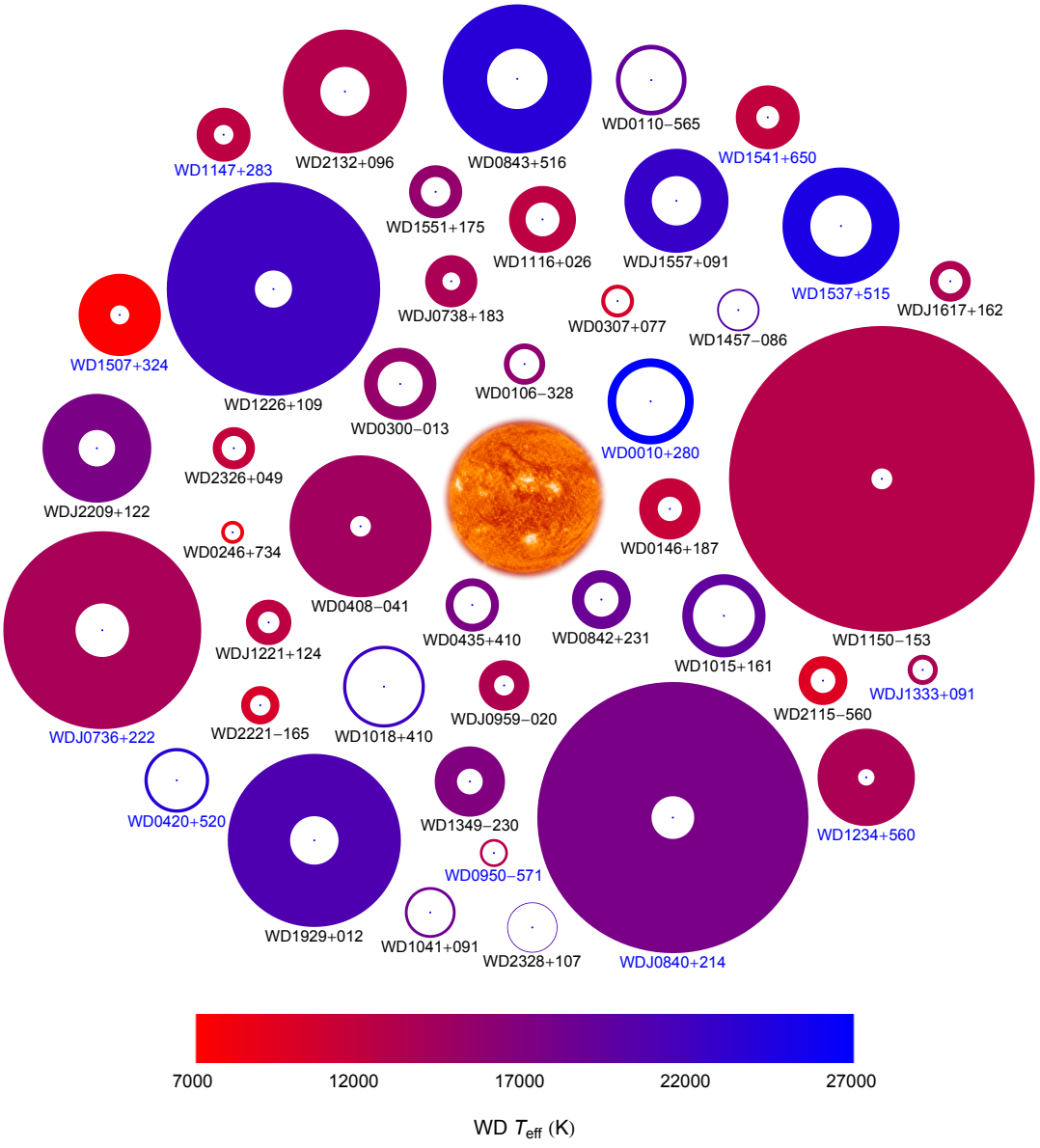


Figure 6.3: All 42 debris disks with published disk parameters. Debris disks pictured to scale relative to the sun. The colors of the disks indicate the WD effective temperature. Blue WD names indicate disks presented by this work.

Table 6.1. White Dwarfs with Debris Disks

WD	Other Name	Type	T_{eff} (K)	Mass ($M_\odot$)	T_{in} (K)	T_{out} (K)	Incl. (°)	Ref.
0010+280	PG	DA	27220	0.57	1300	1100	80	1
0106−328	HE 0106−3253	DAZ	15700	0.62	1400	1100	81	12
0110−565	HE 0110−5630	DBAZ	19200	0.71	1000	900	60	7
0146+187	GD 16	DABZ	11500	0.59	1200	600	48	15
0246+734	G245−58	DZ	8250	···	1200	900	80	5
0300−013	GD 40	DBZ	15200	0.59	1000	700	66	19
0307+077	HS 0307+0746	DAZ	10200	0.66	1050	850	66	12
0408−041	GD 56	DAZ	14400	0.60	1700	400	0	19
0420+520	KPD 0420+5203	DA	23950	0.69	1300	1200	0	1
0435+410	GD 61	DBAZ	17280	0.71	1300	1000	79	10
J0736+2229	SDSS J073612.36+222937.2	DA	13858	0.90	800	300	70	1
J0738+1835	SDSS J073842.56+183509.6	DBZ	13600	0.84	1800	800	58	13
0837+218	SDSS J084031.46+214042.7	DA	17549	0.86	1200	300	30	1
0842+231	Ton 345	DBZ	18600	0.70	1500	1000	66	14
0843+516	PG; SDSS J084702.28+512853.4	DA	23900	···	1260	640	82	6
0950−572	BPM 19738	DA	12790	0.50	1400	1200	80	1
J0959−0200	SDSS J095904.69−020047.6	DAZ	13280	0.64	1600	800	0	8
1015+161	PG	DAZ	19300	0.61	1000	800	53	19
1018+410	PG; SDSS J102155.50+405014.8	DA	22390	0.65	1000	940	40	4
1041+091	SDSS J104341.53+085558.2	DAZ	18330	0.66	1200	1100	60	14
1116+026	GD 133	DAZ	12200	0.66	1000	600	66	19
1147+283	WD 1145+288	DA	12290	0.70	1500	700	60	3

Table 6.1 (cont'd)

WD	Other Name	Type	T_{eff} (K)	Mass ($M_\odot$)	T_{in} (K)	T_{out} (K)	Incl. (°)	Ref.
1150−153	EC11507−1519	DAVZ	12800	0.60	1500	200	0	16
J1221+1245	SDSS J122150.81+124513.3	DAZ	12250	0.73	1400	800	46	8
1225079*	PG	DZAB	10500	0.58	···	···	···	12
1226+109	SDSS J122859.92+104033.0	DAZ	22000	0.59	1670	450	70	17
J1234+5606	SDSS J123432.62+560643.0	DB_{DB}	13567	1.04	1900	500	70	3
J1333+0917	SDSS J133336.04+091704.9	DA	13508	0.82	1600	1200	0	1
1349−230	HE 1349−2305	DBAZ	17000	0.67	1700	800	85	7
1455+298	G166−58	DAZ	7400	0.58	400	···	···	18
1457−086	PG	DAZ	20400	0.62	1500	1400	73	15
J1507+3245	SDSS J150701.98+324545.1	DA	7177	0.63	900	300	0	3
1537+515	WD 1536+520	DBA	24926	0.73	1300	800	30	3
1541+650	KX Dra	DAV	11880	0.67	1300	600	60	2
1551+175	KUV 15519+1730	DBAZ	15500	···	1400	900	85	5
J1557+0916	SDSS J155720.77+091624.7	DAZ	22810	0.42	1400	800	60	8
J1617+1620	SDSS J161717.04+162022.3	WD	13432	···	1400	950	50	9
1729+371	GD 362	DAZ	9740	0.73	1000	···	···	20
1929+012	GALEX J193156.8+011745	DAZ	20890	···	1300	500	70	11
2115−560	LTT 8452	DAZ	9700	0.66	1000	600	80	21
2132+096	HS 2132+0941	DAZ	13000	···	800	400	85	5
J2209+1223	SDSS J220934.84+122336.5	DBZ	17300	···	1340	590	57	6
2221−165	HE 2221−1630	DAZ	10100	0.73	1200	750	60	12
2326+049	G29−38	DAZ	11600	0.62	1200	800	45	21

Table 6.1 (cont'd)

WD	Other Name	Type	T_{eff} (K)	Mass ($M_\odot$)	T_{in} (K)	T_{out} (K)	Incl. (°)	Ref.
2328+107	PG; SDSS J233041.62+110206.0	DA	21000	0.51	1300	1270	75	4

References. — (1) This work. (2) Kilic et al. 2012 ; (3) Barber et al. 2014 ; (4) Rocchetto et al. 2014 ; (5) Bergfors et al. 2014 ; (6) Xu & Jura 2012 ; (7) Girven et al. 2012 ; (8) Farihi et al. 2012 ; (9) Brinkworth et al. 2012 ; (10) Farihi et al. 2011 ; (11) Debes et al. 2011a ; (12) Farihi et al. 2010 ; (13) Dufour et al. 2010 ; (14) Melis et al. 2010 ; (15) Farihi et al. 2009 ; (16) Jura et al. 2009 ; (17) Brinkworth et al. 2009; (18) Farihi et al. 2008 ; (19) Jura et al. 2007a ; (20) Jura et al. 2007b ; (21) von Hippel et al. 2007

Bibliography

C. P. Ahn et al. 2014, ApJS, 211:17, 17

Y. Alibert, C. Mordasini, and W. Benz. 2011, A&A, 526:A63, A63

S. D. Barber et al. 2014, ApJ, 786:77, 77

—. 2012, ApJ, 760:26, 26

E. E. Becklin et al. 2005, ApJ, 632:L119–L122, L119

P. Bergeron et al. 2011, ApJ, 737:28, 28

C. Bergfors et al. 2014, MNRAS, 444:2147–2156, 2147

J. S. Bloom et al. 2006, in ASP Conference Series, Vol. 351, 751

A. Bonsor and M. C. Wyatt. 2012, MNRAS, 420:2990–3002, 2990

B. P. Bowler et al. 2010, ApJ, 709:396–410, 396

C. S. Brinkworth et al. 2012, ApJ, 750:86, 86

—. 2009, ApJ, 696:1402–1406, 1402

W. R. Brown et al. 2008, in SPIE Conference Series, Vol. 7014, 2

A. J. Burgasser et al. 2003, ApJ, 586:512–526, 512

M. Burleigh, F. Clarke, and S. Hodgkin. 2003, in ASP Conference Series, Vol. 294, 111–116

M. R. Burleigh, F. J. Clarke, and S. T. Hodgkin. 2002, MNRAS, 331:L41–L45, L41

M. Casali et al. 2007, A&A, 467:777–784, 777

M. C. Cushing, W. D. Vacca, and J. T. Rayner. 2004, PASP, 116:362–376, 362

R. M. Cutri et al. 2003, 2MASS All Sky Catalog of point sources.

J. H. Debes et al. 2011a, ApJ, 729:4, 4

—. 2011b, ApJS, 197:38, 38

J. H. Debes and S. Sigurdsson. 2002, ApJ, 572:556–565, 556

J. H. Debes, K. J. Walsh, and C. Stark. 2012, ApJ, 747:148, 148

P. Dufour et al. 2010, ApJ, 719:803–809, 803

—. 2012, ApJ, 749:6, 6

X. Dumusque et al. 2012, Nature, 491:207–211, 207

J. Farihi, E. E. Becklin, and B. Zuckerman. 2005, ApJS, 161:394–428, 394

J. Farihi et al. 2011, ApJ, 728:L8, L8

—. 2012, MNRAS, 421:1635–1643, 1635

—. 2010, ApJ, 714:1386–1397, 1386

J. Farihi, M. Jura, and B. Zuckerman. 2009, ApJ, 694:805–819, 805

J. Farihi, B. Zuckerman, and E. E. Becklin. 2008, ApJ, 674:431–446, 431

G. G. Fazio et al. 2004a, ApJS, 154:39–43, 39

—. 2004b, ApJS, 154:10–17, 10

S. Friedrich et al. 2007, in ASP Conference Series, Vol. 372, 343

J. Frith et al. 2013, MNRAS, 435:2161–2170, 2161

A. Gianninas, P. Bergeron, and M. T. Ruiz. 2011, ApJ, 743:138, 138

J. Girven et al. 2012, ApJ, 749:154, 154

A. Gould and M. Kilic. 2008, ApJ, 673:L75–L78, L75

J. R. Graham et al. 1990, ApJ, 357:216–223, 216

R. F. Green, M. Schmidt, and J. Liebert. 1986, ApJS, 61:305–352, 305

N. C. Hambly et al. 2008, MNRAS, 384:637–662, 637

E. Han et al. 2014, PASP, 126:827–837, 827

B. M. S. Hansen, S. Kulkarni, and S. Wiktorowicz. 2006, AJ, 131:1106–1118, 1106

J. J. Hermes. 2013, in AAS Meeting Abstracts, Vol. 221, 424.04

P. C. Hewett et al. 2006, MNRAS, 367:454–468, 454

D. W. Hoard et al. 2013, ApJ, 770:21, 21

K. W. Hodapp et al. 2003, PASP, 115:1388–1406, 1388

S. T. Hodgkin et al. 2009, MNRAS, 394:675–692, 675

J. B. Holberg and P. Bergeron. 2006, AJ, 132:1221–1233, 1221

J. A. Johnson et al. 2010, PASP, 122:905–915, 905

M. Jura. 2003, ApJ, 584:L91–L94, L91

—. 2006, ApJ, 653:613–620, 613

—. 2008, AJ, 135:1785–1792, 1785

M. Jura, J. Farihi, and B. Zuckerman. 2007a, ApJ, 663:1285–1290, 1285

—. 2009, AJ, 137:3191–3197, 3191

M. Jura et al. 2007b, AJ, 133:1927–1933, 1927

M. Jura and S. Xu. 2012, AJ, 143:6, 6

M. Jura and E. D. Young. 2014, Annu. Rev. of Earth Planet. Sci., 42:45–67, 45

J. S. Kalirai et al. 2008, ApJ, 676:594–609, 594

G. M. Kennedy and S. J. Kenyon. 2008, ApJ, 673:502–512, 502

M. Kilic, W. R. Brown, and B. McLeod. 2010, ApJ, 708:411–418, 411

M. Kilic et al. 2008, AJ, 136:111–117, 111

M. Kilic, A. Gould, and D. Koester. 2009a, ApJ, 705:1219–1225, 1219

M. Kilic et al. 2009b, ApJ, 696:2094–2103, 2094

—. 2012, MNRAS, 419:L59–L63, L59

—. 2005, ApJ, 632:L115–L118, L115

—. 2006, ApJ, 646:474–479, 474

J. D. Kirkpatrick et al. 2011, ApJS, 197:19, 19

B. Klein et al. 2010, ApJ, 709:950–962, 950

S. J. Kleinman et al. 2013, ApJS, 204:5, 5

D. Koester, B. T. Gänsicke, and J. Farihi. 2014, A&A, 566:A34, A34

P. M. Kowalski and D. Saumon. 2006, ApJ, 651:L137–L140, L137

A. Lawrence et al. 2007, MNRAS, 379:1599–1617, 1599

S. K. Leggett et al. 2003, MNRAS, 345:144–152, 144

S. Lépine and E. Gaidos. 2011, AJ, 142:138, 138

J. Liebert, P. Bergeron, and J. B. Holberg. 2005, ApJS, 156:47–68, 47

M. Livio, J. E. Pringle, and K. Wood. 2005, ApJ, 632:L37–L39, L37

P. Lorén-Aguilar, J. Isern, and E. García-Berro. 2009, A&A, 500:1193–1205, 1193

J. W. Mason. 2008, Exoplanets, doi:10.1007/978-3-540-74008-7

G. P. McCook and E. M. Sion. 1999, ApJS, 121:1–130, 1

C. Melis et al. 2011, ApJ, 732:90, 90

—. 2010, ApJ, 722:1078–1091, 1078

B. D. Metzger, R. R. Rafikov, and K. V. Bochkarev. 2012, MNRAS, 423:505–528, 505

F. Mullally et al. 2007, ApJS, 171:206–218, 206

E. R. Newton et al. 2014, AJ, 147:20, 20

R. R. Rafikov. 2011a, ApJ, 732:L3, L3

—. 2011b, MNRAS, 416:L55–L59, L55

R. R. Rafikov and J. A. Garmilla. 2012, ApJ, 760:123, 123

J. T. Rayner et al. 2003, PASP, 115:362–382, 362

W. T. Reach et al. 2005a, ApJ, 635:L161–L164, L161

—. 2009, ApJ, 693:697–712, 697

—. 2005b, PASP, 117:978–990, 978

M. Rocchetto et al. 2014, ArXiv e-prints, arXiv:1410.6527

M. F. Skrutskie et al. 2006, AJ, 131:1163–1183, 1163

P. R. Steele et al. 2009, A&A, 500:1207–1210, 1207

P.-E. Tremblay and P. Bergeron. 2009, ApJ, 696:1755–1770, 1755

P.-E. Tremblay, P. Bergeron, and A. Gianninas. 2011, ApJ, 730:128, 128

P.-E. Tremblay et al. 2010, ApJ, 712:1345–1358, 1345

S. Vennes, A. Kawka, and P. Németh. 2010, MNRAS, 404:L40–L44, L40

D. Veras, S. A. Jacobson, and B. T. Gänsicke. 2014a, MNRAS, 445:2794–2799, 2794

D. Veras et al. 2014b, MNRAS, 445:2244–2255, 2244

—. 2013, MNRAS, 431:1686–1708, 1686

T. von Hippel et al. 2007, ApJ, 662:544–551, 544

Z. Wang, A. Tziamtzis, and X. Wang. 2014, ApJ, 782:20, 20

S. J. Warren et al. 2007, ArXiv Astrophysics e-prints, astro-ph/0703037

M. W. Werner et al. 2004, ApJS, 154:1–9, 1

A. A. West et al. 2011, AJ, 141:97, 97

K. A. Williams, M. Bolte, and D. Koester. 2009, ApJ, 693:355–369, 355

E. L. Wright et al. 2010, AJ, 140:1868–1881, 1868

S. Xu and M. Jura. 2012, ApJ, 745:88, 88

S. Xu et al. 2014, ApJ, 783:79, 79

B. Zuckerman and E. E. Becklin. 1987, Nature, 330:138–140, 138

—. 1992, ApJ, 386:260–264, 260

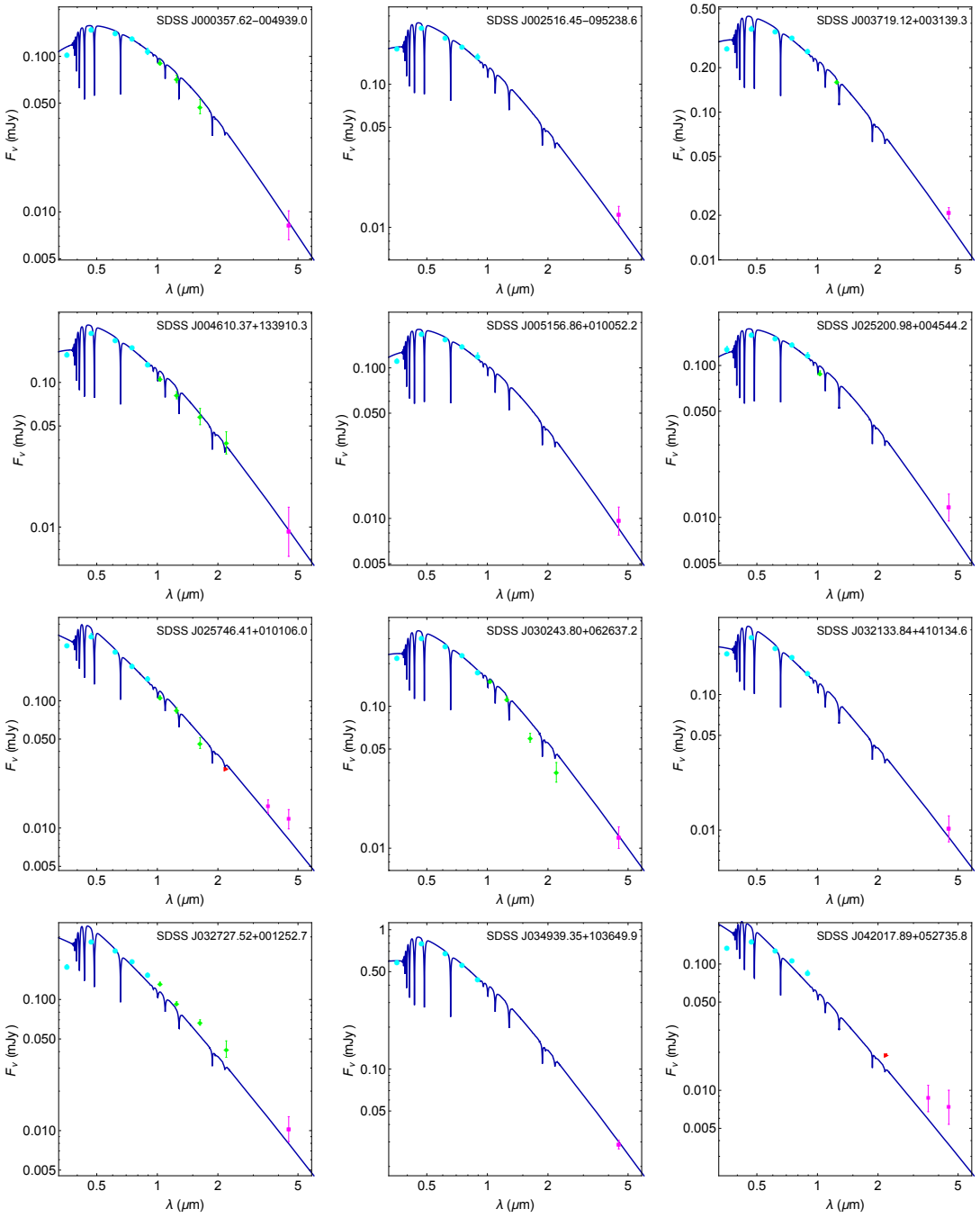
B. Zuckerman et al. 2007, ApJ, 671:872–877, 872

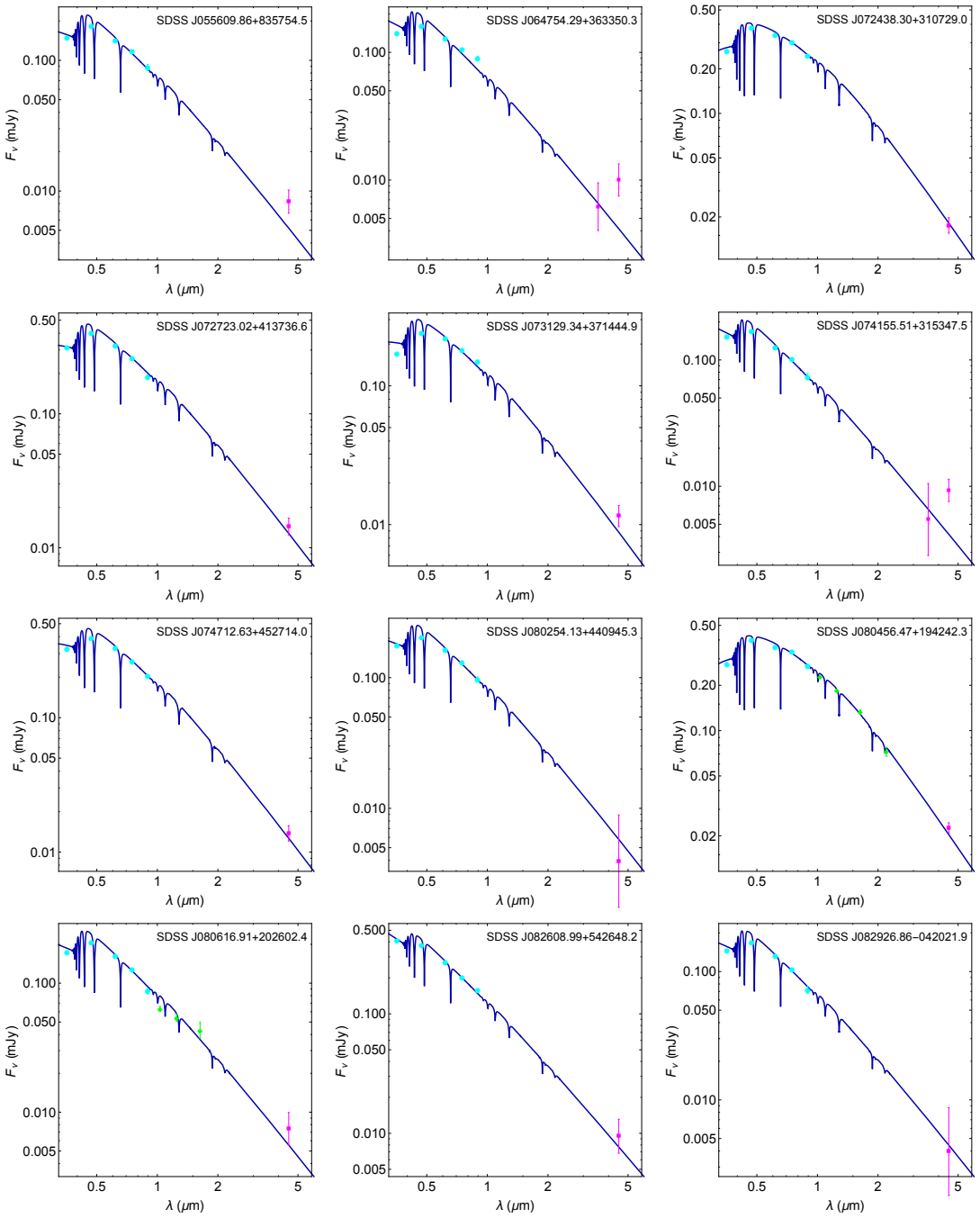
—. 2003, ApJ, 596:477–495, 477

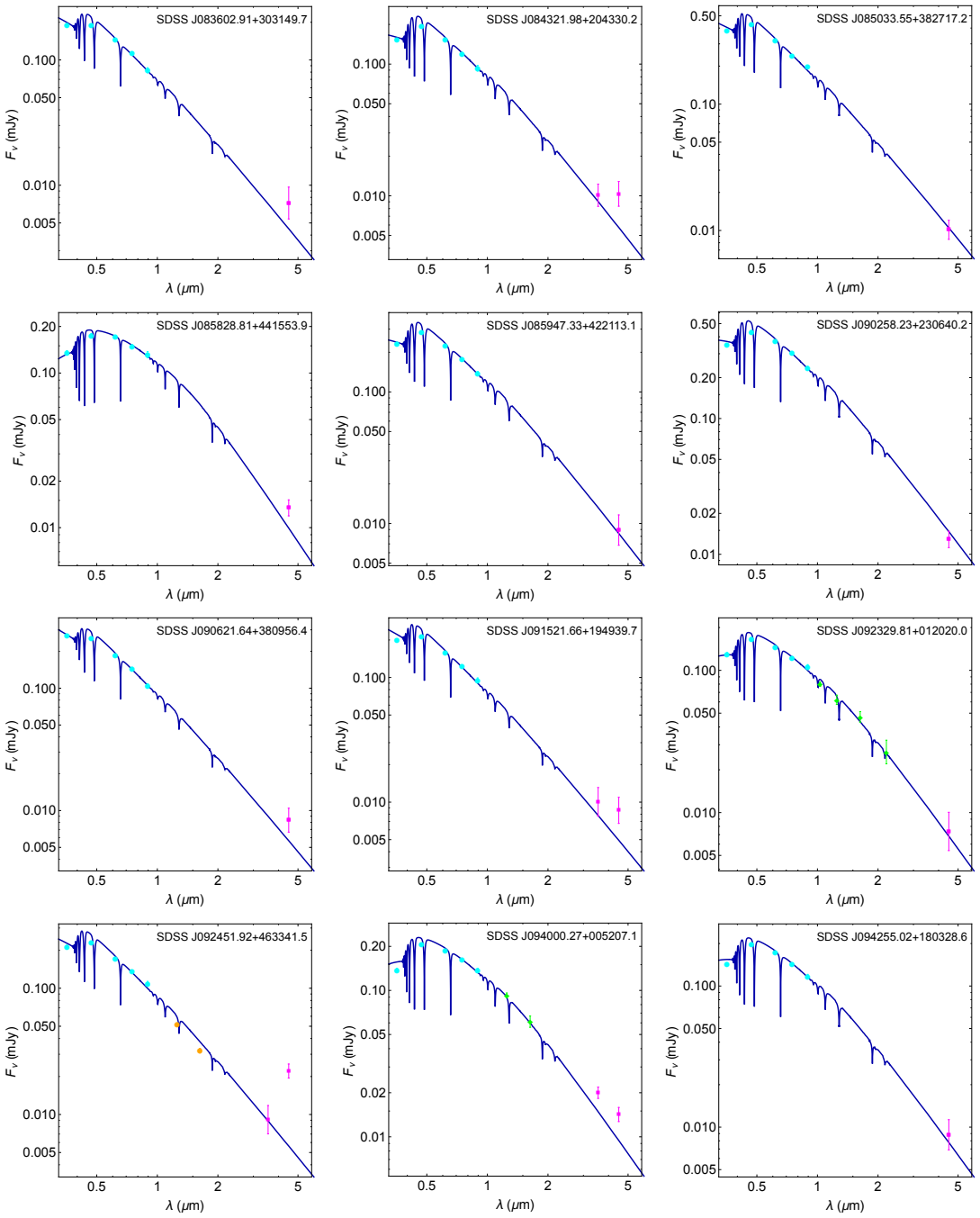
—. 2010, ApJ, 722:725–736, 725

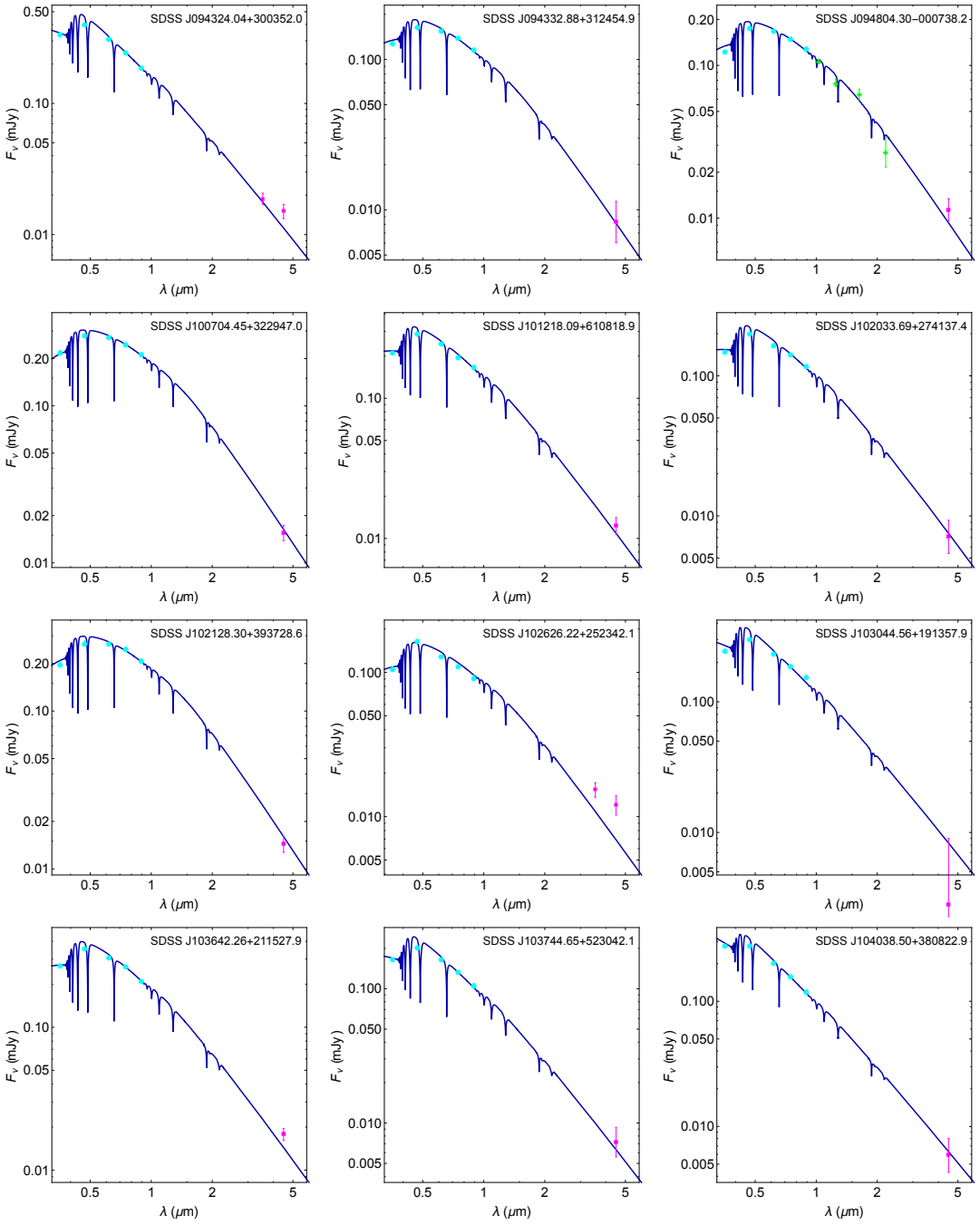
Appendix A

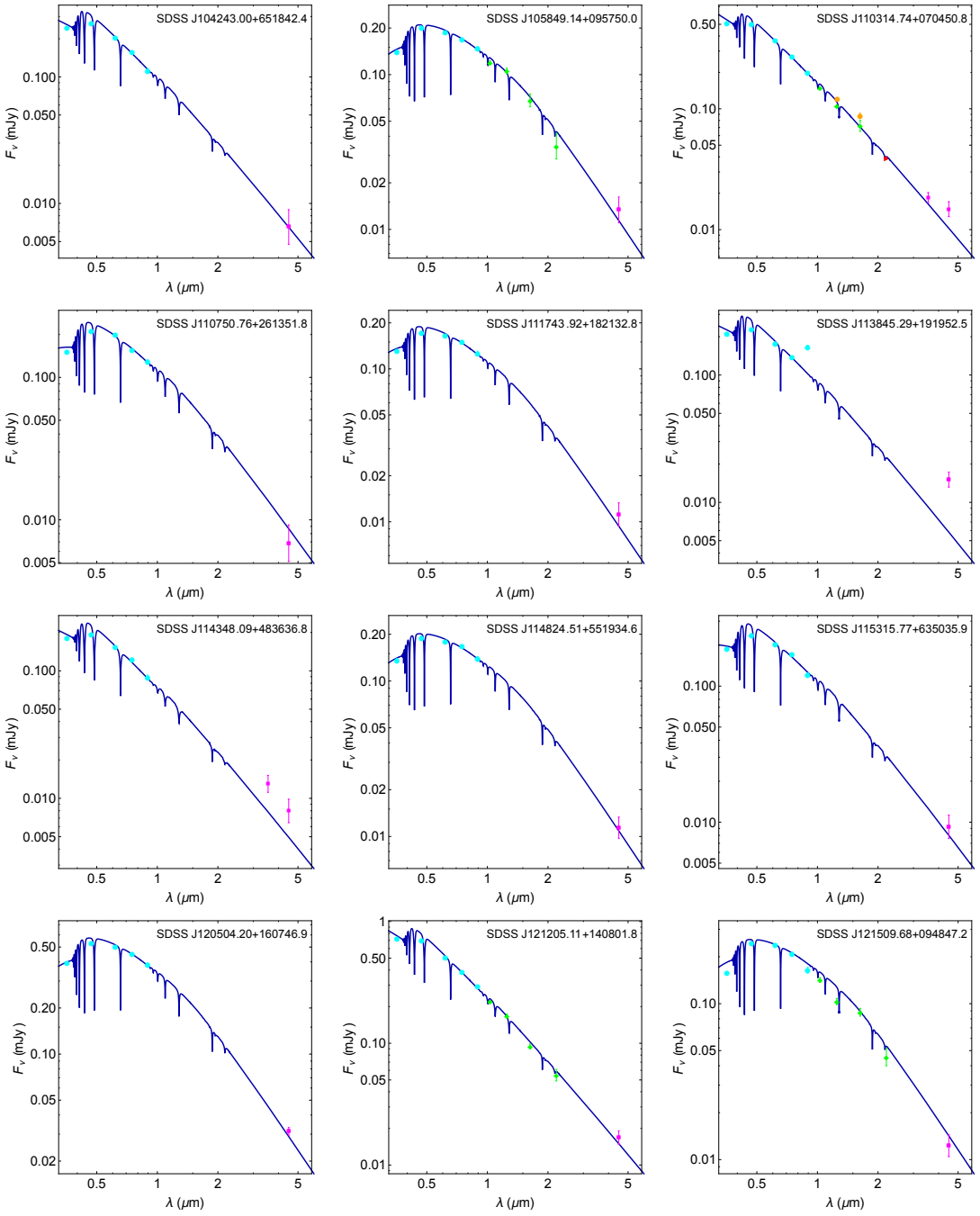
Massive WD SEDs

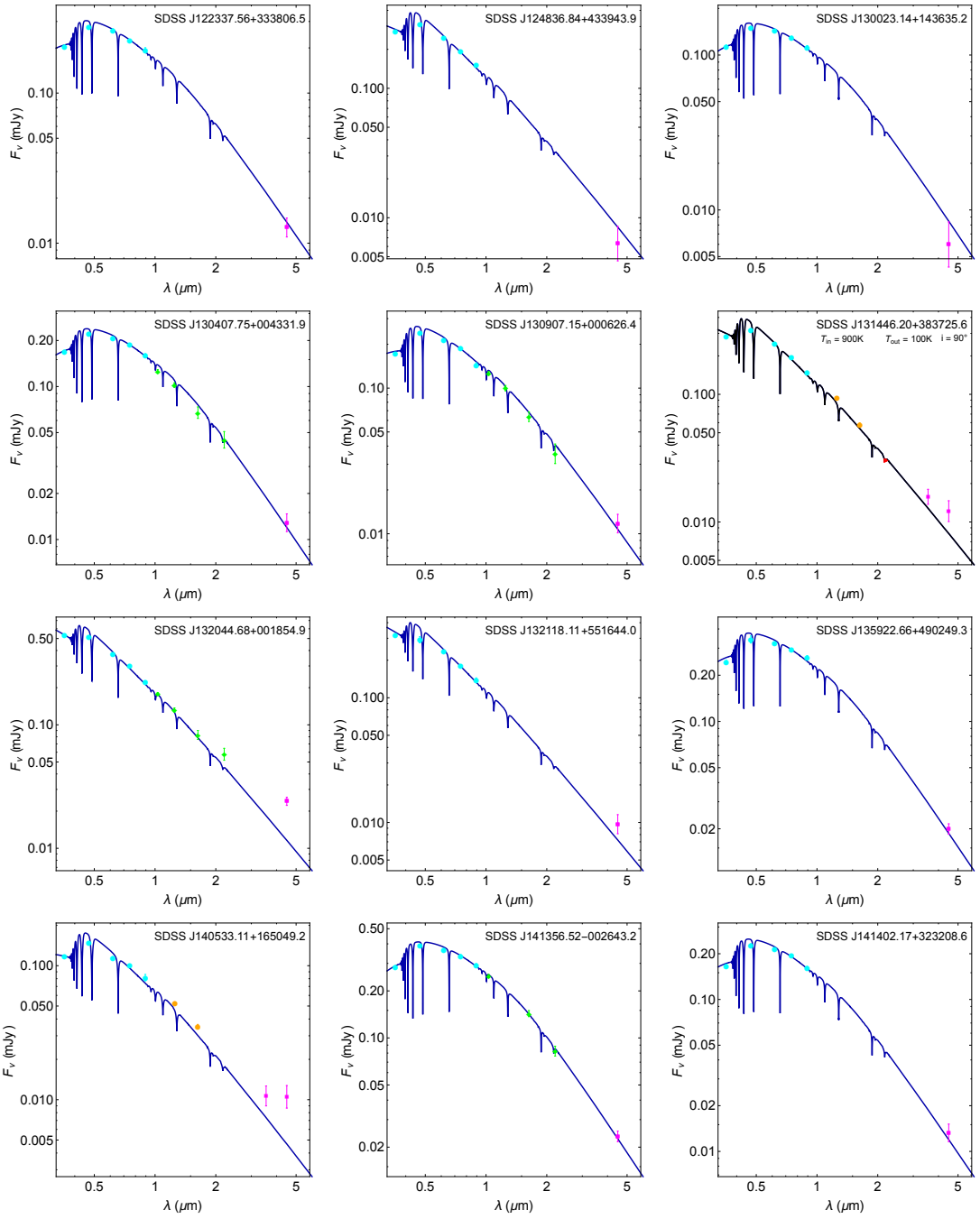

SDSS J000357.62−004939.0
SDSS J002516.45−095238.6
SDSS J003719.12+003139.3
SDSS J004610.37+133910.3
SDSS J005156.86+010052.2
SDSS J025200.98+004544.2
SDSS J025746.41+010106.0
SDSS J030243.80+062637.2
SDSS J032133.84+410134.6
SDSS J032727.52+001252.7
SDSS J034939.35+103649.9
SDSS J042017.89+052735.8
F_ν (mJy)
λ (μm)

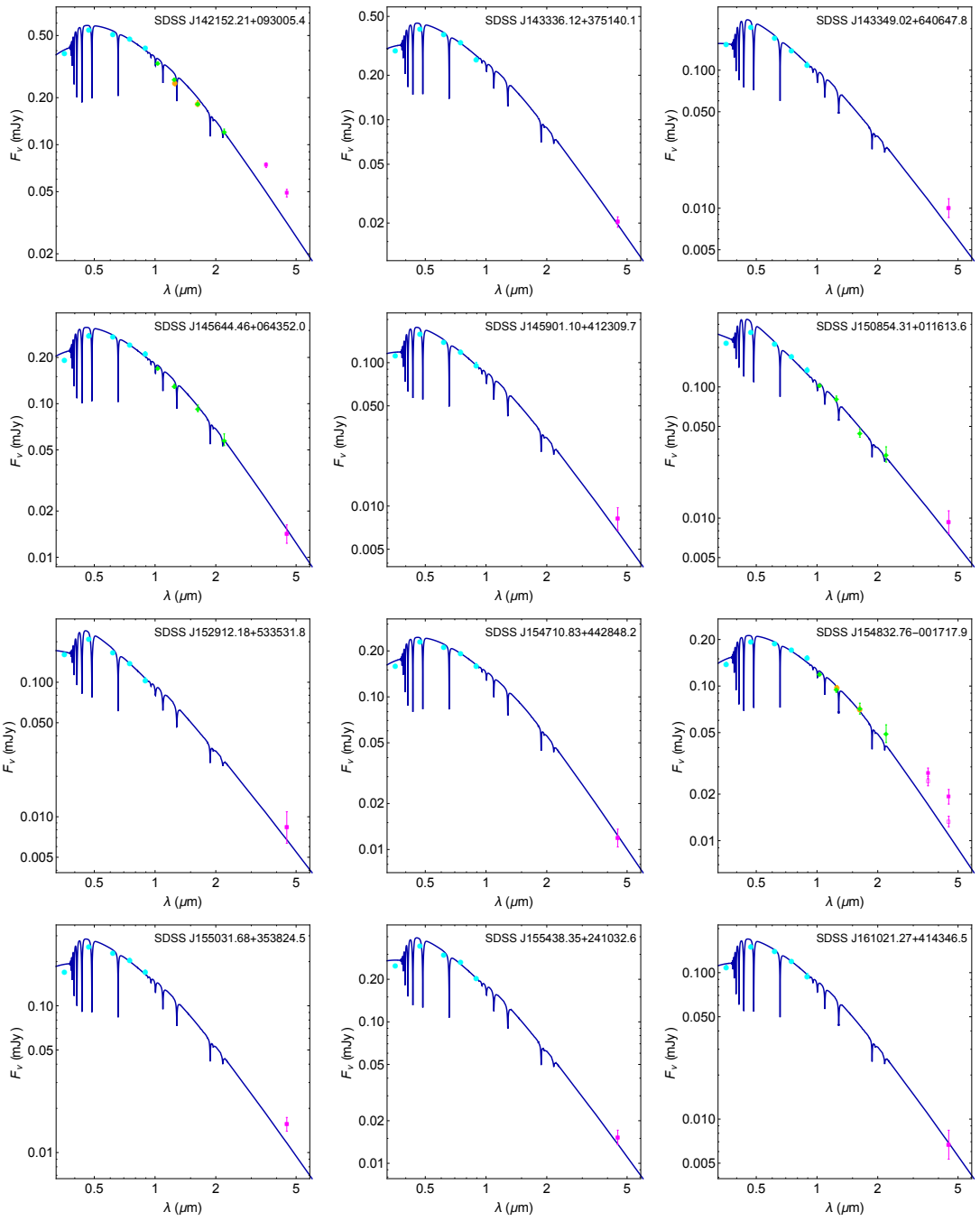

SDSS J055609.86+835754.5
SDSS J064754.29+363350.3
SDSS J072438.30+310729.0
SDSS J072723.02+413736.6
SDSS J073129.34+371444.9
SDSS J074155.51+315347.5
SDSS J074712.63+452714.0
SDSS J080254.13+440945.3
SDSS J080456.47+194242.3
SDSS J080616.91+202602.4
SDSS J082608.99+542648.2
SDSS J082926.86−042021.9
F_ν (mJy)
λ (μm)

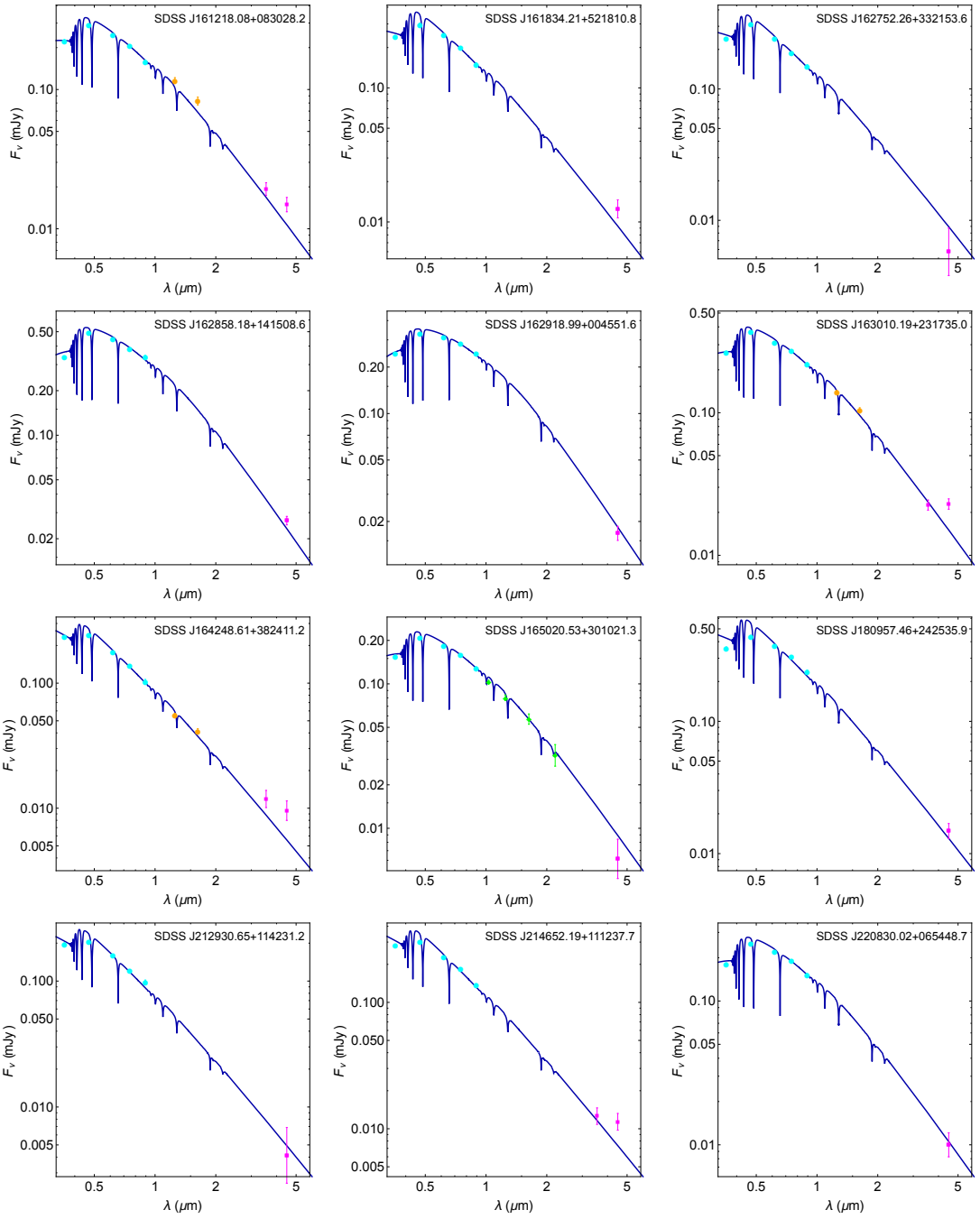

SDSS J083602.91+303149.7
SDSS J084321.98+204330.2
SDSS J085033.55+382717.2
SDSS J085828.81+441553.9
SDSS J085947.33+422113.1
SDSS J090258.23+230640.2
SDSS J090621.64+380956.4
SDSS J091521.66+194939.7
SDSS J092329.81+012020.0
SDSS J092451.92+463341.5
SDSS J094000.27+005207.1
SDSS J094255.02+180328.6
F_ν (mJy)
λ (μm)

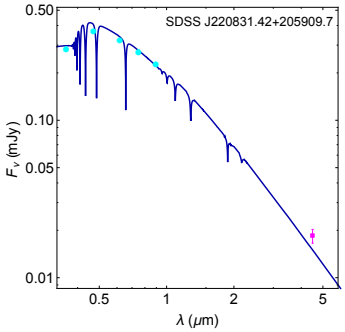

SDSS J094324.04+300352.0
SDSS J094332.88+312454.9
SDSS J094804.30−000738.2
SDSS J100704.45+322947.0
SDSS J101218.09+610818.9
SDSS J102033.69+274137.4
SDSS J102128.30+393728.6
SDSS J102626.22+252342.1
SDSS J103044.56+191357.9
SDSS J103642.26+211527.9
SDSS J103744.65+523042.1
SDSS J104038.50+380822.9
F_ν (mJy)
λ (μm)


SDSS J104243.00+651842.4
SDSS J105849.14+095750.0
SDSS J110314.74+070450.8
SDSS J110750.76+261351.8
SDSS J111743.92+182132.8
SDSS J113845.29+191952.5
SDSS J114348.09+483636.8
SDSS J114824.51+551934.6
SDSS J115315.77+635035.9
SDSS J120504.20+160746.9
SDSS J121205.11+140801.8
SDSS J121509.68+094847.2
F_ν (mJy)
λ (μm)


SDSS J122337.56+333806.5
SDSS J124836.84+433943.9
SDSS J130023.14+143635.2
SDSS J130407.75+004331.9
SDSS J130907.15+000626.4
SDSS J131446.20+383725.6
T_{in} = 900K T_{out} = 100K i = 90°
SDSS J132044.68+001854.9
SDSS J132118.11+551644.0
SDSS J135922.66+490249.3
SDSS J140533.11+165049.2
SDSS J141356.52−002643.2
SDSS J141402.17+323208.6
F_ν (mJy)
λ (μm)


SDSS J142152.21+093005.4
SDSS J143336.12+375140.1
SDSS J143349.02+640647.8
SDSS J145644.46+064352.0
SDSS J145901.10+412309.7
SDSS J150854.31+011613.6
SDSS J152912.18+533531.8
SDSS J154710.83+442848.2
SDSS J154832.76−001717.9
SDSS J155031.68+353824.5
SDSS J155438.35+241032.6
SDSS J161021.27+414346.5
F_ν (mJy)
λ (μm)


SDSS J161218.08+083028.2
SDSS J161834.21+521810.8
SDSS J162752.26+332153.6
SDSS J162858.18+141508.6
SDSS J162918.99+004551.6
SDSS J163010.19+231735.0
SDSS J164248.61+382411.2
SDSS J165020.53+301021.3
SDSS J180957.46+242535.9
SDSS J212930.65+114231.2
SDSS J214652.19+111237.7
SDSS J220830.02+065448.7
F_ν (mJy)
λ (μm)


SDSS J220831.42+205909.7
0.50
0.10
0.05
0.01
F_ν (mJy)
0.5
1
2
5
λ (μm)

Appendix B

McCook & Sion IRAC Photometry

Table B.1. IRAC Ch1 and Ch2 Photometry

WD	$F_{3.6\ \mu m}$ (mJy)	$F_{4.5\ \mu m}$ (mJy)	$F_{5.8\ \mu m}$ (mJy)	$F_{8\ \mu m}$ (mJy)
0000+171	0.066±0.001	0.044±0.001	··· ± ···	··· ± ···
0001+433	0.019±0.002	0.017±0.003	0.030±0.014	0.068±0.014
0004+330	··· ± ···	0.208±0.004	··· ± ···	0.053±0.013
0009+501	··· ± ···	0.969±0.003	··· ± ···	0.339±0.013
0010+280	0.137±0.002	0.088±0.002	0.085±0.009	0.067±0.012
0011+000	0.235±0.006	0.152±0.004	··· ± ···	··· ± ···
0013−241	0.104±0.002	0.066±0.001	··· ± ···	··· ± ···
0018−339	0.189±0.002	0.120±0.002	··· ± ···	··· ± ···
0028−474	0.163±0.002	0.105±0.001	··· ± ···	··· ± ···
0032−175	0.336±0.002	0.217±0.002	0.126±0.006	0.079±0.009
0047−524	··· ± ···	0.203±0.003	··· ± ···	0.073±0.014
0048+202	0.101±0.002	0.063±0.001	··· ± ···	··· ± ···
0050−332	··· ± ···	0.309±0.005	··· ± ···	0.132±0.012
0059+257	0.069±0.002	0.046±0.001	··· ± ···	··· ± ···
0101+048	··· ± ···	0.775±0.003	··· ± ···	0.322±0.018
0102+095	0.228±0.002	0.145±0.002	··· ± ···	··· ± ···
0110−139	0.060±0.001	0.041±0.001	··· ± ···	··· ± ···
0124−257	0.035±0.001	0.024±0.001	··· ± ···	··· ± ···
0126−532	··· ± ···	0.178±0.003	··· ± ···	0.060±0.012
0126+101	··· ± ···	0.460±0.002	··· ± ···	0.192±0.016
0127+270	0.055±0.001	0.033±0.002	0.036±0.010	0.232±0.018
0127+581	0.230±0.005	0.058±0.003	0.437±0.014	0.232±0.018
0129−205	0.103±0.002	0.069±0.001	··· ± ···	··· ± ···
0132+254	0.055±0.001	0.035±0.001	0.024±0.005	0.045±0.015
0133−116	0.456±0.002	0.293±0.001	0.184±0.008	0.112±0.005
0134+833	··· ± ···	0.543±0.004	··· ± ···	0.220±0.010
0136+251	0.044±0.002	0.022±0.004	0.052±0.018	0.052±0.025
0140−392	0.250±0.002	0.165±0.002	··· ± ···	··· ± ···
0141−675	2.549±0.009	1.673±0.004	1.039±0.017	0.618±0.014
0142+312	0.456±0.004	0.298±0.004	··· ± ···	··· ± ···
0145−221	0.967±0.003	0.619±0.003	0.479±0.008	0.327±0.008

Table B.1 (cont'd)

WD	$F_{3.6\ \mu m}$ (mJy)	$F_{4.5\ \mu m}$ (mJy)	$F_{5.8\ \mu m}$ (mJy)	$F_{8\ \mu m}$ (mJy)
0148+467	··· ± ···	1.182±0.005	··· ± ···	0.421±0.015
0148+641	1.594±0.008	1.583±0.006	0.793±0.029	0.831±0.048
0155+069	0.106±0.002	0.069±0.001	··· ± ···	··· ± ···
0208+396	0.376±0.001	0.590±0.002	2.788±0.009	1.591±0.005
0209+085	0.262±0.002	0.162±0.002	0.107±0.008	0.082±0.012
0214+568	0.474±0.004	0.298±0.004	0.181±0.012	0.240±0.015
0216+143	0.206±0.004	0.128±0.004	0.107±0.022	0.042±0.030
0227+050	··· ± ···	0.747±0.007	··· ± ···	0.261±0.015
0229+270	0.079±0.001	0.052±0.001	··· ± ···	··· ± ···
0231−054	··· ± ···	0.231±0.002	··· ± ···	0.099±0.022
0235−125	0.111±0.003	0.065±0.003	0.084±0.014	0.077±0.022
0235+064	0.968±0.022	0.286±0.004	0.111±0.014	0.077±0.015
0236+498	0.139±0.002	0.099±0.003	0.168±0.014	1.136±0.013
0237+241	0.051±0.001	0.035±0.001	0.021±0.008	0.045±0.013
0242−174	0.097±0.002	0.062±0.001	··· ± ···	··· ± ···
0243−026	0.454±0.001	0.295±0.001	0.191±0.003	0.108±0.003
0243+155	0.045±0.001	0.030±0.002	0.044±0.015	0.329±0.021
0255−705	··· ± ···	0.406±0.002	··· ± ···	0.147±0.013
0307+149	0.110±0.002	0.071±0.001	··· ± ···	··· ± ···
0308+188	0.317±0.002	0.206±0.002	··· ± ···	··· ± ···
0310−688	··· ± ···	2.939±0.008	··· ± ···	1.063±0.015
0316+345	··· ± ···	0.236±0.004	··· ± ···	0.080±0.035
0326−273	19.062±0.010	24.240±0.013	··· ± ···	··· ± ···
0339+523	0.188±0.002	0.141±0.002	0.135±0.007	0.154±0.012
0341+021	0.100±0.002	0.063±0.001	··· ± ···	··· ± ···
0349+247	0.026±0.001	0.017±0.002	0.063±0.017	0.061±0.019
0352+018	0.078±0.002	0.048±0.001	··· ± ···	··· ± ···
0352+096	0.276±0.003	0.178±0.002	0.105±0.009	0.061±0.013
0354+556	0.113±0.008	0.086±0.007	··· ± ···	··· ± ···
0402+543	0.124±0.007	0.092±0.006	··· ± ···	··· ± ···
0406+169	0.125±0.002	0.079±0.001	0.069±0.010	0.057±0.014

Table B.1 (cont'd)

WD	$F_{3.6\ \mu m}$ (mJy)	$F_{4.5\ \mu m}$ (mJy)	$F_{5.8\ \mu m}$ (mJy)	$F_{8\ \mu m}$ (mJy)
0407+179	··· ± ···	0.269±0.003	··· ± ···	0.086±0.014
0408−041	1.028±0.002	1.170±0.002	1.168±0.006	1.092±0.006
0410+117	··· ± ···	0.248±0.003	··· ± ···	0.084±0.025
0415+271	0.235±0.002	0.149±0.002	0.099±0.008	0.073±0.012
0418+153	0.051±0.001	0.043±0.001	0.196±0.015	0.073±0.013
0419−487	43.000±0.108	28.944±0.118	19.785±0.211	11.482±0.108
0420+520	0.407±0.014	··· ± ···	··· ± ···	··· ± ···
0421+162	0.274±0.002	0.170±0.002	0.115±0.008	0.075±0.012
0425+168	0.302±0.002	0.189±0.002	0.127±0.007	0.107±0.012
0429+176	37.457±0.047	26.014±0.042	··· ± ···	··· ± ···
0431+126	··· ± ···	0.174±0.002	··· ± ···	0.067±0.019
0437+152	0.080±0.080	0.051±0.001	0.296±0.009	0.600±0.014
0438+108	··· ± ···	0.210±0.004	··· ± ···	0.091±0.024
0439+466	0.812±0.005	0.505±0.004	0.325±0.014	0.198±0.016
0440−038	0.022±0.002	0.021±0.003	0.043±0.021	0.061±0.019
0446−789	··· ± ···	0.339±0.004	··· ± ···	··· ± ···
0453+418	0.450±0.450	0.292±0.004	0.167±0.016	0.141±0.018
0455−282	··· ± ···	0.487±0.006	··· ± ···	0.172±0.014
0458+407	0.079±0.008	0.058±0.007	··· ± ···	··· ± ···
0501+527	1.960±0.002	1.241±0.003	0.792±0.006	0.428±0.006
0507+045.1	··· ± ···	0.102±0.002	··· ± ···	0.083±0.015
0507+045.2	··· ± ···	0.102±0.002	··· ± ···	0.083±0.015
0509−007	0.334±0.004	0.216±0.004	0.145±0.011	0.085±0.018
0516+365	0.081±0.008	0.054±0.007	··· ± ···	··· ± ···
0517+307	0.133±0.001	0.085±0.001	0.050±0.006	0.024±0.005
0518−105	0.049±0.002	0.034±0.002	0.046±0.019	0.050±0.025
0531−022	0.044±0.001	0.025±0.001	0.037±0.011	0.017±0.011
0533+322	0.211±0.012	0.150±0.009	··· ± ···	··· ± ···
0543+579	0.178±0.001	0.112±0.001	··· ± ···	··· ± ···
0546+265	0.021±0.007	··· ± ···	··· ± ···	··· ± ···
0549+158	0.665±0.002	0.425±0.002	0.285±0.005	0.162±0.009

Table B.1 (cont'd)

WD	$F_{3.6\ \mu m}$ (mJy)	$F_{4.5\ \mu m}$ (mJy)	$F_{5.8\ \mu m}$ (mJy)	$F_{8\ \mu m}$ (mJy)
0557+237	0.069±0.008	0.044±0.008	··· ± ···	··· ± ···
0612+177	0.614±0.014	0.395±0.003	··· ± ···	0.221±0.022
0618+067	0.347±0.004	0.235±0.003	··· ± ···	··· ± ···
0618+134	0.122±0.009	0.078±0.007	··· ± ···	··· ± ···
0621−376	··· ± ···	0.896±0.008	··· ± ···	0.272±0.016
0642−166	211.786±4.663	287.220±2.373	1069.530±6.934	228.837±7.349
0644+025	0.383±0.011	0.127±0.014	··· ± ···	··· ± ···
0644+375	··· ± ···	1.310±0.004	··· ± ···	0.455±0.016
0648+641	0.233±0.004	0.156±0.003	··· ± ···	··· ± ···
0651−020	0.134±0.009	0.096±0.009	··· ± ···	··· ± ···
0659−063	0.101±0.007	0.081±0.006	··· ± ···	··· ± ···
0730+487	0.202±0.002	0.128±0.001	0.092±0.007	0.067±0.013
0732−427	··· ± ···	0.241±0.002	··· ± ···	0.105±0.018
0752−676	··· ± ···	2.165±0.005	··· ± ···	1.007±0.024
0752+365	0.189±0.003	0.117±0.003	··· ± ···	··· ± ···
0808+595	0.046±0.001	0.031±0.001	0.658±0.019	0.010±0.011
0816+297	0.078±0.002	0.052±0.002	0.046±0.010	0.057±0.018
0817+386	0.071±0.002	0.048±0.002	··· ± ···	··· ± ···
0819+363	0.114±0.002	0.093±0.002	··· ± ···	··· ± ···
0823+316	0.046±0.001	0.028±0.001	0.037±0.006	0.058±0.007
0824+288	5.787±0.022	4.544±0.029	2.996±0.043	1.880±0.030
0826+455	0.272±0.003	0.173±0.003	··· ± ···	··· ± ···
0839−327	··· ± ···	0.012±0.003	··· ± ···	··· ± ···
0843+516	0.134±0.002	0.123±0.002	0.110±0.009	0.161±0.011
0846+346	0.308±0.002	0.200±0.002	0.121±0.007	0.087±0.010
0847+354	0.026±0.003	··· ± ···	··· ± ···	··· ± ···
0848+122	0.032±0.001	0.023±0.002	0.048±0.011	0.128±0.014
0852+658	0.099±0.001	0.066±0.001	0.049±0.006	0.018±0.013
0854+404	0.155±0.001	0.098±0.001	··· ± ···	··· ± ···
0859−039	0.697±0.003	0.437±0.002	··· ± ···	··· ± ···
0914−195	0.697±0.003	0.015±0.006	0.100±0.026	0.090±0.022

Table B.1 (cont'd)

WD	$F_{3.6\ \mu m}$ (mJy)	$F_{4.5\ \mu m}$ (mJy)	$F_{5.8\ \mu m}$ (mJy)	$F_{8\ \mu m}$ (mJy)
0920+306	0.067±0.002	0.048±0.003	0.060±0.019	0.042±0.033
0920+363	0.056±0.001	0.037±0.001	··· ± ···	··· ± ···
0930+294	0.174±0.003	0.114±0.003	··· ± ···	··· ± ···
0933+025	3.530±0.006	2.442±0.005	··· ± ···	··· ± ···
0937+505	3.530±0.006	0.029±0.002	0.031±0.010	0.022±0.015
0938+550	0.195±0.002	0.124±0.002	··· ± ···	··· ± ···
0943+441	0.882±0.006	0.556±0.004	0.361±0.014	0.230±0.015
0947+325	0.088±0.001	0.057±0.001	··· ± ···	··· ± ···
0950−572	0.286±0.007	0.182±0.005	0.135±0.024	··· ± ···
0950+139	0.923±0.006	1.171±0.007	1.682±0.022	3.703±0.023
0954+697	0.064±0.001	0.045±0.001	··· ± ···	··· ± ···
0955+247	0.385±0.004	0.247±0.004	··· ± ···	··· ± ···
0956+020	0.087±0.001	0.056±0.000	··· ± ···	··· ± ···
0956+045	1.097±0.007	0.764±0.007	0.527±0.020	0.278±0.019
1003−023	0.112±0.001	0.073±0.001	··· ± ···	··· ± ···
1005+642	0.457±0.003	0.288±0.002	··· ± ···	··· ± ···
1013+256	0.041±0.001	0.025±0.001	··· ± ···	··· ± ···
1015+161	0.193±0.001	0.166±0.002	0.143±0.006	0.129±0.008
1017+125	0.072±0.002	0.045±0.002	0.062±0.013	0.040±0.022
1018+410	0.085±0.001	0.076±0.001	··· ± ···	··· ± ···
1019+637	0.966±0.006	0.638±0.005	··· ± ···	··· ± ···
1022−301	0.035±0.002	0.028±0.004	0.085±0.026	0.065±0.024
1029+537	0.173±0.001	0.108±0.001	0.068±0.003	0.060±0.006
1031−114	··· ± ···	0.473±0.002	··· ± ···	0.175±0.015
1034+492	0.094±0.001	0.059±0.001	0.039±0.007	0.096±0.012
1036+085	0.041±0.001	0.026±0.001	··· ± ···	··· ± ···
1038+633	0.105±0.001	0.067±0.002	0.067±0.007	0.267±0.008
1040+451	··· ± ···	0.071±0.069	··· ± ···	··· ± ···
1041+580	0.157±0.001	0.100±0.001	0.077±0.013	0.071±0.014
1052+273	0.302±0.004	0.193±0.004	0.137±0.013	0.080±0.015
1053−550	··· ± ···	0.411±0.002	··· ± ···	0.140±0.016

Table B.1 (cont'd)

WD	$F_{3.6\ \mu m}$ (mJy)	$F_{4.5\ \mu m}$ (mJy)	$F_{5.8\ \mu m}$ (mJy)	$F_{8\ \mu m}$ (mJy)
1057+719	0.134±0.001	0.085±0.001	0.061±0.003	0.063±0.005
1058−129	0.128±0.003	0.082±0.004	0.084±0.021	0.062±0.046
1102−183	0.213±0.002	0.140±0.002	0.092±0.007	0.075±0.012
1102+748	0.134±0.002	0.089±0.001	··· ± ···	··· ± ···
1105−048	··· ± ···	0.639±0.003	··· ± ···	0.270±0.017
1108+475	0.139±0.002	0.089±0.002	0.067±0.008	0.076±0.026
1109+244	0.056±0.002	0.035±0.002	0.198±0.018	0.251±0.021
1113+413	0.139±0.001	0.173±0.001	··· ± ···	··· ± ···
1115+166	0.131±0.002	0.085±0.002	0.392±0.015	0.072±0.018
1116+026	0.572±0.002	0.516±0.002	0.470±0.007	0.446±0.008
1120+439	0.085±0.003	0.047±0.003	0.074±0.020	0.161±0.026
1121+216	··· ± ···	1.669±0.004	··· ± ···	0.668±0.017
1122−324	0.061±0.001	0.041±0.001	··· ± ···	··· ± ···
1122+546	0.120±0.002	0.078±0.002	··· ± ···	··· ± ···
1124−293	0.327±0.002	0.208±0.001	0.139±0.006	0.088±0.007
1126+384	0.127±0.001	0.080±0.001	··· ± ···	··· ± ···
1129+155	0.372±0.004	0.233±0.004	0.160±0.014	0.100±0.018
1132+470	0.064±0.001	0.043±0.001	··· ± ···	··· ± ···
1133+293	0.143±0.003	0.092±0.004	0.101±0.017	0.061±0.030
1134+300	··· ± ···	0.862±0.004	··· ± ···	0.360±0.015
1145+187	0.232±0.002	0.145±0.001	··· ± ···	··· ± ···
1149+057	0.251±0.003	0.164±0.003	··· ± ···	··· ± ···
1150−153	0.504±0.002	0.580±0.003	0.602±0.007	0.587±0.008
1202−232	··· ± ···	1.993±0.004	··· ± ···	0.708±0.014
1202+608	0.350±0.002	0.219±0.002	0.142±0.006	0.077±0.009
1204−136	0.152±0.001	0.098±0.001	0.079±0.004	0.046±0.008
1204−322	0.080±0.002	0.054±0.001	··· ± ···	··· ± ···
1208+576	0.548±0.002	0.362±0.002	0.232±0.006	0.140±0.006
1210+533	0.225±0.001	0.146±0.001	0.104±0.004	0.082±0.007
1213+528	73.499±0.031	··· ± ···	39.643±0.055	··· ± ···
1214+267	0.054±0.001	0.036±0.002	0.285±0.016	0.044±0.015

Table B.1 (cont'd)

WD	$F_{3.6\ \mu m}$ (mJy)	$F_{4.5\ \mu m}$ (mJy)	$F_{5.8\ \mu m}$ (mJy)	$F_{8\ \mu m}$ (mJy)
1216+036	0.075±0.002	0.046±0.002	0.034±0.010	0.041±0.014
1218+497	0.981±0.004	0.682±0.003	··· ± ···	··· ± ···
1220+234	0.066±0.001	0.044±0.001	··· ± ···	··· ± ···
1223−659	··· ± ···	0.933±0.010	··· ± ···	··· ± ···
1229−012	0.238±0.003	0.150±0.004	0.237±0.016	0.067±0.035
1230−308	0.071±0.001	0.046±0.001	··· ± ···	··· ± ···
1233−164	0.114±0.002	0.073±0.001	··· ± ···	··· ± ···
1234+481	··· ± ···	0.206±0.003	··· ± ···	0.121±0.020
1236−495	··· ± ···	0.452±0.002	··· ± ···	0.168±0.012
1241−010	0.878±0.008	0.532±0.006	0.360±0.019	0.485±0.031
1241+235	0.076±0.001	0.052±0.001	··· ± ···	··· ± ···
1249+160	0.172±0.002	··· ± ···	··· ± ···	··· ± ···
1249+182	0.096±0.002	0.060±0.001	··· ± ···	··· ± ···
1253+105	··· ± ···	0.278±0.004	··· ± ···	··· ± ···
1253+378	0.247±0.001	0.179±0.001	0.114±0.006	0.092±0.008
1254+223	0.479±0.001	0.303±0.001	0.205±0.006	0.129±0.007
1257+032	0.085±0.002	0.052±0.002	0.049±0.011	0.033±0.017
1257+047	0.147±0.001	0.093±0.001	··· ± ···	··· ± ···
1257+278	0.277±0.001	0.178±0.001	0.118±0.002	0.074±0.003
1307+354	0.192±0.003	0.120±0.003	0.104±0.011	··· ± ···
1310−305	0.226±0.002	0.143±0.002	··· ± ···	··· ± ···
1310+583	0.659±0.005	0.424±0.005	0.290±0.011	0.317±0.191
1319+466	0.280±0.003	0.180±0.002	0.114±0.010	0.126±0.019
1323−514	0.118±0.002	0.085±0.002	··· ± ···	··· ± ···
1325+167	0.065±0.001	0.042±0.001	··· ± ···	··· ± ···
1325+279	0.094±0.001	0.061±0.001	··· ± ···	··· ± ···
1325+581	0.155±0.003	0.103±0.002	··· ± ···	··· ± ···
1327−083	··· ± ···	1.324±0.004	··· ± ···	0.468±0.016
1330+473	0.110±0.001	0.078±0.001	··· ± ···	··· ± ···
1333+497	0.057±0.001	0.090±0.001	··· ± ···	··· ± ···
1334−160	0.129±0.002	0.141±0.002	··· ± ···	··· ± ···

Table B.1 (cont'd)

WD	$F_{3.6\ \mu m}$ (mJy)	$F_{4.5\ \mu m}$ (mJy)	$F_{5.8\ \mu m}$ (mJy)	$F_{8\ \mu m}$ (mJy)
1335+369	2.039±0.005	1.317±0.004	··· ± ···	··· ± ···
1335+700	0.093±0.001	0.057±0.001	0.184±0.009	0.064±0.040
1337+705	··· ± ···	0.701±0.003	··· ± ···	0.263±0.012
1342+443	0.031±0.004	0.028±0.005	··· ± ···	··· ± ···
1344+106	0.633±0.003	0.409±0.002	0.270±0.007	0.147±0.009
1344+509	0.056±0.001	0.037±0.001	··· ± ···	··· ± ···
1350+656	0.137±0.001	0.089±0.000	0.057±0.003	0.049±0.002
1353+409	0.079±0.002	0.050±0.003	0.069±0.017	0.061±0.021
1407−475	··· ± ···	0.206±0.004	··· ± ···	0.084±0.017
1407+425	0.281±0.002	0.181±0.002	0.118±0.006	0.074±0.009
1408+323	··· ± ···	0.251±0.002	··· ± ···	0.306±0.013
1412−109	0.705±0.006	0.480±0.006	0.332±0.019	0.237±0.023
1413+231	··· ± ···	0.021±0.002	··· ± ···	0.052±0.029
1421+318	0.082±0.001	0.053±0.001	··· ± ···	··· ± ···
1422+095	1.558±0.007	0.920±0.005	0.725±0.015	0.410±0.014
1422+336	0.035±0.002	0.023±0.001	0.073±0.017	0.037±0.011
1425−811	0.914±0.005	0.585±0.002	0.373±0.012	0.213±0.006
1433+538	0.917±0.003	0.645±0.003	··· ± ···	··· ± ···
1446+286	0.194±0.002	0.123±0.003	0.101±0.008	0.075±0.012
1449+168	0.090±0.001	0.059±0.001	··· ± ···	··· ± ···
1451+006.1	0.100±0.001	0.064±0.001	··· ± ···	··· ± ···
1452−042	0.202±0.002	0.161±0.002	··· ± ···	··· ± ···
1455+298	0.367±0.002	0.256±0.001	0.187±0.006	0.179±0.007
1457−086	0.111±0.002	0.074±0.002	0.070±0.010	··· ± ···
1459+347	0.065±0.001	0.041±0.001	··· ± ···	··· ± ···
1503−070	0.330±0.004	0.218±0.003	··· ± ···	··· ± ···
1507+021	0.041±0.001	0.026±0.002	0.044±0.010	0.051±0.021
1507+220	0.149±0.002	0.096±0.001	··· ± ···	··· ± ···
1509+322	··· ± ···	0.258±0.003	··· ± ···	0.111±0.011
1511+009	0.056±0.001	0.034±0.001	··· ± ···	··· ± ···
1513+442	0.082±0.001	0.053±0.001	··· ± ···	··· ± ···

Table B.1 (cont'd)

WD	$F_{3.6\ \mu m}$ (mJy)	$F_{4.5\ \mu m}$ (mJy)	$F_{5.8\ \mu m}$ (mJy)	$F_{8\ \mu m}$ (mJy)
1515+668	0.197±0.003	0.123±0.003	0.096±0.013	··· ± ···
1521+310	0.106±0.001	0.068±0.001	··· ± ···	··· ± ···
1524−749	0.070±0.003	0.051±0.002	··· ± ···	··· ± ···
1525+257	0.069±0.001	0.044±0.001	··· ± ···	··· ± ···
1527+090	0.257±0.001	0.163±0.001	··· ± ···	··· ± ···
1531−022	··· ± ···	0.245±0.003	··· ± ···	0.095±0.015
1535+293	0.050±0.001	0.031±0.001	··· ± ···	··· ± ···
1541+650	0.434±0.004	0.483±0.004	··· ± ···	··· ± ···
1543−366	0.052±0.001	0.030±0.002	0.050±0.008	0.068±0.015
1547+057	0.058±0.001	0.036±0.001	··· ± ···	··· ± ···
1548+149	0.122±0.001	0.077±0.001	··· ± ···	··· ± ···
1550+183	0.218±0.003	0.138±0.003	0.100±0.010	0.060±0.014
1553+353	0.167±0.002	0.105±0.002	0.073±0.011	0.138±0.013
1554+215	0.106±0.001	0.074±0.001	··· ± ···	··· ± ···
1559+128	0.021±0.001	0.011±0.002	0.031±0.012	0.032±0.011
1559+369	··· ± ···	0.268±0.002	··· ± ···	0.194±0.025
1603+432	··· ± ···	0.077±0.002	··· ± ···	0.064±0.013
1605+683	0.062±0.002	0.041±0.002	··· ± ···	0.064±0.013
1606+422	··· ± ···	0.405±0.004	··· ± ···	0.487±0.201
1608+419	0.038±0.004	0.025±0.005	··· ± ···	··· ± ···
1609+044	0.094±0.001	0.060±0.001	··· ± ···	··· ± ···
1609+135	0.313±0.002	0.198±0.001	0.129±0.006	0.076±0.007
1609+631	0.024±0.001	0.016±0.002	0.033±0.011	0.073±0.012
1611−084	··· ± ···	0.184±0.004	··· ± ···	0.106±0.016
1612+554	0.180±0.003	0.156±0.001	0.126±0.010	0.230±0.011
1614+136	0.113±0.002	0.067±0.003	0.086±0.017	0.020±0.059
1614+160	··· ± ···	0.061±0.000	··· ± ···	0.036±0.004
1615−154	··· ± ···	0.304±0.002	··· ± ···	0.096±0.015
1620+260	0.073±0.001	0.046±0.001	··· ± ···	··· ± ···
1620+513	0.069±0.002	0.044±0.002	0.030±0.010	0.042±0.014
1625+093	0.249±0.004	0.168±0.003	··· ± ···	··· ± ···

Table B.1 (cont'd)

WD	$F_{3.6\ \mu m}$ (mJy)	$F_{4.5\ \mu m}$ (mJy)	$F_{5.8\ \mu m}$ (mJy)	$F_{8\ \mu m}$ (mJy)
1626+409	0.047±0.001	0.030±0.001	··· ± ···	··· ± ···
1631+396	··· ± ···	0.160±0.003	··· ± ···	0.057±0.017
1632+177	1.626±0.004	1.037±0.004	0.663±0.008	0.374±0.007
1633+433	0.933±0.003	0.608±0.002	0.394±0.007	0.226±0.006
1633+676	0.033±0.001	0.021±0.001	··· ± ···	··· ± ···
1635+137	0.118±0.003	0.101±0.003	··· ± ···	··· ± ···
1635+608	0.055±0.001	0.036±0.002	0.028±0.014	0.018±0.012
1637+335	··· ± ···	0.260±0.002	··· ± ···	0.089±0.019
1642+413	0.036±0.001	0.021±0.001	0.042±0.013	0.036±0.015
1647+375	0.135±0.001	0.086±0.001	··· ± ···	··· ± ···
1647+591	··· ± ···	1.682±0.004	··· ± ···	0.609±0.013
1654+637	0.086±0.001	0.054±0.001	0.769±0.012	··· ± ···
1655+215	··· ± ···	0.503±0.002	··· ± ···	0.166±0.014
1658+440	0.128±0.002	0.080±0.002	0.086±0.014	0.043±0.017
1659−531	··· ± ···	0.421±0.005	··· ± ···	0.088±0.017
1707+475	0.131±0.002	0.083±0.002	0.066±0.007	··· ± ···
1713+332	··· ± ···	0.184±0.002	··· ± ···	0.073±0.013
1716+020	··· ± ···	0.331±0.002	··· ± ···	0.148±0.024
1720+360	0.158±0.003	0.098±0.002	··· ± ···	··· ± ···
1724−359	10.276±0.164	6.472±0.144	5.180±0.317	2.494±0.298
1735+610	0.093±0.005	0.068±0.006	··· ± ···	··· ± ···
1738+669	0.146±0.001	0.093±0.001	0.061±0.003	0.059±0.004
1740−706	0.026±0.001	0.015±0.001	0.045±0.009	0.022±0.013
1755+194	0.200±0.002	0.129±0.002	··· ± ···	··· ± ···
1756+827	··· ± ···	0.074±0.002	··· ± ···	0.176±0.017
1821−131	2.807±0.076	1.208±0.048	1.111±0.714	··· ± ···
1826−045	··· ± ···	0.255±0.008	0.988±0.025	1.634±0.025
1827−106	2.850±0.272	0.826±0.221	··· ± ···	··· ± ···
1840−111	··· ± ···	0.141±0.009	··· ± ···	··· ± ···
1840+042	0.485±0.005	0.302±0.004	0.179±0.009	0.171±0.010
1844−223	0.390±0.002	0.244±0.002	0.140±0.006	0.086±0.008

Table B.1 (cont'd)

WD	$F_{3.6\ \mu m}$ (mJy)	$F_{4.5\ \mu m}$ (mJy)	$F_{5.8\ \mu m}$ (mJy)	$F_{8\ \mu m}$ (mJy)
1845+019	9.424±0.032	6.479±0.015	··· ± ···	··· ± ···
1858+393	0.189±0.001	0.122±0.001	0.073±0.006	0.006±0.009
1911+135	0.586±0.027	0.420±0.015	0.226±0.038	0.117±0.043
1914−598	0.339±0.003	0.237±0.003	··· ± ···	··· ± ···
1918+110	2.704±0.390	0.346±0.397	0.278±0.076	0.757±0.526
1919+145	2.431±0.032	1.370±0.029	1.335±0.065	0.685±0.069
1935+276	··· ± ···	0.855±0.003	··· ± ···	0.297±0.017
1936+327	··· ± ···	0.324±0.003	··· ± ···	0.110±0.017
1942+499	··· ± ···	0.094±0.003	··· ± ···	0.052±0.015
1943+163	··· ± ···	0.525±0.004	··· ± ···	0.147±0.022
1953−011	··· ± ···	1.198±0.007	··· ± ···	0.421±0.017
1953−715	0.130±0.002	0.084±0.001	··· ± ···	··· ± ···
1957+225	0.494±0.011	0.492±0.011	1.095±0.032	1.539±0.024
2004−605	··· ± ···	0.302±0.003	··· ± ···	0.153±0.021
2007−219	0.542±0.003	0.351±0.003	0.222±0.010	0.144±0.011
2007−303	··· ± ···	1.407±0.004	··· ± ···	0.500±0.016
2011+398	4.235±0.017	2.763±0.019	1.867±0.059	0.987±0.198
2014−575	··· ± ···	0.227±0.004	··· ± ···	0.088±0.015
2021−128	0.112±0.002	0.071±0.001	··· ± ···	··· ± ···
2028+390	0.157±0.010	0.089±0.005	0.875±0.063	0.392±0.067
2032+188	0.124±0.002	0.079±0.001	··· ± ···	··· ± ···
2032+248	··· ± ···	2.240±0.005	··· ± ···	0.778±0.015
2039−202	··· ± ···	1.032±0.003	··· ± ···	0.381±0.018
2039−682	··· ± ···	0.486±0.002	··· ± ···	0.186±0.014
2046−220	0.087±0.002	0.055±0.001	··· ± ···	··· ± ···
2046+396	··· ± ···	0.343±0.007	··· ± ···	0.133±0.025
2047+372	··· ± ···	0.759±0.005	··· ± ···	0.208±0.016
2056+033	0.050±0.001	0.037±0.002	0.057±0.011	0.161±0.018
2058+181	0.148±0.002	0.096±0.001	··· ± ···	··· ± ···
2058+499	0.076±0.007	0.034±0.010	0.064±0.053	··· ± ···
2058+506	0.305±0.009	0.209±0.007	··· ± ···	··· ± ···

Table B.1 (cont'd)

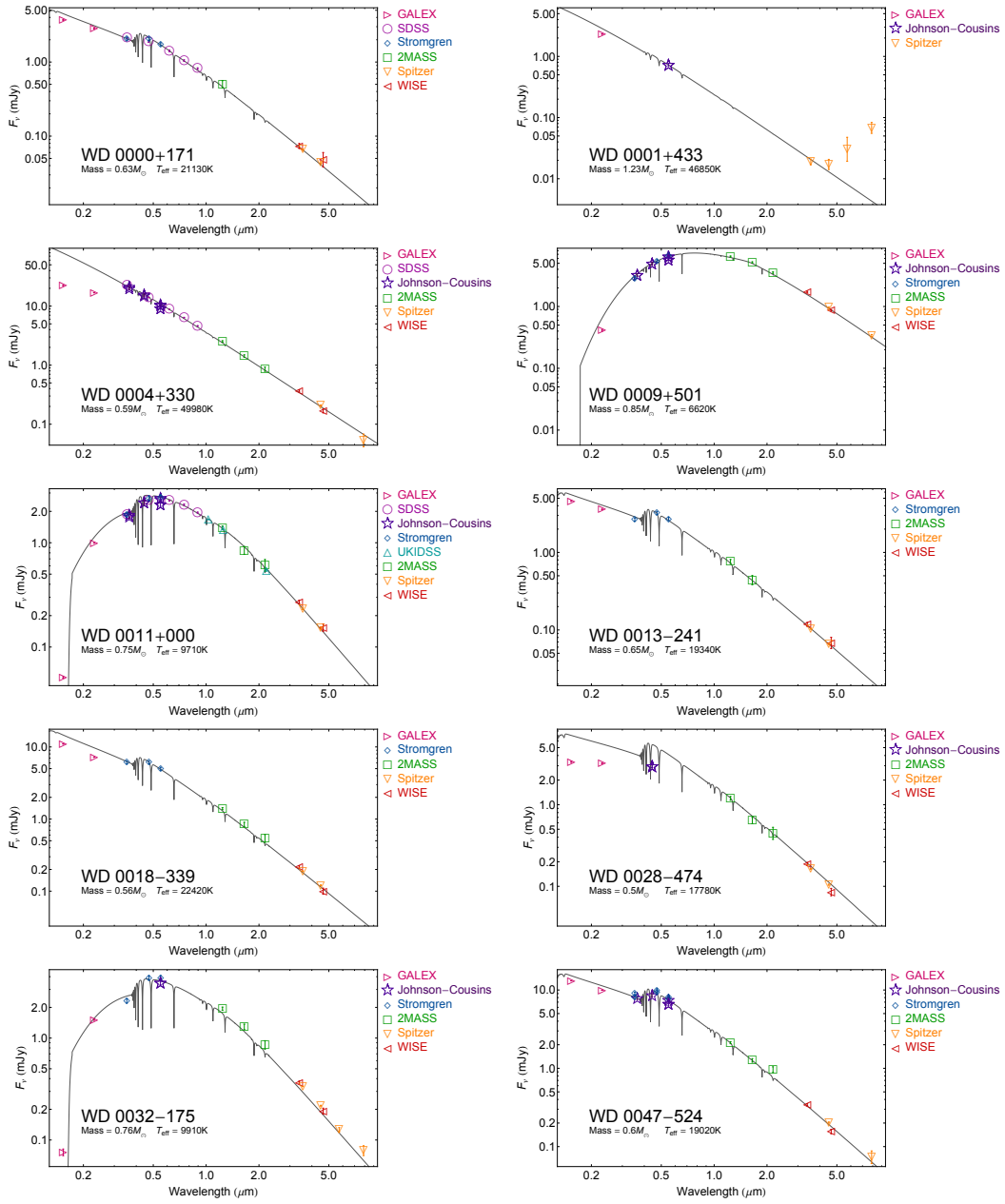
WD	$F_{3.6\ \mu m}$ (mJy)	$F_{4.5\ \mu m}$ (mJy)	$F_{5.8\ \mu m}$ (mJy)	$F_{8\ \mu m}$ (mJy)
2059+190	0.240±0.004	0.149±0.003	··· ± ···	··· ± ···
2059+247	0.244±0.004	0.153±0.003	··· ± ···	··· ± ···
2105−820	··· ± ···	0.726±0.003	··· ± ···	··· ± ···
2111+261	0.615±0.005	0.397±0.004	··· ± ···	··· ± ···
2111+498	0.659±0.017	0.417±0.004	··· ± ···	0.138±0.022
2115−560	1.100±0.003	1.037±0.002	0.989±0.007	0.912±0.007
2115+010	0.069±0.001	0.043±0.001	··· ± ···	··· ± ···
2117+539	1.883±0.020	1.286±0.004	··· ± ···	0.487±0.018
2120+054	0.046±0.001	0.027±0.002	0.245±0.017	0.047±0.014
2124+550	0.205±0.011	··· ± ···	··· ± ···	··· ± ···
2126+734	··· ± ···	0.951±0.003	··· ± ···	0.351±0.012
2134+218	··· ± ···	0.161±0.003	··· ± ···	0.192±0.013
2136+828	0.963±0.006	0.611±0.003	0.393±0.013	0.223±0.012
2152−045	0.082±0.001	0.051±0.001	··· ± ···	··· ± ···
2200−136	0.104±0.002	0.065±0.001	··· ± ···	··· ± ···
2204+070	0.065±0.001	0.046±0.001	··· ± ···	··· ± ···
2207+142	0.309±0.004	0.201±0.003	··· ± ···	··· ± ···
2211−495	··· ± ···	1.304±0.008	··· ± ···	0.463±0.015
2218+706	0.136±0.001	0.087±0.001	0.052±0.004	0.078±0.005
2220+133	0.073±0.001	0.045±0.001	··· ± ···	··· ± ···
2226−210	0.325±0.003	0.213±0.004	0.148±0.011	0.160±0.012
2226+061	0.202±0.002	0.124±0.002	0.079±0.010	0.062±0.018
2246+223	··· ± ···	0.306±0.002	··· ± ···	0.131±0.012
2248+293	0.761±0.005	0.502±0.004	0.345±0.013	0.191±0.012
2257+162	0.413±0.003	0.286±0.003	0.179±0.012	0.130±0.012
2303+242	0.173±0.003	0.112±0.002	··· ± ···	··· ± ···
2306+124	0.123±0.002	0.076±0.001	··· ± ···	··· ± ···
2306+130	0.148±0.003	0.092±0.002	··· ± ···	··· ± ···
2309+105	0.601±0.005	0.380±0.004	0.251±0.012	0.186±0.018
2321−549	0.089±0.002	0.057±0.003	0.470±0.022	0.228±0.019
2322−181	0.097±0.001	0.061±0.001	··· ± ···	··· ± ···

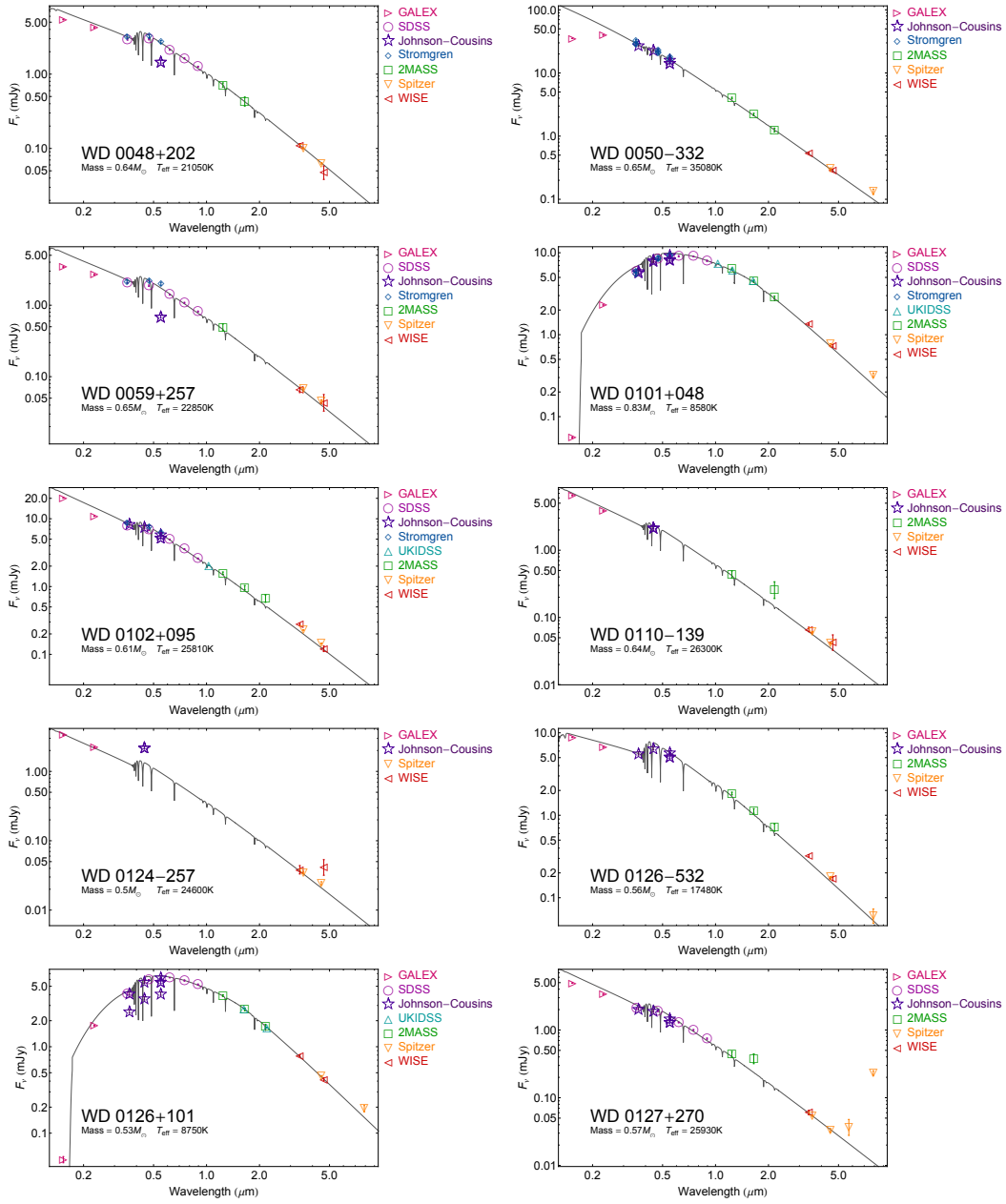
Table B.1 (cont'd)

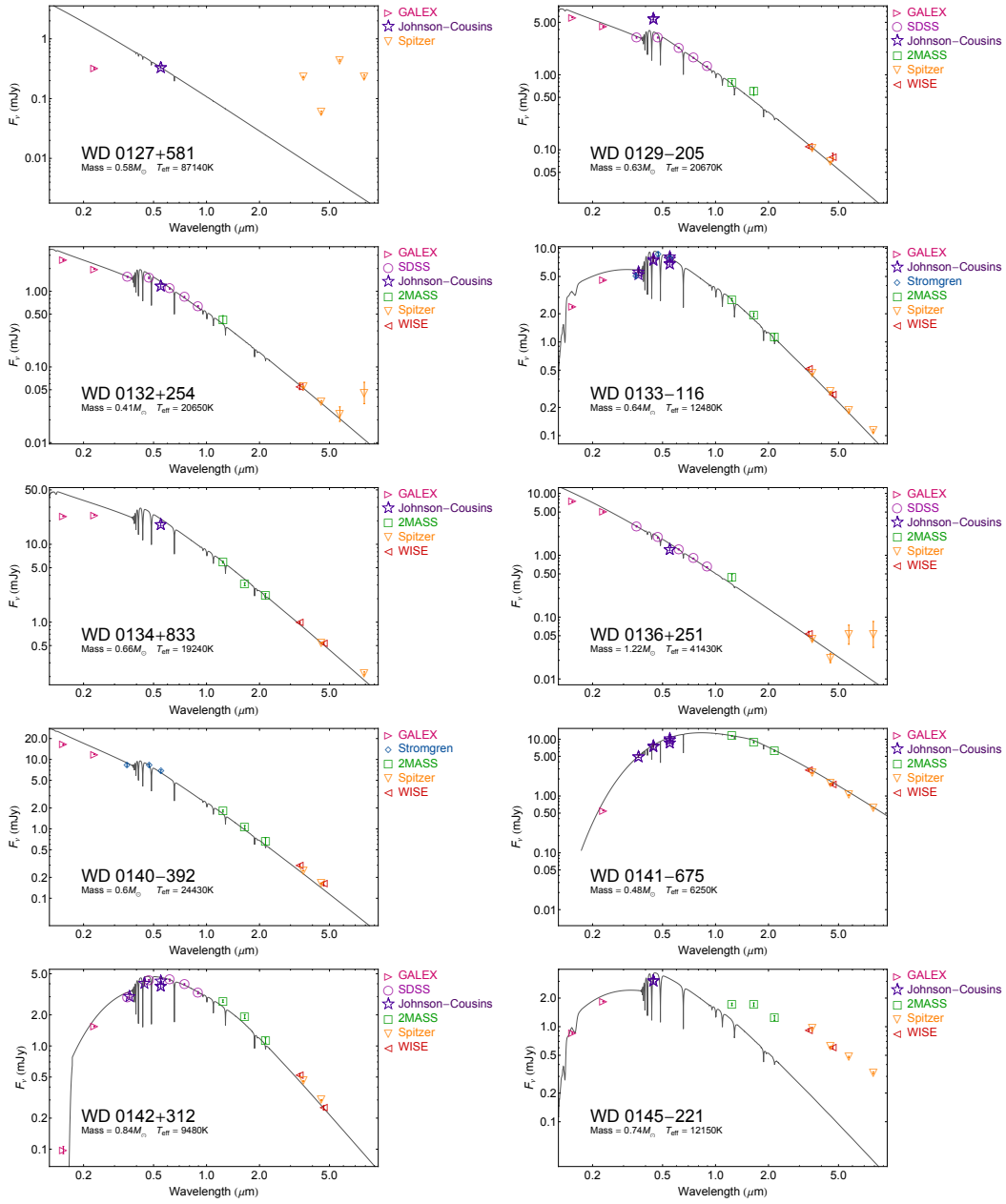
WD	$F_{3.6\ \mu m}$ (mJy)	$F_{4.5\ \mu m}$ (mJy)	$F_{5.8\ \mu m}$ (mJy)	$F_{8\ \mu m}$ (mJy)
2326+049	8.104±0.005	8.730±0.005	8.261±0.013	8.537±0.010
2328+107	0.114±0.001	0.079±0.001	··· ± ···	··· ± ···
2331−475	0.447±0.004	0.290±0.004	0.178±0.013	0.120±0.013
2331+290	0.067±0.002	0.044±0.002	0.032±0.011	0.036±0.010
2342+806	0.169±0.001	0.103±0.001	0.067±0.004	0.073±0.006
2349−031	0.046±0.002	0.042±0.003	··· ± ···	··· ± ···
2351−335	··· ± ···	48.100±0.048	··· ± ···	33.300±0.055
2353+026	0.050±0.001	0.031±0.002	0.048±0.010	0.328±0.015
2359−434	··· ± ···	1.777±0.004	··· ± ···	0.650±0.016

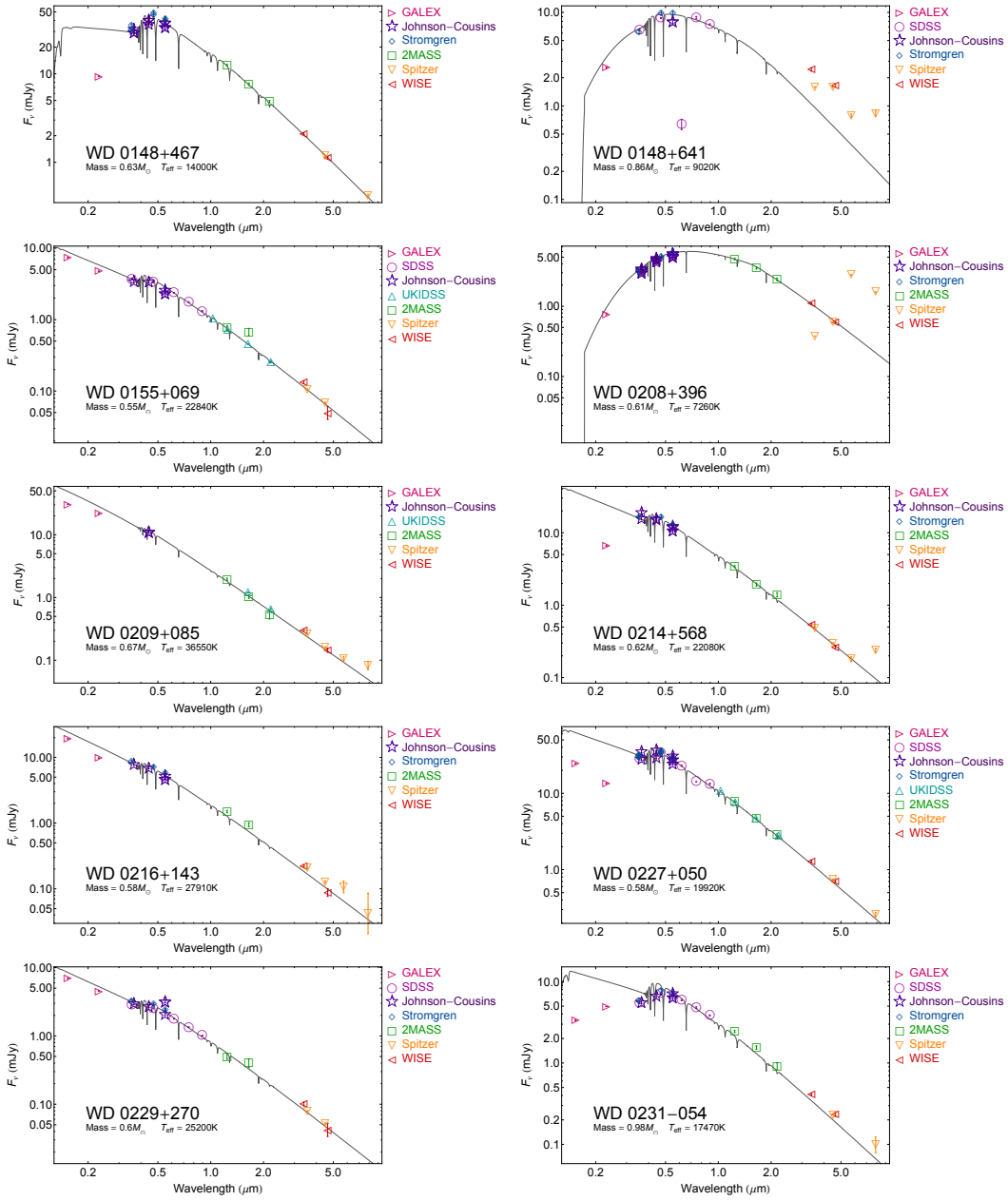
Appendix C

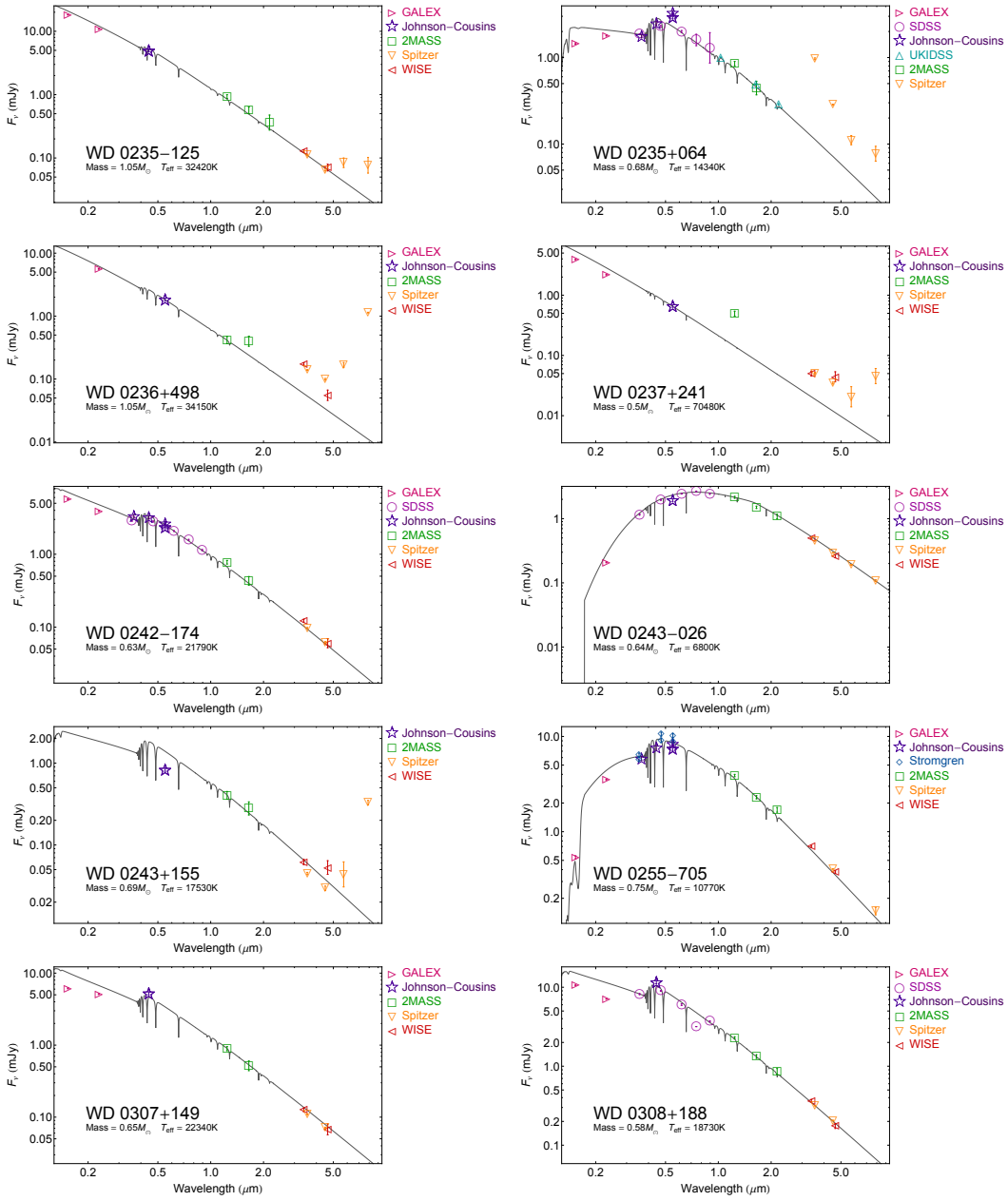
McCook & Sion IRAC SEDs

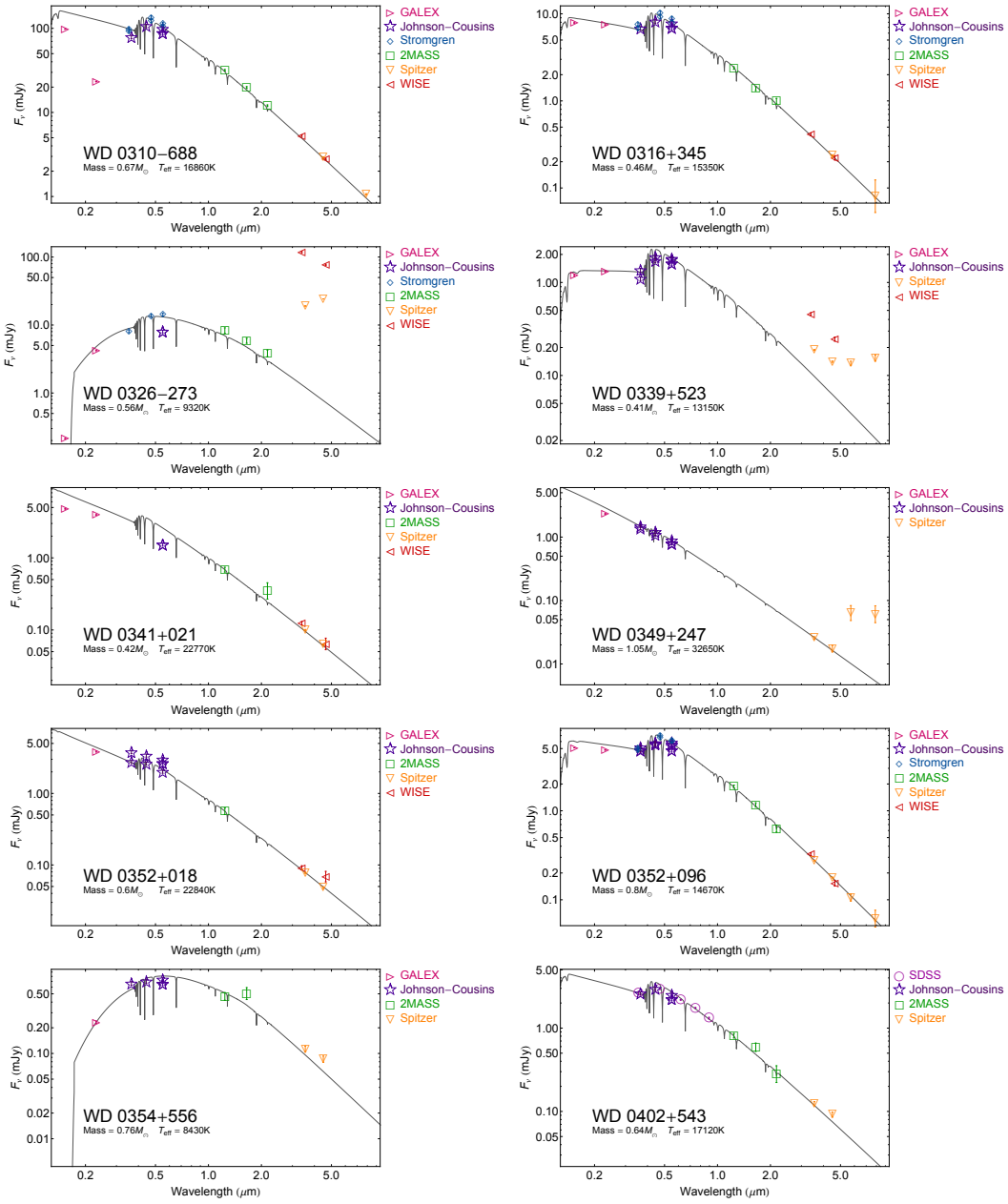

WD 0000+171
Mass = 0.63$M_\odot$ $T_{\rm eff}$ = 21130K
WD 0001+433
Mass = 1.23$M_\odot$ $T_{\rm eff}$ = 46850K
WD 0004+330
Mass = 0.59$M_\odot$ $T_{\rm eff}$ = 49980K
WD 0009+501
Mass = 0.85$M_\odot$ $T_{\rm eff}$ = 6620K
WD 0011+000
Mass = 0.75$M_\odot$ $T_{\rm eff}$ = 9710K
WD 0013−241
Mass = 0.65$M_\odot$ $T_{\rm eff}$ = 19340K
WD 0018−339
Mass = 0.56$M_\odot$ $T_{\rm eff}$ = 22420K
WD 0028−474
Mass = 0.5$M_\odot$ $T_{\rm eff}$ = 17780K
WD 0032−175
Mass = 0.76$M_\odot$ $T_{\rm eff}$ = 9910K
WD 0047−524
Mass = 0.6$M_\odot$ $T_{\rm eff}$ = 19020K
F_ν (mJy)
Wavelength (μm)
GALEX
SDSS
Stromgren
Johnson−Cousins
UKIDSS
2MASS
Spitzer
WISE

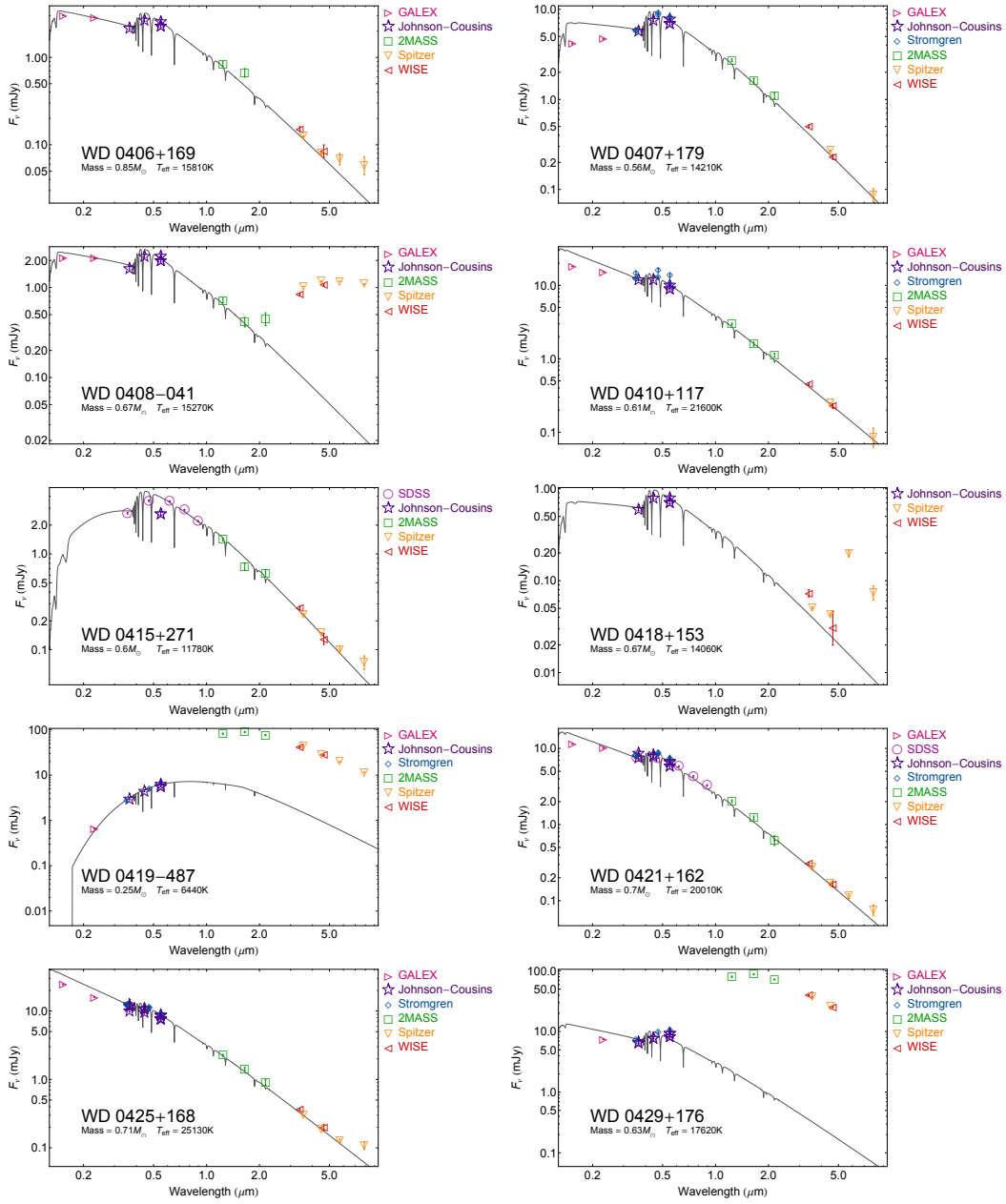

WD 0048+202
Mass = 0.64$M_\odot$ $T_{\rm eff}$ = 21050K
WD 0050−332
Mass = 0.65$M_\odot$ $T_{\rm eff}$ = 35080K
WD 0059+257
Mass = 0.65$M_\odot$ $T_{\rm eff}$ = 22850K
WD 0101+048
Mass = 0.83$M_\odot$ $T_{\rm eff}$ = 8580K
WD 0102+095
Mass = 0.61$M_\odot$ $T_{\rm eff}$ = 25810K
WD 0110−139
Mass = 0.64$M_\odot$ $T_{\rm eff}$ = 26300K
WD 0124−257
Mass = 0.5$M_\odot$ $T_{\rm eff}$ = 24600K
WD 0126−532
Mass = 0.56$M_\odot$ $T_{\rm eff}$ = 17480K
WD 0126+101
Mass = 0.53$M_\odot$ $T_{\rm eff}$ = 8750K
WD 0127+270
Mass = 0.57$M_\odot$ $T_{\rm eff}$ = 25930K
F_ν (mJy)
Wavelength (μm)
GALEX
SDSS
Johnson−Cousins
Stromgren
UKIDSS
2MASS
Spitzer
WISE

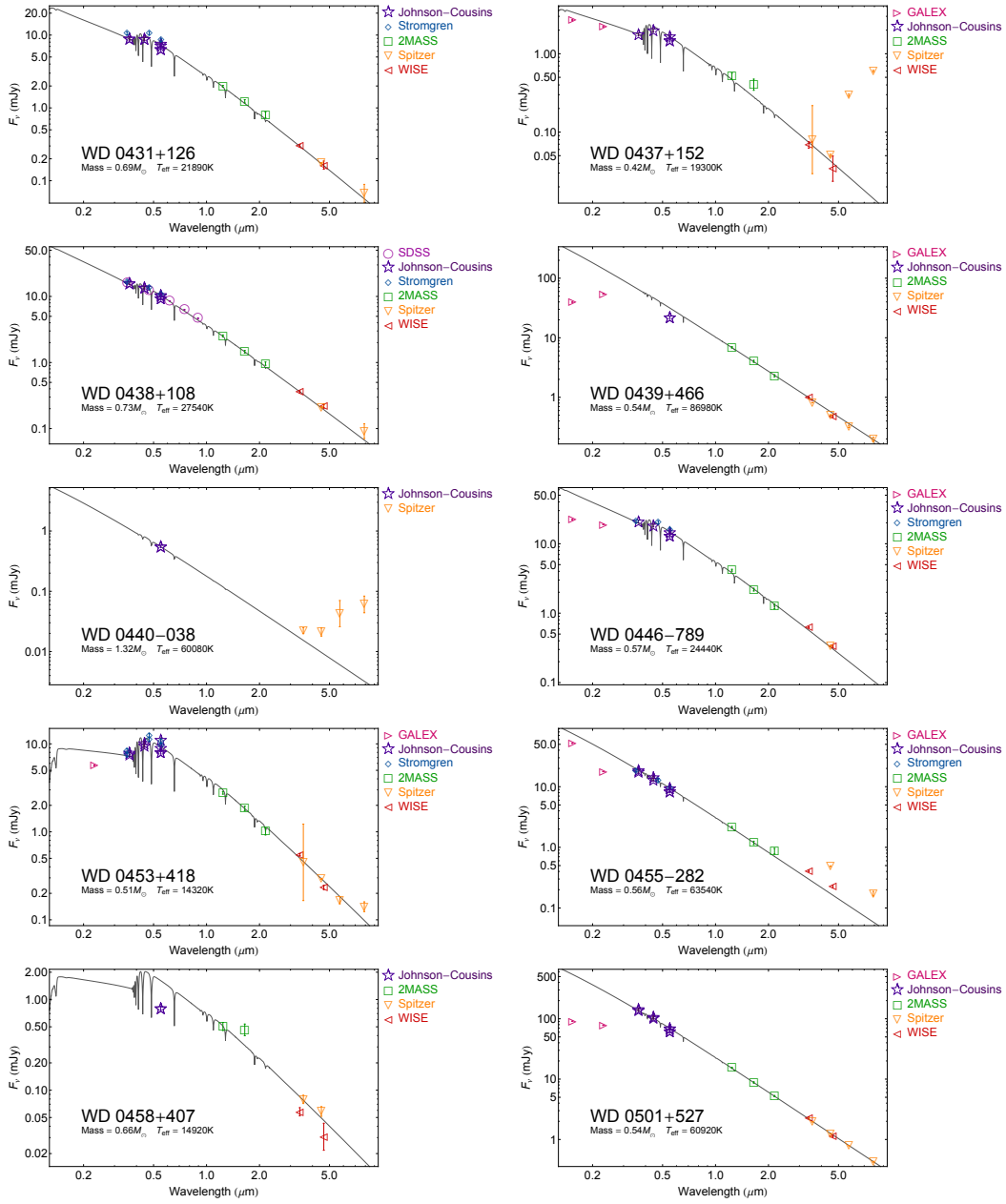

WD 0127+581
Mass = 0.58$M_\odot$ $T_{\rm eff}$ = 87140K
WD 0129−205
Mass = 0.63$M_\odot$ $T_{\rm eff}$ = 20670K
WD 0132+254
Mass = 0.41$M_\odot$ $T_{\rm eff}$ = 20650K
WD 0133−116
Mass = 0.64$M_\odot$ $T_{\rm eff}$ = 12480K
WD 0134+833
Mass = 0.66$M_\odot$ $T_{\rm eff}$ = 19240K
WD 0136+251
Mass = 1.22$M_\odot$ $T_{\rm eff}$ = 41430K
WD 0140−392
Mass = 0.6$M_\odot$ $T_{\rm eff}$ = 24430K
WD 0141−675
Mass = 0.48$M_\odot$ $T_{\rm eff}$ = 6250K
WD 0142+312
Mass = 0.84$M_\odot$ $T_{\rm eff}$ = 9480K
WD 0145−221
Mass = 0.74$M_\odot$ $T_{\rm eff}$ = 12150K
F_ν (mJy)
Wavelength (μm)
GALEX
SDSS
Johnson−Cousins
Stromgren
2MASS
Spitzer
WISE

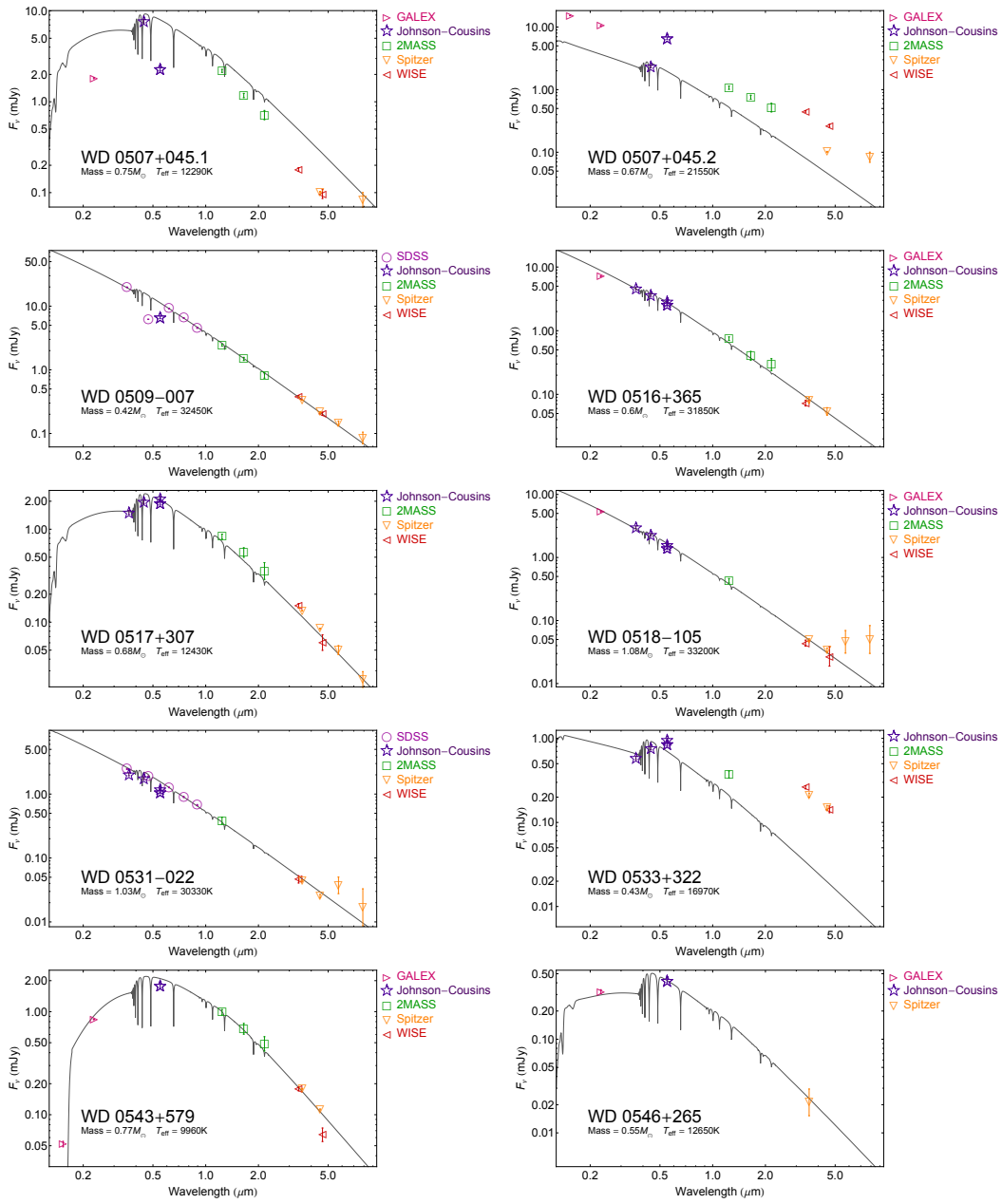

WD 0148+467
Mass = 0.63$M_\odot$ $T_{\rm eff}$ = 14000K
WD 0148+641
Mass = 0.86$M_\odot$ $T_{\rm eff}$ = 9020K
WD 0155+069
Mass = 0.55$M_\odot$ $T_{\rm eff}$ = 22840K
WD 0208+396
Mass = 0.61$M_\odot$ $T_{\rm eff}$ = 7260K
WD 0209+085
Mass = 0.67$M_\odot$ $T_{\rm eff}$ = 36550K
WD 0214+568
Mass = 0.62$M_\odot$ $T_{\rm eff}$ = 22080K
WD 0216+143
Mass = 0.58$M_\odot$ $T_{\rm eff}$ = 27910K
WD 0227+050
Mass = 0.58$M_\odot$ $T_{\rm eff}$ = 19920K
WD 0229+270
Mass = 0.6$M_\odot$ $T_{\rm eff}$ = 25200K
WD 0231−054
Mass = 0.98$M_\odot$ $T_{\rm eff}$ = 17470K
F_ν (mJy)
Wavelength (μm)
GALEX
SDSS
Johnson−Cousins
Stromgren
UKIDSS
2MASS
Spitzer
WISE

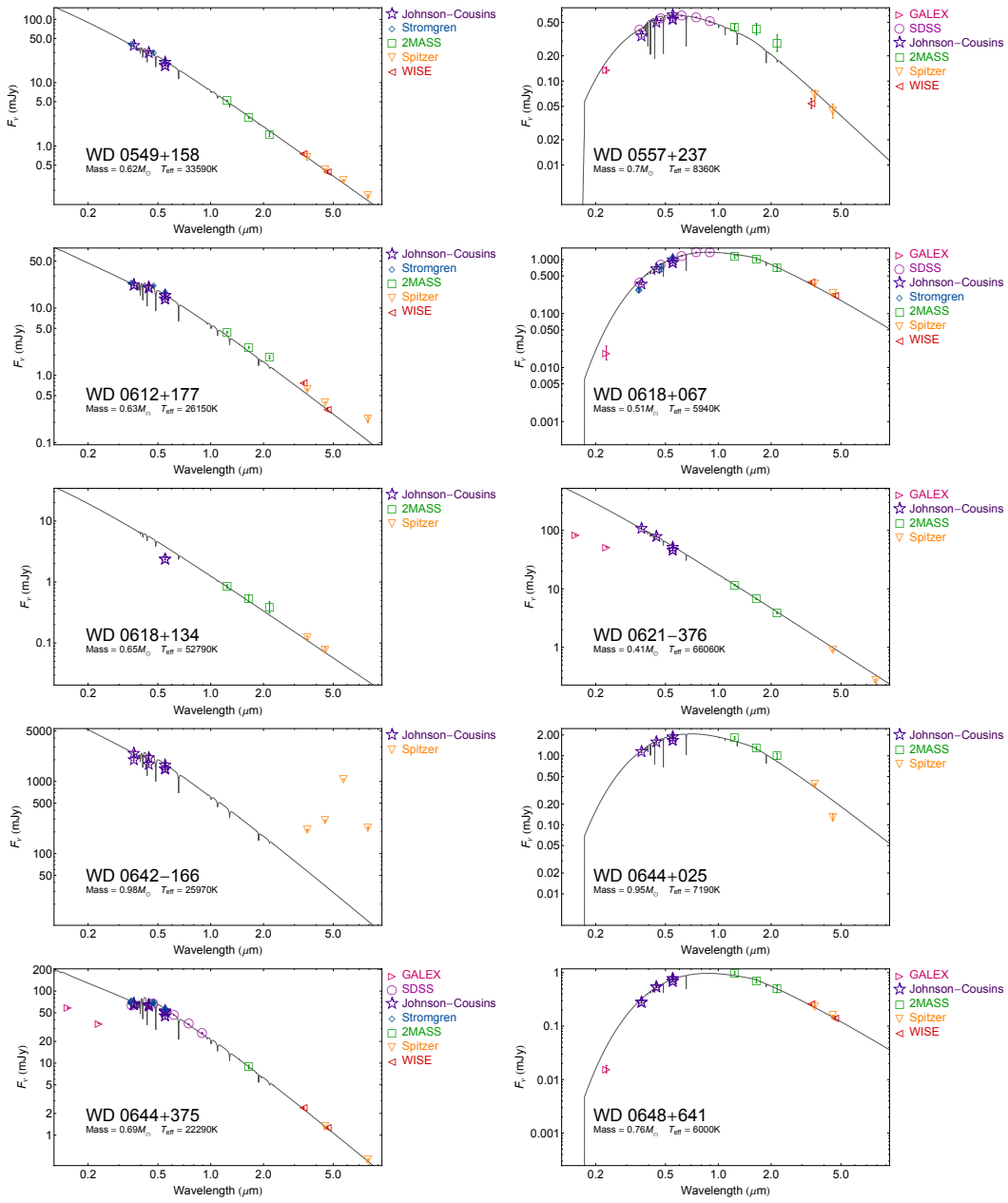

WD 0235−125
Mass = 1.05$M_\odot$ $T_{\rm eff}$ = 32420K
GALEX
Johnson−Cousins
2MASS
Spitzer
WISE
WD 0235+064
Mass = 0.68$M_\odot$ $T_{\rm eff}$ = 14340K
GALEX
SDSS
Johnson−Cousins
UKIDSS
2MASS
Spitzer
WD 0236+498
Mass = 1.05$M_\odot$ $T_{\rm eff}$ = 34150K
GALEX
Johnson−Cousins
2MASS
Spitzer
WISE
WD 0237+241
Mass = 0.5$M_\odot$ $T_{\rm eff}$ = 70480K
GALEX
Johnson−Cousins
2MASS
Spitzer
WISE
WD 0242−174
Mass = 0.63$M_\odot$ $T_{\rm eff}$ = 21790K
GALEX
SDSS
Johnson−Cousins
2MASS
Spitzer
WISE
WD 0243−026
Mass = 0.64$M_\odot$ $T_{\rm eff}$ = 6800K
GALEX
SDSS
Johnson−Cousins
2MASS
Spitzer
WISE
WD 0243+155
Mass = 0.69$M_\odot$ $T_{\rm eff}$ = 17530K
Johnson−Cousins
2MASS
Spitzer
WISE
WD 0255−705
Mass = 0.75$M_\odot$ $T_{\rm eff}$ = 10770K
GALEX
Johnson−Cousins
Stromgren
2MASS
Spitzer
WISE
WD 0307+149
Mass = 0.65$M_\odot$ $T_{\rm eff}$ = 22340K
GALEX
Johnson−Cousins
2MASS
Spitzer
WISE
WD 0308+188
Mass = 0.58$M_\odot$ $T_{\rm eff}$ = 18730K
GALEX
SDSS
Johnson−Cousins
2MASS
Spitzer
WISE
F_ν (mJy)
Wavelength (μm)

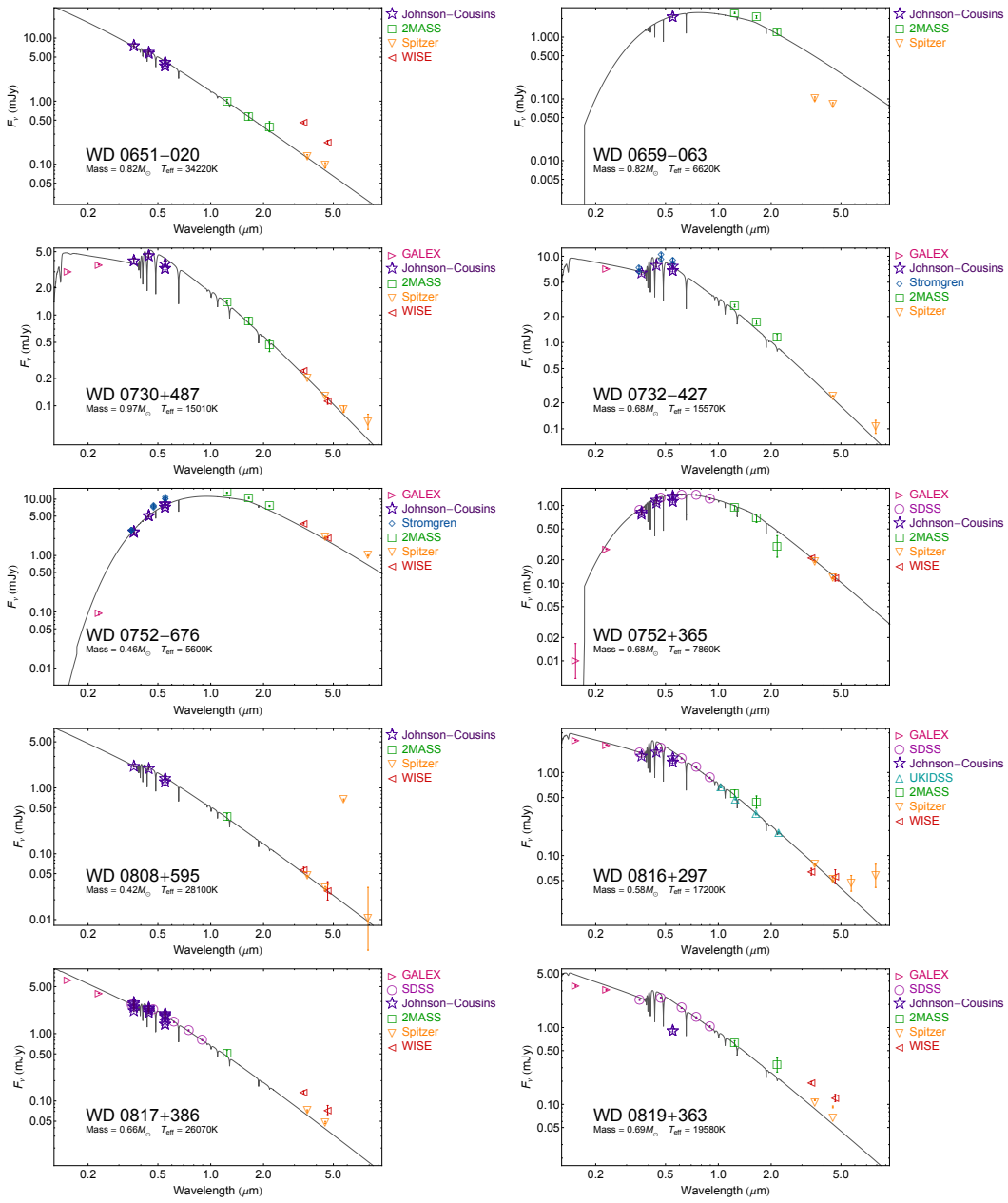

WD 0310−688
Mass = 0.67$M_\odot$ $T_{\rm eff}$ = 16860K
WD 0316+345
Mass = 0.46$M_\odot$ $T_{\rm eff}$ = 15350K
WD 0326−273
Mass = 0.56$M_\odot$ $T_{\rm eff}$ = 9320K
WD 0339+523
Mass = 0.41$M_\odot$ $T_{\rm eff}$ = 13150K
WD 0341+021
Mass = 0.42$M_\odot$ $T_{\rm eff}$ = 22770K
WD 0349+247
Mass = 1.05$M_\odot$ $T_{\rm eff}$ = 32650K
WD 0352+018
Mass = 0.6$M_\odot$ $T_{\rm eff}$ = 22840K
WD 0352+096
Mass = 0.8$M_\odot$ $T_{\rm eff}$ = 14670K
WD 0354+556
Mass = 0.76$M_\odot$ $T_{\rm eff}$ = 8430K
WD 0402+543
Mass = 0.64$M_\odot$ $T_{\rm eff}$ = 17120K
F_ν (mJy)
Wavelength (μm)
GALEX
Johnson−Cousins
Stromgren
2MASS
Spitzer
WISE
SDSS

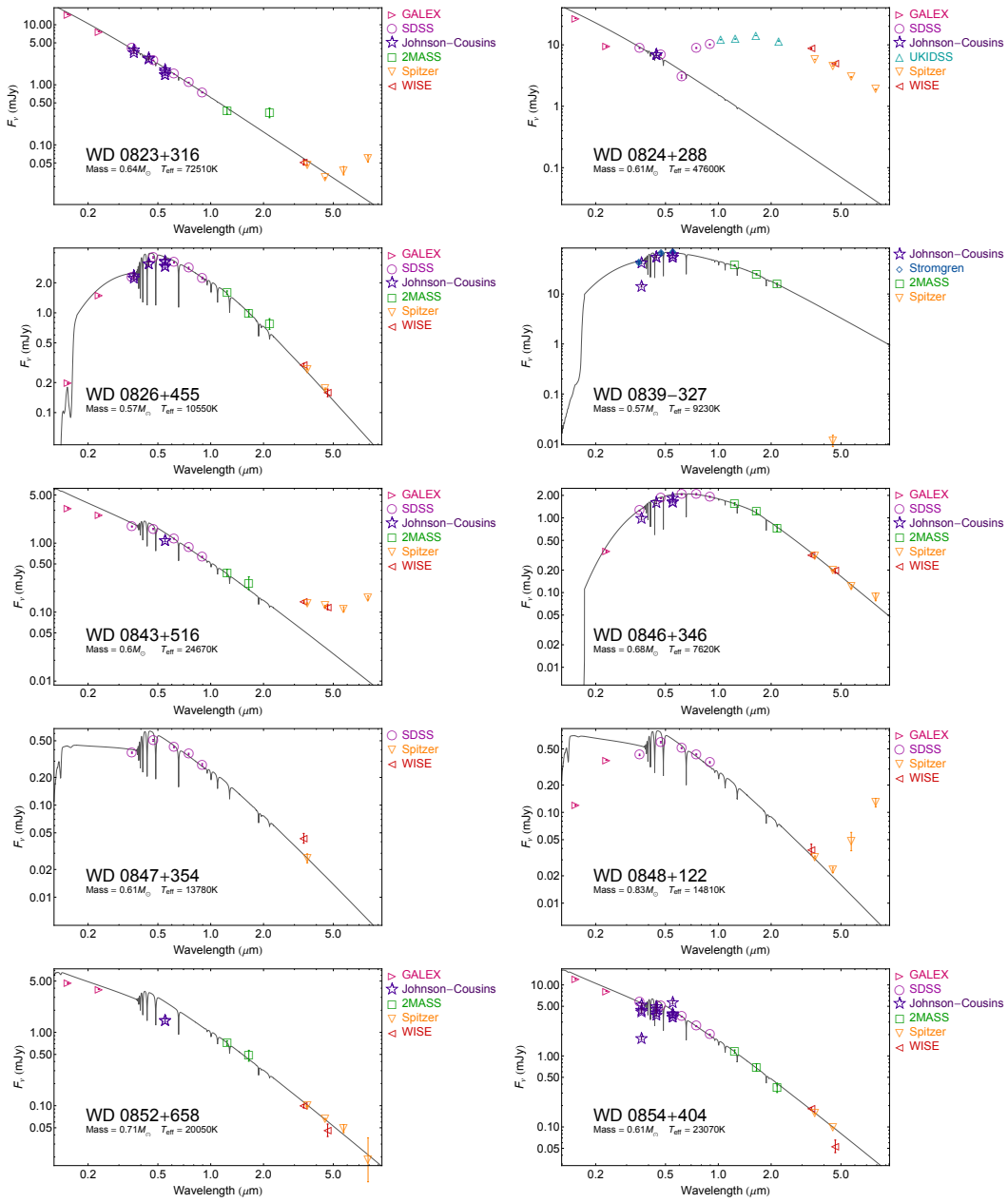

WD 0406+169
Mass = 0.85$M_\odot$ $T_{\rm eff}$ = 15810K
WD 0407+179
Mass = 0.56$M_\odot$ $T_{\rm eff}$ = 14210K
WD 0408−041
Mass = 0.67$M_\odot$ $T_{\rm eff}$ = 15270K
WD 0410+117
Mass = 0.61$M_\odot$ $T_{\rm eff}$ = 21600K
WD 0415+271
Mass = 0.6$M_\odot$ $T_{\rm eff}$ = 11780K
WD 0418+153
Mass = 0.67$M_\odot$ $T_{\rm eff}$ = 14060K
WD 0419−487
Mass = 0.25$M_\odot$ $T_{\rm eff}$ = 6440K
WD 0421+162
Mass = 0.7$M_\odot$ $T_{\rm eff}$ = 20010K
WD 0425+168
Mass = 0.71$M_\odot$ $T_{\rm eff}$ = 25130K
WD 0429+176
Mass = 0.63$M_\odot$ $T_{\rm eff}$ = 17620K
F_ν (mJy)
Wavelength (μm)
GALEX
SDSS
Johnson−Cousins
Stromgren
2MASS
Spitzer
WISE

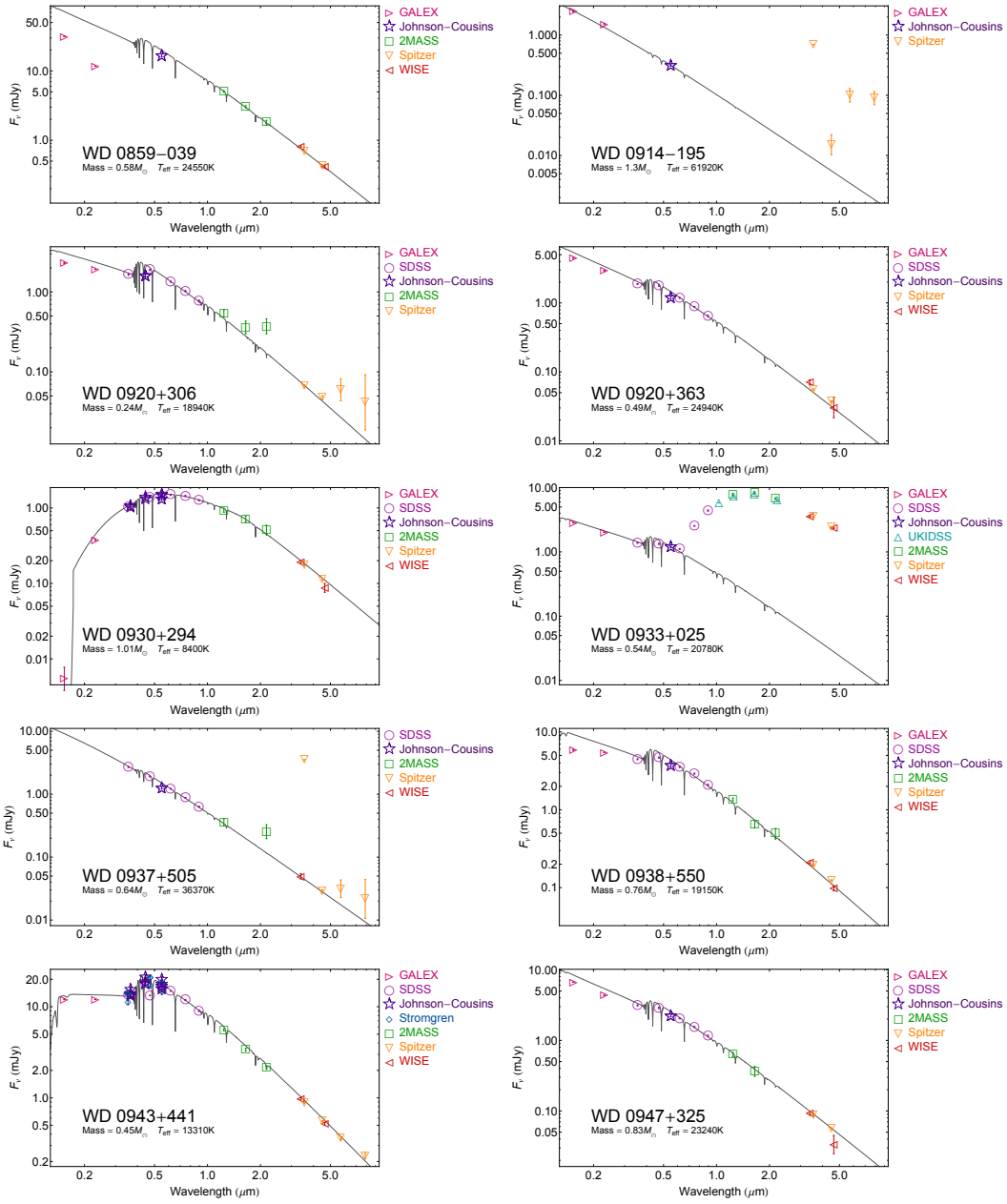

WD 0431+126
Mass = 0.69$M_\odot$ $T_{\rm eff}$ = 21890K
WD 0437+152
Mass = 0.42$M_\odot$ $T_{\rm eff}$ = 19300K
WD 0438+108
Mass = 0.73$M_\odot$ $T_{\rm eff}$ = 27540K
WD 0439+466
Mass = 0.54$M_\odot$ $T_{\rm eff}$ = 86980K
WD 0440−038
Mass = 1.32$M_\odot$ $T_{\rm eff}$ = 60080K
WD 0446−789
Mass = 0.57$M_\odot$ $T_{\rm eff}$ = 24440K
WD 0453+418
Mass = 0.51$M_\odot$ $T_{\rm eff}$ = 14320K
WD 0455−282
Mass = 0.56$M_\odot$ $T_{\rm eff}$ = 63540K
WD 0458+407
Mass = 0.66$M_\odot$ $T_{\rm eff}$ = 14920K
WD 0501+527
Mass = 0.54$M_\odot$ $T_{\rm eff}$ = 60920K
F_ν (mJy)
Wavelength (μm)
GALEX
SDSS
Johnson−Cousins
Stromgren
2MASS
Spitzer
WISE

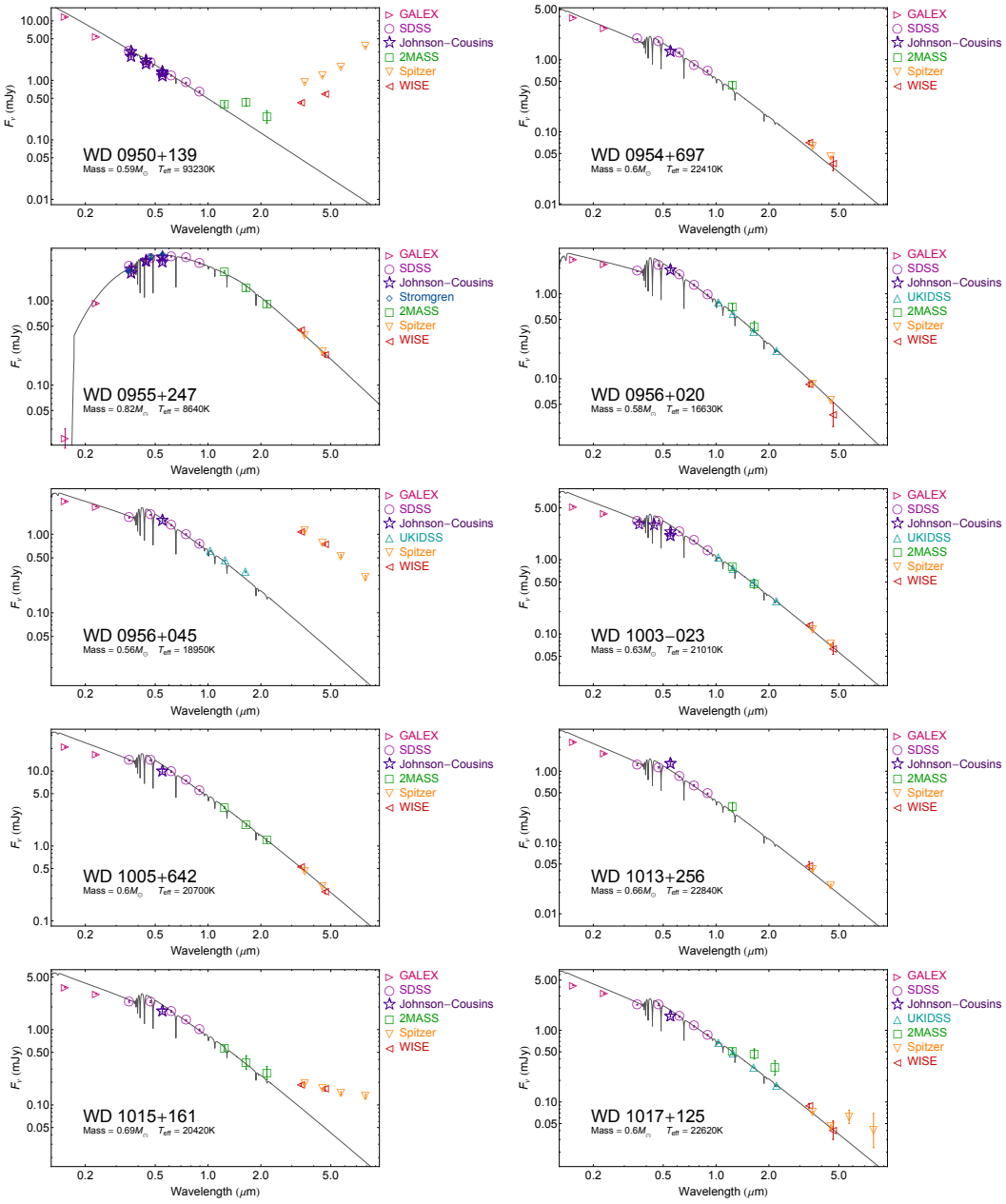

WD 0507+045.1
Mass = 0.75$M_\odot$ $T_{\rm eff}$ = 12290K
WD 0507+045.2
Mass = 0.67$M_\odot$ $T_{\rm eff}$ = 21550K
WD 0509−007
Mass = 0.42$M_\odot$ $T_{\rm eff}$ = 32450K
WD 0516+365
Mass = 0.6$M_\odot$ $T_{\rm eff}$ = 31850K
WD 0517+307
Mass = 0.68$M_\odot$ $T_{\rm eff}$ = 12430K
WD 0518−105
Mass = 1.08$M_\odot$ $T_{\rm eff}$ = 33200K
WD 0531−022
Mass = 1.03$M_\odot$ $T_{\rm eff}$ = 30330K
WD 0533+322
Mass = 0.43$M_\odot$ $T_{\rm eff}$ = 16970K
WD 0543+579
Mass = 0.77$M_\odot$ $T_{\rm eff}$ = 9960K
WD 0546+265
Mass = 0.55$M_\odot$ $T_{\rm eff}$ = 12650K
F_ν (mJy)
Wavelength (μm)
GALEX
SDSS
Johnson−Cousins
2MASS
Spitzer
WISE

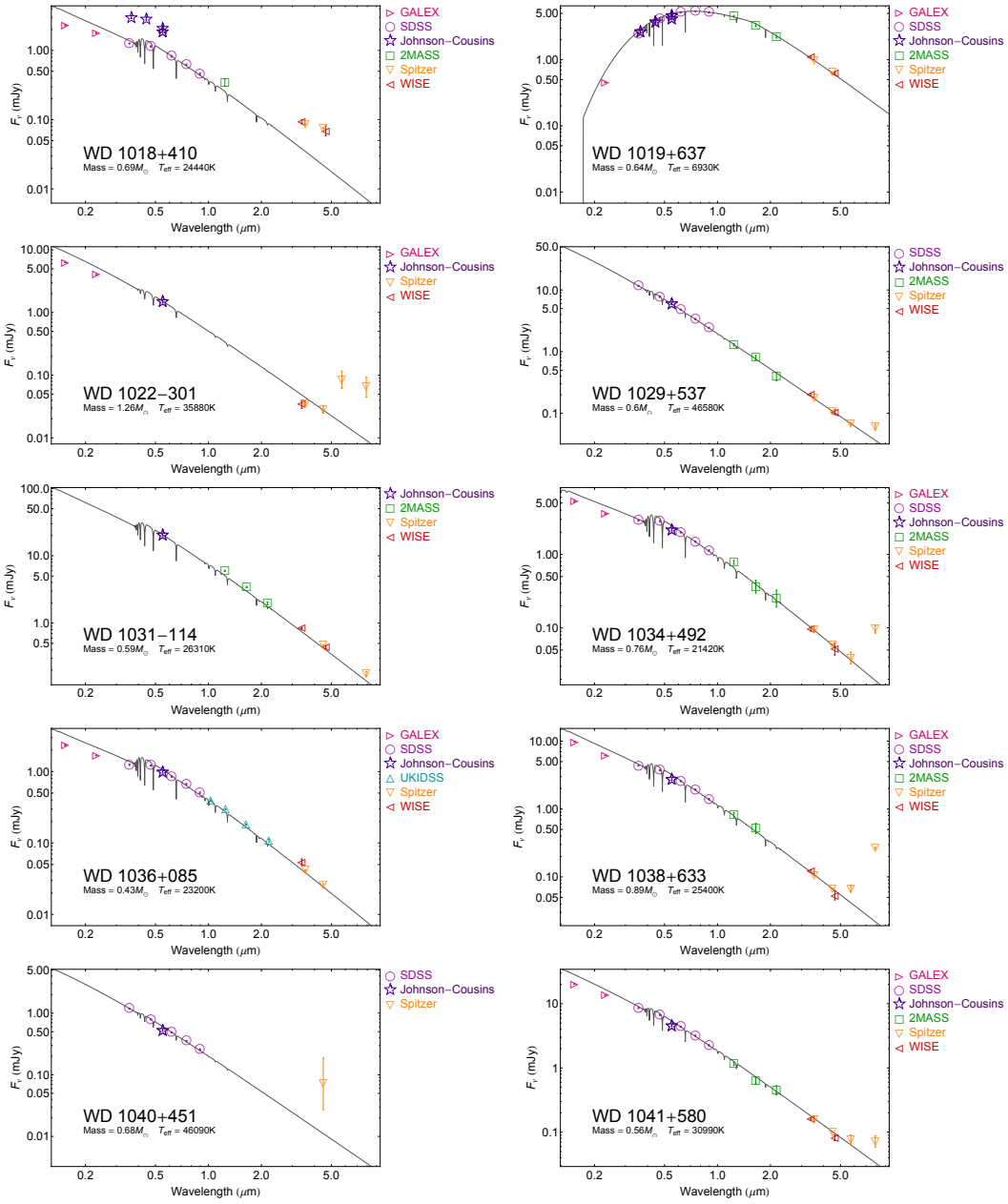

WD 0549+158
Mass = 0.62$M_\odot$ $T_{\rm eff}$ = 33590K
WD 0557+237
Mass = 0.7$M_\odot$ $T_{\rm eff}$ = 8360K
WD 0612+177
Mass = 0.63$M_\odot$ $T_{\rm eff}$ = 26150K
WD 0618+067
Mass = 0.51$M_\odot$ $T_{\rm eff}$ = 5940K
WD 0618+134
Mass = 0.65$M_\odot$ $T_{\rm eff}$ = 52790K
WD 0621−376
Mass = 0.41$M_\odot$ $T_{\rm eff}$ = 66060K
WD 0642−166
Mass = 0.98$M_\odot$ $T_{\rm eff}$ = 25970K
WD 0644+025
Mass = 0.95$M_\odot$ $T_{\rm eff}$ = 7190K
WD 0644+375
Mass = 0.69$M_\odot$ $T_{\rm eff}$ = 22290K
WD 0648+641
Mass = 0.76$M_\odot$ $T_{\rm eff}$ = 6000K
F_ν (mJy)
Wavelength (μm)
GALEX
SDSS
Johnson−Cousins
Stromgren
2MASS
Spitzer
WISE

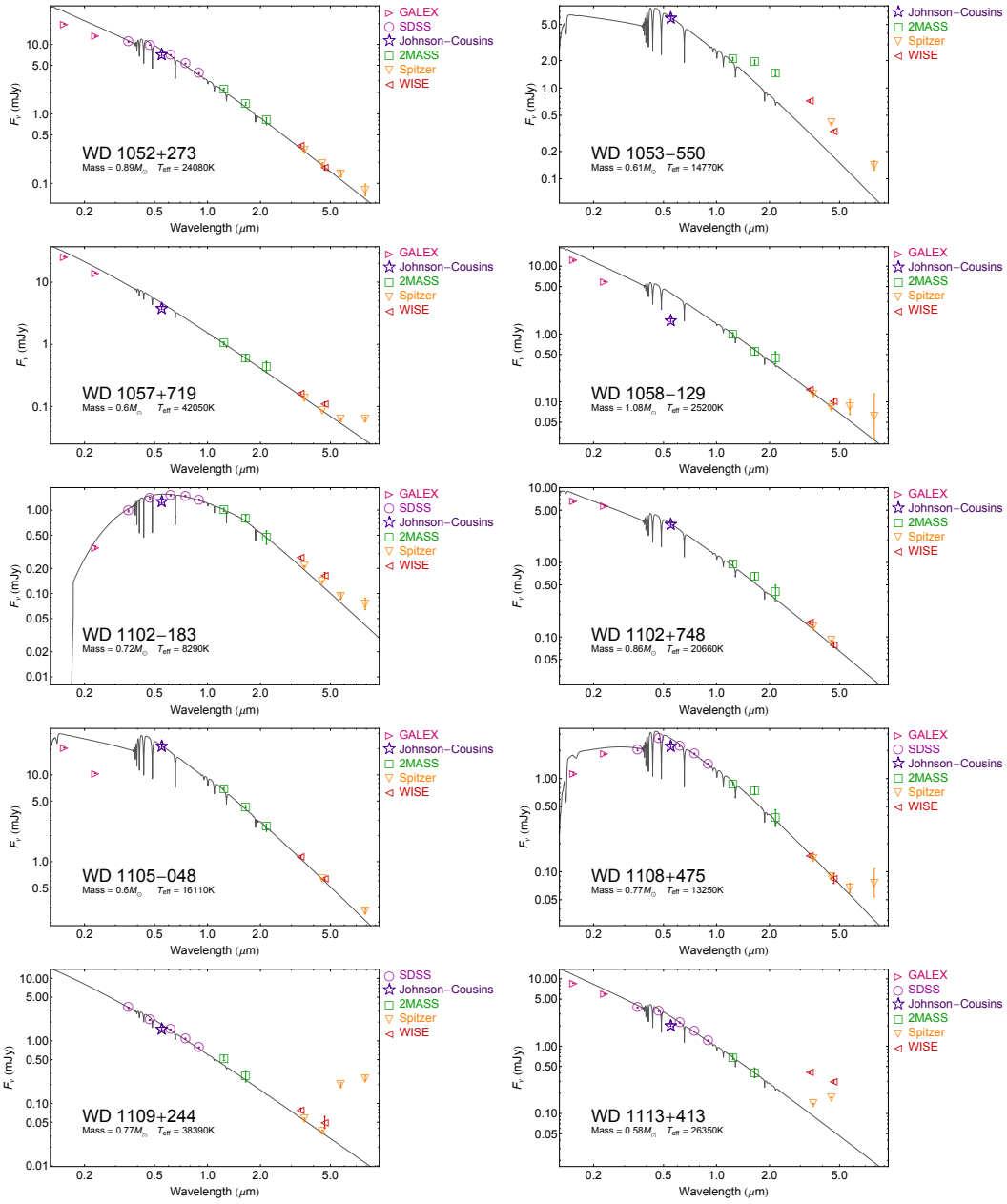

WD 0651−020
Mass = 0.82$M_\odot$ $T_{\rm eff}$ = 34220K
WD 0659−063
Mass = 0.82$M_\odot$ $T_{\rm eff}$ = 6620K
WD 0730+487
Mass = 0.97$M_\odot$ $T_{\rm eff}$ = 15010K
WD 0732−427
Mass = 0.68$M_\odot$ $T_{\rm eff}$ = 15570K
WD 0752−676
Mass = 0.46$M_\odot$ $T_{\rm eff}$ = 5600K
WD 0752+365
Mass = 0.68$M_\odot$ $T_{\rm eff}$ = 7860K
WD 0808+595
Mass = 0.42$M_\odot$ $T_{\rm eff}$ = 28100K
WD 0816+297
Mass = 0.58$M_\odot$ $T_{\rm eff}$ = 17200K
WD 0817+386
Mass = 0.66$M_\odot$ $T_{\rm eff}$ = 26070K
WD 0819+363
Mass = 0.69$M_\odot$ $T_{\rm eff}$ = 19580K
F_ν (mJy)
Wavelength (μm)
GALEX
SDSS
Johnson−Cousins
Stromgren
UKIDSS
2MASS
Spitzer
WISE

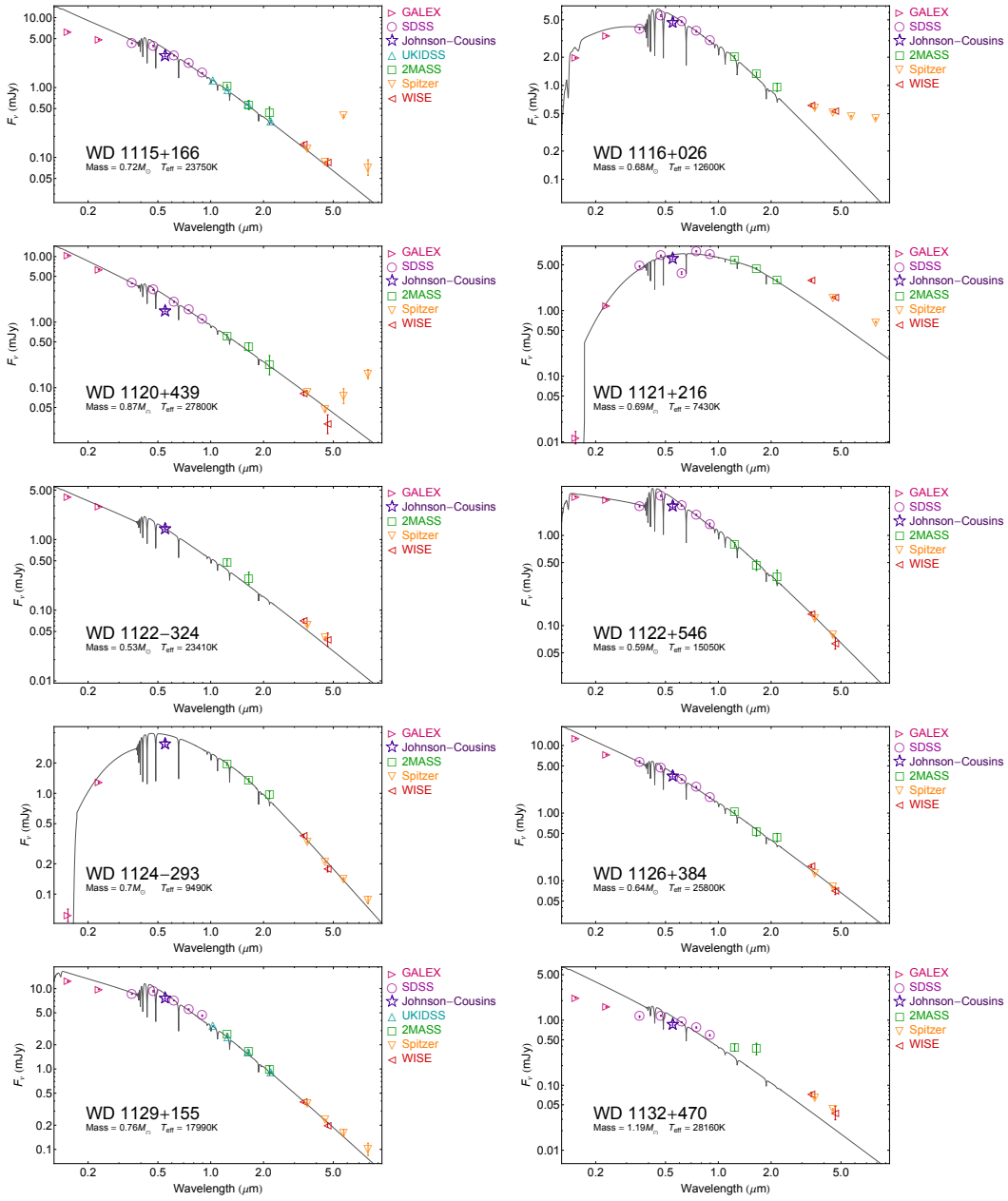

WD 0823+316
Mass = 0.64$M_\odot$ $T_{\rm eff}$ = 72510K
WD 0824+288
Mass = 0.61$M_\odot$ $T_{\rm eff}$ = 47600K
WD 0826+455
Mass = 0.57$M_\odot$ $T_{\rm eff}$ = 10550K
WD 0839−327
Mass = 0.57$M_\odot$ $T_{\rm eff}$ = 9230K
WD 0843+516
Mass = 0.6$M_\odot$ $T_{\rm eff}$ = 24670K
WD 0846+346
Mass = 0.68$M_\odot$ $T_{\rm eff}$ = 7620K
WD 0847+354
Mass = 0.61$M_\odot$ $T_{\rm eff}$ = 13780K
WD 0848+122
Mass = 0.83$M_\odot$ $T_{\rm eff}$ = 14810K
WD 0852+658
Mass = 0.71$M_\odot$ $T_{\rm eff}$ = 20050K
WD 0854+404
Mass = 0.61$M_\odot$ $T_{\rm eff}$ = 23070K
F_ν (mJy)
Wavelength (μm)
GALEX
SDSS
Johnson−Cousins
Stromgren
2MASS
UKIDSS
Spitzer
WISE

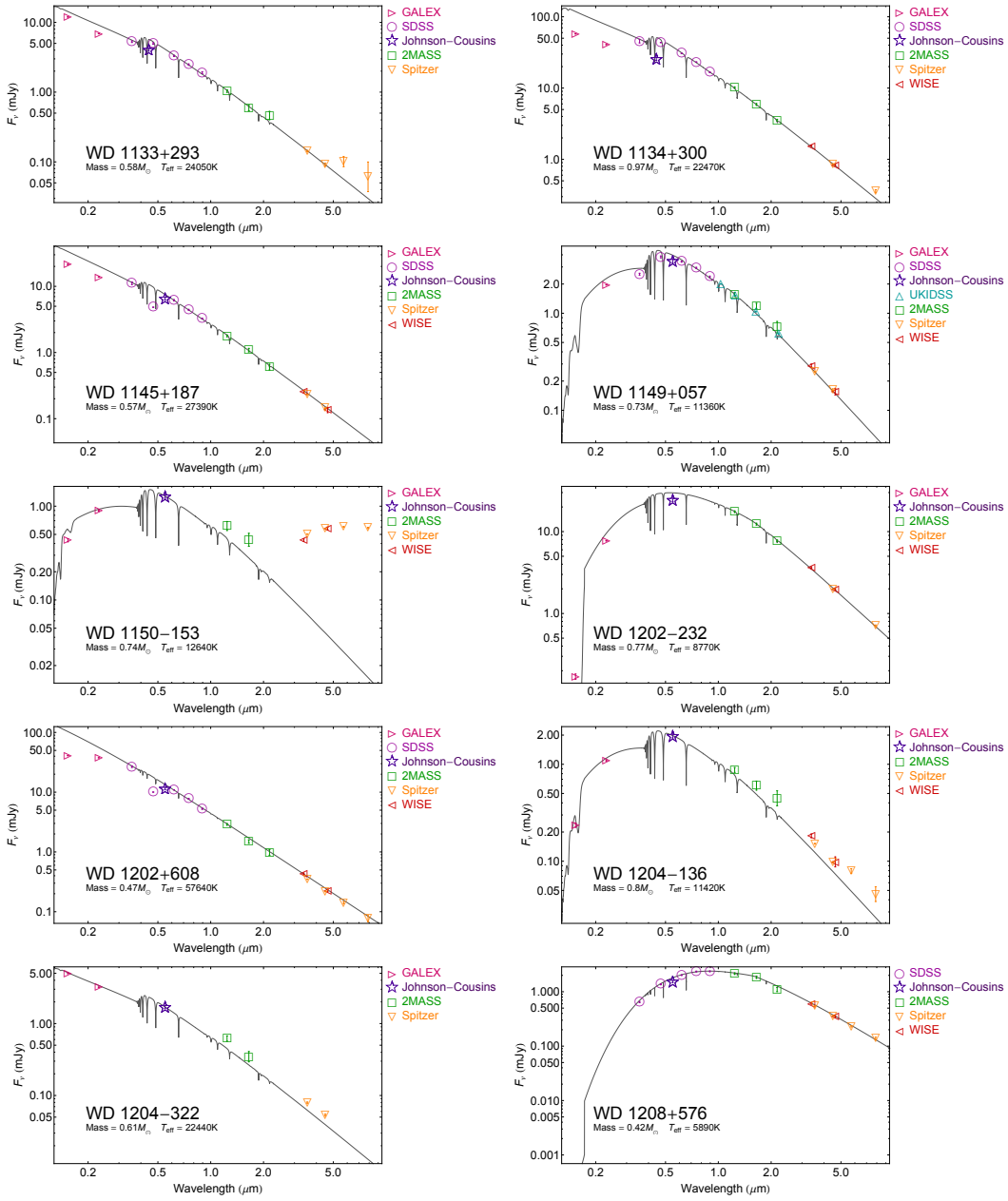

WD 0859−039
Mass = 0.58$M_\odot$ $T_{\rm eff}$ = 24550K
GALEX
Johnson−Cousins
2MASS
Spitzer
WISE
WD 0914−195
Mass = 1.3$M_\odot$ $T_{\rm eff}$ = 61920K
GALEX
Johnson−Cousins
Spitzer
WD 0920+306
Mass = 0.24$M_\odot$ $T_{\rm eff}$ = 18940K
GALEX
SDSS
Johnson−Cousins
2MASS
Spitzer
WD 0920+363
Mass = 0.49$M_\odot$ $T_{\rm eff}$ = 24940K
GALEX
SDSS
Johnson−Cousins
Spitzer
WISE
WD 0930+294
Mass = 1.01$M_\odot$ $T_{\rm eff}$ = 8400K
GALEX
SDSS
Johnson−Cousins
2MASS
Spitzer
WISE
WD 0933+025
Mass = 0.54$M_\odot$ $T_{\rm eff}$ = 20780K
GALEX
SDSS
Johnson−Cousins
UKIDSS
2MASS
Spitzer
WISE
WD 0937+505
Mass = 0.64$M_\odot$ $T_{\rm eff}$ = 36370K
SDSS
Johnson−Cousins
2MASS
Spitzer
WISE
WD 0938+550
Mass = 0.76$M_\odot$ $T_{\rm eff}$ = 19150K
GALEX
SDSS
Johnson−Cousins
2MASS
Spitzer
WISE
WD 0943+441
Mass = 0.45$M_\odot$ $T_{\rm eff}$ = 13310K
GALEX
SDSS
Johnson−Cousins
Stromgren
2MASS
Spitzer
WISE
WD 0947+325
Mass = 0.83$M_\odot$ $T_{\rm eff}$ = 23240K
GALEX
SDSS
Johnson−Cousins
2MASS
Spitzer
WISE
F_ν (mJy)
Wavelength (μm)

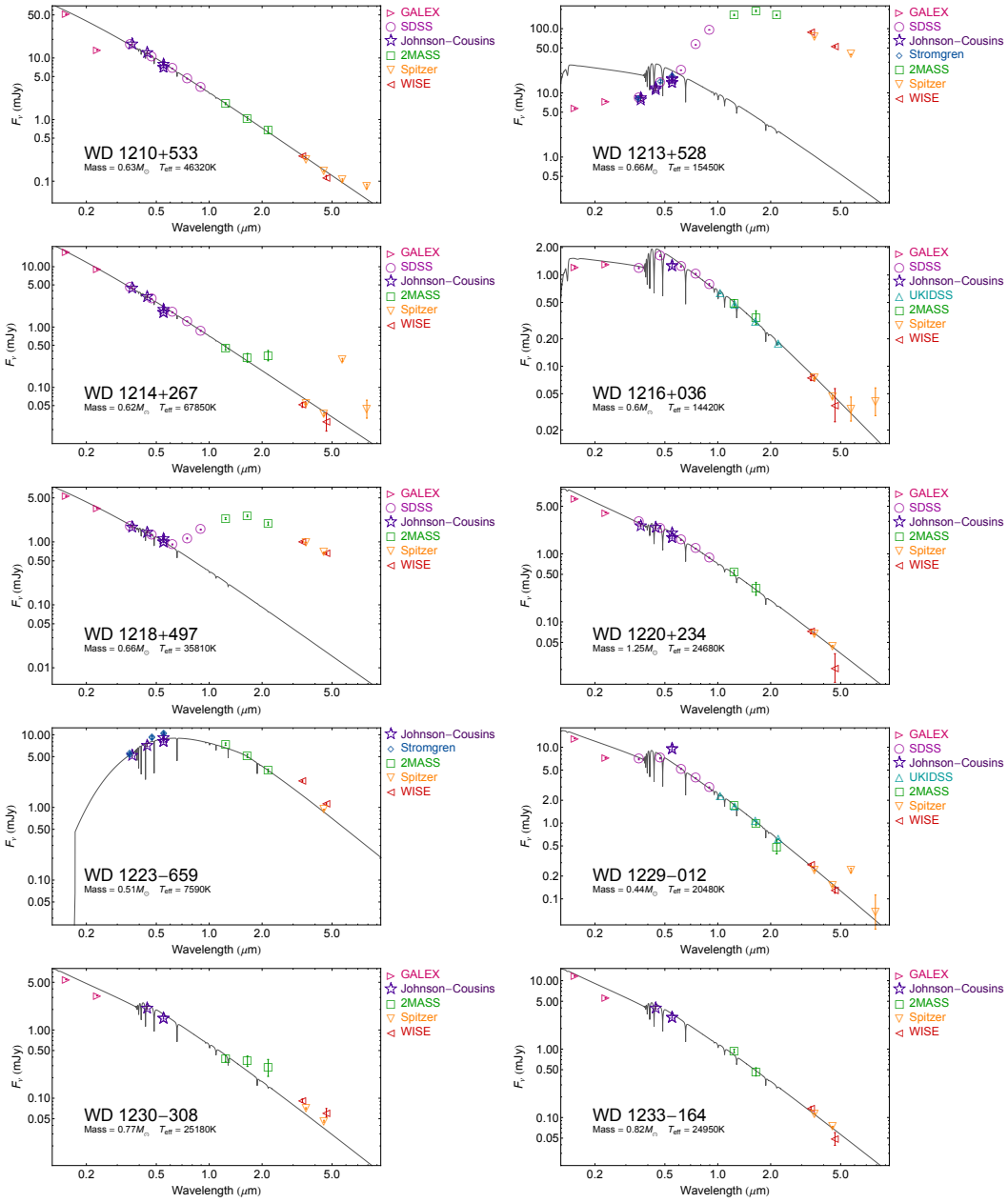

WD 0950+139
Mass = 0.59$M_\odot$ $T_{\rm eff}$ = 93230K
WD 0954+697
Mass = 0.6$M_\odot$ $T_{\rm eff}$ = 22410K
WD 0955+247
Mass = 0.82$M_\odot$ $T_{\rm eff}$ = 8640K
WD 0956+020
Mass = 0.58$M_\odot$ $T_{\rm eff}$ = 16630K
WD 0956+045
Mass = 0.56$M_\odot$ $T_{\rm eff}$ = 18950K
WD 1003−023
Mass = 0.63$M_\odot$ $T_{\rm eff}$ = 21010K
WD 1005+642
Mass = 0.6$M_\odot$ $T_{\rm eff}$ = 20700K
WD 1013+256
Mass = 0.66$M_\odot$ $T_{\rm eff}$ = 22840K
WD 1015+161
Mass = 0.69$M_\odot$ $T_{\rm eff}$ = 20420K
WD 1017+125
Mass = 0.6$M_\odot$ $T_{\rm eff}$ = 22620K
F_ν (mJy)
Wavelength (μm)
GALEX
SDSS
Johnson−Cousins
Stromgren
UKIDSS
2MASS
Spitzer
WISE

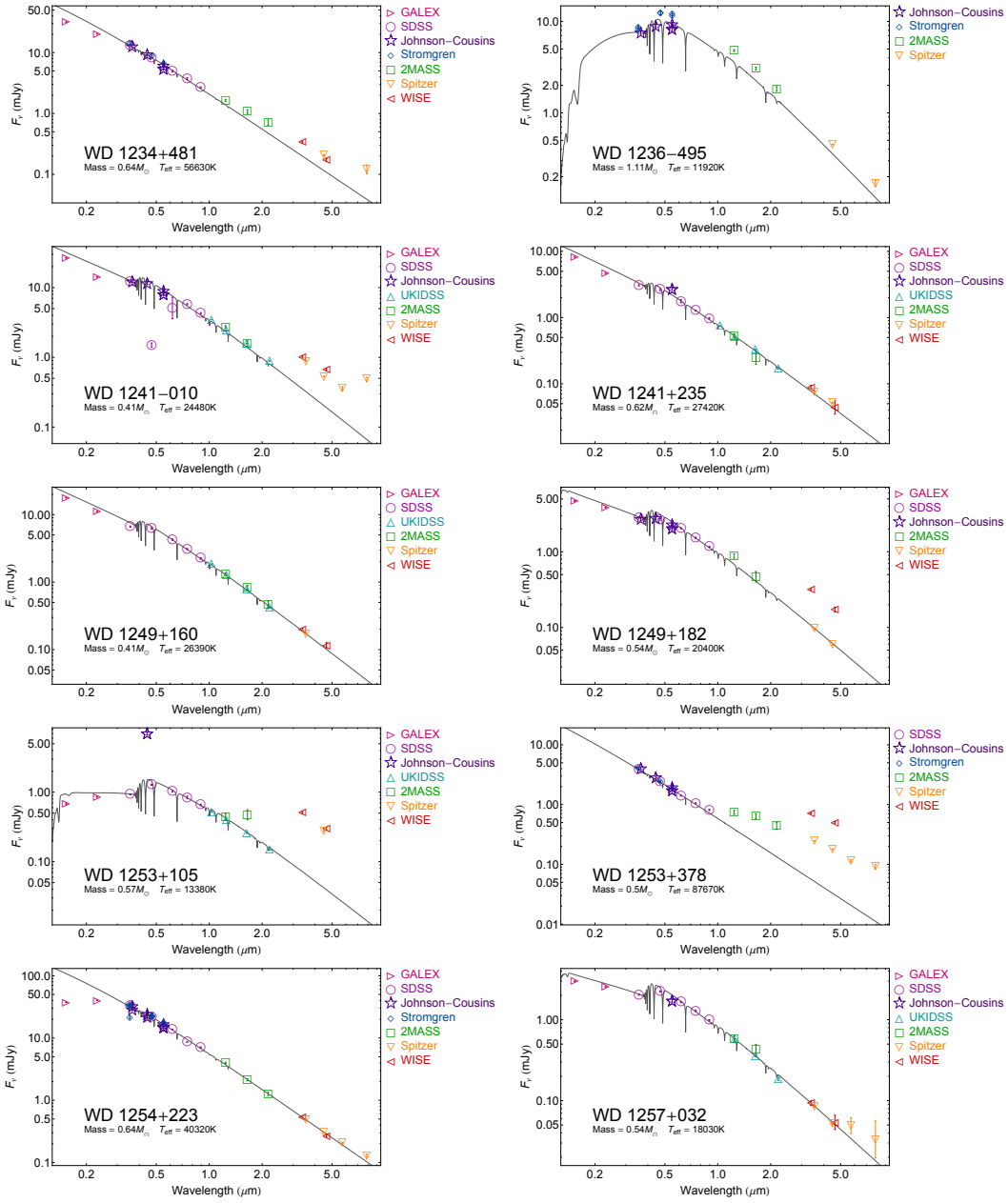

WD 1018+410
Mass = 0.69$M_\odot$ $T_{\rm eff}$ = 24440K
WD 1019+637
Mass = 0.64$M_\odot$ $T_{\rm eff}$ = 6930K
WD 1022−301
Mass = 1.26$M_\odot$ $T_{\rm eff}$ = 35880K
WD 1029+537
Mass = 0.6$M_\odot$ $T_{\rm eff}$ = 46580K
WD 1031−114
Mass = 0.59$M_\odot$ $T_{\rm eff}$ = 26310K
WD 1034+492
Mass = 0.76$M_\odot$ $T_{\rm eff}$ = 21420K
WD 1036+085
Mass = 0.43$M_\odot$ $T_{\rm eff}$ = 23200K
WD 1038+633
Mass = 0.89$M_\odot$ $T_{\rm eff}$ = 25400K
WD 1040+451
Mass = 0.68$M_\odot$ $T_{\rm eff}$ = 46090K
WD 1041+580
Mass = 0.56$M_\odot$ $T_{\rm eff}$ = 30990K
F_ν (mJy)
Wavelength (μm)
GALEX
SDSS
Johnson−Cousins
2MASS
UKIDSS
Spitzer
WISE

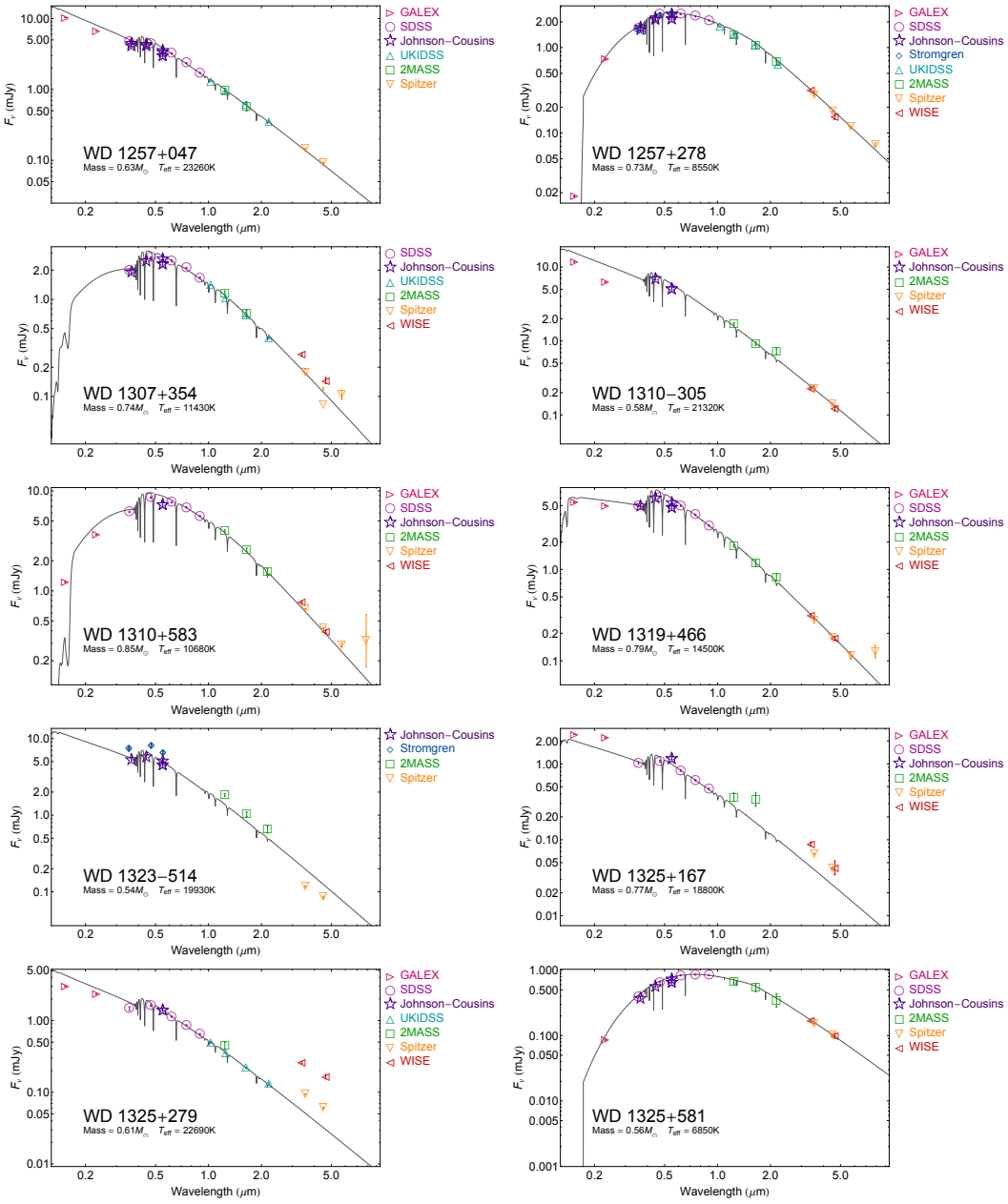

WD 1052+273
Mass = 0.89$M_\odot$ $T_{\rm eff}$ = 24080K
WD 1053−550
Mass = 0.61$M_\odot$ $T_{\rm eff}$ = 14770K
WD 1057+719
Mass = 0.6$M_\odot$ $T_{\rm eff}$ = 42050K
WD 1058−129
Mass = 1.08$M_\odot$ $T_{\rm eff}$ = 25200K
WD 1102−183
Mass = 0.72$M_\odot$ $T_{\rm eff}$ = 8290K
WD 1102+748
Mass = 0.86$M_\odot$ $T_{\rm eff}$ = 20660K
WD 1105−048
Mass = 0.6$M_\odot$ $T_{\rm eff}$ = 16110K
WD 1108+475
Mass = 0.77$M_\odot$ $T_{\rm eff}$ = 13250K
WD 1109+244
Mass = 0.77$M_\odot$ $T_{\rm eff}$ = 38390K
WD 1113+413
Mass = 0.58$M_\odot$ $T_{\rm eff}$ = 26350K
F_ν (mJy)
Wavelength (μm)
GALEX
SDSS
Johnson−Cousins
2MASS
Spitzer
WISE

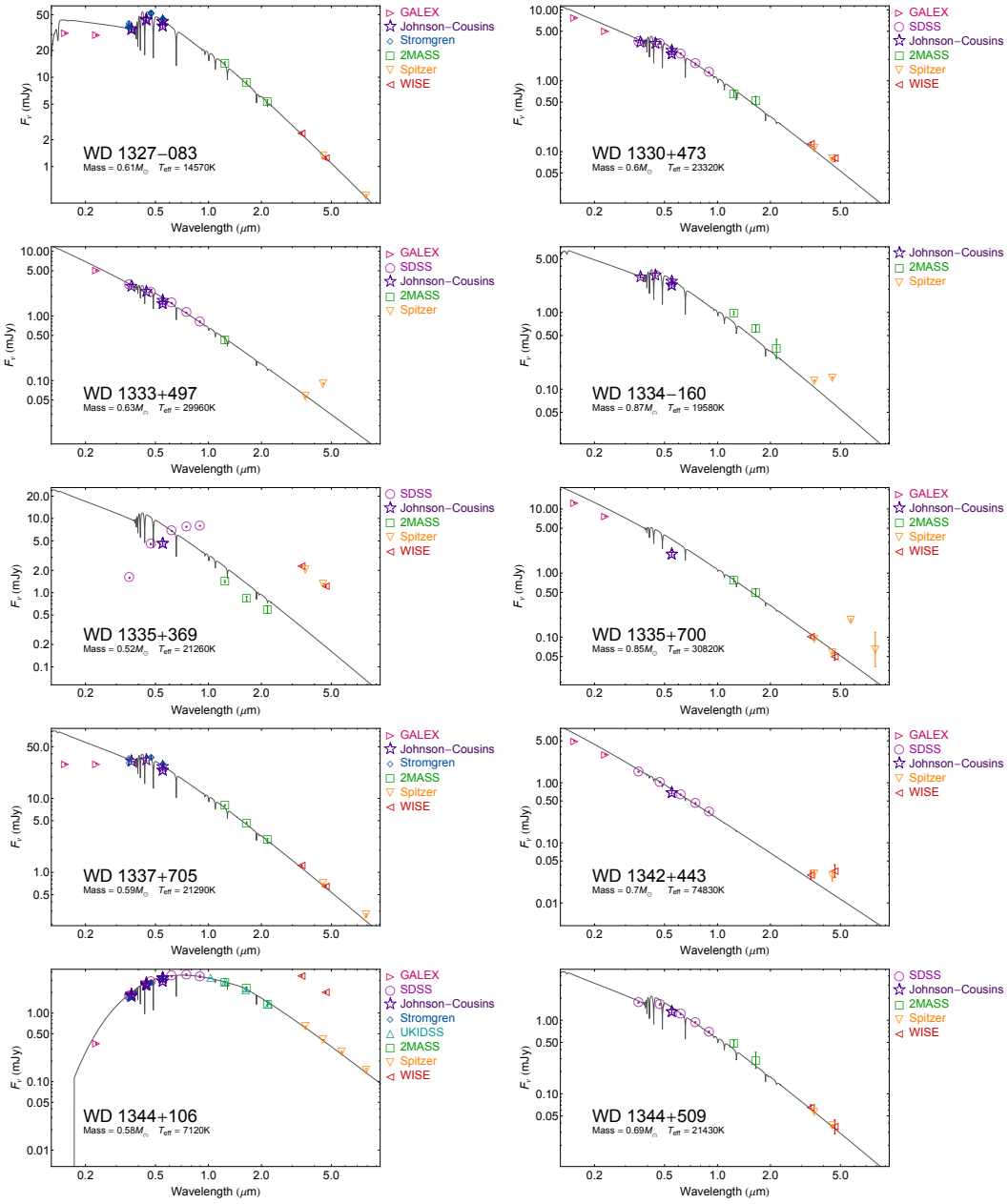

WD 1115+166
Mass = 0.72$M_\odot$ $T_{\rm eff}$ = 23750K
WD 1116+026
Mass = 0.68$M_\odot$ $T_{\rm eff}$ = 12600K
WD 1120+439
Mass = 0.87$M_\odot$ $T_{\rm eff}$ = 27800K
WD 1121+216
Mass = 0.69$M_\odot$ $T_{\rm eff}$ = 7430K
WD 1122−324
Mass = 0.53$M_\odot$ $T_{\rm eff}$ = 23410K
WD 1122+546
Mass = 0.59$M_\odot$ $T_{\rm eff}$ = 15050K
WD 1124−293
Mass = 0.7$M_\odot$ $T_{\rm eff}$ = 9490K
WD 1126+384
Mass = 0.64$M_\odot$ $T_{\rm eff}$ = 25800K
WD 1129+155
Mass = 0.76$M_\odot$ $T_{\rm eff}$ = 17990K
WD 1132+470
Mass = 1.19$M_\odot$ $T_{\rm eff}$ = 28160K
F_ν (mJy)
Wavelength (μm)
GALEX
SDSS
Johnson−Cousins
UKIDSS
2MASS
Spitzer
WISE

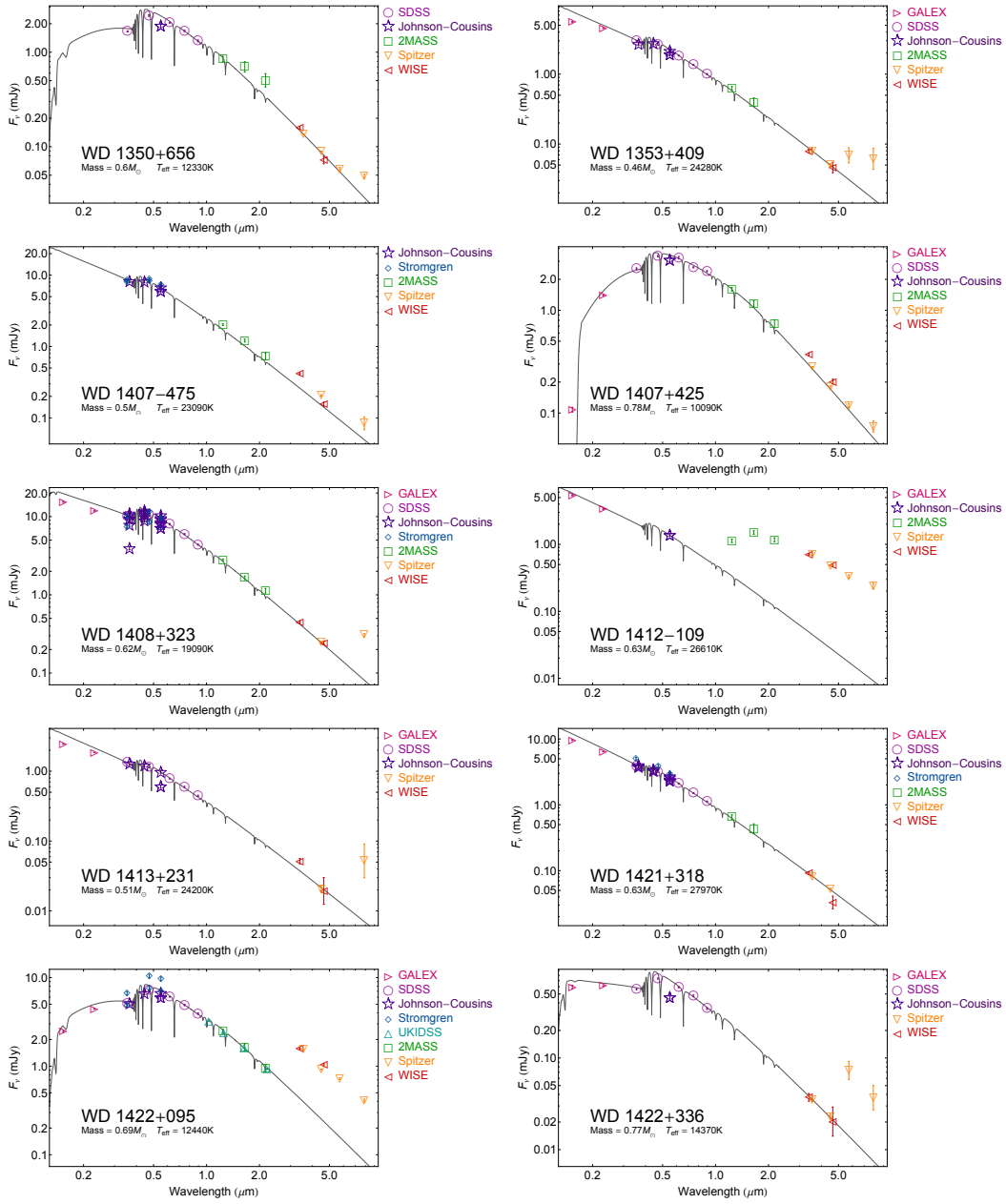

WD 1133+293
Mass = 0.58$M_\odot$ $T_{\rm eff}$ = 24050K
WD 1134+300
Mass = 0.97$M_\odot$ $T_{\rm eff}$ = 22470K
WD 1145+187
Mass = 0.57$M_\odot$ $T_{\rm eff}$ = 27390K
WD 1149+057
Mass = 0.73$M_\odot$ $T_{\rm eff}$ = 11360K
WD 1150−153
Mass = 0.74$M_\odot$ $T_{\rm eff}$ = 12640K
WD 1202−232
Mass = 0.77$M_\odot$ $T_{\rm eff}$ = 8770K
WD 1202+608
Mass = 0.47$M_\odot$ $T_{\rm eff}$ = 57640K
WD 1204−136
Mass = 0.8$M_\odot$ $T_{\rm eff}$ = 11420K
WD 1204−322
Mass = 0.61$M_\odot$ $T_{\rm eff}$ = 22440K
WD 1208+576
Mass = 0.42$M_\odot$ $T_{\rm eff}$ = 5890K
F_ν (mJy)
Wavelength (μm)
GALEX
SDSS
Johnson−Cousins
UKIDSS
2MASS
Spitzer
WISE

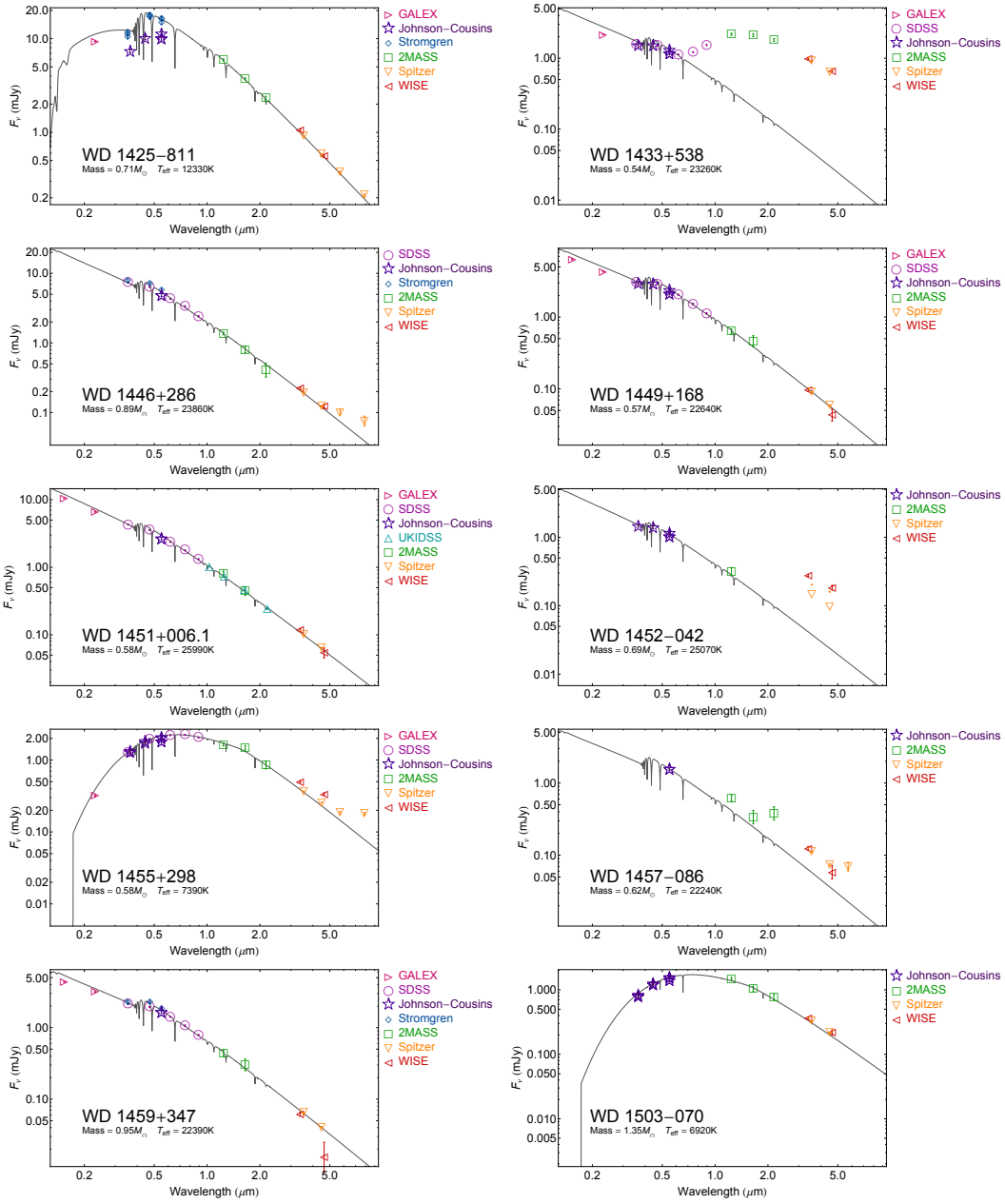

WD 1210+533
Mass = 0.63$M_\odot$ $T_{\rm eff}$ = 46320K
WD 1213+528
Mass = 0.66$M_\odot$ $T_{\rm eff}$ = 15450K
WD 1214+267
Mass = 0.62$M_\odot$ $T_{\rm eff}$ = 67850K
WD 1216+036
Mass = 0.6$M_\odot$ $T_{\rm eff}$ = 14420K
WD 1218+497
Mass = 0.66$M_\odot$ $T_{\rm eff}$ = 35810K
WD 1220+234
Mass = 1.25$M_\odot$ $T_{\rm eff}$ = 24680K
WD 1223−659
Mass = 0.51$M_\odot$ $T_{\rm eff}$ = 7590K
WD 1229−012
Mass = 0.44$M_\odot$ $T_{\rm eff}$ = 20480K
WD 1230−308
Mass = 0.77$M_\odot$ $T_{\rm eff}$ = 25180K
WD 1233−164
Mass = 0.82$M_\odot$ $T_{\rm eff}$ = 24950K
F_ν (mJy)
Wavelength (μm)
GALEX
SDSS
Johnson−Cousins
Stromgren
UKIDSS
2MASS
Spitzer
WISE

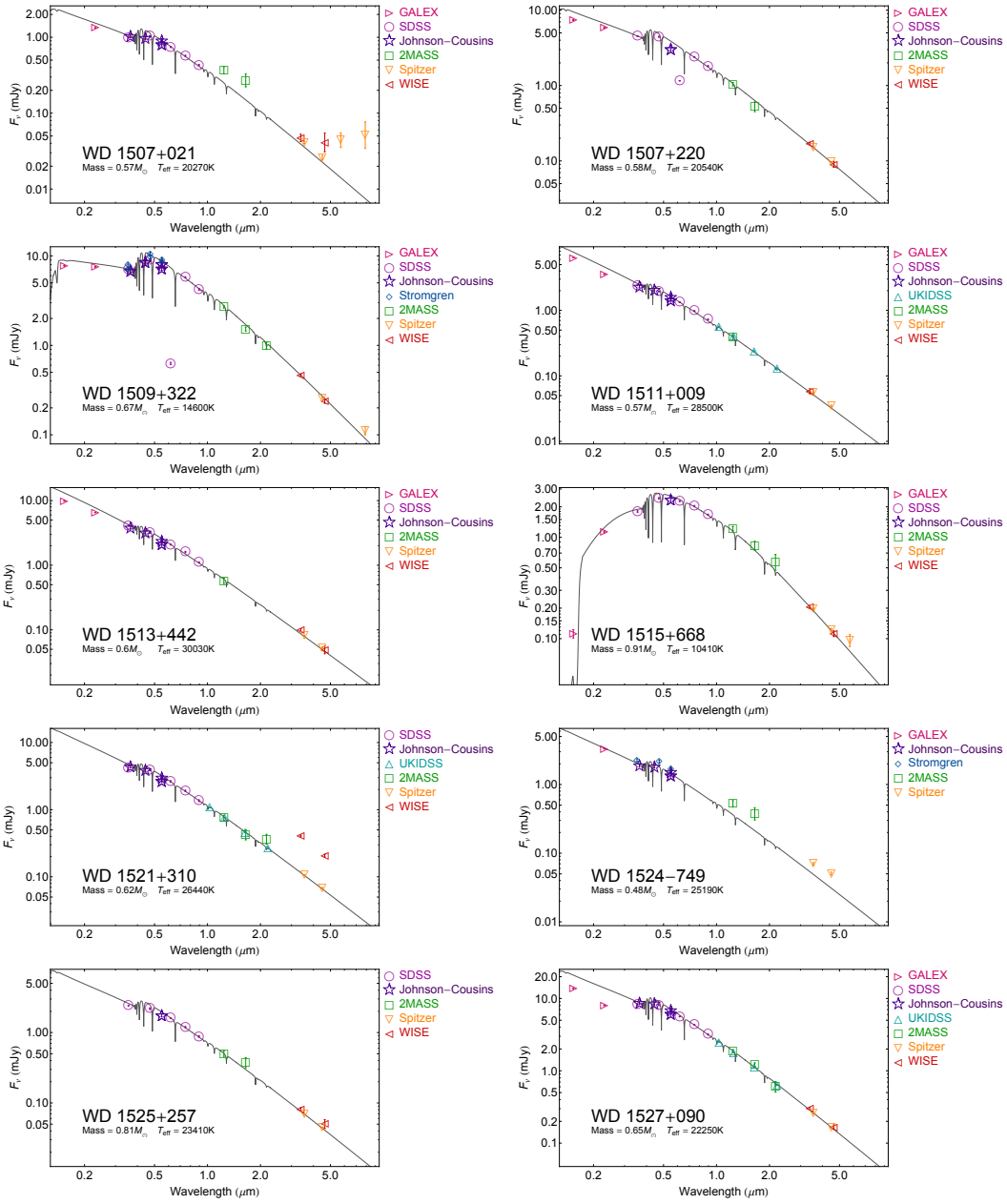

WD 1234+481
Mass = 0.64$M_\odot$ $T_{\rm eff}$ = 56630K
WD 1236−495
Mass = 1.11$M_\odot$ $T_{\rm eff}$ = 11920K
WD 1241−010
Mass = 0.41$M_\odot$ $T_{\rm eff}$ = 24480K
WD 1241+235
Mass = 0.62$M_\odot$ $T_{\rm eff}$ = 27420K
WD 1249+160
Mass = 0.41$M_\odot$ $T_{\rm eff}$ = 26390K
WD 1249+182
Mass = 0.54$M_\odot$ $T_{\rm eff}$ = 20400K
WD 1253+105
Mass = 0.57$M_\odot$ $T_{\rm eff}$ = 13380K
WD 1253+378
Mass = 0.5$M_\odot$ $T_{\rm eff}$ = 87670K
WD 1254+223
Mass = 0.64$M_\odot$ $T_{\rm eff}$ = 40320K
WD 1257+032
Mass = 0.54$M_\odot$ $T_{\rm eff}$ = 18030K
F_ν (mJy)
Wavelength (μm)
GALEX
SDSS
Johnson−Cousins
Stromgren
UKIDSS
2MASS
Spitzer
WISE

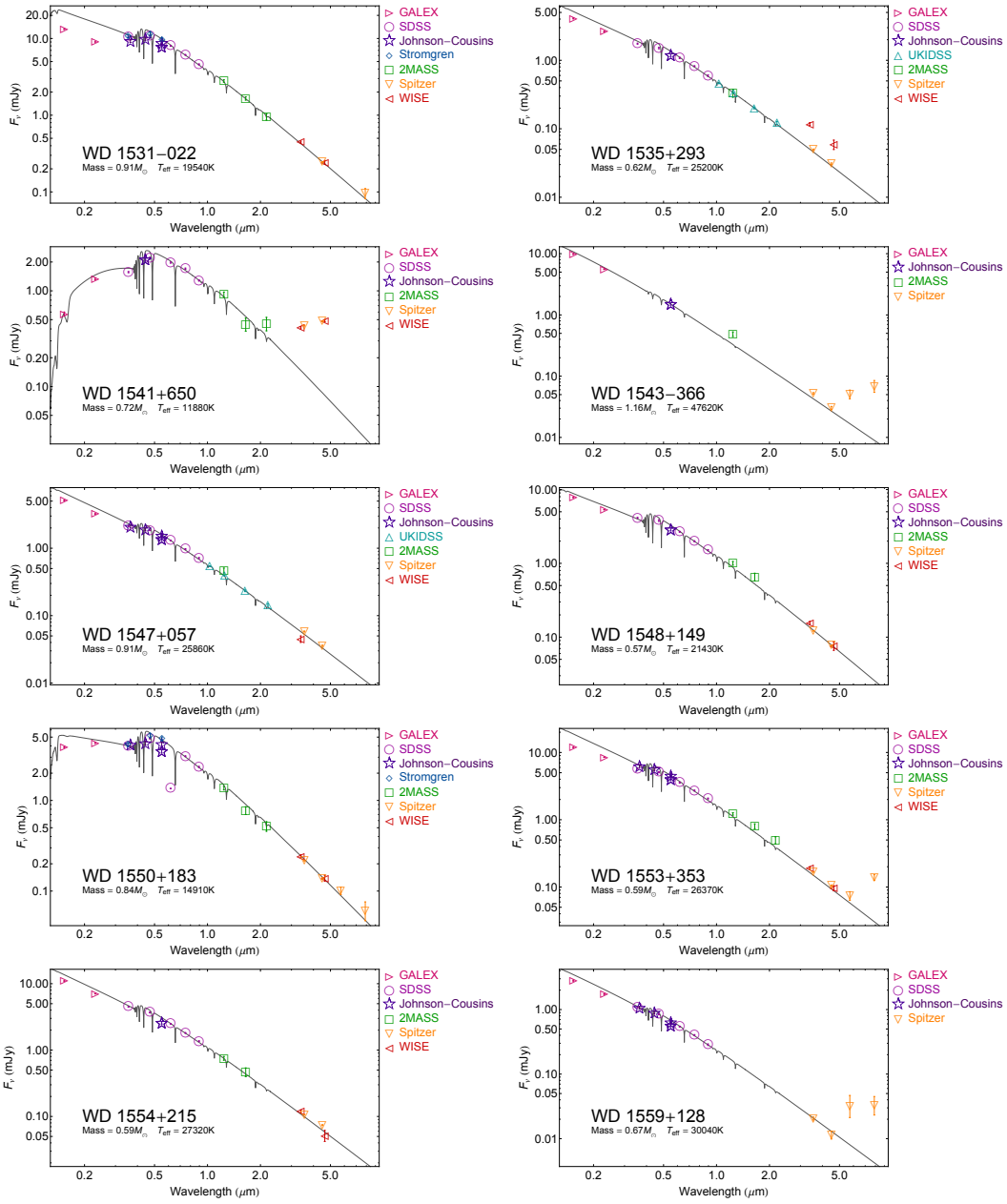

WD 1257+047
Mass = 0.63$M_\odot$ $T_{\rm eff}$ = 23260K
WD 1257+278
Mass = 0.73$M_\odot$ $T_{\rm eff}$ = 8550K
WD 1307+354
Mass = 0.74$M_\odot$ $T_{\rm eff}$ = 11430K
WD 1310−305
Mass = 0.58$M_\odot$ $T_{\rm eff}$ = 21320K
WD 1310+583
Mass = 0.85$M_\odot$ $T_{\rm eff}$ = 10680K
WD 1319+466
Mass = 0.79$M_\odot$ $T_{\rm eff}$ = 14500K
WD 1323−514
Mass = 0.54$M_\odot$ $T_{\rm eff}$ = 19930K
WD 1325+167
Mass = 0.77$M_\odot$ $T_{\rm eff}$ = 18800K
WD 1325+279
Mass = 0.61$M_\odot$ $T_{\rm eff}$ = 22690K
WD 1325+581
Mass = 0.56$M_\odot$ $T_{\rm eff}$ = 6850K
F_ν (mJy)
Wavelength (μm)
GALEX
SDSS
Johnson−Cousins
Stromgren
UKIDSS
2MASS
Spitzer
WISE

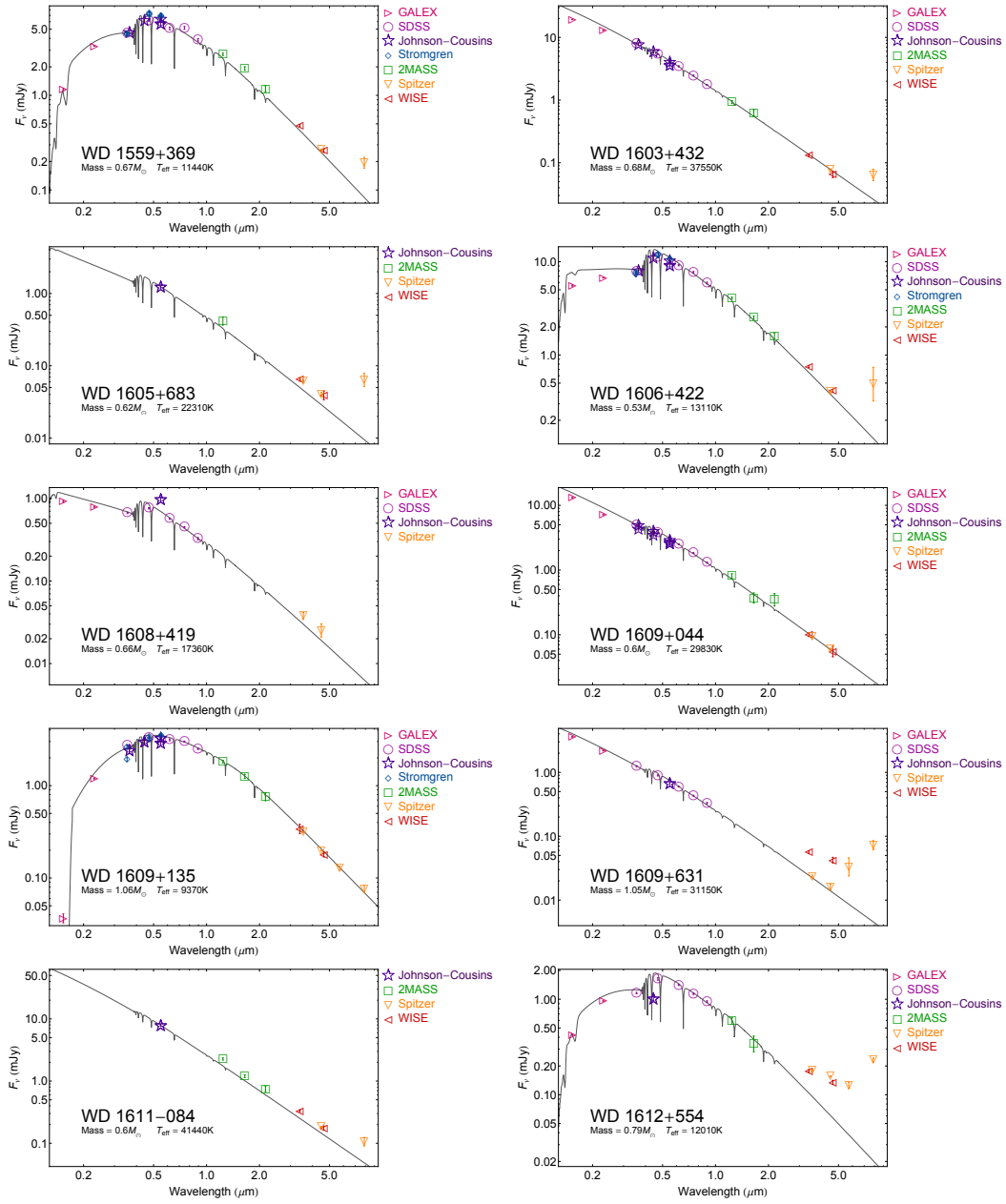

WD 1327−083
Mass = 0.61$M_\odot$ $T_{\rm eff}$ = 14570K
WD 1330+473
Mass = 0.6$M_\odot$ $T_{\rm eff}$ = 23320K
WD 1333+497
Mass = 0.63$M_\odot$ $T_{\rm eff}$ = 29960K
WD 1334−160
Mass = 0.87$M_\odot$ $T_{\rm eff}$ = 19580K
WD 1335+369
Mass = 0.52$M_\odot$ $T_{\rm eff}$ = 21260K
WD 1335+700
Mass = 0.85$M_\odot$ $T_{\rm eff}$ = 30820K
WD 1337+705
Mass = 0.59$M_\odot$ $T_{\rm eff}$ = 21290K
WD 1342+443
Mass = 0.7$M_\odot$ $T_{\rm eff}$ = 74830K
WD 1344+106
Mass = 0.58$M_\odot$ $T_{\rm eff}$ = 7120K
WD 1344+509
Mass = 0.69$M_\odot$ $T_{\rm eff}$ = 21430K
F_ν (mJy)
Wavelength (μm)
GALEX
SDSS
Johnson−Cousins
Stromgren
UKIDSS
2MASS
Spitzer
WISE

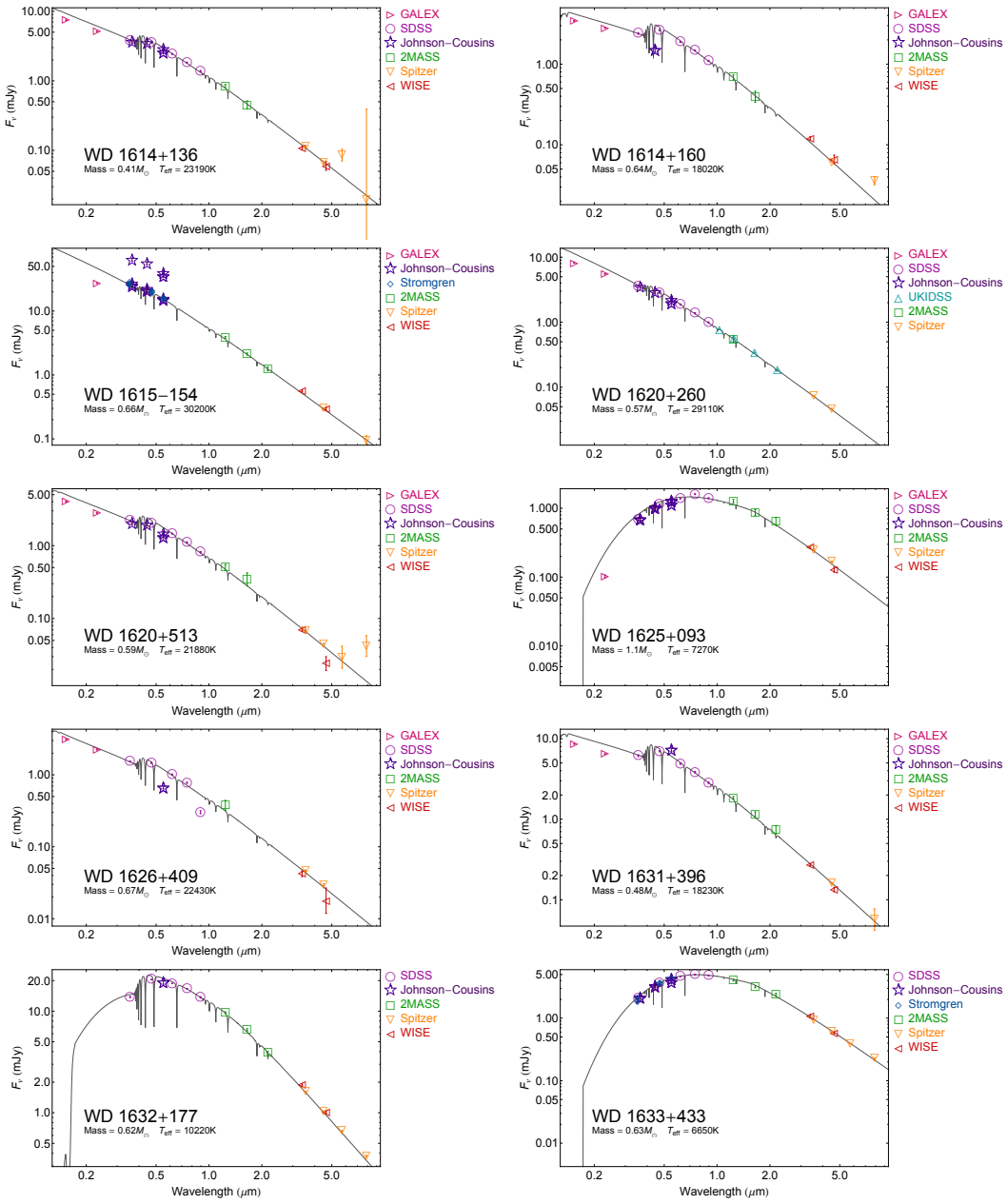

WD 1350+656
Mass = 0.6$M_\odot$ $T_{\rm eff}$ = 12330K
SDSS
Johnson−Cousins
2MASS
Spitzer
WISE
WD 1353+409
Mass = 0.46$M_\odot$ $T_{\rm eff}$ = 24280K
GALEX
SDSS
Johnson−Cousins
2MASS
Spitzer
WISE
WD 1407−475
Mass = 0.5$M_\odot$ $T_{\rm eff}$ = 23090K
Johnson−Cousins
Stromgren
2MASS
Spitzer
WISE
WD 1407+425
Mass = 0.78$M_\odot$ $T_{\rm eff}$ = 10090K
GALEX
SDSS
Johnson−Cousins
2MASS
Spitzer
WISE
WD 1408+323
Mass = 0.62$M_\odot$ $T_{\rm eff}$ = 19090K
GALEX
SDSS
Johnson−Cousins
Stromgren
2MASS
Spitzer
WISE
WD 1412−109
Mass = 0.63$M_\odot$ $T_{\rm eff}$ = 26610K
GALEX
SDSS
Johnson−Cousins
2MASS
Spitzer
WISE
WD 1413+231
Mass = 0.51$M_\odot$ $T_{\rm eff}$ = 24200K
GALEX
SDSS
Johnson−Cousins
Spitzer
WISE
WD 1421+318
Mass = 0.63$M_\odot$ $T_{\rm eff}$ = 27970K
GALEX
SDSS
Johnson−Cousins
Stromgren
2MASS
Spitzer
WISE
WD 1422+095
Mass = 0.69$M_\odot$ $T_{\rm eff}$ = 12440K
GALEX
SDSS
Johnson−Cousins
Stromgren
UKIDSS
2MASS
Spitzer
WISE
WD 1422+336
Mass = 0.77$M_\odot$ $T_{\rm eff}$ = 14370K
GALEX
SDSS
Johnson−Cousins
Spitzer
WISE
F_ν (mJy)
Wavelength (μm)

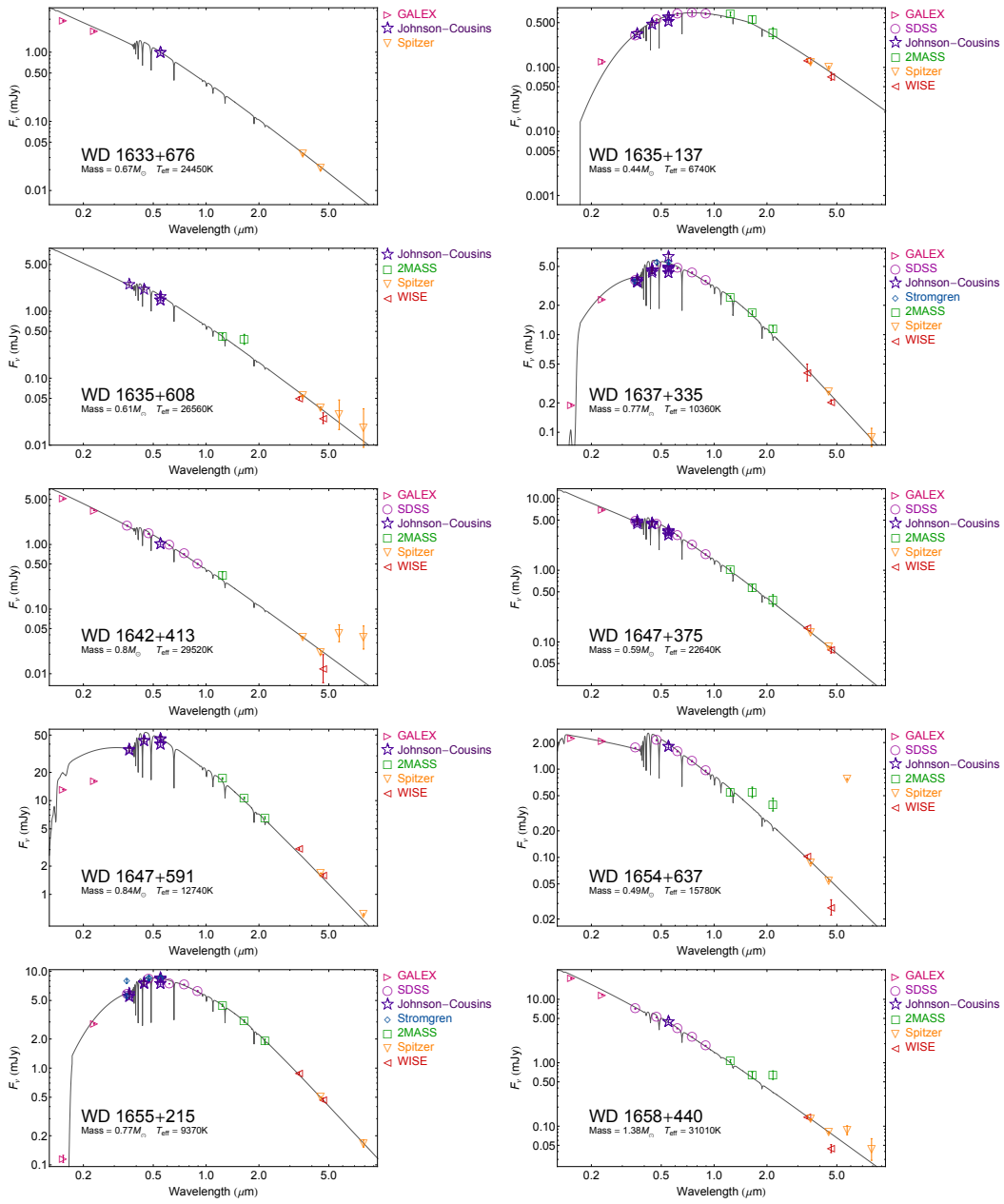

WD 1425−811
Mass = 0.71$M_\odot$ $T_{\rm eff}$ = 12330K
WD 1433+538
Mass = 0.54$M_\odot$ $T_{\rm eff}$ = 23260K
WD 1446+286
Mass = 0.89$M_\odot$ $T_{\rm eff}$ = 23860K
WD 1449+168
Mass = 0.57$M_\odot$ $T_{\rm eff}$ = 22640K
WD 1451+006.1
Mass = 0.58$M_\odot$ $T_{\rm eff}$ = 25990K
WD 1452−042
Mass = 0.69$M_\odot$ $T_{\rm eff}$ = 25070K
WD 1455+298
Mass = 0.58$M_\odot$ $T_{\rm eff}$ = 7390K
WD 1457−086
Mass = 0.62$M_\odot$ $T_{\rm eff}$ = 22240K
WD 1459+347
Mass = 0.95$M_\odot$ $T_{\rm eff}$ = 22390K
WD 1503−070
Mass = 1.35$M_\odot$ $T_{\rm eff}$ = 6920K
F_ν (mJy)
Wavelength (μm)
GALEX
SDSS
Johnson−Cousins
Stromgren
UKIDSS
2MASS
Spitzer
WISE

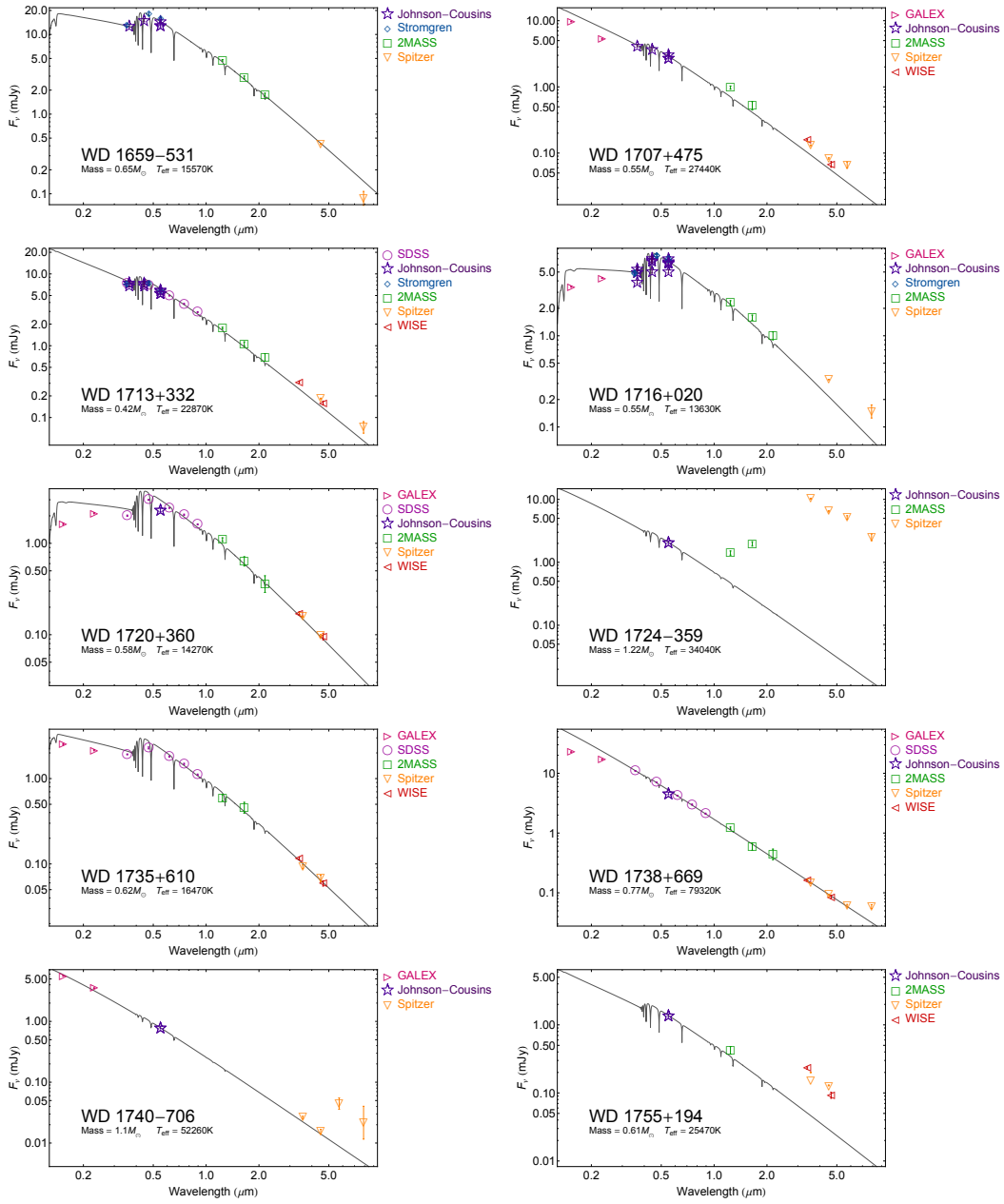

WD 1507+021
Mass = 0.57$M_\odot$ $T_{\rm eff}$ = 20270K
WD 1507+220
Mass = 0.58$M_\odot$ $T_{\rm eff}$ = 20540K
WD 1509+322
Mass = 0.67$M_\odot$ $T_{\rm eff}$ = 14600K
WD 1511+009
Mass = 0.57$M_\odot$ $T_{\rm eff}$ = 28500K
WD 1513+442
Mass = 0.6$M_\odot$ $T_{\rm eff}$ = 30030K
WD 1515+668
Mass = 0.91$M_\odot$ $T_{\rm eff}$ = 10410K
WD 1521+310
Mass = 0.62$M_\odot$ $T_{\rm eff}$ = 26440K
WD 1524−749
Mass = 0.48$M_\odot$ $T_{\rm eff}$ = 25190K
WD 1525+257
Mass = 0.81$M_\odot$ $T_{\rm eff}$ = 23410K
WD 1527+090
Mass = 0.65$M_\odot$ $T_{\rm eff}$ = 22250K
F_ν (mJy)
Wavelength (μm)
GALEX
SDSS
Johnson−Cousins
Stromgren
UKIDSS
2MASS
Spitzer
WISE

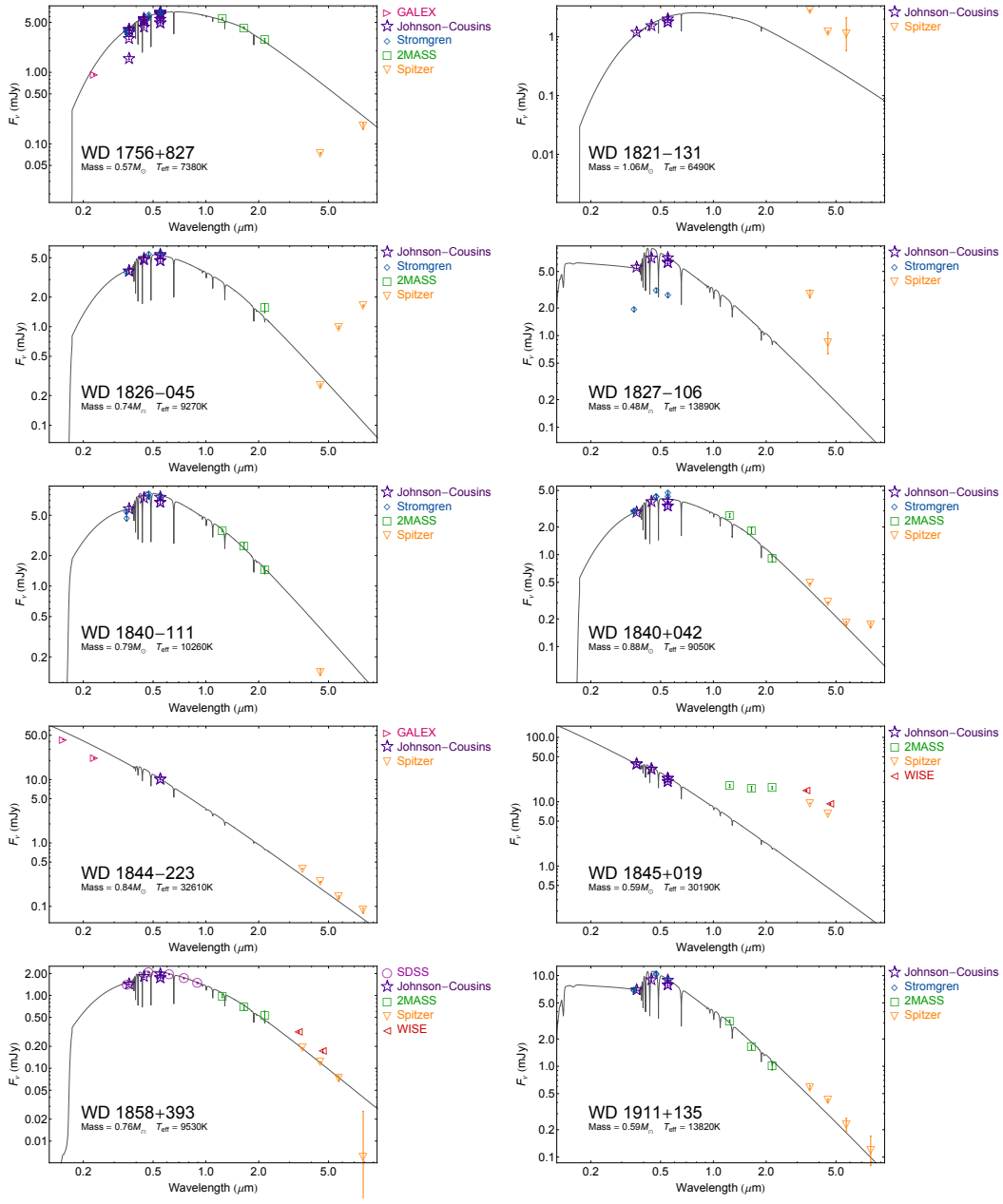

WD 1531−022
Mass = 0.91$M_\odot$ $T_{\rm eff}$ = 19540K
WD 1535+293
Mass = 0.62$M_\odot$ $T_{\rm eff}$ = 25200K
WD 1541+650
Mass = 0.72$M_\odot$ $T_{\rm eff}$ = 11880K
WD 1543−366
Mass = 1.16$M_\odot$ $T_{\rm eff}$ = 47620K
WD 1547+057
Mass = 0.91$M_\odot$ $T_{\rm eff}$ = 25860K
WD 1548+149
Mass = 0.57$M_\odot$ $T_{\rm eff}$ = 21430K
WD 1550+183
Mass = 0.84$M_\odot$ $T_{\rm eff}$ = 14910K
WD 1553+353
Mass = 0.59$M_\odot$ $T_{\rm eff}$ = 26370K
WD 1554+215
Mass = 0.59$M_\odot$ $T_{\rm eff}$ = 27320K
WD 1559+128
Mass = 0.67$M_\odot$ $T_{\rm eff}$ = 30040K
F_ν (mJy)
Wavelength (μm)
GALEX
SDSS
Johnson−Cousins
Stromgren
UKIDSS
2MASS
Spitzer
WISE

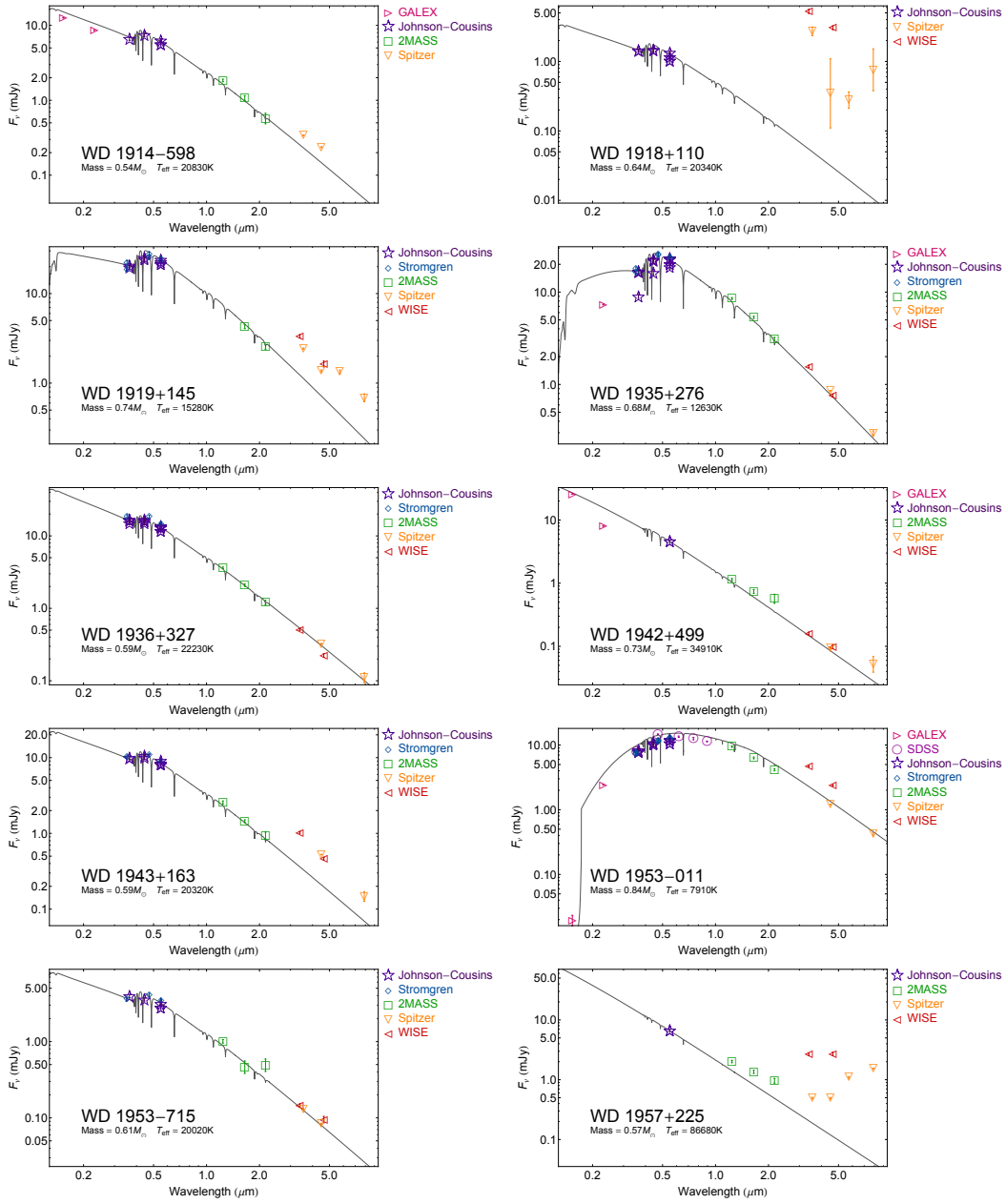

WD 1559+369
Mass = 0.67$M_\odot$ $T_{\rm eff}$ = 11440K
WD 1603+432
Mass = 0.68$M_\odot$ $T_{\rm eff}$ = 37550K
WD 1605+683
Mass = 0.62$M_\odot$ $T_{\rm eff}$ = 22310K
WD 1606+422
Mass = 0.53$M_\odot$ $T_{\rm eff}$ = 13110K
WD 1608+419
Mass = 0.66$M_\odot$ $T_{\rm eff}$ = 17360K
WD 1609+044
Mass = 0.6$M_\odot$ $T_{\rm eff}$ = 29830K
WD 1609+135
Mass = 1.06$M_\odot$ $T_{\rm eff}$ = 9370K
WD 1609+631
Mass = 1.05$M_\odot$ $T_{\rm eff}$ = 31150K
WD 1611−084
Mass = 0.6$M_\odot$ $T_{\rm eff}$ = 41440K
WD 1612+554
Mass = 0.79$M_\odot$ $T_{\rm eff}$ = 12010K
F_ν (mJy)
Wavelength (μm)
GALEX
SDSS
Johnson−Cousins
Stromgren
2MASS
Spitzer
WISE

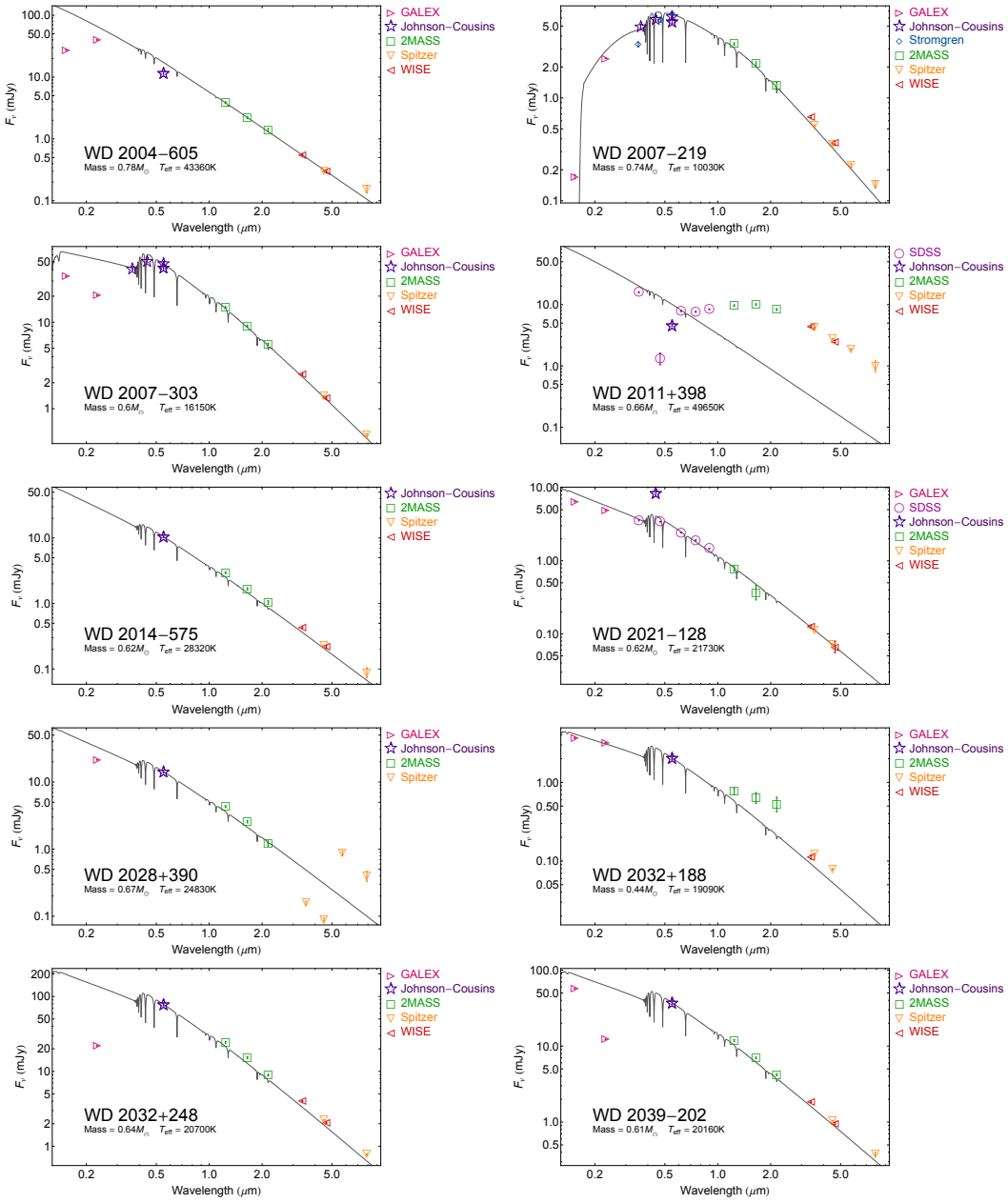

WD 1614+136
Mass = 0.41$M_\odot$ $T_{\rm eff}$ = 23190K
WD 1614+160
Mass = 0.64$M_\odot$ $T_{\rm eff}$ = 18020K
WD 1615−154
Mass = 0.66$M_\odot$ $T_{\rm eff}$ = 30200K
WD 1620+260
Mass = 0.57$M_\odot$ $T_{\rm eff}$ = 29110K
WD 1620+513
Mass = 0.59$M_\odot$ $T_{\rm eff}$ = 21880K
WD 1625+093
Mass = 1.1$M_\odot$ $T_{\rm eff}$ = 7270K
WD 1626+409
Mass = 0.67$M_\odot$ $T_{\rm eff}$ = 22430K
WD 1631+396
Mass = 0.48$M_\odot$ $T_{\rm eff}$ = 18230K
WD 1632+177
Mass = 0.62$M_\odot$ $T_{\rm eff}$ = 10220K
WD 1633+433
Mass = 0.63$M_\odot$ $T_{\rm eff}$ = 6650K
F_ν (mJy)
Wavelength (μm)
GALEX
SDSS
Johnson−Cousins
Stromgren
UKIDSS
2MASS
Spitzer
WISE

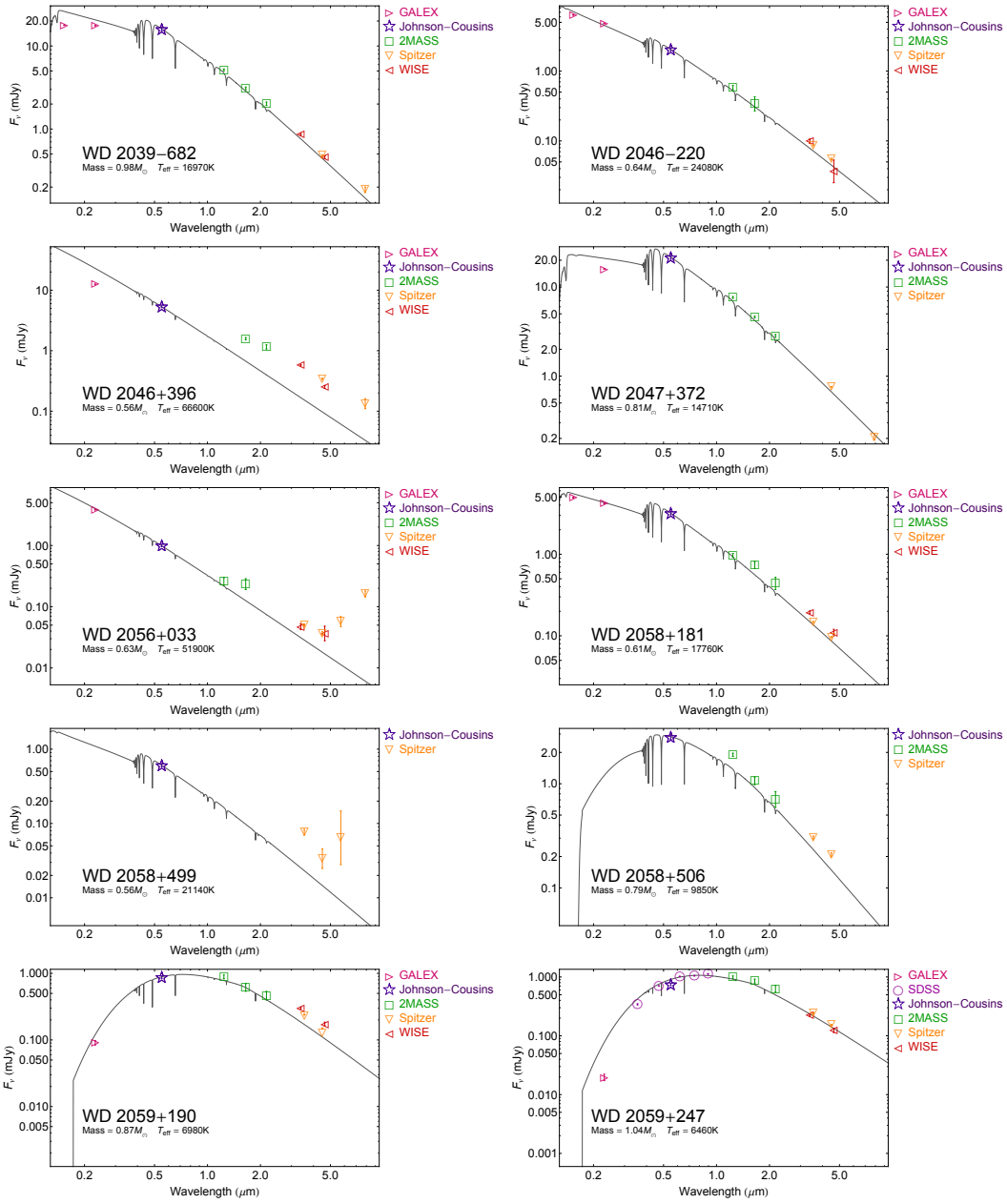

WD 1633+676
Mass = 0.67$M_\odot$ $T_{\rm eff}$ = 24450K
WD 1635+137
Mass = 0.44$M_\odot$ $T_{\rm eff}$ = 6740K
WD 1635+608
Mass = 0.61$M_\odot$ $T_{\rm eff}$ = 26560K
WD 1637+335
Mass = 0.77$M_\odot$ $T_{\rm eff}$ = 10360K
WD 1642+413
Mass = 0.8$M_\odot$ $T_{\rm eff}$ = 29520K
WD 1647+375
Mass = 0.59$M_\odot$ $T_{\rm eff}$ = 22640K
WD 1647+591
Mass = 0.84$M_\odot$ $T_{\rm eff}$ = 12740K
WD 1654+637
Mass = 0.49$M_\odot$ $T_{\rm eff}$ = 15780K
WD 1655+215
Mass = 0.77$M_\odot$ $T_{\rm eff}$ = 9370K
WD 1658+440
Mass = 1.38$M_\odot$ $T_{\rm eff}$ = 31010K
F_ν (mJy)
Wavelength (μm)
GALEX
SDSS
Johnson–Cousins
Stromgren
2MASS
Spitzer
WISE

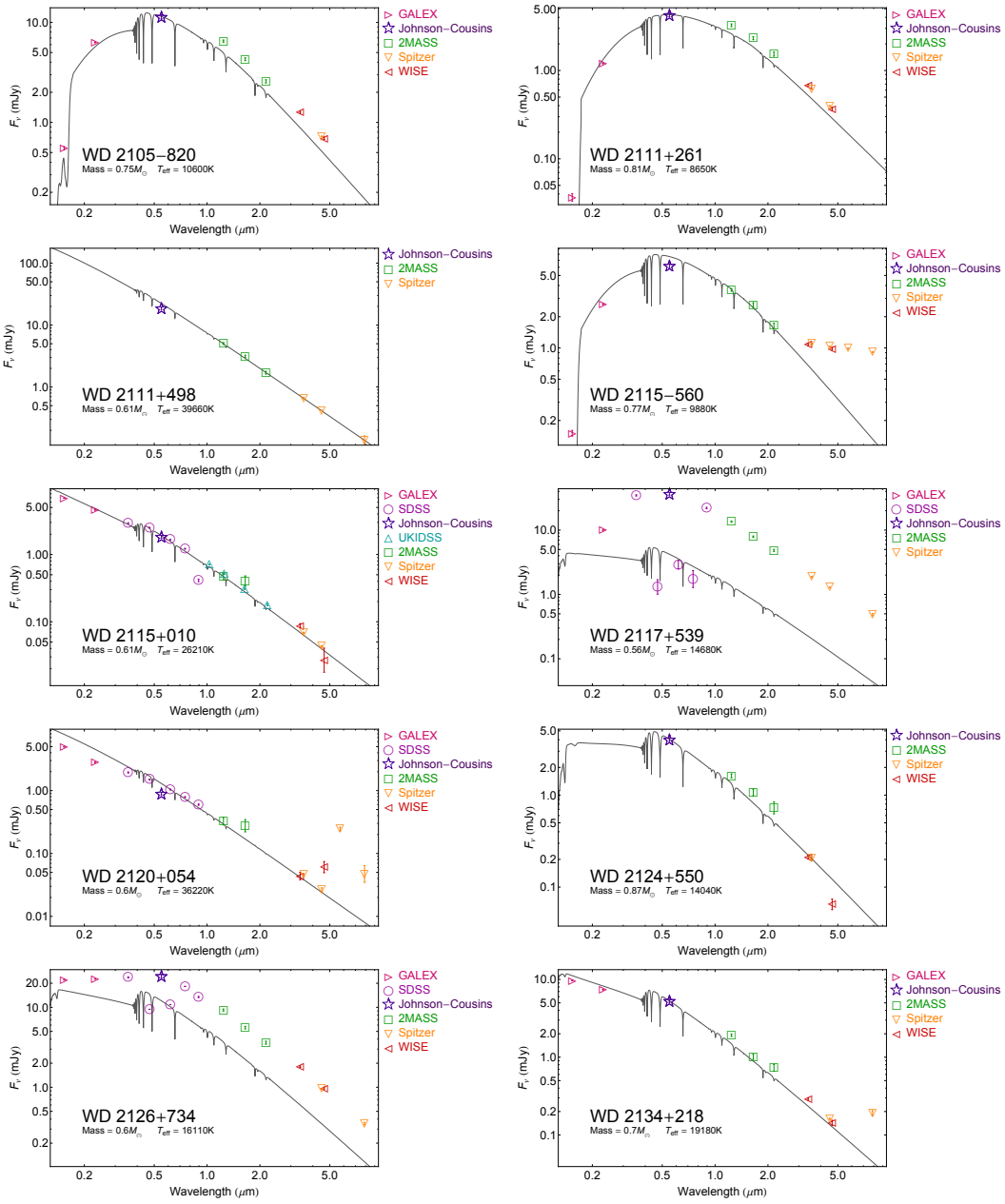

WD 1659−531
Mass = 0.65$M_\odot$ $T_{\rm eff}$ = 15570K
Johnson−Cousins
Stromgren
2MASS
Spitzer
WD 1707+475
Mass = 0.55$M_\odot$ $T_{\rm eff}$ = 27440K
GALEX
Johnson−Cousins
2MASS
Spitzer
WISE
WD 1713+332
Mass = 0.42$M_\odot$ $T_{\rm eff}$ = 22870K
SDSS
Johnson−Cousins
Stromgren
2MASS
Spitzer
WISE
WD 1716+020
Mass = 0.55$M_\odot$ $T_{\rm eff}$ = 13630K
GALEX
Johnson−Cousins
Stromgren
2MASS
Spitzer
WD 1720+360
Mass = 0.58$M_\odot$ $T_{\rm eff}$ = 14270K
GALEX
SDSS
Johnson−Cousins
2MASS
Spitzer
WISE
WD 1724−359
Mass = 1.22$M_\odot$ $T_{\rm eff}$ = 34040K
Johnson−Cousins
2MASS
Spitzer
WD 1735+610
Mass = 0.62$M_\odot$ $T_{\rm eff}$ = 16470K
GALEX
SDSS
2MASS
Spitzer
WISE
WD 1738+669
Mass = 0.77$M_\odot$ $T_{\rm eff}$ = 79320K
GALEX
SDSS
Johnson−Cousins
2MASS
Spitzer
WISE
WD 1740−706
Mass = 1.1$M_\odot$ $T_{\rm eff}$ = 52260K
GALEX
Johnson−Cousins
Spitzer
WD 1755+194
Mass = 0.61$M_\odot$ $T_{\rm eff}$ = 25470K
Johnson−Cousins
2MASS
Spitzer
WISE
F_ν (mJy)
Wavelength (μm)

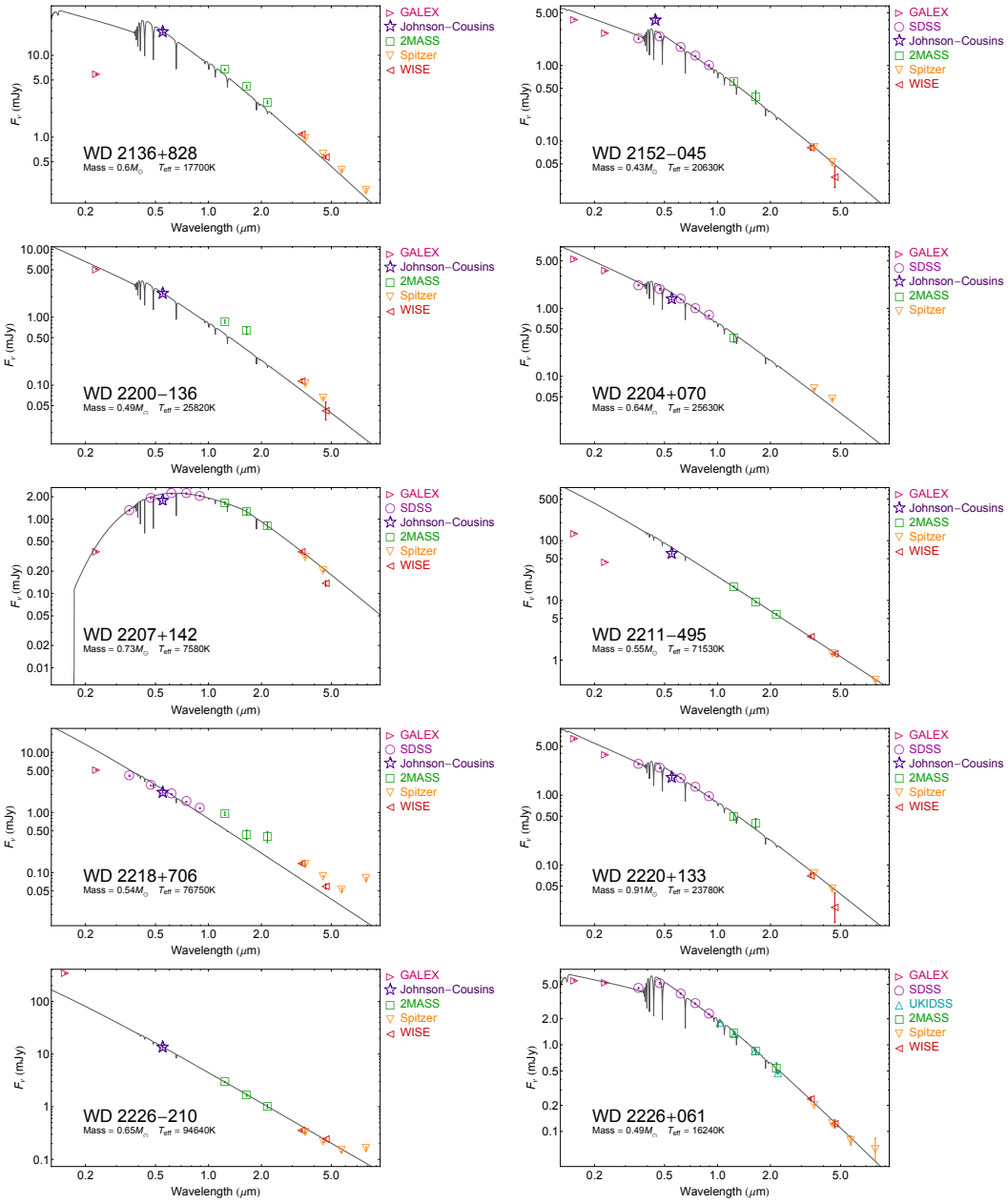

WD 1756+827
Mass = 0.57$M_\odot$ $T_{\rm eff}$ = 7380K
GALEX
Johnson−Cousins
Stromgren
2MASS
Spitzer
WD 1821−131
Mass = 1.06$M_\odot$ $T_{\rm eff}$ = 6490K
Johnson−Cousins
Spitzer
WD 1826−045
Mass = 0.74$M_\odot$ $T_{\rm eff}$ = 9270K
Johnson−Cousins
Stromgren
2MASS
Spitzer
WD 1827−106
Mass = 0.48$M_\odot$ $T_{\rm eff}$ = 13890K
Johnson−Cousins
Stromgren
Spitzer
WD 1840−111
Mass = 0.79$M_\odot$ $T_{\rm eff}$ = 10260K
Johnson−Cousins
Stromgren
2MASS
Spitzer
WD 1840+042
Mass = 0.88$M_\odot$ $T_{\rm eff}$ = 9050K
Johnson−Cousins
Stromgren
2MASS
Spitzer
WD 1844−223
Mass = 0.84$M_\odot$ $T_{\rm eff}$ = 32610K
GALEX
Johnson−Cousins
Spitzer
WD 1845+019
Mass = 0.59$M_\odot$ $T_{\rm eff}$ = 30190K
Johnson−Cousins
2MASS
Spitzer
WISE
WD 1858+393
Mass = 0.76$M_\odot$ $T_{\rm eff}$ = 9530K
SDSS
Johnson−Cousins
2MASS
Spitzer
WISE
WD 1911+135
Mass = 0.59$M_\odot$ $T_{\rm eff}$ = 13820K
Johnson−Cousins
Stromgren
2MASS
Spitzer
F_ν (mJy)
Wavelength (μm)

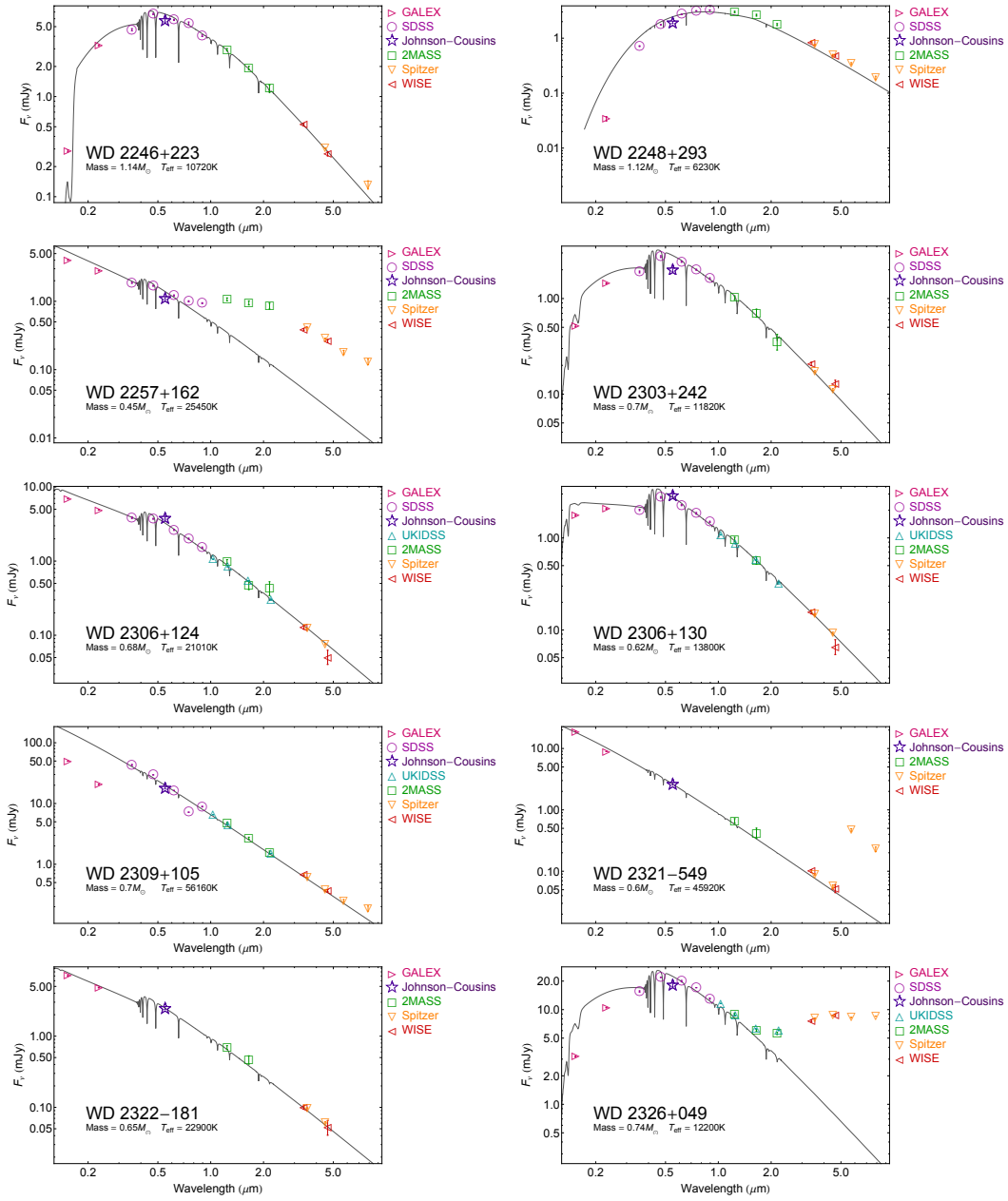

WD 1914−598
Mass = 0.54$M_\odot$ $T_{\rm eff}$ = 20830K
WD 1918+110
Mass = 0.64$M_\odot$ $T_{\rm eff}$ = 20340K
WD 1919+145
Mass = 0.74$M_\odot$ $T_{\rm eff}$ = 15280K
WD 1935+276
Mass = 0.68$M_\odot$ $T_{\rm eff}$ = 12630K
WD 1936+327
Mass = 0.59$M_\odot$ $T_{\rm eff}$ = 22230K
WD 1942+499
Mass = 0.73$M_\odot$ $T_{\rm eff}$ = 34910K
WD 1943+163
Mass = 0.59$M_\odot$ $T_{\rm eff}$ = 20320K
WD 1953−011
Mass = 0.84$M_\odot$ $T_{\rm eff}$ = 7910K
WD 1953−715
Mass = 0.61$M_\odot$ $T_{\rm eff}$ = 20020K
WD 1957+225
Mass = 0.57$M_\odot$ $T_{\rm eff}$ = 86680K
F_ν (mJy)
Wavelength (μm)
GALEX
SDSS
Johnson−Cousins
Stromgren
2MASS
Spitzer
WISE

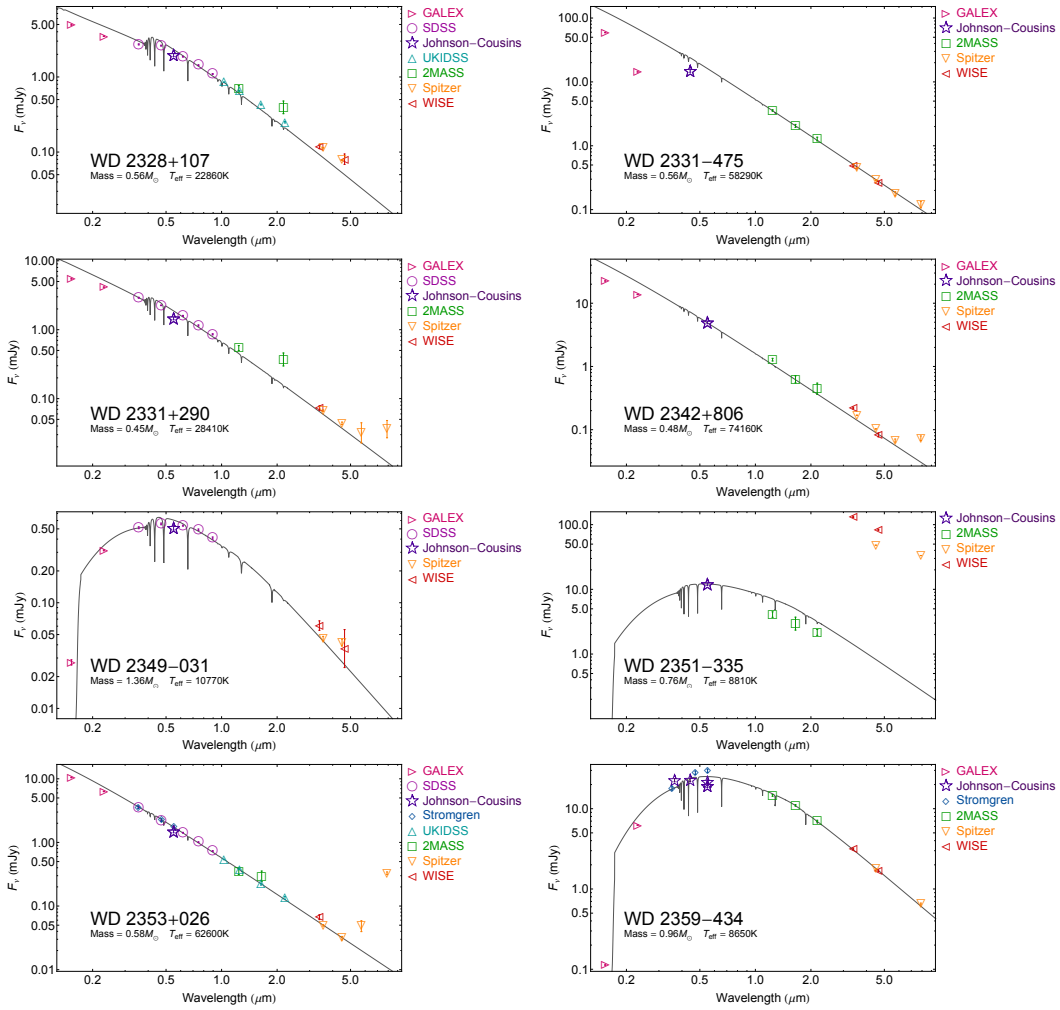

WD 2004−605
Mass = 0.78$M_\odot$ $T_{\rm eff}$ = 43360K
WD 2007−219
Mass = 0.74$M_\odot$ $T_{\rm eff}$ = 10030K
WD 2007−303
Mass = 0.6$M_\odot$ $T_{\rm eff}$ = 16150K
WD 2011+398
Mass = 0.66$M_\odot$ $T_{\rm eff}$ = 49650K
WD 2014−575
Mass = 0.62$M_\odot$ $T_{\rm eff}$ = 28320K
WD 2021−128
Mass = 0.62$M_\odot$ $T_{\rm eff}$ = 21730K
WD 2028+390
Mass = 0.67$M_\odot$ $T_{\rm eff}$ = 24830K
WD 2032+188
Mass = 0.44$M_\odot$ $T_{\rm eff}$ = 19090K
WD 2032+248
Mass = 0.64$M_\odot$ $T_{\rm eff}$ = 20700K
WD 2039−202
Mass = 0.61$M_\odot$ $T_{\rm eff}$ = 20160K
F_ν (mJy)
Wavelength (μm)
GALEX
SDSS
Johnson−Cousins
Stromgren
2MASS
Spitzer
WISE


WD 2039−682
Mass = 0.98$M_\odot$ $T_{\rm eff}$ = 16970K
WD 2046−220
Mass = 0.64$M_\odot$ $T_{\rm eff}$ = 24080K
WD 2046+396
Mass = 0.56$M_\odot$ $T_{\rm eff}$ = 66600K
WD 2047+372
Mass = 0.81$M_\odot$ $T_{\rm eff}$ = 14710K
WD 2056+033
Mass = 0.63$M_\odot$ $T_{\rm eff}$ = 51900K
WD 2058+181
Mass = 0.61$M_\odot$ $T_{\rm eff}$ = 17760K
WD 2058+499
Mass = 0.56$M_\odot$ $T_{\rm eff}$ = 21140K
WD 2058+506
Mass = 0.79$M_\odot$ $T_{\rm eff}$ = 9850K
WD 2059+190
Mass = 0.87$M_\odot$ $T_{\rm eff}$ = 6980K
WD 2059+247
Mass = 1.04$M_\odot$ $T_{\rm eff}$ = 6460K
F_ν (mJy)
Wavelength (μm)
GALEX
SDSS
Johnson−Cousins
2MASS
Spitzer
WISE


WD 2105−820
Mass = 0.75$M_\odot$ $T_{\rm eff}$ = 10600K
WD 2111+261
Mass = 0.81$M_\odot$ $T_{\rm eff}$ = 8650K
WD 2111+498
Mass = 0.61$M_\odot$ $T_{\rm eff}$ = 39660K
WD 2115−560
Mass = 0.77$M_\odot$ $T_{\rm eff}$ = 9880K
WD 2115+010
Mass = 0.61$M_\odot$ $T_{\rm eff}$ = 26210K
WD 2117+539
Mass = 0.56$M_\odot$ $T_{\rm eff}$ = 14680K
WD 2120+054
Mass = 0.6$M_\odot$ $T_{\rm eff}$ = 36220K
WD 2124+550
Mass = 0.87$M_\odot$ $T_{\rm eff}$ = 14040K
WD 2126+734
Mass = 0.6$M_\odot$ $T_{\rm eff}$ = 16110K
WD 2134+218
Mass = 0.7$M_\odot$ $T_{\rm eff}$ = 19180K
F_ν (mJy)
Wavelength (μm)
GALEX
SDSS
Johnson−Cousins
UKIDSS
2MASS
Spitzer
WISE

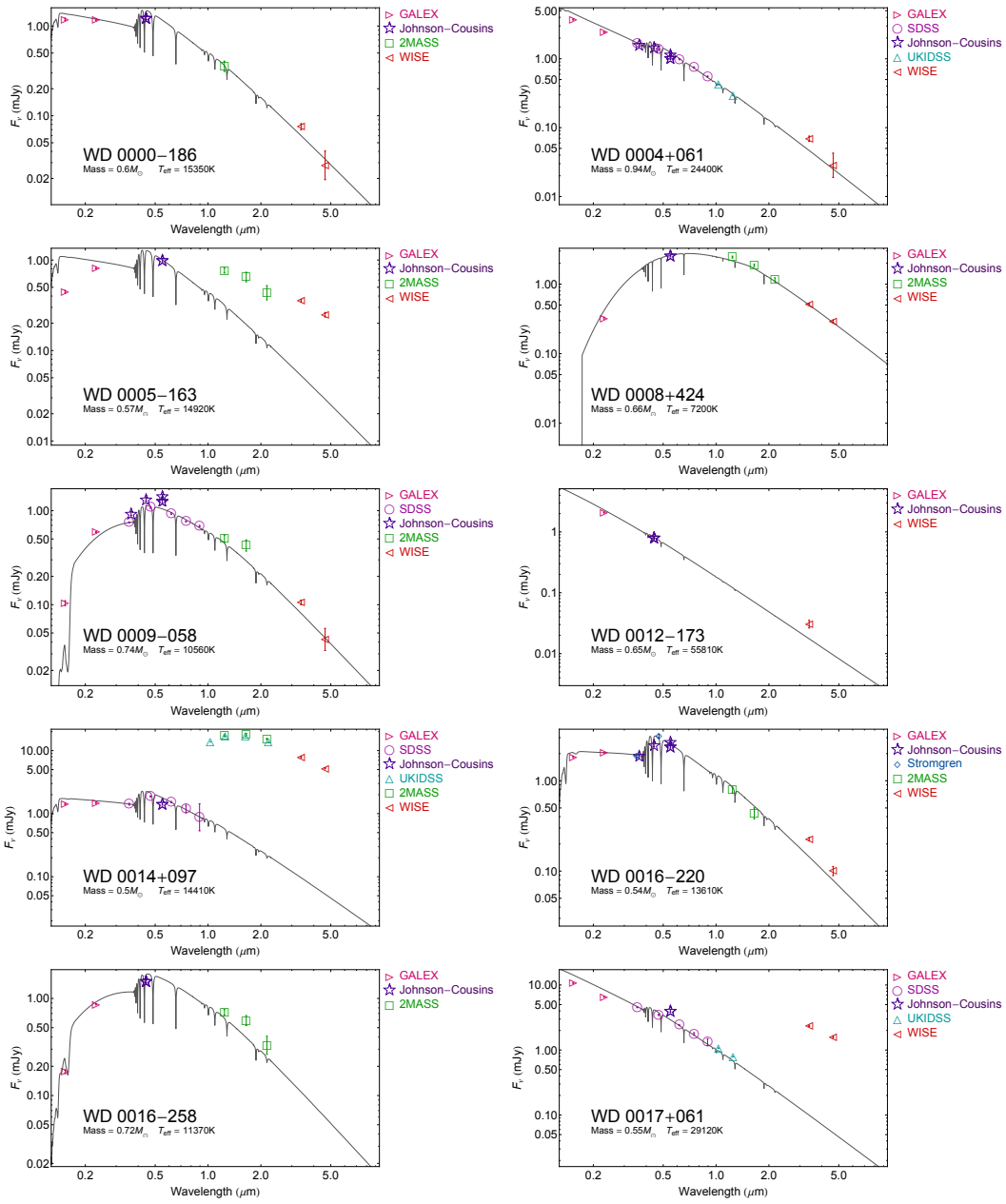

WD 2136+828
Mass = 0.6$M_\odot$ $T_{\rm eff}$ = 17700K
WD 2152−045
Mass = 0.43$M_\odot$ $T_{\rm eff}$ = 20630K
WD 2200−136
Mass = 0.49$M_\odot$ $T_{\rm eff}$ = 25820K
WD 2204+070
Mass = 0.64$M_\odot$ $T_{\rm eff}$ = 25630K
WD 2207+142
Mass = 0.73$M_\odot$ $T_{\rm eff}$ = 7580K
WD 2211−495
Mass = 0.55$M_\odot$ $T_{\rm eff}$ = 71530K
WD 2218+706
Mass = 0.54$M_\odot$ $T_{\rm eff}$ = 76750K
WD 2220+133
Mass = 0.91$M_\odot$ $T_{\rm eff}$ = 23780K
WD 2226−210
Mass = 0.65$M_\odot$ $T_{\rm eff}$ = 94640K
WD 2226+061
Mass = 0.49$M_\odot$ $T_{\rm eff}$ = 16240K
F_ν (mJy)
Wavelength (μm)
GALEX
SDSS
Johnson−Cousins
2MASS
UKIDSS
Spitzer
WISE

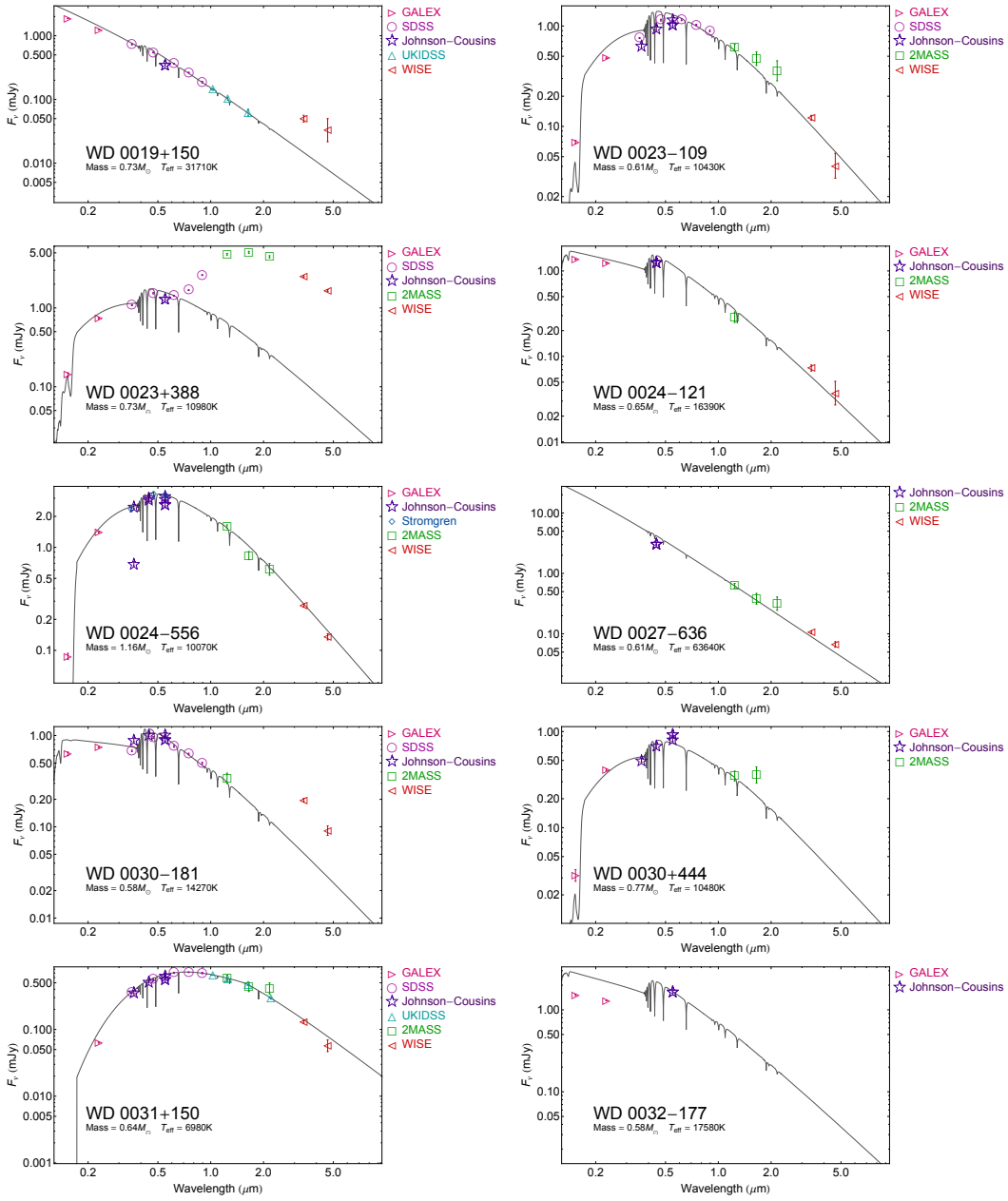

WD 2246+223
Mass = 1.14$M_\odot$ $T_{\rm eff}$ = 10720K
WD 2248+293
Mass = 1.12$M_\odot$ $T_{\rm eff}$ = 6230K
WD 2257+162
Mass = 0.45$M_\odot$ $T_{\rm eff}$ = 25450K
WD 2303+242
Mass = 0.7$M_\odot$ $T_{\rm eff}$ = 11820K
WD 2306+124
Mass = 0.68$M_\odot$ $T_{\rm eff}$ = 21010K
WD 2306+130
Mass = 0.62$M_\odot$ $T_{\rm eff}$ = 13800K
WD 2309+105
Mass = 0.7$M_\odot$ $T_{\rm eff}$ = 56160K
WD 2321−549
Mass = 0.6$M_\odot$ $T_{\rm eff}$ = 45920K
WD 2322−181
Mass = 0.65$M_\odot$ $T_{\rm eff}$ = 22900K
WD 2326+049
Mass = 0.74$M_\odot$ $T_{\rm eff}$ = 12200K
F_ν (mJy)
Wavelength (μm)
GALEX
SDSS
Johnson−Cousins
UKIDSS
2MASS
Spitzer
WISE

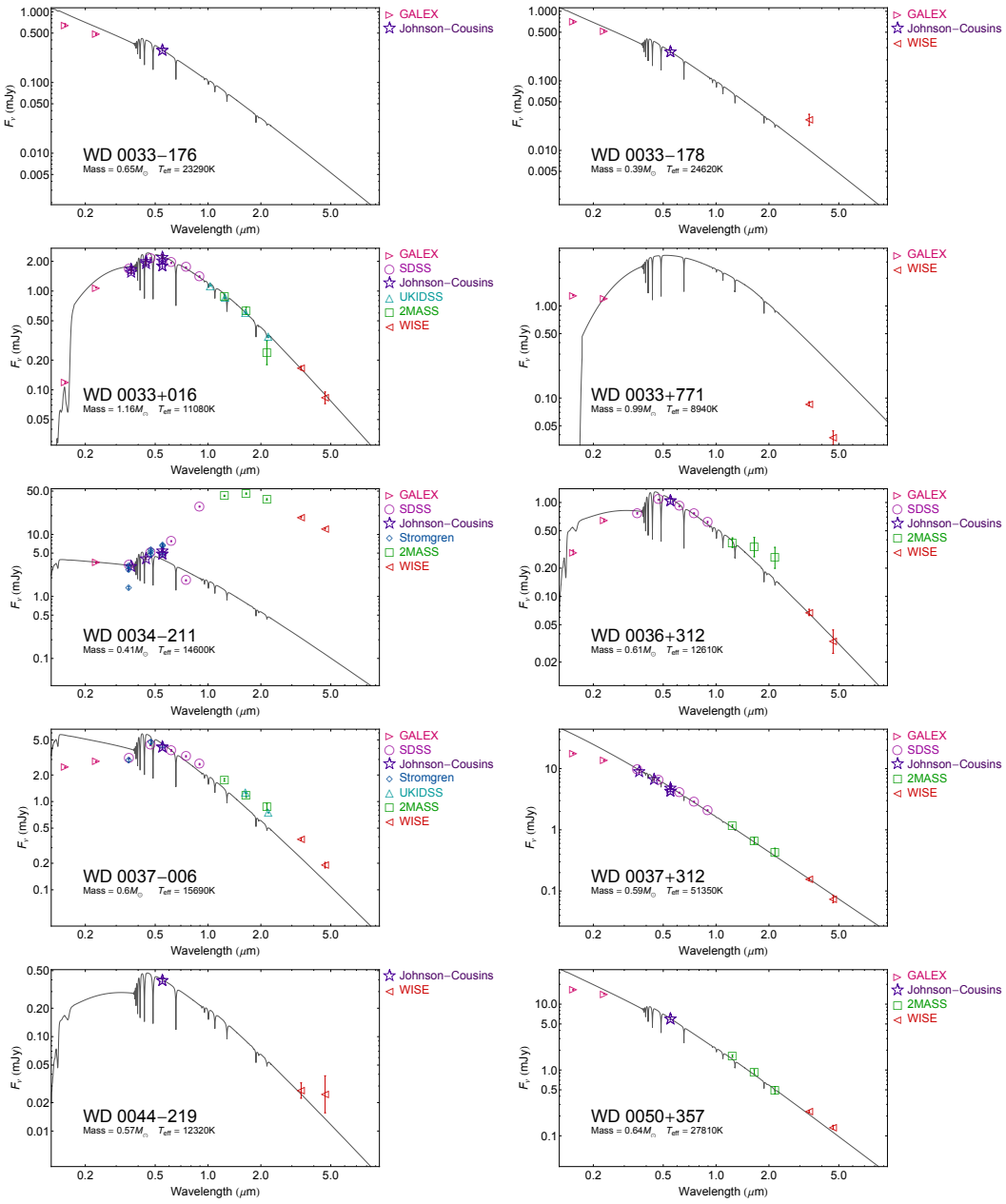

WD 2328+107
Mass = 0.56$M_\odot$ $T_{\rm eff}$ = 22860K
WD 2331−475
Mass = 0.56$M_\odot$ $T_{\rm eff}$ = 58290K
WD 2331+290
Mass = 0.45$M_\odot$ $T_{\rm eff}$ = 28410K
WD 2342+806
Mass = 0.48$M_\odot$ $T_{\rm eff}$ = 74160K
WD 2349−031
Mass = 1.36$M_\odot$ $T_{\rm eff}$ = 10770K
WD 2351−335
Mass = 0.76$M_\odot$ $T_{\rm eff}$ = 8810K
WD 2353+026
Mass = 0.58$M_\odot$ $T_{\rm eff}$ = 62600K
WD 2359−434
Mass = 0.96$M_\odot$ $T_{\rm eff}$ = 8650K
F_ν (mJy)
Wavelength (μm)
GALEX
SDSS
Johnson−Cousins
Stromgren
UKIDSS
2MASS
Spitzer
WISE

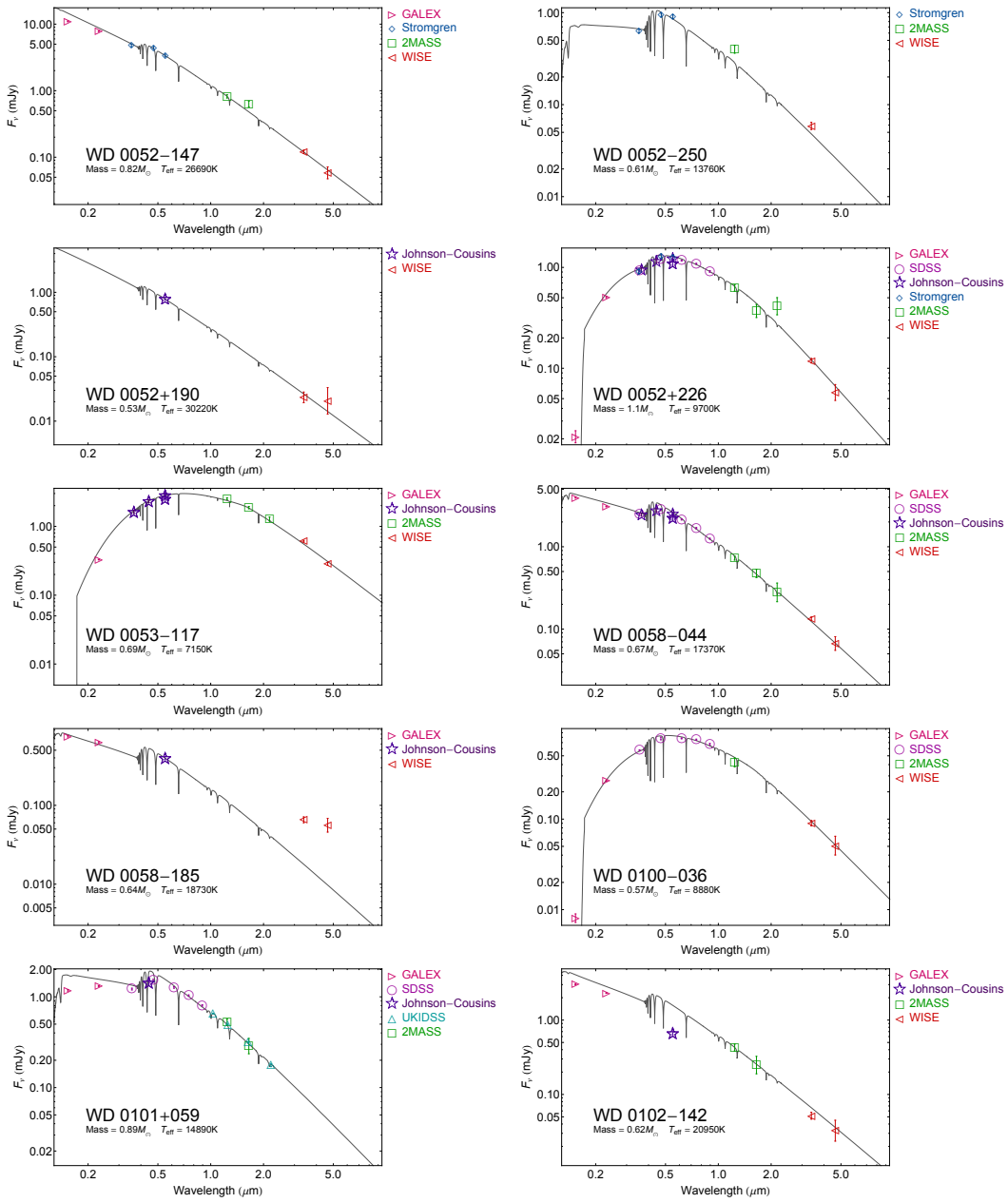
Appendix D

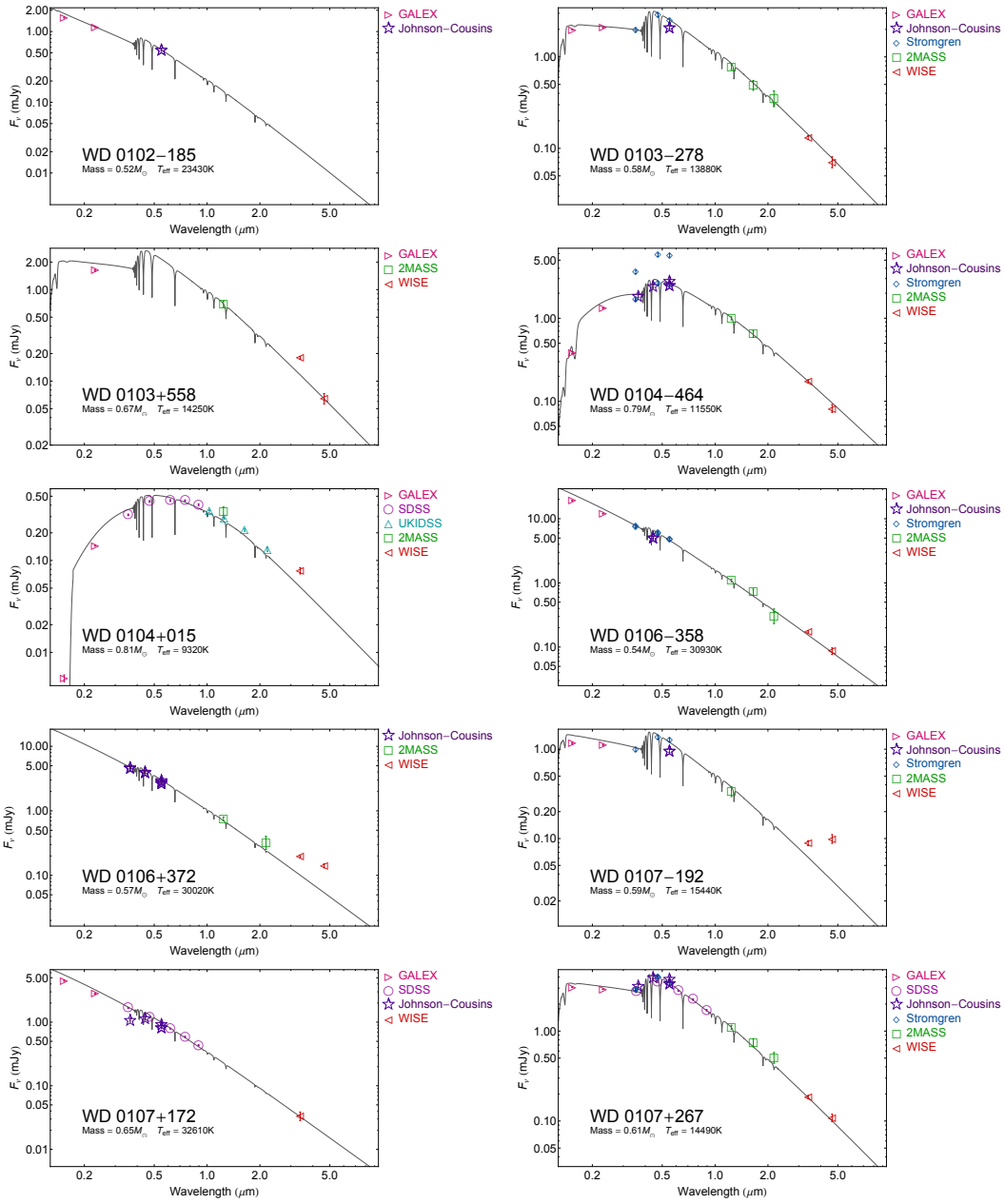
McCook & Sion non-IRAC SEDs

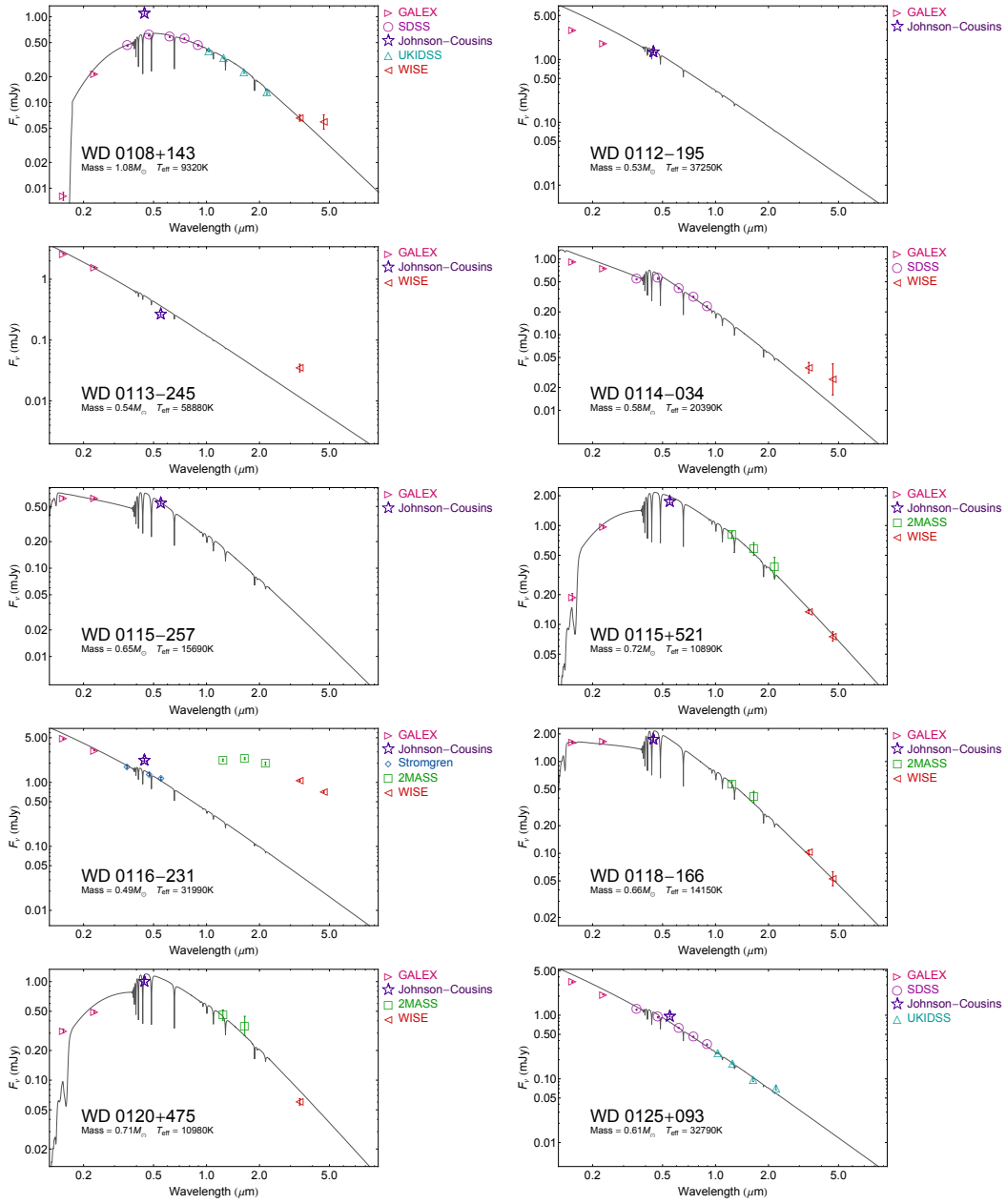

WD 0000−186
Mass = 0.6$M_\odot$ $T_{\rm eff}$ = 15350K
WD 0004+061
Mass = 0.94$M_\odot$ $T_{\rm eff}$ = 24400K
WD 0005−163
Mass = 0.57$M_\odot$ $T_{\rm eff}$ = 14920K
WD 0008+424
Mass = 0.66$M_\odot$ $T_{\rm eff}$ = 7200K
WD 0009−058
Mass = 0.74$M_\odot$ $T_{\rm eff}$ = 10560K
WD 0012−173
Mass = 0.65$M_\odot$ $T_{\rm eff}$ = 55810K
WD 0014+097
Mass = 0.5$M_\odot$ $T_{\rm eff}$ = 14410K
WD 0016−220
Mass = 0.54$M_\odot$ $T_{\rm eff}$ = 13610K
WD 0016−258
Mass = 0.72$M_\odot$ $T_{\rm eff}$ = 11370K
WD 0017+061
Mass = 0.55$M_\odot$ $T_{\rm eff}$ = 29120K
F_ν (mJy)
Wavelength (μm)
GALEX
SDSS
Johnson−Cousins
Stromgren
2MASS
UKIDSS
WISE

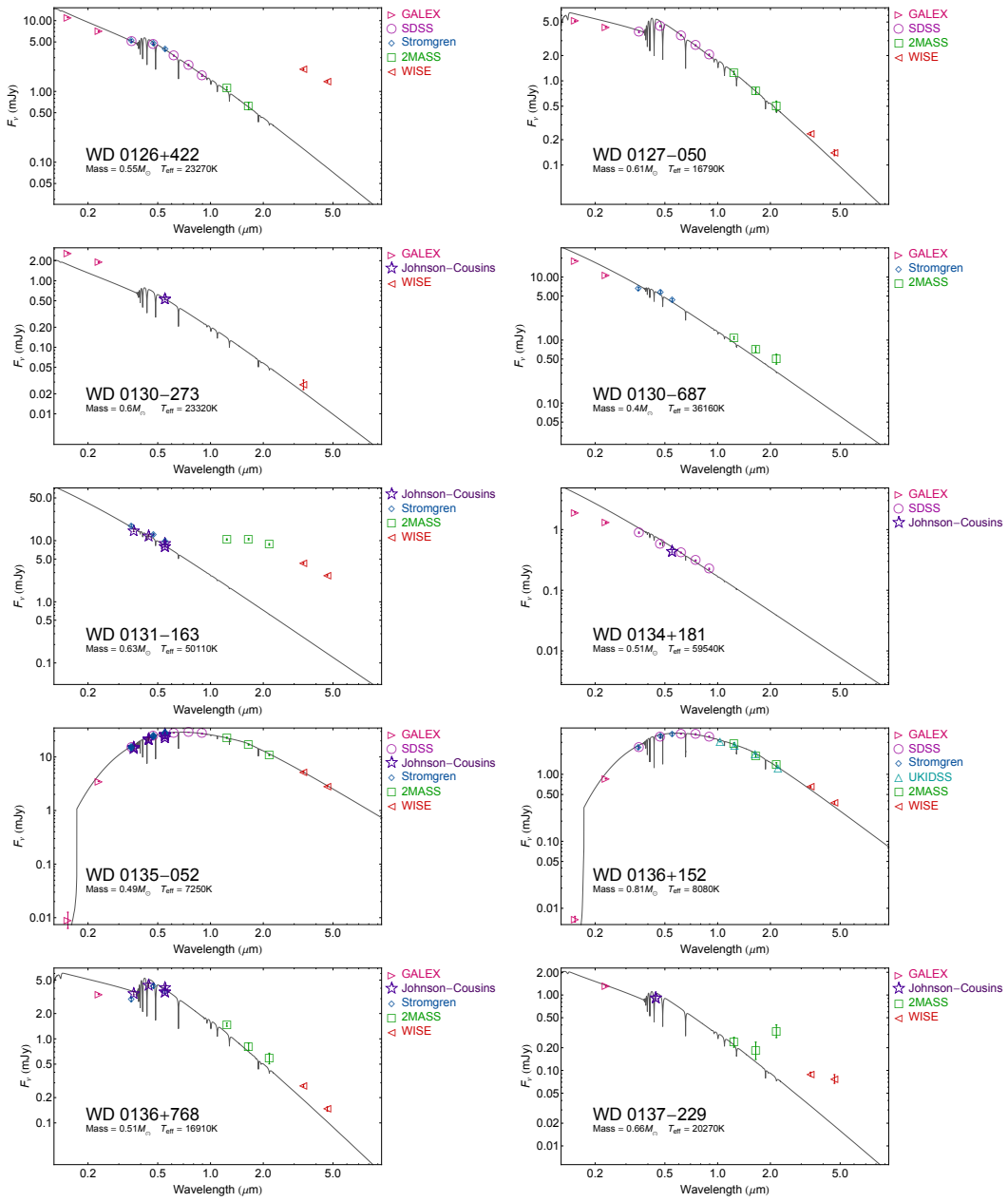

WD 0019+150
Mass = 0.73$M_\odot$ $T_{\rm eff}$ = 31710K
WD 0023−109
Mass = 0.61$M_\odot$ $T_{\rm eff}$ = 10430K
WD 0023+388
Mass = 0.73$M_\odot$ $T_{\rm eff}$ = 10980K
WD 0024−121
Mass = 0.65$M_\odot$ $T_{\rm eff}$ = 16390K
WD 0024−556
Mass = 1.16$M_\odot$ $T_{\rm eff}$ = 10070K
WD 0027−636
Mass = 0.61$M_\odot$ $T_{\rm eff}$ = 63640K
WD 0030−181
Mass = 0.58$M_\odot$ $T_{\rm eff}$ = 14270K
WD 0030+444
Mass = 0.77$M_\odot$ $T_{\rm eff}$ = 10480K
WD 0031+150
Mass = 0.64$M_\odot$ $T_{\rm eff}$ = 6980K
WD 0032−177
Mass = 0.58$M_\odot$ $T_{\rm eff}$ = 17580K
F_ν (mJy)
Wavelength (μm)
GALEX
SDSS
Johnson−Cousins
Stromgren
UKIDSS
2MASS
WISE

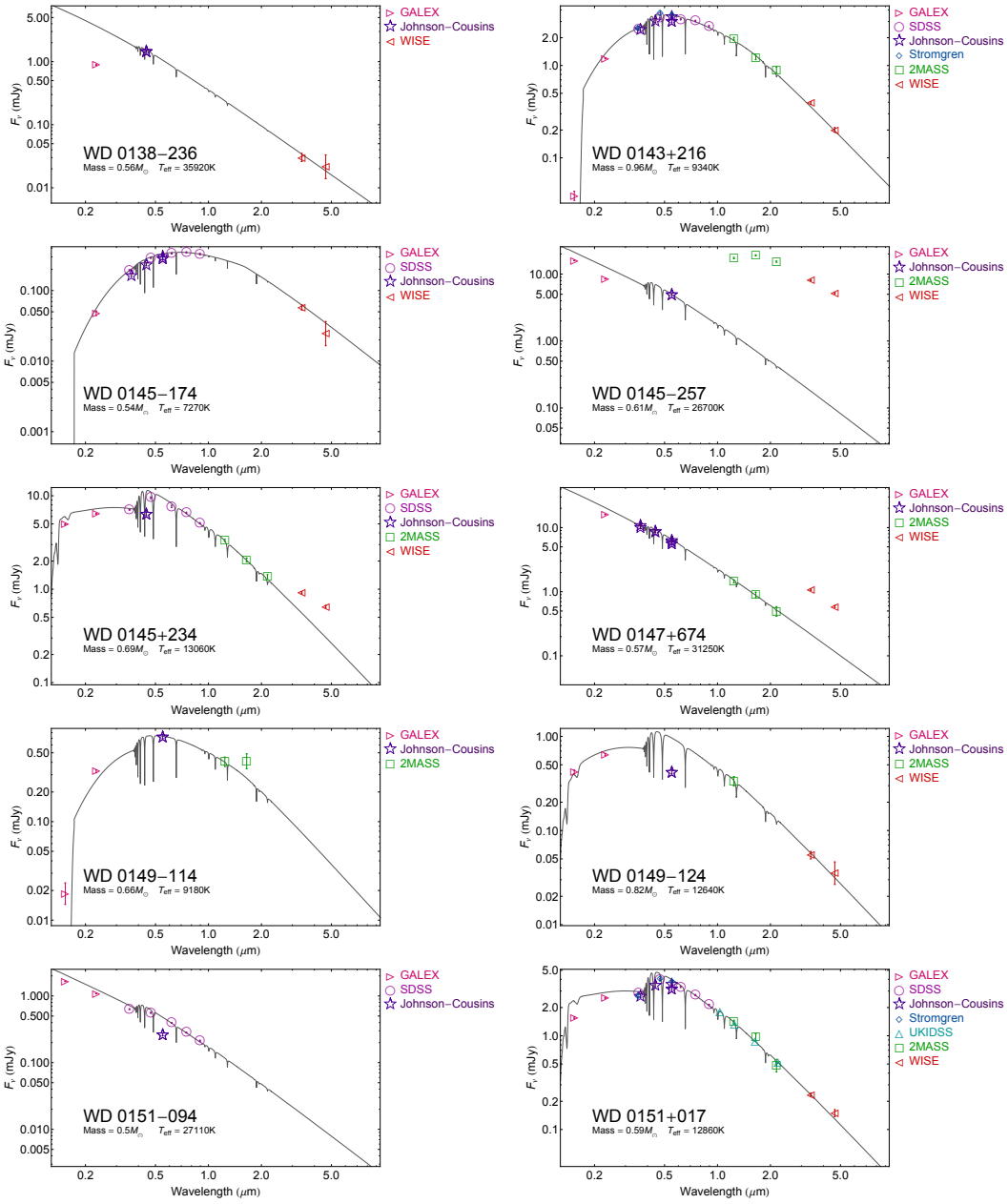

WD 0033−176
Mass = 0.65$M_\odot$ $T_{\rm eff}$ = 23290K
GALEX
Johnson−Cousins
WD 0033−178
Mass = 0.39$M_\odot$ $T_{\rm eff}$ = 24620K
GALEX
Johnson−Cousins
WISE
WD 0033+016
Mass = 1.16$M_\odot$ $T_{\rm eff}$ = 11080K
GALEX
SDSS
Johnson−Cousins
UKIDSS
2MASS
WISE
WD 0033+771
Mass = 0.99$M_\odot$ $T_{\rm eff}$ = 8940K
GALEX
WISE
WD 0034−211
Mass = 0.41$M_\odot$ $T_{\rm eff}$ = 14600K
GALEX
SDSS
Johnson−Cousins
Stromgren
2MASS
WISE
WD 0036+312
Mass = 0.61$M_\odot$ $T_{\rm eff}$ = 12610K
GALEX
SDSS
Johnson−Cousins
2MASS
WISE
WD 0037−006
Mass = 0.6$M_\odot$ $T_{\rm eff}$ = 15690K
GALEX
SDSS
Johnson−Cousins
Stromgren
UKIDSS
2MASS
WISE
WD 0037+312
Mass = 0.59$M_\odot$ $T_{\rm eff}$ = 51350K
GALEX
SDSS
Johnson−Cousins
2MASS
WISE
WD 0044−219
Mass = 0.57$M_\odot$ $T_{\rm eff}$ = 12320K
Johnson−Cousins
WISE
WD 0050+357
Mass = 0.64$M_\odot$ $T_{\rm eff}$ = 27810K
GALEX
Johnson−Cousins
2MASS
WISE
F_ν (mJy)
Wavelength (μm)

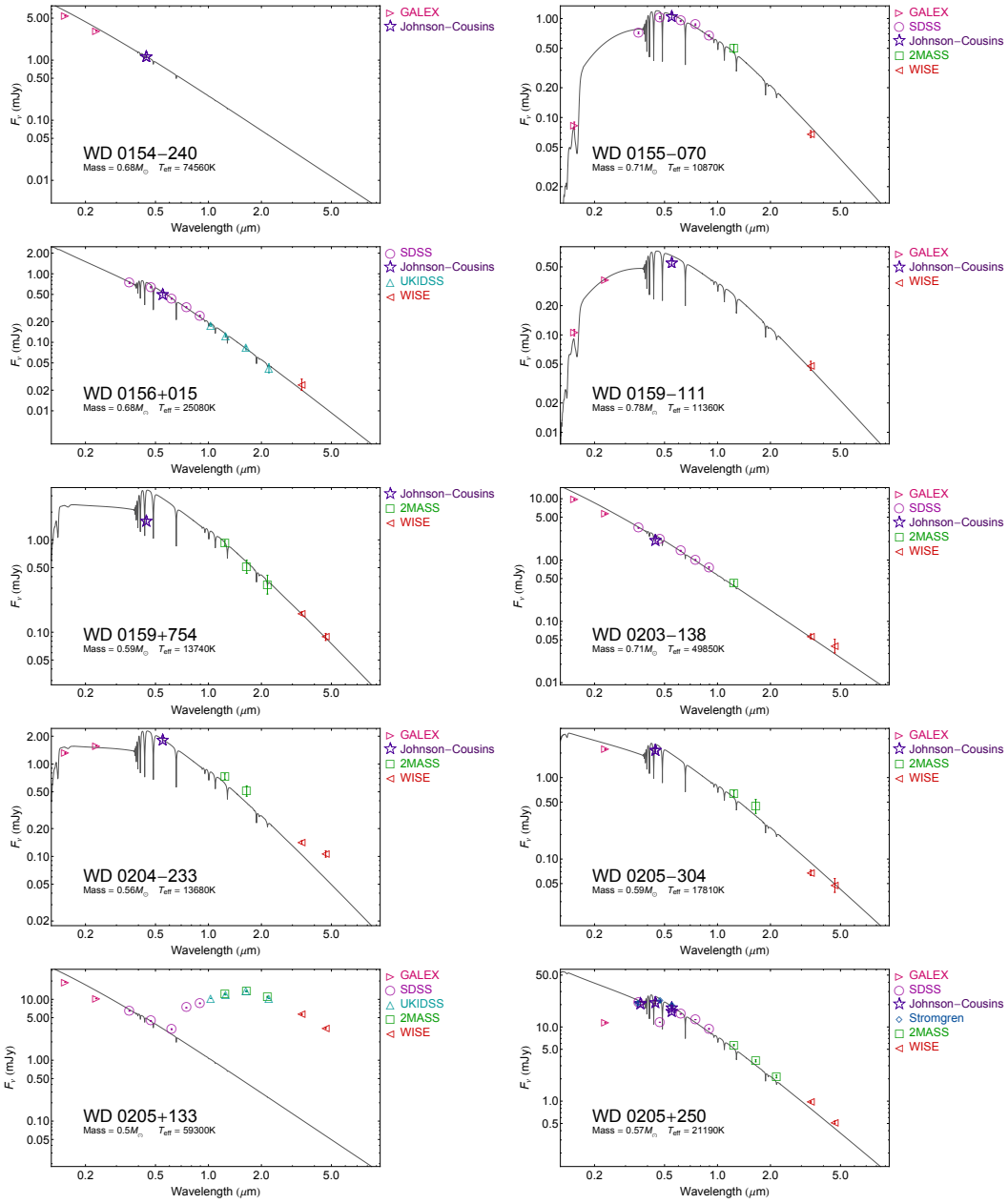

WD 0052−147
Mass = 0.82$M_\odot$ $T_{\rm eff}$ = 26690K
GALEX
Stromgren
2MASS
WISE
WD 0052−250
Mass = 0.61$M_\odot$ $T_{\rm eff}$ = 13760K
Stromgren
2MASS
WISE
WD 0052+190
Mass = 0.53$M_\odot$ $T_{\rm eff}$ = 30220K
Johnson−Cousins
WISE
WD 0052+226
Mass = 1.1$M_\odot$ $T_{\rm eff}$ = 9700K
GALEX
SDSS
Johnson−Cousins
Stromgren
2MASS
WISE
WD 0053−117
Mass = 0.69$M_\odot$ $T_{\rm eff}$ = 7150K
GALEX
Johnson−Cousins
2MASS
WISE
WD 0058−044
Mass = 0.67$M_\odot$ $T_{\rm eff}$ = 17370K
GALEX
SDSS
Johnson−Cousins
2MASS
WISE
WD 0058−185
Mass = 0.64$M_\odot$ $T_{\rm eff}$ = 18730K
GALEX
Johnson−Cousins
WISE
WD 0100−036
Mass = 0.57$M_\odot$ $T_{\rm eff}$ = 8880K
GALEX
SDSS
2MASS
WISE
WD 0101+059
Mass = 0.89$M_\odot$ $T_{\rm eff}$ = 14890K
GALEX
SDSS
Johnson−Cousins
UKIDSS
2MASS
WD 0102−142
Mass = 0.62$M_\odot$ $T_{\rm eff}$ = 20950K
GALEX
Johnson−Cousins
2MASS
WISE
F_ν (mJy)
Wavelength (μm)

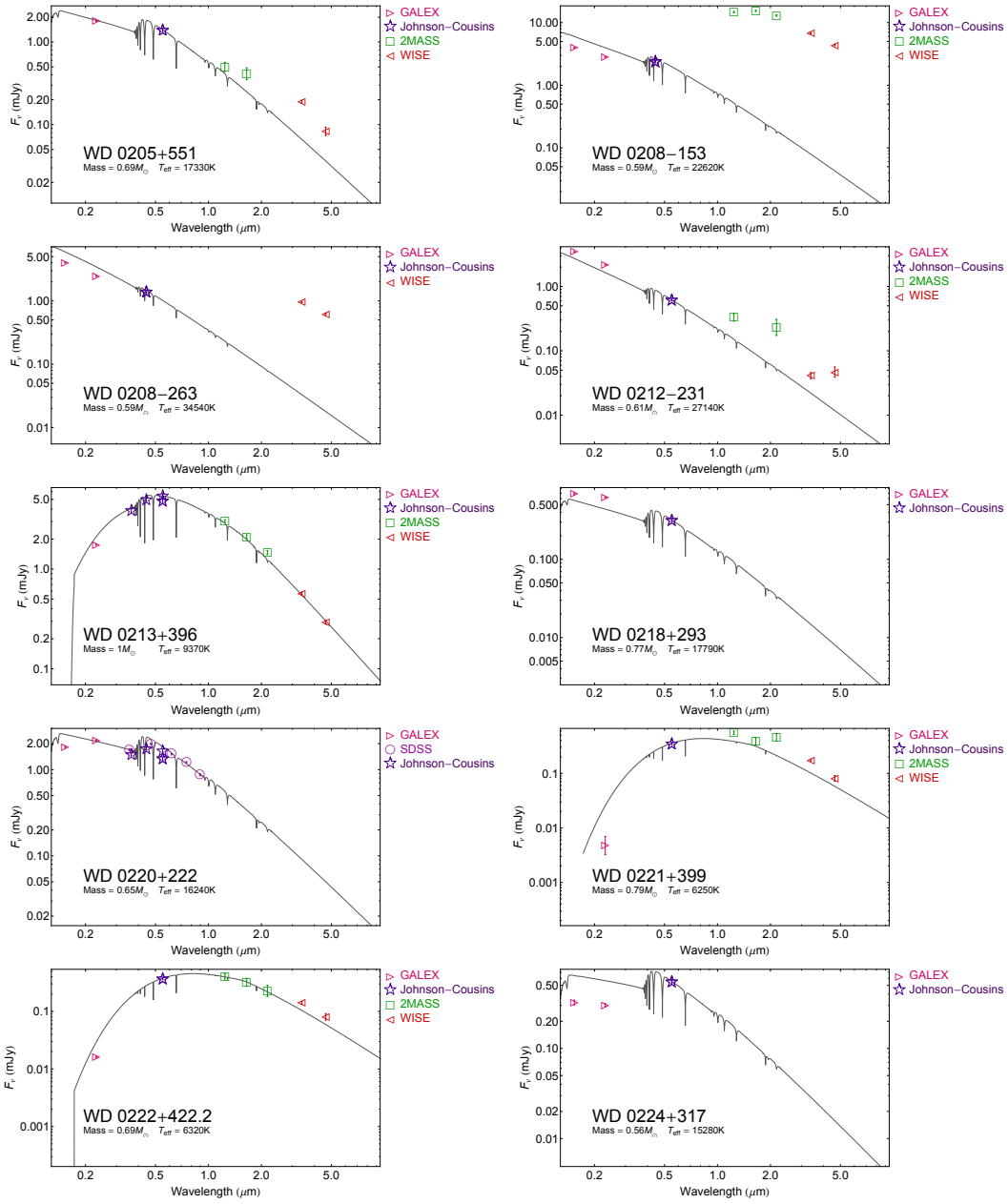

WD 0102−185
Mass = 0.52$M_\odot$ $T_{\rm eff}$ = 23430K
GALEX
Johnson−Cousins
WD 0103−278
Mass = 0.58$M_\odot$ $T_{\rm eff}$ = 13880K
GALEX
Johnson−Cousins
Stromgren
2MASS
WISE
WD 0103+558
Mass = 0.67$M_\odot$ $T_{\rm eff}$ = 14250K
GALEX
2MASS
WISE
WD 0104−464
Mass = 0.79$M_\odot$ $T_{\rm eff}$ = 11550K
GALEX
Johnson−Cousins
Stromgren
2MASS
WISE
WD 0104+015
Mass = 0.81$M_\odot$ $T_{\rm eff}$ = 9320K
GALEX
SDSS
UKIDSS
2MASS
WISE
WD 0106−358
Mass = 0.54$M_\odot$ $T_{\rm eff}$ = 30930K
GALEX
Johnson−Cousins
Stromgren
2MASS
WISE
WD 0106+372
Mass = 0.57$M_\odot$ $T_{\rm eff}$ = 30020K
Johnson−Cousins
2MASS
WISE
WD 0107−192
Mass = 0.59$M_\odot$ $T_{\rm eff}$ = 15440K
GALEX
Johnson−Cousins
Stromgren
2MASS
WISE
WD 0107+172
Mass = 0.65$M_\odot$ $T_{\rm eff}$ = 32610K
GALEX
SDSS
Johnson−Cousins
WISE
WD 0107+267
Mass = 0.61$M_\odot$ $T_{\rm eff}$ = 14490K
GALEX
SDSS
Johnson−Cousins
Stromgren
2MASS
WISE
F_ν (mJy)
Wavelength (μm)

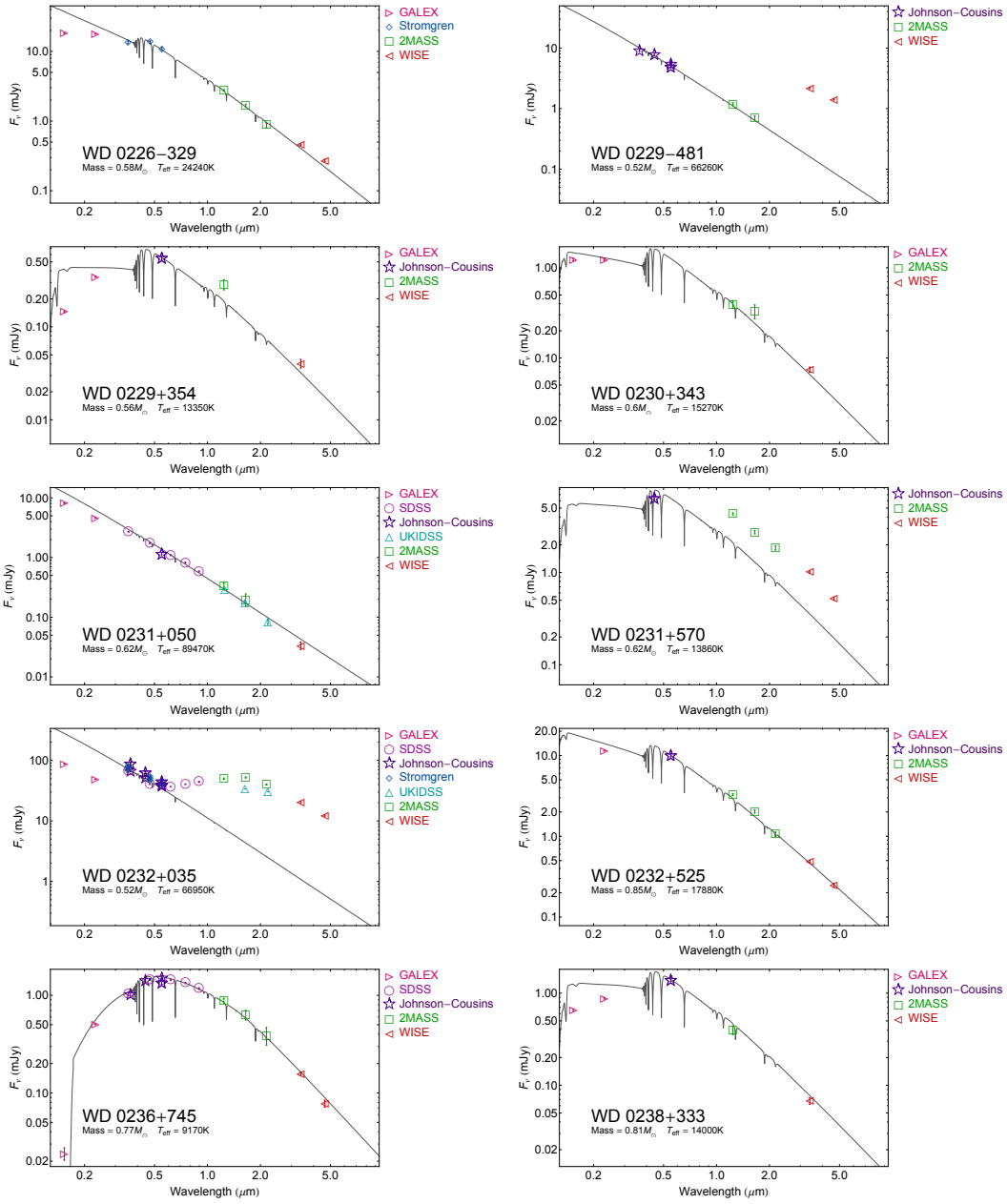

WD 0108+143
Mass = 1.08$M_\odot$ $T_{\rm eff}$ = 9320K
GALEX
SDSS
Johnson−Cousins
UKIDSS
WISE
WD 0112−195
Mass = 0.53$M_\odot$ $T_{\rm eff}$ = 37250K
GALEX
Johnson−Cousins
WD 0113−245
Mass = 0.54$M_\odot$ $T_{\rm eff}$ = 58880K
GALEX
Johnson−Cousins
WISE
WD 0114−034
Mass = 0.58$M_\odot$ $T_{\rm eff}$ = 20390K
GALEX
SDSS
WISE
WD 0115−257
Mass = 0.65$M_\odot$ $T_{\rm eff}$ = 15690K
GALEX
Johnson−Cousins
WD 0115+521
Mass = 0.72$M_\odot$ $T_{\rm eff}$ = 10890K
GALEX
Johnson−Cousins
2MASS
WISE
WD 0116−231
Mass = 0.49$M_\odot$ $T_{\rm eff}$ = 31990K
GALEX
Johnson−Cousins
Stromgren
2MASS
WISE
WD 0118−166
Mass = 0.66$M_\odot$ $T_{\rm eff}$ = 14150K
GALEX
Johnson−Cousins
2MASS
WISE
WD 0120+475
Mass = 0.71$M_\odot$ $T_{\rm eff}$ = 10980K
GALEX
Johnson−Cousins
2MASS
WISE
WD 0125+093
Mass = 0.61$M_\odot$ $T_{\rm eff}$ = 32790K
GALEX
SDSS
Johnson−Cousins
UKIDSS
F_ν (mJy)
Wavelength (μm)

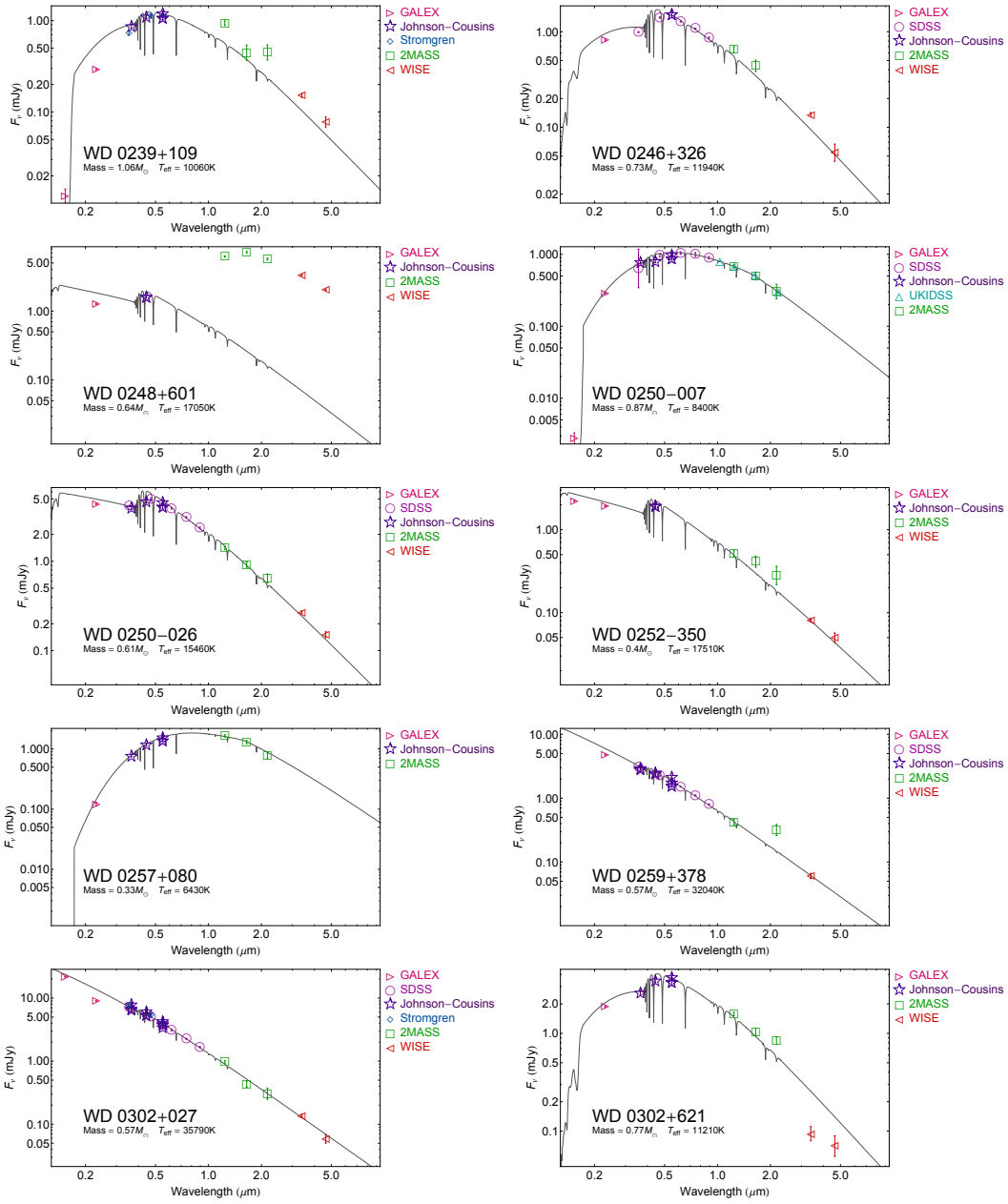

WD 0126+422
Mass = 0.55$M_\odot$ $T_{\rm eff}$ = 23270K
GALEX
SDSS
Stromgren
2MASS
WISE
WD 0127−050
Mass = 0.61$M_\odot$ $T_{\rm eff}$ = 16790K
GALEX
SDSS
2MASS
WISE
WD 0130−273
Mass = 0.6$M_\odot$ $T_{\rm eff}$ = 23320K
GALEX
Johnson−Cousins
WISE
WD 0130−687
Mass = 0.4$M_\odot$ $T_{\rm eff}$ = 36160K
GALEX
Stromgren
2MASS
WD 0131−163
Mass = 0.63$M_\odot$ $T_{\rm eff}$ = 50110K
Johnson−Cousins
Stromgren
2MASS
WISE
WD 0134+181
Mass = 0.51$M_\odot$ $T_{\rm eff}$ = 59540K
GALEX
SDSS
Johnson−Cousins
WD 0135−052
Mass = 0.49$M_\odot$ $T_{\rm eff}$ = 7250K
GALEX
SDSS
Johnson−Cousins
Stromgren
2MASS
WISE
WD 0136+152
Mass = 0.81$M_\odot$ $T_{\rm eff}$ = 8080K
GALEX
SDSS
Stromgren
UKIDSS
2MASS
WISE
WD 0136+768
Mass = 0.51$M_\odot$ $T_{\rm eff}$ = 16910K
GALEX
Johnson−Cousins
Stromgren
2MASS
WISE
WD 0137−229
Mass = 0.66$M_\odot$ $T_{\rm eff}$ = 20270K
GALEX
Johnson−Cousins
2MASS
WISE
F_ν (mJy)
Wavelength (μm)

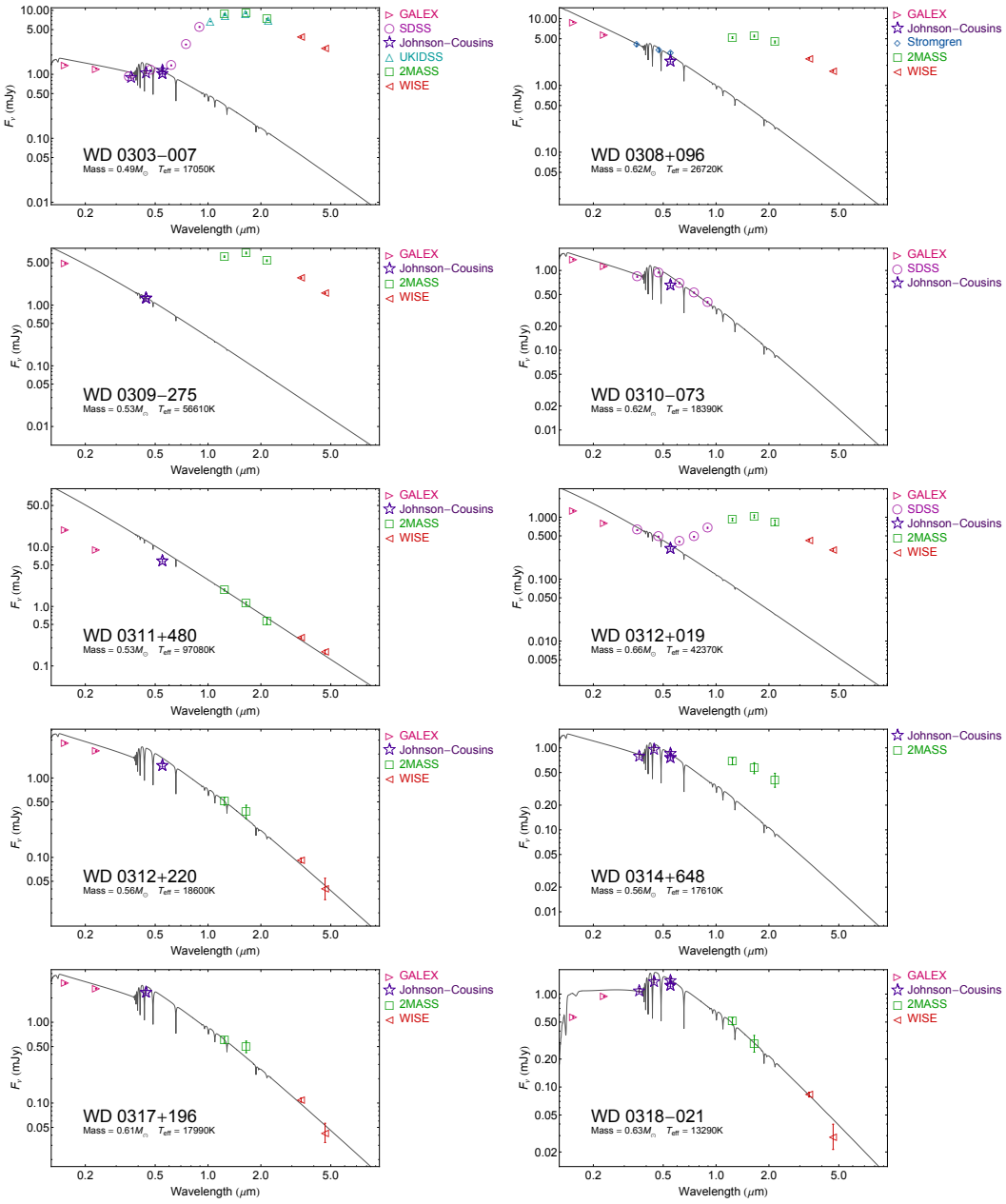

WD 0138−236
Mass = 0.56$M_\odot$ $T_{\rm eff}$ = 35920K
GALEX
Johnson−Cousins
WISE
WD 0143+216
Mass = 0.96$M_\odot$ $T_{\rm eff}$ = 9340K
GALEX
SDSS
Johnson−Cousins
Stromgren
2MASS
WISE
WD 0145−174
Mass = 0.54$M_\odot$ $T_{\rm eff}$ = 7270K
GALEX
SDSS
Johnson−Cousins
WISE
WD 0145−257
Mass = 0.61$M_\odot$ $T_{\rm eff}$ = 26700K
GALEX
Johnson−Cousins
2MASS
WISE
WD 0145+234
Mass = 0.69$M_\odot$ $T_{\rm eff}$ = 13060K
GALEX
SDSS
Johnson−Cousins
2MASS
WISE
WD 0147+674
Mass = 0.57$M_\odot$ $T_{\rm eff}$ = 31250K
GALEX
Johnson−Cousins
2MASS
WISE
WD 0149−114
Mass = 0.66$M_\odot$ $T_{\rm eff}$ = 9180K
GALEX
Johnson−Cousins
2MASS
WD 0149−124
Mass = 0.82$M_\odot$ $T_{\rm eff}$ = 12640K
GALEX
Johnson−Cousins
2MASS
WISE
WD 0151−094
Mass = 0.5$M_\odot$ $T_{\rm eff}$ = 27110K
GALEX
SDSS
Johnson−Cousins
WD 0151+017
Mass = 0.59$M_\odot$ $T_{\rm eff}$ = 12860K
GALEX
SDSS
Johnson−Cousins
Stromgren
UKIDSS
2MASS
WISE
F_ν (mJy)
Wavelength (μm)

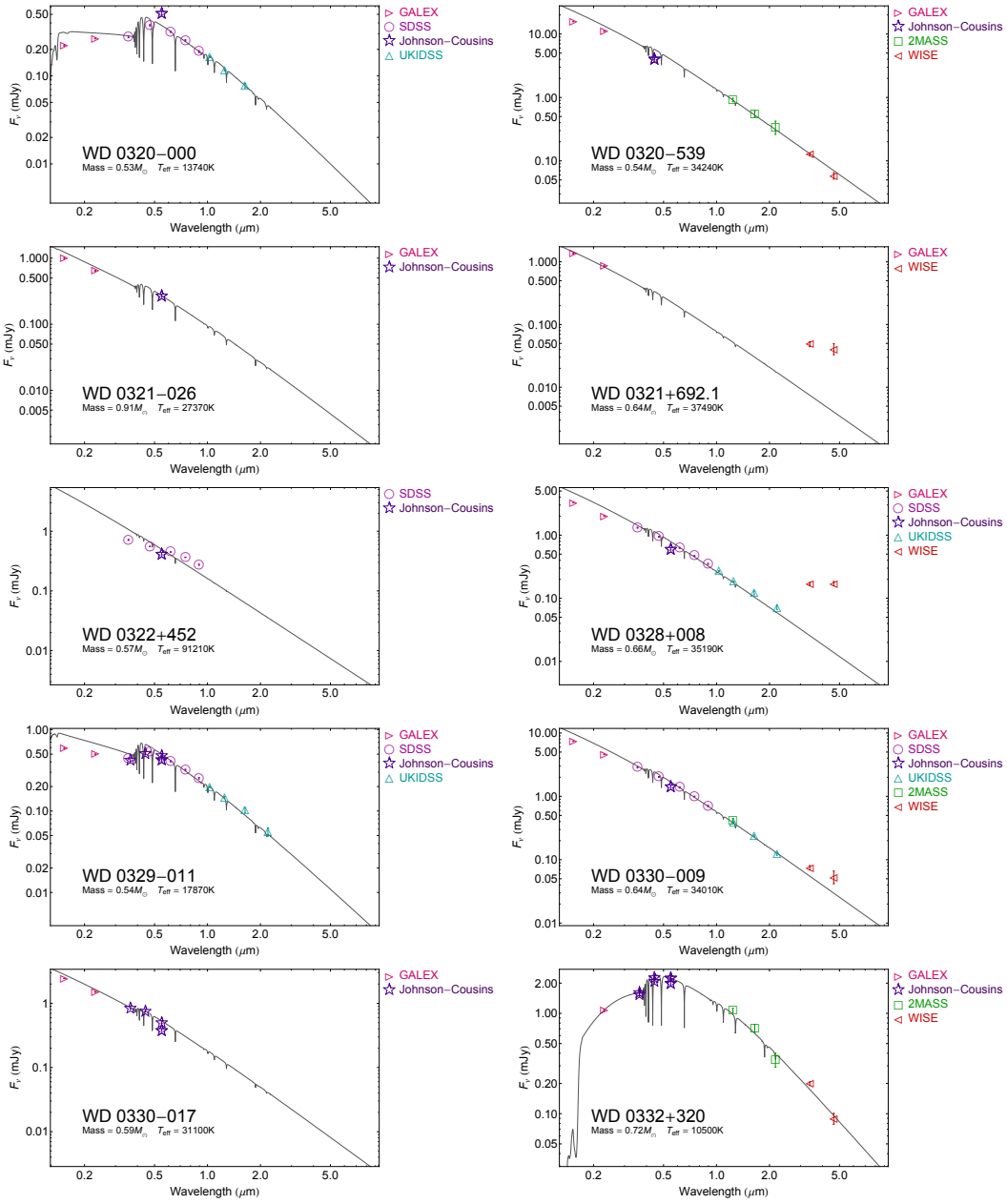

WD 0154−240
Mass = 0.68$M_\odot$ $T_{\rm eff}$ = 74560K
GALEX
Johnson−Cousins
WD 0155−070
Mass = 0.71$M_\odot$ $T_{\rm eff}$ = 10870K
GALEX
SDSS
Johnson−Cousins
2MASS
WISE
WD 0156+015
Mass = 0.68$M_\odot$ $T_{\rm eff}$ = 25080K
SDSS
Johnson−Cousins
UKIDSS
WISE
WD 0159−111
Mass = 0.78$M_\odot$ $T_{\rm eff}$ = 11360K
GALEX
Johnson−Cousins
WISE
WD 0159+754
Mass = 0.59$M_\odot$ $T_{\rm eff}$ = 13740K
Johnson−Cousins
2MASS
WISE
WD 0203−138
Mass = 0.71$M_\odot$ $T_{\rm eff}$ = 49850K
GALEX
SDSS
Johnson−Cousins
2MASS
WISE
WD 0204−233
Mass = 0.56$M_\odot$ $T_{\rm eff}$ = 13680K
GALEX
Johnson−Cousins
2MASS
WISE
WD 0205−304
Mass = 0.59$M_\odot$ $T_{\rm eff}$ = 17810K
GALEX
Johnson−Cousins
2MASS
WISE
WD 0205+133
Mass = 0.5$M_\odot$ $T_{\rm eff}$ = 59300K
GALEX
SDSS
UKIDSS
2MASS
WISE
WD 0205+250
Mass = 0.57$M_\odot$ $T_{\rm eff}$ = 21190K
GALEX
SDSS
Johnson−Cousins
Stromgren
2MASS
WISE
F_ν (mJy)
Wavelength (μm)

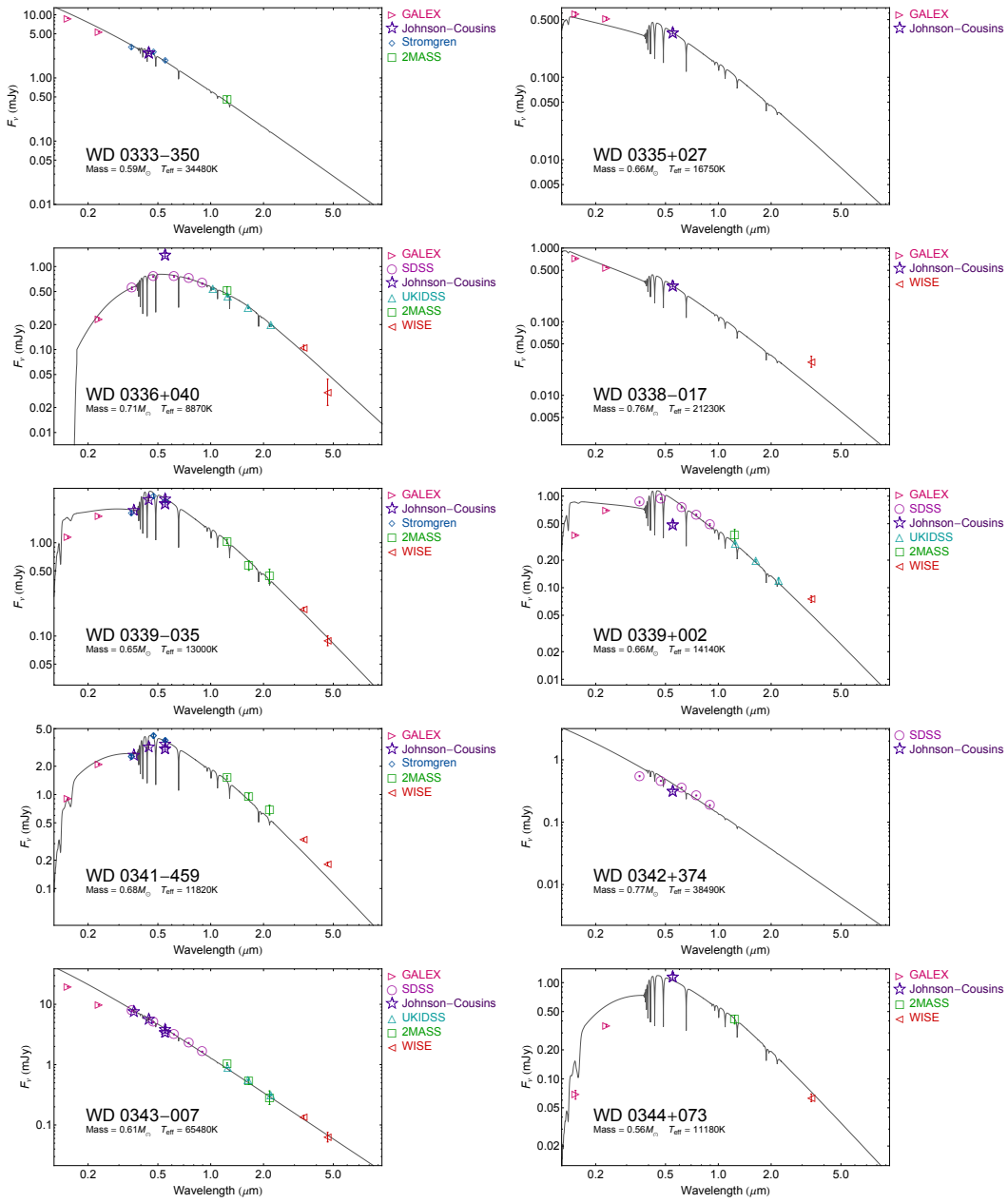

WD 0205+551
Mass = 0.69$M_\odot$ $T_{\rm eff}$ = 17330K
WD 0208−153
Mass = 0.59$M_\odot$ $T_{\rm eff}$ = 22620K
WD 0208−263
Mass = 0.59$M_\odot$ $T_{\rm eff}$ = 34540K
WD 0212−231
Mass = 0.61$M_\odot$ $T_{\rm eff}$ = 27140K
WD 0213+396
Mass = 1$M_\odot$ $T_{\rm eff}$ = 9370K
WD 0218+293
Mass = 0.77$M_\odot$ $T_{\rm eff}$ = 17790K
WD 0220+222
Mass = 0.65$M_\odot$ $T_{\rm eff}$ = 16240K
WD 0221+399
Mass = 0.79$M_\odot$ $T_{\rm eff}$ = 6250K
WD 0222+422.2
Mass = 0.69$M_\odot$ $T_{\rm eff}$ = 6320K
WD 0224+317
Mass = 0.56$M_\odot$ $T_{\rm eff}$ = 15280K
F_ν (mJy)
Wavelength (μm)
GALEX
Johnson−Cousins
2MASS
WISE
SDSS

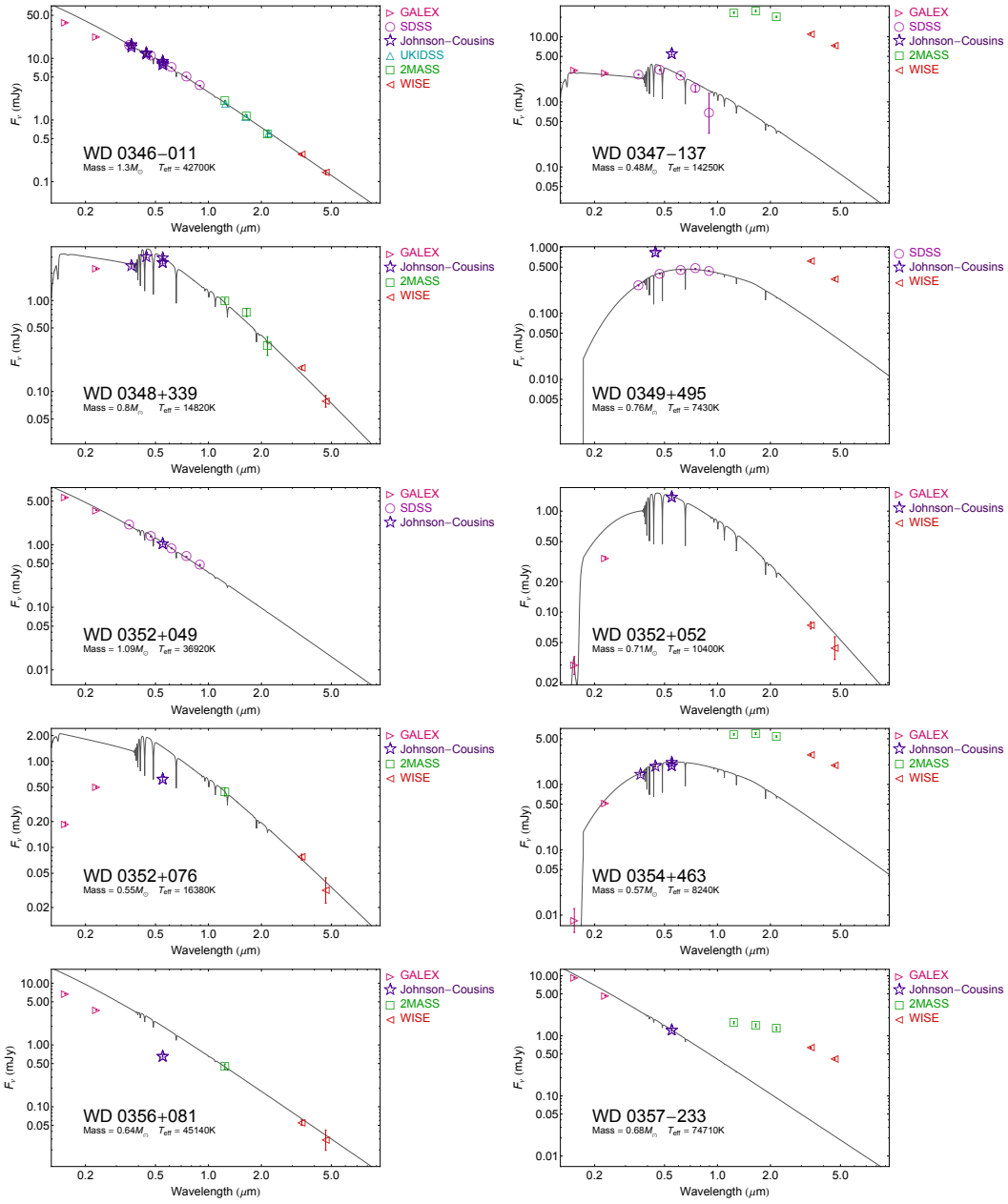

WD 0226−329
Mass = 0.58$M_\odot$ $T_{\rm eff}$ = 24240K
GALEX
Stromgren
2MASS
WISE
WD 0229−481
Mass = 0.52$M_\odot$ $T_{\rm eff}$ = 66260K
Johnson−Cousins
2MASS
WISE
WD 0229+354
Mass = 0.56$M_\odot$ $T_{\rm eff}$ = 13350K
GALEX
Johnson−Cousins
2MASS
WISE
WD 0230+343
Mass = 0.6$M_\odot$ $T_{\rm eff}$ = 15270K
GALEX
2MASS
WISE
WD 0231+050
Mass = 0.62$M_\odot$ $T_{\rm eff}$ = 89470K
GALEX
SDSS
Johnson−Cousins
UKIDSS
2MASS
WISE
WD 0231+570
Mass = 0.62$M_\odot$ $T_{\rm eff}$ = 13860K
Johnson−Cousins
2MASS
WISE
WD 0232+035
Mass = 0.52$M_\odot$ $T_{\rm eff}$ = 66950K
GALEX
SDSS
Johnson−Cousins
Stromgren
UKIDSS
2MASS
WISE
WD 0232+525
Mass = 0.85$M_\odot$ $T_{\rm eff}$ = 17880K
GALEX
Johnson−Cousins
2MASS
WISE
WD 0236+745
Mass = 0.77$M_\odot$ $T_{\rm eff}$ = 9170K
GALEX
SDSS
Johnson−Cousins
2MASS
WISE
WD 0238+333
Mass = 0.81$M_\odot$ $T_{\rm eff}$ = 14000K
GALEX
Johnson−Cousins
2MASS
WISE
F_ν (mJy)
Wavelength (μm)

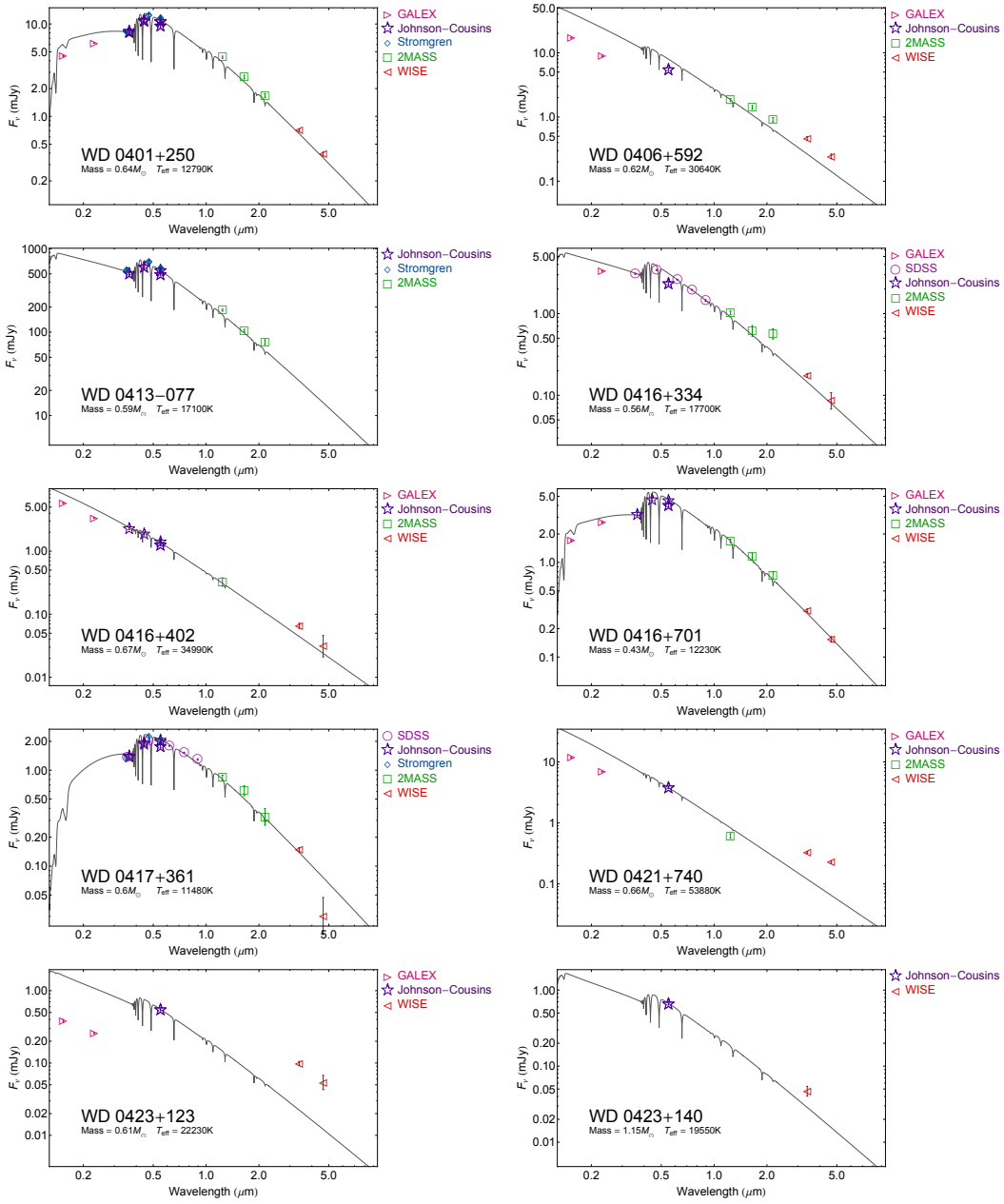

WD 0239+109
Mass = 1.06$M_\odot$ $T_{\rm eff}$ = 10060K
WD 0246+326
Mass = 0.73$M_\odot$ $T_{\rm eff}$ = 11940K
WD 0248+601
Mass = 0.64$M_\odot$ $T_{\rm eff}$ = 17050K
WD 0250−007
Mass = 0.87$M_\odot$ $T_{\rm eff}$ = 8400K
WD 0250−026
Mass = 0.61$M_\odot$ $T_{\rm eff}$ = 15460K
WD 0252−350
Mass = 0.4$M_\odot$ $T_{\rm eff}$ = 17510K
WD 0257+080
Mass = 0.33$M_\odot$ $T_{\rm eff}$ = 6430K
WD 0259+378
Mass = 0.57$M_\odot$ $T_{\rm eff}$ = 32040K
WD 0302+027
Mass = 0.57$M_\odot$ $T_{\rm eff}$ = 35790K
WD 0302+621
Mass = 0.77$M_\odot$ $T_{\rm eff}$ = 11210K
F_ν (mJy)
Wavelength (μm)
GALEX
SDSS
Johnson−Cousins
Stromgren
UKIDSS
2MASS
WISE

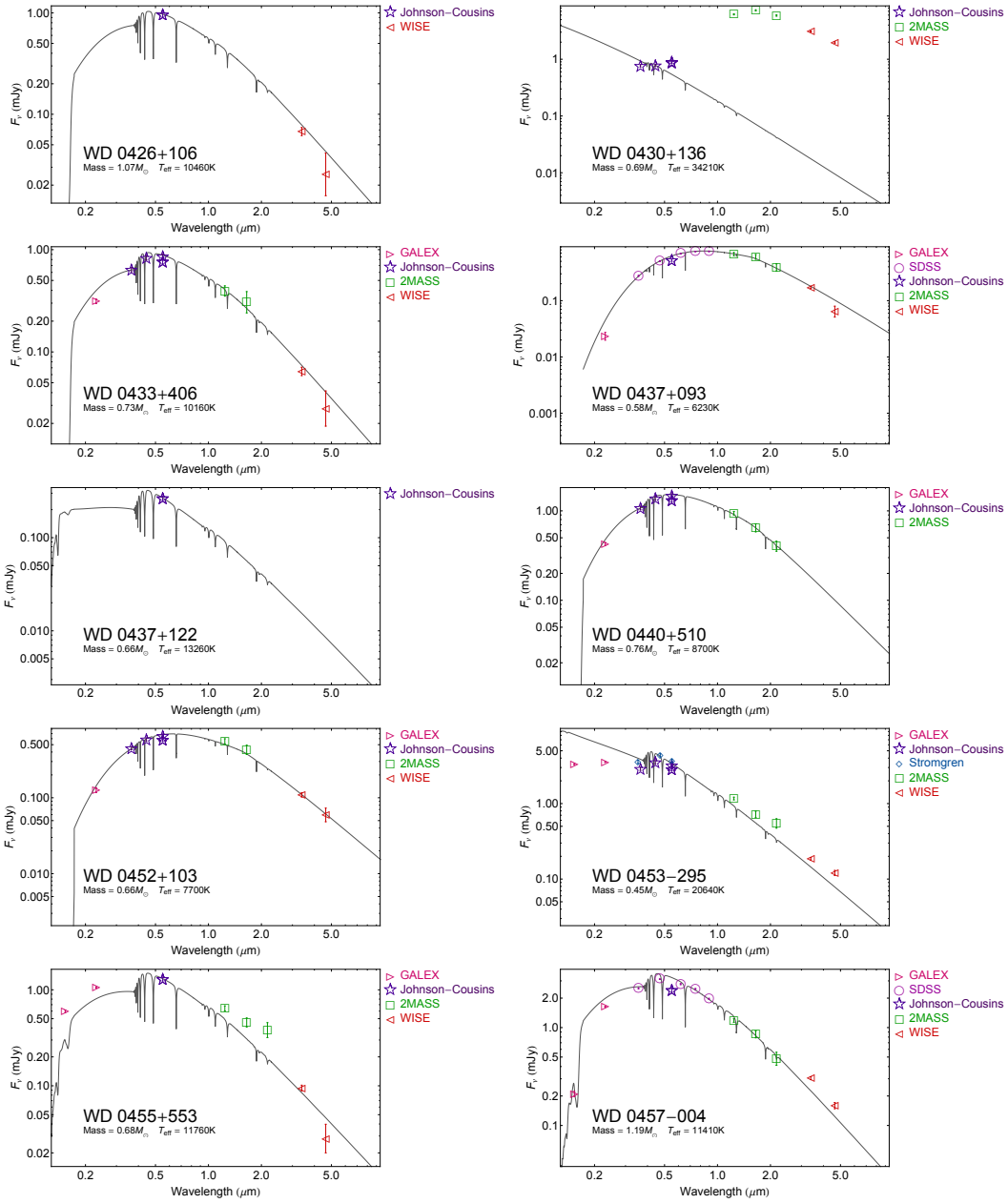

WD 0303−007
Mass = 0.49$M_\odot$ $T_{\rm eff}$ = 17050K
GALEX
SDSS
Johnson−Cousins
UKIDSS
2MASS
WISE
WD 0308+096
Mass = 0.62$M_\odot$ $T_{\rm eff}$ = 26720K
GALEX
Johnson−Cousins
Stromgren
2MASS
WISE
WD 0309−275
Mass = 0.53$M_\odot$ $T_{\rm eff}$ = 56610K
GALEX
Johnson−Cousins
2MASS
WISE
WD 0310−073
Mass = 0.62$M_\odot$ $T_{\rm eff}$ = 18390K
GALEX
SDSS
Johnson−Cousins
WD 0311+480
Mass = 0.53$M_\odot$ $T_{\rm eff}$ = 97080K
GALEX
Johnson−Cousins
2MASS
WISE
WD 0312+019
Mass = 0.66$M_\odot$ $T_{\rm eff}$ = 42370K
GALEX
SDSS
Johnson−Cousins
2MASS
WISE
WD 0312+220
Mass = 0.56$M_\odot$ $T_{\rm eff}$ = 18600K
GALEX
Johnson−Cousins
2MASS
WISE
WD 0314+648
Mass = 0.56$M_\odot$ $T_{\rm eff}$ = 17610K
Johnson−Cousins
2MASS
WD 0317+196
Mass = 0.61$M_\odot$ $T_{\rm eff}$ = 17990K
GALEX
Johnson−Cousins
2MASS
WISE
WD 0318−021
Mass = 0.63$M_\odot$ $T_{\rm eff}$ = 13290K
GALEX
Johnson−Cousins
2MASS
WISE
F_ν (mJy)
Wavelength (μm)

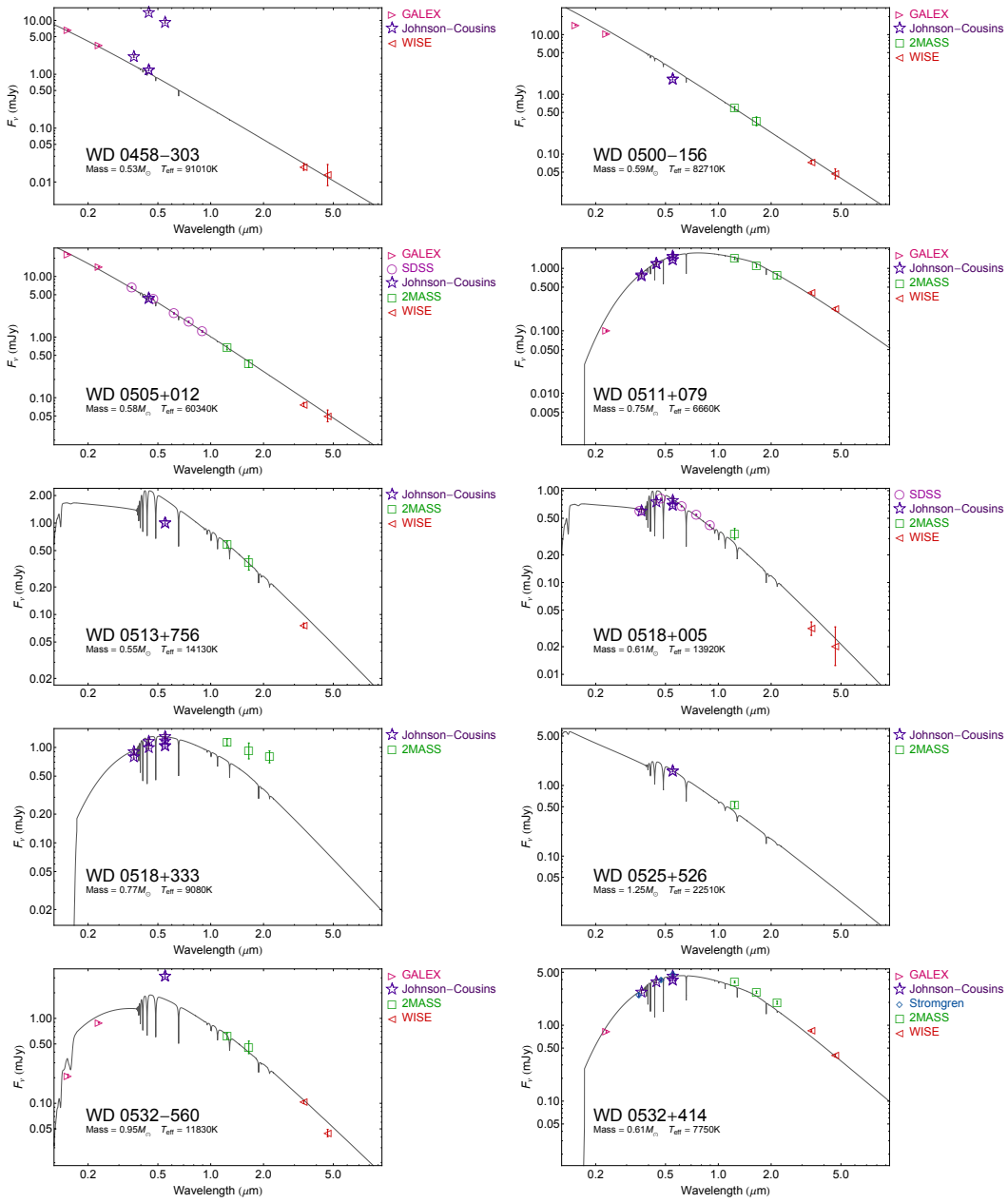

WD 0320−000
Mass = 0.53$M_\odot$ $T_{\rm eff}$ = 13740K
GALEX
SDSS
Johnson−Cousins
UKIDSS
WD 0320−539
Mass = 0.54$M_\odot$ $T_{\rm eff}$ = 34240K
GALEX
Johnson−Cousins
2MASS
WISE
WD 0321−026
Mass = 0.91$M_\odot$ $T_{\rm eff}$ = 27370K
GALEX
Johnson−Cousins
WD 0321+692.1
Mass = 0.64$M_\odot$ $T_{\rm eff}$ = 37490K
GALEX
WISE
WD 0322+452
Mass = 0.57$M_\odot$ $T_{\rm eff}$ = 91210K
SDSS
Johnson−Cousins
WD 0328+008
Mass = 0.66$M_\odot$ $T_{\rm eff}$ = 35190K
GALEX
SDSS
Johnson−Cousins
UKIDSS
WISE
WD 0329−011
Mass = 0.54$M_\odot$ $T_{\rm eff}$ = 17870K
GALEX
SDSS
Johnson−Cousins
UKIDSS
WD 0330−009
Mass = 0.64$M_\odot$ $T_{\rm eff}$ = 34010K
GALEX
SDSS
Johnson−Cousins
UKIDSS
2MASS
WISE
WD 0330−017
Mass = 0.59$M_\odot$ $T_{\rm eff}$ = 31100K
GALEX
Johnson−Cousins
WD 0332+320
Mass = 0.72$M_\odot$ $T_{\rm eff}$ = 10500K
GALEX
Johnson−Cousins
2MASS
WISE
F_ν (mJy)
Wavelength (μm)

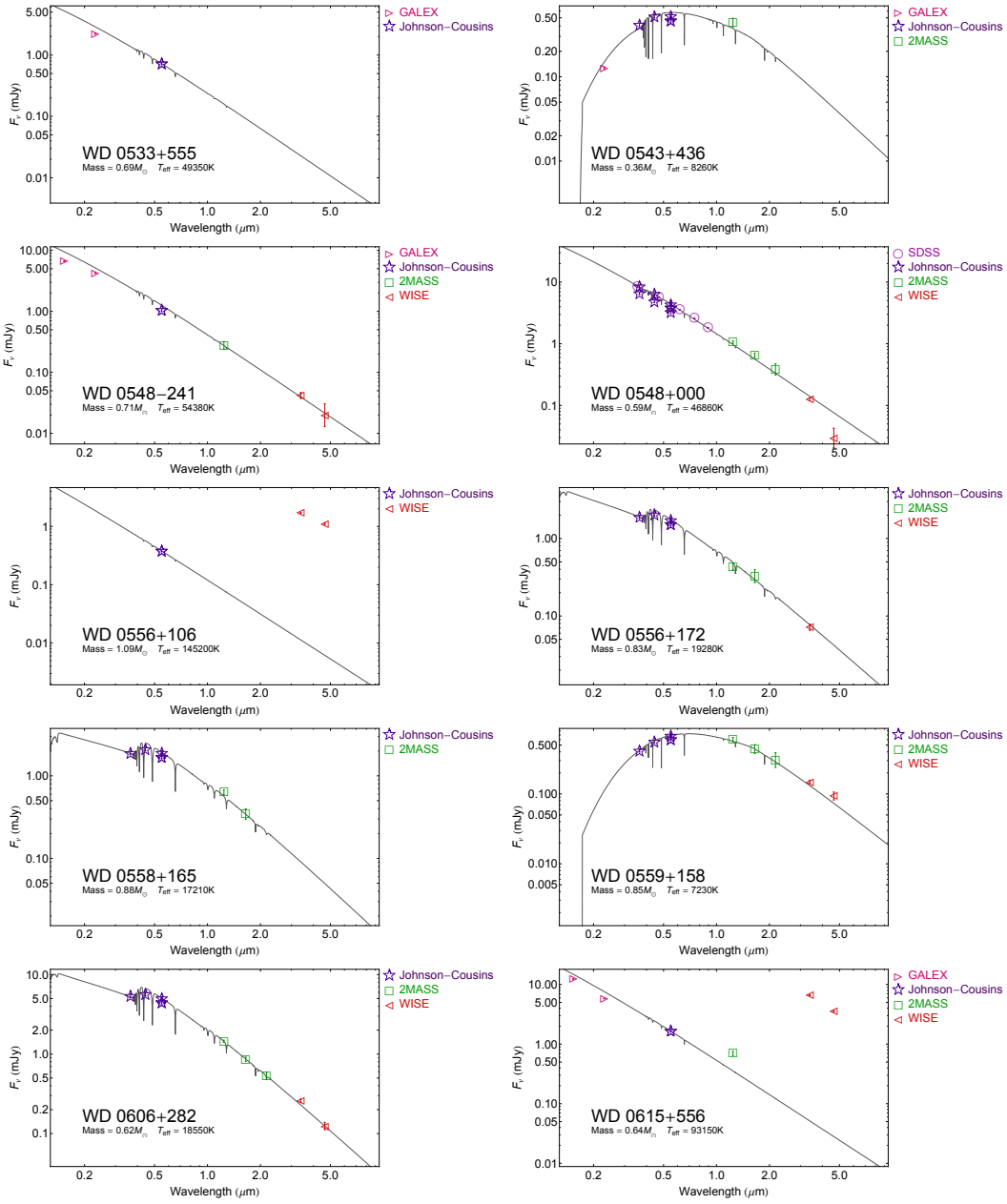

WD 0333−350
Mass = 0.59$M_\odot$ $T_{\rm eff}$ = 34480K
GALEX
Johnson−Cousins
Stromgren
2MASS
WD 0335+027
Mass = 0.66$M_\odot$ $T_{\rm eff}$ = 16750K
GALEX
Johnson−Cousins
WD 0336+040
Mass = 0.71$M_\odot$ $T_{\rm eff}$ = 8870K
GALEX
SDSS
Johnson−Cousins
UKIDSS
2MASS
WISE
WD 0338−017
Mass = 0.76$M_\odot$ $T_{\rm eff}$ = 21230K
GALEX
Johnson−Cousins
WISE
WD 0339−035
Mass = 0.65$M_\odot$ $T_{\rm eff}$ = 13000K
GALEX
Johnson−Cousins
Stromgren
2MASS
WISE
WD 0339+002
Mass = 0.66$M_\odot$ $T_{\rm eff}$ = 14140K
GALEX
SDSS
Johnson−Cousins
UKIDSS
2MASS
WISE
WD 0341−459
Mass = 0.68$M_\odot$ $T_{\rm eff}$ = 11820K
GALEX
Johnson−Cousins
Stromgren
2MASS
WISE
WD 0342+374
Mass = 0.77$M_\odot$ $T_{\rm eff}$ = 38490K
SDSS
Johnson−Cousins
WD 0343−007
Mass = 0.61$M_\odot$ $T_{\rm eff}$ = 65480K
GALEX
SDSS
Johnson−Cousins
UKIDSS
2MASS
WISE
WD 0344+073
Mass = 0.56$M_\odot$ $T_{\rm eff}$ = 11180K
GALEX
Johnson−Cousins
2MASS
WISE
F_ν (mJy)
Wavelength (μm)

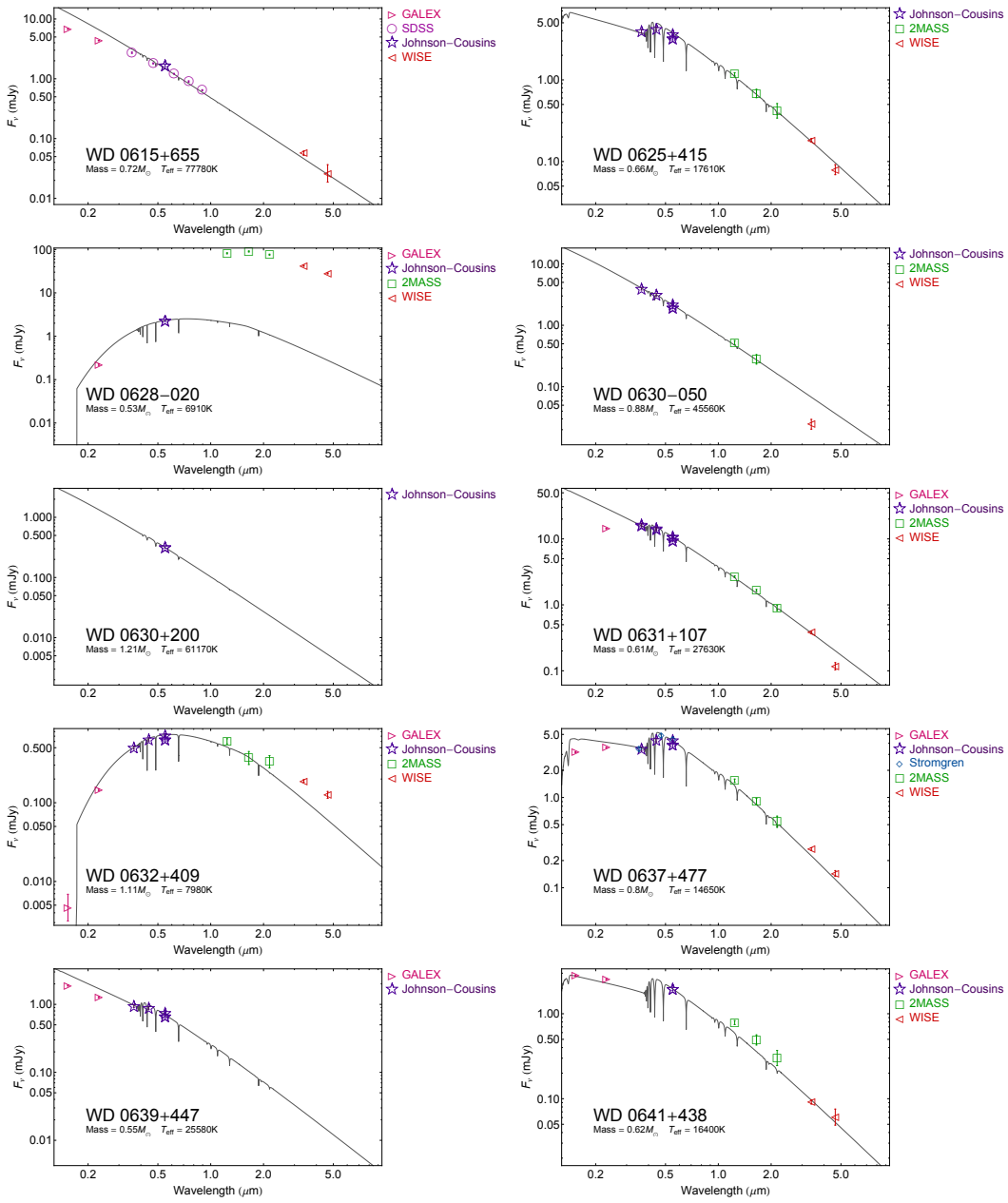

WD 0346−011
Mass = 1.3$M_\odot$ $T_{\rm eff}$ = 42700K
WD 0347−137
Mass = 0.48$M_\odot$ $T_{\rm eff}$ = 14250K
WD 0348+339
Mass = 0.8$M_\odot$ $T_{\rm eff}$ = 14820K
WD 0349+495
Mass = 0.76$M_\odot$ $T_{\rm eff}$ = 7430K
WD 0352+049
Mass = 1.09$M_\odot$ $T_{\rm eff}$ = 36920K
WD 0352+052
Mass = 0.71$M_\odot$ $T_{\rm eff}$ = 10400K
WD 0352+076
Mass = 0.55$M_\odot$ $T_{\rm eff}$ = 16380K
WD 0354+463
Mass = 0.57$M_\odot$ $T_{\rm eff}$ = 8240K
WD 0356+081
Mass = 0.64$M_\odot$ $T_{\rm eff}$ = 45140K
WD 0357−233
Mass = 0.68$M_\odot$ $T_{\rm eff}$ = 74710K
GALEX
SDSS
Johnson−Cousins
UKIDSS
2MASS
WISE
F_ν (mJy)
Wavelength (μm)

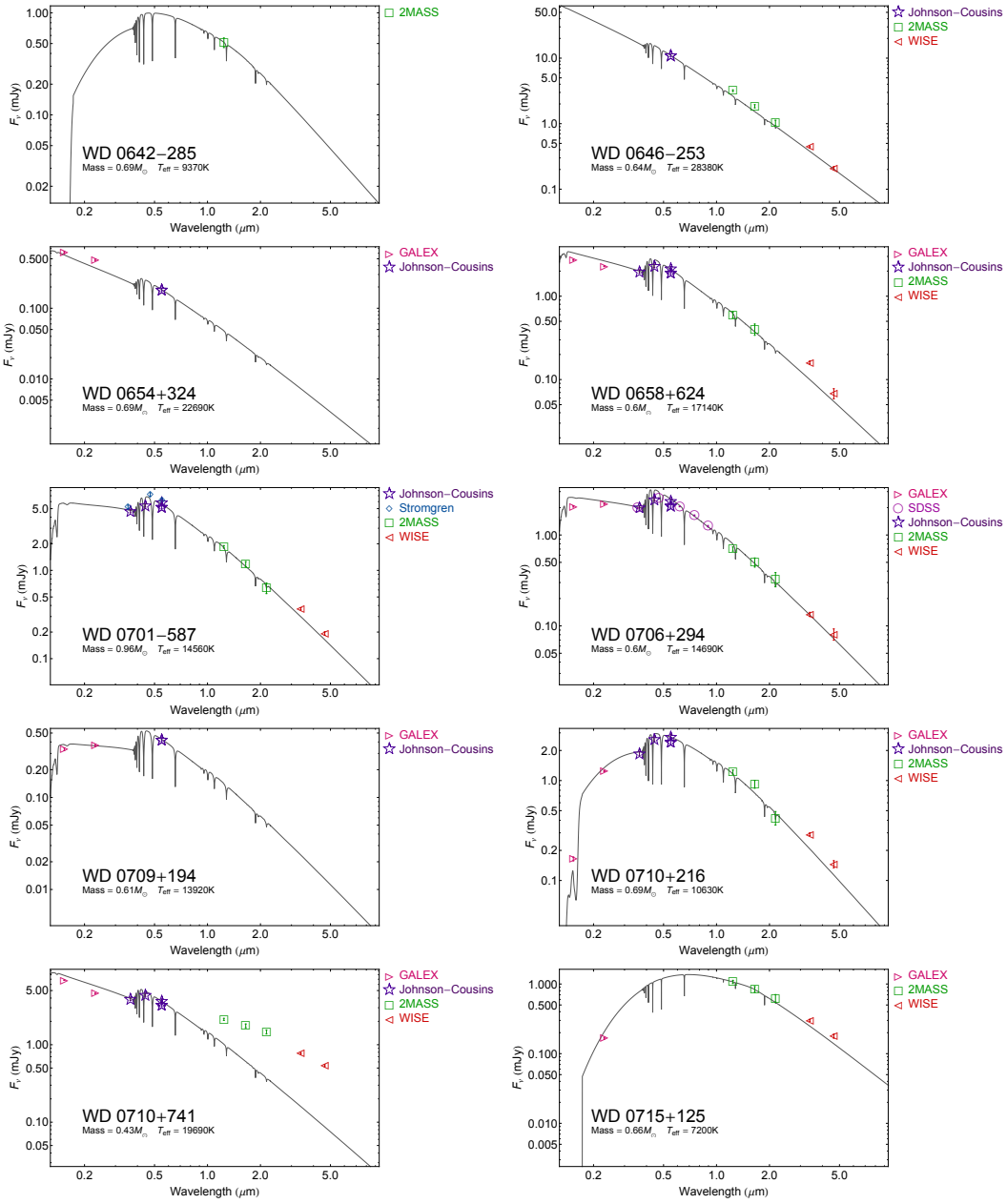

WD 0401+250
Mass = 0.64$M_\odot$ $T_{\rm eff}$ = 12790K
GALEX
Johnson−Cousins
Stromgren
2MASS
WISE
WD 0406+592
Mass = 0.62$M_\odot$ $T_{\rm eff}$ = 30640K
GALEX
Johnson−Cousins
2MASS
WISE
WD 0413−077
Mass = 0.59$M_\odot$ $T_{\rm eff}$ = 17100K
Johnson−Cousins
Stromgren
2MASS
WD 0416+334
Mass = 0.56$M_\odot$ $T_{\rm eff}$ = 17700K
GALEX
SDSS
Johnson−Cousins
2MASS
WISE
WD 0416+402
Mass = 0.67$M_\odot$ $T_{\rm eff}$ = 34990K
GALEX
Johnson−Cousins
2MASS
WISE
WD 0416+701
Mass = 0.43$M_\odot$ $T_{\rm eff}$ = 12230K
GALEX
Johnson−Cousins
2MASS
WISE
WD 0417+361
Mass = 0.6$M_\odot$ $T_{\rm eff}$ = 11480K
SDSS
Johnson−Cousins
Stromgren
2MASS
WISE
WD 0421+740
Mass = 0.66$M_\odot$ $T_{\rm eff}$ = 53880K
GALEX
Johnson−Cousins
2MASS
WISE
WD 0423+123
Mass = 0.61$M_\odot$ $T_{\rm eff}$ = 22230K
GALEX
Johnson−Cousins
WISE
WD 0423+140
Mass = 1.15$M_\odot$ $T_{\rm eff}$ = 19550K
Johnson−Cousins
WISE
F_ν (mJy)
Wavelength (μm)

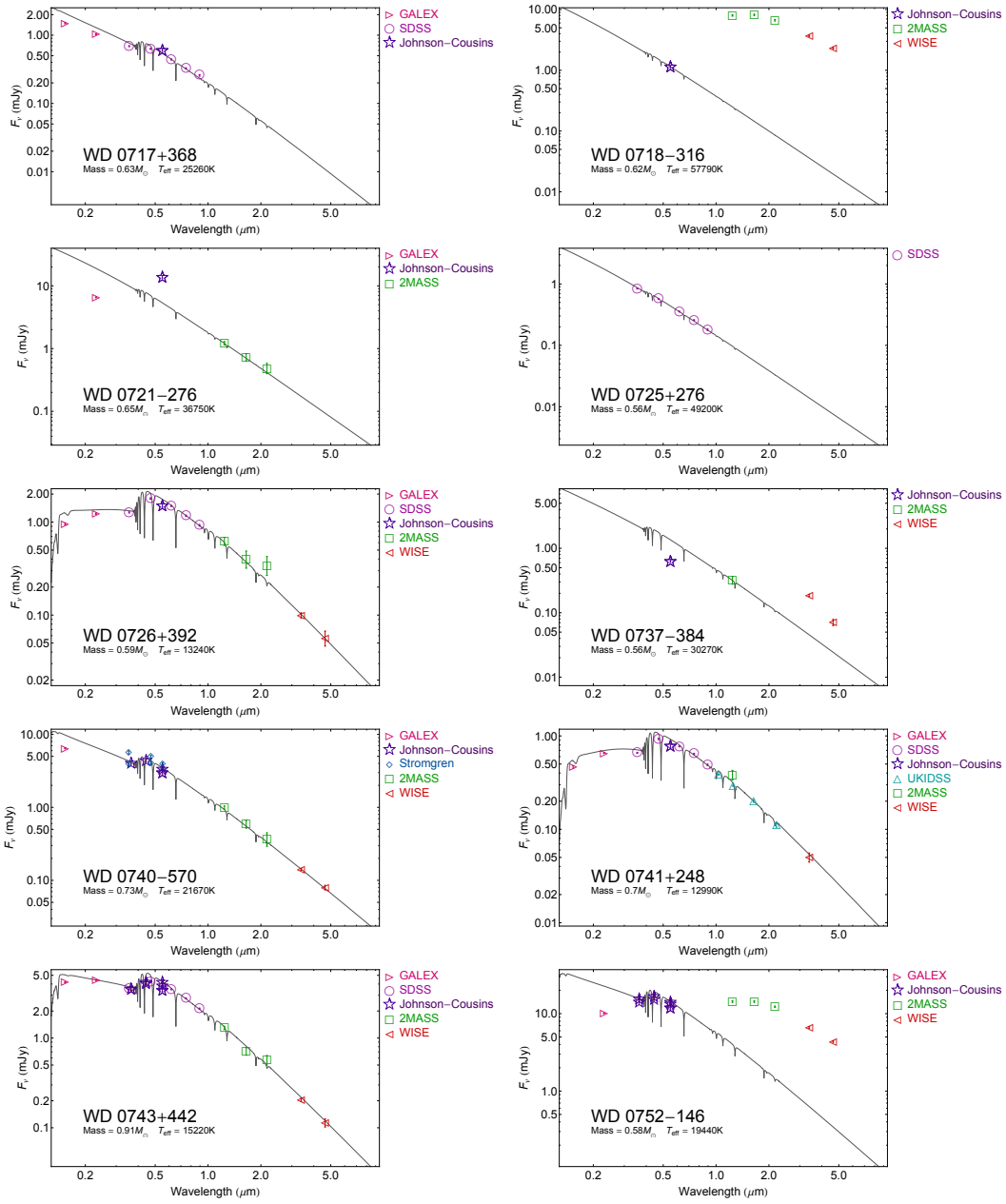

WD 0426+106
Mass = 1.07$M_\odot$ $T_{\rm eff}$ = 10460K
Johnson–Cousins
WISE
WD 0430+136
Mass = 0.69$M_\odot$ $T_{\rm eff}$ = 34210K
Johnson–Cousins
2MASS
WISE
WD 0433+406
Mass = 0.73$M_\odot$ $T_{\rm eff}$ = 10160K
GALEX
Johnson–Cousins
2MASS
WISE
WD 0437+093
Mass = 0.58$M_\odot$ $T_{\rm eff}$ = 6230K
GALEX
SDSS
Johnson–Cousins
2MASS
WISE
WD 0437+122
Mass = 0.66$M_\odot$ $T_{\rm eff}$ = 13260K
Johnson–Cousins
WD 0440+510
Mass = 0.76$M_\odot$ $T_{\rm eff}$ = 8700K
GALEX
Johnson–Cousins
2MASS
WD 0452+103
Mass = 0.66$M_\odot$ $T_{\rm eff}$ = 7700K
GALEX
Johnson–Cousins
2MASS
WISE
WD 0453−295
Mass = 0.45$M_\odot$ $T_{\rm eff}$ = 20640K
GALEX
Johnson–Cousins
Stromgren
2MASS
WISE
WD 0455+553
Mass = 0.68$M_\odot$ $T_{\rm eff}$ = 11760K
GALEX
Johnson–Cousins
2MASS
WISE
WD 0457−004
Mass = 1.19$M_\odot$ $T_{\rm eff}$ = 11410K
GALEX
SDSS
Johnson–Cousins
2MASS
WISE
F_ν (mJy)
Wavelength (μm)

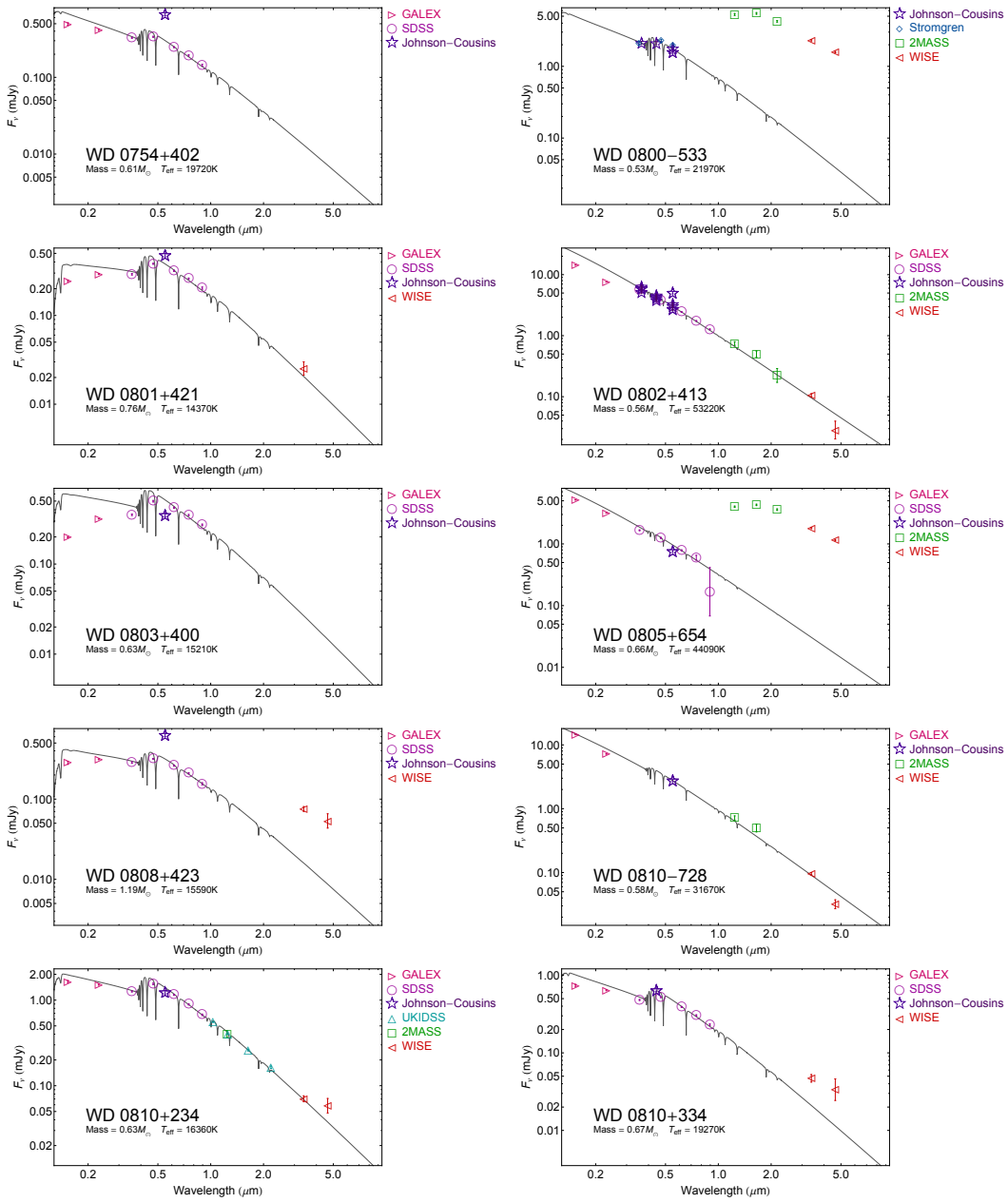

WD 0458−303
Mass = 0.53$M_\odot$ $T_{\rm eff}$ = 91010K
WD 0500−156
Mass = 0.59$M_\odot$ $T_{\rm eff}$ = 82710K
WD 0505+012
Mass = 0.58$M_\odot$ $T_{\rm eff}$ = 60340K
WD 0511+079
Mass = 0.75$M_\odot$ $T_{\rm eff}$ = 6660K
WD 0513+756
Mass = 0.55$M_\odot$ $T_{\rm eff}$ = 14130K
WD 0518+005
Mass = 0.61$M_\odot$ $T_{\rm eff}$ = 13920K
WD 0518+333
Mass = 0.77$M_\odot$ $T_{\rm eff}$ = 9080K
WD 0525+526
Mass = 1.25$M_\odot$ $T_{\rm eff}$ = 22510K
WD 0532−560
Mass = 0.95$M_\odot$ $T_{\rm eff}$ = 11830K
WD 0532+414
Mass = 0.61$M_\odot$ $T_{\rm eff}$ = 7750K
F_ν (mJy)
Wavelength (μm)
GALEX
SDSS
Johnson−Cousins
Stromgren
2MASS
WISE

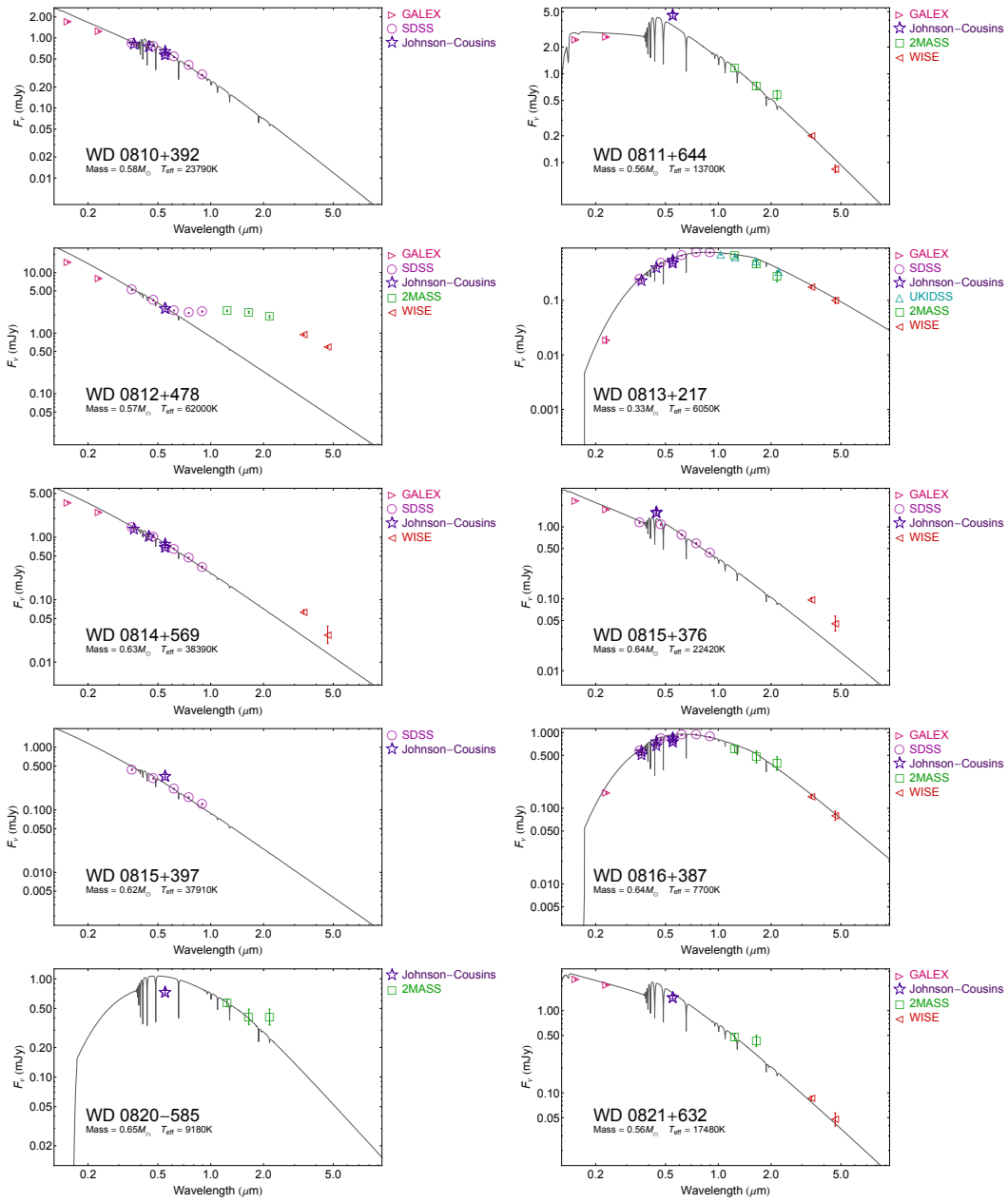

WD 0533+555
Mass = 0.69$M_\odot$ $T_{\rm eff}$ = 49350K
GALEX
Johnson–Cousins
WD 0543+436
Mass = 0.36$M_\odot$ $T_{\rm eff}$ = 8260K
GALEX
Johnson–Cousins
2MASS
WD 0548–241
Mass = 0.71$M_\odot$ $T_{\rm eff}$ = 54380K
GALEX
Johnson–Cousins
2MASS
WISE
WD 0548+000
Mass = 0.59$M_\odot$ $T_{\rm eff}$ = 46860K
SDSS
Johnson–Cousins
2MASS
WISE
WD 0556+106
Mass = 1.09$M_\odot$ $T_{\rm eff}$ = 145200K
Johnson–Cousins
WISE
WD 0556+172
Mass = 0.83$M_\odot$ $T_{\rm eff}$ = 19280K
Johnson–Cousins
2MASS
WISE
WD 0558+165
Mass = 0.88$M_\odot$ $T_{\rm eff}$ = 17210K
Johnson–Cousins
2MASS
WD 0559+158
Mass = 0.85$M_\odot$ $T_{\rm eff}$ = 7230K
Johnson–Cousins
2MASS
WISE
WD 0606+282
Mass = 0.62$M_\odot$ $T_{\rm eff}$ = 18550K
Johnson–Cousins
2MASS
WISE
WD 0615+556
Mass = 0.64$M_\odot$ $T_{\rm eff}$ = 93150K
GALEX
Johnson–Cousins
2MASS
WISE
F_ν (mJy)
Wavelength (μm)

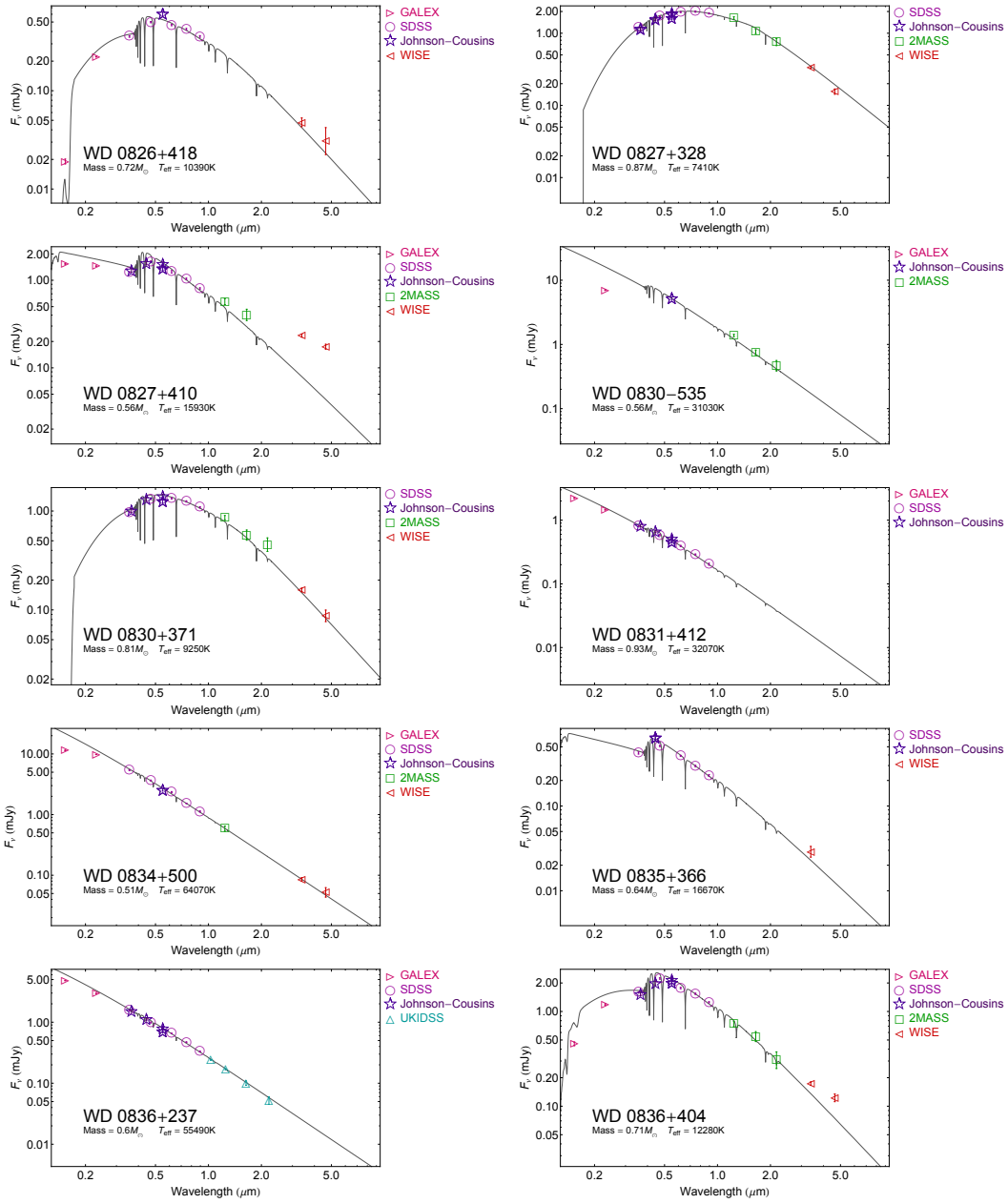

GALEX
SDSS
Johnson−Cousins
WISE
WD 0615+655
Mass = 0.72$M_\odot$ $T_{\rm eff}$ = 77780K
WD 0625+415
Mass = 0.66$M_\odot$ $T_{\rm eff}$ = 17610K
WD 0628−020
Mass = 0.53$M_\odot$ $T_{\rm eff}$ = 6910K
WD 0630−050
Mass = 0.88$M_\odot$ $T_{\rm eff}$ = 45560K
WD 0630+200
Mass = 1.21$M_\odot$ $T_{\rm eff}$ = 61170K
WD 0631+107
Mass = 0.61$M_\odot$ $T_{\rm eff}$ = 27630K
WD 0632+409
Mass = 1.11$M_\odot$ $T_{\rm eff}$ = 7980K
WD 0637+477
Mass = 0.8$M_\odot$ $T_{\rm eff}$ = 14650K
Stromgren
2MASS
WD 0639+447
Mass = 0.55$M_\odot$ $T_{\rm eff}$ = 25580K
WD 0641+438
Mass = 0.62$M_\odot$ $T_{\rm eff}$ = 16400K
F_ν (mJy)
Wavelength (μm)

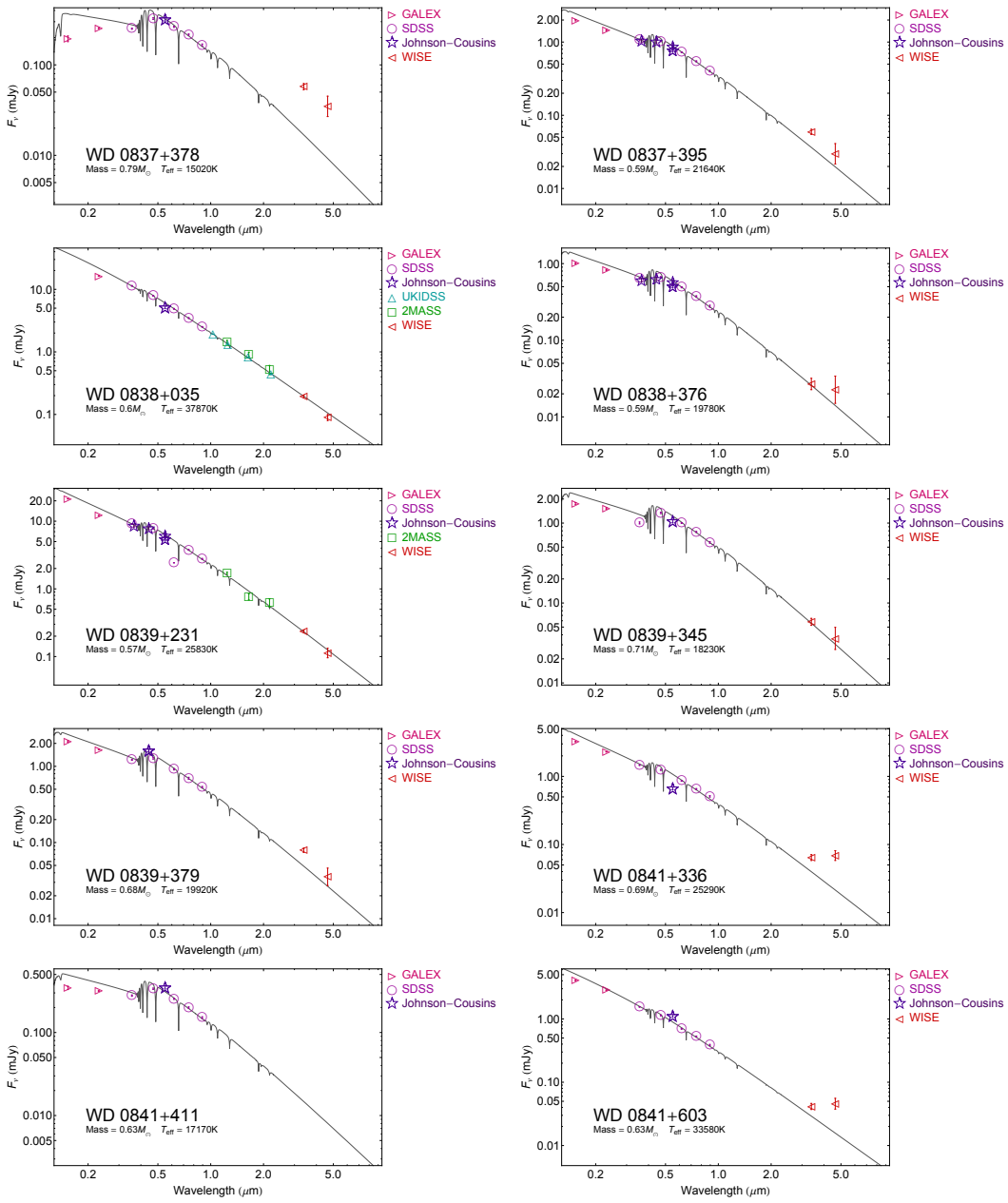

WD 0642−285
Mass = 0.69$M_\odot$ $T_{\rm eff}$ = 9370K
2MASS
WD 0646−253
Mass = 0.64$M_\odot$ $T_{\rm eff}$ = 28380K
Johnson−Cousins
2MASS
WISE
WD 0654+324
Mass = 0.69$M_\odot$ $T_{\rm eff}$ = 22690K
GALEX
Johnson−Cousins
WD 0658+624
Mass = 0.6$M_\odot$ $T_{\rm eff}$ = 17140K
GALEX
Johnson−Cousins
2MASS
WISE
WD 0701−587
Mass = 0.96$M_\odot$ $T_{\rm eff}$ = 14560K
Johnson−Cousins
Stromgren
2MASS
WISE
WD 0706+294
Mass = 0.6$M_\odot$ $T_{\rm eff}$ = 14690K
GALEX
SDSS
Johnson−Cousins
2MASS
WISE
WD 0709+194
Mass = 0.61$M_\odot$ $T_{\rm eff}$ = 13920K
GALEX
Johnson−Cousins
WD 0710+216
Mass = 0.69$M_\odot$ $T_{\rm eff}$ = 10630K
GALEX
Johnson−Cousins
2MASS
WISE
WD 0710+741
Mass = 0.43$M_\odot$ $T_{\rm eff}$ = 19690K
GALEX
Johnson−Cousins
2MASS
WISE
WD 0715+125
Mass = 0.66$M_\odot$ $T_{\rm eff}$ = 7200K
GALEX
2MASS
WISE
F_ν (mJy)
Wavelength (μm)

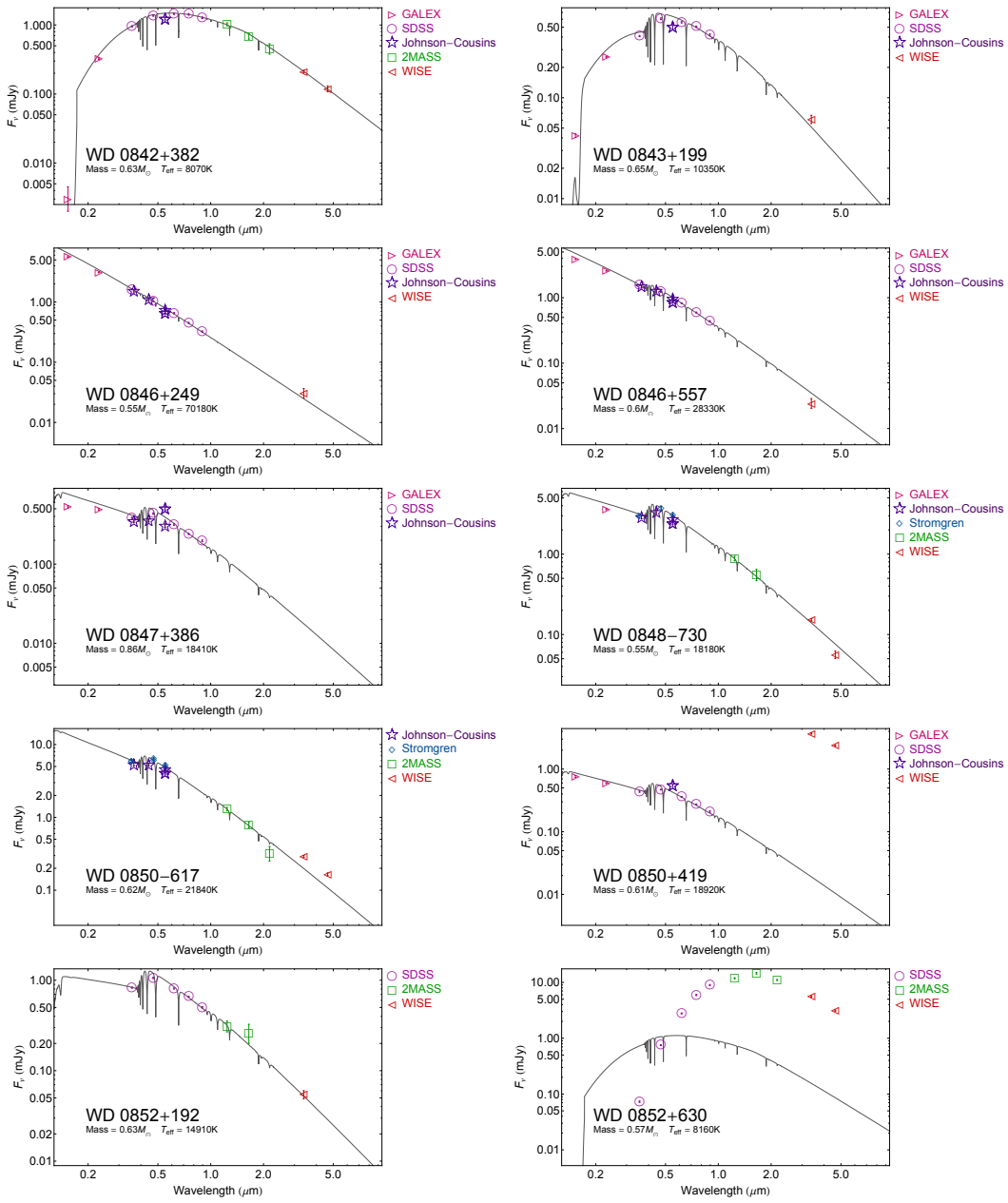

WD 0717+368
Mass = 0.63$M_\odot$ $T_{\rm eff}$ = 25260K
GALEX
SDSS
Johnson−Cousins
WD 0718−316
Mass = 0.62$M_\odot$ $T_{\rm eff}$ = 57790K
Johnson−Cousins
2MASS
WISE
WD 0721−276
Mass = 0.65$M_\odot$ $T_{\rm eff}$ = 36750K
GALEX
Johnson−Cousins
2MASS
WD 0725+276
Mass = 0.56$M_\odot$ $T_{\rm eff}$ = 49200K
SDSS
WD 0726+392
Mass = 0.59$M_\odot$ $T_{\rm eff}$ = 13240K
GALEX
SDSS
Johnson−Cousins
2MASS
WISE
WD 0737−384
Mass = 0.56$M_\odot$ $T_{\rm eff}$ = 30270K
Johnson−Cousins
2MASS
WISE
WD 0740−570
Mass = 0.73$M_\odot$ $T_{\rm eff}$ = 21670K
GALEX
Johnson−Cousins
Stromgren
2MASS
WISE
WD 0741+248
Mass = 0.7$M_\odot$ $T_{\rm eff}$ = 12990K
GALEX
SDSS
Johnson−Cousins
UKIDSS
2MASS
WISE
WD 0743+442
Mass = 0.91$M_\odot$ $T_{\rm eff}$ = 15220K
GALEX
SDSS
Johnson−Cousins
2MASS
WISE
WD 0752−146
Mass = 0.58$M_\odot$ $T_{\rm eff}$ = 19440K
GALEX
Johnson−Cousins
2MASS
WISE
F_ν (mJy)
Wavelength (μm)

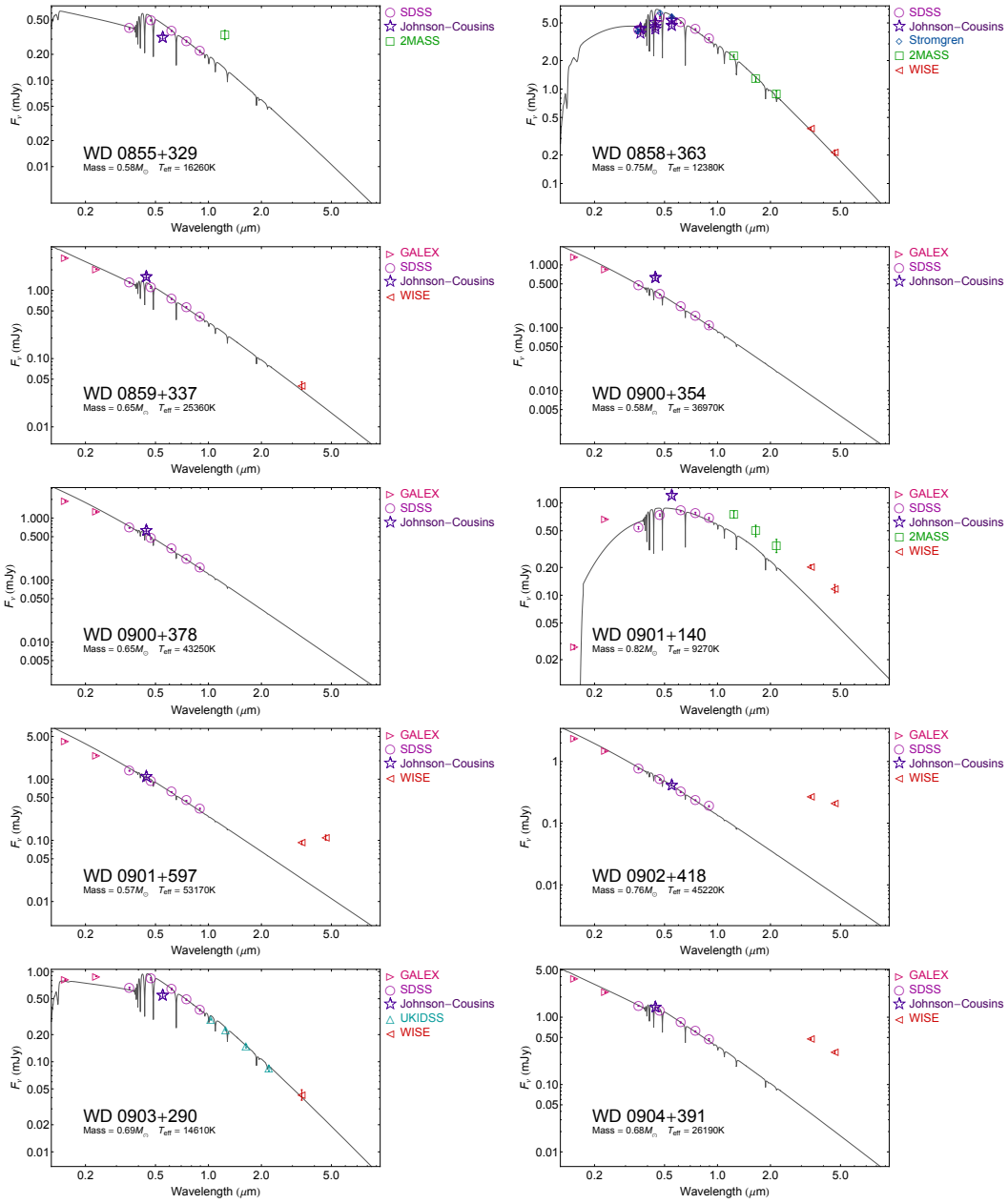

WD 0754+402
Mass = 0.61$M_\odot$ $T_{\rm eff}$ = 19720K
WD 0800−533
Mass = 0.53$M_\odot$ $T_{\rm eff}$ = 21970K
WD 0801+421
Mass = 0.76$M_\odot$ $T_{\rm eff}$ = 14370K
WD 0802+413
Mass = 0.56$M_\odot$ $T_{\rm eff}$ = 53220K
WD 0803+400
Mass = 0.63$M_\odot$ $T_{\rm eff}$ = 15210K
WD 0805+654
Mass = 0.66$M_\odot$ $T_{\rm eff}$ = 44090K
WD 0808+423
Mass = 1.19$M_\odot$ $T_{\rm eff}$ = 15590K
WD 0810−728
Mass = 0.58$M_\odot$ $T_{\rm eff}$ = 31670K
WD 0810+234
Mass = 0.63$M_\odot$ $T_{\rm eff}$ = 16360K
WD 0810+334
Mass = 0.67$M_\odot$ $T_{\rm eff}$ = 19270K
F_ν (mJy)
Wavelength (μm)
GALEX
SDSS
Johnson−Cousins
Stromgren
2MASS
UKIDSS
WISE

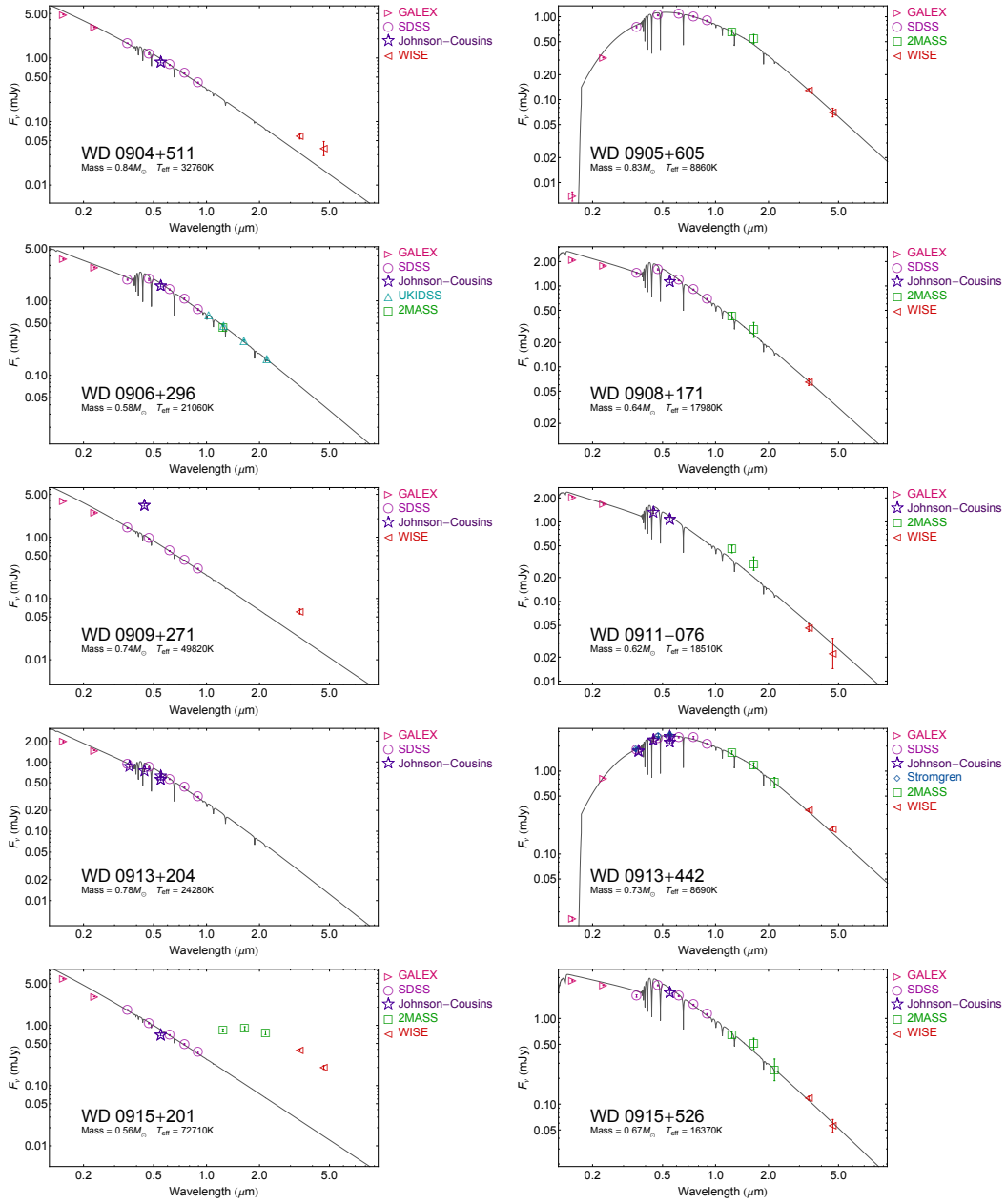

WD 0810+392
Mass = 0.58$M_\odot$ $T_{\rm eff}$ = 23790K
GALEX
SDSS
Johnson–Cousins
WD 0811+644
Mass = 0.56$M_\odot$ $T_{\rm eff}$ = 13700K
GALEX
Johnson–Cousins
2MASS
WISE
WD 0812+478
Mass = 0.57$M_\odot$ $T_{\rm eff}$ = 62000K
GALEX
SDSS
Johnson–Cousins
2MASS
WISE
WD 0813+217
Mass = 0.33$M_\odot$ $T_{\rm eff}$ = 6050K
GALEX
SDSS
Johnson–Cousins
UKIDSS
2MASS
WISE
WD 0814+569
Mass = 0.63$M_\odot$ $T_{\rm eff}$ = 38390K
GALEX
SDSS
Johnson–Cousins
WISE
WD 0815+376
Mass = 0.64$M_\odot$ $T_{\rm eff}$ = 22420K
GALEX
SDSS
Johnson–Cousins
WISE
WD 0815+397
Mass = 0.62$M_\odot$ $T_{\rm eff}$ = 37910K
SDSS
Johnson–Cousins
WD 0816+387
Mass = 0.64$M_\odot$ $T_{\rm eff}$ = 7700K
GALEX
SDSS
Johnson–Cousins
2MASS
WISE
WD 0820−585
Mass = 0.65$M_\odot$ $T_{\rm eff}$ = 9180K
Johnson–Cousins
2MASS
WD 0821+632
Mass = 0.56$M_\odot$ $T_{\rm eff}$ = 17480K
GALEX
Johnson–Cousins
2MASS
WISE
F_ν (mJy)
Wavelength (μm)

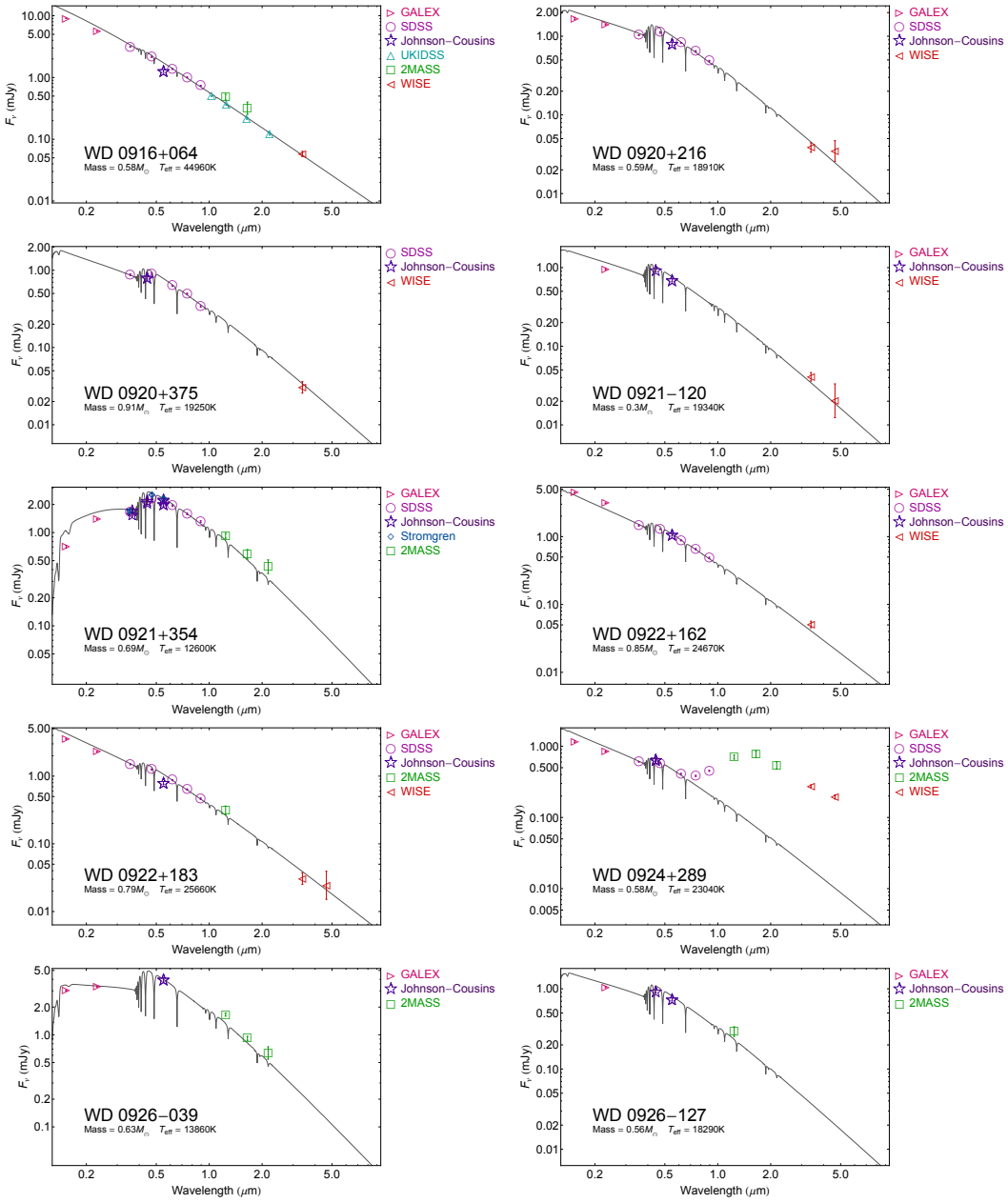

WD 0826+418
Mass = 0.72$M_\odot$ $T_{\rm eff}$ = 10390K
GALEX
SDSS
Johnson–Cousins
WISE
WD 0827+328
Mass = 0.87$M_\odot$ $T_{\rm eff}$ = 7410K
SDSS
Johnson–Cousins
2MASS
WISE
WD 0827+410
Mass = 0.56$M_\odot$ $T_{\rm eff}$ = 15930K
GALEX
SDSS
Johnson–Cousins
2MASS
WISE
WD 0830–535
Mass = 0.56$M_\odot$ $T_{\rm eff}$ = 31030K
GALEX
Johnson–Cousins
2MASS
WD 0830+371
Mass = 0.81$M_\odot$ $T_{\rm eff}$ = 9250K
SDSS
Johnson–Cousins
2MASS
WISE
WD 0831+412
Mass = 0.93$M_\odot$ $T_{\rm eff}$ = 32070K
GALEX
SDSS
Johnson–Cousins
WD 0834+500
Mass = 0.51$M_\odot$ $T_{\rm eff}$ = 64070K
GALEX
SDSS
Johnson–Cousins
2MASS
WISE
WD 0835+366
Mass = 0.64$M_\odot$ $T_{\rm eff}$ = 16670K
SDSS
Johnson–Cousins
WISE
WD 0836+237
Mass = 0.6$M_\odot$ $T_{\rm eff}$ = 55490K
GALEX
SDSS
Johnson–Cousins
UKIDSS
WD 0836+404
Mass = 0.71$M_\odot$ $T_{\rm eff}$ = 12280K
GALEX
SDSS
Johnson–Cousins
2MASS
WISE
F_ν (mJy)
Wavelength (μm)

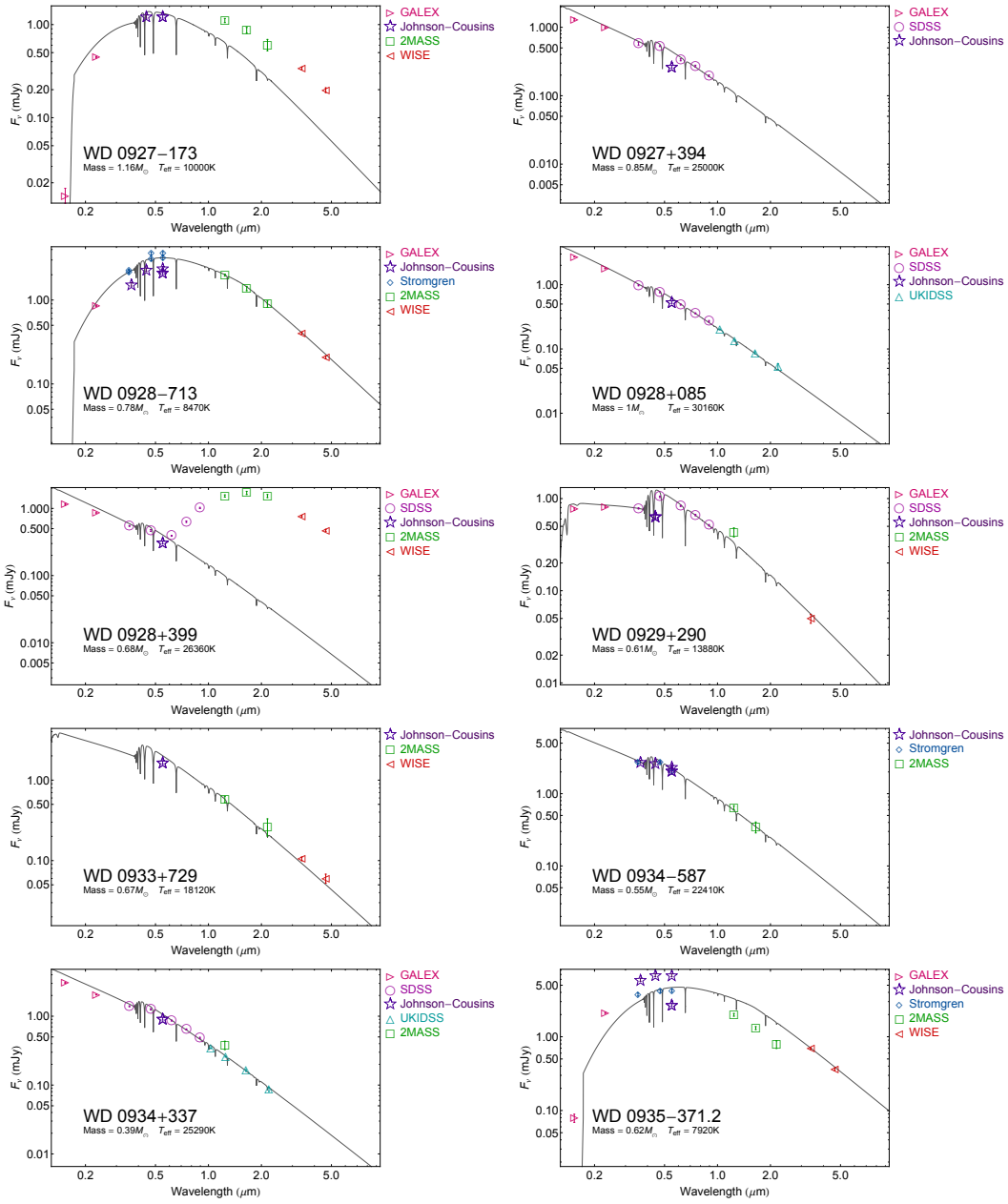

WD 0837+378
Mass = 0.79$M_\odot$ $T_{\rm eff}$ = 15020K
WD 0837+395
Mass = 0.59$M_\odot$ $T_{\rm eff}$ = 21640K
WD 0838+035
Mass = 0.6$M_\odot$ $T_{\rm eff}$ = 37870K
WD 0838+376
Mass = 0.59$M_\odot$ $T_{\rm eff}$ = 19780K
WD 0839+231
Mass = 0.57$M_\odot$ $T_{\rm eff}$ = 25830K
WD 0839+345
Mass = 0.71$M_\odot$ $T_{\rm eff}$ = 18230K
WD 0839+379
Mass = 0.68$M_\odot$ $T_{\rm eff}$ = 19920K
WD 0841+336
Mass = 0.69$M_\odot$ $T_{\rm eff}$ = 25290K
WD 0841+411
Mass = 0.63$M_\odot$ $T_{\rm eff}$ = 17170K
WD 0841+603
Mass = 0.63$M_\odot$ $T_{\rm eff}$ = 33580K
GALEX
SDSS
Johnson–Cousins
UKIDSS
2MASS
WISE
F_ν (mJy)
Wavelength (μm)

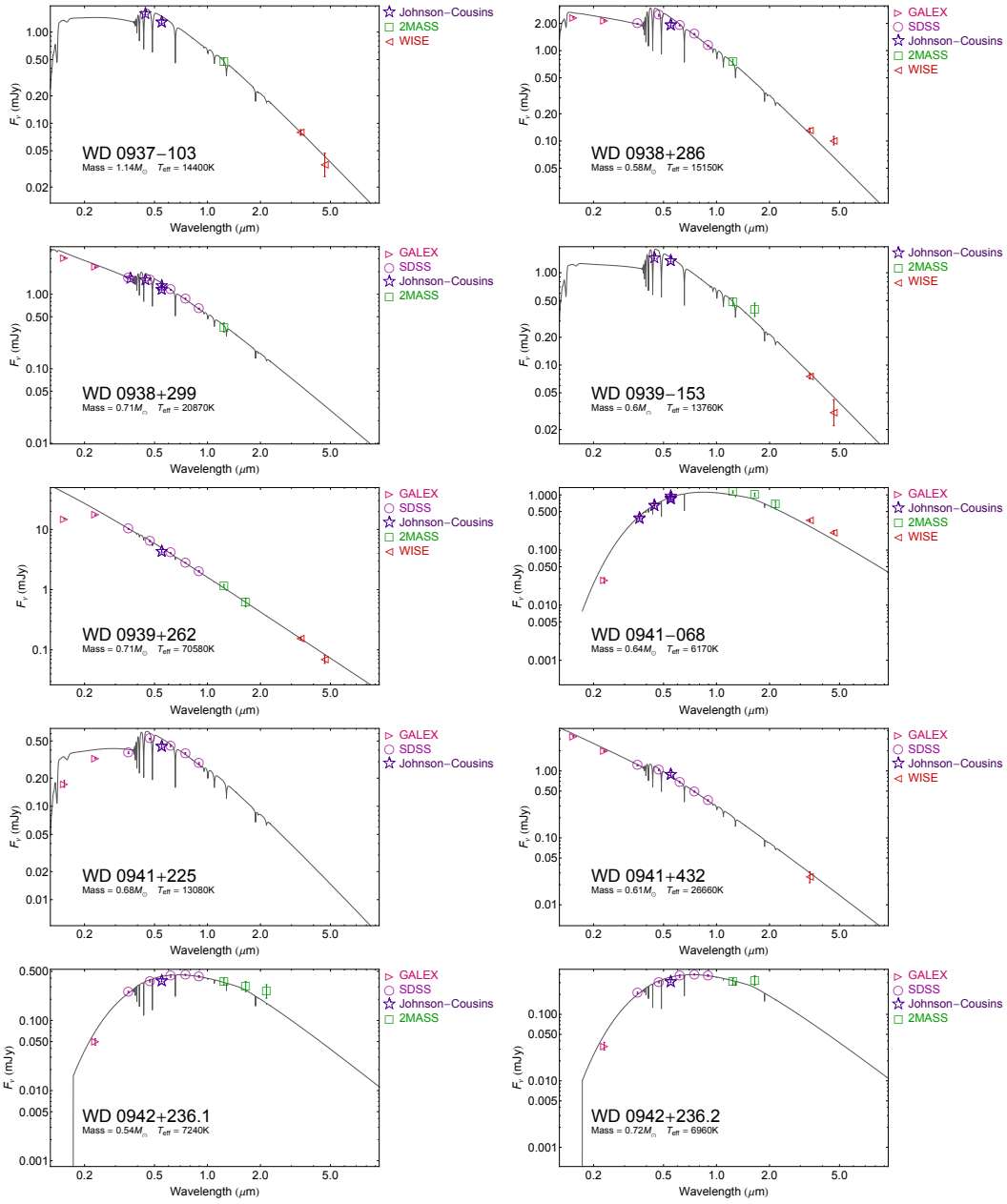

WD 0842+382
Mass = 0.63$M_\odot$ $T_{\rm eff}$ = 8070K
WD 0843+199
Mass = 0.65$M_\odot$ $T_{\rm eff}$ = 10350K
WD 0846+249
Mass = 0.55$M_\odot$ $T_{\rm eff}$ = 70180K
WD 0846+557
Mass = 0.6$M_\odot$ $T_{\rm eff}$ = 28330K
WD 0847+386
Mass = 0.86$M_\odot$ $T_{\rm eff}$ = 18410K
WD 0848−730
Mass = 0.55$M_\odot$ $T_{\rm eff}$ = 18180K
WD 0850−617
Mass = 0.62$M_\odot$ $T_{\rm eff}$ = 21840K
WD 0850+419
Mass = 0.61$M_\odot$ $T_{\rm eff}$ = 18920K
WD 0852+192
Mass = 0.63$M_\odot$ $T_{\rm eff}$ = 14910K
WD 0852+630
Mass = 0.57$M_\odot$ $T_{\rm eff}$ = 8160K
F_ν (mJy)
Wavelength (μm)
GALEX
SDSS
Johnson−Cousins
Stromgren
2MASS
WISE

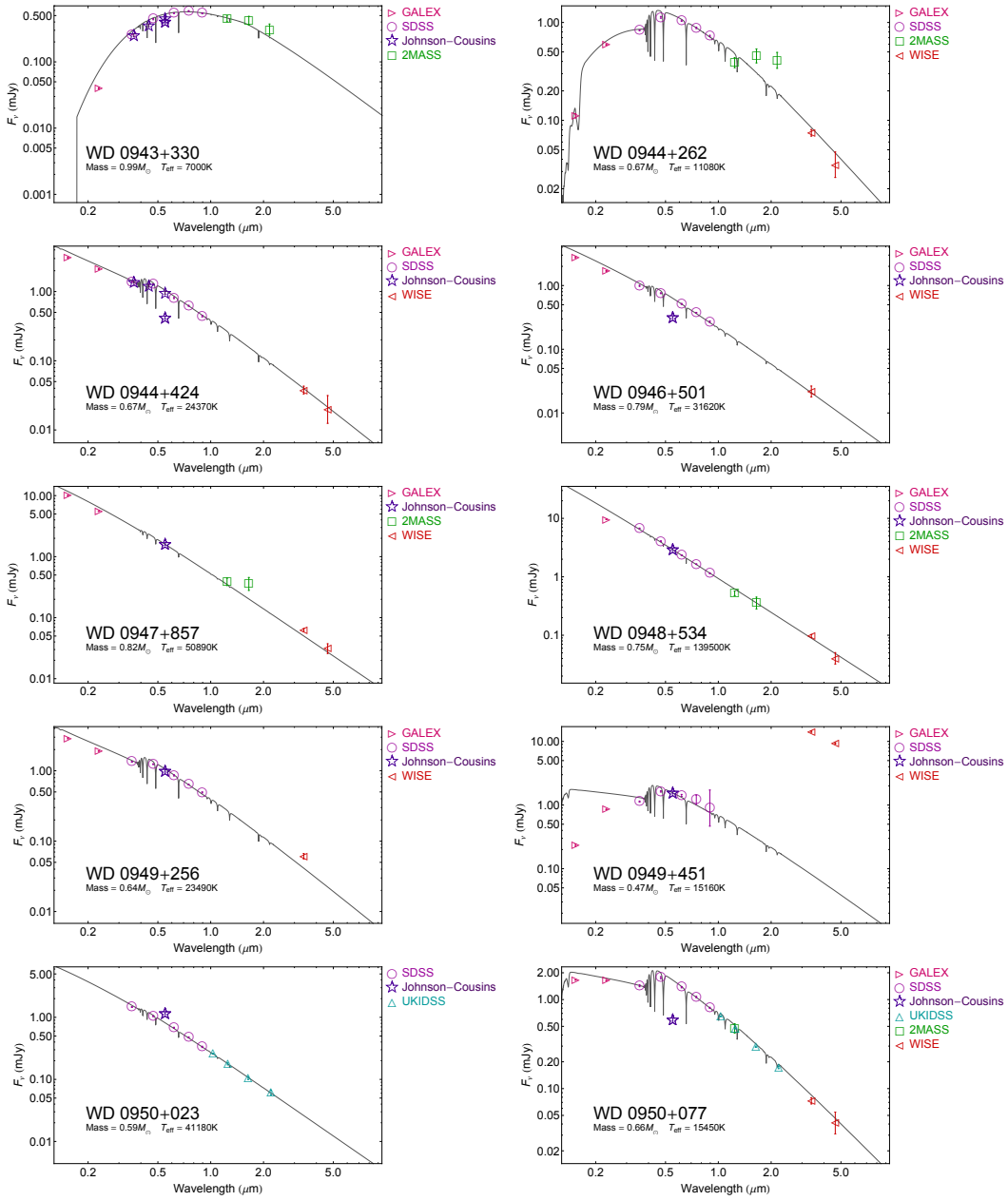

WD 0855+329
Mass = 0.58$M_\odot$ $T_{\rm eff}$ = 16260K
SDSS
Johnson−Cousins
2MASS
WD 0858+363
Mass = 0.75$M_\odot$ $T_{\rm eff}$ = 12380K
SDSS
Johnson−Cousins
Stromgren
2MASS
WISE
WD 0859+337
Mass = 0.65$M_\odot$ $T_{\rm eff}$ = 25360K
GALEX
SDSS
Johnson−Cousins
WISE
WD 0900+354
Mass = 0.58$M_\odot$ $T_{\rm eff}$ = 36970K
GALEX
SDSS
Johnson−Cousins
WD 0900+378
Mass = 0.65$M_\odot$ $T_{\rm eff}$ = 43250K
GALEX
SDSS
Johnson−Cousins
WD 0901+140
Mass = 0.82$M_\odot$ $T_{\rm eff}$ = 9270K
GALEX
SDSS
Johnson−Cousins
2MASS
WISE
WD 0901+597
Mass = 0.57$M_\odot$ $T_{\rm eff}$ = 53170K
GALEX
SDSS
Johnson−Cousins
WISE
WD 0902+418
Mass = 0.76$M_\odot$ $T_{\rm eff}$ = 45220K
GALEX
SDSS
Johnson−Cousins
WISE
WD 0903+290
Mass = 0.69$M_\odot$ $T_{\rm eff}$ = 14610K
GALEX
SDSS
Johnson−Cousins
UKIDSS
WISE
WD 0904+391
Mass = 0.68$M_\odot$ $T_{\rm eff}$ = 26190K
GALEX
SDSS
Johnson−Cousins
WISE
F_ν (mJy)
Wavelength (μm)

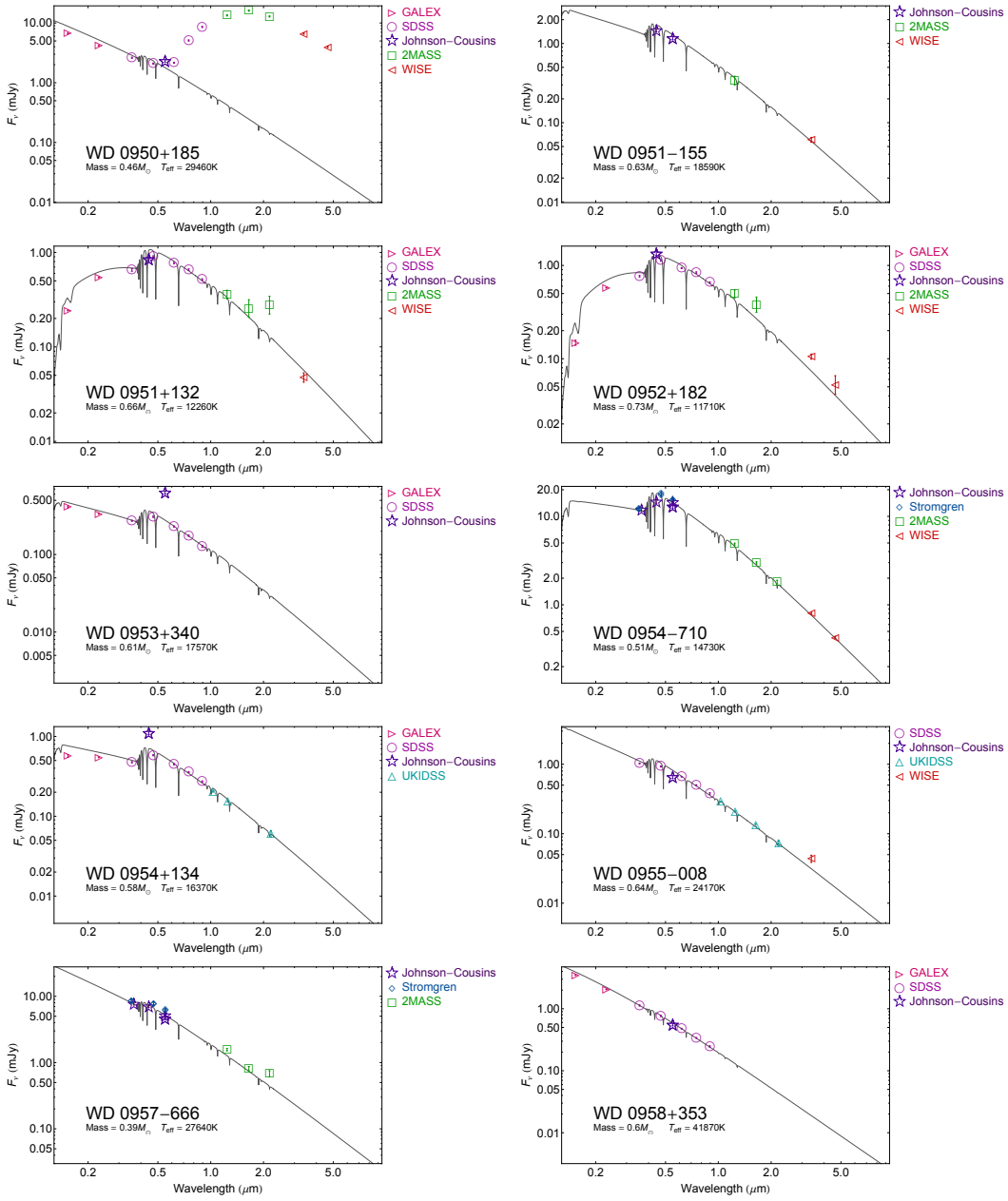

WD 0904+511
Mass = 0.84$M_\odot$ $T_{\rm eff}$ = 32760K
WD 0905+605
Mass = 0.83$M_\odot$ $T_{\rm eff}$ = 8860K
WD 0906+296
Mass = 0.58$M_\odot$ $T_{\rm eff}$ = 21060K
WD 0908+171
Mass = 0.64$M_\odot$ $T_{\rm eff}$ = 17980K
WD 0909+271
Mass = 0.74$M_\odot$ $T_{\rm eff}$ = 49820K
WD 0911−076
Mass = 0.62$M_\odot$ $T_{\rm eff}$ = 18510K
WD 0913+204
Mass = 0.78$M_\odot$ $T_{\rm eff}$ = 24280K
WD 0913+442
Mass = 0.73$M_\odot$ $T_{\rm eff}$ = 8690K
WD 0915+201
Mass = 0.56$M_\odot$ $T_{\rm eff}$ = 72710K
WD 0915+526
Mass = 0.67$M_\odot$ $T_{\rm eff}$ = 16370K
F_ν (mJy)
Wavelength (μm)
GALEX
SDSS
Johnson−Cousins
Stromgren
UKIDSS
2MASS
WISE

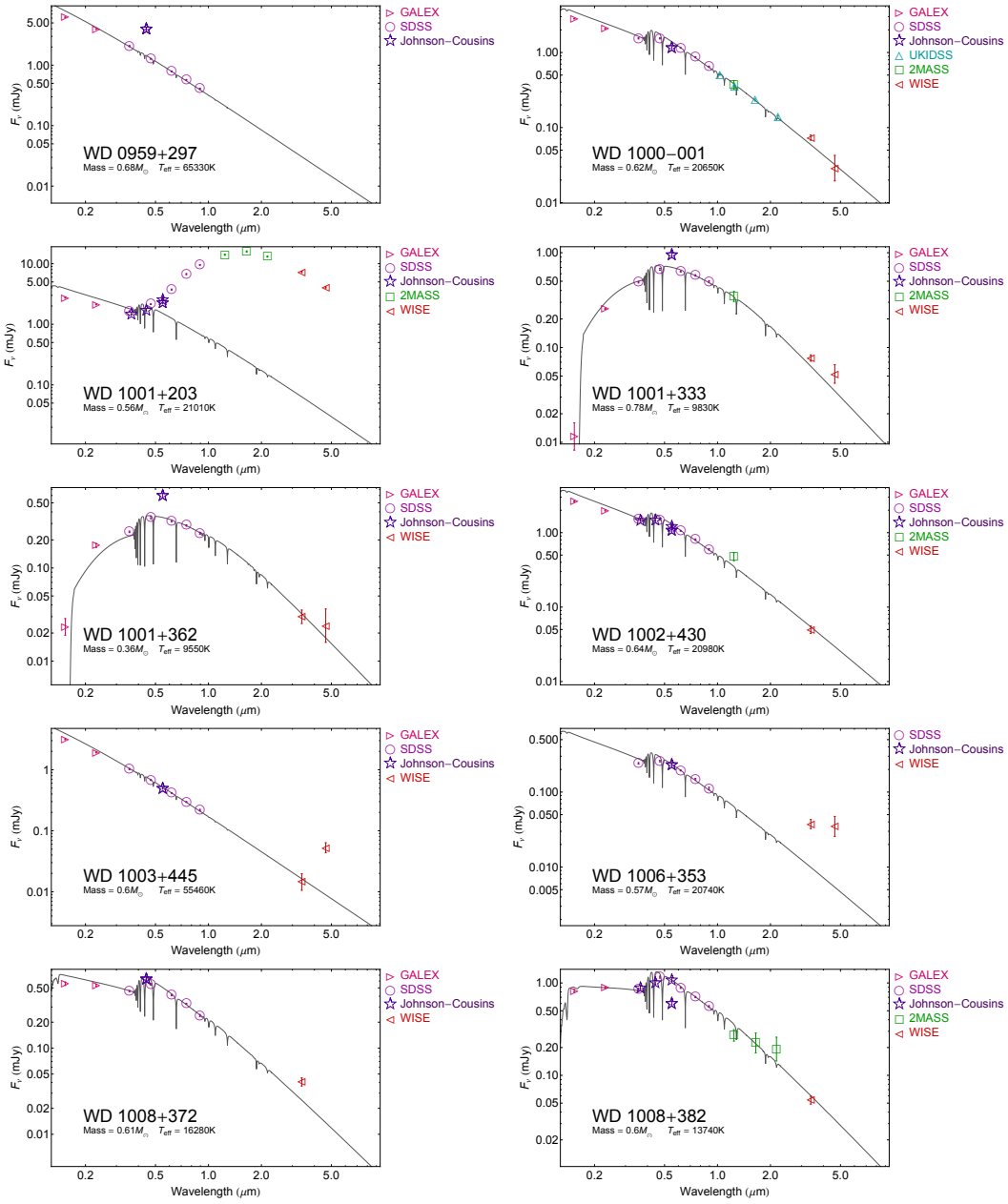

WD 0916+064
Mass = 0.58$M_\odot$ $T_{\rm eff}$ = 44960K
GALEX
SDSS
Johnson−Cousins
UKIDSS
2MASS
WISE
WD 0920+216
Mass = 0.59$M_\odot$ $T_{\rm eff}$ = 18910K
GALEX
SDSS
Johnson−Cousins
WISE
WD 0920+375
Mass = 0.91$M_\odot$ $T_{\rm eff}$ = 19250K
SDSS
Johnson−Cousins
WISE
WD 0921−120
Mass = 0.3$M_\odot$ $T_{\rm eff}$ = 19340K
GALEX
Johnson−Cousins
WISE
WD 0921+354
Mass = 0.69$M_\odot$ $T_{\rm eff}$ = 12600K
GALEX
SDSS
Johnson−Cousins
Stromgren
2MASS
WD 0922+162
Mass = 0.85$M_\odot$ $T_{\rm eff}$ = 24670K
GALEX
SDSS
Johnson−Cousins
WISE
WD 0922+183
Mass = 0.79$M_\odot$ $T_{\rm eff}$ = 25660K
GALEX
SDSS
Johnson−Cousins
2MASS
WISE
WD 0924+289
Mass = 0.58$M_\odot$ $T_{\rm eff}$ = 23040K
GALEX
SDSS
Johnson−Cousins
2MASS
WISE
WD 0926−039
Mass = 0.63$M_\odot$ $T_{\rm eff}$ = 13860K
GALEX
Johnson−Cousins
2MASS
WD 0926−127
Mass = 0.56$M_\odot$ $T_{\rm eff}$ = 18290K
GALEX
Johnson−Cousins
2MASS
F_ν (mJy)
Wavelength (μm)

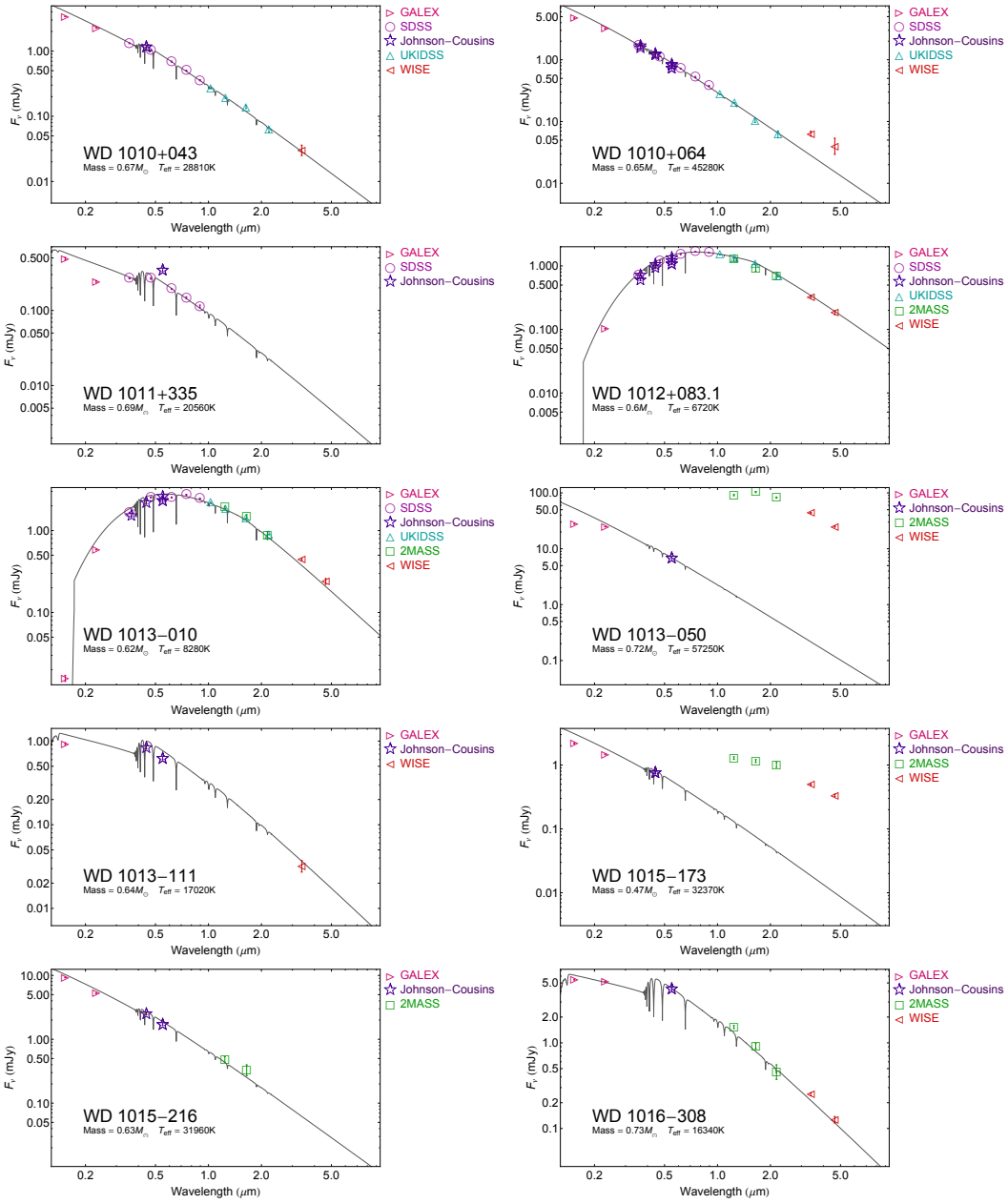

WD 0927−173
Mass = 1.16$M_\odot$ $T_{\rm eff}$ = 10000K
GALEX
Johnson−Cousins
2MASS
WISE
WD 0927+394
Mass = 0.85$M_\odot$ $T_{\rm eff}$ = 25000K
GALEX
SDSS
Johnson−Cousins
WD 0928−713
Mass = 0.78$M_\odot$ $T_{\rm eff}$ = 8470K
GALEX
Johnson−Cousins
Stromgren
2MASS
WISE
WD 0928+085
Mass = 1$M_\odot$ $T_{\rm eff}$ = 30160K
GALEX
SDSS
Johnson−Cousins
UKIDSS
WD 0928+399
Mass = 0.68$M_\odot$ $T_{\rm eff}$ = 26360K
GALEX
SDSS
Johnson−Cousins
2MASS
WISE
WD 0929+290
Mass = 0.61$M_\odot$ $T_{\rm eff}$ = 13880K
GALEX
SDSS
Johnson−Cousins
2MASS
WISE
WD 0933+729
Mass = 0.67$M_\odot$ $T_{\rm eff}$ = 18120K
Johnson−Cousins
2MASS
WISE
WD 0934−587
Mass = 0.55$M_\odot$ $T_{\rm eff}$ = 22410K
Johnson−Cousins
Stromgren
2MASS
WD 0934+337
Mass = 0.39$M_\odot$ $T_{\rm eff}$ = 25290K
GALEX
SDSS
Johnson−Cousins
UKIDSS
2MASS
WD 0935−371.2
Mass = 0.62$M_\odot$ $T_{\rm eff}$ = 7920K
GALEX
Johnson−Cousins
Stromgren
2MASS
WISE
F_ν (mJy)
Wavelength (μm)

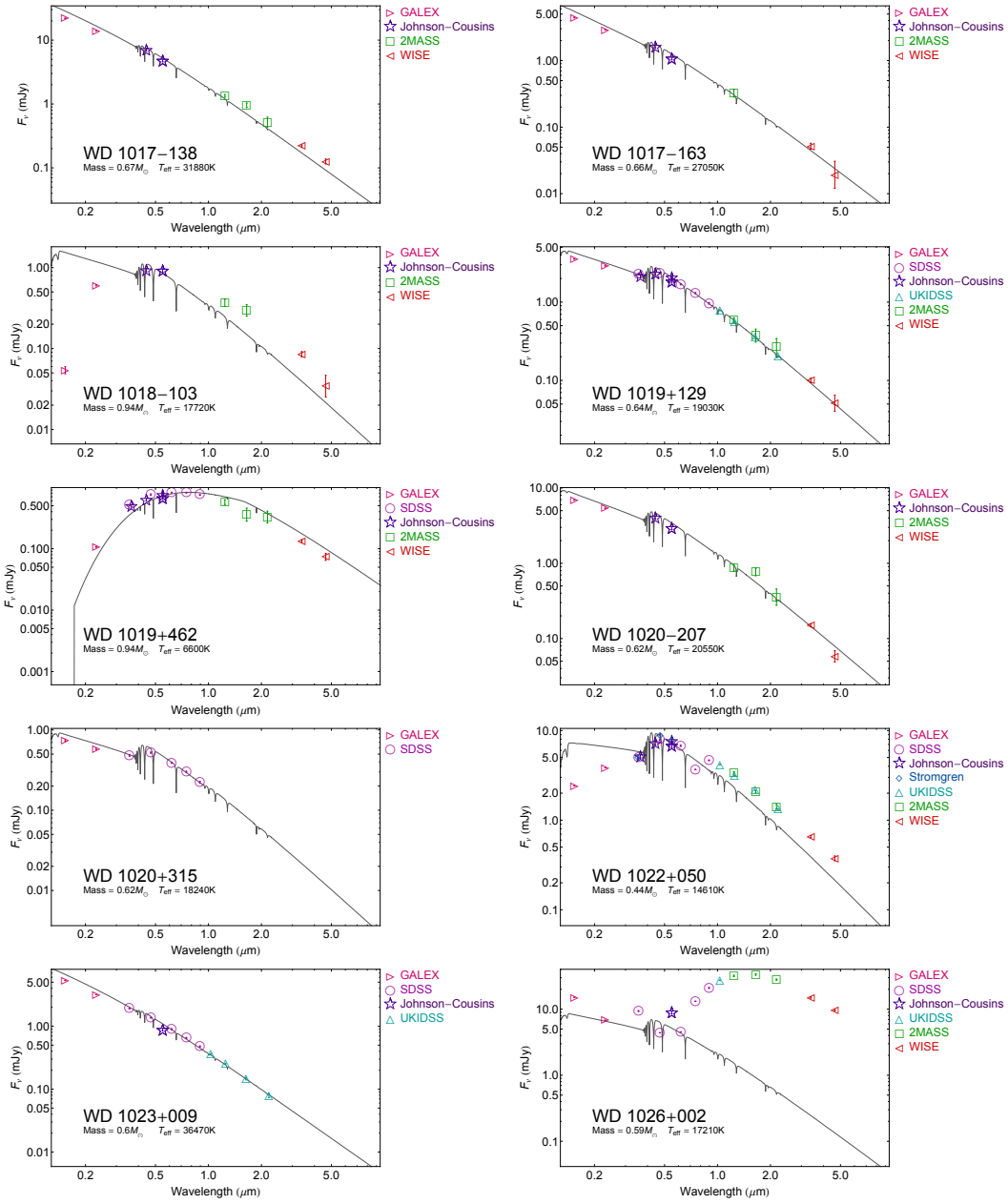

WD 0937−103
Mass = 1.14$M_\odot$ $T_{\rm eff}$ = 14400K
WD 0938+286
Mass = 0.58$M_\odot$ $T_{\rm eff}$ = 15150K
WD 0938+299
Mass = 0.71$M_\odot$ $T_{\rm eff}$ = 20870K
WD 0939−153
Mass = 0.6$M_\odot$ $T_{\rm eff}$ = 13760K
WD 0939+262
Mass = 0.71$M_\odot$ $T_{\rm eff}$ = 70580K
WD 0941−068
Mass = 0.64$M_\odot$ $T_{\rm eff}$ = 6170K
WD 0941+225
Mass = 0.68$M_\odot$ $T_{\rm eff}$ = 13080K
WD 0941+432
Mass = 0.61$M_\odot$ $T_{\rm eff}$ = 26660K
WD 0942+236.1
Mass = 0.54$M_\odot$ $T_{\rm eff}$ = 7240K
WD 0942+236.2
Mass = 0.72$M_\odot$ $T_{\rm eff}$ = 6960K
GALEX
SDSS
Johnson−Cousins
2MASS
WISE
F_ν (mJy)
Wavelength (μm)

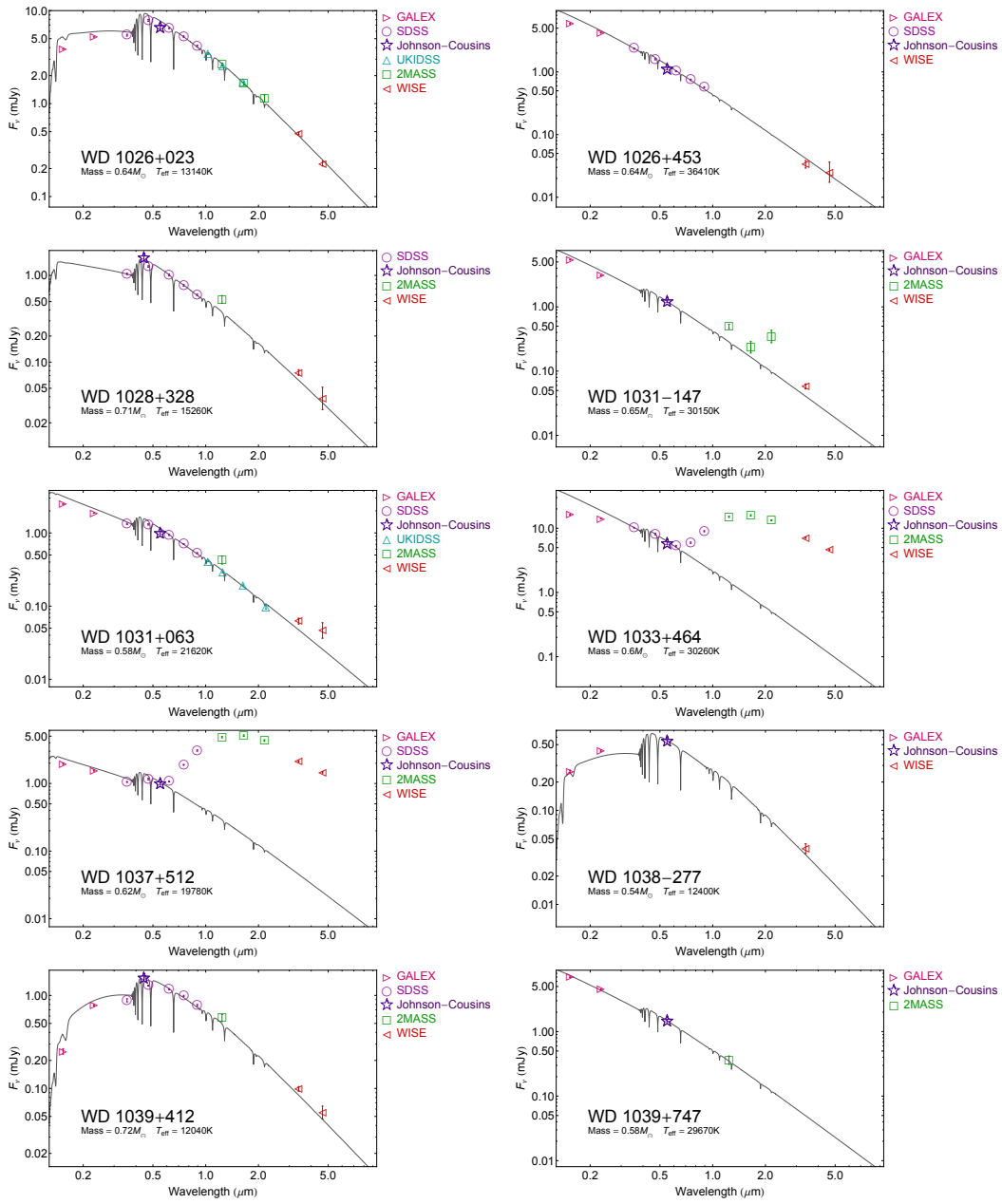

WD 0943+330
Mass = 0.99$M_\odot$ $T_{\rm eff}$ = 7000K
GALEX
SDSS
Johnson–Cousins
2MASS
WD 0944+262
Mass = 0.67$M_\odot$ $T_{\rm eff}$ = 11080K
GALEX
SDSS
2MASS
WISE
WD 0944+424
Mass = 0.67$M_\odot$ $T_{\rm eff}$ = 24370K
GALEX
SDSS
Johnson–Cousins
WISE
WD 0946+501
Mass = 0.79$M_\odot$ $T_{\rm eff}$ = 31620K
GALEX
SDSS
Johnson–Cousins
WISE
WD 0947+857
Mass = 0.82$M_\odot$ $T_{\rm eff}$ = 50890K
GALEX
Johnson–Cousins
2MASS
WISE
WD 0948+534
Mass = 0.75$M_\odot$ $T_{\rm eff}$ = 139500K
GALEX
SDSS
Johnson–Cousins
2MASS
WISE
WD 0949+256
Mass = 0.64$M_\odot$ $T_{\rm eff}$ = 23490K
GALEX
SDSS
Johnson–Cousins
WISE
WD 0949+451
Mass = 0.47$M_\odot$ $T_{\rm eff}$ = 15160K
GALEX
SDSS
Johnson–Cousins
WISE
WD 0950+023
Mass = 0.59$M_\odot$ $T_{\rm eff}$ = 41180K
SDSS
Johnson–Cousins
UKIDSS
WD 0950+077
Mass = 0.66$M_\odot$ $T_{\rm eff}$ = 15450K
GALEX
SDSS
Johnson–Cousins
UKIDSS
2MASS
WISE
F_ν (mJy)
Wavelength (μm)

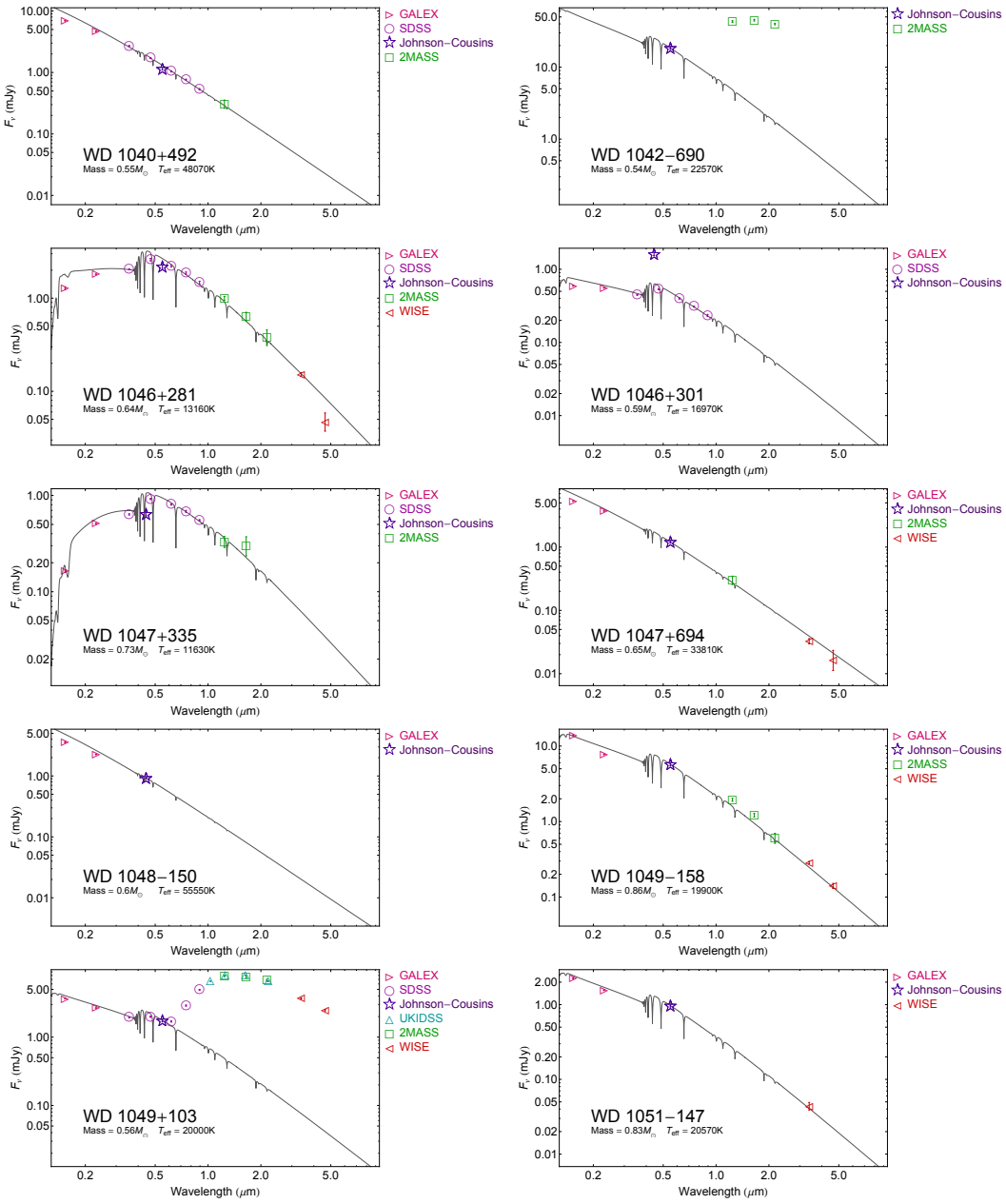

WD 0950+185
Mass = 0.46$M_\odot$ $T_{\rm eff}$ = 29460K
WD 0951−155
Mass = 0.63$M_\odot$ $T_{\rm eff}$ = 18590K
WD 0951+132
Mass = 0.66$M_\odot$ $T_{\rm eff}$ = 12260K
WD 0952+182
Mass = 0.73$M_\odot$ $T_{\rm eff}$ = 11710K
WD 0953+340
Mass = 0.61$M_\odot$ $T_{\rm eff}$ = 17570K
WD 0954−710
Mass = 0.51$M_\odot$ $T_{\rm eff}$ = 14730K
WD 0954+134
Mass = 0.58$M_\odot$ $T_{\rm eff}$ = 16370K
WD 0955−008
Mass = 0.64$M_\odot$ $T_{\rm eff}$ = 24170K
WD 0957−666
Mass = 0.39$M_\odot$ $T_{\rm eff}$ = 27640K
WD 0958+353
Mass = 0.6$M_\odot$ $T_{\rm eff}$ = 41870K
F_ν (mJy)
Wavelength (μm)
GALEX
SDSS
Johnson−Cousins
Stromgren
2MASS
UKIDSS
WISE

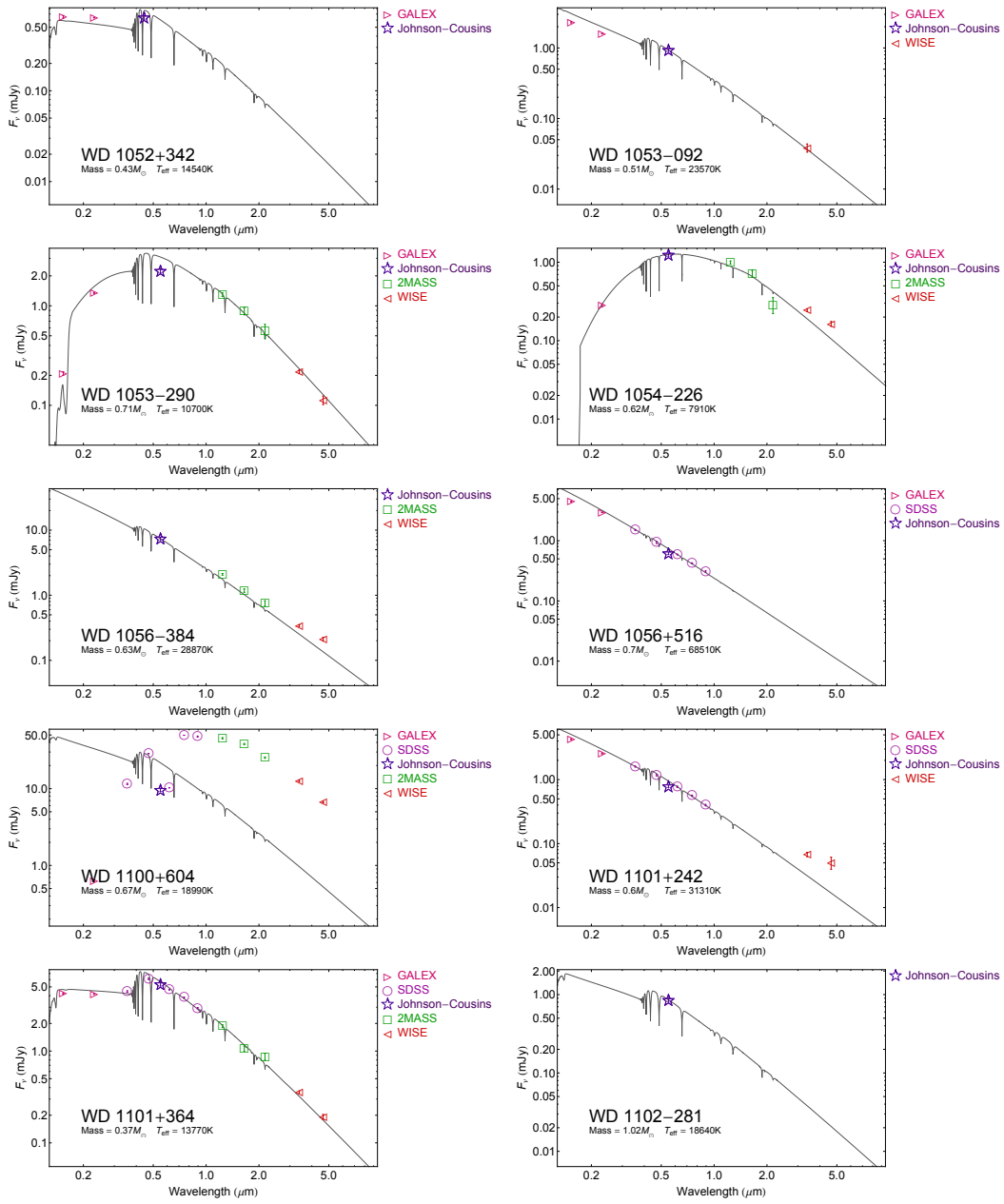

WD 0959+297
Mass = 0.68$M_\odot$ $T_{\rm eff}$ = 65330K
WD 1000−001
Mass = 0.62$M_\odot$ $T_{\rm eff}$ = 20650K
WD 1001+203
Mass = 0.56$M_\odot$ $T_{\rm eff}$ = 21010K
WD 1001+333
Mass = 0.78$M_\odot$ $T_{\rm eff}$ = 9830K
WD 1001+362
Mass = 0.36$M_\odot$ $T_{\rm eff}$ = 9550K
WD 1002+430
Mass = 0.64$M_\odot$ $T_{\rm eff}$ = 20980K
WD 1003+445
Mass = 0.6$M_\odot$ $T_{\rm eff}$ = 55460K
WD 1006+353
Mass = 0.57$M_\odot$ $T_{\rm eff}$ = 20740K
WD 1008+372
Mass = 0.61$M_\odot$ $T_{\rm eff}$ = 16280K
WD 1008+382
Mass = 0.6$M_\odot$ $T_{\rm eff}$ = 13740K
GALEX
SDSS
Johnson−Cousins
UKIDSS
2MASS
WISE
F_ν (mJy)
Wavelength (μm)

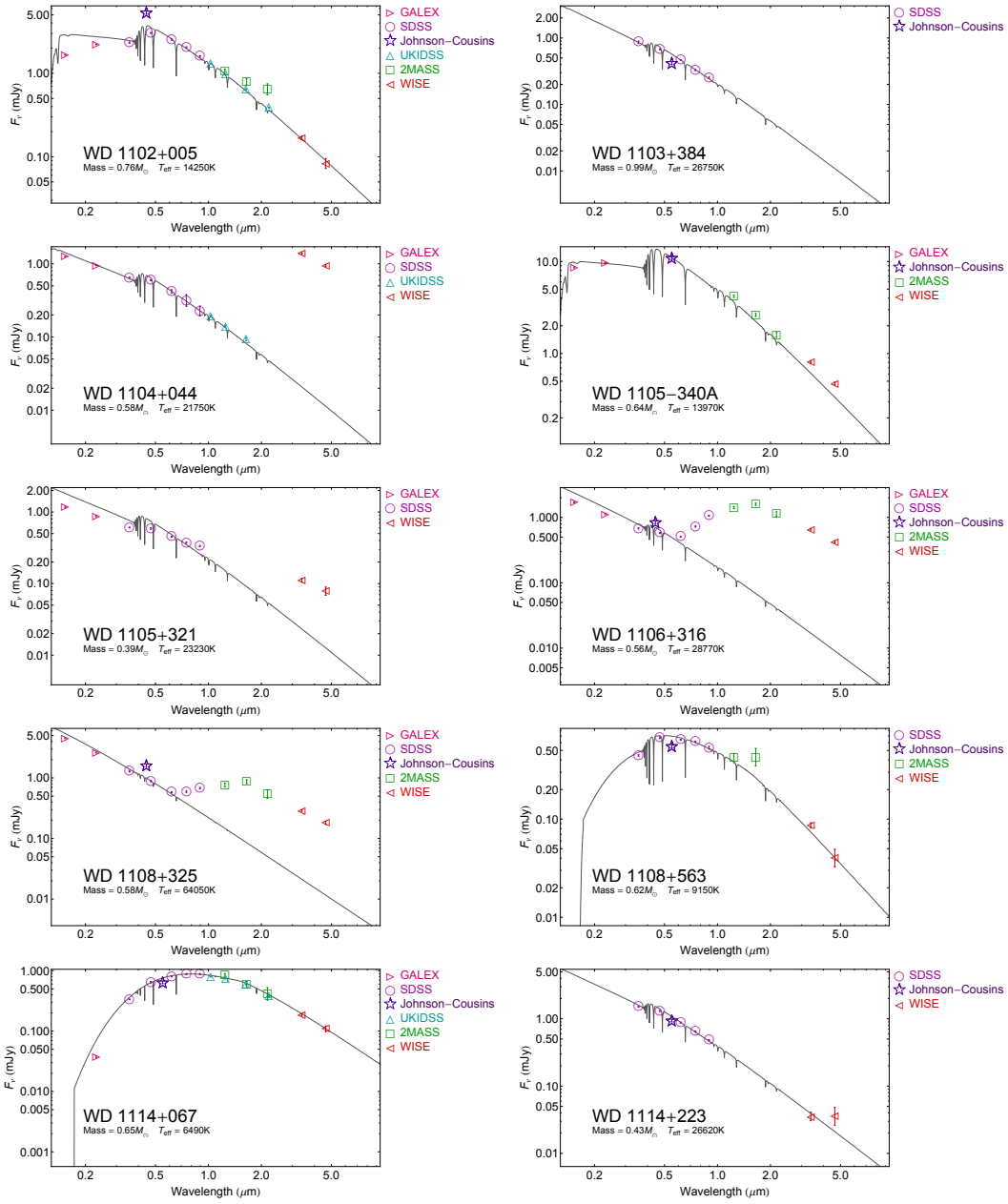

WD 1010+043
Mass = 0.67$M_\odot$ $T_{\rm eff}$ = 28810K
WD 1010+064
Mass = 0.65$M_\odot$ $T_{\rm eff}$ = 45280K
WD 1011+335
Mass = 0.69$M_\odot$ $T_{\rm eff}$ = 20560K
WD 1012+083.1
Mass = 0.6$M_\odot$ $T_{\rm eff}$ = 6720K
WD 1013−010
Mass = 0.62$M_\odot$ $T_{\rm eff}$ = 8280K
WD 1013−050
Mass = 0.72$M_\odot$ $T_{\rm eff}$ = 57250K
WD 1013−111
Mass = 0.64$M_\odot$ $T_{\rm eff}$ = 17020K
WD 1015−173
Mass = 0.47$M_\odot$ $T_{\rm eff}$ = 32370K
WD 1015−216
Mass = 0.63$M_\odot$ $T_{\rm eff}$ = 31960K
WD 1016−308
Mass = 0.73$M_\odot$ $T_{\rm eff}$ = 16340K
F_ν (mJy)
Wavelength (μm)
GALEX
SDSS
Johnson−Cousins
UKIDSS
2MASS
WISE

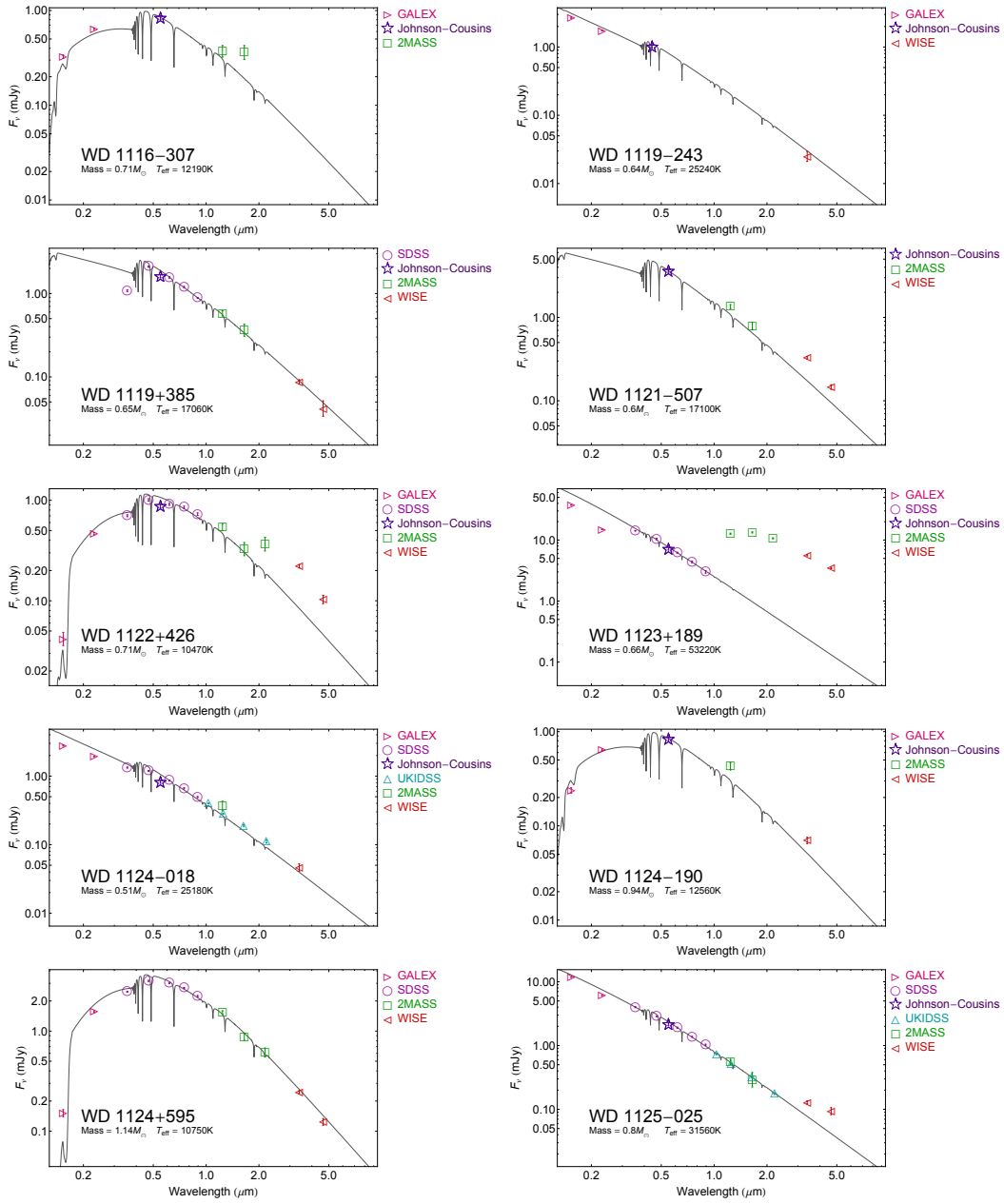

WD 1017−138
Mass = 0.67$M_\odot$ $T_{\rm eff}$ = 31880K
WD 1017−163
Mass = 0.66$M_\odot$ $T_{\rm eff}$ = 27050K
WD 1018−103
Mass = 0.94$M_\odot$ $T_{\rm eff}$ = 17720K
WD 1019+129
Mass = 0.64$M_\odot$ $T_{\rm eff}$ = 19030K
WD 1019+462
Mass = 0.94$M_\odot$ $T_{\rm eff}$ = 6600K
WD 1020−207
Mass = 0.62$M_\odot$ $T_{\rm eff}$ = 20550K
WD 1020+315
Mass = 0.62$M_\odot$ $T_{\rm eff}$ = 18240K
WD 1022+050
Mass = 0.44$M_\odot$ $T_{\rm eff}$ = 14610K
WD 1023+009
Mass = 0.6$M_\odot$ $T_{\rm eff}$ = 36470K
WD 1026+002
Mass = 0.59$M_\odot$ $T_{\rm eff}$ = 17210K
F_ν (mJy)
Wavelength (μm)
GALEX
SDSS
Johnson−Cousins
Stromgren
UKIDSS
2MASS
WISE

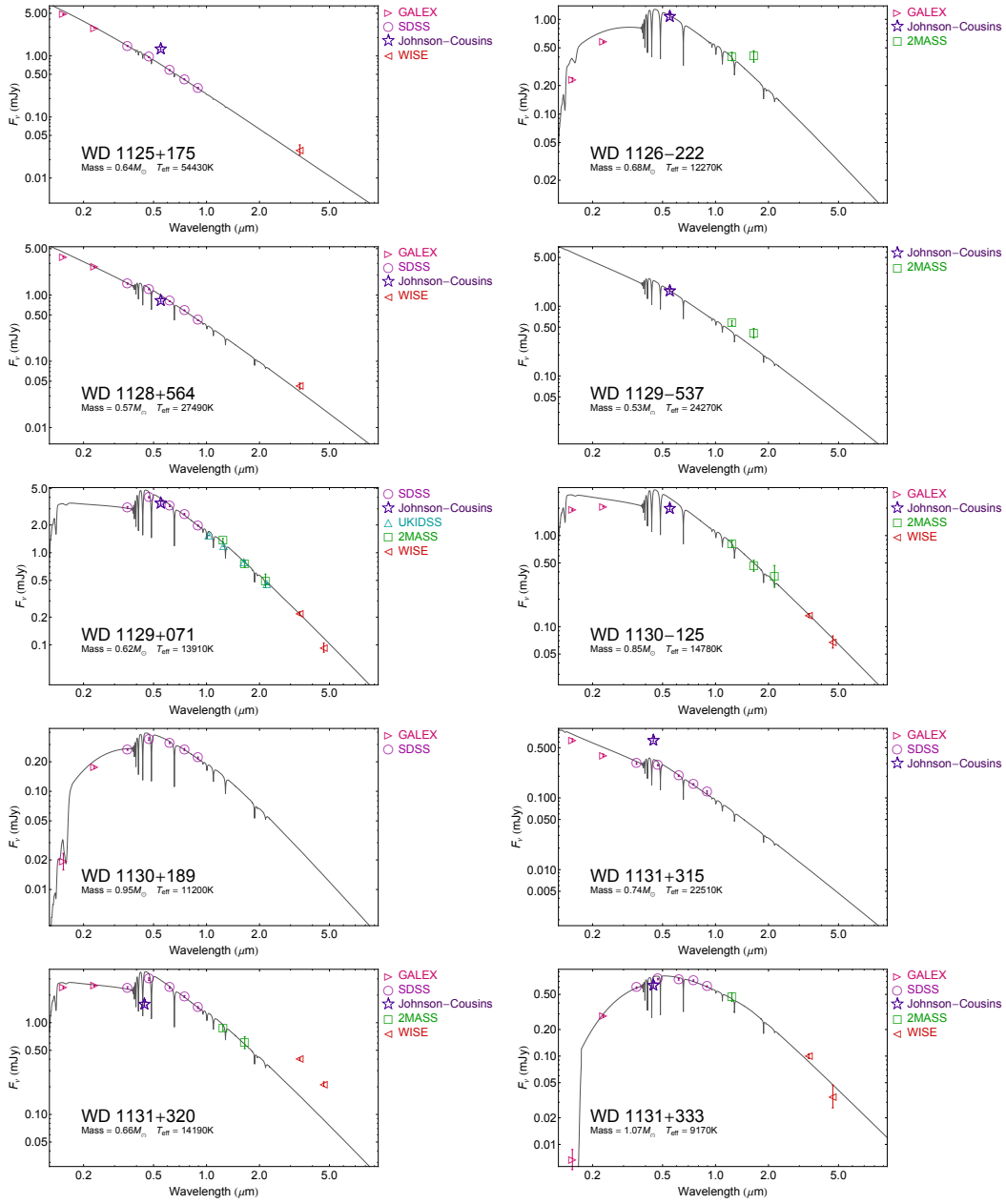

WD 1026+023
Mass = 0.64$M_\odot$ $T_{\rm eff}$ = 13140K
WD 1026+453
Mass = 0.64$M_\odot$ $T_{\rm eff}$ = 36410K
WD 1028+328
Mass = 0.71$M_\odot$ $T_{\rm eff}$ = 15260K
WD 1031−147
Mass = 0.65$M_\odot$ $T_{\rm eff}$ = 30150K
WD 1031+063
Mass = 0.58$M_\odot$ $T_{\rm eff}$ = 21620K
WD 1033+464
Mass = 0.6$M_\odot$ $T_{\rm eff}$ = 30260K
WD 1037+512
Mass = 0.62$M_\odot$ $T_{\rm eff}$ = 19780K
WD 1038−277
Mass = 0.54$M_\odot$ $T_{\rm eff}$ = 12400K
WD 1039+412
Mass = 0.72$M_\odot$ $T_{\rm eff}$ = 12040K
WD 1039+747
Mass = 0.58$M_\odot$ $T_{\rm eff}$ = 29670K
F_ν (mJy)
Wavelength (μm)
GALEX
SDSS
Johnson−Cousins
UKIDSS
2MASS
WISE

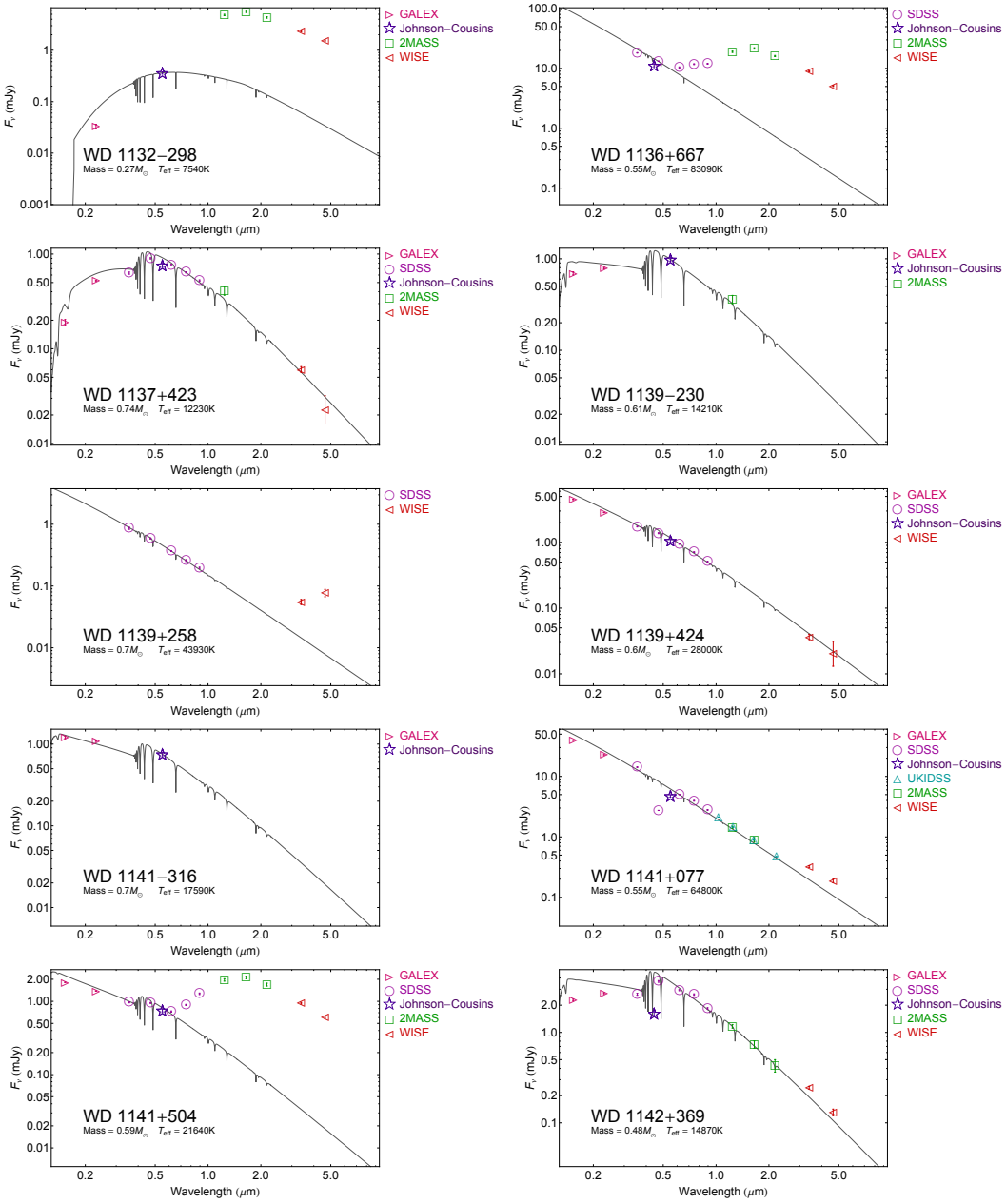

WD 1040+492
Mass = 0.55$M_\odot$ $T_{\rm eff}$ = 48070K
GALEX
SDSS
Johnson−Cousins
2MASS
WD 1042−690
Mass = 0.54$M_\odot$ $T_{\rm eff}$ = 22570K
Johnson−Cousins
2MASS
WD 1046+281
Mass = 0.64$M_\odot$ $T_{\rm eff}$ = 13160K
GALEX
SDSS
Johnson−Cousins
2MASS
WISE
WD 1046+301
Mass = 0.59$M_\odot$ $T_{\rm eff}$ = 16970K
GALEX
SDSS
Johnson−Cousins
WD 1047+335
Mass = 0.73$M_\odot$ $T_{\rm eff}$ = 11630K
GALEX
SDSS
Johnson−Cousins
2MASS
WD 1047+694
Mass = 0.65$M_\odot$ $T_{\rm eff}$ = 33810K
GALEX
Johnson−Cousins
2MASS
WISE
WD 1048−150
Mass = 0.6$M_\odot$ $T_{\rm eff}$ = 55550K
GALEX
Johnson−Cousins
WD 1049−158
Mass = 0.86$M_\odot$ $T_{\rm eff}$ = 19900K
GALEX
Johnson−Cousins
2MASS
WISE
WD 1049+103
Mass = 0.56$M_\odot$ $T_{\rm eff}$ = 20000K
GALEX
SDSS
Johnson−Cousins
UKIDSS
2MASS
WISE
WD 1051−147
Mass = 0.83$M_\odot$ $T_{\rm eff}$ = 20570K
GALEX
Johnson−Cousins
WISE
F_ν (mJy)
Wavelength (μm)

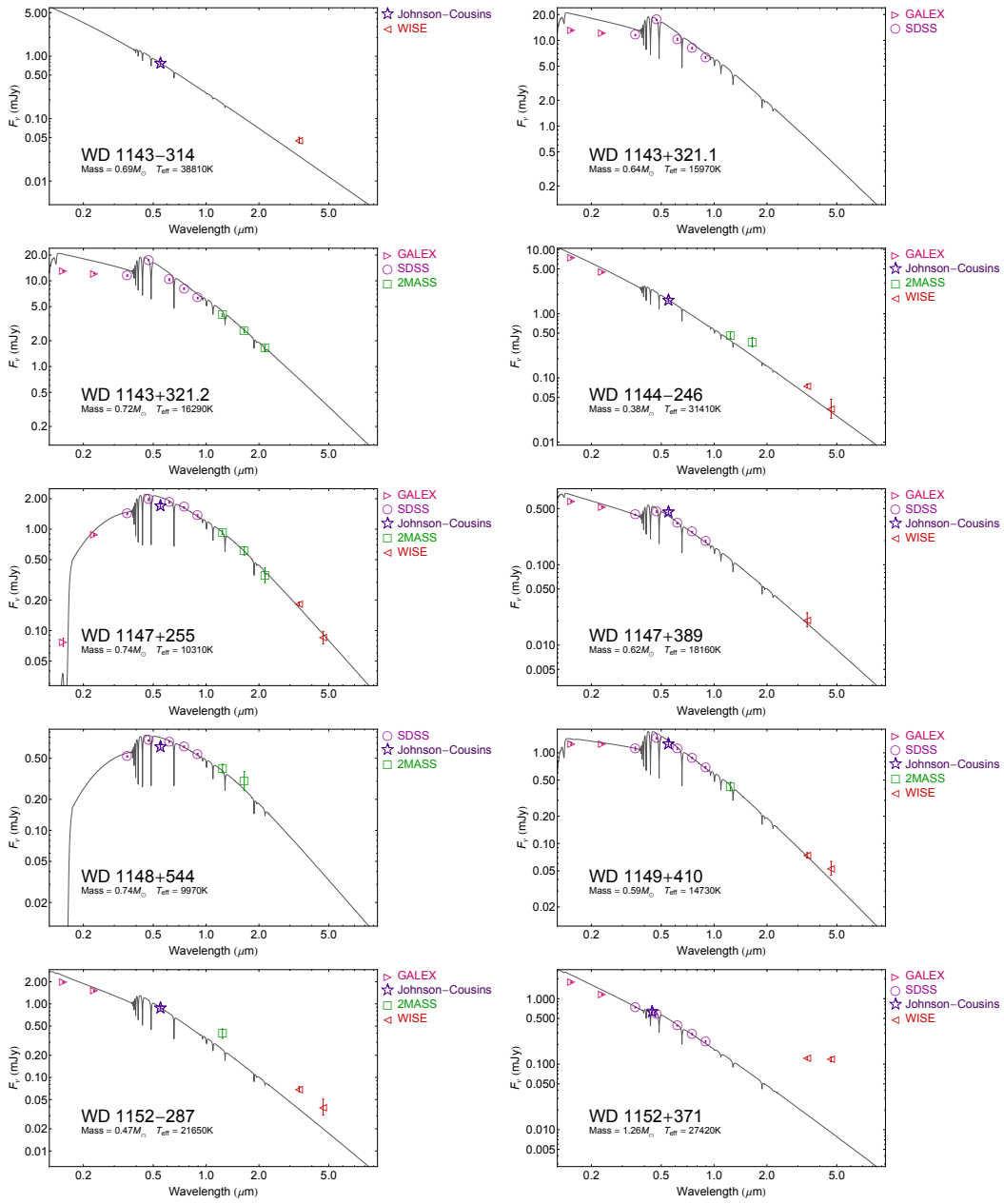

WD 1052+342
Mass = 0.43$M_\odot$ $T_{\rm eff}$ = 14540K
GALEX
Johnson–Cousins
WD 1053–092
Mass = 0.51$M_\odot$ $T_{\rm eff}$ = 23570K
GALEX
Johnson–Cousins
WISE
WD 1053–290
Mass = 0.71$M_\odot$ $T_{\rm eff}$ = 10700K
GALEX
Johnson–Cousins
2MASS
WISE
WD 1054–226
Mass = 0.62$M_\odot$ $T_{\rm eff}$ = 7910K
GALEX
Johnson–Cousins
2MASS
WISE
WD 1056–384
Mass = 0.63$M_\odot$ $T_{\rm eff}$ = 28870K
Johnson–Cousins
2MASS
WISE
WD 1056+516
Mass = 0.7$M_\odot$ $T_{\rm eff}$ = 68510K
GALEX
SDSS
Johnson–Cousins
WD 1100+604
Mass = 0.67$M_\odot$ $T_{\rm eff}$ = 18990K
GALEX
SDSS
Johnson–Cousins
2MASS
WISE
WD 1101+242
Mass = 0.6$M_\odot$ $T_{\rm eff}$ = 31310K
GALEX
SDSS
Johnson–Cousins
WISE
WD 1101+364
Mass = 0.37$M_\odot$ $T_{\rm eff}$ = 13770K
GALEX
SDSS
Johnson–Cousins
2MASS
WISE
WD 1102–281
Mass = 1.02$M_\odot$ $T_{\rm eff}$ = 18640K
Johnson–Cousins
F_ν (mJy)
Wavelength (μm)

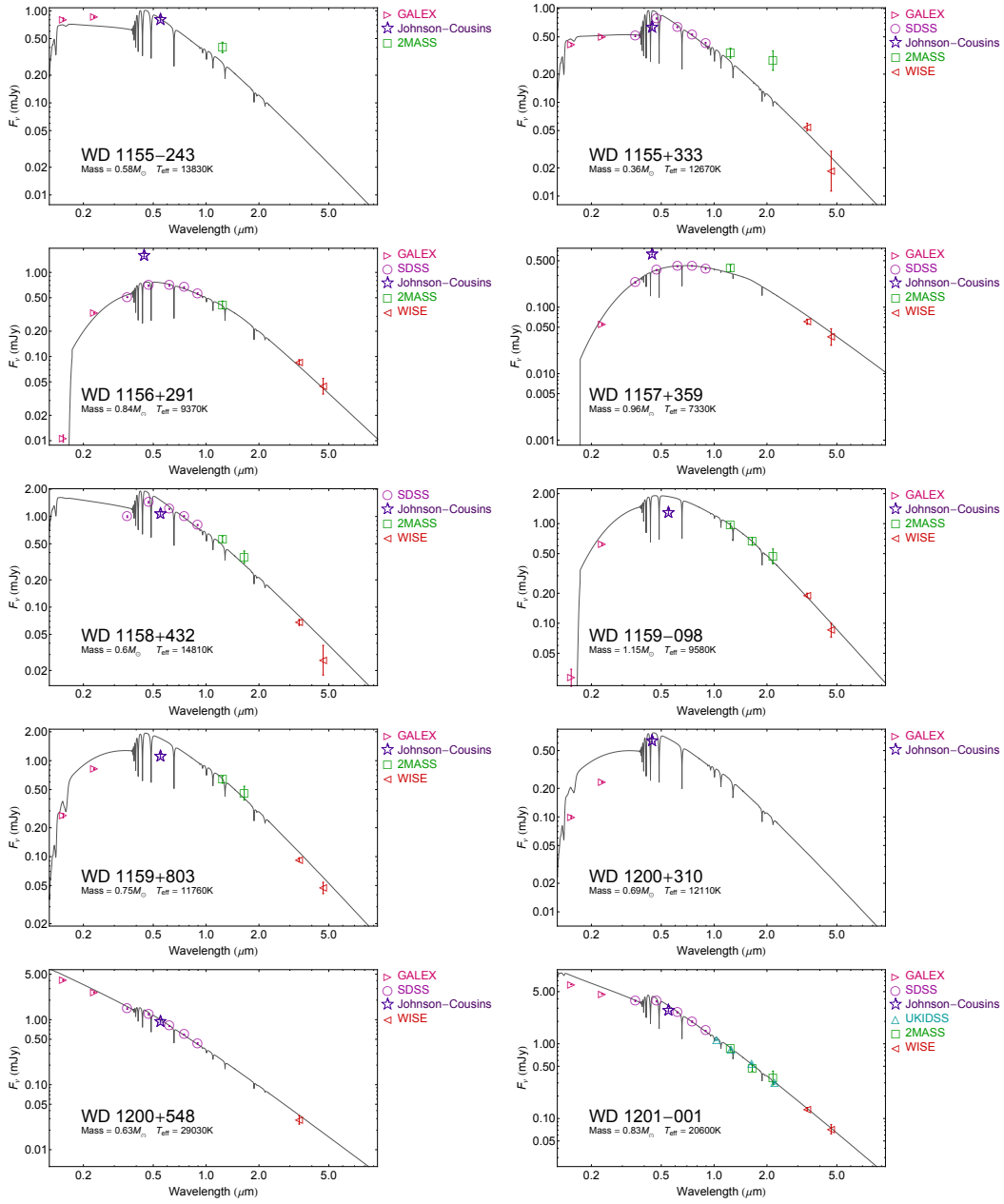

WD 1102+005
Mass = 0.76$M_\odot$ $T_{\rm eff}$ = 14250K
WD 1103+384
Mass = 0.99$M_\odot$ $T_{\rm eff}$ = 26750K
WD 1104+044
Mass = 0.58$M_\odot$ $T_{\rm eff}$ = 21750K
WD 1105−340A
Mass = 0.64$M_\odot$ $T_{\rm eff}$ = 13970K
WD 1105+321
Mass = 0.39$M_\odot$ $T_{\rm eff}$ = 23230K
WD 1106+316
Mass = 0.56$M_\odot$ $T_{\rm eff}$ = 28770K
WD 1108+325
Mass = 0.58$M_\odot$ $T_{\rm eff}$ = 64050K
WD 1108+563
Mass = 0.62$M_\odot$ $T_{\rm eff}$ = 9150K
WD 1114+067
Mass = 0.65$M_\odot$ $T_{\rm eff}$ = 6490K
WD 1114+223
Mass = 0.43$M_\odot$ $T_{\rm eff}$ = 26620K
F_ν (mJy)
Wavelength (μm)
GALEX
SDSS
Johnson−Cousins
UKIDSS
2MASS
WISE

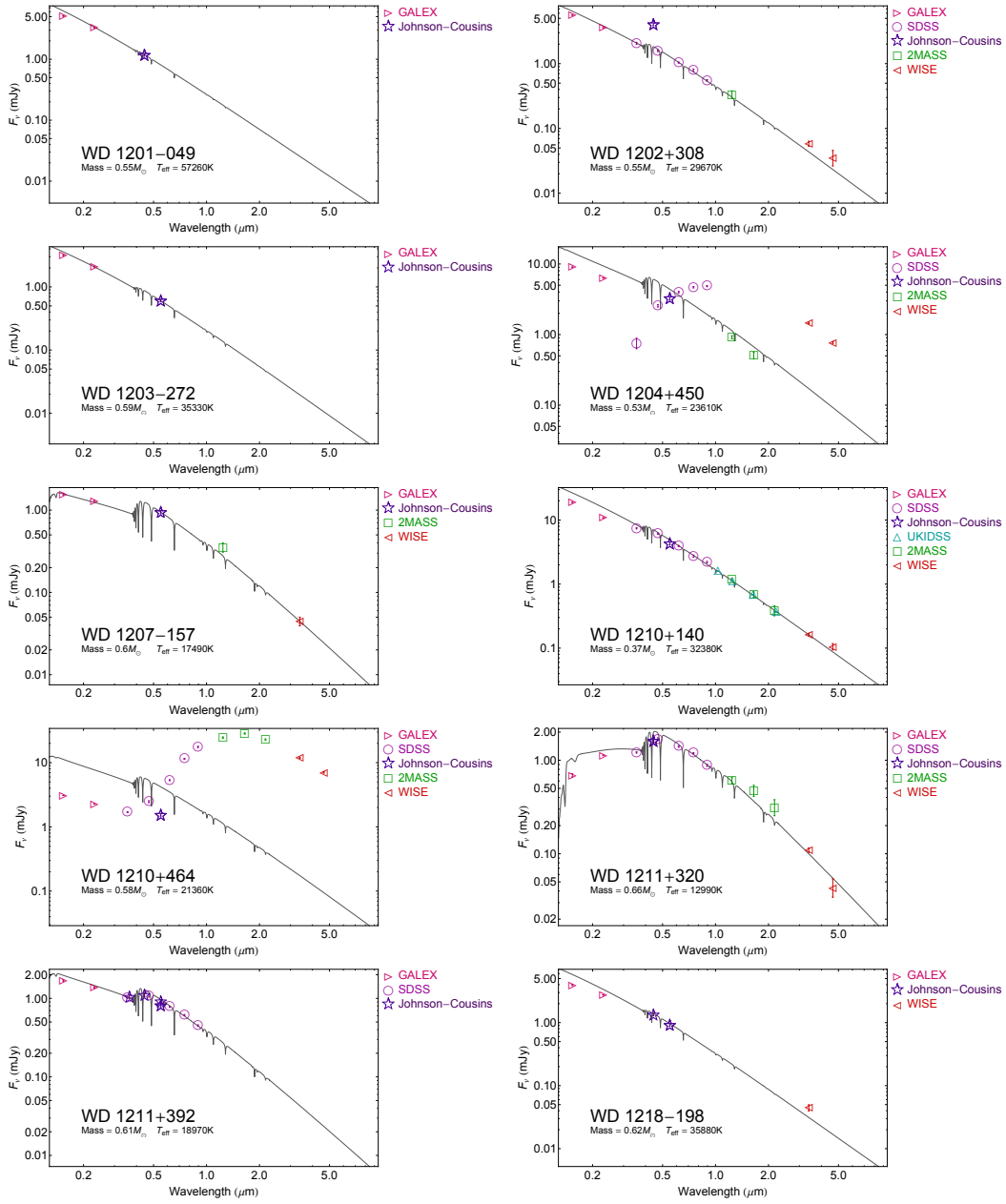

WD 1116−307
Mass = 0.71$M_\odot$ $T_{\rm eff}$ = 12190K
GALEX
Johnson−Cousins
2MASS
WD 1119−243
Mass = 0.64$M_\odot$ $T_{\rm eff}$ = 25240K
GALEX
Johnson−Cousins
WISE
WD 1119+385
Mass = 0.65$M_\odot$ $T_{\rm eff}$ = 17060K
SDSS
Johnson−Cousins
2MASS
WISE
WD 1121−507
Mass = 0.6$M_\odot$ $T_{\rm eff}$ = 17100K
Johnson−Cousins
2MASS
WISE
WD 1122+426
Mass = 0.71$M_\odot$ $T_{\rm eff}$ = 10470K
GALEX
SDSS
Johnson−Cousins
2MASS
WISE
WD 1123+189
Mass = 0.66$M_\odot$ $T_{\rm eff}$ = 53220K
GALEX
SDSS
Johnson−Cousins
2MASS
WISE
WD 1124−018
Mass = 0.51$M_\odot$ $T_{\rm eff}$ = 25180K
GALEX
SDSS
Johnson−Cousins
UKIDSS
2MASS
WISE
WD 1124−190
Mass = 0.94$M_\odot$ $T_{\rm eff}$ = 12560K
GALEX
Johnson−Cousins
2MASS
WISE
WD 1124+595
Mass = 1.14$M_\odot$ $T_{\rm eff}$ = 10750K
GALEX
SDSS
2MASS
WISE
WD 1125−025
Mass = 0.8$M_\odot$ $T_{\rm eff}$ = 31560K
GALEX
SDSS
Johnson−Cousins
UKIDSS
2MASS
WISE
F_ν (mJy)
Wavelength (μm)

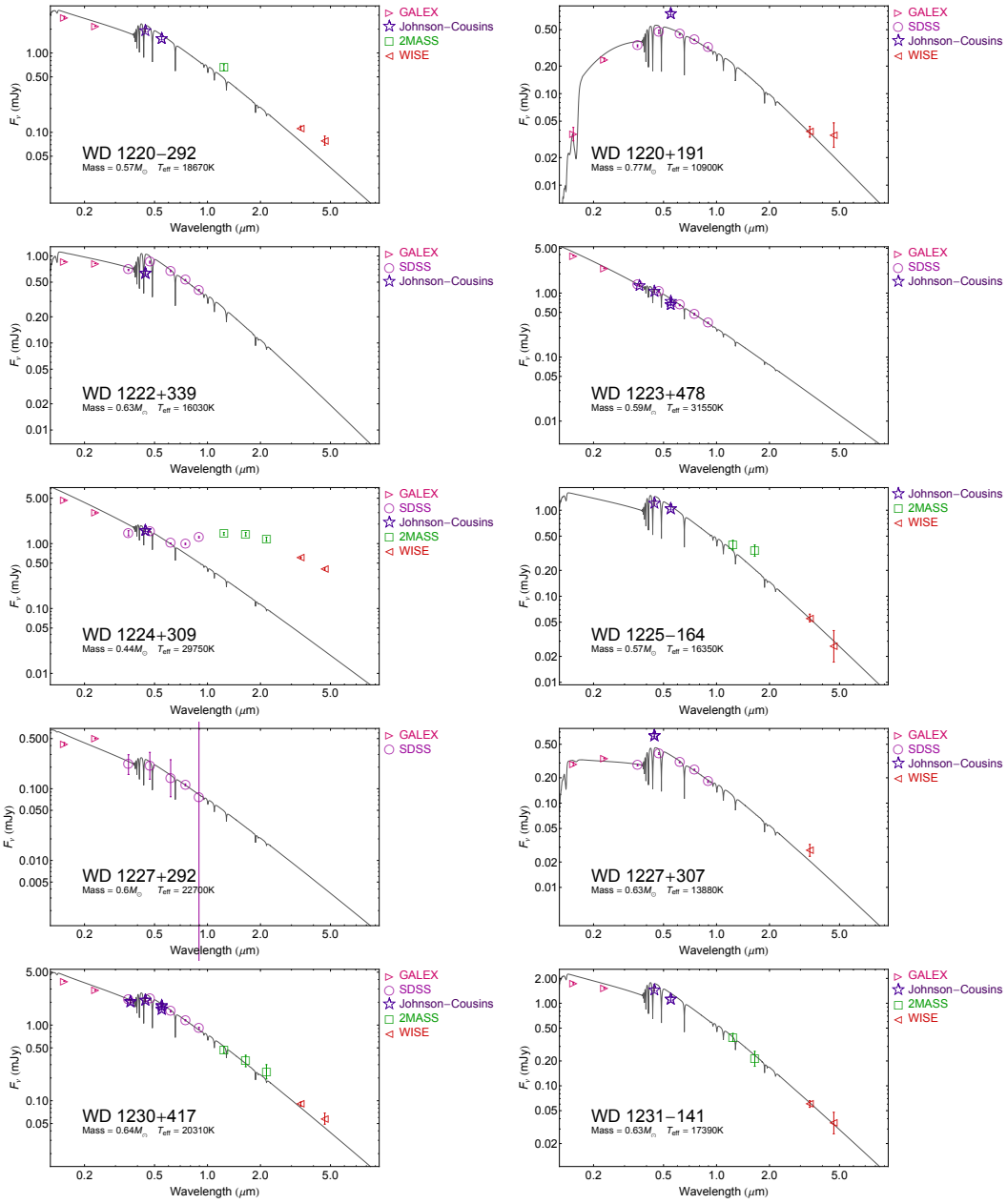

WD 1125+175
Mass = 0.64$M_\odot$ $T_{\rm eff}$ = 54430K
GALEX
SDSS
Johnson−Cousins
WISE
WD 1126−222
Mass = 0.68$M_\odot$ $T_{\rm eff}$ = 12270K
GALEX
Johnson−Cousins
2MASS
WD 1128+564
Mass = 0.57$M_\odot$ $T_{\rm eff}$ = 27490K
GALEX
SDSS
Johnson−Cousins
WISE
WD 1129−537
Mass = 0.53$M_\odot$ $T_{\rm eff}$ = 24270K
Johnson−Cousins
2MASS
WD 1129+071
Mass = 0.62$M_\odot$ $T_{\rm eff}$ = 13910K
SDSS
Johnson−Cousins
UKIDSS
2MASS
WISE
WD 1130−125
Mass = 0.85$M_\odot$ $T_{\rm eff}$ = 14780K
GALEX
Johnson−Cousins
2MASS
WISE
WD 1130+189
Mass = 0.95$M_\odot$ $T_{\rm eff}$ = 11200K
GALEX
SDSS
WD 1131+315
Mass = 0.74$M_\odot$ $T_{\rm eff}$ = 22510K
GALEX
SDSS
Johnson−Cousins
WD 1131+320
Mass = 0.66$M_\odot$ $T_{\rm eff}$ = 14190K
GALEX
SDSS
Johnson−Cousins
2MASS
WISE
WD 1131+333
Mass = 1.07$M_\odot$ $T_{\rm eff}$ = 9170K
GALEX
SDSS
Johnson−Cousins
2MASS
WISE
F_ν (mJy)
Wavelength (μm)

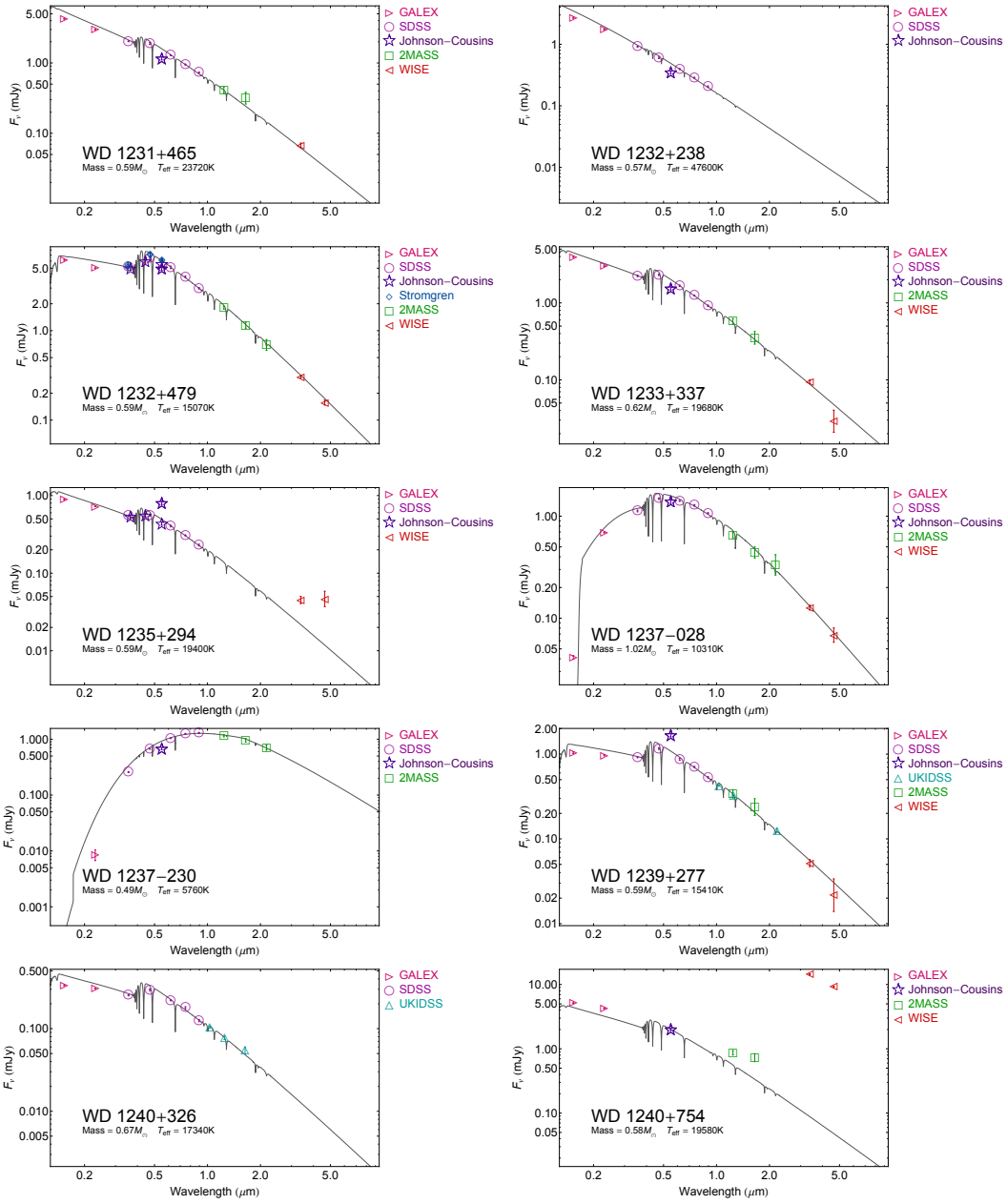

WD 1132−298
Mass = 0.27$M_\odot$ $T_{\rm eff}$ = 7540K
GALEX
Johnson−Cousins
2MASS
WISE
WD 1136+667
Mass = 0.55$M_\odot$ $T_{\rm eff}$ = 83090K
SDSS
Johnson−Cousins
2MASS
WISE
WD 1137+423
Mass = 0.74$M_\odot$ $T_{\rm eff}$ = 12230K
GALEX
SDSS
Johnson−Cousins
2MASS
WISE
WD 1139−230
Mass = 0.61$M_\odot$ $T_{\rm eff}$ = 14210K
GALEX
Johnson−Cousins
2MASS
WD 1139+258
Mass = 0.7$M_\odot$ $T_{\rm eff}$ = 43930K
SDSS
WISE
WD 1139+424
Mass = 0.6$M_\odot$ $T_{\rm eff}$ = 28000K
GALEX
SDSS
Johnson−Cousins
WISE
WD 1141−316
Mass = 0.7$M_\odot$ $T_{\rm eff}$ = 17590K
GALEX
Johnson−Cousins
WD 1141+077
Mass = 0.55$M_\odot$ $T_{\rm eff}$ = 64800K
GALEX
SDSS
Johnson−Cousins
UKIDSS
2MASS
WISE
WD 1141+504
Mass = 0.59$M_\odot$ $T_{\rm eff}$ = 21640K
GALEX
SDSS
Johnson−Cousins
2MASS
WISE
WD 1142+369
Mass = 0.48$M_\odot$ $T_{\rm eff}$ = 14870K
GALEX
SDSS
Johnson−Cousins
2MASS
WISE
F_ν (mJy)
Wavelength (μm)

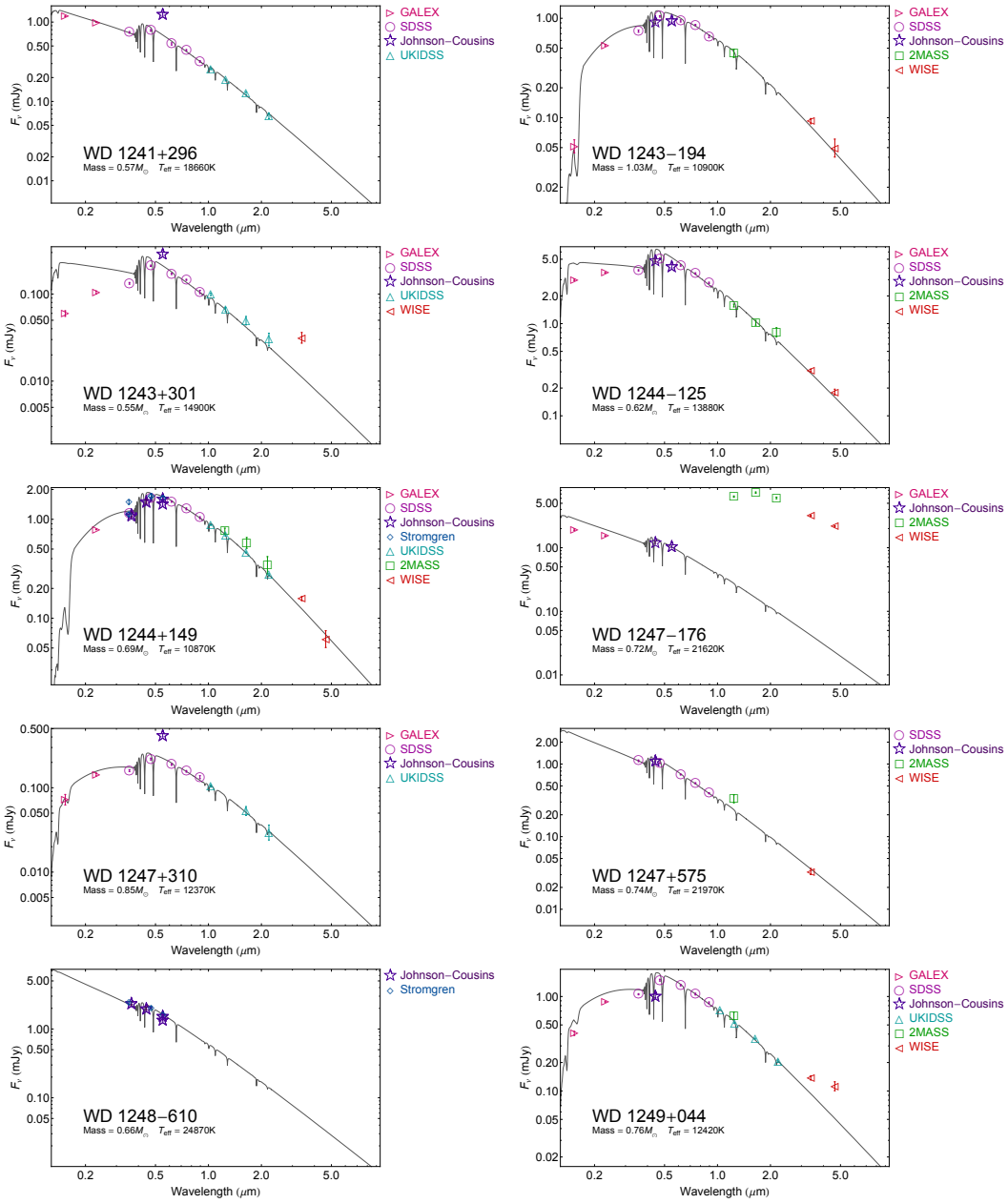

WD 1143−314
Mass = 0.69$M_\odot$ $T_{\rm eff}$ = 38810K
Johnson−Cousins
WISE
WD 1143+321.1
Mass = 0.64$M_\odot$ $T_{\rm eff}$ = 15970K
GALEX
SDSS
WD 1143+321.2
Mass = 0.72$M_\odot$ $T_{\rm eff}$ = 16290K
GALEX
SDSS
2MASS
WD 1144−246
Mass = 0.38$M_\odot$ $T_{\rm eff}$ = 31410K
GALEX
Johnson−Cousins
2MASS
WISE
WD 1147+255
Mass = 0.74$M_\odot$ $T_{\rm eff}$ = 10310K
GALEX
SDSS
Johnson−Cousins
2MASS
WISE
WD 1147+389
Mass = 0.62$M_\odot$ $T_{\rm eff}$ = 18160K
GALEX
SDSS
Johnson−Cousins
WISE
WD 1148+544
Mass = 0.74$M_\odot$ $T_{\rm eff}$ = 9970K
SDSS
Johnson−Cousins
2MASS
WD 1149+410
Mass = 0.59$M_\odot$ $T_{\rm eff}$ = 14730K
GALEX
SDSS
Johnson−Cousins
2MASS
WISE
WD 1152−287
Mass = 0.47$M_\odot$ $T_{\rm eff}$ = 21650K
GALEX
Johnson−Cousins
2MASS
WISE
WD 1152+371
Mass = 1.26$M_\odot$ $T_{\rm eff}$ = 27420K
GALEX
SDSS
Johnson−Cousins
WISE
F_ν (mJy)
Wavelength (μm)

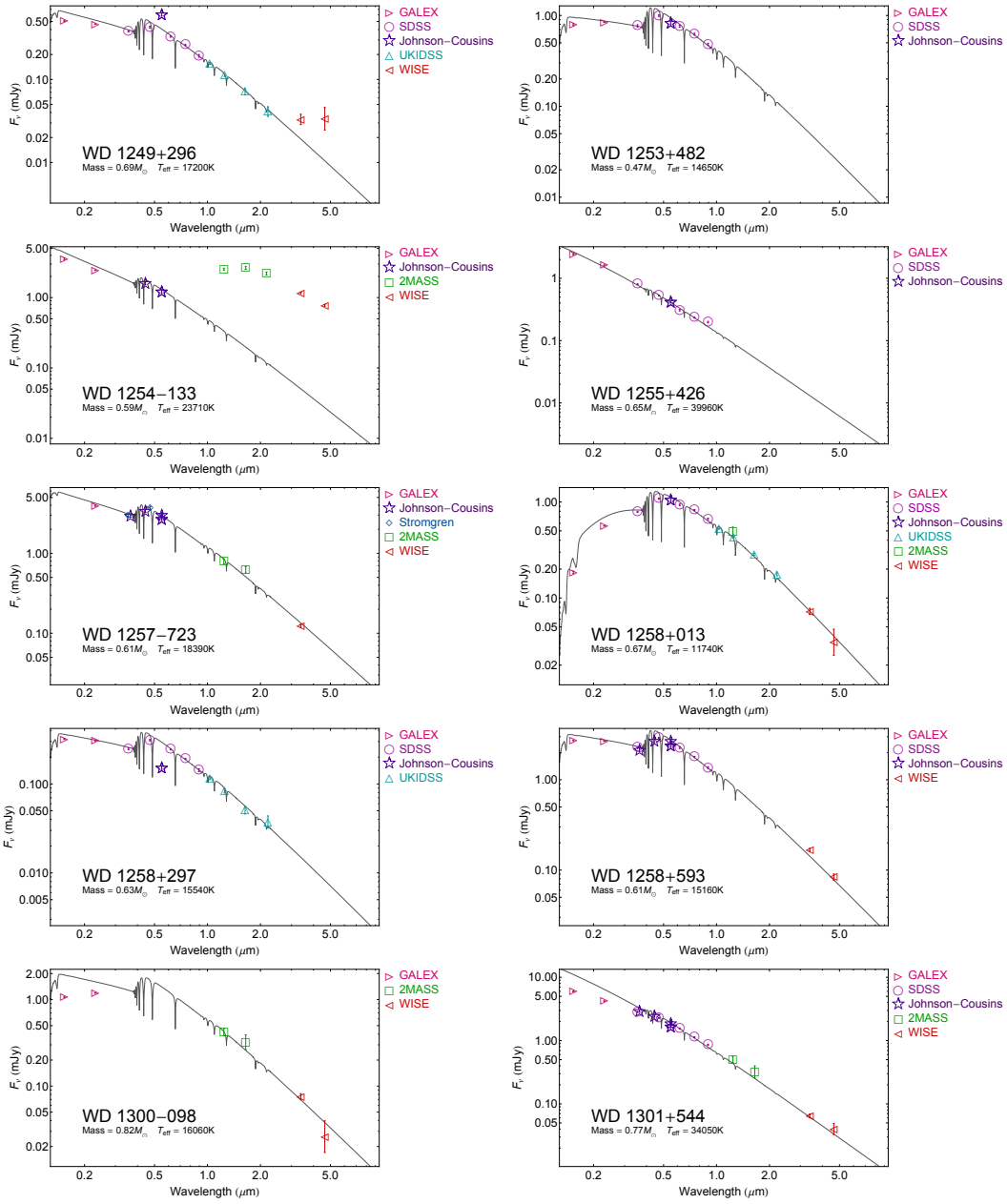

WD 1155−243
Mass = 0.58$M_\odot$ $T_{\rm eff}$ = 13830K
GALEX
Johnson−Cousins
2MASS
WD 1155+333
Mass = 0.36$M_\odot$ $T_{\rm eff}$ = 12670K
GALEX
SDSS
Johnson−Cousins
2MASS
WISE
WD 1156+291
Mass = 0.84$M_\odot$ $T_{\rm eff}$ = 9370K
GALEX
SDSS
Johnson−Cousins
2MASS
WISE
WD 1157+359
Mass = 0.96$M_\odot$ $T_{\rm eff}$ = 7330K
GALEX
SDSS
Johnson−Cousins
2MASS
WISE
WD 1158+432
Mass = 0.6$M_\odot$ $T_{\rm eff}$ = 14810K
SDSS
Johnson−Cousins
2MASS
WISE
WD 1159−098
Mass = 1.15$M_\odot$ $T_{\rm eff}$ = 9580K
GALEX
Johnson−Cousins
2MASS
WISE
WD 1159+803
Mass = 0.75$M_\odot$ $T_{\rm eff}$ = 11760K
GALEX
Johnson−Cousins
2MASS
WISE
WD 1200+310
Mass = 0.69$M_\odot$ $T_{\rm eff}$ = 12110K
GALEX
Johnson−Cousins
WD 1200+548
Mass = 0.63$M_\odot$ $T_{\rm eff}$ = 29030K
GALEX
SDSS
Johnson−Cousins
WISE
WD 1201−001
Mass = 0.83$M_\odot$ $T_{\rm eff}$ = 20600K
GALEX
SDSS
Johnson−Cousins
UKIDSS
2MASS
WISE
F_ν (mJy)
Wavelength (μm)

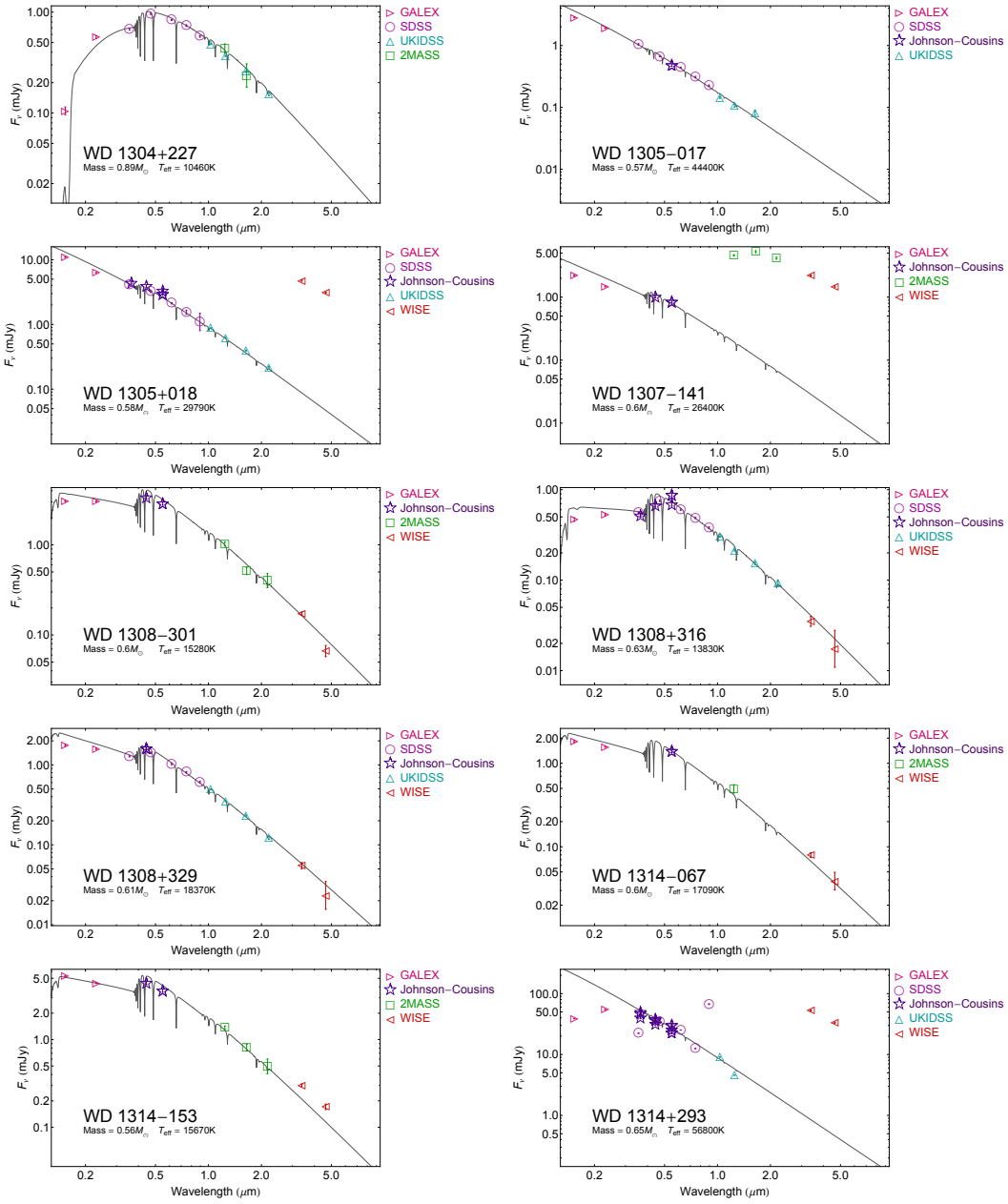

WD 1201−049
Mass = 0.55$M_\odot$ $T_{\rm eff}$ = 57260K
WD 1202+308
Mass = 0.55$M_\odot$ $T_{\rm eff}$ = 29670K
WD 1203−272
Mass = 0.59$M_\odot$ $T_{\rm eff}$ = 35330K
WD 1204+450
Mass = 0.53$M_\odot$ $T_{\rm eff}$ = 23610K
WD 1207−157
Mass = 0.6$M_\odot$ $T_{\rm eff}$ = 17490K
WD 1210+140
Mass = 0.37$M_\odot$ $T_{\rm eff}$ = 32380K
WD 1210+464
Mass = 0.58$M_\odot$ $T_{\rm eff}$ = 21360K
WD 1211+320
Mass = 0.66$M_\odot$ $T_{\rm eff}$ = 12990K
WD 1211+392
Mass = 0.61$M_\odot$ $T_{\rm eff}$ = 18970K
WD 1218−198
Mass = 0.62$M_\odot$ $T_{\rm eff}$ = 35880K
F_ν (mJy)
Wavelength (μm)
GALEX
SDSS
Johnson−Cousins
UKIDSS
2MASS
WISE

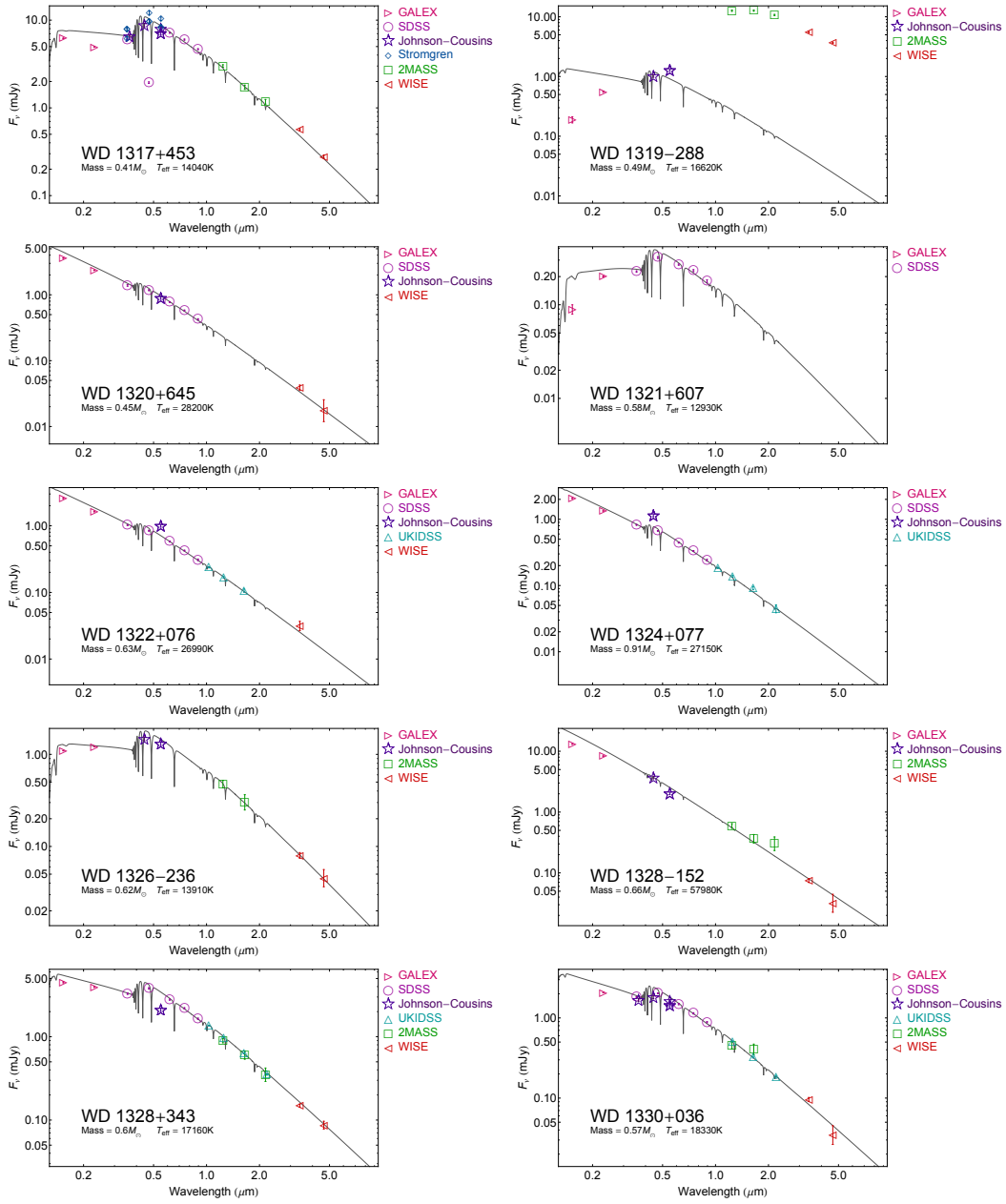

WD 1220−292
Mass = 0.57$M_\odot$ $T_{\rm eff}$ = 18670K
WD 1220+191
Mass = 0.77$M_\odot$ $T_{\rm eff}$ = 10900K
WD 1222+339
Mass = 0.63$M_\odot$ $T_{\rm eff}$ = 16030K
WD 1223+478
Mass = 0.59$M_\odot$ $T_{\rm eff}$ = 31550K
WD 1224+309
Mass = 0.44$M_\odot$ $T_{\rm eff}$ = 29750K
WD 1225−164
Mass = 0.57$M_\odot$ $T_{\rm eff}$ = 16350K
WD 1227+292
Mass = 0.6$M_\odot$ $T_{\rm eff}$ = 22700K
WD 1227+307
Mass = 0.63$M_\odot$ $T_{\rm eff}$ = 13880K
WD 1230+417
Mass = 0.64$M_\odot$ $T_{\rm eff}$ = 20310K
WD 1231−141
Mass = 0.63$M_\odot$ $T_{\rm eff}$ = 17390K
F_ν (mJy)
Wavelength (μm)
GALEX
SDSS
Johnson−Cousins
2MASS
WISE

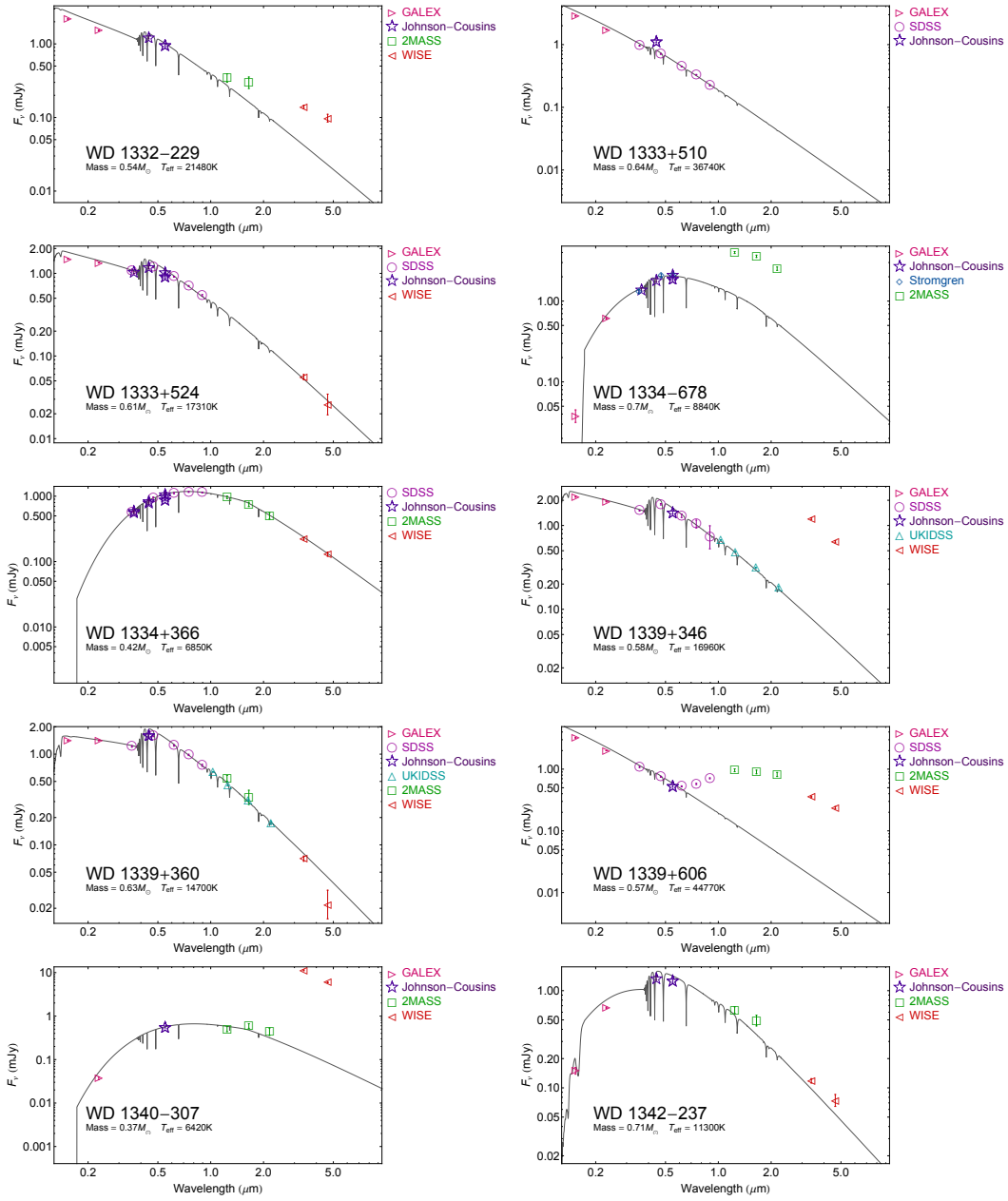

WD 1231+465
Mass = 0.59$M_\odot$ $T_{\rm eff}$ = 23720K
WD 1232+238
Mass = 0.57$M_\odot$ $T_{\rm eff}$ = 47600K
WD 1232+479
Mass = 0.59$M_\odot$ $T_{\rm eff}$ = 15070K
WD 1233+337
Mass = 0.62$M_\odot$ $T_{\rm eff}$ = 19680K
WD 1235+294
Mass = 0.59$M_\odot$ $T_{\rm eff}$ = 19400K
WD 1237−028
Mass = 1.02$M_\odot$ $T_{\rm eff}$ = 10310K
WD 1237−230
Mass = 0.49$M_\odot$ $T_{\rm eff}$ = 5760K
WD 1239+277
Mass = 0.59$M_\odot$ $T_{\rm eff}$ = 15410K
WD 1240+326
Mass = 0.67$M_\odot$ $T_{\rm eff}$ = 17340K
WD 1240+754
Mass = 0.58$M_\odot$ $T_{\rm eff}$ = 19580K
F_ν (mJy)
Wavelength (μm)
GALEX
SDSS
Johnson−Cousins
Stromgren
2MASS
UKIDSS
WISE

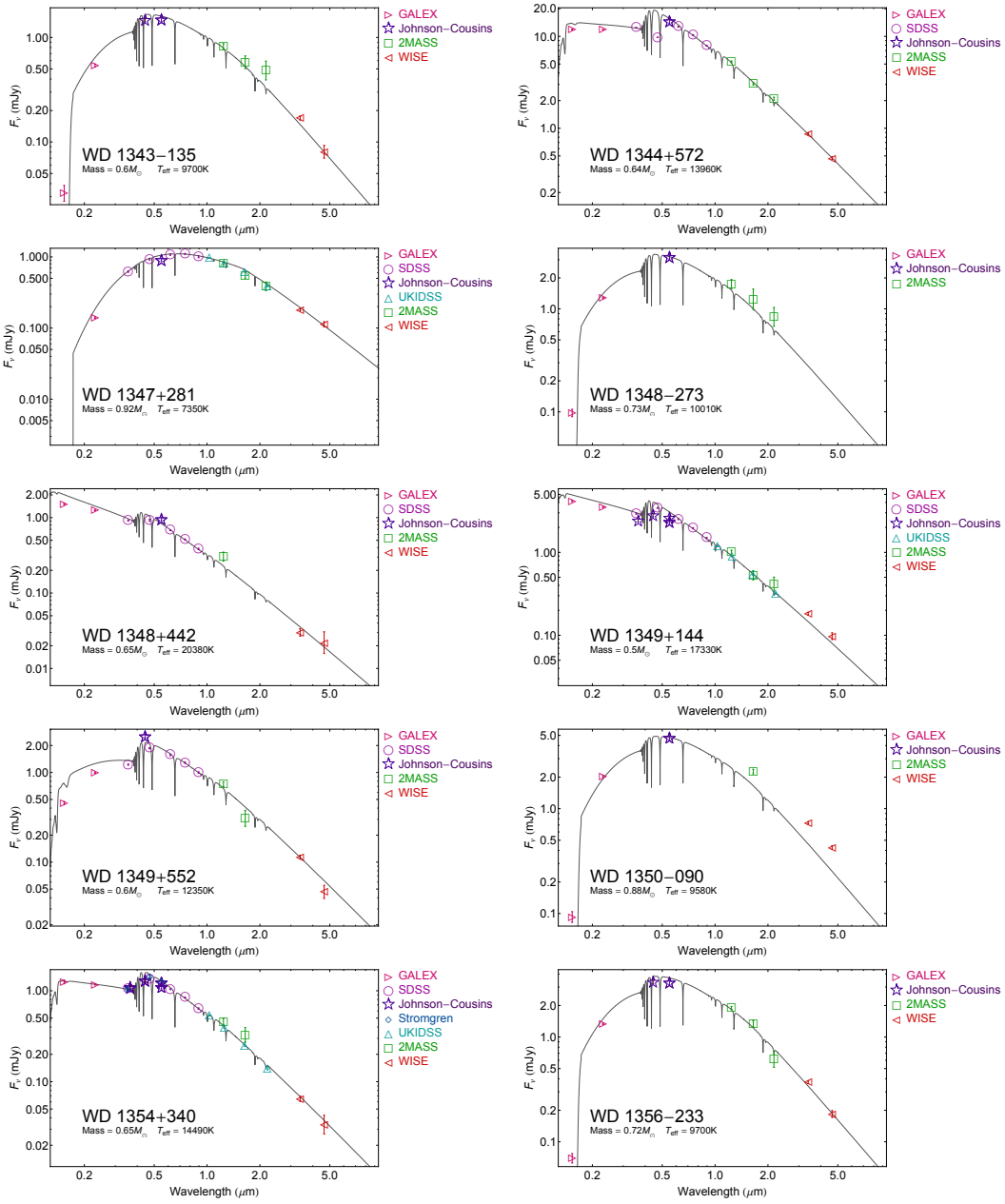

WD 1241+296
Mass = 0.57$M_\odot$ $T_{\rm eff}$ = 18660K
GALEX
SDSS
Johnson–Cousins
UKIDSS
WD 1243–194
Mass = 1.03$M_\odot$ $T_{\rm eff}$ = 10900K
GALEX
SDSS
Johnson–Cousins
2MASS
WISE
WD 1243+301
Mass = 0.55$M_\odot$ $T_{\rm eff}$ = 14900K
GALEX
SDSS
Johnson–Cousins
UKIDSS
WISE
WD 1244–125
Mass = 0.62$M_\odot$ $T_{\rm eff}$ = 13880K
GALEX
SDSS
Johnson–Cousins
2MASS
WISE
WD 1244+149
Mass = 0.69$M_\odot$ $T_{\rm eff}$ = 10870K
GALEX
SDSS
Johnson–Cousins
Stromgren
UKIDSS
2MASS
WISE
WD 1247–176
Mass = 0.72$M_\odot$ $T_{\rm eff}$ = 21620K
GALEX
Johnson–Cousins
2MASS
WISE
WD 1247+310
Mass = 0.85$M_\odot$ $T_{\rm eff}$ = 12370K
GALEX
SDSS
Johnson–Cousins
UKIDSS
WD 1247+575
Mass = 0.74$M_\odot$ $T_{\rm eff}$ = 21970K
SDSS
Johnson–Cousins
2MASS
WISE
WD 1248–610
Mass = 0.66$M_\odot$ $T_{\rm eff}$ = 24870K
Johnson–Cousins
Stromgren
WD 1249+044
Mass = 0.76$M_\odot$ $T_{\rm eff}$ = 12420K
GALEX
SDSS
Johnson–Cousins
UKIDSS
2MASS
WISE
F_ν (mJy)
Wavelength (μm)

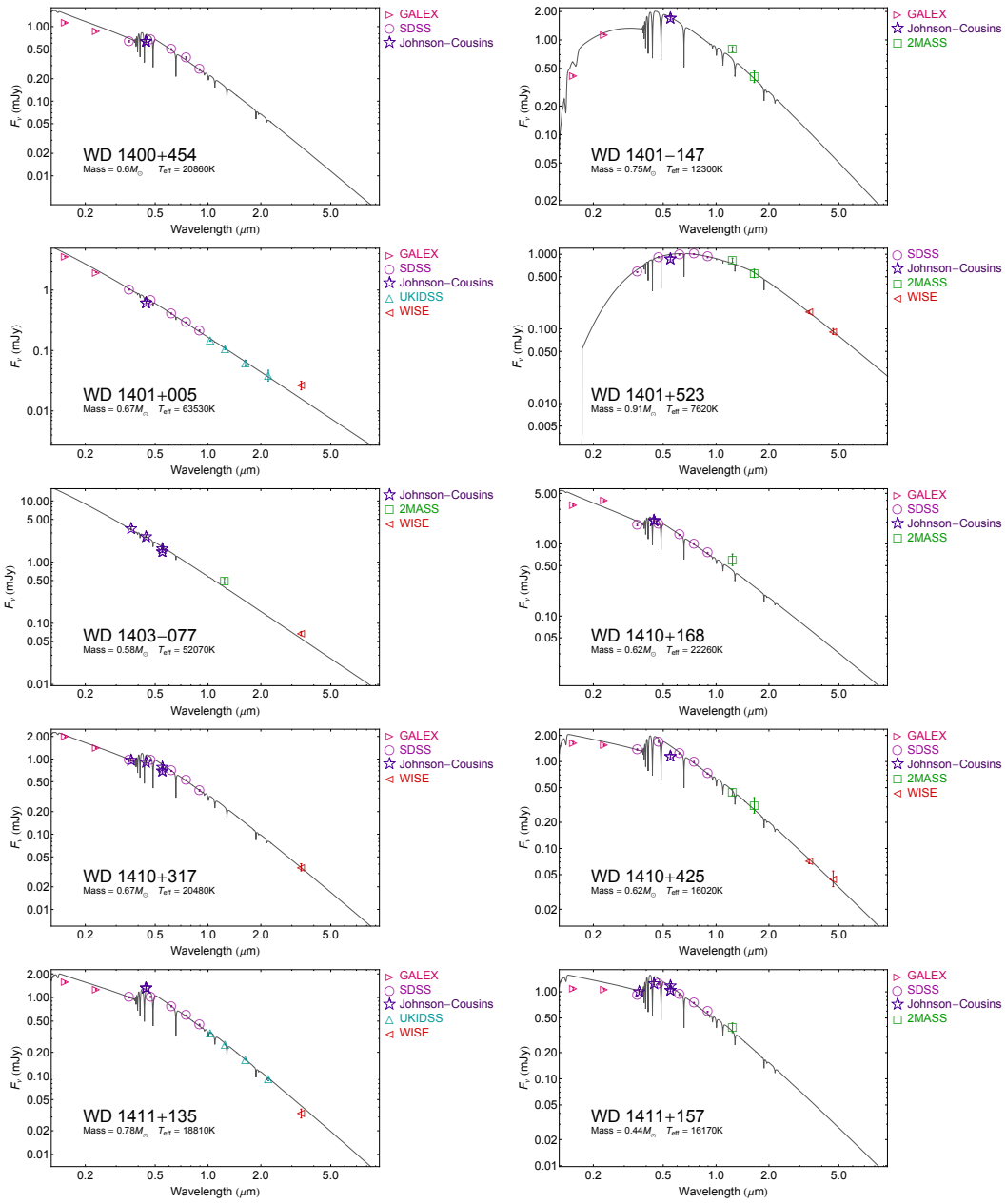

WD 1249+296
Mass = 0.69$M_\odot$ $T_{\rm eff}$ = 17200K
GALEX
SDSS
Johnson–Cousins
UKIDSS
WISE
WD 1253+482
Mass = 0.47$M_\odot$ $T_{\rm eff}$ = 14650K
GALEX
SDSS
Johnson–Cousins
WD 1254–133
Mass = 0.59$M_\odot$ $T_{\rm eff}$ = 23710K
GALEX
Johnson–Cousins
2MASS
WISE
WD 1255+426
Mass = 0.65$M_\odot$ $T_{\rm eff}$ = 39960K
GALEX
SDSS
Johnson–Cousins
WD 1257–723
Mass = 0.61$M_\odot$ $T_{\rm eff}$ = 18390K
GALEX
Johnson–Cousins
Stromgren
2MASS
WISE
WD 1258+013
Mass = 0.67$M_\odot$ $T_{\rm eff}$ = 11740K
GALEX
SDSS
Johnson–Cousins
UKIDSS
2MASS
WISE
WD 1258+297
Mass = 0.63$M_\odot$ $T_{\rm eff}$ = 15540K
GALEX
SDSS
Johnson–Cousins
UKIDSS
WD 1258+593
Mass = 0.61$M_\odot$ $T_{\rm eff}$ = 15160K
GALEX
SDSS
Johnson–Cousins
WISE
WD 1300–098
Mass = 0.82$M_\odot$ $T_{\rm eff}$ = 16060K
GALEX
2MASS
WISE
WD 1301+544
Mass = 0.77$M_\odot$ $T_{\rm eff}$ = 34050K
GALEX
SDSS
Johnson–Cousins
2MASS
WISE
F_ν (mJy)
Wavelength (μm)

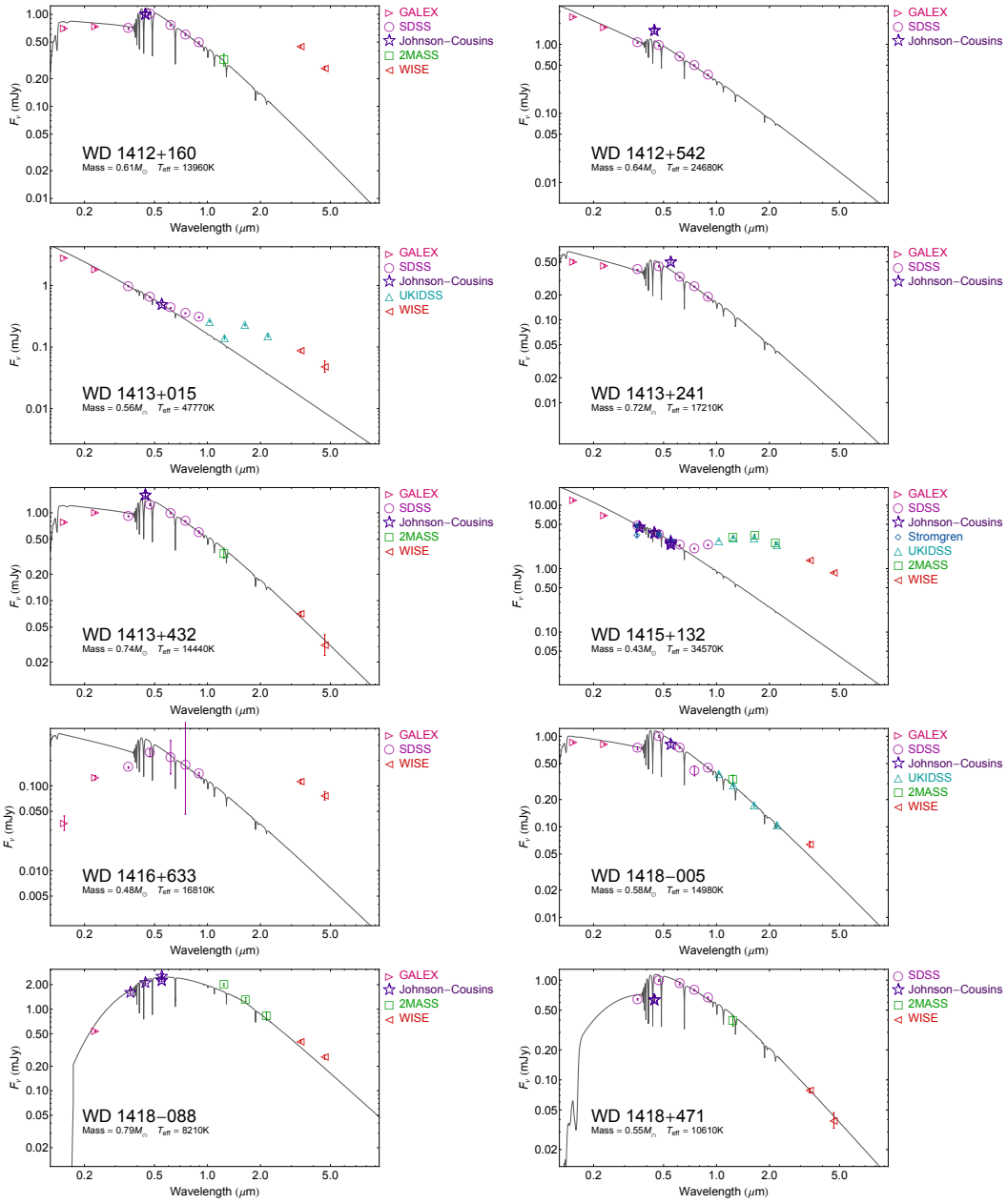

WD 1304+227
Mass = 0.89$M_\odot$ $T_{\rm eff}$ = 10460K
GALEX
SDSS
UKIDSS
2MASS
WD 1305−017
Mass = 0.57$M_\odot$ $T_{\rm eff}$ = 44400K
GALEX
SDSS
Johnson−Cousins
UKIDSS
WD 1305+018
Mass = 0.58$M_\odot$ $T_{\rm eff}$ = 29790K
GALEX
SDSS
Johnson−Cousins
UKIDSS
WISE
WD 1307−141
Mass = 0.6$M_\odot$ $T_{\rm eff}$ = 26400K
GALEX
Johnson−Cousins
2MASS
WISE
WD 1308−301
Mass = 0.6$M_\odot$ $T_{\rm eff}$ = 15280K
GALEX
Johnson−Cousins
2MASS
WISE
WD 1308+316
Mass = 0.63$M_\odot$ $T_{\rm eff}$ = 13830K
GALEX
SDSS
Johnson−Cousins
UKIDSS
WISE
WD 1308+329
Mass = 0.61$M_\odot$ $T_{\rm eff}$ = 18370K
GALEX
SDSS
Johnson−Cousins
UKIDSS
WISE
WD 1314−067
Mass = 0.6$M_\odot$ $T_{\rm eff}$ = 17090K
GALEX
Johnson−Cousins
2MASS
WISE
WD 1314−153
Mass = 0.56$M_\odot$ $T_{\rm eff}$ = 15670K
GALEX
Johnson−Cousins
2MASS
WISE
WD 1314+293
Mass = 0.65$M_\odot$ $T_{\rm eff}$ = 56800K
GALEX
SDSS
Johnson−Cousins
UKIDSS
WISE
F_ν (mJy)
Wavelength (μm)

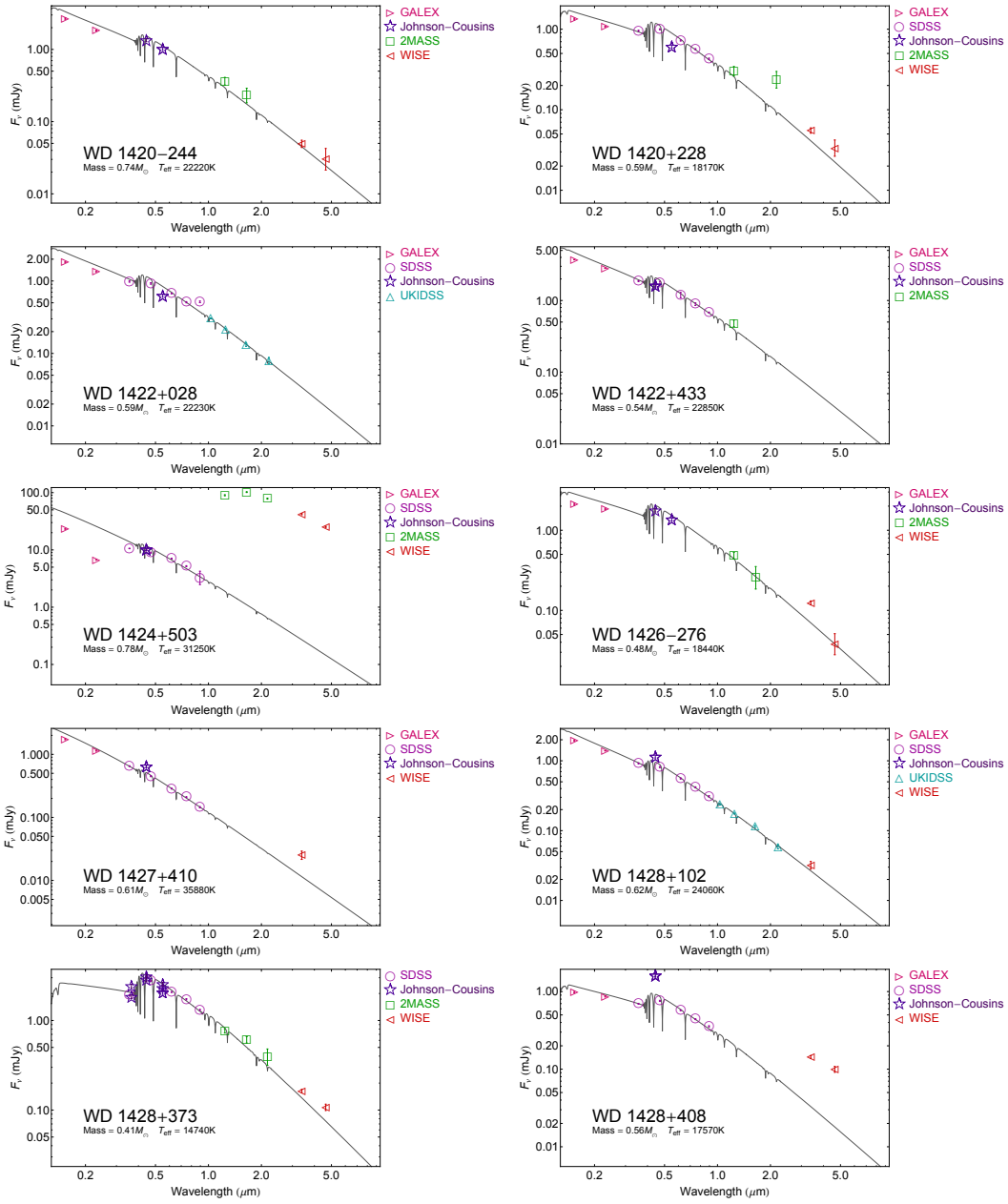

WD 1317+453
Mass = 0.41$M_\odot$ $T_{\rm eff}$ = 14040K
GALEX
SDSS
Johnson−Cousins
Stromgren
2MASS
WISE
WD 1319−288
Mass = 0.49$M_\odot$ $T_{\rm eff}$ = 16620K
GALEX
Johnson−Cousins
2MASS
WISE
WD 1320+645
Mass = 0.45$M_\odot$ $T_{\rm eff}$ = 28200K
GALEX
SDSS
Johnson−Cousins
WISE
WD 1321+607
Mass = 0.58$M_\odot$ $T_{\rm eff}$ = 12930K
GALEX
SDSS
WD 1322+076
Mass = 0.63$M_\odot$ $T_{\rm eff}$ = 26990K
GALEX
SDSS
Johnson−Cousins
UKIDSS
WISE
WD 1324+077
Mass = 0.91$M_\odot$ $T_{\rm eff}$ = 27150K
GALEX
SDSS
Johnson−Cousins
UKIDSS
WD 1326−236
Mass = 0.62$M_\odot$ $T_{\rm eff}$ = 13910K
GALEX
Johnson−Cousins
2MASS
WISE
WD 1328−152
Mass = 0.66$M_\odot$ $T_{\rm eff}$ = 57980K
GALEX
Johnson−Cousins
2MASS
WISE
WD 1328+343
Mass = 0.6$M_\odot$ $T_{\rm eff}$ = 17160K
GALEX
SDSS
Johnson−Cousins
UKIDSS
2MASS
WISE
WD 1330+036
Mass = 0.57$M_\odot$ $T_{\rm eff}$ = 18330K
GALEX
SDSS
Johnson−Cousins
UKIDSS
2MASS
WISE
F_ν (mJy)
Wavelength (μm)

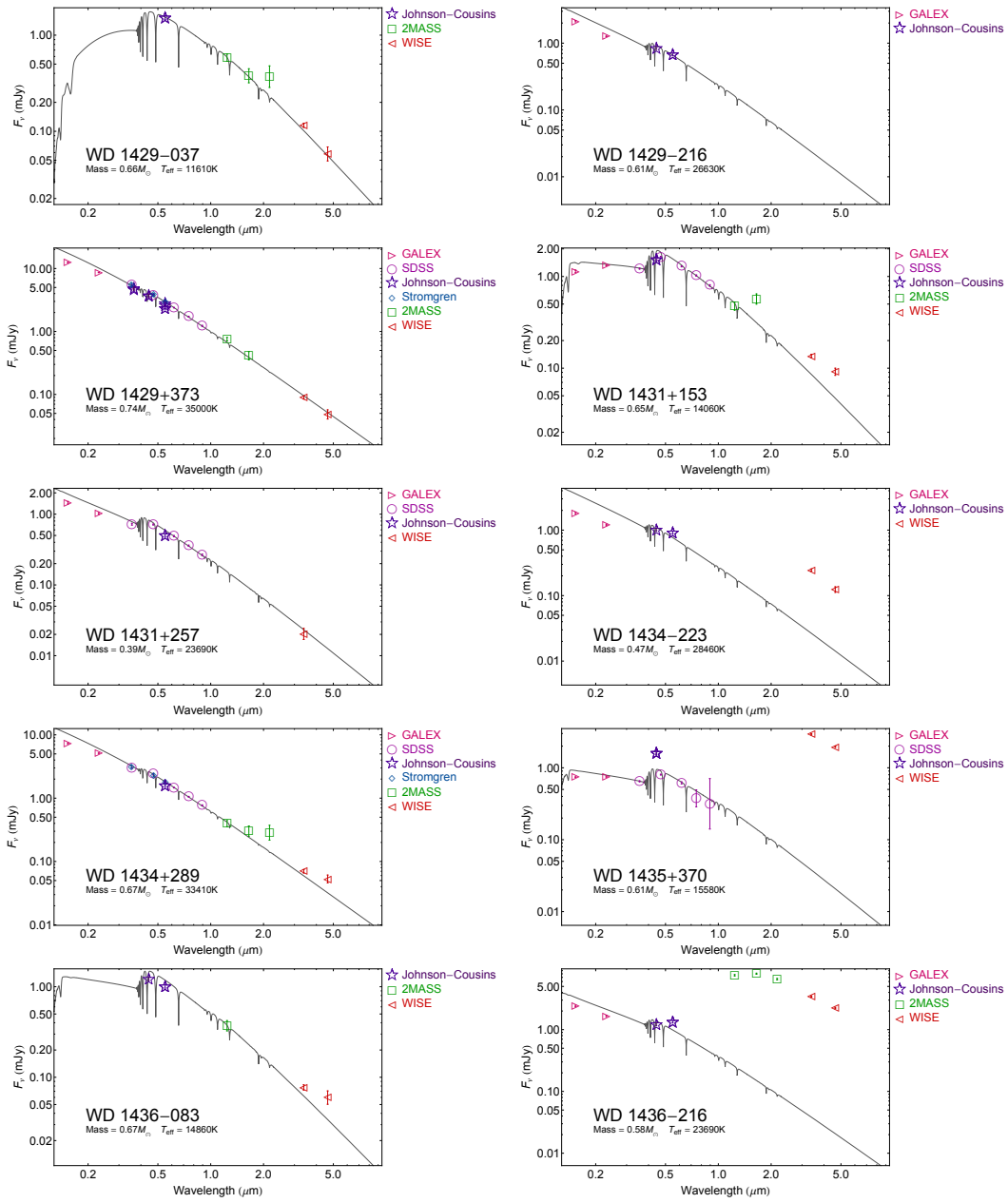

WD 1332−229
Mass = 0.54$M_\odot$ $T_{\rm eff}$ = 21480K
GALEX
Johnson−Cousins
2MASS
WISE
WD 1333+510
Mass = 0.64$M_\odot$ $T_{\rm eff}$ = 36740K
GALEX
SDSS
Johnson−Cousins
WD 1333+524
Mass = 0.61$M_\odot$ $T_{\rm eff}$ = 17310K
GALEX
SDSS
Johnson−Cousins
WISE
WD 1334−678
Mass = 0.7$M_\odot$ $T_{\rm eff}$ = 8840K
GALEX
Johnson−Cousins
Stromgren
2MASS
WD 1334+366
Mass = 0.42$M_\odot$ $T_{\rm eff}$ = 6850K
SDSS
Johnson−Cousins
2MASS
WISE
WD 1339+346
Mass = 0.58$M_\odot$ $T_{\rm eff}$ = 16960K
GALEX
SDSS
Johnson−Cousins
UKIDSS
WISE
WD 1339+360
Mass = 0.63$M_\odot$ $T_{\rm eff}$ = 14700K
GALEX
SDSS
Johnson−Cousins
UKIDSS
2MASS
WISE
WD 1339+606
Mass = 0.57$M_\odot$ $T_{\rm eff}$ = 44770K
GALEX
SDSS
Johnson−Cousins
2MASS
WISE
WD 1340−307
Mass = 0.37$M_\odot$ $T_{\rm eff}$ = 6420K
GALEX
Johnson−Cousins
2MASS
WISE
WD 1342−237
Mass = 0.71$M_\odot$ $T_{\rm eff}$ = 11300K
GALEX
Johnson−Cousins
2MASS
WISE
F_ν (mJy)
Wavelength (μm)

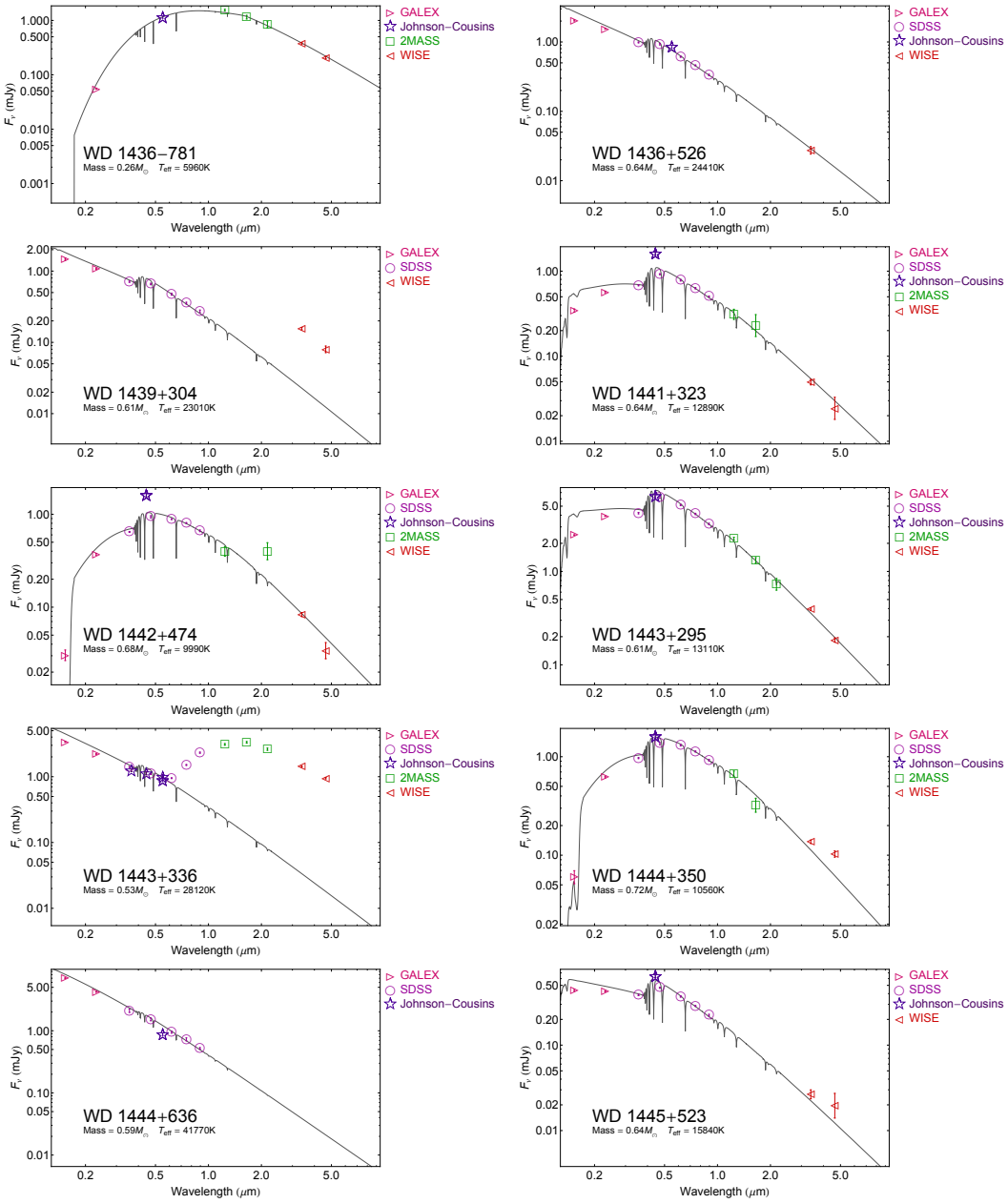

WD 1343−135
Mass = 0.6$M_\odot$ $T_{\rm eff}$ = 9700K
WD 1344+572
Mass = 0.64$M_\odot$ $T_{\rm eff}$ = 13960K
WD 1347+281
Mass = 0.92$M_\odot$ $T_{\rm eff}$ = 7350K
WD 1348−273
Mass = 0.73$M_\odot$ $T_{\rm eff}$ = 10010K
WD 1348+442
Mass = 0.65$M_\odot$ $T_{\rm eff}$ = 20380K
WD 1349+144
Mass = 0.5$M_\odot$ $T_{\rm eff}$ = 17330K
WD 1349+552
Mass = 0.6$M_\odot$ $T_{\rm eff}$ = 12350K
WD 1350−090
Mass = 0.88$M_\odot$ $T_{\rm eff}$ = 9580K
WD 1354+340
Mass = 0.65$M_\odot$ $T_{\rm eff}$ = 14490K
WD 1356−233
Mass = 0.72$M_\odot$ $T_{\rm eff}$ = 9700K
F_ν (mJy)
Wavelength (μm)
GALEX
SDSS
Johnson−Cousins
Stromgren
UKIDSS
2MASS
WISE

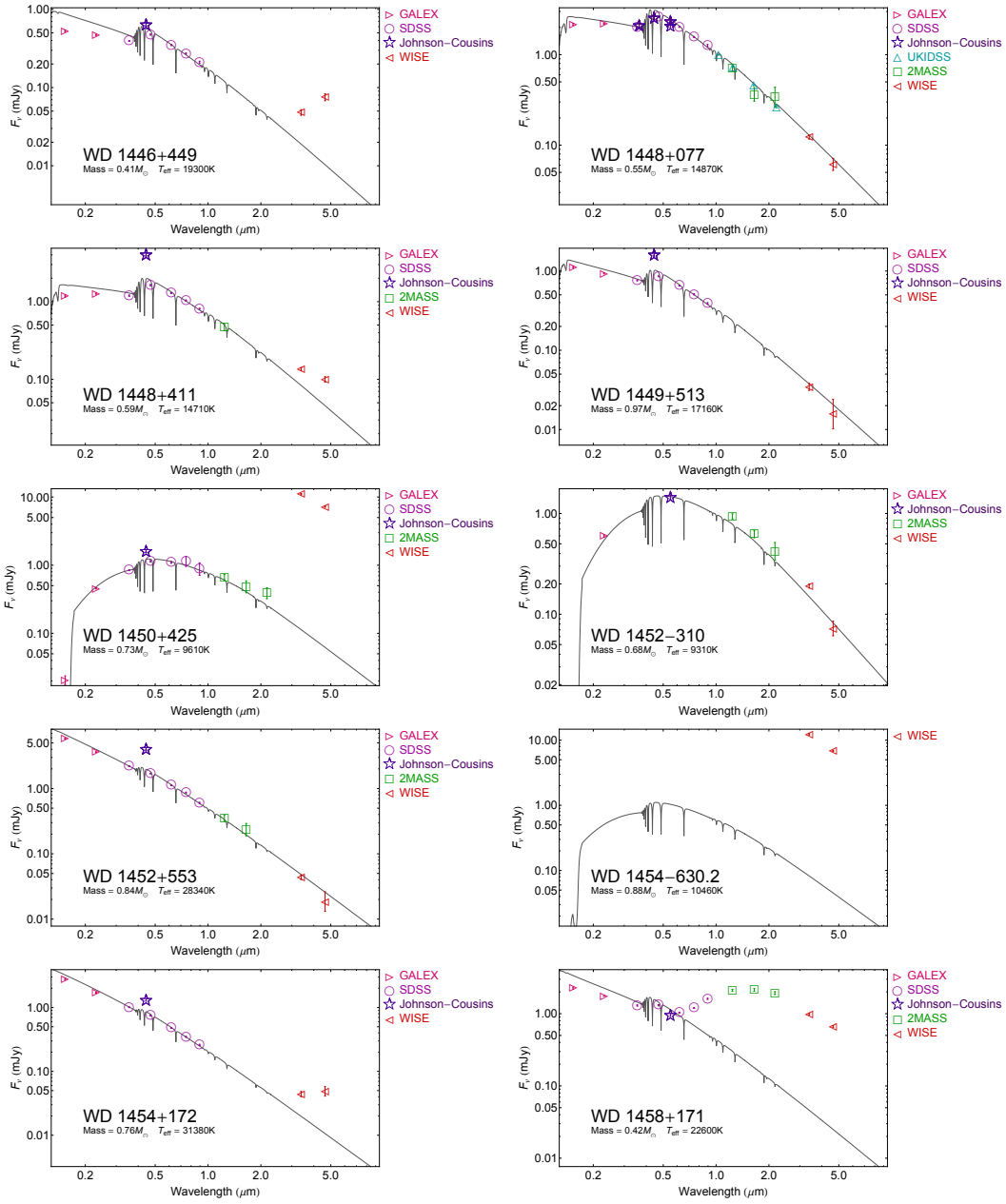

WD 1400+454
Mass = 0.6$M_\odot$ $T_{\rm eff}$ = 20860K
GALEX
SDSS
Johnson–Cousins
WD 1401–147
Mass = 0.75$M_\odot$ $T_{\rm eff}$ = 12300K
GALEX
Johnson–Cousins
2MASS
WD 1401+005
Mass = 0.67$M_\odot$ $T_{\rm eff}$ = 63530K
GALEX
SDSS
Johnson–Cousins
UKIDSS
WISE
WD 1401+523
Mass = 0.91$M_\odot$ $T_{\rm eff}$ = 7620K
SDSS
Johnson–Cousins
2MASS
WISE
WD 1403–077
Mass = 0.58$M_\odot$ $T_{\rm eff}$ = 52070K
Johnson–Cousins
2MASS
WISE
WD 1410+168
Mass = 0.62$M_\odot$ $T_{\rm eff}$ = 22260K
GALEX
SDSS
Johnson–Cousins
2MASS
WD 1410+317
Mass = 0.67$M_\odot$ $T_{\rm eff}$ = 20480K
GALEX
SDSS
Johnson–Cousins
WISE
WD 1410+425
Mass = 0.62$M_\odot$ $T_{\rm eff}$ = 16020K
GALEX
SDSS
Johnson–Cousins
2MASS
WISE
WD 1411+135
Mass = 0.78$M_\odot$ $T_{\rm eff}$ = 18810K
GALEX
SDSS
Johnson–Cousins
UKIDSS
WISE
WD 1411+157
Mass = 0.44$M_\odot$ $T_{\rm eff}$ = 16170K
GALEX
SDSS
Johnson–Cousins
2MASS
F_ν (mJy)
Wavelength (μm)

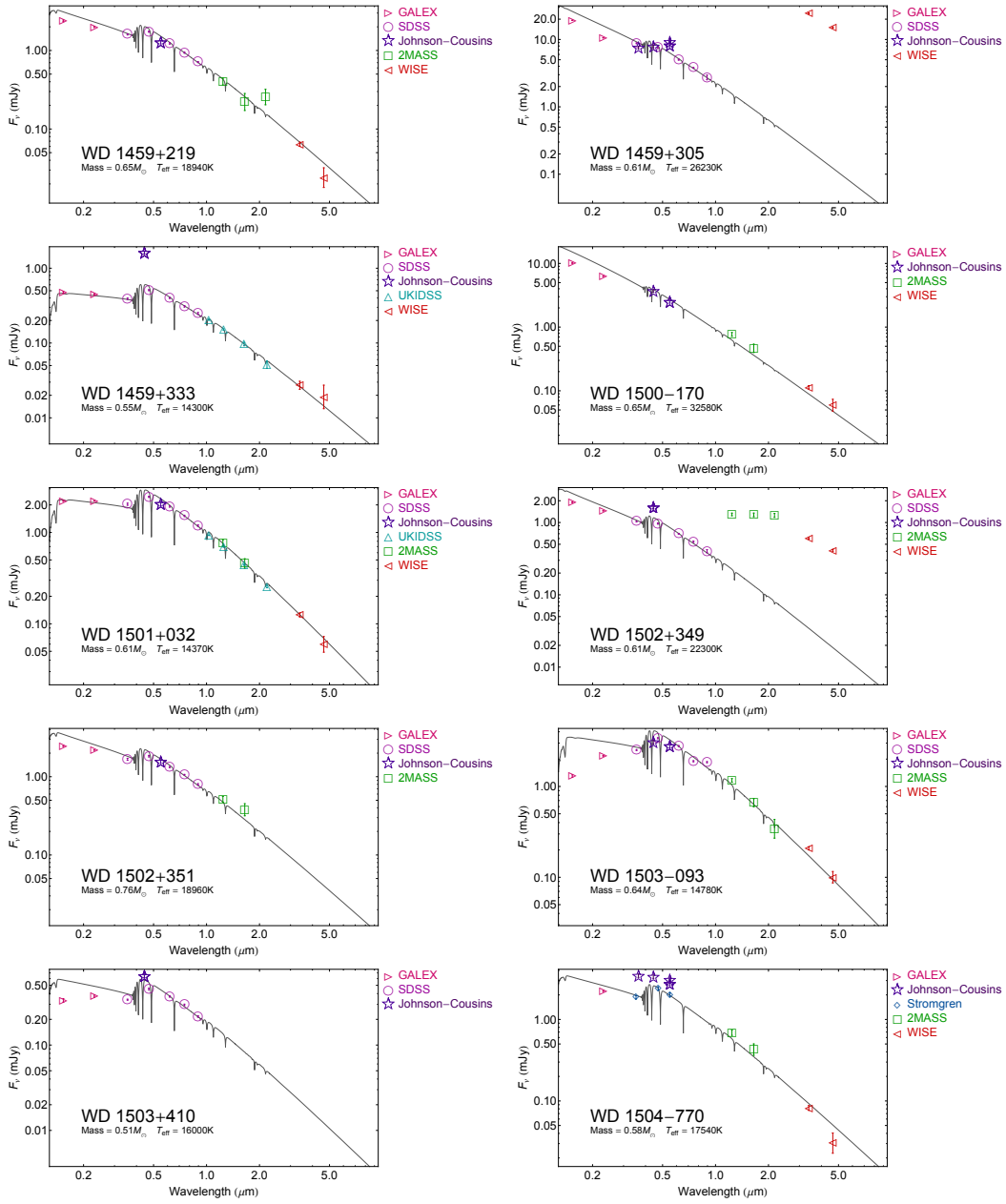

WD 1412+160
Mass = 0.61$M_\odot$ $T_{\rm eff}$ = 13960K
GALEX
SDSS
Johnson−Cousins
2MASS
WISE
WD 1412+542
Mass = 0.64$M_\odot$ $T_{\rm eff}$ = 24680K
GALEX
SDSS
Johnson−Cousins
WD 1413+015
Mass = 0.56$M_\odot$ $T_{\rm eff}$ = 47770K
GALEX
SDSS
Johnson−Cousins
UKIDSS
WISE
WD 1413+241
Mass = 0.72$M_\odot$ $T_{\rm eff}$ = 17210K
GALEX
SDSS
Johnson−Cousins
WD 1413+432
Mass = 0.74$M_\odot$ $T_{\rm eff}$ = 14440K
GALEX
SDSS
Johnson−Cousins
2MASS
WISE
WD 1415+132
Mass = 0.43$M_\odot$ $T_{\rm eff}$ = 34570K
GALEX
SDSS
Johnson−Cousins
Stromgren
UKIDSS
2MASS
WISE
WD 1416+633
Mass = 0.48$M_\odot$ $T_{\rm eff}$ = 16810K
GALEX
SDSS
WISE
WD 1418−005
Mass = 0.58$M_\odot$ $T_{\rm eff}$ = 14980K
GALEX
SDSS
Johnson−Cousins
UKIDSS
2MASS
WISE
WD 1418−088
Mass = 0.79$M_\odot$ $T_{\rm eff}$ = 8210K
GALEX
Johnson−Cousins
2MASS
WISE
WD 1418+471
Mass = 0.55$M_\odot$ $T_{\rm eff}$ = 10610K
SDSS
Johnson−Cousins
2MASS
WISE
F_ν (mJy)
Wavelength (μm)

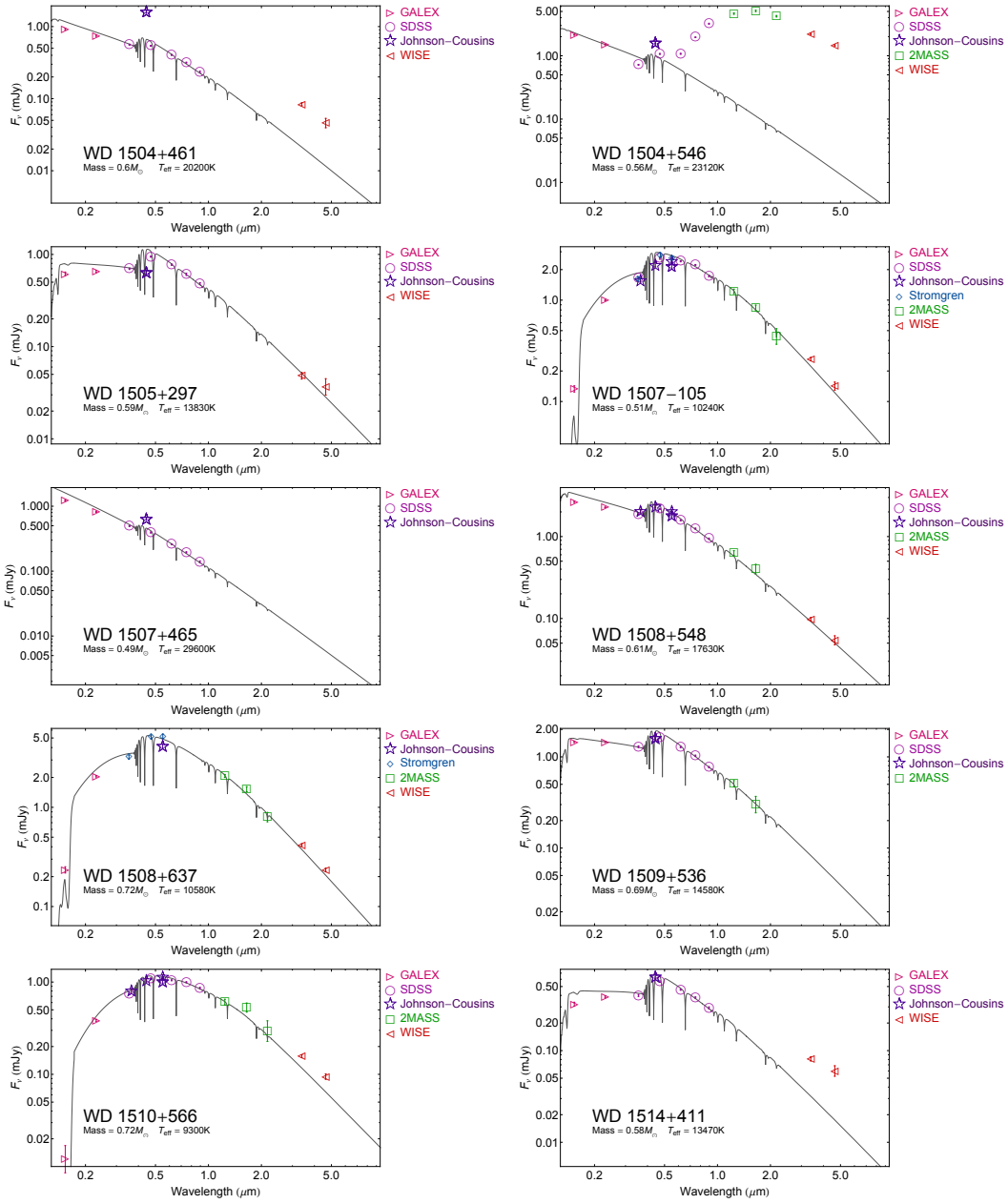

WD 1420−244
Mass = 0.74$M_\odot$ $T_{\rm eff}$ = 22220K
GALEX
Johnson−Cousins
2MASS
WISE
WD 1420+228
Mass = 0.59$M_\odot$ $T_{\rm eff}$ = 18170K
GALEX
SDSS
Johnson−Cousins
2MASS
WISE
WD 1422+028
Mass = 0.59$M_\odot$ $T_{\rm eff}$ = 22230K
GALEX
SDSS
Johnson−Cousins
UKIDSS
WD 1422+433
Mass = 0.54$M_\odot$ $T_{\rm eff}$ = 22850K
GALEX
SDSS
Johnson−Cousins
2MASS
WD 1424+503
Mass = 0.78$M_\odot$ $T_{\rm eff}$ = 31250K
GALEX
SDSS
Johnson−Cousins
2MASS
WISE
WD 1426−276
Mass = 0.48$M_\odot$ $T_{\rm eff}$ = 18440K
GALEX
Johnson−Cousins
2MASS
WISE
WD 1427+410
Mass = 0.61$M_\odot$ $T_{\rm eff}$ = 35880K
GALEX
SDSS
Johnson−Cousins
WISE
WD 1428+102
Mass = 0.62$M_\odot$ $T_{\rm eff}$ = 24060K
GALEX
SDSS
Johnson−Cousins
UKIDSS
WISE
WD 1428+373
Mass = 0.41$M_\odot$ $T_{\rm eff}$ = 14740K
SDSS
Johnson−Cousins
2MASS
WISE
WD 1428+408
Mass = 0.56$M_\odot$ $T_{\rm eff}$ = 17570K
GALEX
SDSS
Johnson−Cousins
WISE
F_ν (mJy)
Wavelength (μm)

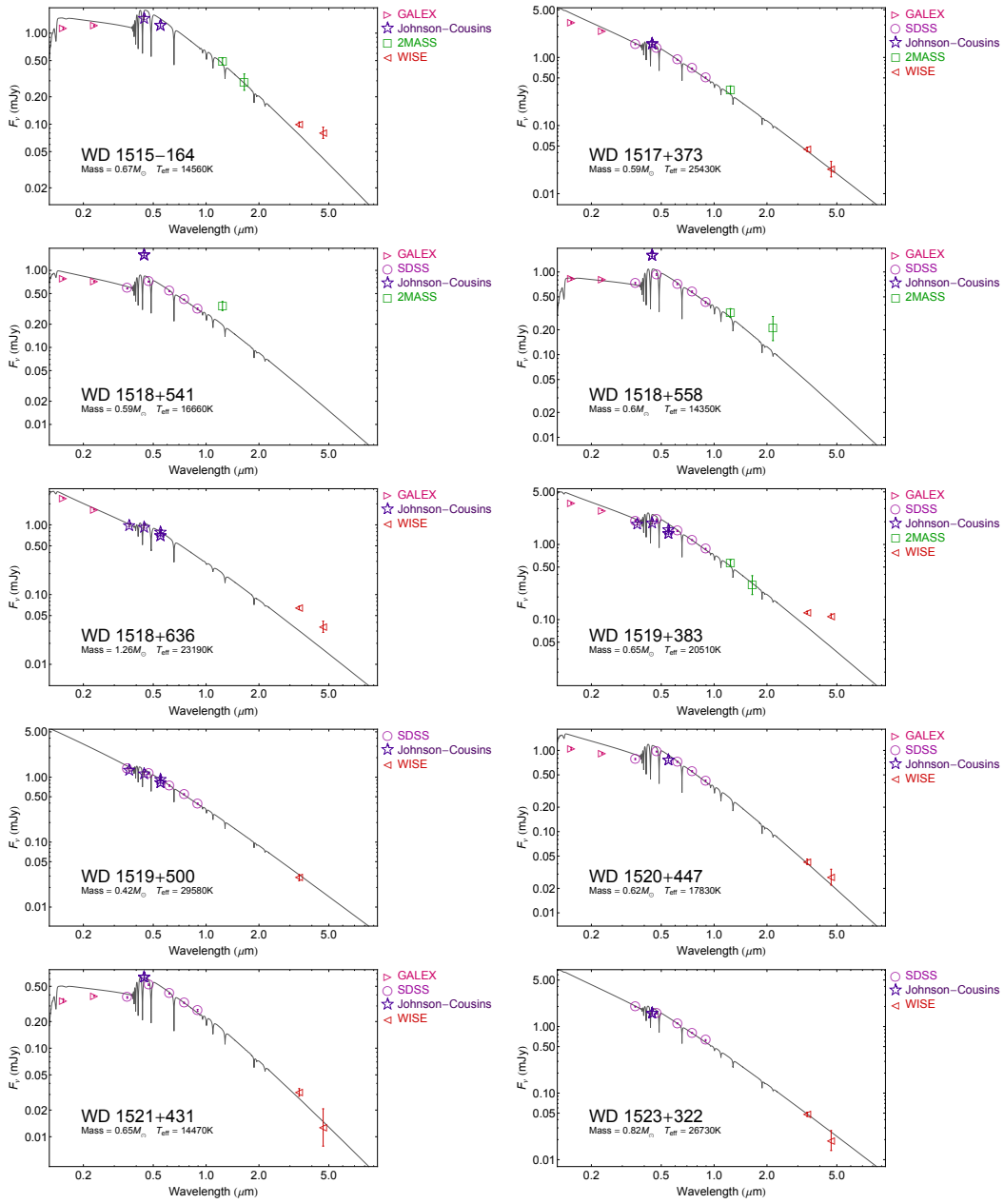

WD 1429−037
Mass = 0.66$M_\odot$ $T_{\rm eff}$ = 11610K
Johnson−Cousins
2MASS
WISE
WD 1429−216
Mass = 0.61$M_\odot$ $T_{\rm eff}$ = 26630K
GALEX
Johnson−Cousins
WD 1429+373
Mass = 0.74$M_\odot$ $T_{\rm eff}$ = 35000K
GALEX
SDSS
Johnson−Cousins
Stromgren
2MASS
WISE
WD 1431+153
Mass = 0.65$M_\odot$ $T_{\rm eff}$ = 14060K
GALEX
SDSS
Johnson−Cousins
2MASS
WISE
WD 1431+257
Mass = 0.39$M_\odot$ $T_{\rm eff}$ = 23690K
GALEX
SDSS
Johnson−Cousins
WISE
WD 1434−223
Mass = 0.47$M_\odot$ $T_{\rm eff}$ = 28460K
GALEX
Johnson−Cousins
WISE
WD 1434+289
Mass = 0.67$M_\odot$ $T_{\rm eff}$ = 33410K
GALEX
SDSS
Johnson−Cousins
Stromgren
2MASS
WISE
WD 1435+370
Mass = 0.61$M_\odot$ $T_{\rm eff}$ = 15580K
GALEX
SDSS
Johnson−Cousins
WISE
WD 1436−083
Mass = 0.67$M_\odot$ $T_{\rm eff}$ = 14860K
Johnson−Cousins
2MASS
WISE
WD 1436−216
Mass = 0.58$M_\odot$ $T_{\rm eff}$ = 23690K
GALEX
Johnson−Cousins
2MASS
WISE
F_ν (mJy)
Wavelength (μm)

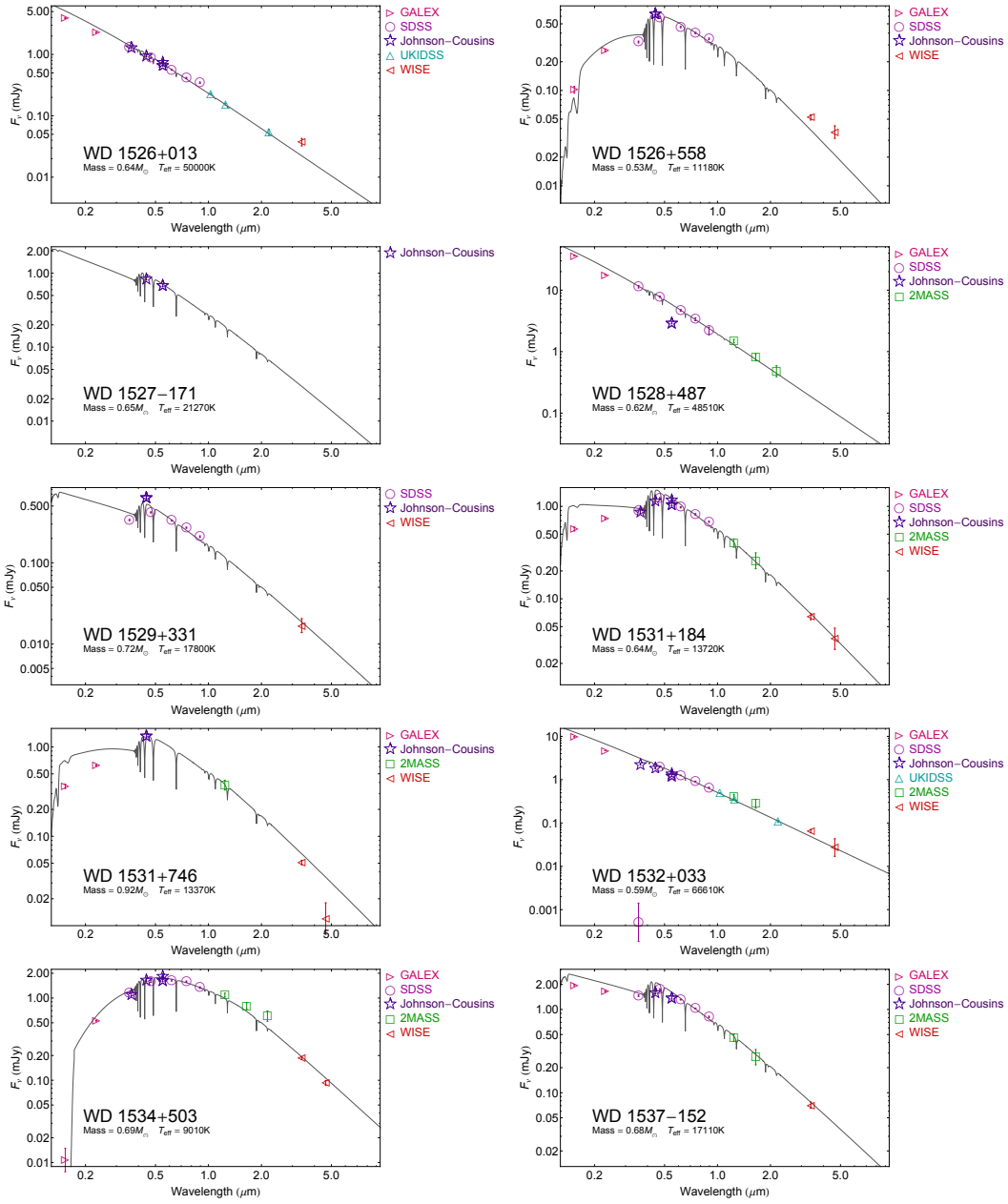

WD 1436−781
Mass = 0.26$M_\odot$ $T_{\rm eff}$ = 5960K
WD 1436+526
Mass = 0.64$M_\odot$ $T_{\rm eff}$ = 24410K
WD 1439+304
Mass = 0.61$M_\odot$ $T_{\rm eff}$ = 23010K
WD 1441+323
Mass = 0.64$M_\odot$ $T_{\rm eff}$ = 12890K
WD 1442+474
Mass = 0.68$M_\odot$ $T_{\rm eff}$ = 9990K
WD 1443+295
Mass = 0.61$M_\odot$ $T_{\rm eff}$ = 13110K
WD 1443+336
Mass = 0.53$M_\odot$ $T_{\rm eff}$ = 28120K
WD 1444+350
Mass = 0.72$M_\odot$ $T_{\rm eff}$ = 10560K
WD 1444+636
Mass = 0.59$M_\odot$ $T_{\rm eff}$ = 41770K
WD 1445+523
Mass = 0.64$M_\odot$ $T_{\rm eff}$ = 15840K
F_ν (mJy)
Wavelength (μm)
GALEX
SDSS
Johnson−Cousins
2MASS
WISE

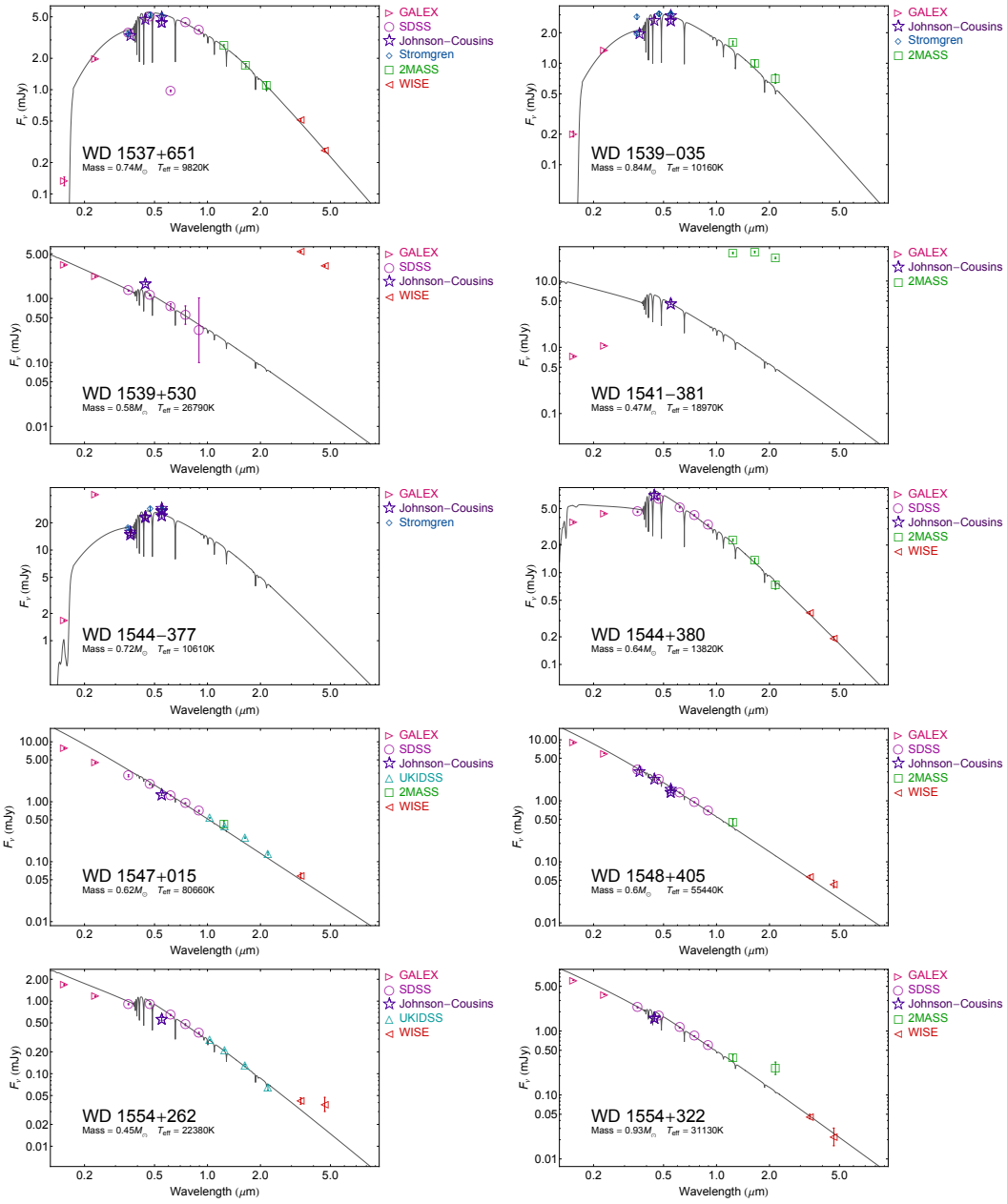

WD 1446+449
Mass = 0.41$M_\odot$ $T_{\rm eff}$ = 19300K
WD 1448+077
Mass = 0.55$M_\odot$ $T_{\rm eff}$ = 14870K
WD 1448+411
Mass = 0.59$M_\odot$ $T_{\rm eff}$ = 14710K
WD 1449+513
Mass = 0.97$M_\odot$ $T_{\rm eff}$ = 17160K
WD 1450+425
Mass = 0.73$M_\odot$ $T_{\rm eff}$ = 9610K
WD 1452−310
Mass = 0.68$M_\odot$ $T_{\rm eff}$ = 9310K
WD 1452+553
Mass = 0.84$M_\odot$ $T_{\rm eff}$ = 28340K
WD 1454−630.2
Mass = 0.88$M_\odot$ $T_{\rm eff}$ = 10460K
WD 1454+172
Mass = 0.76$M_\odot$ $T_{\rm eff}$ = 31380K
WD 1458+171
Mass = 0.42$M_\odot$ $T_{\rm eff}$ = 22600K
F_ν (mJy)
Wavelength (μm)
GALEX
SDSS
Johnson−Cousins
UKIDSS
2MASS
WISE

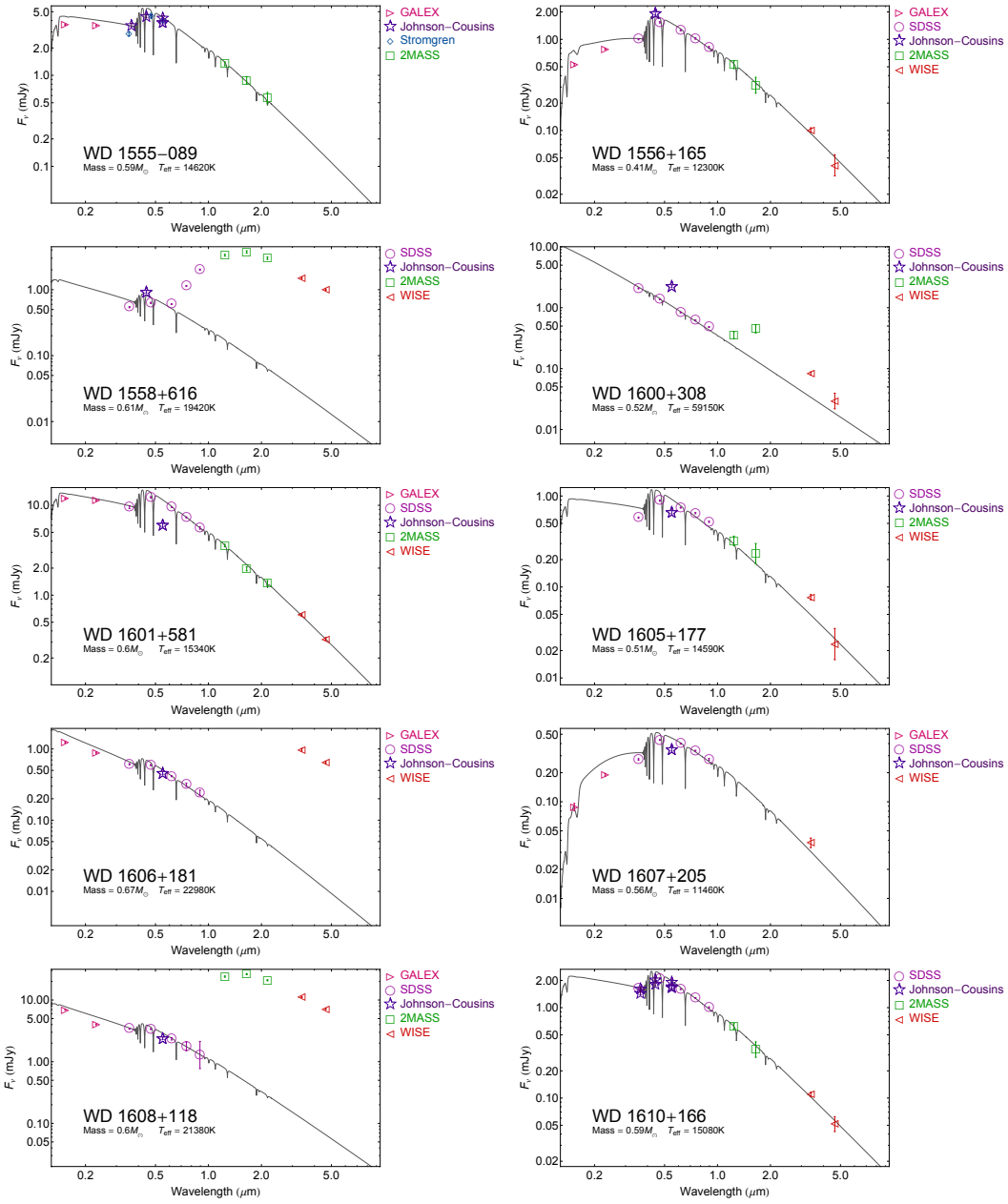

WD 1459+219
Mass = 0.65$M_\odot$ $T_{\rm eff}$ = 18940K
WD 1459+305
Mass = 0.61$M_\odot$ $T_{\rm eff}$ = 26230K
WD 1459+333
Mass = 0.55$M_\odot$ $T_{\rm eff}$ = 14300K
WD 1500−170
Mass = 0.65$M_\odot$ $T_{\rm eff}$ = 32580K
WD 1501+032
Mass = 0.61$M_\odot$ $T_{\rm eff}$ = 14370K
WD 1502+349
Mass = 0.61$M_\odot$ $T_{\rm eff}$ = 22300K
WD 1502+351
Mass = 0.76$M_\odot$ $T_{\rm eff}$ = 18960K
WD 1503−093
Mass = 0.64$M_\odot$ $T_{\rm eff}$ = 14780K
WD 1503+410
Mass = 0.51$M_\odot$ $T_{\rm eff}$ = 16000K
WD 1504−770
Mass = 0.58$M_\odot$ $T_{\rm eff}$ = 17540K
F_ν (mJy)
Wavelength (μm)
GALEX
SDSS
Johnson−Cousins
Stromgren
2MASS
UKIDSS
WISE

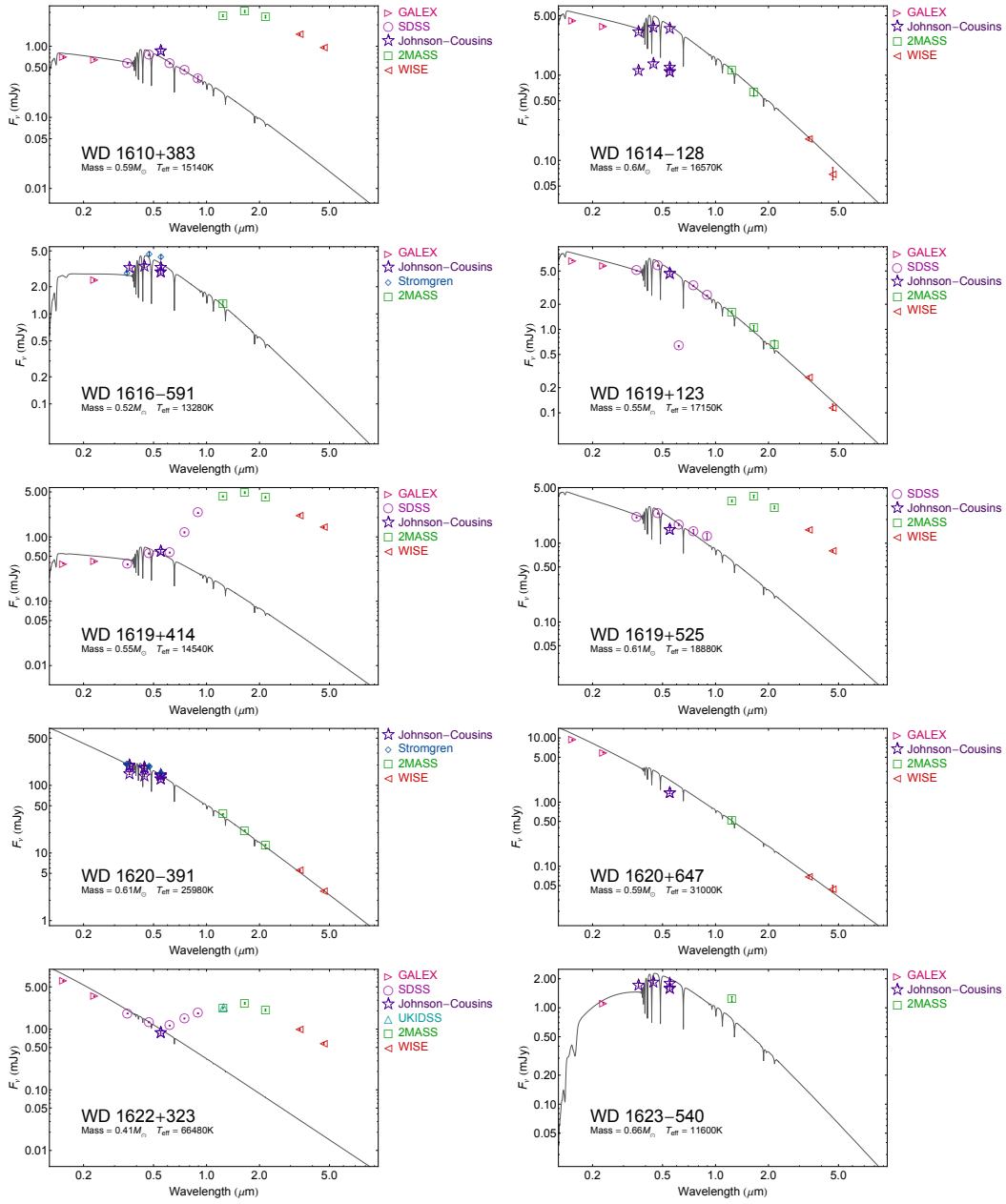

WD 1504+461
Mass = 0.6$M_\odot$ $T_{\rm eff}$ = 20200K
WD 1504+546
Mass = 0.56$M_\odot$ $T_{\rm eff}$ = 23120K
WD 1505+297
Mass = 0.59$M_\odot$ $T_{\rm eff}$ = 13830K
WD 1507−105
Mass = 0.51$M_\odot$ $T_{\rm eff}$ = 10240K
WD 1507+465
Mass = 0.49$M_\odot$ $T_{\rm eff}$ = 29600K
WD 1508+548
Mass = 0.61$M_\odot$ $T_{\rm eff}$ = 17630K
WD 1508+637
Mass = 0.72$M_\odot$ $T_{\rm eff}$ = 10580K
WD 1509+536
Mass = 0.69$M_\odot$ $T_{\rm eff}$ = 14580K
WD 1510+566
Mass = 0.72$M_\odot$ $T_{\rm eff}$ = 9300K
WD 1514+411
Mass = 0.58$M_\odot$ $T_{\rm eff}$ = 13470K
F_ν (mJy)
Wavelength (μm)
GALEX
SDSS
Johnson−Cousins
Stromgren
2MASS
WISE

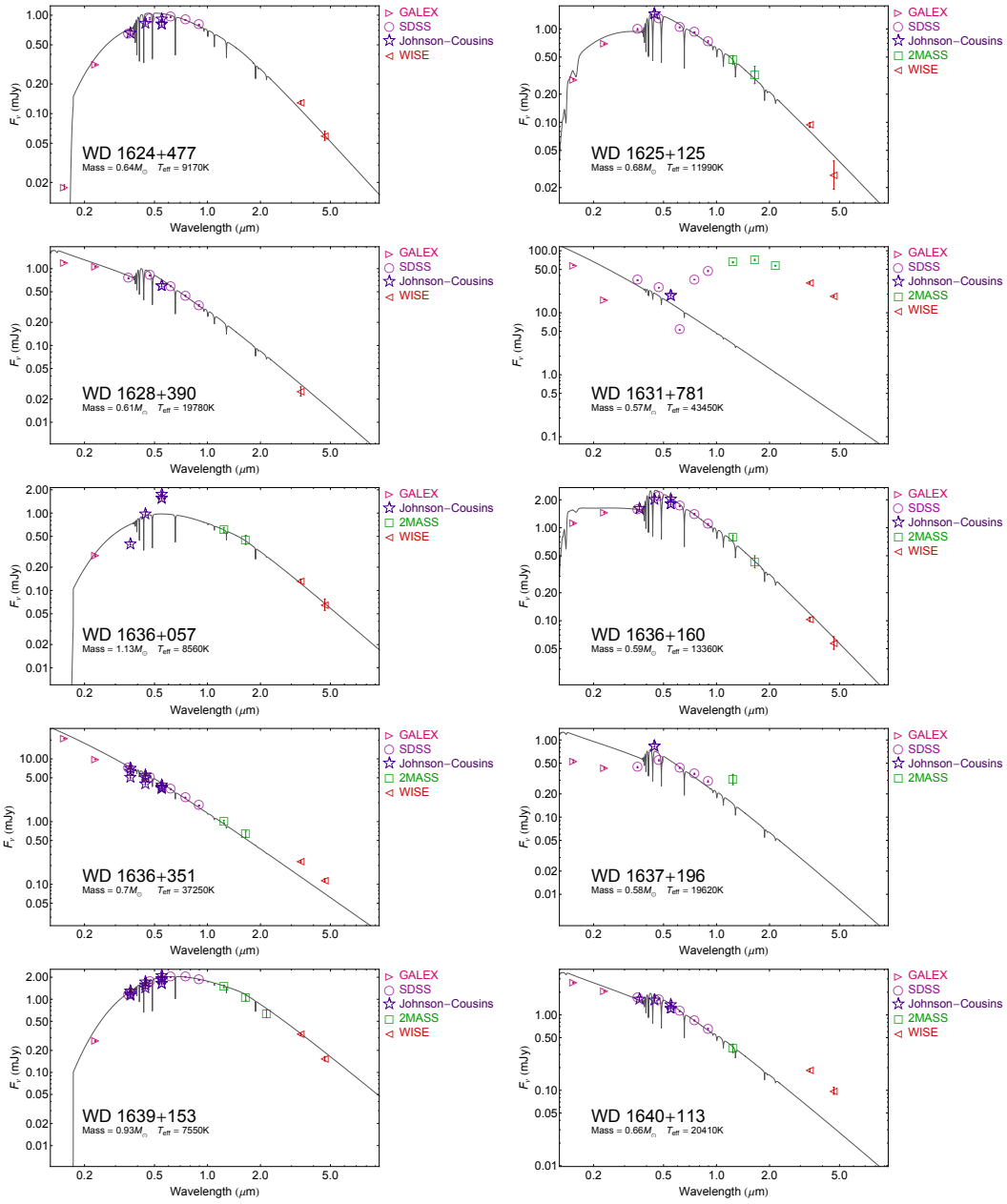

WD 1515−164
Mass = 0.67$M_\odot$ $T_{\rm eff}$ = 14560K
GALEX
Johnson−Cousins
2MASS
WISE
WD 1517+373
Mass = 0.59$M_\odot$ $T_{\rm eff}$ = 25430K
GALEX
SDSS
Johnson−Cousins
2MASS
WISE
WD 1518+541
Mass = 0.59$M_\odot$ $T_{\rm eff}$ = 16660K
GALEX
SDSS
Johnson−Cousins
2MASS
WD 1518+558
Mass = 0.6$M_\odot$ $T_{\rm eff}$ = 14350K
GALEX
SDSS
Johnson−Cousins
2MASS
WD 1518+636
Mass = 1.26$M_\odot$ $T_{\rm eff}$ = 23190K
GALEX
Johnson−Cousins
WISE
WD 1519+383
Mass = 0.65$M_\odot$ $T_{\rm eff}$ = 20510K
GALEX
SDSS
Johnson−Cousins
2MASS
WISE
WD 1519+500
Mass = 0.42$M_\odot$ $T_{\rm eff}$ = 29580K
SDSS
Johnson−Cousins
WISE
WD 1520+447
Mass = 0.62$M_\odot$ $T_{\rm eff}$ = 17830K
GALEX
SDSS
Johnson−Cousins
WISE
WD 1521+431
Mass = 0.65$M_\odot$ $T_{\rm eff}$ = 14470K
GALEX
SDSS
Johnson−Cousins
WISE
WD 1523+322
Mass = 0.82$M_\odot$ $T_{\rm eff}$ = 26730K
SDSS
Johnson−Cousins
WISE
F_ν (mJy)
Wavelength (μm)

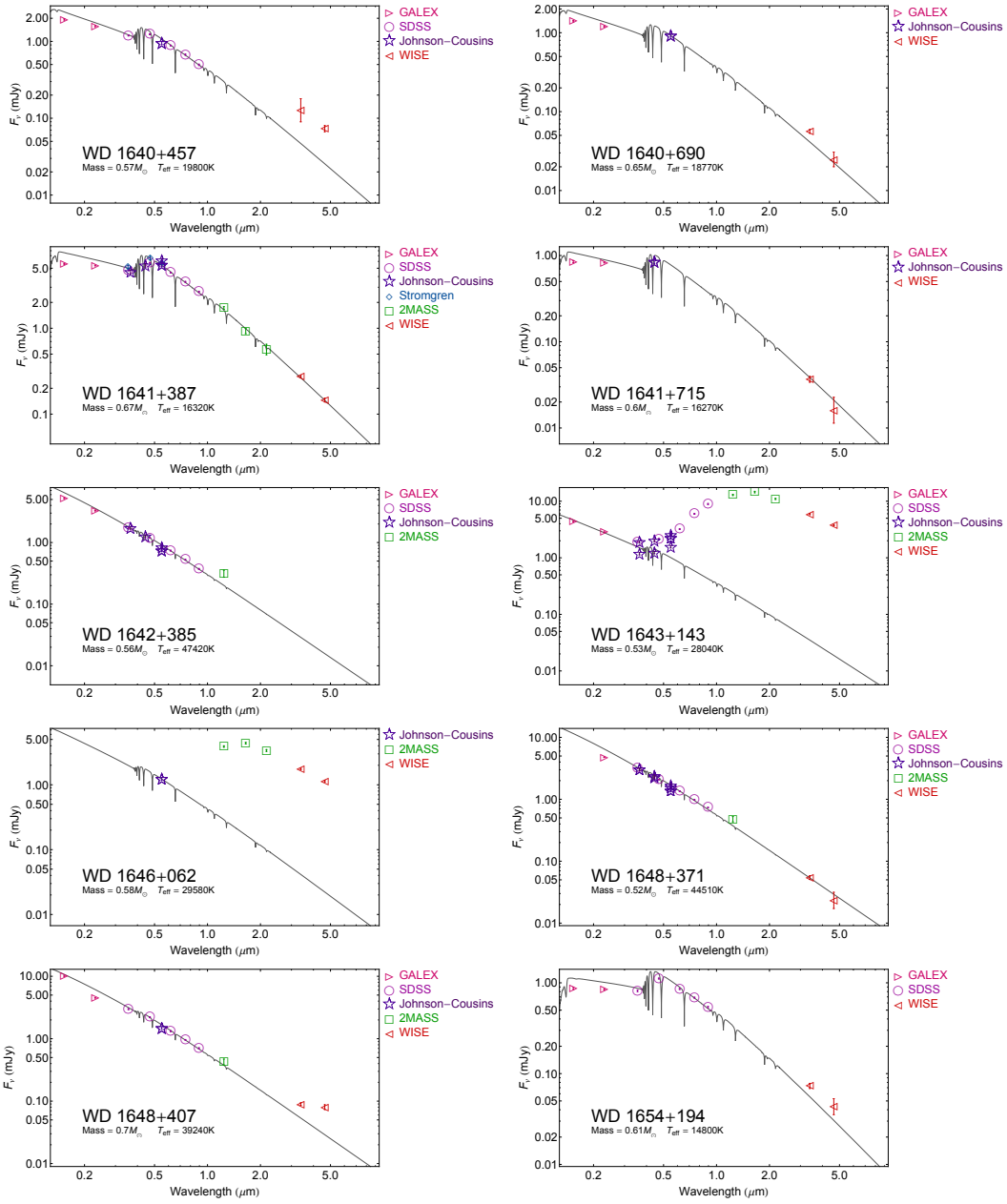

WD 1526+013
Mass = 0.64$M_\odot$ $T_{\rm eff}$ = 50000K
GALEX
SDSS
Johnson−Cousins
UKIDSS
WISE
WD 1526+558
Mass = 0.53$M_\odot$ $T_{\rm eff}$ = 11180K
GALEX
SDSS
Johnson−Cousins
WISE
WD 1527−171
Mass = 0.65$M_\odot$ $T_{\rm eff}$ = 21270K
Johnson−Cousins
WD 1528+487
Mass = 0.62$M_\odot$ $T_{\rm eff}$ = 48510K
GALEX
SDSS
Johnson−Cousins
2MASS
WD 1529+331
Mass = 0.72$M_\odot$ $T_{\rm eff}$ = 17800K
SDSS
Johnson−Cousins
WISE
WD 1531+184
Mass = 0.64$M_\odot$ $T_{\rm eff}$ = 13720K
GALEX
SDSS
Johnson−Cousins
2MASS
WISE
WD 1531+746
Mass = 0.92$M_\odot$ $T_{\rm eff}$ = 13370K
GALEX
Johnson−Cousins
2MASS
WISE
WD 1532+033
Mass = 0.59$M_\odot$ $T_{\rm eff}$ = 66610K
GALEX
SDSS
Johnson−Cousins
UKIDSS
2MASS
WISE
WD 1534+503
Mass = 0.69$M_\odot$ $T_{\rm eff}$ = 9010K
GALEX
SDSS
Johnson−Cousins
2MASS
WISE
WD 1537−152
Mass = 0.68$M_\odot$ $T_{\rm eff}$ = 17110K
GALEX
SDSS
Johnson−Cousins
2MASS
WISE
F_ν (mJy)
Wavelength (μm)

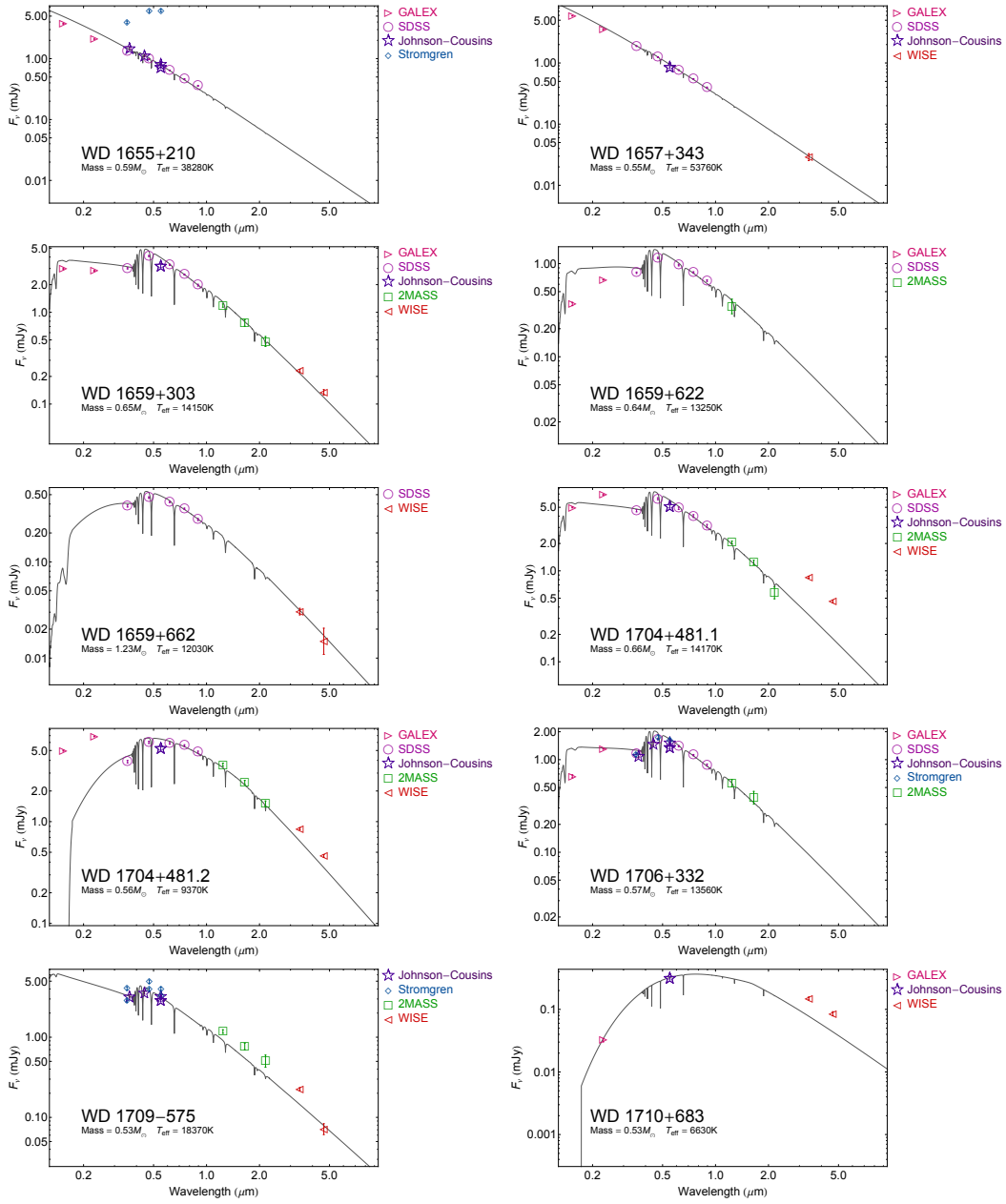

WD 1537+651
Mass = 0.74$M_\odot$ $T_{\rm eff}$ = 9820K
WD 1539−035
Mass = 0.84$M_\odot$ $T_{\rm eff}$ = 10160K
WD 1539+530
Mass = 0.58$M_\odot$ $T_{\rm eff}$ = 26790K
WD 1541−381
Mass = 0.47$M_\odot$ $T_{\rm eff}$ = 18970K
WD 1544−377
Mass = 0.72$M_\odot$ $T_{\rm eff}$ = 10610K
WD 1544+380
Mass = 0.64$M_\odot$ $T_{\rm eff}$ = 13820K
WD 1547+015
Mass = 0.62$M_\odot$ $T_{\rm eff}$ = 80660K
WD 1548+405
Mass = 0.6$M_\odot$ $T_{\rm eff}$ = 55440K
WD 1554+262
Mass = 0.45$M_\odot$ $T_{\rm eff}$ = 22380K
WD 1554+322
Mass = 0.93$M_\odot$ $T_{\rm eff}$ = 31130K
F_ν (mJy)
Wavelength (μm)
GALEX
SDSS
Johnson−Cousins
Stromgren
UKIDSS
2MASS
WISE

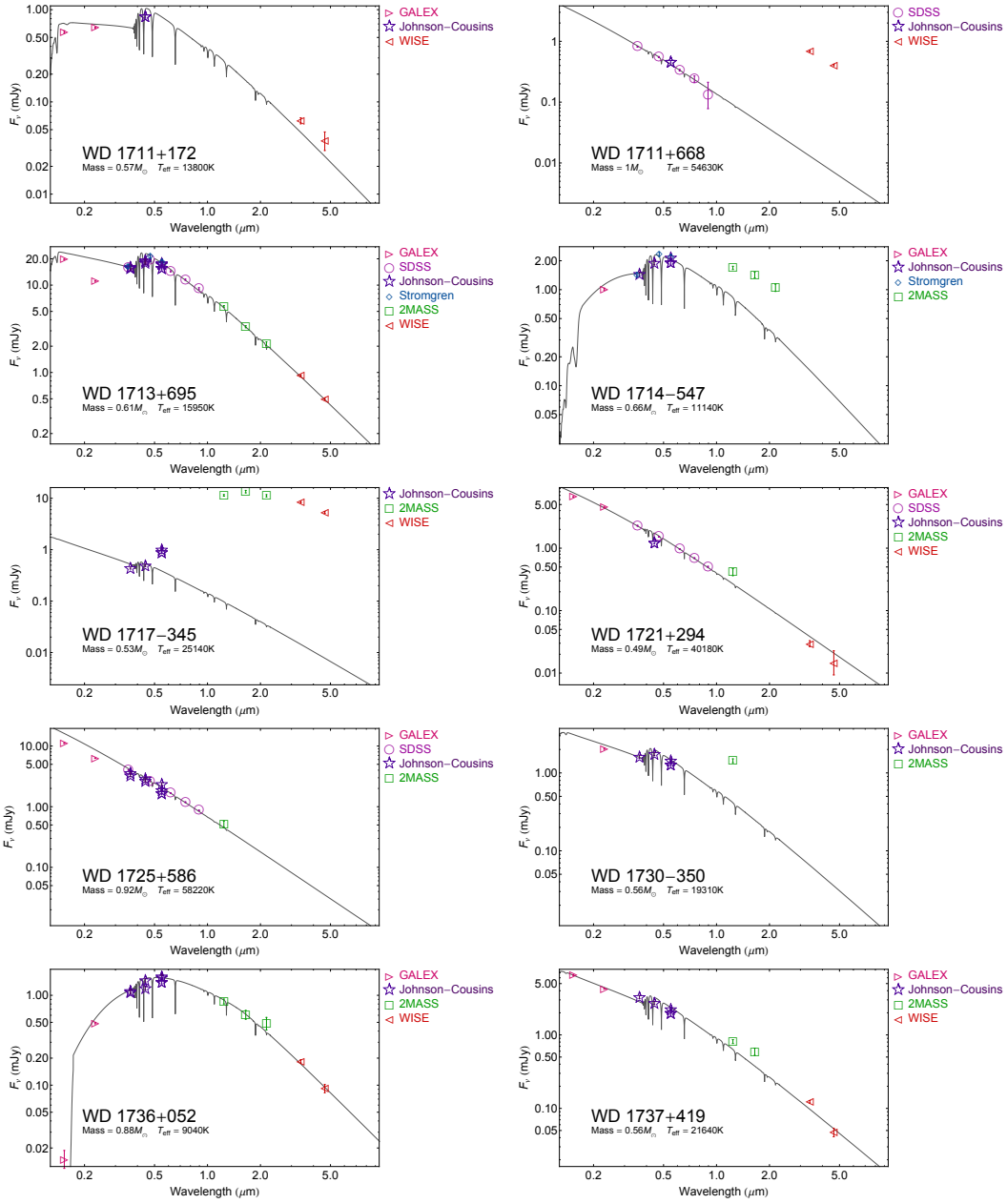

WD 1555−089
Mass = 0.59$M_\odot$ $T_{\rm eff}$ = 14620K
GALEX
Johnson−Cousins
Stromgren
2MASS
WD 1556+165
Mass = 0.41$M_\odot$ $T_{\rm eff}$ = 12300K
GALEX
SDSS
Johnson−Cousins
2MASS
WISE
WD 1558+616
Mass = 0.61$M_\odot$ $T_{\rm eff}$ = 19420K
SDSS
Johnson−Cousins
2MASS
WISE
WD 1600+308
Mass = 0.52$M_\odot$ $T_{\rm eff}$ = 59150K
SDSS
Johnson−Cousins
2MASS
WISE
WD 1601+581
Mass = 0.6$M_\odot$ $T_{\rm eff}$ = 15340K
GALEX
SDSS
Johnson−Cousins
2MASS
WISE
WD 1605+177
Mass = 0.51$M_\odot$ $T_{\rm eff}$ = 14590K
SDSS
Johnson−Cousins
2MASS
WISE
WD 1606+181
Mass = 0.67$M_\odot$ $T_{\rm eff}$ = 22980K
GALEX
SDSS
Johnson−Cousins
WISE
WD 1607+205
Mass = 0.56$M_\odot$ $T_{\rm eff}$ = 11460K
GALEX
SDSS
Johnson−Cousins
WISE
WD 1608+118
Mass = 0.6$M_\odot$ $T_{\rm eff}$ = 21380K
GALEX
SDSS
Johnson−Cousins
2MASS
WISE
WD 1610+166
Mass = 0.59$M_\odot$ $T_{\rm eff}$ = 15080K
SDSS
Johnson−Cousins
2MASS
WISE
F_ν (mJy)
Wavelength (μm)

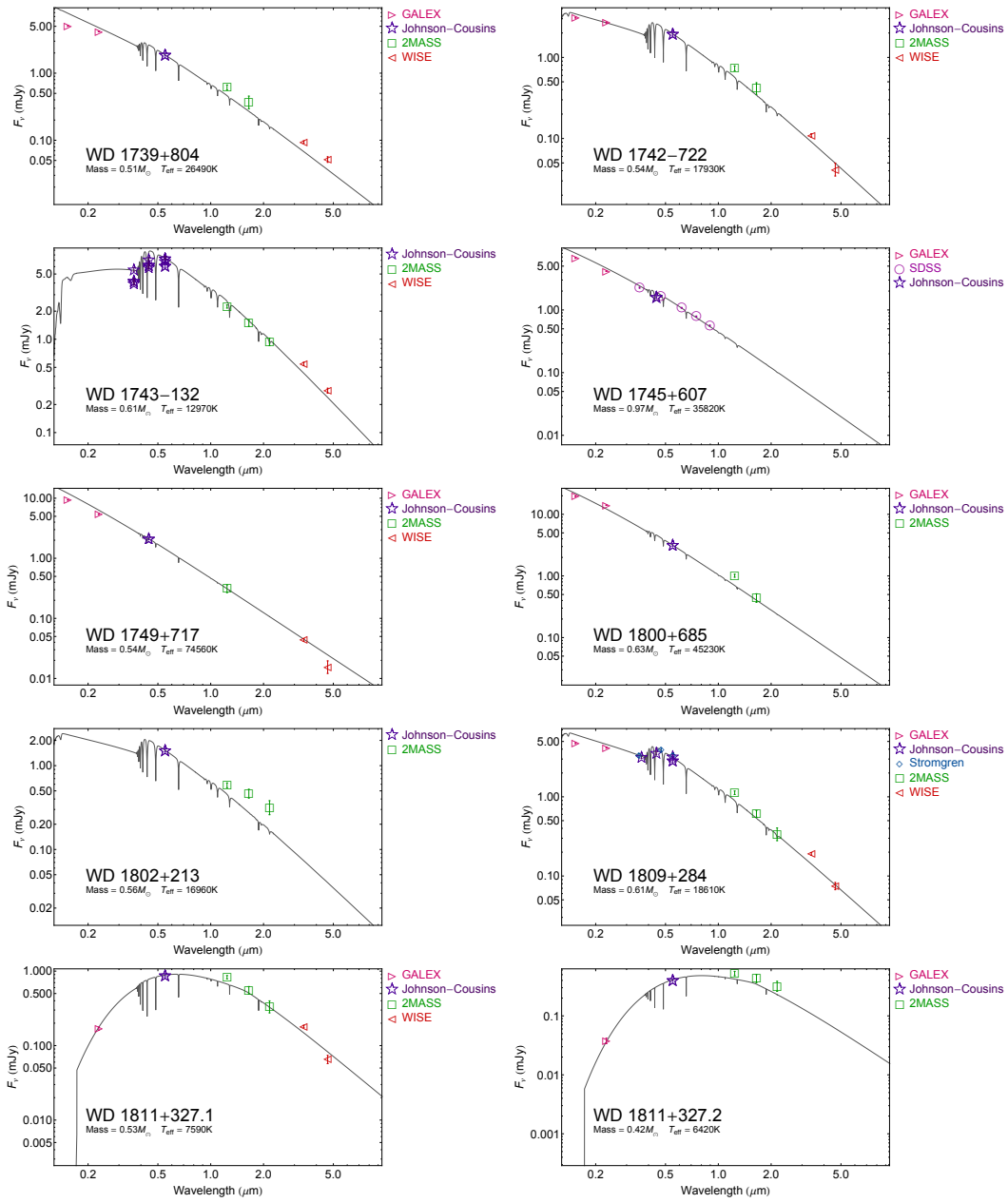

WD 1610+383
Mass = 0.59$M_\odot$ $T_{\rm eff}$ = 15140K
GALEX
SDSS
Johnson−Cousins
2MASS
WISE
WD 1614−128
Mass = 0.6$M_\odot$ $T_{\rm eff}$ = 16570K
GALEX
Johnson−Cousins
2MASS
WISE
WD 1616−591
Mass = 0.52$M_\odot$ $T_{\rm eff}$ = 13280K
GALEX
Johnson−Cousins
Stromgren
2MASS
WD 1619+123
Mass = 0.55$M_\odot$ $T_{\rm eff}$ = 17150K
GALEX
SDSS
Johnson−Cousins
2MASS
WISE
WD 1619+414
Mass = 0.55$M_\odot$ $T_{\rm eff}$ = 14540K
GALEX
SDSS
Johnson−Cousins
2MASS
WISE
WD 1619+525
Mass = 0.61$M_\odot$ $T_{\rm eff}$ = 18880K
SDSS
Johnson−Cousins
2MASS
WISE
WD 1620−391
Mass = 0.61$M_\odot$ $T_{\rm eff}$ = 25980K
Johnson−Cousins
Stromgren
2MASS
WISE
WD 1620+647
Mass = 0.59$M_\odot$ $T_{\rm eff}$ = 31000K
GALEX
Johnson−Cousins
2MASS
WISE
WD 1622+323
Mass = 0.41$M_\odot$ $T_{\rm eff}$ = 66480K
GALEX
SDSS
Johnson−Cousins
UKIDSS
2MASS
WISE
WD 1623−540
Mass = 0.66$M_\odot$ $T_{\rm eff}$ = 11600K
GALEX
Johnson−Cousins
2MASS
F_ν (mJy)
Wavelength (μm)

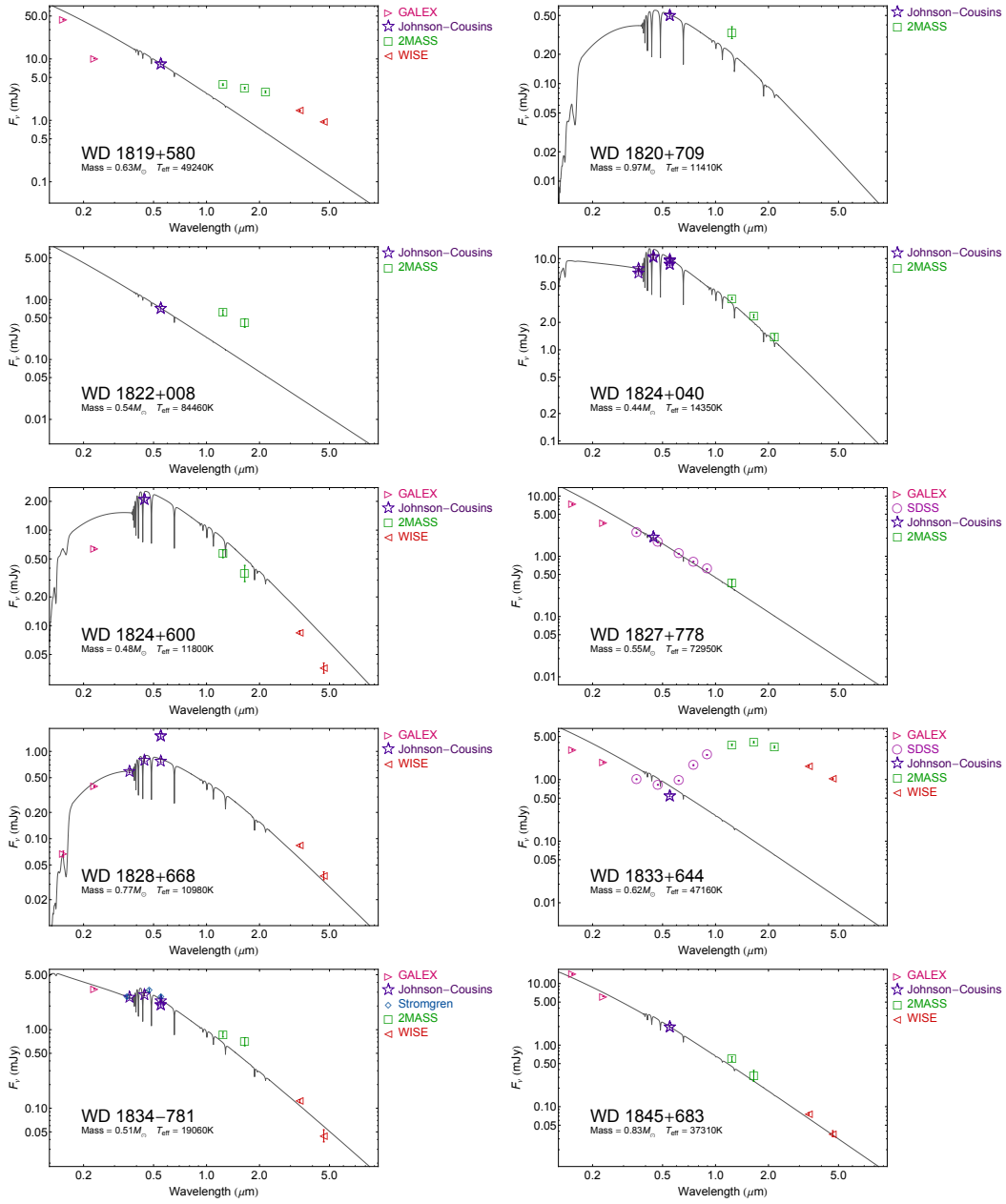

WD 1624+477
Mass = 0.64$M_\odot$ $T_{\rm eff}$ = 9170K
WD 1625+125
Mass = 0.68$M_\odot$ $T_{\rm eff}$ = 11990K
WD 1628+390
Mass = 0.61$M_\odot$ $T_{\rm eff}$ = 19780K
WD 1631+781
Mass = 0.57$M_\odot$ $T_{\rm eff}$ = 43450K
WD 1636+057
Mass = 1.13$M_\odot$ $T_{\rm eff}$ = 8560K
WD 1636+160
Mass = 0.59$M_\odot$ $T_{\rm eff}$ = 13360K
WD 1636+351
Mass = 0.7$M_\odot$ $T_{\rm eff}$ = 37250K
WD 1637+196
Mass = 0.58$M_\odot$ $T_{\rm eff}$ = 19620K
WD 1639+153
Mass = 0.93$M_\odot$ $T_{\rm eff}$ = 7550K
WD 1640+113
Mass = 0.66$M_\odot$ $T_{\rm eff}$ = 20410K
F_ν (mJy)
Wavelength (μm)
GALEX
SDSS
Johnson–Cousins
2MASS
WISE

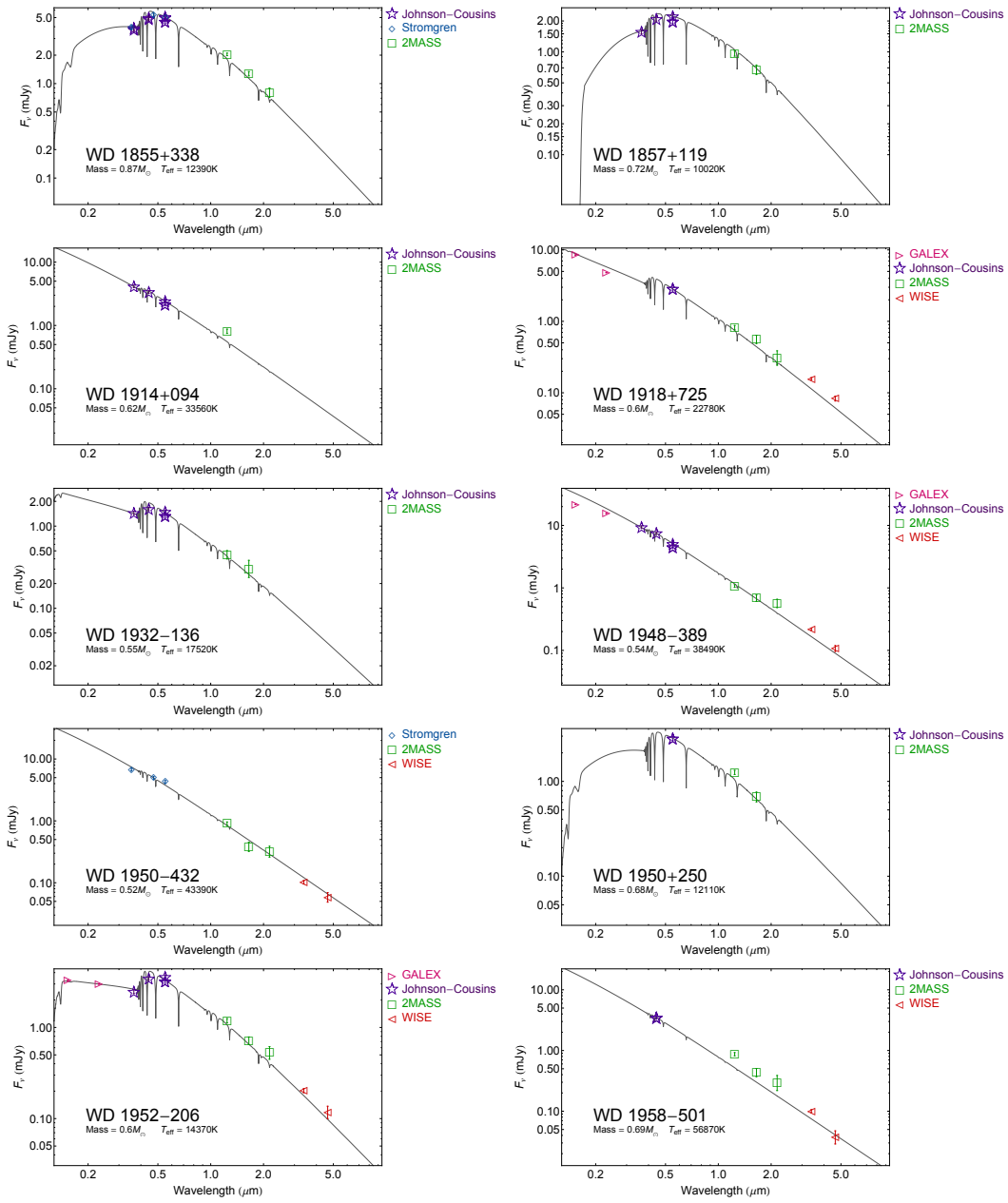

WD 1640+457
Mass = 0.57$M_\odot$ $T_{\rm eff}$ = 19800K
WD 1640+690
Mass = 0.65$M_\odot$ $T_{\rm eff}$ = 18770K
WD 1641+387
Mass = 0.67$M_\odot$ $T_{\rm eff}$ = 16320K
WD 1641+715
Mass = 0.6$M_\odot$ $T_{\rm eff}$ = 16270K
WD 1642+385
Mass = 0.56$M_\odot$ $T_{\rm eff}$ = 47420K
WD 1643+143
Mass = 0.53$M_\odot$ $T_{\rm eff}$ = 28040K
WD 1646+062
Mass = 0.58$M_\odot$ $T_{\rm eff}$ = 29580K
WD 1648+371
Mass = 0.52$M_\odot$ $T_{\rm eff}$ = 44510K
WD 1648+407
Mass = 0.7$M_\odot$ $T_{\rm eff}$ = 39240K
WD 1654+194
Mass = 0.61$M_\odot$ $T_{\rm eff}$ = 14800K
F_ν (mJy)
Wavelength (μm)
GALEX
SDSS
Johnson−Cousins
Stromgren
2MASS
WISE

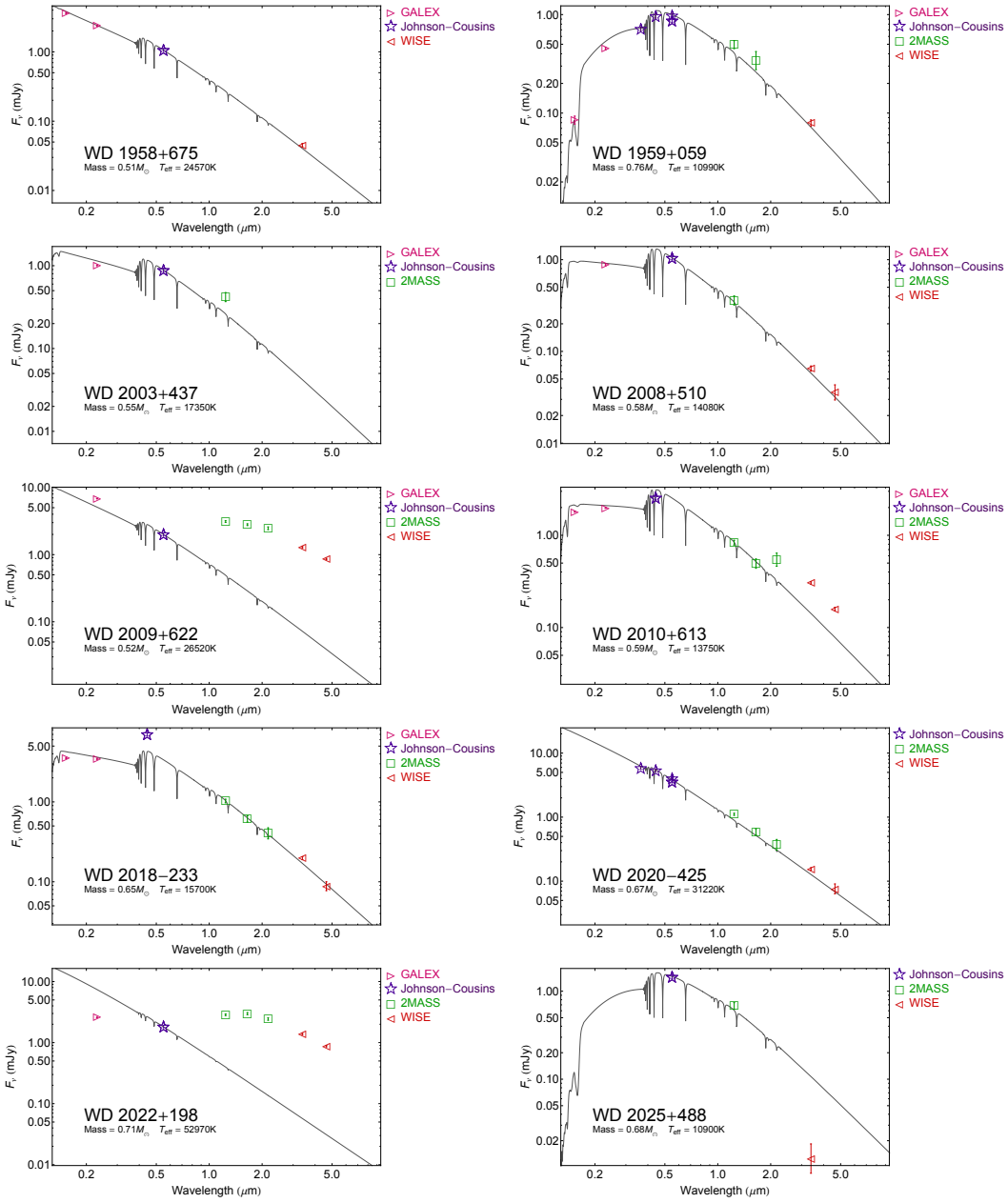

WD 1655+210
Mass = 0.59$M_\odot$ $T_{\rm eff}$ = 38280K
GALEX
SDSS
Johnson−Cousins
Stromgren
WD 1657+343
Mass = 0.55$M_\odot$ $T_{\rm eff}$ = 53760K
GALEX
SDSS
Johnson−Cousins
WISE
WD 1659+303
Mass = 0.65$M_\odot$ $T_{\rm eff}$ = 14150K
GALEX
SDSS
Johnson−Cousins
2MASS
WISE
WD 1659+622
Mass = 0.64$M_\odot$ $T_{\rm eff}$ = 13250K
GALEX
SDSS
2MASS
WD 1659+662
Mass = 1.23$M_\odot$ $T_{\rm eff}$ = 12030K
SDSS
WISE
WD 1704+481.1
Mass = 0.66$M_\odot$ $T_{\rm eff}$ = 14170K
GALEX
SDSS
Johnson−Cousins
2MASS
WISE
WD 1704+481.2
Mass = 0.56$M_\odot$ $T_{\rm eff}$ = 9370K
GALEX
SDSS
Johnson−Cousins
2MASS
WISE
WD 1706+332
Mass = 0.57$M_\odot$ $T_{\rm eff}$ = 13560K
GALEX
SDSS
Johnson−Cousins
Stromgren
2MASS
WD 1709−575
Mass = 0.53$M_\odot$ $T_{\rm eff}$ = 18370K
Johnson−Cousins
Stromgren
2MASS
WISE
WD 1710+683
Mass = 0.53$M_\odot$ $T_{\rm eff}$ = 6630K
GALEX
Johnson−Cousins
WISE
F_ν (mJy)
Wavelength (μm)

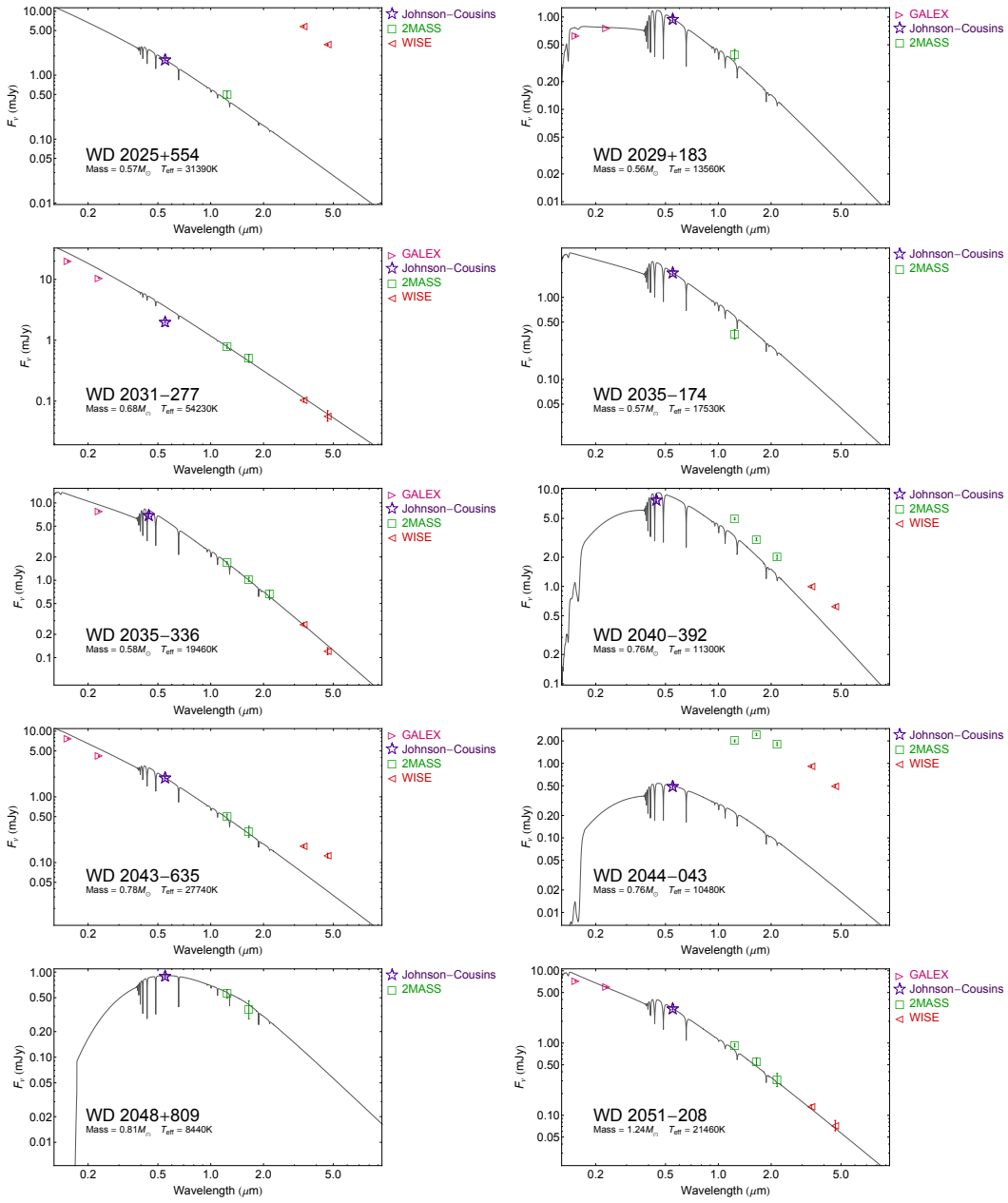

WD 1711+172
Mass = 0.57$M_\odot$ $T_{\rm eff}$ = 13800K
GALEX
Johnson–Cousins
WISE
WD 1711+668
Mass = 1$M_\odot$ $T_{\rm eff}$ = 54630K
SDSS
Johnson–Cousins
WISE
WD 1713+695
Mass = 0.61$M_\odot$ $T_{\rm eff}$ = 15950K
GALEX
SDSS
Johnson–Cousins
Stromgren
2MASS
WISE
WD 1714−547
Mass = 0.66$M_\odot$ $T_{\rm eff}$ = 11140K
GALEX
Johnson–Cousins
Stromgren
2MASS
WD 1717−345
Mass = 0.53$M_\odot$ $T_{\rm eff}$ = 25140K
Johnson–Cousins
2MASS
WISE
WD 1721+294
Mass = 0.49$M_\odot$ $T_{\rm eff}$ = 40180K
GALEX
SDSS
Johnson–Cousins
2MASS
WISE
WD 1725+586
Mass = 0.92$M_\odot$ $T_{\rm eff}$ = 58220K
GALEX
SDSS
Johnson–Cousins
2MASS
WD 1730−350
Mass = 0.56$M_\odot$ $T_{\rm eff}$ = 19310K
GALEX
Johnson–Cousins
2MASS
WD 1736+052
Mass = 0.88$M_\odot$ $T_{\rm eff}$ = 9040K
GALEX
Johnson–Cousins
2MASS
WISE
WD 1737+419
Mass = 0.56$M_\odot$ $T_{\rm eff}$ = 21640K
GALEX
Johnson–Cousins
2MASS
WISE
F_ν (mJy)
Wavelength (μm)

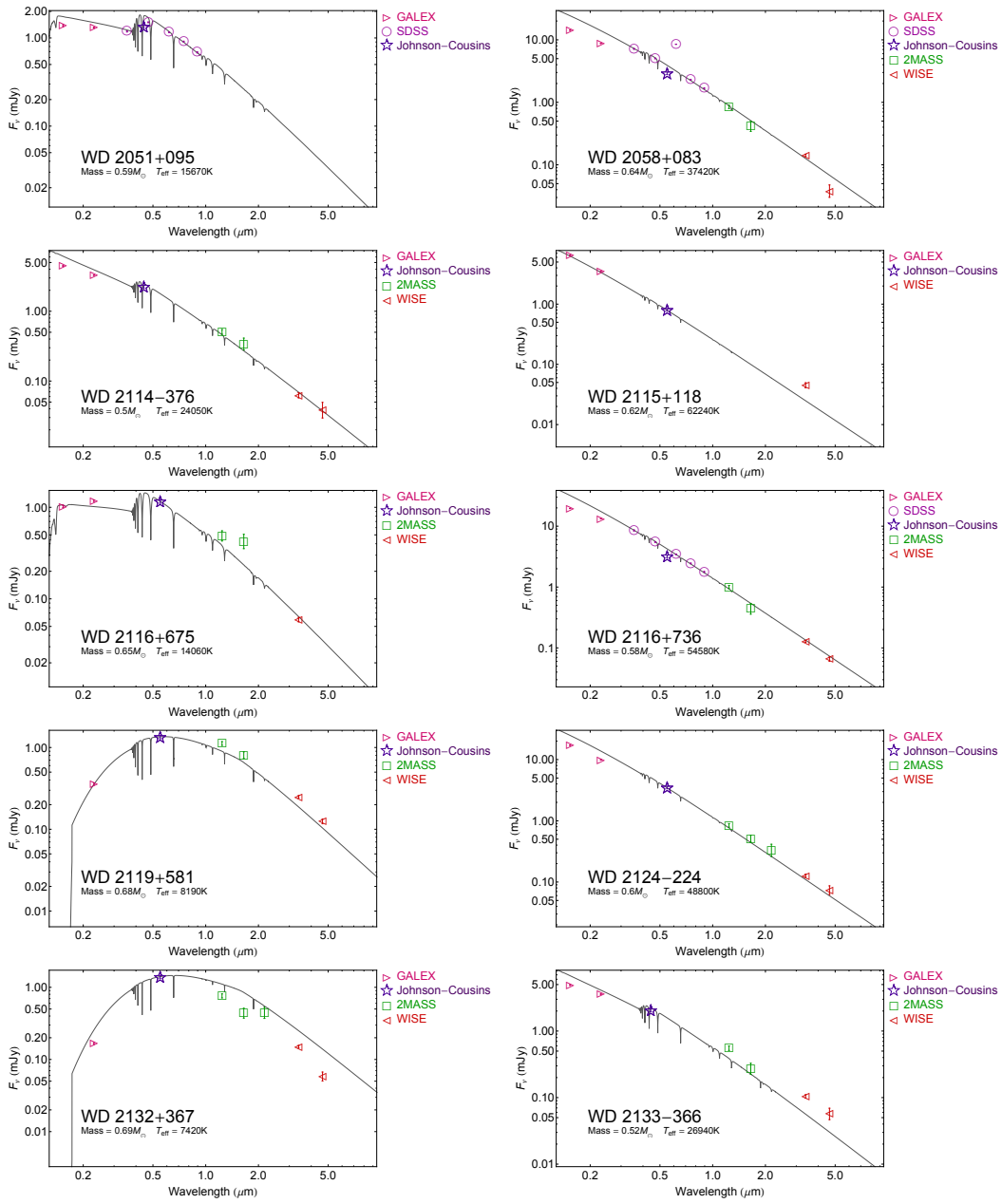

WD 1739+804
Mass = 0.51$M_\odot$ $T_{\rm eff}$ = 26490K
WD 1742−722
Mass = 0.54$M_\odot$ $T_{\rm eff}$ = 17930K
WD 1743−132
Mass = 0.61$M_\odot$ $T_{\rm eff}$ = 12970K
WD 1745+607
Mass = 0.97$M_\odot$ $T_{\rm eff}$ = 35820K
WD 1749+717
Mass = 0.54$M_\odot$ $T_{\rm eff}$ = 74560K
WD 1800+685
Mass = 0.63$M_\odot$ $T_{\rm eff}$ = 45230K
WD 1802+213
Mass = 0.56$M_\odot$ $T_{\rm eff}$ = 16960K
WD 1809+284
Mass = 0.61$M_\odot$ $T_{\rm eff}$ = 18610K
WD 1811+327.1
Mass = 0.53$M_\odot$ $T_{\rm eff}$ = 7590K
WD 1811+327.2
Mass = 0.42$M_\odot$ $T_{\rm eff}$ = 6420K
F_ν (mJy)
Wavelength (μm)
GALEX
Johnson−Cousins
SDSS
Stromgren
2MASS
WISE

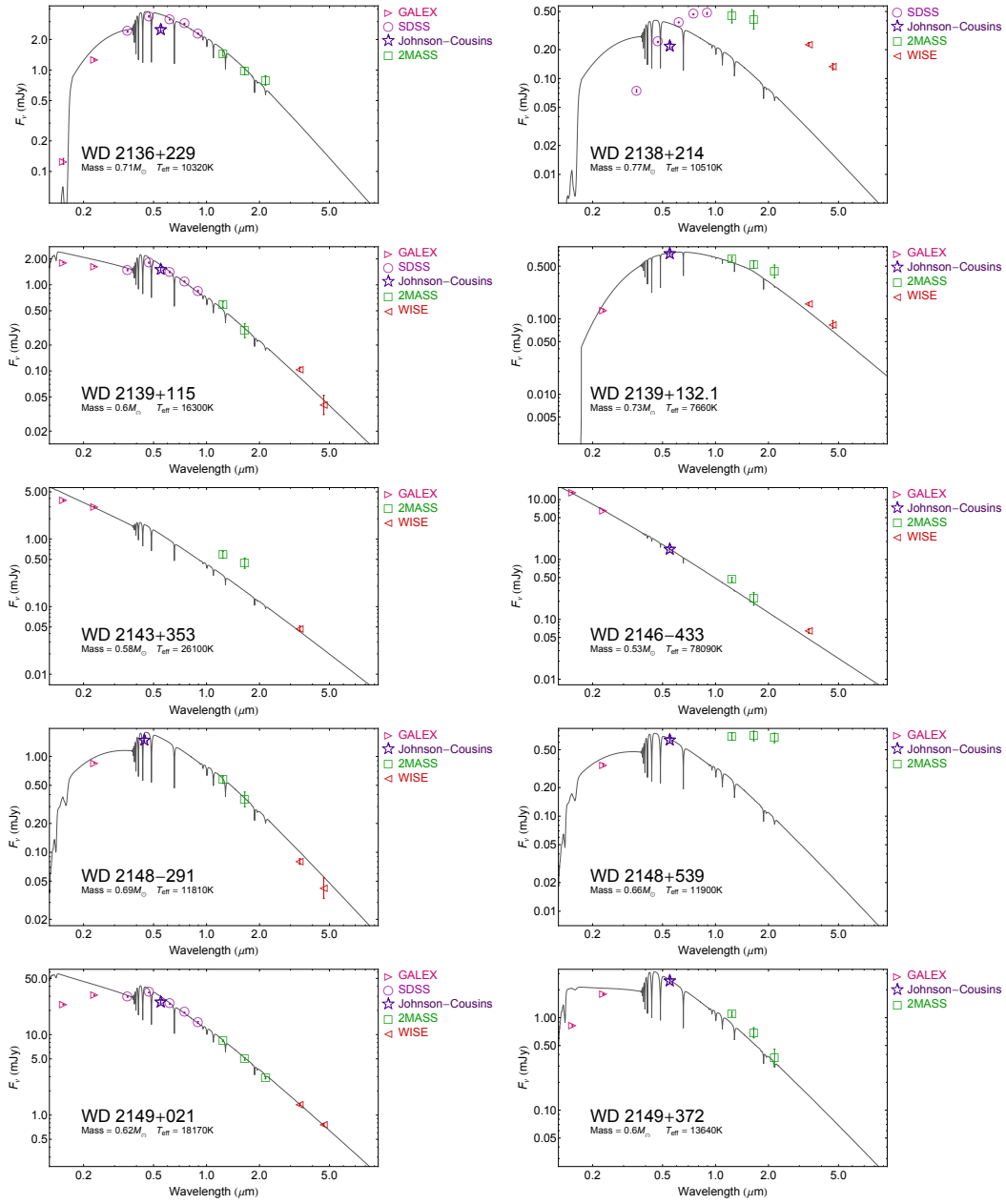

WD 1819+580
Mass = 0.63$M_\odot$ $T_{\rm eff}$ = 49240K
GALEX
Johnson−Cousins
2MASS
WISE
WD 1820+709
Mass = 0.97$M_\odot$ $T_{\rm eff}$ = 11410K
Johnson−Cousins
2MASS
WD 1822+008
Mass = 0.54$M_\odot$ $T_{\rm eff}$ = 84460K
Johnson−Cousins
2MASS
WD 1824+040
Mass = 0.44$M_\odot$ $T_{\rm eff}$ = 14350K
Johnson−Cousins
2MASS
WD 1824+600
Mass = 0.48$M_\odot$ $T_{\rm eff}$ = 11800K
GALEX
Johnson−Cousins
2MASS
WISE
WD 1827+778
Mass = 0.55$M_\odot$ $T_{\rm eff}$ = 72950K
GALEX
SDSS
Johnson−Cousins
2MASS
WD 1828+668
Mass = 0.77$M_\odot$ $T_{\rm eff}$ = 10980K
GALEX
Johnson−Cousins
WISE
WD 1833+644
Mass = 0.62$M_\odot$ $T_{\rm eff}$ = 47160K
GALEX
SDSS
Johnson−Cousins
2MASS
WISE
WD 1834−781
Mass = 0.51$M_\odot$ $T_{\rm eff}$ = 19060K
GALEX
Johnson−Cousins
Stromgren
2MASS
WISE
WD 1845+683
Mass = 0.83$M_\odot$ $T_{\rm eff}$ = 37310K
GALEX
Johnson−Cousins
2MASS
WISE
F_ν (mJy)
Wavelength (μm)

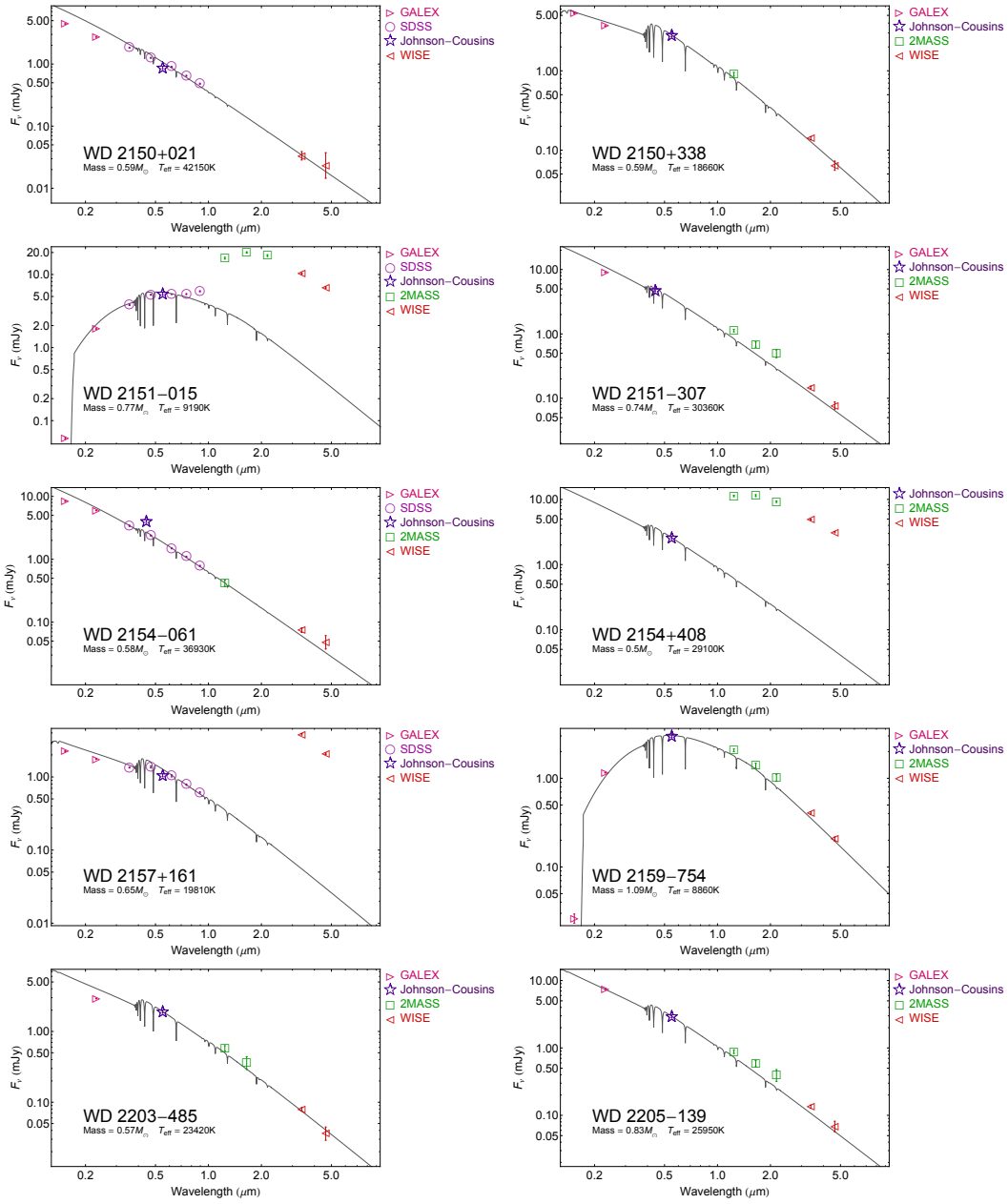

WD 1855+338
Mass = 0.87$M_\odot$ $T_{\rm eff}$ = 12390K
Johnson−Cousins
Stromgren
2MASS
WD 1857+119
Mass = 0.72$M_\odot$ $T_{\rm eff}$ = 10020K
Johnson−Cousins
2MASS
WD 1914+094
Mass = 0.62$M_\odot$ $T_{\rm eff}$ = 33560K
Johnson−Cousins
2MASS
WD 1918+725
Mass = 0.6$M_\odot$ $T_{\rm eff}$ = 22780K
GALEX
Johnson−Cousins
2MASS
WISE
WD 1932−136
Mass = 0.55$M_\odot$ $T_{\rm eff}$ = 17520K
Johnson−Cousins
2MASS
WD 1948−389
Mass = 0.54$M_\odot$ $T_{\rm eff}$ = 38490K
GALEX
Johnson−Cousins
2MASS
WISE
WD 1950−432
Mass = 0.52$M_\odot$ $T_{\rm eff}$ = 43390K
Stromgren
2MASS
WISE
WD 1950+250
Mass = 0.68$M_\odot$ $T_{\rm eff}$ = 12110K
Johnson−Cousins
2MASS
WD 1952−206
Mass = 0.6$M_\odot$ $T_{\rm eff}$ = 14370K
GALEX
Johnson−Cousins
2MASS
WISE
WD 1958−501
Mass = 0.69$M_\odot$ $T_{\rm eff}$ = 56870K
Johnson−Cousins
2MASS
WISE
F_ν (mJy)
Wavelength (μm)

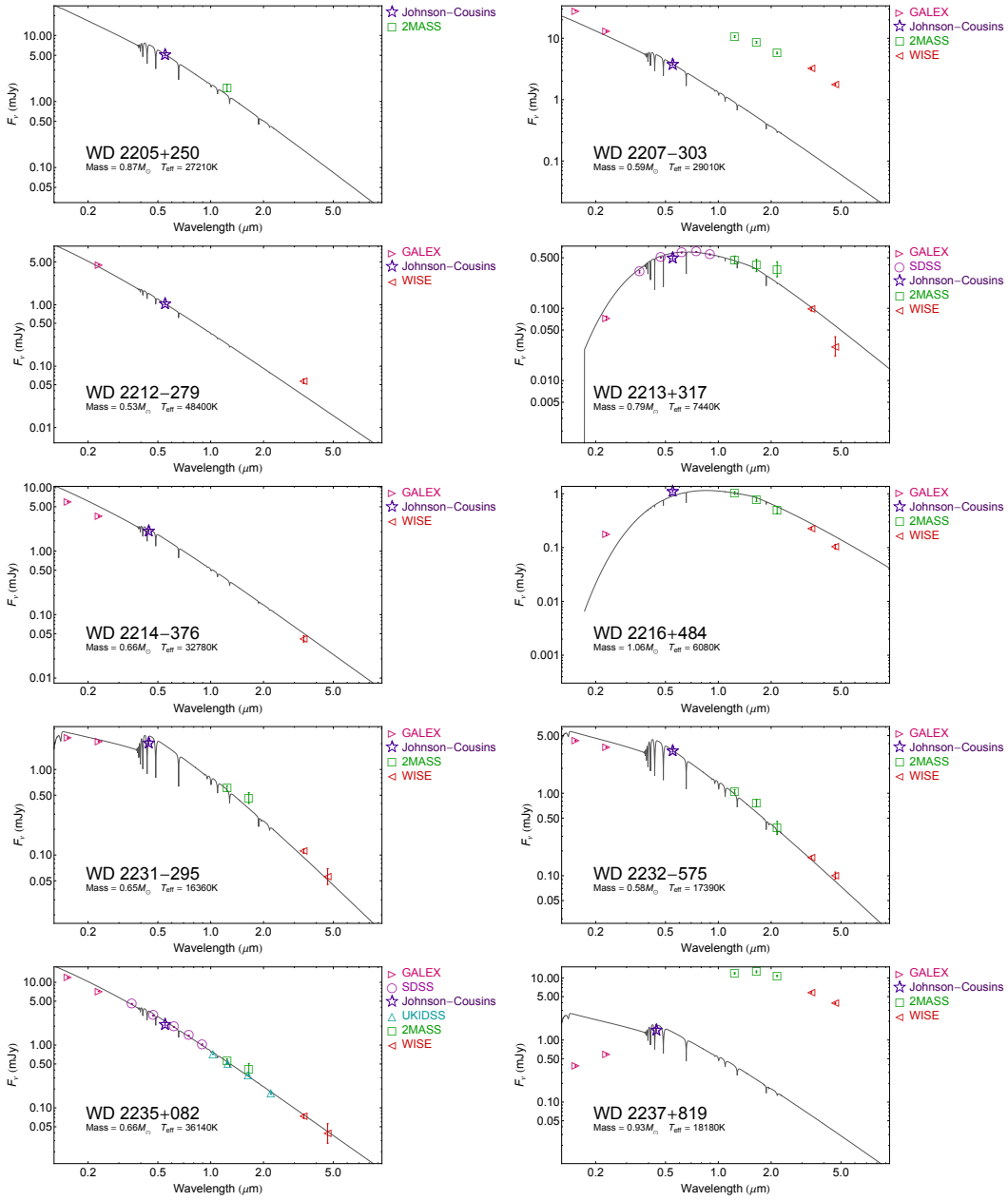

GALEX
Johnson−Cousins
2MASS
WISE
WD 1958+675
Mass = 0.51$M_\odot$ $T_{\rm eff}$ = 24570K
WD 1959+059
Mass = 0.76$M_\odot$ $T_{\rm eff}$ = 10990K
WD 2003+437
Mass = 0.55$M_\odot$ $T_{\rm eff}$ = 17350K
WD 2008+510
Mass = 0.58$M_\odot$ $T_{\rm eff}$ = 14080K
WD 2009+622
Mass = 0.52$M_\odot$ $T_{\rm eff}$ = 26520K
WD 2010+613
Mass = 0.59$M_\odot$ $T_{\rm eff}$ = 13750K
WD 2018−233
Mass = 0.65$M_\odot$ $T_{\rm eff}$ = 15700K
WD 2020−425
Mass = 0.67$M_\odot$ $T_{\rm eff}$ = 31220K
WD 2022+198
Mass = 0.71$M_\odot$ $T_{\rm eff}$ = 52970K
WD 2025+488
Mass = 0.68$M_\odot$ $T_{\rm eff}$ = 10900K
F_ν (mJy)
Wavelength (μm)

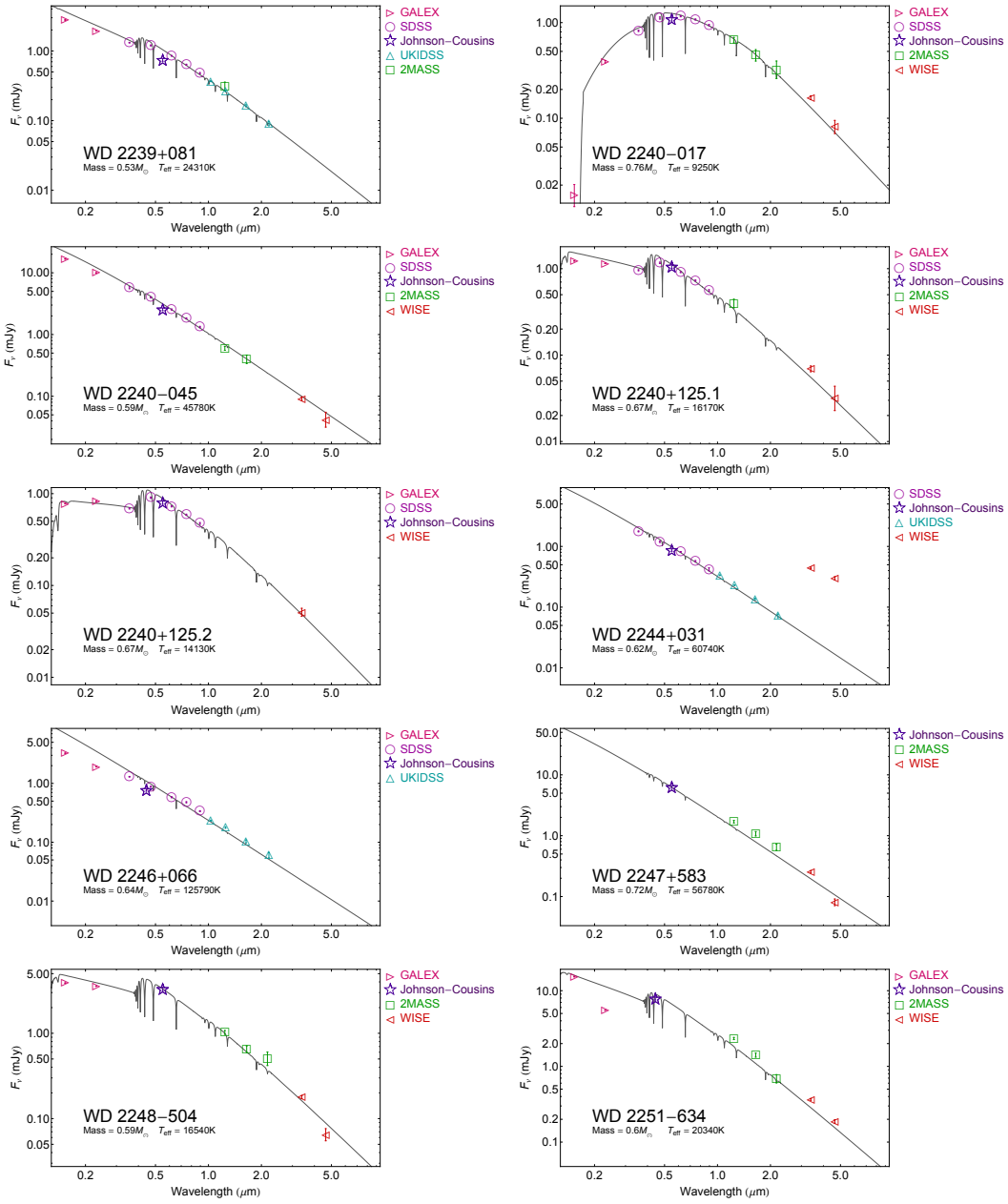

WD 2025+554
Mass = 0.57$M_\odot$ $T_{\rm eff}$ = 31390K
WD 2029+183
Mass = 0.56$M_\odot$ $T_{\rm eff}$ = 13560K
WD 2031−277
Mass = 0.68$M_\odot$ $T_{\rm eff}$ = 54230K
WD 2035−174
Mass = 0.57$M_\odot$ $T_{\rm eff}$ = 17530K
WD 2035−336
Mass = 0.58$M_\odot$ $T_{\rm eff}$ = 19460K
WD 2040−392
Mass = 0.76$M_\odot$ $T_{\rm eff}$ = 11300K
WD 2043−635
Mass = 0.78$M_\odot$ $T_{\rm eff}$ = 27740K
WD 2044−043
Mass = 0.76$M_\odot$ $T_{\rm eff}$ = 10480K
WD 2048+809
Mass = 0.81$M_\odot$ $T_{\rm eff}$ = 8440K
WD 2051−208
Mass = 1.24$M_\odot$ $T_{\rm eff}$ = 21460K
GALEX
Johnson−Cousins
2MASS
WISE
F_ν (mJy)
Wavelength (μm)

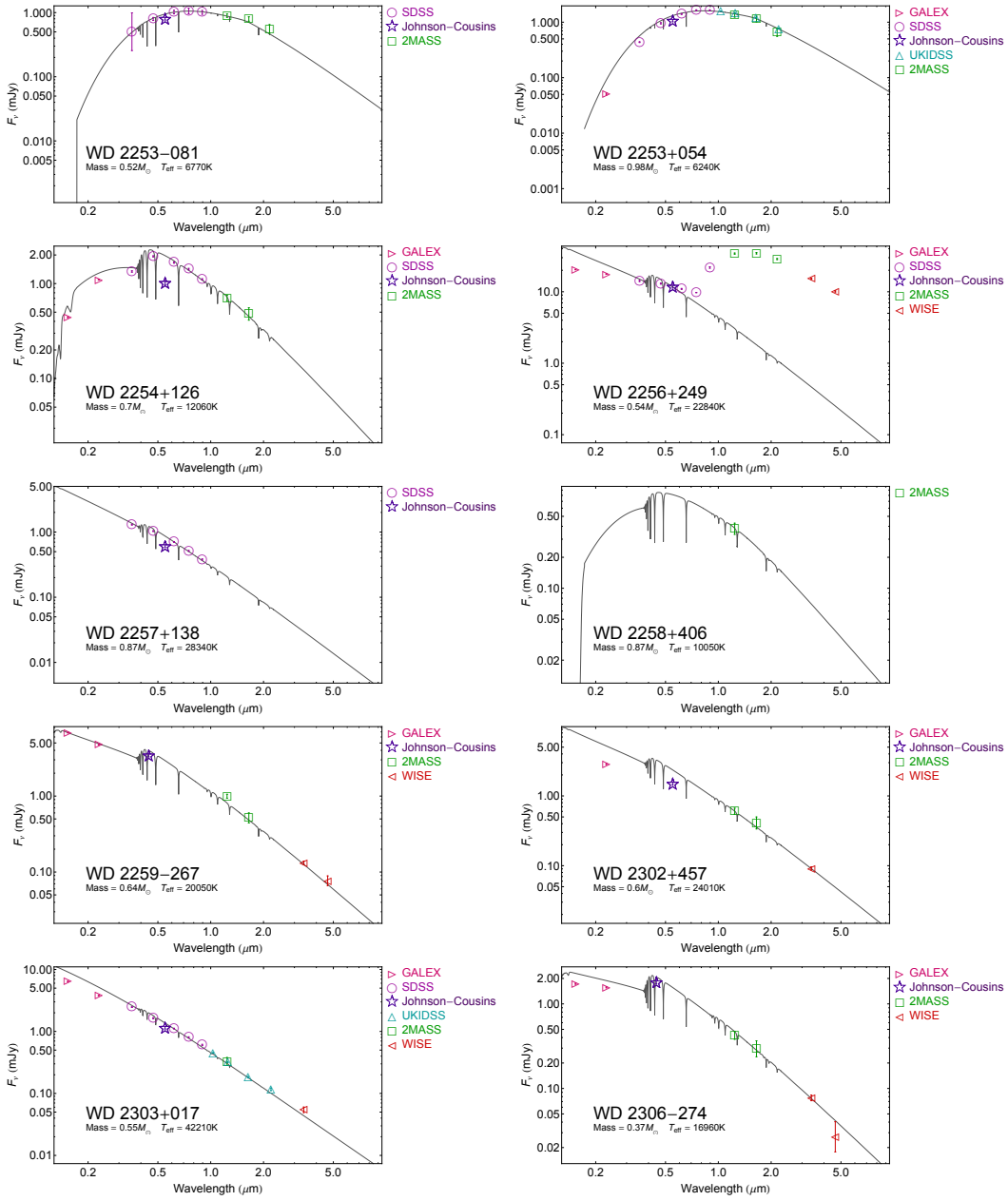

WD 2051+095
Mass = 0.59$M_\odot$ $T_{\rm eff}$ = 15670K
WD 2058+083
Mass = 0.64$M_\odot$ $T_{\rm eff}$ = 37420K
WD 2114−376
Mass = 0.5$M_\odot$ $T_{\rm eff}$ = 24050K
WD 2115+118
Mass = 0.62$M_\odot$ $T_{\rm eff}$ = 62240K
WD 2116+675
Mass = 0.65$M_\odot$ $T_{\rm eff}$ = 14060K
WD 2116+736
Mass = 0.58$M_\odot$ $T_{\rm eff}$ = 54580K
WD 2119+581
Mass = 0.68$M_\odot$ $T_{\rm eff}$ = 8190K
WD 2124−224
Mass = 0.6$M_\odot$ $T_{\rm eff}$ = 48800K
WD 2132+367
Mass = 0.69$M_\odot$ $T_{\rm eff}$ = 7420K
WD 2133−366
Mass = 0.52$M_\odot$ $T_{\rm eff}$ = 26940K
F_ν (mJy)
Wavelength (μm)
GALEX
SDSS
Johnson−Cousins
2MASS
WISE

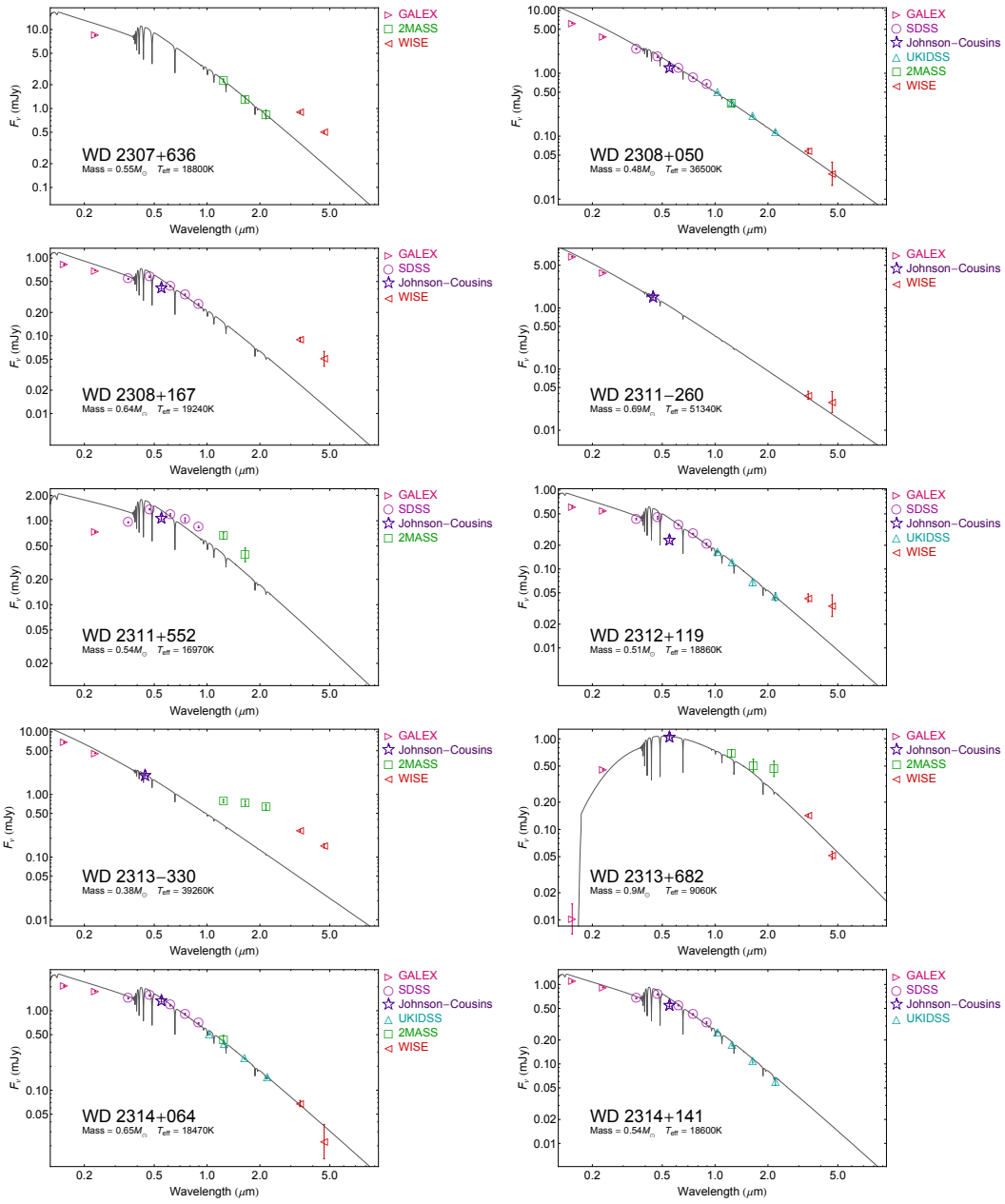

WD 2136+229
Mass = 0.71$M_\odot$ $T_{\rm eff}$ = 10320K
WD 2138+214
Mass = 0.77$M_\odot$ $T_{\rm eff}$ = 10510K
WD 2139+115
Mass = 0.6$M_\odot$ $T_{\rm eff}$ = 16300K
WD 2139+132.1
Mass = 0.73$M_\odot$ $T_{\rm eff}$ = 7660K
WD 2143+353
Mass = 0.58$M_\odot$ $T_{\rm eff}$ = 26100K
WD 2146−433
Mass = 0.53$M_\odot$ $T_{\rm eff}$ = 78090K
WD 2148−291
Mass = 0.69$M_\odot$ $T_{\rm eff}$ = 11810K
WD 2148+539
Mass = 0.66$M_\odot$ $T_{\rm eff}$ = 11900K
WD 2149+021
Mass = 0.62$M_\odot$ $T_{\rm eff}$ = 18170K
WD 2149+372
Mass = 0.6$M_\odot$ $T_{\rm eff}$ = 13640K
GALEX
SDSS
Johnson−Cousins
2MASS
WISE
F_ν (mJy)
Wavelength (μm)

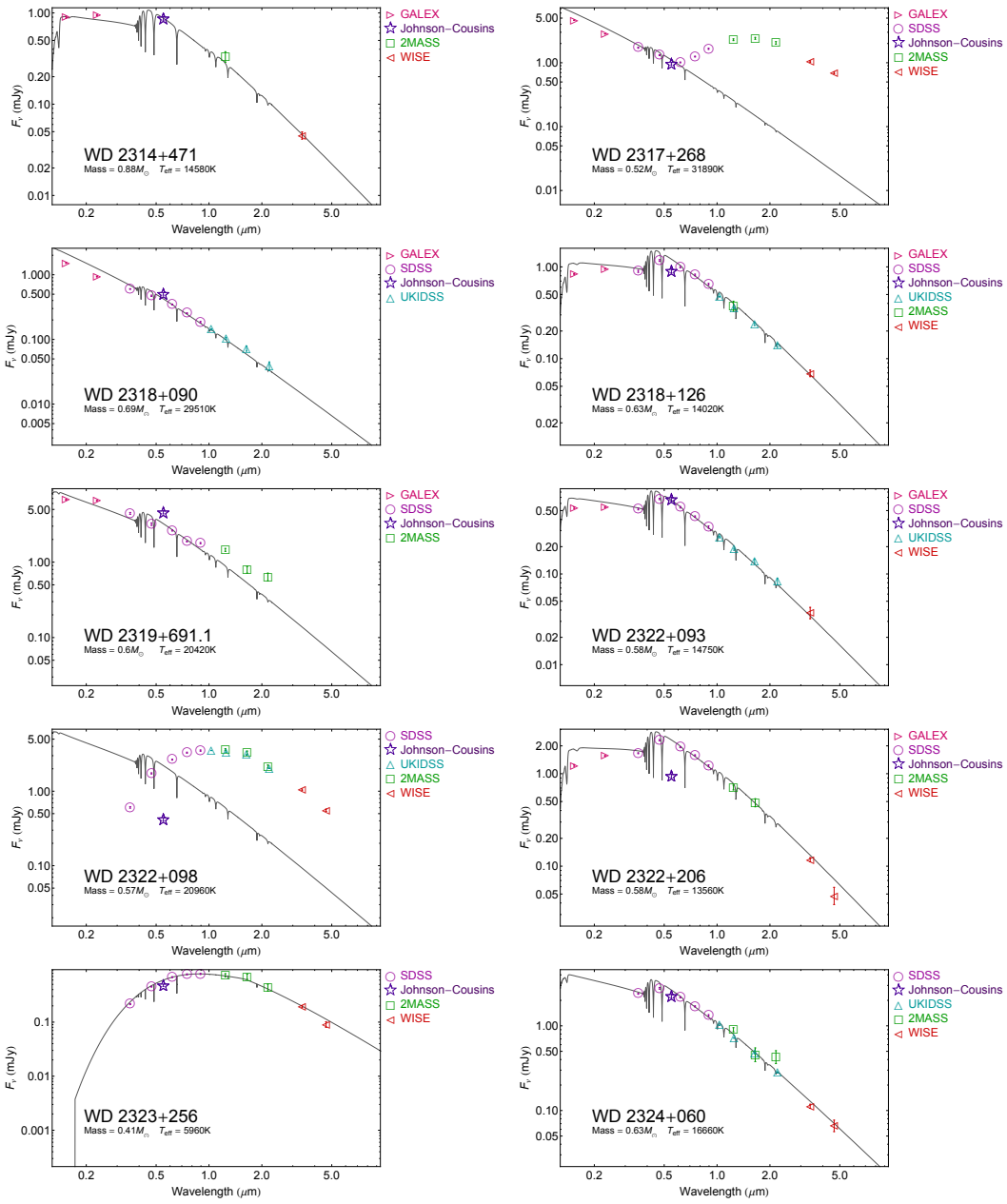

WD 2150+021
Mass = 0.59$M_\odot$ $T_{\rm eff}$ = 42150K
WD 2150+338
Mass = 0.59$M_\odot$ $T_{\rm eff}$ = 18660K
WD 2151−015
Mass = 0.77$M_\odot$ $T_{\rm eff}$ = 9190K
WD 2151−307
Mass = 0.74$M_\odot$ $T_{\rm eff}$ = 30360K
WD 2154−061
Mass = 0.58$M_\odot$ $T_{\rm eff}$ = 36930K
WD 2154+408
Mass = 0.5$M_\odot$ $T_{\rm eff}$ = 29100K
WD 2157+161
Mass = 0.65$M_\odot$ $T_{\rm eff}$ = 19810K
WD 2159−754
Mass = 1.09$M_\odot$ $T_{\rm eff}$ = 8860K
WD 2203−485
Mass = 0.57$M_\odot$ $T_{\rm eff}$ = 23420K
WD 2205−139
Mass = 0.83$M_\odot$ $T_{\rm eff}$ = 25950K
F_ν (mJy)
Wavelength (μm)
GALEX
SDSS
Johnson−Cousins
2MASS
WISE

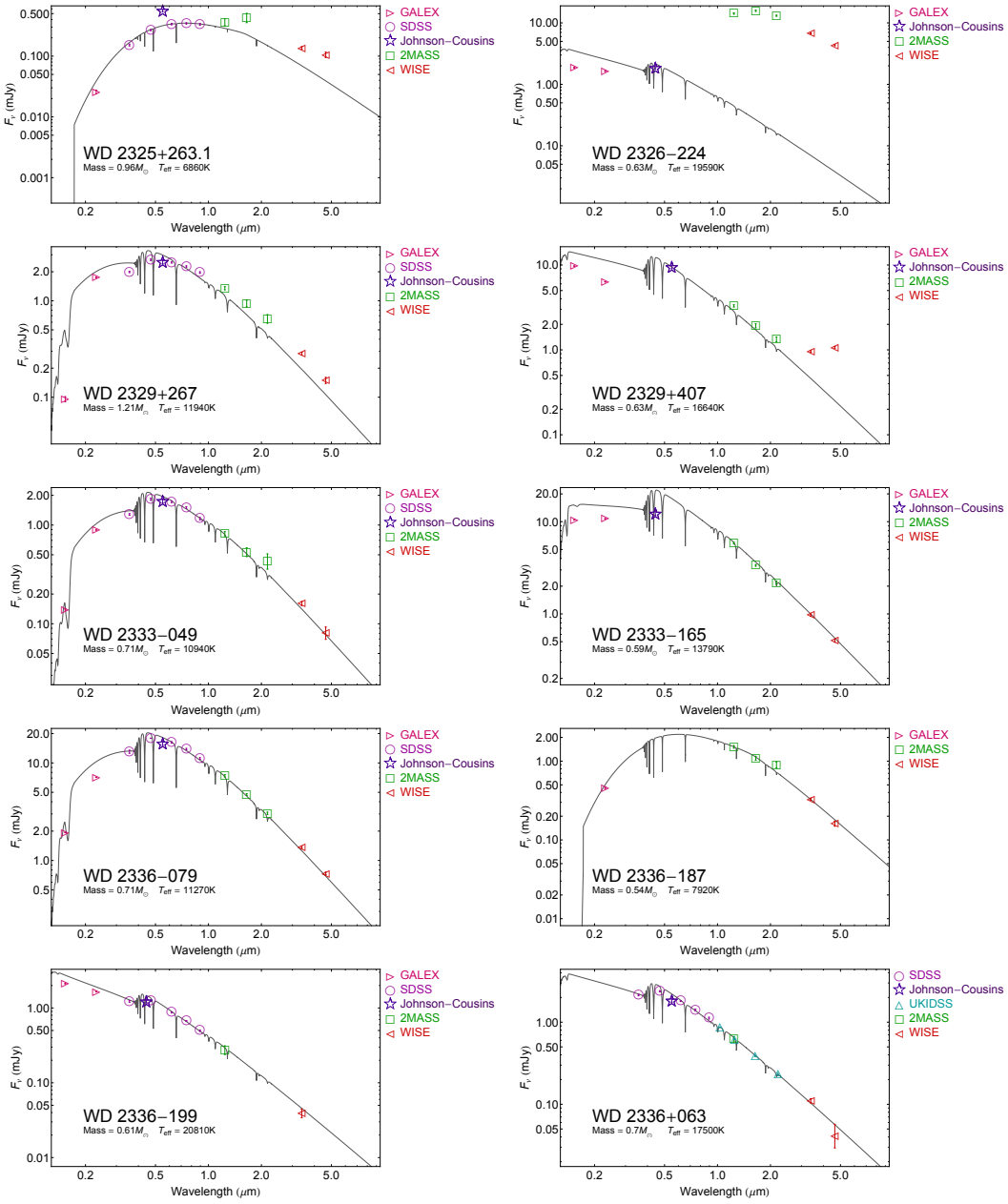

WD 2205+250
Mass = 0.87$M_\odot$ $T_{\rm eff}$ = 27210K
Johnson−Cousins
2MASS
WD 2207−303
Mass = 0.59$M_\odot$ $T_{\rm eff}$ = 29010K
GALEX
Johnson−Cousins
2MASS
WISE
WD 2212−279
Mass = 0.53$M_\odot$ $T_{\rm eff}$ = 48400K
GALEX
Johnson−Cousins
WISE
WD 2213+317
Mass = 0.79$M_\odot$ $T_{\rm eff}$ = 7440K
GALEX
SDSS
Johnson−Cousins
2MASS
WISE
WD 2214−376
Mass = 0.66$M_\odot$ $T_{\rm eff}$ = 32780K
GALEX
Johnson−Cousins
WISE
WD 2216+484
Mass = 1.06$M_\odot$ $T_{\rm eff}$ = 6080K
GALEX
Johnson−Cousins
2MASS
WISE
WD 2231−295
Mass = 0.65$M_\odot$ $T_{\rm eff}$ = 16360K
GALEX
Johnson−Cousins
2MASS
WISE
WD 2232−575
Mass = 0.58$M_\odot$ $T_{\rm eff}$ = 17390K
GALEX
Johnson−Cousins
2MASS
WISE
WD 2235+082
Mass = 0.66$M_\odot$ $T_{\rm eff}$ = 36140K
GALEX
SDSS
Johnson−Cousins
UKIDSS
2MASS
WISE
WD 2237+819
Mass = 0.93$M_\odot$ $T_{\rm eff}$ = 18180K
GALEX
Johnson−Cousins
2MASS
WISE
F_ν (mJy)
Wavelength (μm)

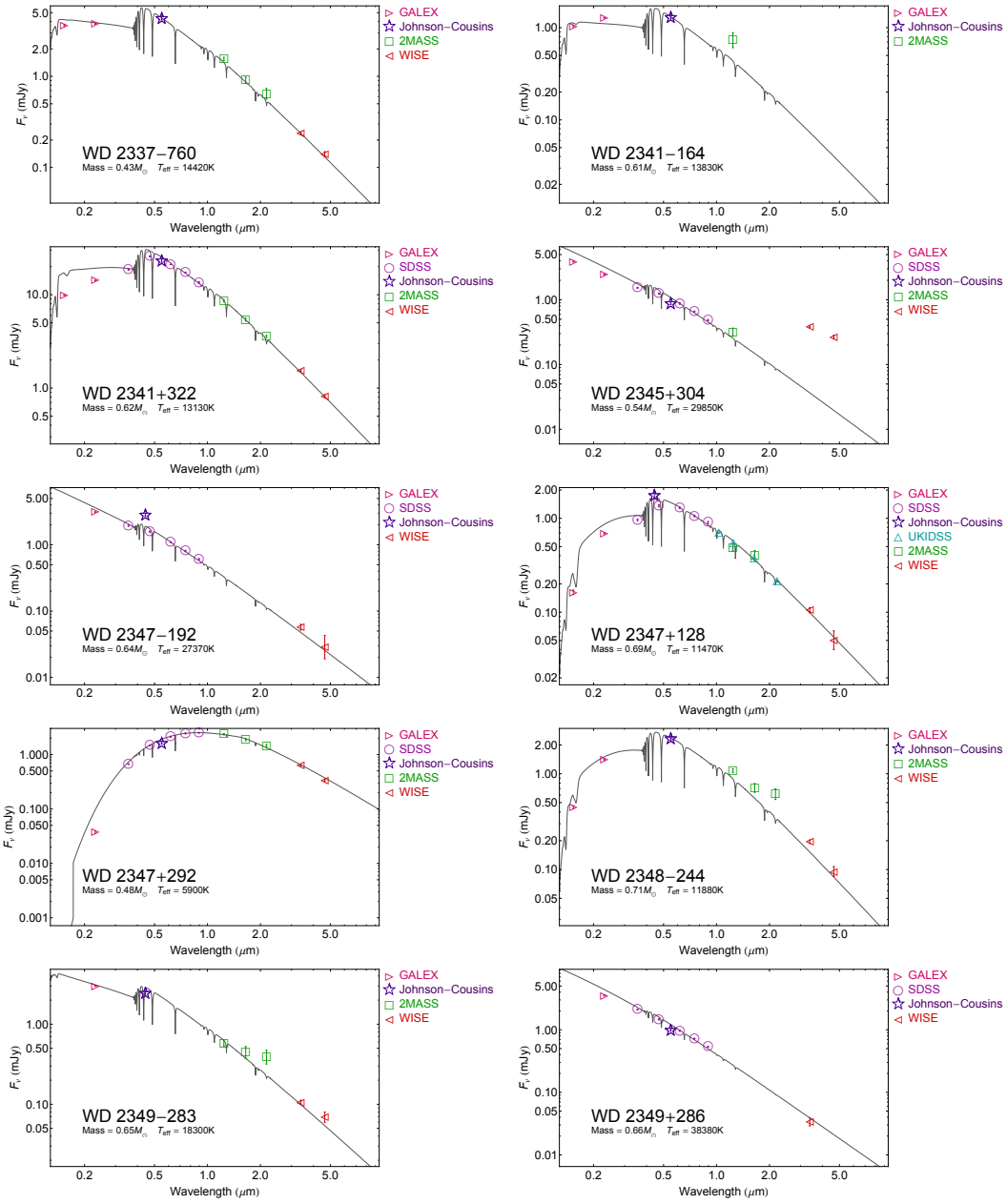

WD 2239+081
Mass = 0.53$M_\odot$ $T_{\rm eff}$ = 24310K
GALEX
SDSS
Johnson–Cousins
UKIDSS
2MASS
WD 2240–017
Mass = 0.76$M_\odot$ $T_{\rm eff}$ = 9250K
GALEX
SDSS
Johnson–Cousins
2MASS
WISE
WD 2240–045
Mass = 0.59$M_\odot$ $T_{\rm eff}$ = 45780K
GALEX
SDSS
Johnson–Cousins
2MASS
WISE
WD 2240+125.1
Mass = 0.67$M_\odot$ $T_{\rm eff}$ = 16170K
GALEX
SDSS
Johnson–Cousins
2MASS
WISE
WD 2240+125.2
Mass = 0.67$M_\odot$ $T_{\rm eff}$ = 14130K
GALEX
SDSS
Johnson–Cousins
WISE
WD 2244+031
Mass = 0.62$M_\odot$ $T_{\rm eff}$ = 60740K
SDSS
Johnson–Cousins
UKIDSS
WISE
WD 2246+066
Mass = 0.64$M_\odot$ $T_{\rm eff}$ = 125790K
GALEX
SDSS
Johnson–Cousins
UKIDSS
WD 2247+583
Mass = 0.72$M_\odot$ $T_{\rm eff}$ = 56780K
Johnson–Cousins
2MASS
WISE
WD 2248–504
Mass = 0.59$M_\odot$ $T_{\rm eff}$ = 16540K
GALEX
Johnson–Cousins
2MASS
WISE
WD 2251–634
Mass = 0.6$M_\odot$ $T_{\rm eff}$ = 20340K
GALEX
Johnson–Cousins
2MASS
WISE
F_ν (mJy)
Wavelength (μm)

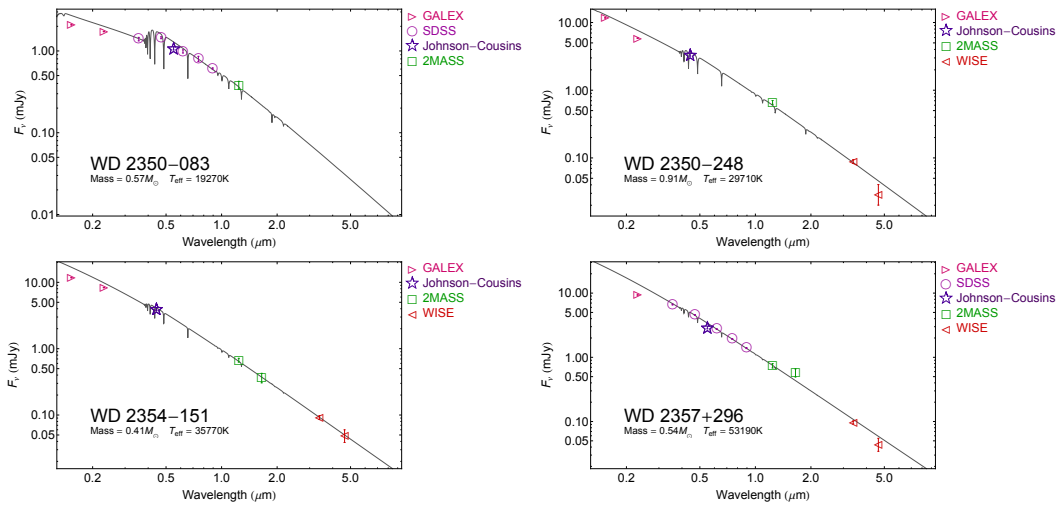

WD 2253−081
Mass = 0.52$M_\odot$ $T_{\rm eff}$ = 6770K
SDSS
Johnson−Cousins
2MASS
WD 2253+054
Mass = 0.98$M_\odot$ $T_{\rm eff}$ = 6240K
GALEX
SDSS
Johnson−Cousins
UKIDSS
2MASS
WD 2254+126
Mass = 0.7$M_\odot$ $T_{\rm eff}$ = 12060K
GALEX
SDSS
Johnson−Cousins
2MASS
WD 2256+249
Mass = 0.54$M_\odot$ $T_{\rm eff}$ = 22840K
GALEX
SDSS
Johnson−Cousins
2MASS
WISE
WD 2257+138
Mass = 0.87$M_\odot$ $T_{\rm eff}$ = 28340K
SDSS
Johnson−Cousins
WD 2258+406
Mass = 0.87$M_\odot$ $T_{\rm eff}$ = 10050K
2MASS
WD 2259−267
Mass = 0.64$M_\odot$ $T_{\rm eff}$ = 20050K
GALEX
Johnson−Cousins
2MASS
WISE
WD 2302+457
Mass = 0.6$M_\odot$ $T_{\rm eff}$ = 24010K
GALEX
Johnson−Cousins
2MASS
WISE
WD 2303+017
Mass = 0.55$M_\odot$ $T_{\rm eff}$ = 42210K
GALEX
SDSS
Johnson−Cousins
UKIDSS
2MASS
WISE
WD 2306−274
Mass = 0.37$M_\odot$ $T_{\rm eff}$ = 16960K
GALEX
Johnson−Cousins
2MASS
WISE
F_ν (mJy)
Wavelength (μm)


WD 2307+636
Mass = 0.55$M_\odot$ $T_{\rm eff}$ = 18800K
GALEX
2MASS
WISE
WD 2308+050
Mass = 0.48$M_\odot$ $T_{\rm eff}$ = 36500K
GALEX
SDSS
Johnson–Cousins
UKIDSS
2MASS
WISE
WD 2308+167
Mass = 0.64$M_\odot$ $T_{\rm eff}$ = 19240K
GALEX
SDSS
Johnson–Cousins
WISE
WD 2311–260
Mass = 0.69$M_\odot$ $T_{\rm eff}$ = 51340K
GALEX
Johnson–Cousins
WISE
WD 2311+552
Mass = 0.54$M_\odot$ $T_{\rm eff}$ = 16970K
GALEX
SDSS
Johnson–Cousins
2MASS
WD 2312+119
Mass = 0.51$M_\odot$ $T_{\rm eff}$ = 18860K
GALEX
SDSS
Johnson–Cousins
UKIDSS
WISE
WD 2313–330
Mass = 0.38$M_\odot$ $T_{\rm eff}$ = 39260K
GALEX
Johnson–Cousins
2MASS
WISE
WD 2313+682
Mass = 0.9$M_\odot$ $T_{\rm eff}$ = 9060K
GALEX
Johnson–Cousins
2MASS
WISE
WD 2314+064
Mass = 0.65$M_\odot$ $T_{\rm eff}$ = 18470K
GALEX
SDSS
Johnson–Cousins
UKIDSS
2MASS
WISE
WD 2314+141
Mass = 0.54$M_\odot$ $T_{\rm eff}$ = 18600K
GALEX
SDSS
Johnson–Cousins
UKIDSS
F_ν (mJy)
Wavelength (μm)


WD 2314+471
Mass = 0.88$M_\odot$ $T_{\rm eff}$ = 14580K
WD 2317+268
Mass = 0.52$M_\odot$ $T_{\rm eff}$ = 31890K
WD 2318+090
Mass = 0.69$M_\odot$ $T_{\rm eff}$ = 29510K
WD 2318+126
Mass = 0.63$M_\odot$ $T_{\rm eff}$ = 14020K
WD 2319+691.1
Mass = 0.6$M_\odot$ $T_{\rm eff}$ = 20420K
WD 2322+093
Mass = 0.58$M_\odot$ $T_{\rm eff}$ = 14750K
WD 2322+098
Mass = 0.57$M_\odot$ $T_{\rm eff}$ = 20960K
WD 2322+206
Mass = 0.58$M_\odot$ $T_{\rm eff}$ = 13560K
WD 2323+256
Mass = 0.41$M_\odot$ $T_{\rm eff}$ = 5960K
WD 2324+060
Mass = 0.63$M_\odot$ $T_{\rm eff}$ = 16660K
F_ν (mJy)
Wavelength (μm)
GALEX
SDSS
Johnson–Cousins
UKIDSS
2MASS
WISE


WD 2325+263.1
Mass = 0.96$M_\odot$ $T_{\rm eff}$ = 6860K
WD 2326−224
Mass = 0.63$M_\odot$ $T_{\rm eff}$ = 19590K
WD 2329+267
Mass = 1.21$M_\odot$ $T_{\rm eff}$ = 11940K
WD 2329+407
Mass = 0.63$M_\odot$ $T_{\rm eff}$ = 16640K
WD 2333−049
Mass = 0.71$M_\odot$ $T_{\rm eff}$ = 10940K
WD 2333−165
Mass = 0.59$M_\odot$ $T_{\rm eff}$ = 13790K
WD 2336−079
Mass = 0.71$M_\odot$ $T_{\rm eff}$ = 11270K
WD 2336−187
Mass = 0.54$M_\odot$ $T_{\rm eff}$ = 7920K
WD 2336−199
Mass = 0.61$M_\odot$ $T_{\rm eff}$ = 20810K
WD 2336+063
Mass = 0.7$M_\odot$ $T_{\rm eff}$ = 17500K
F_ν (mJy)
Wavelength (μm)
GALEX
SDSS
Johnson−Cousins
2MASS
WISE
UKIDSS


WD 2337−760
Mass = 0.43$M_\odot$ $T_{\rm eff}$ = 14420K
WD 2341−164
Mass = 0.61$M_\odot$ $T_{\rm eff}$ = 13830K
WD 2341+322
Mass = 0.62$M_\odot$ $T_{\rm eff}$ = 13130K
WD 2345+304
Mass = 0.54$M_\odot$ $T_{\rm eff}$ = 29850K
WD 2347−192
Mass = 0.64$M_\odot$ $T_{\rm eff}$ = 27370K
WD 2347+128
Mass = 0.69$M_\odot$ $T_{\rm eff}$ = 11470K
WD 2347+292
Mass = 0.48$M_\odot$ $T_{\rm eff}$ = 5900K
WD 2348−244
Mass = 0.71$M_\odot$ $T_{\rm eff}$ = 11880K
WD 2349−283
Mass = 0.65$M_\odot$ $T_{\rm eff}$ = 18300K
WD 2349+286
Mass = 0.66$M_\odot$ $T_{\rm eff}$ = 38380K
F_ν (mJy)
Wavelength (μm)
GALEX
SDSS
Johnson−Cousins
UKIDSS
2MASS
WISE


GALEX
SDSS
Johnson−Cousins
2MASS
WISE
WD 2350−083
Mass = 0.57$M_\odot$ $T_{\rm eff}$ = 19270K
WD 2350−248
Mass = 0.91$M_\odot$ $T_{\rm eff}$ = 29710K
WD 2354−151
Mass = 0.41$M_\odot$ $T_{\rm eff}$ = 35770K
WD 2357+296
Mass = 0.54$M_\odot$ $T_{\rm eff}$ = 53190K
F_ν (mJy)
Wavelength (μm)